APPLIED GEOPHYSICS
U.S.S.R.

Edited by

NICHOLAS RAST, B.Sc., Ph.D., F.G.S.

Liverpool University

PERGAMON PRESS

OXFORD • LONDON • NEW YORK • PARIS

1962

PERGAMON PRESS LTD.
Headington Hill Hall, Oxford
4 and 5 Fitzroy Square, London W. 1

PERGAMON PRESS INC.
122 East 55th Street, New York 22, N.Y.
1404 New York Avenue N. W., Washington 5, D. C.

PERGAMON PRESS S.A.R.L.
*24 Rue des Écoles, Paris V^e^*

PERGAMON PRESS G.m.b.H.
Kaiserstrasse 75, Frankfurt am Main

Library of Congress Card Number 60–53385

Printed in Poland
to the order of PWN — Polish Scientific Publishers
by Drukarnia Narodowa, Cracow

EDITOR'S FOREWORD

SPECTACULAR successes achieved by the Soviet scientists in the field of applied physics have focused attention on the vigour of scientific research in the U.S.S.R. As a result a concerted attempt is being made to make the extensive Soviet scientific literature available to Western readers. Although, at present, several institutions are concerned with translations from Russian only rarely are aspects of applied, as distinct from pure, science given their rightful place. Thus, the attempts of the Pergamon Institute to redress this situation are especially welcome. It must be remembered that in the U.S.S.R. scientific workers often follow what can be called an American tradition in not separating sharply the fundamental research from its technological applications. As a consequence many Russian papers dealing with specific industrial problems contain much of general scientific interest. This is especially true with respect to geophysics. Every new method of geophysical exploration is valuable since it provides a new possibility of inspecting the unseen parts of the Earth. In any case in a new science practically every investigation is of some significance if only because it adds to the relatively meagre store of factual data.

In the U.S.S.R. the methods of geophysical research have been extensively applied not only in an effort to find useful minerals, but also in order to accumulate information on the geological structure of that vast country. Furthermore, the accuracy and reproducibility of the geophysical methods has been widely checked with the aid of numerous bore-holes systematically located at critical points. As a result very notable advances have been made in developing the so-called electrical, seismic and gravimetric methods, while the existence of the numerous bore-holes has led to an extensive, application and improvement of the geophysical methods of logging. In the present compendium a selection of papers published in the volumes 18 and 20 of the Soviet journal "Applied Geophysics" are being presented to the Western scientists. The intention is to illustrate some of the achievements of the Russian applied geophysicists by translating their recent publications. Although a fairly wide range of topics is being covered there is a bias towards the application of geophysical methods to the search for oil. In this respect the editor, who was responsible for selecting the papers to be translated, followed the tendency discernible in the original journals. Nonetheless the orientation of many of the included articles on seismic, electrical, gravimetric methods and logging techniques is such that the

volume should appeal not only to the oil geophysicists and geologists but to everyone interested in modern developments in geophysical methodology.

Since the translation of Soviet scientific literature is as yet in a pioneering stage it is, perhaps, not inappropriate to add a few remarks of a purely linguistic nature. The relatively prolonged isolation of Russian scientists from their western colleagues has led to differences in terminology. For instance, the Russian term *equatorialnyi sond* does not mean an equatorial sonde, but probes with a quadrilateral arrangement, while the word *podniatie* in various contexts implies an elevation, a culmination or an upfold. In the present volume, where necessary, the Russian usage is indicated and it is hoped that such editorial remarks will be of use to the translators of scientific Russian. Responsibility for these remarks rests with the editor, but in certain instances Professor R. M. Shackleton and Dr. C. D. V. Wilson of the University of Liverpool were consulted and made suggestions, for which the editor wishes to express his gratitude.

NICHOLAS RAST

CHAPTER 1

INTENSITIES OF REFRACTED AND REFLECTED LONGITUDINAL WAVES AT ANGLES OF INCIDENCE BELOW CRITICAL

V. P. GORBATOVA

THE dynamic properties of waves can be effectively utilized in interpreting seismic prospecting data, since these properties, in conjunction with the velocity components enable us to recognize the nature of any particular wave recorded on the seismogram.

The solution of problems connected with the dynamic propagation of waves presents difficulties which are well known. While part of the work done in this field by PETRASHEN' and the team of mathematicians headed by him has already been published, the theory which we have in mind has been fully worked out only for ideally elastic horizontally laminated media.

Each of the layers is presumed to be sufficiently "dense", that is to say the travel time of a disturbance in the layer is substantially longer than the duration of the pulse transmitted. The velocity of propagation of longitudinal and transverse waves, however, as well as the densities, is constant inside the layer and assume new values on the boundaries of the layers.

Quantitative comparisons made up to date have not revealed any sharp discrepancy between theory and experiment. The theoretically discovered qualitative laws also show good agreement with seismic prospecting practice. We suggest that there would be undoubted advantage in introducing the theory, in the form in which it has been worked out to date, into the interpretation of field data.

A method for calculating the intensities and shapes of seismic traces for different waves propagated in media with plane-parallel boundaries has been worked out in detail in the Leningrad Section of the Institute of Mathematics (Academy of Sciences of the U.S.S.R.) [2,3]. The Section has also compiled tables for fairly accurate calculations.

In this paper we offer a number of simplified methods for determining the intensities of purely longitudinal waves (in the media referred to) and discuss how the different parameters of the medium affect their frequency rate.

In the main these simplifications mean that the frequency rates of the waves under consideration are determined not by accurate tables but simply by a small number of typical graphs, which we shall give later. Further, the assumption has been made that layers possessing a higher longitudinal velocity have also a higher ratio of transverse velocity to longitudinal velocity and a greater density. This would appear to be true for most real media.

The elastic properties of two neighbouring media (the ith and the $i+1$th) are characterized by the following parameters: α—the ratio of the lower longitudinal velocity to the higher; γ—the ratio of the transverse velocity to the longitudinal velocity in the layer where v_p is the smaller; Δ—the ratio of the transverse velocity to the longitudinal velocity in a layer where v_p is the greater; σ—the ratio of the lower density to the higher.

If $v_{i,p} < v_{i+1,p}$,

$$\alpha = \frac{v_{i,p}}{v_{i+1,p}}, \quad \gamma = \frac{v_{i,s}}{v_{i,p}}, \quad \Delta = \frac{v_{i+1,s}}{v_{i+1,p}}, \quad \sigma = \frac{\varrho_i}{\varrho_{i+1}}.$$

If $v_{i,p} > v_{i+1,p}$,

$$\alpha = \frac{v_{i+1,p}}{v_{i,p}}, \quad \gamma = \frac{v_{i+1,s}}{v_{i+1,p}}, \quad \Delta = \frac{v_{i,s}}{v_{i,p}}, \quad \sigma = \frac{\varrho_{i+1}}{\varrho_i};$$

That is, $\gamma \leqslant \Delta$, $\sigma \leqslant 1{,}0$, $\alpha < 1$, on all occasions.

The parameters α, γ, Δ and σ of adjacent layers, on whose boundaries refraction occurs, are chosen within the following limits:

$$0.3 \leqslant \alpha < 0.9, \; 0.3 \leqslant \gamma < 0.6, \quad 0.4 \leqslant \Delta \leqslant 0.6, \; 0.7 \leqslant \sigma \leqslant 1.0$$

But the boundaries of adjacent layers characterized by the parameters $\gamma = 0.3$, $\Delta = 0.6$ are excluded. For the ratio of transverse velocities in the boundary media therefore we shall always assume: $0.3 \leqslant \delta \leqslant 0.9$,

where

$$\delta = \begin{cases} \dfrac{v_{i,s}}{v_{i+1,s}}, & \text{if } v_{i,p} < v_{i+1,p} \\ \dfrac{v_{i+1,s}}{v_{i,s}}, & \text{if } v_{i,p} > v_{i+1,p}. \end{cases}$$

Table 1 shows values for the parameters of adjacent layers on whose boundary reflection occurs if the reflection takes place from the layer in which the travel velocity of longitudinal waves is higher than in the layer through which the wave has passed. If the reflection occurs from the layer with the lower group velocity the values for the parameters will be found in Table 2.

TABLE 1

γ	0.6	0.5	0.4	0.6	0.5	0.4	0.5	0.4	0.3	0.4	0.3
Δ	0.6	0.5	0.4	0.6	0.5	0.4	0.6	0.5	0.4	0.6	0.5
α	0.3–0.7	0.3–0.7	0.3–0.7	0.7–0.9	0.7–0.9	0.7–0.9	0.36–0.6	0.375–0.625	0.4–0.667	$\alpha \leqslant 0.45$	$\alpha \leqslant 0.5$
σ	0.7–1.0	0.7–1.0	0.7–1.0	1.0	1.0	1.0	0.7–1.0	0.7–1.0	0.7–1.0	0.7–1.0	0.7–1.0

TABLE 2

γ	0.6	0.5	0.4	0.6	0.5	0.4	0.5	0.4	0.3
Δ	0.6	0.5	0.4	0.6	0.5	0.4	0.6	0.5	0.4
α	0.3–0.7	0.3–0.7	0.3–0.7	0.7–0.9	0.7–0.9	0.7–0.9	0.36–0.6	0.375–0.625	0.4–0.667
σ	0.7–1.0	0.7–1.0	0.7–1.0	1.0	1.0	1.0	0.7–1.0	0.7–1.0	0.7–1.0

The angles at which simple and multiple waves strike the reflecting boundaries are assumed to vary from zero to the value of α_1 where $\sin \alpha_1 = 0.75 \sin \alpha_{cr}$. But in the case of reflection from media where the group velocity wave is travelling, the angles of incidence onto the reflecting boundary are treated as having a sine less than or equal to 0.6.

In this way then, we can investigate the intensity* and shape of vertical displacements of points on a free surface caused by the arrival of purely longitudinal waves. The source of excitation chosen will be a shot fired in the upper layer of the medium.

In our analysis of the intensities of the head and reflected waves we shall always assume that the conditions of the excitation remain unchanged and that the velocity of propagation of the longitudinal waves and the density of the medium in the layer where the shot is fired are kept constant. The head waves are examined at a distance from their points of emergence, while the simple reflected waves will be examined at a distance from the points of emergence of the head waves formed at the same interfaces as the simple reflected wave under consideration.

By the expression "at a distance from the points of emergence" of a head wave, we mean all points on the ground surface lying at a distance r from the shot point, which satisfy the inequality (1).

$$|r - r_0| \geqslant 0.7 \sqrt{\lambda_b \left[\sum_{i=0}^{n-1} \frac{2h_i \tan \alpha_i}{\cos^2 \alpha_i} - \frac{h_{sd} \tan \alpha_0}{\cos^2 \alpha_0} \right]}, \qquad (1)$$

Where r_0 is the abscissa of the point of origin of the head wave under consideration:

λ_b is the wave-length when the wave is travelling along the refracting boundary; $\lambda_b = v_b T$. Here T is the predominant period of the vibration being propagated, and v_b is the boundary velocity of the head wave under consideration;

h_i is the thickness of the ith layer of the covering medium;

α_i is the angle at which the wave under consideration (head or reflected) passes through the ith layer;

h_{sd} is the shot depth.

* By intensity we mean a quantity proportional to the amount of maximum displacement of points on the ground surface caused by the arrival of the wave under consideration. If the same conditions of excitation are maintained, the coefficient of proportionality is constant for all primary waves. It is also constant for all reflected waves, but is not the same as for primary waves.

Multiple reflected waves are examined at a distance from the points of emergence of like reflected-refracted waves. We evaluate the distance with the help of inequalities similar to (1), where only in the term $\sum \frac{h_i \tan \alpha_i}{\cos^2 \alpha_i}$ is each of the items repeated as many times as the multiple wave under consideration passes through the ith layer.

METHODS FOR CALCULATING INTENSITIES

Head Waves

The intensity of a head wave propagated in a medium (Fig. 1) from the $n-1$th and nth boundaries of the layers is determined by the expression

$$j_{head} = \frac{C_0 \prod_{i=0}^{n-2} (P_i P_{i+1})(P_{i+1} P_i) \Gamma^{pp}(p)}{4\pi (\lambda_0 + 2\mu_0) \sqrt{r} (r - r_0)^{3/2}}, \qquad (2)$$

where C_0 is some multiplier dependent on the properties of the zero layer*

$\Gamma^{pp}(p)$ is the coefficient of the head wave formation at the boundary of the $n1$th and nth layers;

r is the distance between shot point and the observation point along the free surface;

r_0 is the abscissa of the point of origin of the head wave under consideration;

λ_0, and μ_0 are the Lamé constants for the layer where the shot is fired;

$(P_i P_{i+1})(P_{i+1} P_i)$ are the coefficients of refraction in the intensities when the wave is passing through the boundary between the ith and the $i+1$th layers from above to below and from below to above.

In the product $\prod_{i=0}^{n-2} (P_i P_{i+1})(P_{i+1} P_i)$ in formula (2) the coefficients of refraction of the wave under consideration at all the intermediate interfaces are taken into account.

The coefficients of refraction, the coefficients of head wave formation, and also the multiplier C_0 depend both on the properties of the interfaces themselves and also on the angle at which the primary wave under consideration strikes these boundaries. Values for these coefficients are given in the detailed tables compiled by the team of mathematicians headed by Petrashen' at the Leningrad Section of the Institute of Mathematics. Using these tables to determine the quantities mentioned we have compiled graphs

* The advisability of using this lies in the fact that if the calculations are suffciently approximate, we can assume that $C_0 = 2$ when $\sin \alpha_0 \leqslant 0.9$.

on which the sines of the angles of incidence with which we are concerned are plotted against the quantities which interest us or quantities which differ from these by having different multipliers.

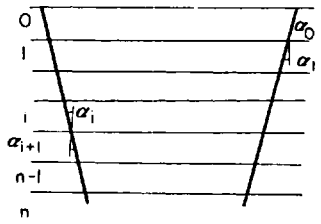

FIG. 1.

The process of calculating the intensities of head waves can be summarized as follows:

1. Using the law of wave refraction we determine the sines of the angles of incidence of the primary wave under consideration at all the interfaces:

$$\sin \alpha_i = \frac{v_{i,\,p}}{v_{n,\,p}}.$$

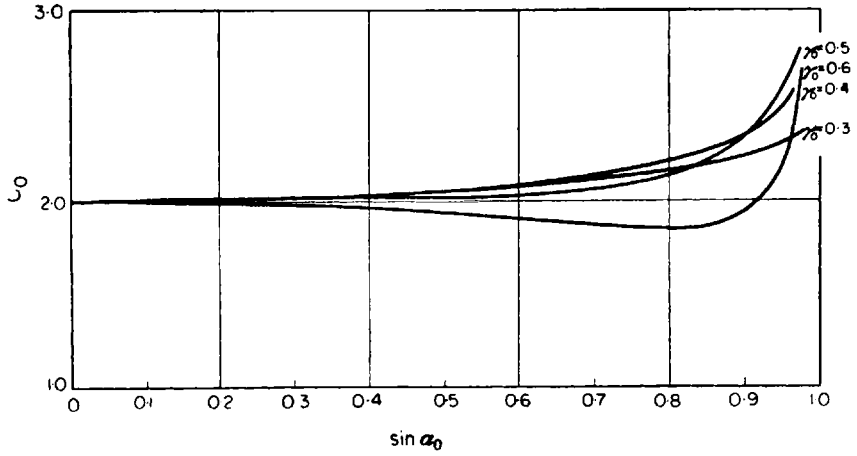

FIG. 2. Curves for the multiplier C_0.

2. From the ordinates of the curve (Fig. 2) which is characterized by the parameter $\gamma_0 = \frac{v_{0,\,s}}{v_{0,\,e}}$ we take the value for the multiplier with C_0 at the point $x = \sin \alpha_0 = \frac{v_{0,\,e}}{v_{n,\,e}}$

3. To determine the value of the coefficient of refraction $(P_i P_{i+1})\ (P_{i+1} P_i)$ at the point $x = \sin \alpha_j$ (where α_j is the lesser of the angles α_i and α_{i+1}) from the curve in Fig. 3 corresponding to the parameter which is the same as at the boundary of the ith and i1th layers, we take the value of the ordinate $[(P_i P_{i+1})\ (P_{i+1} P_i)]$ rel and multiply by $\frac{4\varrho_i v_{i,p}\, \varrho_{i+1} v_{i+1,p}}{(\varrho_i v_{i,p} + \varrho_{i+1} v_{i+1,p})^2}$, which is the product of coefficients of refraction $(P_i P_{i+1})\ (P_{i+1} P_i)$, of the plane waves when incidence is vertical.

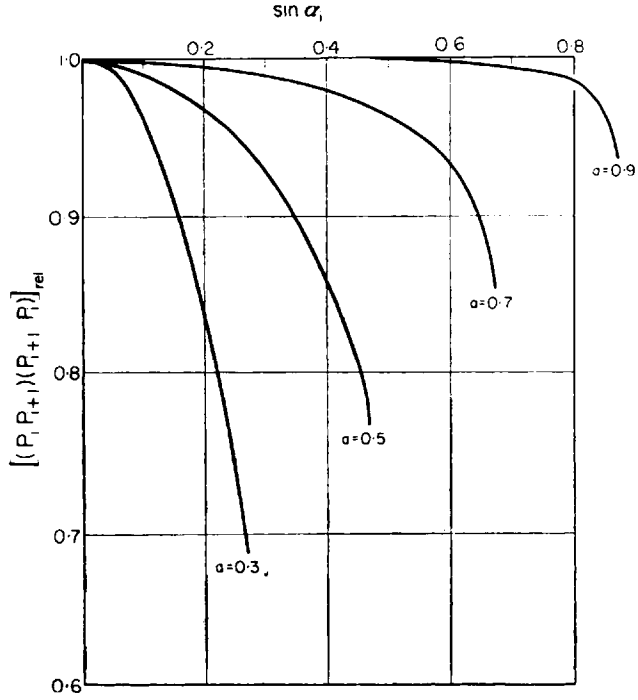

FIG. 3. Curves for determining the coefficient of refraction $[(P_i P_{i+1})\ (P_{i+1} Pi)]$.

The product obtained thus gives the value for the coefficient of refraction $(P_i P_{i+1})\ (P_{i+1} P_i)$.

4. The coefficient $\Gamma^{pp}(p)$ is taken at the point $x = \sin \alpha_{cr} = \frac{v_{n-1,p}}{v_{n,p}}$ from the curve corresponding to the parameters γ, Δ and σ which characterize the boundary of the n1th and nth layers (Fig. 4). Fig. 4 (a and b) shows the $\Gamma^{pp}(p)$ curves for two values of the parameter σ (dotted lines—$\sigma = 0.7$; thick lines—$\sigma = 1.0$).

5. The values obtained for $C_0 (P_i P_{i+1}) (P_{i+1} P_i)$, $\Gamma^{pp}(p)$ and r_0 are inserted in formula (2).

Reflected Simple and Multiple Waves

The intensity of a simple wave reflected from the boundary of the $n1$th and nth layers is determined from formula (3)

$$j_{ref} = \frac{C_0 \prod_{i=0}^{n-2} (P_i P_{i+1}) (P_{i+1} P_i) (P_{n-1} P_{n-1})}{4\pi (\lambda_0 + 2\mu_0) v_{0,p}} \times \frac{\sin \alpha_0}{\sqrt{r \left[\sum_{i=0}^{n-1} 2 \frac{h_i \tan \alpha_i}{\cos^2 \alpha_i} - \frac{h_{sd} \tan \alpha_0}{\cos^2 \alpha_0} \right]}}. \quad (3)$$

Similar formulae are given in MALINOVSKAIA'S work [2].

The intensities of multiple waves are determined from formulae similar to (3). Here again we must take into account all the refractions and reflections at the intermediate interfaces. Therefore if the multiple wave under consideration intersects the interface between the ith and $i+1$th layers while it is travelling from above downwards m times and the same number of times when it is travelling from below upwards, then the multiplier $(P_i P_{i+1})$ $(P_{i+1} P_i)$ is repeated in the product $\Pi (P_i P_{i+1})$ $(P_{i+1} P_i)$ also m times. If the wave suffers n reflections from the given interface, the coefficient of reflection corresponding to this boundary is raised to the nth power. We introduce coefficients raised to the appropriate powers for reflection from all the interfaces at which the wave under consideration suffers further reflections.

We shall henceforward adopt the following notation: if the reflected wave is travelling in the mth layer and is reflected from its lower boundary, the coefficient of reflection will be denoted by $(P_m P_m)$; but if the reflection takes place from the upper boundary of the mth layer the coefficient of reflection will be denoted by $(P_{m'} P_{m'})$.

In the sum $\sum h_i \frac{\tan \alpha_i}{\cos^2 \alpha_i}$ each item is repeated as many times as the multiple wave under consideration passes through the ith layer. If this wave is propagated from the shot point upwards and then is again reflected from the free surface and goes downwards, a further term, $2h_{sd} \frac{\tan \alpha_0}{\cos^2 \alpha_0}$ must be introduced into the sum $\sum 2 \frac{h_i \tan \alpha_i}{\cos^2 \alpha_i} - h_{sd} \frac{\tan \alpha_0}{\cos^2 \alpha_0}$ in formula (3).

The method of calculating the intensities of reflected waves can be summarized as follows.

1. First we determine the sines of the angles of incidence of the reflected wave under consideration at all the interfaces.

These angles will vary from point to point along the ground surface unlike the corresponding angles for the head waves. It is best to have sin α_0

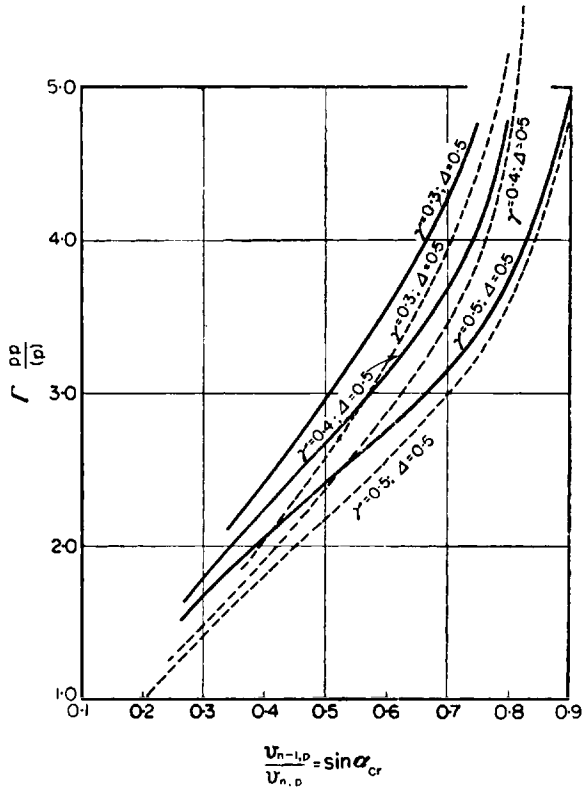

FIG. 4*a*. Curves for the coefficient Γ^{pp} (p) of primary wave formation ($\Delta = 0.6$ and $\Delta = 0.4$)

given and then the angles of incidence of the ray selected will have the same sines at all the interfaces, and these will be determined by expression (4).

$$\sin \alpha_i = \frac{v_{i,\,p}}{v_{0,\,p}} \sin \alpha_0 , \qquad (4)$$

while the point of emergence of the ray under consideration will lie at a distance r, determined by the formula

$$r = \sum_{i=0}^{n-1} 2h_i \tan \alpha_i - h_{sd} \tan \alpha_0. \tag{5}$$

from the shot point along the profile.

In a case of multiple waves, the term $h_i \tan \alpha_i$ in the sum $\sum h_i \tan \alpha_i$ in expression (5) is repeated the same numbers of times as the wave under consideration passes through the ith layer.

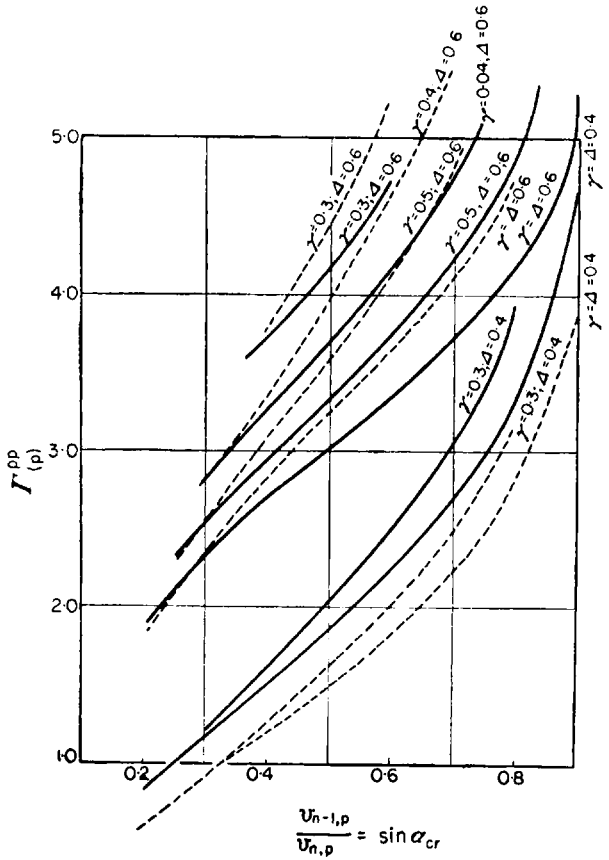

FIG. 4*b*. Curves for the coefficient $I^{pp}(p)$ of primary wave formations ($\Delta = 0.5$).

2. The multiplier C_0 is determined in the same way as for primary waves. Its value is taken at the point $x = \sin \alpha_0$ from the curve (see Fig. 2) corresponding to the parameter $\gamma_0 = \frac{v_{o,p}}{v_{o,p}}$, as for the zero layer of the medium under consideration.

3. The coefficients of refraction $(P_i P_{i+1})$ $(P_{i+1} P_i)$ are determined in the same way as for head waves. Only the ordinates of the curves (see Fig. 3) are now taken at the points $x = \sin \alpha_j = \frac{v_{j,p}}{v_{0,p}} \sin \alpha_0$ where $v_{j,p}$ is the lesser of the velocities $v_{i\,p}$ and $v_{i+1,\,p}$, that is at points equal to the sines of the lesser of the angles at which the ray under consideration meets the boundary between the ith and the $i+1$th layers. The curves are chosen with the same parameter as corresponds to the boundary between the ith and the $i+1$th layers. Then the ordinates are again multiplied by the quantity,

$$\frac{4\varrho_i v_{i,\,p}\, \varrho_{i+1} v_{i+1,\,p}}{(\varrho_i v_{i,\,p} + \varrho_{i+1} v_{i+1,\,p})^2}.$$

The product also immediately gives us the value of the coefficient of refraction $(P_i P_{i+1})$ $(P_{i+1} P_i)$.

4. The coefficients of reflection $(P_m P_m)$ and $(P_{m'} P_{m'})$ depend both on the properties of the reflecting boundary itself and also on the angle at which the wave strikes it. To determine these we have constructed graphs (Figs. 5, 6 and 7) based on the tables drawn up by the PETRASHEN' team; the sines of the angles at which the wave under consideration strikes the given reflecting boundary are plotted against the abscissa, and the parameters of the reflecting boundary are used as the parameters of the curves. We shall deal with each of the following cases separately:

(a) Reflection of a wave from a layer having higher velocity of longitudinal wave propagation than the layer in which the incident ray is travelling;

(b) Reflection of a wave from a layer having a lower velocity of propagation of longitudinal waves;

(c) Reflection of a wave from the free surface of the medium.

Case a. To determine the coefficient $(P_m P_m)$ or $(P_{m'} P_{m'})$ from the curve corresponding to the parameter Δ (see Fig. 5) which characterizes the reflecting interface under consideration, we take the ordinate value $(P_m P_m)_{\text{rel}}$, if $v_{m,\,p} < v_{m+1,\,p}$, or $(P_{m'} P_{m'})_{\text{rel}}$ if v_{mp} is $< v_{m-1,\,p}$ where the abscissa is equal to the sine of the angle at which the wave under consideration strikes the given reflecting boundary. The value of the ordinate is again multiplied by the coefficient of reflection of plane waves when the incidence is vertical.

The product gives the value of the co-efficient of reflection,

$$v_{m,\,p} < v_{m+1,\,p},$$

that is, if

$$(P_m P_m) = -(P_m P_m)_{\text{rel}} \frac{\varrho_m v_{m,\,p} - \varrho_{m+1} v_{m+1,\,p}}{\varrho_m v_{m,\,p} + \varrho_{m+1} v_{m+1,\,p}};$$

and if $v_{m,\,p} < v_{m-1,\,p}$,

$$(P_{m'}\,P_{m'}) = -\,(P_{m'}\,P_{m'})_{\text{rel}}\,\frac{\varrho_m\,v_{m,\,p} - \varrho_{m-1}\,v_{m-1,\,p}}{\varrho_m\,v_{m,\,p} + \varrho_{m-1}\,v_{m-1,\,p}}\,.$$

Case b. From the curve corresponding to the same parameters γ and Δ as on the reflecting boundary (see Fig. 6) at a point with a reading along the

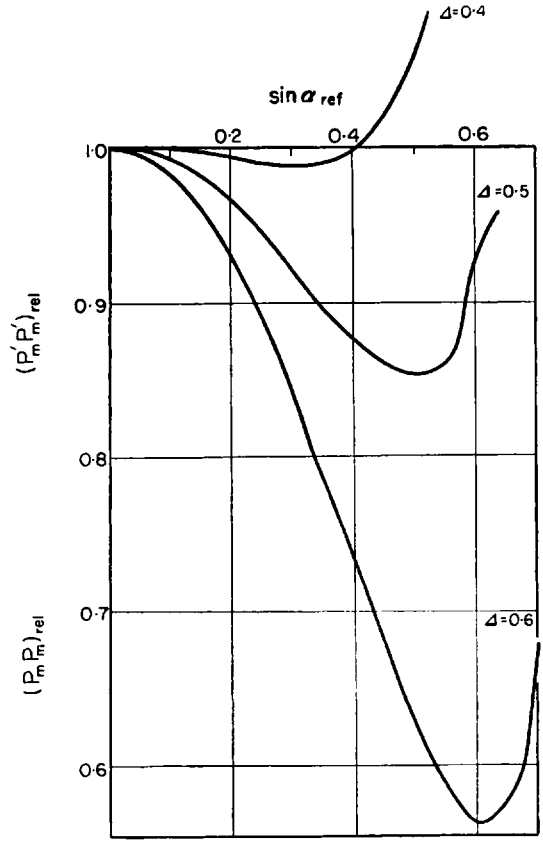

FIG. 5. Curves for calculating the coefficient of reflection of longitudinal waves from the layer boundary with a higher velocity of propagation than in the layer in which the incident ray is travelling.

abscissa equal to the sine of the angle of reflection, we take the ordinate $(P_m\,P_m)_{\text{rel}}$ if $v_{m,\,p} > v_{m+1,\,p}$, or $(P_{m'}\,P_{m'})_{\text{rel}}$, if $v_{m,\,p} > v_{m-1,\,p}$, and multiply it by the coefficient of reflection of planar waves when the incidence is vertical. The product gives the coefficient of reflection, that is if

$$v_{m,\,p} > v_{m+1,\,p}$$

then $$(P_m P_m) = -(P_m P_m)_{\text{rel}} \frac{\varrho_m v_{m,p} - \varrho_{m+1} v_{m+1,p}}{\varrho_m v_{m,p} + \varrho_{m+1} v_{m+1,p}};$$

and if $v_{m,p} < v_{m-1,p}$, then

$$(P'_m P'_m) = -(P'_m P'_m)_{\text{rel}} \frac{\varrho_m v_{m,p} - \varrho_{m-1} v_{m-1,p}}{\varrho_m v_{m,p} + \varrho_{m-1} v_{m-1,p}}.$$

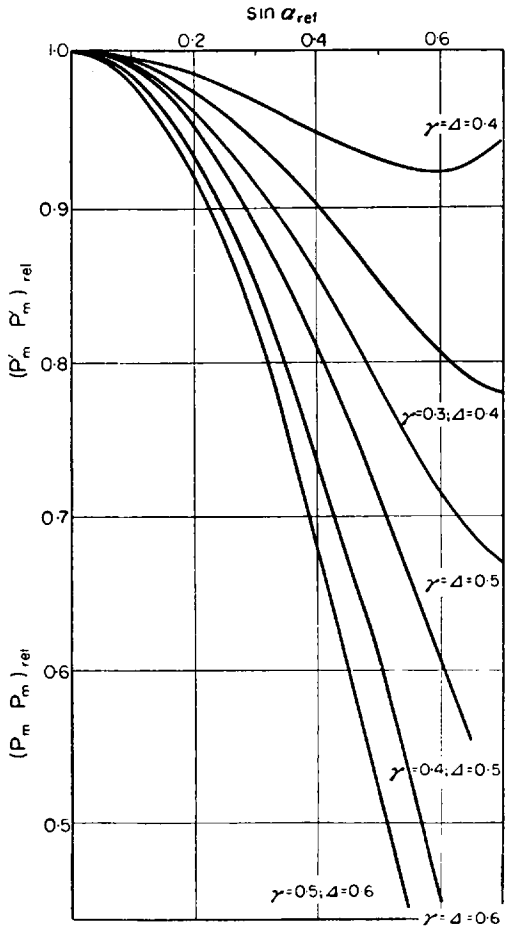

FIG. 6. Curves for calculating the coefficient of reflection of longitudinal waves from the layer boundary with a lower velocity of propagation than in the layer in which the incident ray is travelling.

Case c. The value of the coefficient of reflection $(P_{0'} P_{0'})$ is taken at the point $x = \sin \alpha_0$ along the ordinate from the curve (see Fig. 7) corresponding

to the parameter $\gamma_0 = \frac{v_{0,s}}{v_{0,p}}$ characterizing the zero layer of the medium under consideration.

The values found for the coefficients of refraction and reflection and also for the multiplier C_0 are substituted in the appropriate formulas. The intensity obtained for the wave relates to a point at a distance r from the shot point along the profile calculated from the formula (5).

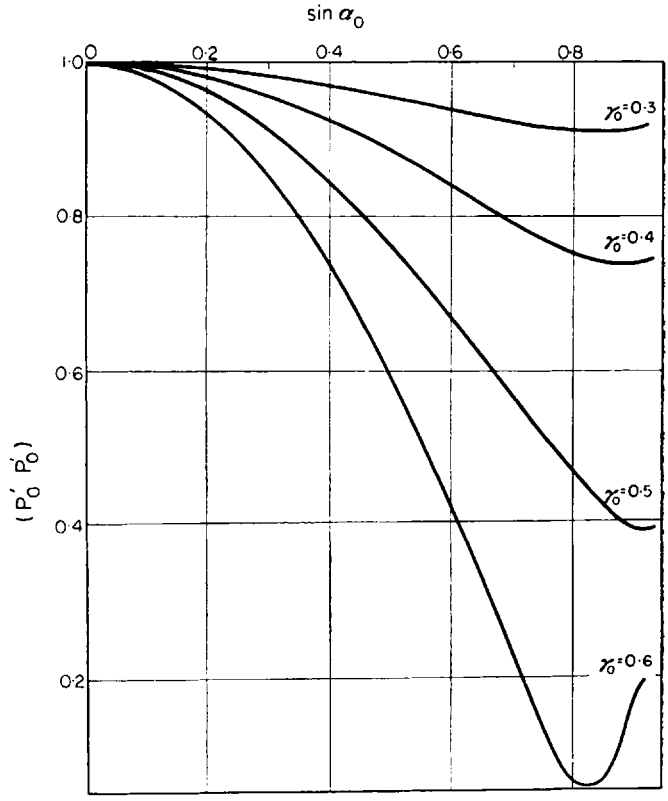

FIG. 7. Curves for the coefficient of reflection $(P_0' P_0')$ from a free surface.

For two-layered media the formula (3) is converted into (6) and (7) for single reflected waves, and into (8) and (9) for waves reflected n times

$$j_{\text{ref}} = \frac{C_0 (P_0 P_0)}{4\pi (\lambda_0 + 2\mu_0) v_{0,p}} \frac{\sin \alpha_0 \cos \alpha_0}{r}, \tag{6}$$

$$j_{\text{ref}} = \frac{C_0 (P_0 P_0)}{4\pi (\lambda_0 + 2\mu_0) v_{0,p}} \frac{\cos^2 \alpha_0}{2h_0 - h_{sd}}, \tag{7}$$

$$j_{ref} = \frac{C_0 (P_0 P_0)^n (P_{0'} P_{0'})^{n-1}}{4\pi (\lambda_0 + 2\mu_0) v_{0,p}} \frac{\sin \alpha_0 \cos \alpha_0}{r}, \tag{8}$$

$$j_{ref} = \frac{C_0 (P_0 P_0)^n (P_{0'} P_{0'})^{n-1}}{4\pi (\lambda_0 + 2\mu_0) v_{0,p}} \frac{\cos^2 \alpha_0}{2nh_0 - h_{sd}}. \tag{9}$$

Here h_0 is the thickness of the upper layer.

For multi-layered media, the multiplier

$$\frac{\sin \alpha_0}{\sqrt{r\left[\sum 2 \frac{h_i \tan \alpha_i}{\cos^2 \alpha_i} - h_{sd} \frac{\tan \alpha_0}{\cos^2 \alpha_0}\right]}}$$

from formula (3) can also be simplified and represented in the form $\frac{\sin \alpha_0}{r}$ when the angles at which the reflected wave under consideration strikes the intermediate interfaces are not too great. The permissible error with such a substitution lies within the limits shown in Table 3, where α_j is the largest of the angles α_i (where $i = 0$ to $n-2$) at which the wave reflected from the $n-1$th and nth layers strikes the intermediate interfaces.

TABLE 3

α_j	5°	10°	15°	17°30′	20°	22°30′	25°	30°
Error, %	0.3	1.5	3.4	4.5	5.7	7.4	9	12.5

It can be seen from the table that if α_j does not exceed 25° the permissible error will not exceed 9%. This degree of error will occur if all the angles $\alpha_i (i = 0$ to $n-2)$ are equal to 25°. If however some of them are smaller than 25° the error will be reduced. Here the true values of the multiplier we are dealing with are lower than the approximate values. If, by analogy with a two-layered medium, we substitute the value $\frac{\sin \alpha_0 \cos \alpha_0}{r}$ for this multiplier, we obtain still better accuracy.

If the angles of incidence onto the intermediate interfaces of multi-layered media are not too great, then the multiplier

$$\frac{\sin \alpha_0}{\sqrt{r\left[\sum 2 \frac{h_i \tan \alpha_i}{\cos^2 \alpha_i} - h_{sd} \frac{\tan \alpha_0}{\cos^2 \alpha_0}\right]}}$$

in the formulas for calculating the intensity of reflected waves (simple and multiple) can be replaced by $\frac{\sin\alpha_0\cos\alpha_0}{r}$. Formula (3) is then converted into (10)

$$j_{\text{ref}} = \frac{C_0 \prod_{i=0}^{n-2} (P_iP_{i+1})\,(P_{i+1}P_i)\,(P_{n-1}P_{n-1})}{4\pi\,(\lambda_0+2\mu_0)\,v_{0,p}} \times \frac{\sin\alpha_0\cos\alpha_0}{r}. \tag{10}$$

If we apply eqn. (4) to eqn. (3) and go over to a single independent variable $\sin\alpha_0$, and then proceed to the limit $\sin\alpha_0 \to 0$ we shall obtain formula (11) for determining the intensity of waves which reflected once above the shot point when reception is vertical:

$$j_{\text{ref}\cdot v} = \frac{2\prod_{i=0}^{n-2} [(P_iP_{i+1})\,(P_{i+1}P_i)]_v\,(P_{n-1}P_{n-1})_v}{4\pi\,(\lambda_0+2\mu_0)\,v_{0,p}\sum_{i=0}^{n-1} h_i\,\frac{v_{i,p}}{v_{0,p}}}, \tag{11}$$

Where $[(P_iP_{i+1})\,(P_{i+1}P_i)]_v$ is the coefficient of refraction of planar waves when the incidence of the wave is vertical; that is

$$[(P_iP_{i+1})\,(P_{i+1}P_i)]_v = \frac{2\varrho_i v_{i,p}}{\varrho_i v_{i,p}+\varrho_{i+1}v_{i+1,p}} \times \frac{2\varrho_{i+1}v_{i+1,p}}{\varrho_i v_{i,p}+\varrho_{i+1}v_{i+1,p}}; \tag{12}$$

$(P_{n-1}P_{n-1})_v$ is the coefficient of reflection of planar waves when the incidence is vertical on to the reflecting boundary under consideration of the $n-1$th and nth layers equal to the following expression

$$(P_{n-1}P_{n-1})_v = \frac{\varrho_{n-1}v_{n-1,p}-\varrho_n v_{n,p}}{\varrho_{n-1}v_{n-1,p}+\varrho_n v_{n,p}}; \tag{13}$$

h_i is the distance traversed by the wave in the i-th layer;

$v_{i,p}$ is the group velocity of longitudinal waves in the i-th layer.

When we determined the intensities of multiple waves above the shot point, formula (11) is transformed in the same way as formula (3). All the coefficients of reflection and refraction of the multiple wave under consideration are introduced into the numerator, each of these coefficients being

equal to the coefficient of reflection or refraction of plane waves with vertical incidence of the wave on a given interface, and being determined from formulas (12) and (13). The distance h_i travelled by the multiple wave under consideration in the ith layer is introduced into the denominator.

The formulas thus obtained add to the knowledge we already have from the theory of plane waves, about the intensitites of simple and multiple reflected waves over a shot point, the possibility of taking into account the weakening of reflected waves due to the divergence of a spherical wave.

ACCURACY OF THE PROPOSED METHOD OF CALCULATION

The method proposed is approximate. We shall now evaluate this method by comparing it with accurate solutions, and with the values obtained when the Leningrad tables and methods were used.

The basic formulas are merely another way of writing out the expressions for intensity which were given in the papers [2,3]; no new errors are therefore introduced. The values obtained from the tables for the multipliers C_0, $\Gamma^{pp}(p)$, $(P_0' P_0')$ have been plotted in figures 2, 4 and 7. We may regard their graphical values as being determined with a sufficient degree of accuracy. The coefficients of refraction and the coefficients of reflection on the other hand have been found approximately by means of the graphs shown.

Let us now evaluate this approximation. The possible error in determining each of the multipliers $(P_i P_{i+1})$ $(P_{i+1} P_i)$ for interfaces characterized by the quantity lying within the limits $0.7 \leqslant a \leqslant 0.9$ does not exceed 2%; if this quantity lies between the limits $0.5 \leqslant a \leqslant 0.7$ the error is 5% and finally if it lies within the limits $0.3 \leqslant a \leqslant 0.5$ the error is 10%. This estimate has been made for refracting boundaries with the parameters indicated above. Only for boundaries with $\gamma = 0.4$ and $\Delta = 0.6$ are the errors in determining the refraction coefficients slightly higher. The refraction coefficients for such boundaries can nevertheless be calculated by the method referred to, the errors being reduced as the angle of incidence becomes smaller or approximates to critical. For boundaries characterized by the parameters $\gamma = \Delta = 0.6$, $\sigma = 0.7$ to 1.0, the error will never exceed 3%.

We shall estimate the error entailed in determining the coefficient of reflection separately for the following cases.

Reflection from a layer with high acoustic rigidity—When the sine of the angles of incidence on the reflecting boundary is equal to $0.75a$ (a being the parameter of the reflecting boundary under consideration), the error in determining the coefficient of reflection does not exceed 10%. The degree of accuracy rises rapidly as the angle of incidence becomes smaller.

The approximation method indicated can be used for reflecting boundaries with the parameters shown in Table 1.

Reflection from a layer with lower acoustic rigidity—For reflecting boundaries with parameters as shown in Table 2, the magnitude of error in determining the coefficient of reflection is given in Table 4, from which it can be seen that when the angles at which the wave under consideration strikes the reflecting boundary are not too great it is permissible to use our approximate method of calculation.

TABLE 4

Values of parameters		Error in determination of coefficient of reflection, %		
γ	Δ	$\sin \alpha_{ref} \leqslant 0.6$	$\sin \alpha_{ref} \leqslant 0.5$	$\sin \alpha_{ref} \leqslant 0.45$
0.6	0.6	5	3	1
0.5	0.5	6	2	1
0.4	0.4	9	5	4
0.5	0.6	33	13	10
0.4	0.5	8	6	5
0.3	0.4	2	2	1.5

ANALYSIS OF THE INTENSITIES OF HEAD (REFRACTED) WAVES

A Two-Layered Medium

The intensity of head waves in two-layered media is determined from the formula

$$j_{head} = \frac{C_0 \Gamma^{pp}(p)}{4\pi(\lambda_0 + 2\mu_0)\sqrt{r}(r-r_0)^{3/2}} \tag{14}$$

The value of the multiplier C_0 (see Fig. 2) depends slightly on the values of the parameter γ_0 and is near to 2 when $\sin \alpha_0 \leqslant 0.9$. The behaviour of $\Gamma^{pp}(p)$ the coefficient of the head wave formation (see Fig. 4) — will therefore illustrate the dependence of the intensity of head waves in two-layered media on the parameters of the interface at distances r, which are sufficiently far from the point of emergence of the head wave, when we can set $\sqrt{r}(r-r_0)^{3/2} \approx r^2$.

It can be seen from Fig. 4, moreover, that when γ, Δ and σ are fixed, the intensity of the head wave increases in inverse proportion to the difference in the longitudinal velocities at the refracting boundary. At distances $r \gg r_0$ the intensity of a refracted wave increases with reduced sharpness of the refracting boundary just as the coefficient $\Gamma^{pp}(p)$ grows. At distances r comparable with r_0, when it is not possible to set $\sqrt{r}(r-r_0)^{3/2} = r^2$,

the increase in intensity of the refracted waves with decrease in the drop in velocities of propagation of the longitudinal waves at the refracting boundary occurs still more rapidly than the growth of the coefficient $\Gamma^{pp}(p)$. Even if the comparison is made at equal distances from the point of emergence, then when $r-r_0 \geqslant 0.8h_0$ refracted waves with higher amplitude will correspond to boundaries with less difference in the velocities of propagation, although for these the points of comparison are at a greater distance from the shot point. For boundaries where the difference in propagation velocities is slight, the intensity of a head wave at some distance from its point of origin will be greater than for a sharp interface at the same distance from its point of origin. The curves shown in Fig. 4 show how the intensity of head waves depends on the values of the parameters γ, Δ and σ at the refracting boundary. We can however choose these parameters to be such that when the drop in the propagation velocities of longitudinal waves is slight, the head waves will have a lower intensity than in a case of greater difference in the velocities of propagation at the interface (but with other parameters γ and Δ). It can be seen that the intensity of the head waves increases in direct proportion to Δ and in inverse proportion to γ.

The density ratio at the interface also affects the intensity of the head waves. For boundaries $\Delta = 0.4$ and $\Delta = 0.5$ the head wave intensity increases as the difference in densities decreases, while for boundaries where $\Delta = 0.6$ and $a \geqslant 0.35$ it decreases.

The damping of the head waves with distance is determined by the multiplier $r^{-1/2}(r-r_0)^{-3/2}$. The influence of the depth of the refracting boundary on the intensity of the head waves has a substantial effect only at distances r comparable with r_0. If the comparison is made for several two-layered media which differ from one another only by the parameter h_0 (r being fixed and the same for all the media), we arrive at what seems to be a contradictory conclusion: namely that the greater the bedding depth of the interface the greater the intensity of the primary waves. If however we compare the intensity of the head waves at uniform distances from their points of origin, everything becomes clear. We find that to get head waves of the same intensity at the same distance from their respective points of origin in the case of much deeper interfaces, a much more violent cause of excitation is required. At distances $r \gg r_0$ the bedding depth of the interface does not influence the intensity of a head wave. The head waves will dampen with distance as r^{-2}.

Multi-layered Media — Of the many problems connected with the origin and propagation of head waves in multi-layered media, we shall here treat only the following:

(a) the influence of the velocities at which transverse waves are propagated on the intensity of longitudinal primary waves;

(b) the effect of adding an ith layer, and changing the longitudinal velocity in it, on the intensity of the head waves excited in layers of greater depth;

(c) the effect of a sharp principal refracting boundary on the intensity of a head wave excited in it;

(d) the damping of the head waves with distance and the influence of the bedding depth of the main refracting boundary on the intensity of these waves.

We shall examine all these questions in order.

(a) Formula (2) is used to determine the intensity of the head waves excited in multi-layer media. As has been shown above the multiplier C_0 as well as the coefficients of refraction $(P_i P_{i+1})$ $(P_{i+1} P_i)$ at all the intermediate interfaces depend only slightly on the parameters γ and Δ, that is on the values of the transverse velocities in the covering layer. The intensity of the the head waves is consequently also only slightly dependent on them. It follows that ignorance or inaccurate knowledge of the transverse velocity values in the covering layer is not an obstacle in the way of calculating the intensities of the longitudinal head waves excited in deep boundaries. In drawing this conclusion we are assuming that the covering layer is characterized by the parameters indicated in the introduction.

The transverse velocity values in layers directly adjacent to the principal refracting boundary, on the other hand, may well exert a considerable influence on the intensity of a head wave excited at this interface. The curves in Fig. 4 show at a glance the possible variation in the theoretical intensity of a head wave according to the assumptions we make about the ratio between the transverse and the longitudinal velocities in the adjacent layers, on the boundary of which the primary wave under consideration is formed.

It can be seen from the curves that the wave intensity increases in inverse proportion to the parameter Δ and in direct proportion to the parameter γ, which characterize the adjacent layers on the boundary of which the head wave forms.

This means that in order to calculate the intensity of the head waves, we must have information about the densities and the values of transverse and longitudinal velocity on both sides of the interface where the head wave is excited, and that we must also know the values of velocity for the longitudinal waves and the densities throughout the covering layer.

(b) We shall now see how the intensity of the refracted waves varies if the longitudinal valocity value changes in one of the upper layers, other than the topmost, which is not directly adjacent to the interface at which

the head wave is excited. All the other parameters of the medium will be regarded as unchanged.

We shall find, for example, the variation in the intensity of a head wave excited in the nth horizon of the medium (see Fig. 1) with $v_{n,p} = 6000$ m/s, if the longitudinal velocity in the ith layer adapts from 1540 to 5150 m/s.

When $v_{i,p}$ in formula (2) changes, the quantity r_0 (the abscissa of the point of emergence of the head wave under consideration) and the value of the coefficient of refraction at the upper and lower boundaries (that is the expressions $(P_{i-1}P_i)(P_iP_{i-1})$ and $(P_iP_{i+1})(P_{i+1}P_i)$) of the ith layer will also change.

We shall regard the intensities as being determined at such distances r from r_0 that we can assume $\sqrt{r(r-r_0)^3} \approx r^2$. Then, when $v_{i,p}$ varies and all the other parameters of the structure of the medium remain unchanged, the intensity of the head waves will vary proportionately to the product of the coefficients of refraction $[(P_{i-1}P_i)(P_iP_{i-1})]\,[(P_iP_{i+1})(P_{i+1}P_i)]$, allowance having been made for the refraction of the wave at the boundaries of the ith layer. The curves in Fig. 8*a* therefore, where the value

$$[(P_{i-1}P_i)(P_iP_{i-1})]\,[(P_iP_{i+1})(P_{i+1}P_i)],$$

is plotted against $\frac{v_{i,p}}{v_{n,p}}$ illustrate the variations in the intensity of the head waves with growth of $v_{i,p}$. The curve determined by the parameter $b = \frac{v_{i-1,p}}{v_{i+1,p}} = 0.35$ characterizes the change in intensity of the head wave excited in the ith layer of the medium with $v_{n,p} = 6000$ m/s and $v_{i-1,p} = 1800$ m/s when $v_{i,p}$ varies within the range 1540–5150 m/s. The curves for cases where the values of the parameter $b = \frac{v_{i-1,p}}{v_{i+1,p}}$ show how the intensity of the head waves excited in the nth layers would vary with variation in $v_{i,p}$, if the medium under consideration were characterized by some other difference in the velocities $v_{i-1,p}$ and $v_{i+1,p}$ and by the same value $\frac{v_{i-1,p}}{v_{n,p}} = 0.3$.

If a medium with a different ratio of $v_{i-1,p}/v_{n,p}$ were considered then different curves would be obtained. Fig. 8*b* shows the $[(P_{i-1}P_i)(P_iP_{i-1})]\,[(P_iP_{i+1})(P_{i+1}P_i)]$ curves for the same parameters $b = v_{i-1,p}/v_{i+1,p}$, but for a ratio $v_{i-1,p}/v_{n,p} = 0.175$.

For a medium which differs from the one discussed above only in having a different value for the velocity $v_{i-1,p}$ ($v_{i-1,p} = 1500$ m/s), the intensity of

the head waves formed in the nth layer with a travel velocity of 6000 m/s would vary with change in the velocity of the ith layer within the range 1500–3500 m/s, as is shown by the curve in Fig. 8*b* which relates to the parameter $b = v_{i-1,p}/v_{i+1,p} = 0.21$. The behaviour of all the curves in Fig. 8*a* and *b*

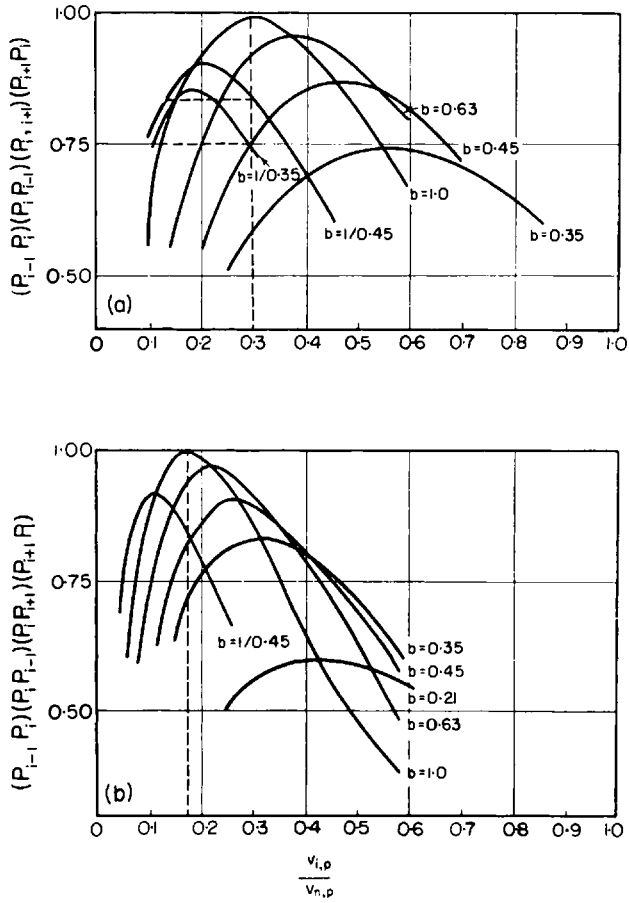

FIG. 8. Curves for the variation in intensity of primary waves if the longitudinal velocity changes in one of the upper layers.

reflects the change in intensity of the heat waves from the low-lying horizons when the velocity in the ith layer changes. We cannot, however, compare the ordinates of the various curves, since they give values for the coefficients of reflection at the boundaries of the ith layer which are proportional but not equal to the intensity values when $v_{i,p}$ changes. The coefficient of

proportionality is constant for each curve but is different for different curves.

From an analysis of the curves shown we may conclude that if we take $(r-r_0')^{3/2} = (r-r_0)^{3/2}$ where r_0' is the abscissa of the point of origin of the head wave under consideration when there is no ith layer, and r_0 is the same when there is such a layer, we shall obtain the following.

1. The addition of an ith layer characterized by a velocity $v_{i,p}$ lying within the interval $v_{i-1,p} < v_{i,p} < v_{i+1,p}$, will cause the intensity of the head waves from the underlying horizons to increase.

2. As $v_{i,p}$ increases from $v_{i-1,p}$ to $v_{i+1,p}$ the intensity of the head waves at first increases and then diminishes. When $v_{i,p} = v_{i-1,p}$ or $v_{i+1,p}$ the intensity of the head waves is of course the same in each case and the same as when there is no ith layer. The bigger the difference between the velocities $v_{i-1,p}$ and $v_{i+1,p}$ that is the greater the interval $v_{i-1,p} < v_{i,p} < v_{i+1,p}$ given a constant $v_{i-1,p}/v_{n,p}$ the greater will be the variations in the intensity values of the head waves excited in the low-lying layers. With a constant value of $b = v_{i-1,p}/v_{i+1,p}$ the intensity of the head waves when $v_{i,p}$ changes may show greater variations the higher the value of the parameter $v_{i-1,p}/v_{n,p}$. The intensity reaches its peak value at values of $v_{i,p}$ near to the mean value of the interval $v_{i-1,p} \leqslant v_{i,p} \leqslant v_{i+1,p}$.

3. The addition of an ith layer with a longitudinal wave travel velocity lower than the lower of the velocities $v_{i-1,p}$, $v_{i+1,p}$, or greater than the greater of the velocities $v_{i-1,p}$, $v_{i+1,p}$, leads to a reduction in the intensity of the head waves formed in the low-lying layers. The reason for this is that we now have an even sharper interface than where there was no ith layer.

(c) We shall now assume that the value of the longitudinal boundary velocity of the head wave changes, and that the density and velocity throughout the whole covering layer, as well as the density ratio and the density between the transverse and longitudinal velocities on both sides of the interface where the wave is excited remain constant. Under these conditions the angles at which the head wave strikes the intermediate interfaces will vary and this will cause variations in the values of the coefficients of refraction and in the multiplier C_0. Furthermore there will be a change in the value of the discontinuity in the longitudinal velocities and the principal refracting boundary and on $I^{pp}(p)$, the coefficient of head wave formation, which depends on it. Lastly the abscissa of the point of emergence of the head wave will also vary.

We shall first assume that the intensity of the head waves is being compared at distances from r_0 such that we can assume $\sqrt{r}(r-r_0)^{3/2} = r^2$.

The head waves emerge towards points on the ground surface at angles such that $\sin\alpha_0 \leqslant 0.9$ for which, as can be seen from Fig. 2, we can take $C_0 \approx 2$. Then the variation in the head wave intensity value with variation of $v_{n,p}$ will depend solely on the behaviour of the multipliers $\Gamma^{pp}(p)$ and $(P_iP_{i+1})(P_{i+1}P_i)$.

As $v_{n,p}$ diminishes, the discontinuity in the longitudinal velocities at the principal refracting boundary will diminish and the coefficient $\Gamma^{pp}(p)$ and the angles of incidence on to the intermediate interfaces will increase, while all the coefficients of refraction at these interfaces will decrease.

We shall now see how the intensity of head waves $P_0P_1P_2P_1P_0$ in a three-layer medium changes as $v_{2,p}$ changes. As can be seen from Fig. 4, the coefficient $\Gamma^{pp}(p)$ for boundaries of layers characterized by the parameters $\gamma = \Delta = 0.6$, $\sigma = 1.0$ increases least rapidly as the sharpness of the refracting boundary diminishes.

Fig. 9 shows curves for the variation in head wave intensity in three-layered media with change in the boundary velocity $v_{2,p}$ at the interface of layers characterized by the parameters $\gamma = \Delta = 0.6$, $\sigma = 1.0$. The intermediate interfaces examined have an upper layer to lower layer longitudinal wave velocity ratio within the limits $0.3 \leqslant a_{01} = \dfrac{v_{0,p}}{v_{1,p}} \leqslant 1/0.3$ and a density ratio equal to unity. The parameter of each of these curves is the ratio $v_{0,p}/v_{1,p} = a_{01}$.

As can be seen from the figure, the intensity of the head wave $P_0P_1P_2P_1P_0$ increases as the difference between the velocities $v_{1,p}$ and $v_{2,p}$ decreases. For three-layered media for which $v_{0,p} > v_{1,p} < v_{2,p}$ this remains true so long as $v_{0,p}$ does not approach $v_{2,p}$; that is, so long as $v_{0,p} \leqslant 0.9v_{2,p}$. With further diminution of $v_{2,p}$ the intensity of head waves diminishes despite the concomitant diminution in the values of $v_{1,p}$ and $v_{2,p}$.

If the adjacent layers are characterized by other parameters, γ, Δ, σ, the intensity of a refracted wave formed on their boundary will increase with diminution of the discontinuity in the values of the longitudinal velocities at this boundary more rapidly than is shown in Fig. 9. A variation in σ at the intermediate interface does not entail changes in the course of the curves shown but only alters their vertical scale.

Accordingly, we may conclude that in three-layered media with the parameters indicated at the start the intensity of the head waves $P_0P_1P_2P_1P_0$ will increase as the difference in the values of the longitudinal velocities $v_{1,p}$ and $v_{2,p}$ decreases. Indeed the intensity of such waves will decrease only for media where $v_{0,p}$ $v_{1,p}$ when the value of $v_{2,p}$ approaches $v_{0,p}$, or in other words when the difference between $v_{1,p}$ and $v_{2,p}$ decreases.

For four-layered media with layer velocities which increase with depth, that is $v_{0,p} < v_{1,p} < v_{2,p} < v_{3,p}$, we can also show that as the difference in the values of $v_{2,p}$ and $v_{3,p}$ decreases the intensity of head waves $P_0P_1P_2P_3P_2P_1P_0$ increases. If in a four-layered medium one or two of the layers have a high speed, that is if the medium is characterized by one of the ratios:

$$v_{0,p} < v_{1,p} > v_{2,p} < v_{3,p},$$

$$v_{0,p} > v_{1,p} > v_{2,p} < v_{3,p},$$

$$v_{0,p} > v_{1,p} < v_{2,p} < v_{3,p}$$

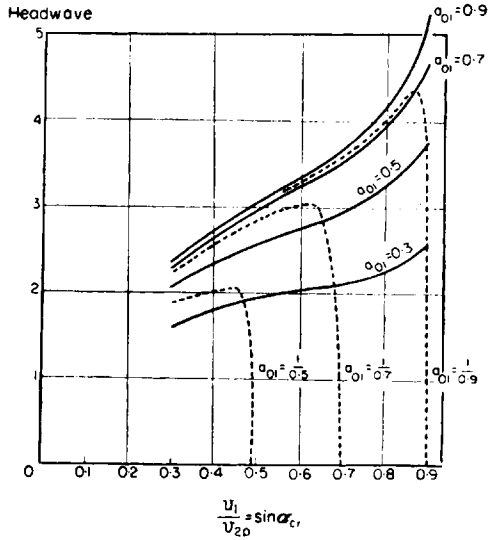

FIG. 9. The increase in intensity of primary waves j_{head} in three-layered media as the sharpness of the interface of layers diminishes at which the primary wave $\left(\frac{v_{1,p}}{v_{2,p}}\right)$ originates.

(but the highest velocity in the overburden does not exceed $0.9\,v_{3,p}$) we can then also show as the ratio $v_{2,p}/v_{3,p}$ increases within the limits 0.3—0.9 the intensity of the head waves $P_0P_1P_2P_3P_2P_1P_0$, although it increases, does not do so by a factor of more than 0.7.

The greater the number of interfaces with $v_{i,p} < v_{i+1,p}$ which separate the intermediate boundary under consideration from the refracting boundary

at which the head wave is produced, the more uniformly will it weaken waves from this boundary with differences v_b. We can therefore assume that in multi-layered media with layered velocities which increase with depth the intensity of the head waves produced at interfaces where the difference in velocity is slight will be fully comparable with the wave intensity which would be found with these velocities and densities of the covering layer, but with a much bigger discontinuity in the velocities of longitudinal waves at the interface where the head wave is formed. We consider the parameters γ, Δ, σ at this boundary to be unchanged.

If the overburden contains one layer with a high velocity which is less than or equal to $0.9\,v_b$ then even under the most favourable conditions of the intensity of the primary waves from the underlying layers will diminish by a factor of not more than 0.45 as the jump in longitudinal velocities in these horizons is reduced (within the limits 0.3–0.9) and provided γ, Δ and σ remain unchanged.

The conclusion we have reached here has been made on the assumptions indicated at the beginning of this section (that is we are assuming that the intensities of the primary waves are being compared at distances from r_0 such that we can regard $\sqrt{r(r-r_0)^3}/_4 \approx r^2$ and that the head waves are emerging towards points on the ground surface at angles such that $\sin\alpha_0 \leqslant 0.9$). But as we can show, these assumptions are not so important.

If for example we make the comparison at a distance r comparable with r_0 then the intensity of the head waves will increase still more rapidly as the discontinuity in longitudinal velocities at the reflecting boundary diminishes than at fairly great distances from r_0. When there are weathered zones present the angles at which the waves emerge at the ground surface are small and, of course, satisfy the inequality $\sin\alpha_0 \leqslant 0.9$. If the longitudinal velocity alone varies in the nth layer on the boundary of which the wave under consideration is formed, while the transverse velocity remains constant, then, as can be seen from Fig. 4, the diminution in the discontinuity in longitudinal velocities at this boundary will be accompanied by a still more rapid increase in the intensity of the head waves formed at it than in the case we considered above, where we assumed that the ratio $v_{n,s}/v_{n,p}$ remained constant. The principal conclusion reached here still holds good. Intensive head waves can be observed coming from refracting boundaries where the difference in velocities is slight. Head waves formed at a weak interface lying above a boundary where the discontinuity in velocities is great can of course be a good deal more intense than waves formed at a sharper boundary lying underneath. It is also possible for refracted waves formed at deeper boundaries, where the difference in velocities is slight, to be more

intense than refracted waves formed at higher boundaries where there is a bigger discontinuity in the velocity values.

It is a widely known fact in practical seismic prospecting that more intensive head waves can be obtained from an interface where the difference in velocities is slight [1]. It has been noted in many works that the head waves excited at boundaries where there is a considerable discontinuity in the velocities are less intense than waves formed at boundaries which lie higher and in which the difference in velocities is slight [1,4].

Our inference that intense head waves, excited at weak interfaces do exist therefore agrees with experimental data.

(d) According to the theory head waves suffer damping with distance as $r^{-1/2}(r-r_0)^{-3/2}$ and at greater distances r, as r^{-2}. But at distances $r = 10r_0$ the replacement of $r^{-1/2}(r-r_0)^{-3/2}$ by r^{-2} leads to an error of 15%. At such distances the intensity of the head waves diminishes more quickly than at r^{-2}. The overall depth of the refracting interface and the ratio between the thicknesses of the individual layers influence the intensity of the refracted waves so long as it is not possible to assume $r^{1/2}(r-r_0)^{3/2} = r^2$.

Any variation in the geometrical structure of the overburden which leads to an increase in r_0 (an increase in the overall depth or thickness of the high velocity layers) also leads to an increase in the intensity of the heads waves at the fixed distance r calculated from the shot point. As r increases this increase falls off, and when $r \gg r_0$ it becomes negligible.

The Form of Refracted Head Waves in Multi-layered Media

All longitudinal head waves excited in multi-layered horizontal layered media as a result of similar shocks have a similar form of trace and phase. The displacements of points on the ground surface repeat the form of the given pulse. Head waves along the profile do not alter the form of the trace.

ANALYSIS OF THE INTENSITY OF REFLECTED WAVES

A Two-Layered Medium

(a) *Single Reflected Waves*—The intensity of single reflected waves above the shot point is equal to the quantity

$$-\frac{2}{4\pi(\lambda_0+2\mu_0)v_{0,p}}\,\frac{\varrho_0 v_{0,p}-\varrho_1 v_{1,p}}{\varrho_0 v_{0,p}+\varrho_1 v_{1,p}}\,\frac{1}{2h_0-h_{sd}*}.$$

* The index *sd* signifies the shot depth.

This increases in proportion to the difference in the acoustic rigidities at the interface, in inverse proportion to the bedding depth h_0 and in direct proportion to h_{sd}.

The intensity of reflected (longitudinal) waves above the shot point does not depend on the value of the transverse velocities. For media where the difference in acoustic rigidities is such that they are uniform but $v_{0,p} < v_{1,p}$ in one while in the other $v_{0,p} > v_{1,p}$ when $v_{0,p}$ and ϱ_0 coincide in both media, the intensity of the reflected waves above the shot point is equal.

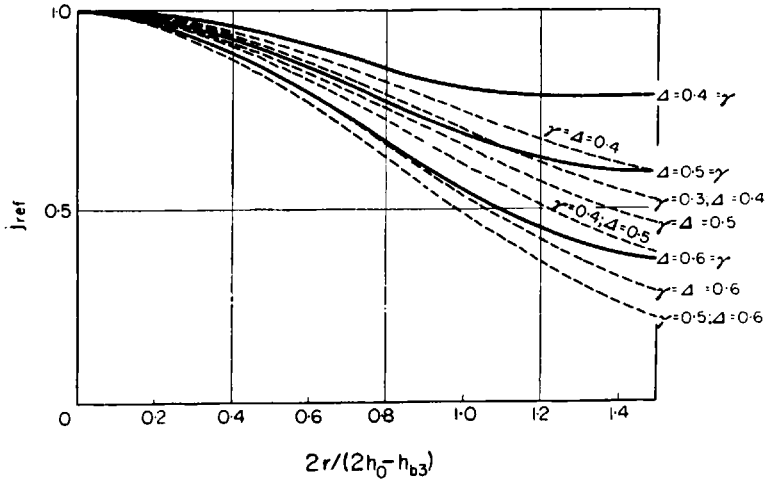

FIG. 10. Curves for the damping of single reflected waves in two-layered media.

It diminishes with distance from the observation point along the free surface of the medium and is determined by formulas (6) and (7). The rate at which the intensity diminishes ceases to be uniform for media where $v_{0,p} < v_{1,p}$ and $v_{0,p} > v_{1,p}$ and depends on the transverse velocity values. For media where $v_{0,p} < v_{1,p}$ it depends on the ratio between the longitudinal and transverse velocities in a half-space and for media where $v_{0,p} > v_{1,p}$ it depends on this value both in a half-space and in a layer.

Figure 10 shows curves for the damping of reflected wave intensity with distance for media where $v_{0,p} < v_{1,p}$ (continuous lines) and for media where $v_{0,p} > v_{1,p}$ (dotted lines); it can be seen that if Δ, the reflected wave will dampen more quickly the greater the parameter. Conversely if $v_{0,p} > v_{1,p}$, the intensity will dampen more rapidly the greater the parameter Δ and the smaller the parameter γ at a fixed Δ. Given the same Δ in media where $v_{0,p} > v_{1,p}$ the reflected waves will dampen with dis-

tance slightly more quickly than in media where $v_{0,p} < v_{1,p}$. As the bedding depth h_0 of the boundary increases the waves reflected from it will dampen more slowly with increase of r. At distances $r = h_0/2$ the intensity of reflected waves when $h_0 \gg h_{sd}$ is not less than 0.8 of the intensity above the shot point when $h_0 \approx h_{sd}$ is not less than 0.5.

(b) *Doubly Reflected Waves*—The intensity of doubly reflected waves above the shot point is equal to

$$\frac{2}{4\pi(\lambda_0+2\mu_0)v_{0,p}} \frac{(\varrho_0 v_{0,p}-\varrho_1 v_{1,p})^2}{(\varrho_0 v_{0,p}+\varrho_1 v_{1,p})^2} \frac{1}{4h_0-h_{sd}}.$$

This does not depend on the value of the transverse wave velocity and takes on higher values the greater the discontinuity in the acoustic rigidities at the interface, the shallower the depth of the bed h_0 and the greater h_{sd}.

The ratio between the intensities of doubly and singly reflected waves above a shot point is equal to

$$\frac{j_{\text{double}}}{j_{\text{single}}} = \frac{\varrho_0 v_{0,p}-\varrho_1 v_{1,p}}{\varrho_0 v_{0,p}+\varrho_1 v_{1,p}} \frac{2h_0-h_{sd}}{4h_0-h_{sd}},$$

when the shot depth varies from $h_{sd} \ll h_0$ to $h_{sd} \approx h_0$ this lies within the limits

$$\frac{1}{3}\left|\frac{\varrho_0 v_{0,p}-\varrho_1 v_{1,p}}{\varrho_0 v_{0,p}+\varrho_1 v_{1,p}}\right| < \frac{j_{\text{double}}}{j_{\text{single}}} < \frac{1}{2}\left|\frac{\varrho_0 v_{0,p}-\varrho_1 v_{1,p}}{\varrho_0 v_{0,p}+\varrho_1 v_{1,p}}\right|.$$

The doubly reflected wave diminishes more slowly than the single reflected wave with growth of r. The rate at which it diminishes also depends on whether the two-layered medium is characterized by the inequality $v_{0,p} < v_{1,p}$ or $v_{0,p} > v_{1,p}$ and on the values of the transverse velocities of the waves. The effect of a change in the transverse velocity on the rate at which the intensity of the doubly reflected waves is damped can be the same as in the case of singly reflected waves.

Figure 11 shows curves for the damping of intensity of doubly reflected waves with distance for media where $v_{0,p} < v_{1,p}$ (continuous lines) determined by the parameter $\Delta = v_{1,s}/v_{1,p}$ (on which the rate of damping also mainly depends) and for media where $v_{0,p} > v_{1,p}$ (dotted lines characterized by the parameters $\gamma = \frac{v_{1,s}}{v_{1,p}}$ and $\Delta = \frac{v_{0,s}}{v_{0,p}}$).

Since doubly reflected waves diminish with distance more slowly than single echoes, the question arises whether they become more intense, at some distance from the shot point, than such single echoes. We shall not

discuss all possible two-layered media in this paper but only those which have parameters with the values shown in Tables 1 and 2. We are taking it that in the case of media where $v_{0,p} < v_{1,p}$ the angles at which the wave strikes the reflecting boundary satisfy the ratio $\sin \alpha_0 \leqslant 0.75 \frac{v_{0,p}}{v_{1,p}}$, and for media where $v_{0,p} > v_{1,p}$ the ratio $\sin \alpha_0 \leqslant 0.6$.

Given these limitations we see by comparing the curves in Figs. 10 and 11 as well as the intensity values for waves reflected above the shot point, that

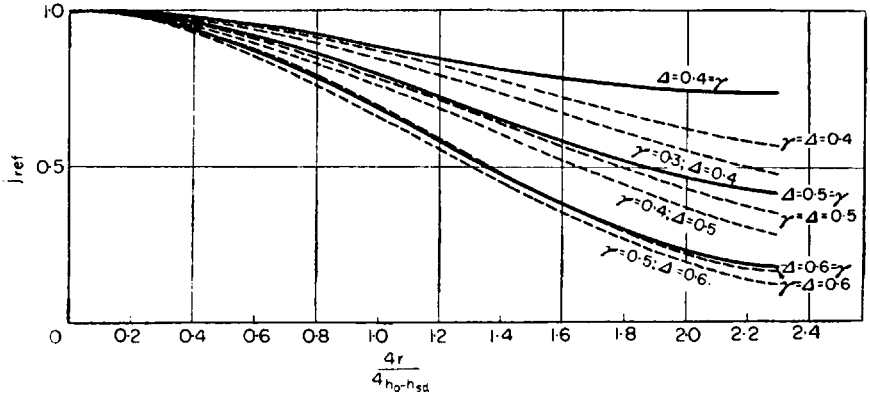

FIG. 11. Curves for the dam ping of doubly reflected waves in two-layered media.

double echoes are always less intense than single ones. The ratio of their intensities is found within the following limits:

$$\frac{1}{3}\left|\frac{\varrho_0 v_{0,p}-\varrho_1 v_{1,p}}{\varrho_0 v_{0,p}+\varrho_1 v_{1,p}}\right| < \frac{j_{\text{double}}}{j_{\text{single}}} \leqslant \left|\frac{\varrho_0, v_{0,p}-\varrho_1 v_{1,p}}{\varrho_0 v_{0,p}+\varrho_1 v_{1,p}}\right| \tag{17}$$

where $0 < h_{sd} < h_0$.

The ratio $j_{\text{double}}/j_{\text{single}}$ for media where $v_{0,p} > v_{1,p}$ will be slightly greater than for media where $v_{0,p} < v_{1,p}$, provided Δ is the same. This ratio increases as Δ increases and as γ decreases but Δ does not alter.

Multi-layered Media

Of the many problems connected with the intensity of reflected waves excited in multi-layered media, we shall here consider only the following:

(a) the influence of the values of transverse velocity on the intensity of reflected waves;

(b) the influence of the overall depth of the reflecting boundary and the ratio between the thicknesses of the different layers on the intensity of reflected waves over a shot point;

(c) comparison of the intensities of single and double echoes above a shot point.

We shall take these problems in the order given.

(a) The intensity of reflected waves in multi-layered media is determined from formula (3) and above a shot point from formula (11). Formula (11)—and so also the intensity of reflected waves above a shot point—do not depend on the transverse velocities in the media under consideration. In formula (3) only one coefficient of reflection depends on the transverse velocity values. When the reflection is from an interface with high acoustic rigidity, it depends mainly on the ratio of transverse to longitudinal velocities in the layer from which the reflection takes place; when the reflection is from an interface with lower acoustic rigidity the coefficient of reflection depends on the transverse velocity values on both sides of the reflecting boundary.

The curves (see Figs. 5, 6 and 7) show the dependence of the coefficient of reflection (and therefore also the intensity of the echoes) on the transverse velocity value at the reflecting boundary. The echoes are more intense the smaller the parameter Δ at the reflecting boundaries, while for waves reflected from media with low travel velocity the intensity of the waves increases (when Δ is fixed) with increase of v. The influence of the transverse velocities on the intensity of the echoes is greater for multiple echoes.

It is becoming clear that to determine the intensities of echoes in multi-layered media we need information only about the values of the transverse velocities at the actual reflecting boundary. If the reflection occurs from a high velocity layer we must take the value of transverse velocity in the layer under the reflecting horizon; but if reflection takes place from a weathered layer we need to know the transverse velocity on both sides of the reflecting boundary. What has been said holds true for media with the above-mentioned parameters when the angles at which the waves strike the reflecting boundaries are lying within the limits indicated.

(b) The intensity of reflected waves above a shot point is determined from formula (11). From this formula it is clear that if the depth of the reflecting boundary increases or diminishes n times the thickness ratio for the different layers, and h_{sd} remaining as before, then the intensity of the echoes above the shot point will diminish or increase n times. If the velocity and density-structure of the medium are unchanged and the depth of the reflecting boundary is also unchanged, the intensity of the waves

reflected from this boundary will be greater in inverse proportion to the thickness of the layers which have the higher velocities and in direct proportion to the thickness of the layers which have the lower velocities. The more the velocity of the ith layer differs from that in the layer where the shot is fired, the greater will be the influence which a change in the thickness of this layer exerts on the intensity of waves reflected from interfaces lying at greater depths.

(c) From formula (11) we can easily obtain expressions for the intensity ratio of multiple echoes above a shot point, when the reflection occurs at the boundary of the $n-1$th and nth layers and the free surface.

If we assume that $h_{sd} \ll \sum_{i=0}^{n-1} 2h_i \frac{v_{i,p}}{v_{0,p}}$, we shall have the following formula for the intensity ratio of waves reflected k and $k-1$ times:

$$\frac{j_{k-1}}{j_k} = \frac{k}{k-1} \prod_{i=0}^{n-2} [(P_i P_{i+1})\,(P_{i+1} P_i)]_v\,(P_{n-1} P_{n-1})_v, \tag{18}$$

where $[(P_i P_{i+1})\,(P_{i+1} P_i)]_v$ and $(P_{n-1} P_{n-1})_v$ are determined from formulas (12) and (13), and k is the number of times the wave is reflected.

As can be seen from (18) the greatest difference in the intensities above the shot point is found to occur between single and double echoes. The greater the number of reflections the smaller the difference between the intensities of waves reflected a neighbouring number of times.

For such multiple echoes where the second reflection has taken place from the free surface, we can easily obtain from (18) the following expression:

$$\frac{j_k^2}{j_{k-1}\, j_{k+1}} = \frac{(k-1)\,(k+1)}{k^2}, \tag{19}$$

where j_k is the intensity above the shot point of a wave reflected k times; j_{k-1} is the intensity above the shot point for a wave reflected k^{-1} times; j_{k+1} is the intensity above the shot point for a wave reflected $k+1$ times.

For example, for the intensity of a a single wave j_1, a double echo j_2 and a triple echo j_3 we have

$$\frac{j_2^2}{j_1 j_3} = 0.75$$

The ratio (19) does not depend only on the values of the transverse velocities but also on the longitudinal velocities. This is true for any type of effect when any component of displacement is being recorded above the point of disturbance.

The intensity of possible interbed echoes above a shot point can also be readily determined by means of formula (11). Comparison of their intensities with the intensity of single echoes from low-lying boundaries can help in recognizing the nature of any particular wave recorded on the seismogram.

THE FORM OF SINGLE AND MULTIPLE ECHOES IN MULTI-LAYERED MEDIA

We can say the following about the form of seismic traces for echoes excited as a result of shots in multi-layered media up to the points of emergence of the corresponding head waves: all reflected waves, whether simple or multiple, have the same trace form when the influences are the same. Their phases cannot be opposite. Displacements of points on the ground surface repeat the form of the given pulse. As to the onset of echoes when the angles at which they strike the reflecting boundaries are small, all the facts that are well known from plane wave theory can be repeated. If the wave is reflected from a layer which has a lower speed than the layer from which the wave has arrived, and if the discontinuity in the transverse velocities at the reflecting layer is greater than that in the longitudinal velocities (that is $\gamma < \Delta$), then when the angle at which the wave strikes such a reflecting boundary increases, the intensity of the echo from it can pass through zero and the wave can change the sign of its onset. For waves reflected from boundaries (with parameters from Table 2) this can occur when the angles at which the wave strikes the reflecting boundary have a sine greater than 0.6 (not discussed in the present paper). If the reflected wave under consideration nowhere undergoes reflection from such boundaries then, as the angles of incidence increase to critical, it does not change its sign of onset and has the same form as it has above the shot point. What we have said does not refer to the vicinity in which the corresponding head waves emerge.

REFERENCES

1. A. M. Epinat'yeva, Experimental data on refracted waves in media with poor speed differentiation. *Izv. Akad. Nauk SSSR, ser. geofiz.* No. 2 (1955).
2. G. I. Petrashen', Problems in Dynamic Theory of Seismic Wave Propagation. Coll. I. Gostoptekhizdat, 1957.
3. G. I. Petrashen', Propagation of elastic waves in layered isotropic media divided by parallel planes. *Sci. Rec. Zhdanov State Univ.*, Leningrad, No. 162, Pt. 26, 1953.
4. D. B. Tal'-Virskii, Tectonics of the Tobolsk Zone from Seismic Prospecting and Deep-drilling Data. Thesis. VNII Geofiz. Foundation.

CHAPTER 2

METHOD AND TECHNIQUES OF USING STEREOGRAPHIC PROJECTIONS FOR SOLVING SPATIAL PROBLEMS IN GEOMETRICAL SEISMICS

E. I. GAL'PERIN, G. A. KRASIL'SHCHIKOVA, V. I. MIRONOVA and A. V. FROLOVA

IN seismic prospecting, as in all geophysical methods of prospecting, the solution of linear problems is of great importance for the purpose of analysing data and is an essential step in the working out of methods for interpreting field observations. The solution of ray problems makes it possible to study the shape of surface hodographs for media of various structures, to compare the surface hodographs of different types of waves and discover the possible regions in which they can interfere, to check on the correctness of the constructions made and estimate the degree of error introduced, to confirm approximate methods of interpretation, to verify the permissibility of any simplified assumptions which have been used in interpreting the seismic data and so forth. Yet it is precisely in seismic prospecting that the solution of linear problems has received comparatively little attention. Until recently opportunities for solving linear problems have been confined to cases where the structure of the medium is very simple, and in the main to two dimensional problems, although all the problems in seismic prospecting are by their very nature spatial ones. The reason for this is largely the difficulty of solving spatial problems in geometrical seismics. In those instances when spatial problems have been examined, the examination has been confined as a rule to one interface. The methods used have been both graphical and analytical [1,6,5].

An earlier paper [3] describes a method for solving linear spatial problems in geometric seismics for multi-layered media with interfaces of arbitrary shape. The method is based on using stereographic projections which make it possible to determine the direction of rays in space after they have struck the interface.

The method is applicable principally to multi-layered media with a constant velocity in each layer, where there is any number of interfaces of arbitrary shape, and can be used equally well for calculating the seismic fields

of reflected and of refracted waves. As the graphical constructions are cumbersome, however, the practical use of the method is confined to three- or four-layered media.

It should be stressed that further development both of the graphical and of the analytical methods of solving linear problems in geometrical seismics is essential. Only by combining both methods of construction is it possible, where necessary, to increase the degree of accuracy by very simple methods.

In seismology a Wulff net is used in processing earthquake records. The construction of spatial fields by means of a Wulff net as applied to problems in seismology has been described in a thesis by N. Bessonova.

The present paper is devoted to a detailed exposition of problems in methodology and technique for the solution of spatial problems in geometrical seismics by means of stereographic projections as applied to problems in seismic prospecting. The first part explains the principal properties of stereographic projections, without demonstration, and describes the technique of working with a Wulff net together with methods for solving problems in geometrical seismics by means of these grids. In the second part we describe the technique for solving linear problems in geometric seismics for multi-layered media with interfaces of arbitrary shape.

STEREOGRAPHIC PROJECTIONS

Stereographic projections were used in astronomy as far back as over two thousand years ago to represent the surface of the heavenly vault on a plane. Later the method began to be used for the same purpose in map making. At the end of last century stereographic projections began to be used successfully for studying the angles between lines and planes in space. This use of stereographic projections is of major interest for geometric seismics since it can be used to solve problems connected with the propagation of seismic waves, which by their very nature are spatial. Here we shall not dwell on the theory of stereographic projection, which has been expounded in a number of works[7], but shall merely describe their main properties which enable them to be used for studying on a drawing the mutual inclinations of rays in space by first projecting them on to a sphere.

1. The entire upper hemisphere can be represented by a circle.

2. The angles between the rays of the great circles in the sphere are equal to the angles between the arcs of their projections.

3. The arcs of the circumferences of both small and great circles are represented in the projection by arcs of circles or in a particular case by straight

lines (in general the latter can be considered as circles of infinitely great radius).

Stereographic projection is equiangular projection, that is, the angle between the projections of lines on the sphere is equal to the angle between the lines on the sphere themselves. This property of stereographic projections, which is also possessed by certain other projections, is a necessary and sufficient condition for a given projection to be conformal, meaning that figures on the sphere which have infinitely small dimensions in all directions are projected as infinitely similar small figures. A further characteristic of stereographic projections is that the projection of a circle is a circle.

The Stereographic Net

A projection onto the diametral plane of a sphere divided into degrees is called a stereographic net. Depending on the position of the projection plane a stereographic net can be polar (when the projection plane coincides with the equator, and the observation point with the nadir—the lower pole) or meridianal, when the observation point lies on the equator and the projection plane is a meridian lying at 90° from the point of observation.

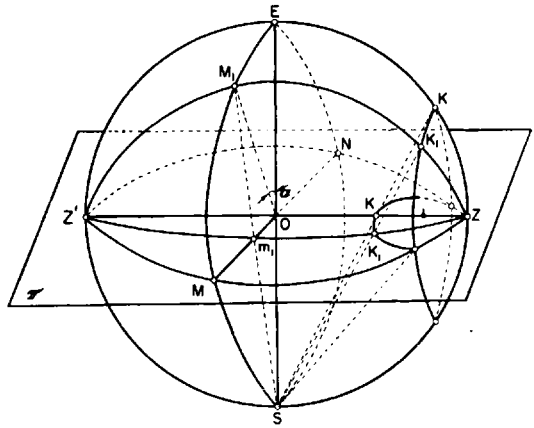

FIG. 1. Construction of a meridianal stereographic net (after M. K. Razumovskii).

For purposes of geometrical seismics the meridional net is the most interesting. Let us now look at this in detail. Fig. 1, which we have taken from Reference [7], shows a construction of a meridianal stereographic net. Here the plane of drawing coincides with the meridian ZEZ', and the plane of projection (π) coincides with the meridian ZMZ'. The point of observation

lies on the equator *EMS* at the point *S*. The equator *EMS* and the meridian *ZEZ'* are represented by two mutually perpendicular diameters *MN* and *ZZ'* of the projection circle, the projection of the meridian coinciding with the polar axis of the sphere *ZZ'*. The remaining meridians are represented by circles passing through the poles *Z* and *Z'* and intersecting the equator.

Let us consider for example the meridian ZM_1Z' for which the angle EOM_1 is $\alpha°$. The projection (m_1) of the point at which the equator intersects the meridian (M_1) will be distant from *O* an amount

$$Om_1 = R \tan \frac{\alpha}{2},$$

where *R* is the radius of the sphere.

The parallel* with the co-ordinate $\varrho = 15° = ZK$ lies at this number of degrees from the pole along all the meridians; we can therefore plot *Z* at 15° from the pole round the circle of the projections on both sides, and we can also plot the segment $ZK = 15°$ along the straight line *OZ* on the stereographic scale from the point *Z*. We thus obtain three points belonging to the parallel. These points are sufficient to enable us to construct the whole parallel.

The meridianal stereographic net constructed through 2° for a sphere $R = 10$ cm, was first introduced into crystallography by Vul'f (2) and bears his name (normally as Wulff in English) (See Fig. 2).

Operations with a Wulff Net

The Wulff net is a transparent sheet by which any construction can be transferred to transparent paper (wax paper or ordinary tracing paper) without the use of compasses or a ruler. The tracing paper is centred and a mark is made on it to indicate the end of a meridian which is the point of origin for counting off the azimuths. This fixes the initial position for the tracing paper, and by means of this index the paper can be subsequently brought back into the initial position.

We shall now consider problems in geometrical seismics which can be solved by means of a Wulff net.

PROBLEMS ENCOUNTERED IN GEOMETRICAL SEISMICS

Every direction in space can be unambiguously determined by two angles. Let these angles be the azimuth (α), that is the angle counted from the northward direction in the clockwise sense which varies from 0 to 360°,

* Throughout the paper the term "parallel" is used as parallel of latitude or small circle [*Editor's note*].

and the angle φ with the vertical, which varies from 0 to 180°. The first essential is to learn to plot on the net the directions of the rays along the co-ordinates so that we can remove the co-ordinates from the net.

Let us examine the main methods of working with a Wulff net.

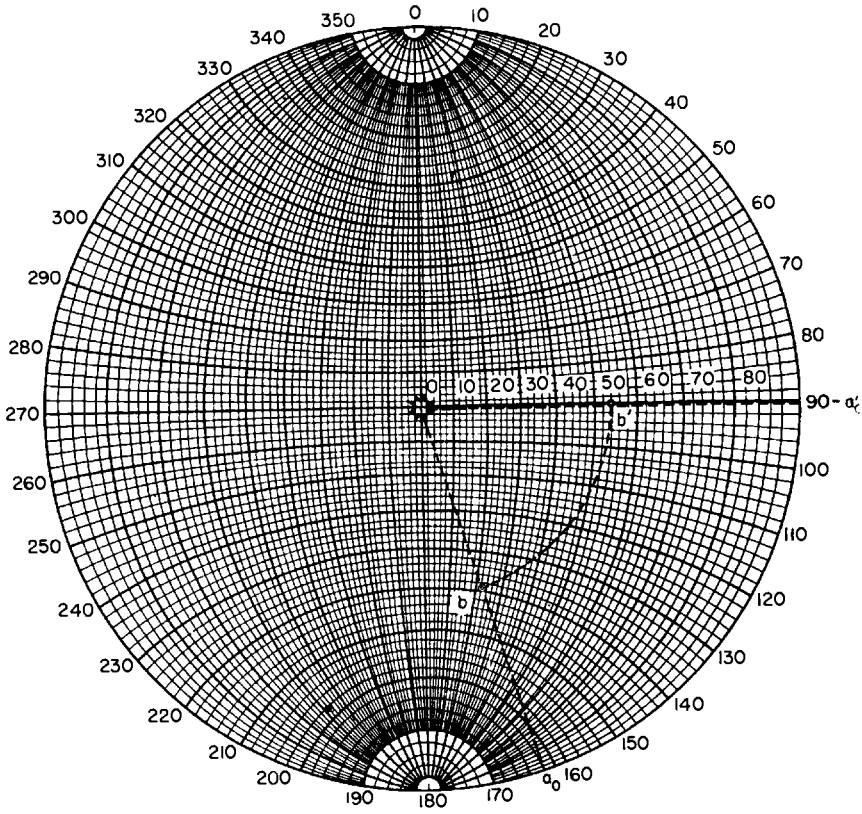

FIG. 2. Constructing the direction from given co-ordinates ($\alpha = 162°$, $\varphi = 54°$) by means of a Wulff net.

1. To construct on the grid directions of which the co-ordinates are given. Let the co-ordinates of direction be $\alpha = 162°$ and $\varphi = 54°$. In order to construct this direction on the net (see Fig. 2) we must count off an angle equal to the azimuth of our direction on the tracing paper in a clockwise direction round the outer circle of the grid, and mark point α with a_0. Rotating the tracing paper we bring the point which we have just obtained onto one of the diameters of the projection circle. For example, let this be the horizontal

diameter with the mark 90° (point a_0') and let us plot the angle $\varphi = 54°$ (point b') from the centre of the projections to the circumference.

When the tracing paper is rotated into the original position (the index coinciding with 0°) the point b' takes up the position b which is also a projection of the trace of the intersection of a direction determined by the given angles $\alpha = 162°$, $\varphi = 54°$ with the sphere.

It must be noted that all the directions for which φ is equal to or less than 90° will be above the plane of drawing, and in this case they will be marked on the grid by points. If $90° \leqslant \varphi \leqslant 180°$, then such directions will be marked on the drawing by means of crosses.

If the angle given is not from the vertical but from the horizontal then it will be calculated not from the centre of the projection but from the outer circumference of the grid towards its centre.

2. To determine the co-ordinates of points given on the net (the problem in reverse). To solve this problem we draw a straight line from the centre through the given point up to its intersection with the circumference of the net, and we count off on the circumference the azimuth α. We then transfer the point to the equator and count off the angle φ from the centre.

We can now pass immediately to the consideration of problems encountered in geometrical seismics.

Problem 1. To determine on the net the plane which includes the direction of the ray and the normal to the boundary.

It is known that incident, reflected and refracted rays and the normal to an interface lie in one plane, which is also the plane of the rays. We shall use this property to find the plane of the rays. Imagine the centre of a stereographic net at the point of incidence of a ray; we now plot on the tracing paper, using the net, the direction of the incident ray and the normal to the interface. We must bear in mind that since the centre of the net is set at the point of incidence of the ray, it will always be essential to take its inverse azimuth when we plot the direction of the incident ray onto the net.

Two directions in space have thus been plotted on the tracing paper and the problem is reduced to finding the plane in which both directions lie. The meridians of the net correspond to an assembly of circles (planes), differently inclined to the plane of drawing. Consequently, if we rotate the tracing paper until both given directions fall on one and the same meridian of the grid, we shall thereby find the plane in which both given directions lie. We produce this meridian and find the pole of arc of the great circle, which will also determine the direction of the normal to the plane of the rays. For this purpose it is sufficient if we count off 90° along the diameter from the arc. Rotating the tracing paper again until it reaches its original

position, we obtain the position of the plane of the rays in space. For purposes of examining these problems the direction of the normal is regarded as given.

For example let the direction of a ray incident from a source be represented by co-ordinates 234° and 31° and the direction of the normal to the interface at the point of incidence of the ray by 112° and 14°. Let the imaginary centre of a projection onto the interface be at the point of incidence of the ray and let us plot on the net the direction of this ray and of the normal. It should be kept in mind that the azimuth of the ray will thereby be inverted.

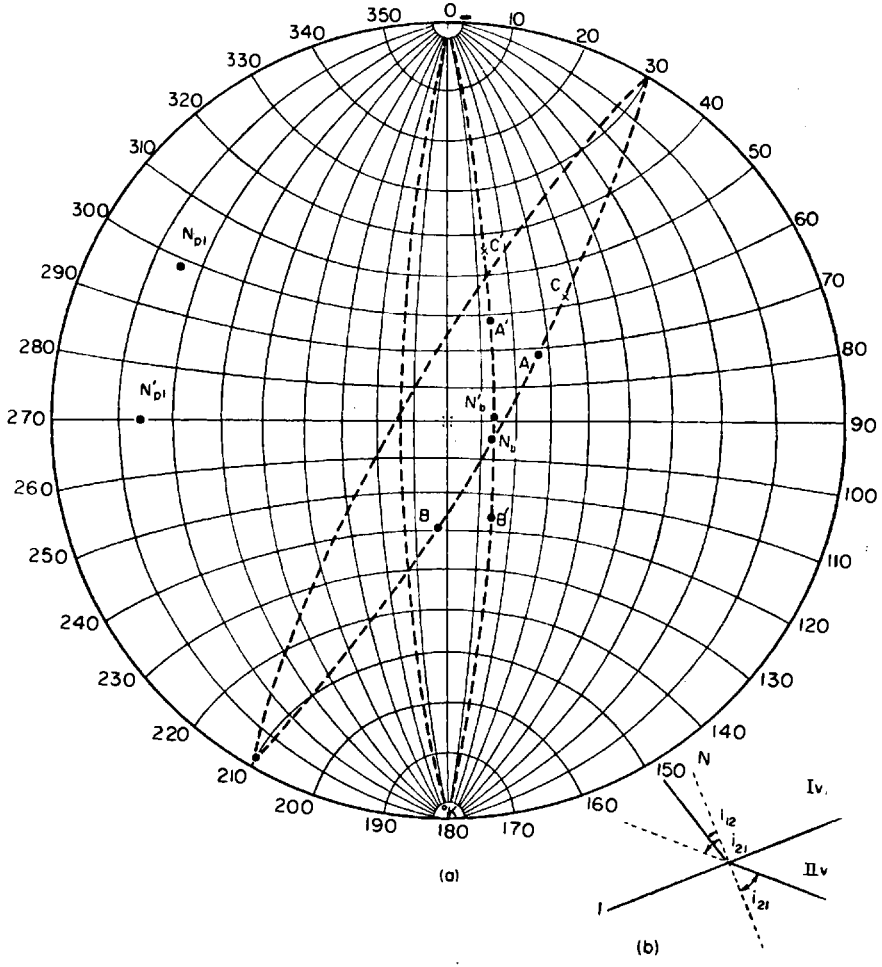

FIG. 3. *a*—determination of direction of reflected, refracted and grazing rays; *b*—towards determination of the direction of the refracted ray.

In Fig. 3 the point A with the co-ordinates 54° and 31° corresponds to the direction of an incident ray, while the point N_b (112° and 14°) corresponds to the normal to the interface at the point of incidence.

To find the plane of the ray by rotating the tracing paper, we plot both points on the same meridian (points A', N_b') and draw it on the tracing paper (lines produced on the tracing paper are shown on the drawing by a dotted line). We mark on the tracing paper the normal to the plane of the circle (the point N_{pl}'). Next we move the tracing paper into its original position and we can determine the position of the plane of the rays in space; in our case the co-ordinates of the normal to the plane of the rays are determined as 300° and 76°*.

If one of the directions is above the plane of drawing and the other is below it then the points will be on symmetrical (equidistant from zero) meridians. This is correct since the lower half of the meridian is projected from the zenith in a symmetrical arc.

Problem 2. To determine the angle between two directions in space. Both directions are plotted by means of the net on tracing paper (points A and B Fig. 3), and by rotating the tracing paper the plane in which both points lie is found. The points under consideration, A and B, take up positions A' and B' respectively. The angle between points A' and B' in this plane are counted off on the net; in our case this is equal to 54°. This angle is also the angle between the given directions in space.

Problem 3. Given the direction of an incident ray and of the normal to the interface at the point of incidence, to determine the direction of a reflected, a refracted and a grazing ray. In order to determine the directions of these rays in space, we must first find the plane of the rays, that is we must first solve Problem 1, after which we can construct the directions of the rays in which we are interested in the plane of the rays. Let a point N_b (see Fig. 3) (112° and 14°) correspond to the direction of the normal to the interface, and a point A (54° and 31°) to the direction of the incident ray (with inverse azimuth). Then the plane of the rays is determined by the points A' and N_b'.

We shall consider separately how to determine the direction of each of the rays which interests us (the reflected, the refracted and the grazing rays) in this plane.

(a) To determine the direction of the reflected ray. Since the angle of reflection is equal to the angle of incidence, it follows that when we have determined the angle between the incident ray and the normal by means

* The Russian original states mistakenly 86°.

of the net (in our case between the points A' and N_b' is equal to 27°) we can plot it in the plane of the rays from the normal in the direction opposite to the incident ray (point B'). We next bring the tracing paper into its original position. The point B' is now transferred to point B which also corresponds to the direction of the ray after its reflection. The direction of the reflected ray in our case is determined by the co-ordinates 185° and 30°.

(b) To determine the direction of the refracted ray. The method is similar to that used for the reflected ray, the only difference being that in this case instead of plotting the angle of reflection, which is equal to the angle of incidence, from the normal we plot the angle of refraction. The angle of refraction is calculated from the angle of incidence and from the ratio of velocities $\frac{v_2}{v_1}$ in the first and in the second layers according to Snell's equation:

$$i_{2,1} = \text{arc sin } i_{1,2} \frac{v_2}{v_1},$$

where: $i_{2,1}$ is the angle of refraction and $i_{1,2}$ is the angle of incidence.

By way of example let $\frac{v_2}{v_1} = 1{\cdot}5$ in our case; then when $i_{1,2} = 27°$ the angle of refraction $i_{2,1}$ will be equal to 43°.

Since the refracted ray will be under the plane of the drawing we shall construct on the grid the direction opposite to it. (As indicated above, we shall for the sake of convenience denote the direction in such cases by a cross and not by a point). For this purpose, as can be seen from the ray diagram (see Fig. 3, *b*) it is sufficient to plot the angle of refraction from the normal in the direction of the incident ray in the plane of the ray. The direction of the refracted ray is denoted in Fig. 3,*a* by the point C'. If we rotate the tracing paper into its original position we shall obtain from the point C the co-ordinates of the refracted ray (43° and 47°). We must not forget, however, that here we are dealing with a direction opposite to the direction of the refracted ray, and therefore when we remove the co-ordinates we must take the inverse azimuth. Then the direction of the refracted ray will be 223° and 47°.

(c) To determine the direction of a grazing ray. To obtain a grazing ray the angle of refraction must be 90°. To determine the direction of the grazing ray it is sufficient to plot an angle of 90° from the normal in the plane of the ray and having restored the tracing paper to its original position to take the co-ordinates of the grazing ray from the net (point K, Fig. 3, *a*).

The problems we have considered are sufficient to enable us to proceed to a description of the methods and techniques used in solving three-dimensional ray problems in geometrical seismics.

GENERAL SCHEME OF SOLUTION

The solution of three-dimensional ray problems resolves itself into studying seismic fields in space. Seismic fronts are traced along the seismic rays. For this purpose, instead of using individual rays, we find it more convenient to use certain aggregations of rays, for example rays emerging from a source and making a known angle with the vertical or intersecting an interface along certain definite lines (isohypses). In the first case these rays will form, in the first medium a conic ray surface, which after striking the very first interface can get deformed. If we take a definite number of such surfaces which differ only in the apical angle of the cone, we can use these to fill in the whole portion of the space which interests us. The behaviour of each such conic ray surface is traced in space along the individual rays forming it, which in the first medium differ from one another only with respect to the azimuth. By tracing consecutively the behaviour of the conic ray surface on all the given interfaces we can find the trace of intersection of the ray surface with the surface or plane of observation.

All the constructions are produced on a plan where trace projections of the ray surface intersections with each of the interfaces in turn are drawn.

The intersection trace of a ray surface with an interface if the latter has a simple shape can be found by ordinary geometrical constructions, the trace being subsequently projected onto the horizontal observation plane.

In cases where the interface is not distinguished by a simple form, the projection of the intersection trace of the ray surface with the interface can be constructed as the geometrical position of the trace projections of the intersection with the interface of the rays forming the ray surface. The point of intersection of the ray with the interface is determined as the point where the interface and the ray have exactly the same depth. Each point of the projection of the ray on the plan corresponds to a particular depth of the ray which can be calculated from the known angle made by the ray with the vertical (the inclination of the ray). Projection points of rays for which the depth along the rays coincide with the interface depths (isohypses) are projections of traces of intersection with the interface of the corresponding rays. The travel times of waves are calculated from the rays separately for each section of the wave path. The length of the section of a ray which is included between interfaces is determined from the angle of inclination of

the ray to the vertical and from the depths of its extreme points. We sum the travel times of the waves for the different sectors and record the points at which each relevant ray emerges onto the observation surface. An isochronous chart is constructed by interpolating the travel time values along each ray. In addition to the time fields we can construct the fields of azimuthal deviations and the angles of emergence [4].

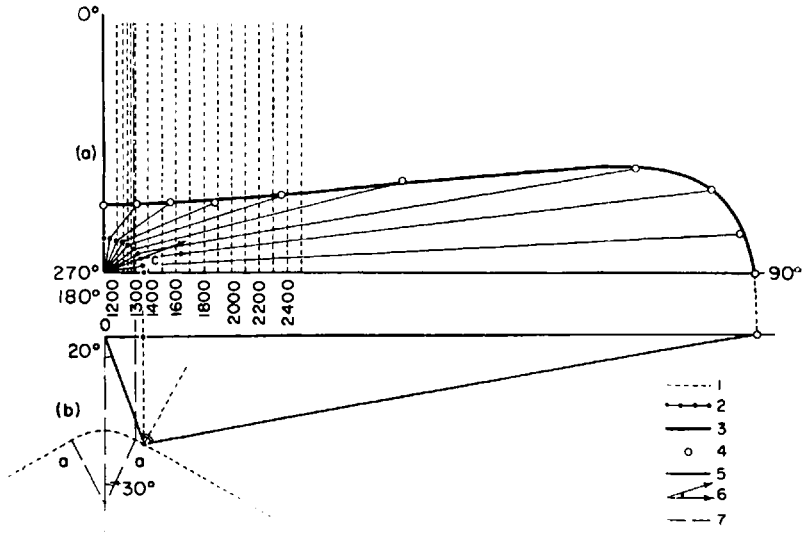

FIG. 4. Construction for radial conic surface formed by rays emerging from source at an angle of 20° with the vertical.

a—plan; *b*—cross-section of structure in vertical plane from 270–90° azimuth. 1—structure contours of interface (for cylindrical surface taken at every 20 m; for plane—at every 100 m); 2—trace projection of intersection of radial conic surface with interface; 3—geometric locus of points of emergence of rays of 20° conic surface on to observation plane; 4—points of emergence of individual rays; 5—projection of rays; 6—azimuthal deviation suffered by the ray on reflection at point c; 7—line joining cylindrical surface and plane.

In order to solve linear problems, therefore, we must have a plan on the appropriate scale with isohypses for all the interfaces. The plan must show the position of the source of vibrations (shot point).

Let us now examine the technique for making the constructions, taking concrete examples first of two layered and then of three layered media.

* Structure contour [*Editor's note*].

CONSTRUCTING A SURFACE HODOGRAPH FOR REFLECTED RAYS IN THE CASE OF A TWO LAYERED MEDIUM

By way of example we shall consider the construction of a surface hodograph or waves reflected from an interface which has a cylindrical form.

Formulation of the problem—To solve a linear problem in geometrical seismics (to construct a chart of isochronous lines) for waves reflected from a cylindrical surface with a horizontal axis of infinite extent. The cylindrical surface is joined to planes. A section of the interface across the extent of its vertical plane is shown in Fig. 4, *b*. The source of vibrations 0 (shot point) is situated above the axis of the cylinder.

Description of the constructions—The reflecting boundary has two mutually perpendicular axes of symmetry, the source being above the point of intersection of these axes. In this case we can limit our consideration of the constructions to one-quarter alone, for the field in the remaining quarters will be symmetrical. Taking the direction in which the structure spreads as the initial azimuth reading, we shall make the constructions within the limits 0 to 90°.

To solve this problem we shall trace several ray surfaces formed by rays emerging from the source at arbitrarily determined angles φ. The section of these surfaces in the vertical plane is shown in Fig. 8, *b*. By way of example we shall consider in detail constructions for any one of these surfaces alone (for example the surface formed by rays which make an angle φ^* equal to 20°). For this purpose we shall consider the rays of which the azimuths differ from one another by a definite quantity for example 10°. The projections of the incident rays in the first medium are shown in Fig. 4, *a* by the lines 5.

The constructions for each ray surface can be broken down into separate stages:

(a) construction of the trace of intersection of the ray surface with the interface on the plane of the projection;

(b) determination by Wulff's net of the directions (azimuth and angle with vertical) of the reflected rays;

(c) construction of the trace of intersection of the ray surface with the observation plane after reflection.

Let us examine these stages for each ray surface separately.

(a) Construction of the projection of the trace of intersection of the ray surface intersection with the interface. Since the interface is not simple in form we shall find the projection of the trace of intersection of the ray

* For the sake of brevity we shall henceforward call such a surface the "φ° ray surface".

surface with the interface as the geometric locus of the projection of traces of intersection with the interface of the individual rays.

Let us take a particular example in order to examine the technique for determining the projection of the points of intersection of the ray with the interface. To do this we shall select from the total number of rays forming the conic surface one ray for example with an azimuth of 70°. Its projection on the horizontal plane is shown in Fig. 5, *a*, and the section of the vertical plane along the lines *I—I*, that is in the direction of the ray in Fig. 5, *b*. Since

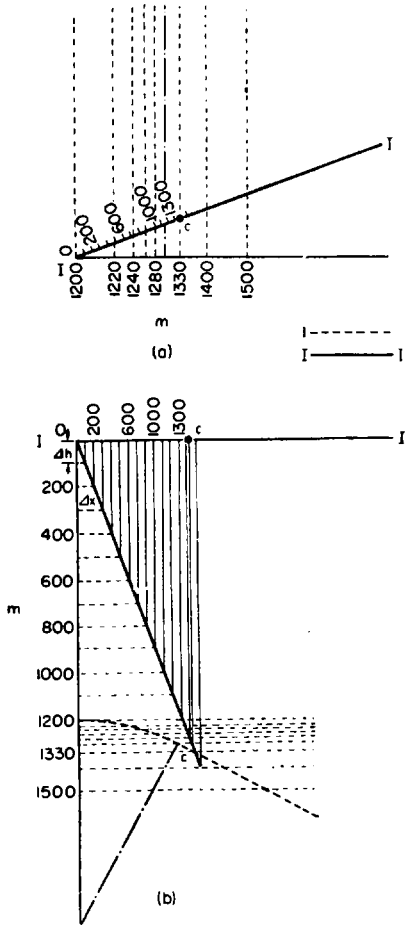

FIG. 5. Projection of point where ray intersects interface. *a*—plan; *b*—vertical cross section along direction of incidence of ray; 1—structure contours of interface; I—I direction of incidence of ray.

according to the assumption this ray makes an angle of 20° with the vertical, it will be projected onto the observation plane in a section $\Delta x = \Delta h \tan 20°$, when it penetrates to a depth Δh. If we now plot on the plan on the scale of the constructions the section Δx in the direction of incidence of the ray, we shall obtain on the projection of the ray a successive series of points corresponding to certain definite depths of the ray: in our case $\Delta h = 100$m and the points will be at 100, 200 and 300m.

Let us suppose that we strike the point marked 1300m, that is at this point the ray has penetrated to a depth of 1300m; while the structure contour of the interface 1320m passes through this point, it is obvious that the ray has not yet reached the interface. We plot the section once again and obtain a point marked 1400m but the structure contour 1340m passes through this point on the plan and consequently our ray has not yet intersected the interface between the contours 1300 and 1400m. Interpolating values for the depths between the structure contours 1300 and 1400m and also the depths of the section Δx 1300—1400m, we obtain a point c in which the depths both along the structure contours of the interface and along the ray are the same—1330m.

The point c is thus a projection of the trace of intersection of our chosen ray with the interface. Having made such constructions for many rays of the conic surface and having joined the points obtained in a smooth curved line we shall obtain on the plan the trace of intersection between the interface and our ray surface (line *2* in Fig. 4). This line is also the projection on to the horizontal plane of the line on which the reflection of the rays making up our ray surface takes place.

(b) Determination of the direction of the reflected rays. Having constructed on the plan projections of the points of incidence of the rays under consideration we find the direction of the rays after reflection. This is done by means of a Wulff net, in the manner indicated above (Problem 3). The centre of the Wulff net is placed at the point of incidence of the ray and the direction of the incident rays and the direction of the normal to the interface at the point of incidence are plotted on the Wulff net. The direction of the normal is determined from the structure contour chart of the interface.

The azimuth of the normal to the boundary at the point of incidence is determined by the direction of maximum inclination of the boundary at this point. This direction corresponds on the plan (Fig. 6, *a*) to the direction of the normal to the structure contour of the interface. The angle of incidence of the normal to the vertical is determined from the value of the angle of incidence of the interface at the point of incidence.

The angle made by the normal with the vertical can be determined

graphically; for this purpose we construct, along the direction of the normal azimuth, a section of the interface of the vertical plane and drop a perpendicular to the point of incidence (Fig. 6, *b*).

In our problem the azimuth of the normal to the interface for all its points is the same, 90°. This is because all the structure contours are rectilinear and have an azimuth of 0°. The angle of incidence of the normal to the interface is constant at 30° in sectors where the interface is represented

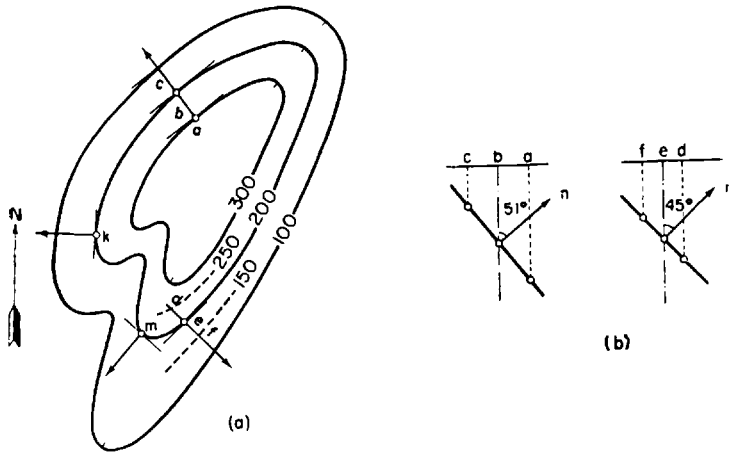

FIG. 6. Determination of the direction of the normal to the interface. *a*—determination of the azimuth of the normal at points *a*, *b*, *c*, *k*, *m*; *b*—determination of the angle with the vertical.

by planes, while in those sectors where the interface is represented by a cylindrical surface the angle of incidence of the normal to the vertical varies from 0 to 30°.

The ray which we are considering which has an azimuth of 70°, strikes the interface at a point which is projected on the plan as point *c* (Figs. 4 and 5). We place an imaginary centre of the net at the point of incidence and construct on the net the directions of the incident ray *A*(70° and 20°) and the normal to the interface (90° and 30°) and then we determine the direction of the reflected ray *B* (83° and 79°)—Fig. 7. Figure 7 also shows the determination of the reflected ray direction for all the remaining rays of the 20° surface which we are considering. The azimuths of the incident rays are separated from one another by 10° (that is 0°, 10°, 20°, 30°, 40°, 50°, 60°, 70°, 80°, 90°). The points are marked on the drawing as 0, 1, 2, 3, 4, and so forth.

(c) Construction of the trace of the intersection between the observation plane and the ray surface after reflection. For this purpose we plot on the plan projections of the reflected rays according to their known azimuths (these are shown in Fig. 4 by the lines 5). As can be seen from the illustration the direction of the projection of the incident ray coincides with the direction of the projection of the reflected ray only along two azimuths (0° and 90°)[4]. In neither case is there any azimuthal deviation; in all the remaining cases azimuthal deviations are observed and the projections of the rays are not straight lines but are broken lines consisting of two parts.

At the point of reflection then the ray suffers an azimuthal deviation which is easily visible when we project the ray onto the horizontal plane

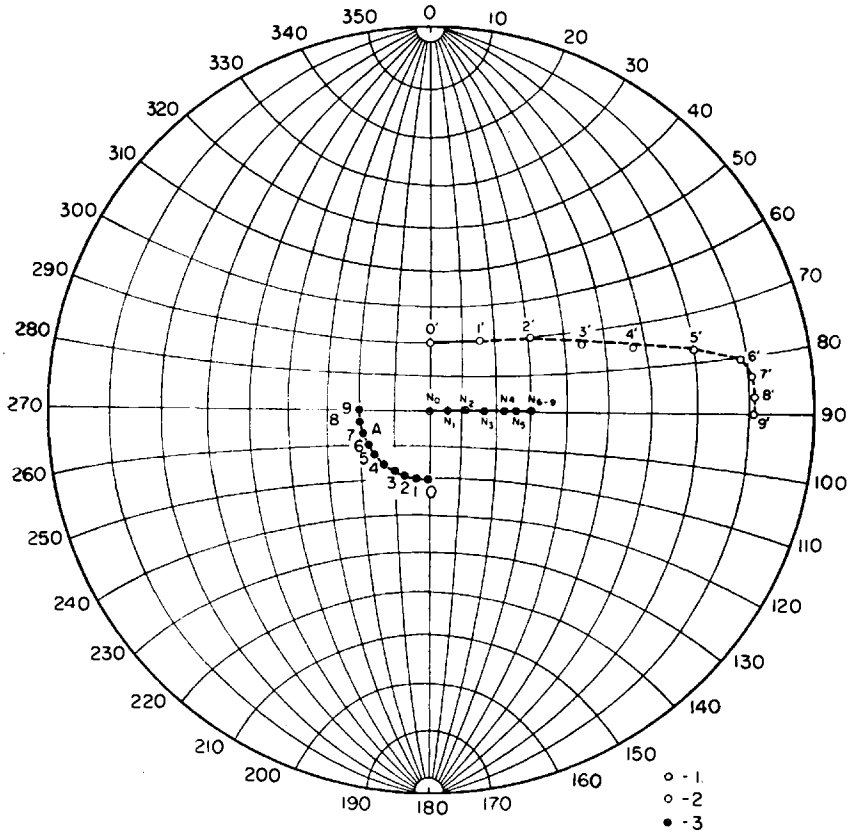

FIG. 7. Determination of the direction of the rays after reflection by means of a Wulff net. 1—direction of incident rays with azimuths 0–90° at every 10°; 2—direction of reflected rays; 3—direction of the normal to the interface at the point of incidence of the corresponding ray.

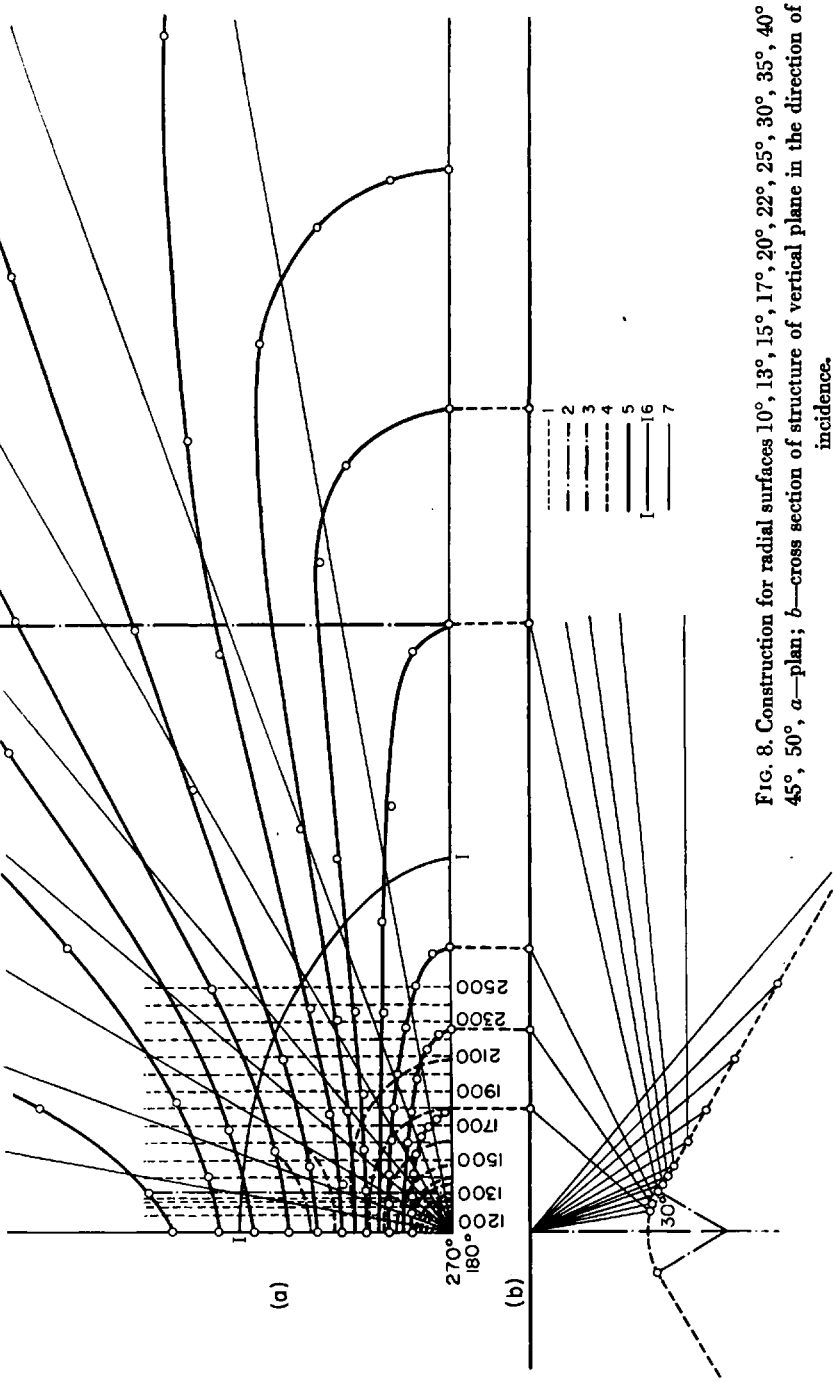

FIG. 8. Construction for radial surfaces 10°, 13°, 15°, 17°, 20°, 22°, 25°, 30°, 35°, 40° 45°, 50°, *a*—plan; *b*—cross section of structure of vertical plane in the direction of incidence.

1—structure contours of interface (given every 20 m within the limits of the cylindrical surface); 2—line where cylindrical surface joins plane; 3—geometrical position of points of emergence of rays reflected from the line of joining of the cylindrical surface with the plane; 4—projection of the traces of intersection of radial conic surfaces with interface; 5—geometrical position of emergence points of rays belonging to one radial surface on the observation plane; 6—critical contour; 7—lines of equal azimuths.

of observation. The azimuthal deviation for a ray with an azimuth in the first medium of 70° is shown in the illustration by means of arrows and is equal to 15°.

We find the intersection trace of the ray surface with the plane of observation as the geometrical position of the points of emergence of rays belonging to one ray surface. These points are calculated for each of the rays of the ray surface from the known depth of the point at which the ray intersects the interface and the angle the ray makes with the vertical after reflection. This angle is taken from the Wulff net when the direction of the

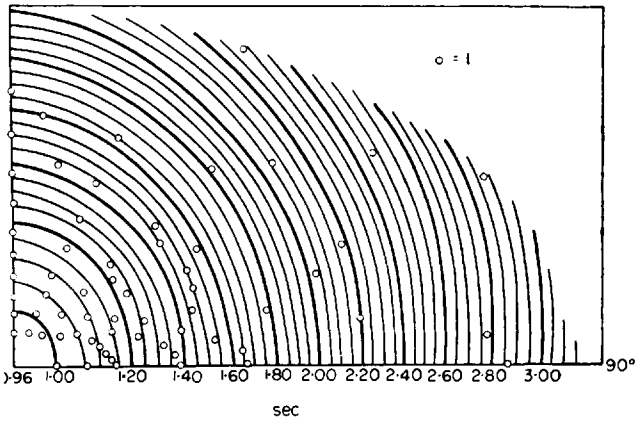

FIG. 9. Chart of isochronous lines.

1—points of emergence of rays from which the field was constructed.

reflected ray is determined. In the general case we can find this point by the same methods as we use for determining the projection trace of a ray intersection with an interface. In contrast to the case analysed above what we are here examining is not "descent" of a ray but its "climb". The point on the projection of the reflected ray which corresponds to zero depth will also be the point of emergence of the corresponding ray (see line *4* in Fig. 4). When we have joined all the ray emergence points by a smooth line we shall obtain the intersection trace of our ray surface with the observation plane.

For every point on line *2*, then, there is a corresponding point on line *3* (see Fig. 4).

Similar constructions can be made for all ray surfaces (Fig. 8), where (*a*) the lines *4* correspond to radial surfaces of 10°, 13°, 15°, 17°, 20°, 22°,

25°, 30°, 35°, 40°, 45°, 50°. Using such constructions we can now pass on directly to calculating the travel times along the rays. The length of the ray's segment required for this is determined from the difference in depth ΔH of the initial and terminal points of the segment of the ray and its angle with the vertical from the formula

$$l = \frac{\Delta H}{\cos \varphi}$$

The times for any ray are calculated separately for each segment in the broken line and then the travel times are summed. The travel time obtained is entered on the plan at the emergence point of the appropriate ray. The chart of isochronous lines is obtained by interpolating the travel time values for all emergence points of the rays under consideration. Fig. 9 shows an isochrones chart constructed by the method described. The isochrones are plotted on this chart at 0.05s. As we might have expected the isochrones form smooth lines extending along the line of the limits of the structure.

We now consider a problem for a three-layered medium.

CONSTRUCTING THE SURFACE HODOGRAPH FOR REFLECTED WAVES IN THE CASE OF A THREE-LAYERED MEDIUM

By way of example we shall analyse in detail an isochrone chart for waves reflected from a dome, making allowance for intermediate refraction on an inclined plane*. The construction of the medium is shown in Fig. 10, *b*. The velocity ratio $\frac{v_2}{v_1}$ in the first and in the second layers is equal to 1.2. The source of excitation is in both cases above the slope of the dome.

The general scheme for solving the problem is the same as for problem 1. The difference is that it is necessary to make allowance for an intermediate interface. We do this by constructing projected traces of the intersections of the ray surfaces with the intermediate interface both before and after its reflection when we are tracing the ray surfaces.

Let us examine the tracing of several ray surfaces. Fig. 10, *a*, shows constructions for a ray surface formed by rays which emerge from a source and make an angle $\varphi = 30°$ with the vertical. It can be seen from the plan that the source is set in relation to the top of the dome. Radial lines emerging from the source are produced at every 10° and correspond to the directions (azimuths) of the rays in the first medium which were used in tracing the ray surfaces.

* The solution of this problem is given in[3].

The point from which the azimuths are read off coincides with the direction of incidence of the inclined refracting boundary. Line *3* is a trace projection of the intersection of the radial surface with the inclined refracting plane.

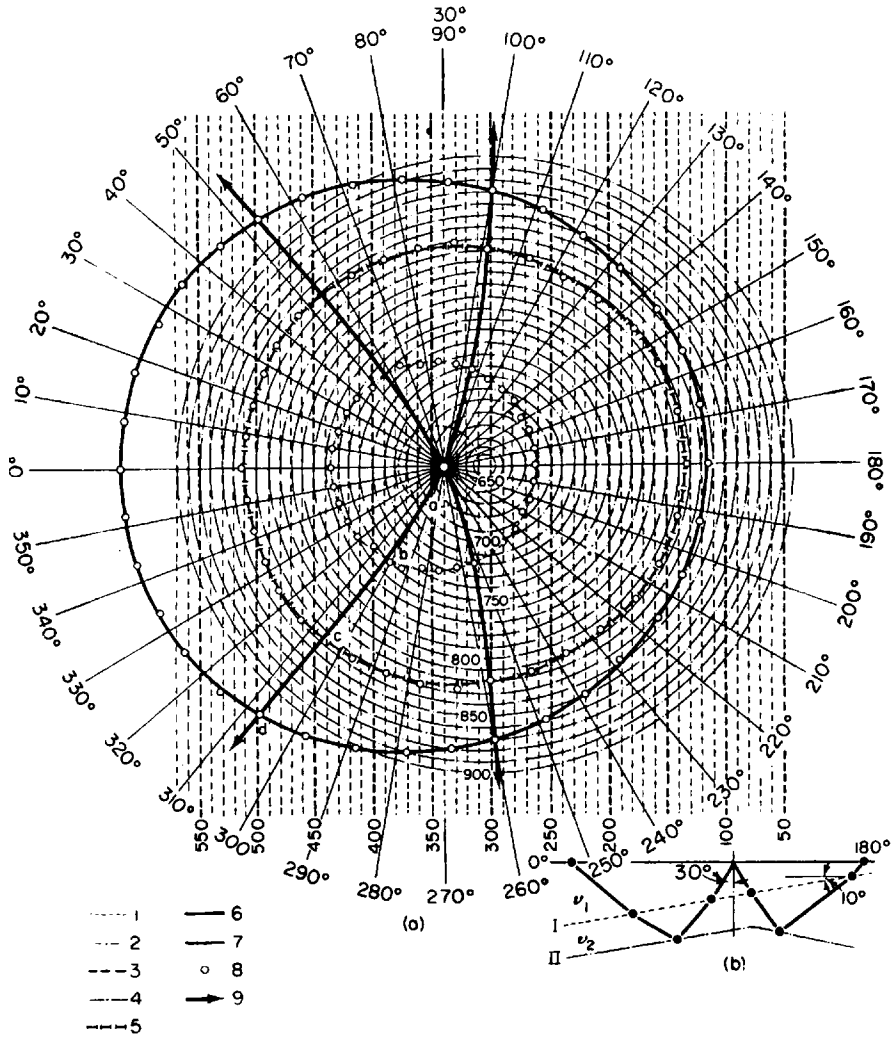

FIG. 10. Determination of points of emergence of rays onto observation plane (30° ray surface). *a*—plan; *b*—cross section in vertical plane containing azimuths 0 and 180° (the generators of the 30° ray surface are shown). 1—structure contours of refracting interface; 2—structure contours of reflecting interface; 3-4-5-6—trace projections of intersection of 30° ray surface with refracting boundary (3), reflecting boundary (4), refracting boundary after reflection (5), and observation plane (6); 7—lines of equal azimuths; 8—points of emergence of rays; 9—projections of separate rays.

This projection is found as the geometric locus of the projected traces of the interface with rays with azimuths 10° apart from one another and with projections shown by the radial lines.

The projection of the traces of intersection of the rays with the interface are found as projections of points on the rays and on the interface, then points having the same depth. A ray with its azimuth in the first medium at 300°, intersects the inclined refracting interface at a depth of 356 m. The projection

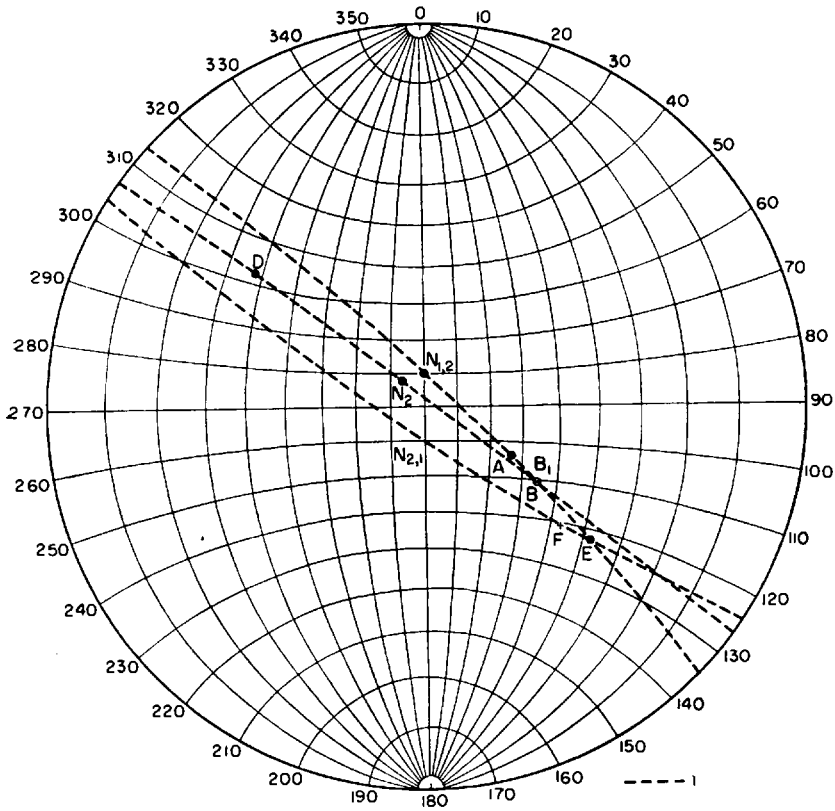

FIG. 11. Example of determination of direction of refracted and reflected rays and of a ray refracted on transition from second medium to first. 1—plane of rays; the points correspond to directions: *A*—of a ray incident on a refracting boundary (120 and 30°); $N_{1,2}$—of the normal to the refracting boundary; *B*—of a refracted ray (125° and 39°); B_1—of a ray striking the reflecting boundary after refraction (125° and 39°); N_2—of the normal to the reflecting boundary (318° and 10°); *D*—of a reflected ray (309° and 59°); *E*—of a ray striking the refracting boundary after reflection (129° and 59°); $N_{2,1}$—of the normal to the refracting boundary (180° and 10°) after reflection; *F*—of the emergent ray (132° and 50°).

of this point on to the observation plane is denoted by the letter a. It must be noted, however, that in this case the trace of the projection of the intersection of the ray surface with the inclined refracting boundary can be found by purely geometrical constructions as an ellipse formed by the intersection of the conical surface with the inclined plane.

The line thus constructed is the geometric locus of the points of refraction of rays belonging to the 30° radial surface under consideration. At these points the rays having been refracted pass into the second medium.

Let us determine the direction of the rays in the second medium (after they have been refracted). This is easily done with a Wulff net by the method described (Problem 3).

Now let us see how to determine the direction of one of the refracted rays, for example a ray with an azimuth in the first medium on emergence from the source equal to 300°. Following the method described above we set the centre of the net at the point of incidence of the ray and plot on the net the direction of the normal to the interface and the direction of the incident ray. Since the refracting interface is a plane the direction of the normal will be the same for all points on this interface. The angle at which the normal inclines to the vertical is equal to the angle of inclination of the plane to the horizontal, namely 10°. The azimuth of the normal is 0°. The direction of the normal (0° and 10°) is shown in Fig. 11 by the letter $N_{1,2}$.

Since the centre of the projection is placed at the point of incidence, in plotting on the Wulff net the direction of an incident ray emerging from the source with an azimuth of 300° we must take the inverse azimuth, that is 120°. The direction of the incident ray under consideration (120° and 30°) is shown in the illustration by the point A. Using tracing paper we plot points corresponding to both directions on one meridian, and then measure the angle of incidence $i_{1,2}$, which is equal to an angle of 30°.

We calculate the angle of refraction from the angle of incidence and the velocity ratio v_2/v_1 according to the formula

$$\sin i_{2,1} = \sin i_{1,2} \frac{v_2}{v_1},$$

where $i_{2,1}$ is the angle of refraction.

$$\sin i_{2,1} = 0.588 \; i_{1,2} = 0.705; \; i_{2,1} = 45°.$$

We plot the angle of refraction we have found in the plane of the ray from the normal in the direction of the incident ray, and mark the point B

obtained by a cross, since the refracted ray lies underneath the observation plane. Rotating the tracing paper to its original position we take the coordinates of point B from the net. It must be remembered, however, that the ray is under the observation plane and therefore we must take the inverse azimuth.

The direction of the refracted ray will accordingly be (305° and 39°). Using similar constructions we can find the directions of all the rays under consideration in the second medium. Figure 12 shows such constructions for a 30° ray surface.

We now turn back to Fig. 10. We plot on the plan the directions (azi-

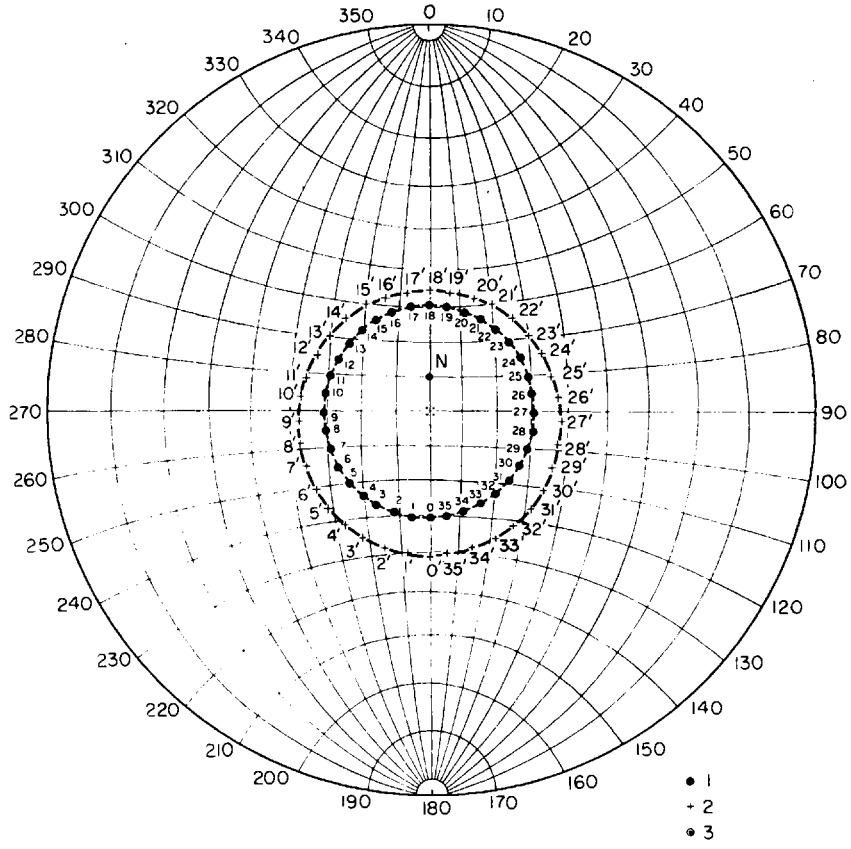

FIG. 12. Determination of the direction of refracted ray for a 30° ray surface. 1—directions of incident rays having azimuths from 0° to 360° at every 10°; 2—directions of the corresponding refracted rays; 3—normal to the interface.

muths) of the rays in the second medium which we have found, for a ray with an azimuth of 300° and an azimuth of 305°. We then obtain the projection of the ray on to the horizontal plane in the second medium. As can be seen from the illustration and also from the values of the direction coordinates, the ray under consideration undergoes azimuthal deviation of +5° during refraction.

Having traced the directions of the rays after refraction in the second medium, we find the trace projection of the intersection of the ray surface

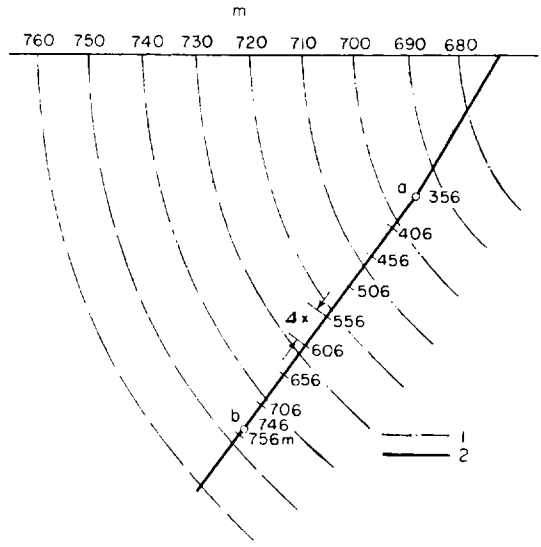

FIG. 13. Determination on plan of projection of point of intersection of a ray with a reflecting interface. 1—structure contours of reflecting interface; 2—direction of incidence of ray.

with the reflecting boundary. This projection is also found to be the geometric locus of the trace projections of the intersection with a reflecting boundary of individual rays of the ray surface, in our case rays with azimuths in the first medium which are 10° from one another.

The traces of the rays' intersection with the reflecting interface are found to be points on the ray and the interface which have the same depth. These traces are then projected onto the observation plane. We determine the trace projection of the intersection for a ray with an azimuth of 300°. After refraction on the inclined interface at point *a*, the ray with the 300° azimuth and the 30° angle with the vertical has changed its direction—the azimuth

is now 305° and the angle with the vertical 39°. In order to make the following discussion clear we show the ray under consideration and the structure contours of the reflecting interface (Fig. 13) on the plan (constructions for all the rays are usually shown on one drawing). The point *a* lies in the plane of the inclined interface and has a depth of 356 m. Knowing the angle the ray makes with the vertical (39°) we calculate the amount of projection of the ray onto the observation plane during its penetration at some depth Δh (in our case $\Delta h = 50$ m) as $\Delta x = 50 \tan 39°$. We plot the segment Δx from the point *a* along the direction of incidence of the ray. We now examine the two points on the projection of the ray which we have thus obtained: 706 and 756 m. At the first point the ray has not yet reached the reflecting boundary, since the 742 m contour passes through this point; at the second point it has intersected the interface since the depth of this point along the 756 m ray is greater than its depth along the 748 m contours. Consequently, the projection of the point of incidence of the ray on to the reflecting boundary lies between the points 706 and 756 m along the ray and between the contours 740 and 750 m and is found by interpolating the depths. Similar constructions can be made for all rays. After joining by a smooth line the trace projections of the intersection of the radial surface with the reflecting interface, along which the rays belonging to our radial surface are reflected (Fig. 10, line *4*), we must next find the direction of the reflected rays.

This again is done by means of a Wulff net. For this purpose the centre of the net is set at the point of incidence of the ray, and the directions of the incident ray and of the normal to the interface are plotted on the grid.

Let us trace the direction, after reflection, of the ray in which we are interested. The ray has emerged from the source with an azimuth of 300° and has been refracted on the inclined interface at a depth of 356 m at a point the projection of which on the plane is denoted by point *a*, and which has struck the reflecting boundary at a point 746 m deep. The projection of the point of incidence on the observation plane is denoted by the point *b*. We have already described how to determine the direction of the reflected ray; we shall now briefly recapitulate this method as it applies to our data.

We imagine the centre of the net placed at the point of incidence, and plot on it the directions of the incident ray and the normal to the interface. The direction of the incident ray is determined as we have shown above, by the co-ordinates (305° and 39°). The point *B* (see Fig. 11) with the reverse azimuth characterizes the direction of the incident ray. The direction of the normal to the interface is in our case determined by the values (318°

and 10°), and the position of the normal to the interface on the net is determined by the point N_2. Making both directions coincide with one of the meridians of the net we find the plane of the ray and in this plane we plot from the normal the angle of reflection, which is equal to the angle of incidence. We now obtain the point D. We rotate the tracing paper to its original position and using the Wulff net we take the co-ordinates (azimuth and angle with the vertical) of the point D. The co-ordinates obtained characterize the direction of the reflected ray.

The ray which we are to examine after reflection has a direction determined by the co-ordinates (309° and 59°) and suffers an azimuthal devia-

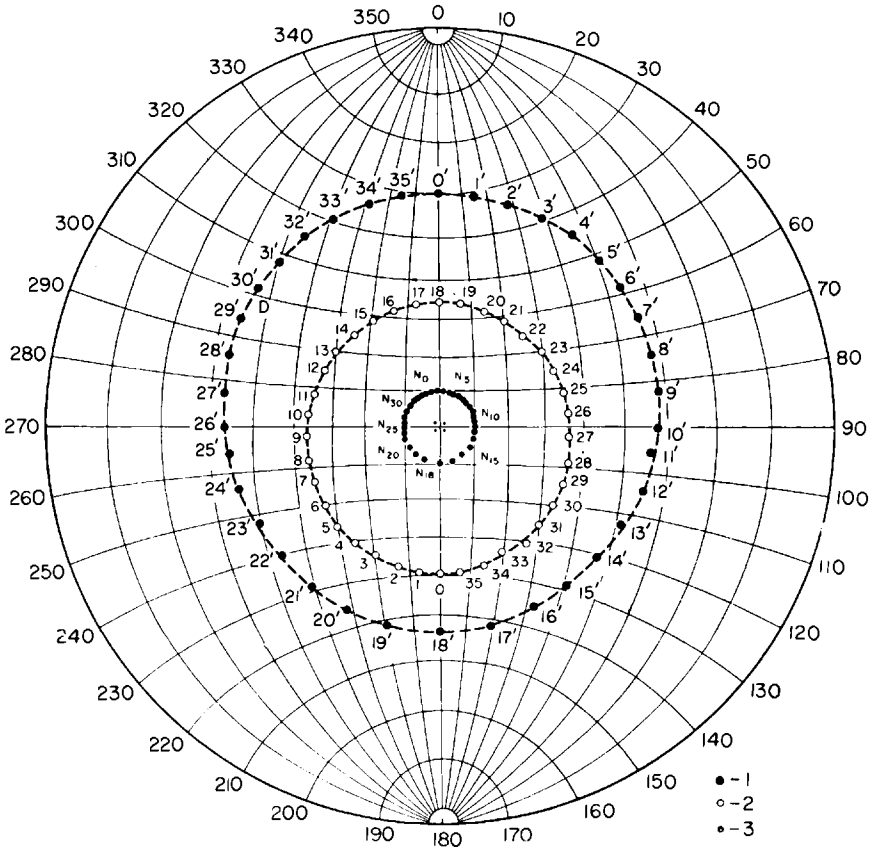

FIG. 14. Determination of the direction of reflected rays for 30° ray surface. 1—directions of incident rays having azimuths from 0 to 360° at every 10°; 2—directions of the corresponding reflected rays; 3—direction of normal to interface at point of incidence of rays.

tion of +4° on reflection. In this way we determine the directions of the remaining rays after reflection.

Having determined the direction of the rays after they have been reflected from the dome and having constructed the projections of these directions on the plane, we can now find the projection of the traces of the intersection of the ray surface under consideration with the inclined refracting boundary. For this purpose we use the methods which have been described to find the projections of the points of intersection of the reflected rays with the refracting interface, and then we join these points on the plan by a smooth line. The ray which we are considering, after emerging from the source with an azimuth of 300° and striking the reflecting boundary at a point the projection of which on the plan is point *b*, intersects the refracting boundary at a depth of 443 m; the projection of this point on the plan is denoted by the letter *c* (see Fig. 10). In Fig. 10 the projection of the trace of intersection with the inclined refracting boundary of the ray surface after reflection is shown by the line *5*. After being refracted at points on the line of intersection of the ray surface with the refracting boundary, the rays strike the first medium. The directions of the rays in the first medium after refraction are determined from the Wulff net. This is shown in Fig. 11 for the ray under consideration.

As we have shown above the ray we are considering has undergone azimuthal deviation on the reflecting boundary and after reflection has an azimuth of 309° and an angle with the vertical of 59°. It must be remembered that the incident ray is plotted with inverse azimuth (309°−180° = = 129°) and that in determining the direction of the refracted ray we take the inverse azimuth. We mark the direction of the incident ray on the tracing paper by means of the Wulff net (point *E*) and also the direction of the normal to the interface $N_{2,1}$ (180 and 10°), and then make both directions coincide with one of the meridians of the net. In the plane of the rays which we have thus obtained, we measure the angle between the normal and the point *E*—angle of incidence—and after calculating the angle of refraction according to the formula given above we plot it from the normal in the direction of the incident ray. The point *F* is marked by a cross since the ray lies under the plane. We now rotate the tracing paper to its original position and take the co-ordinates of the point *F* from the net—the azimuth and the angle with the vertical.

We thus find that the direction of the ray after refraction is 312° and 50°. Consequently, on refraction the ray undergoes an azimuthal deviation equal to 3°. The Fig. 15 shows how the direction of the refracted rays of the 30° ray surface is determined. The points where the ray emerges are determined

as points of a ray having zero depth. For the ray under consideration this point is marked on the plan (Fig. 10) by the letter *d*. After we have determined the points of emergence of all the rays and joined them by a smooth line we obtain the geometrical position of the points of emergence of rays belonging to one ray surface. The intersection trace of the ray surface with the observation plane is shown by the line *6*.

We have now consistently traced in space a ray surface (which in the first medium was conic) formed by rays emerging from a source at an angle of 30° with the vertical, and we have obtained for each of the rays under consideration its projection onto the observation plane. The other ray sur-

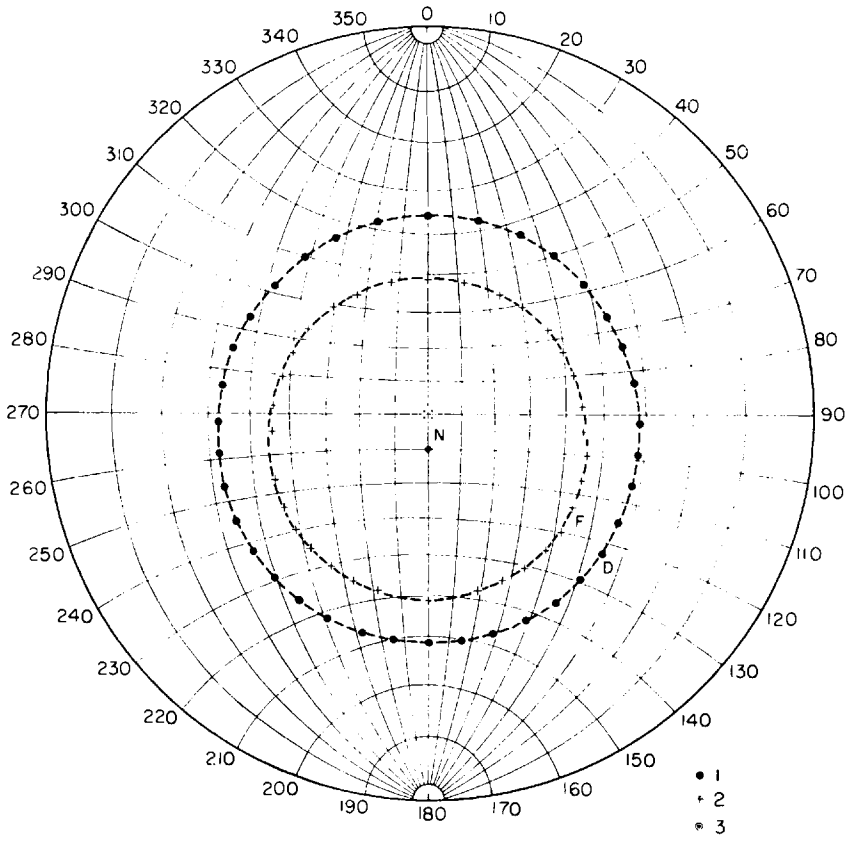

FIG. 15. Determination of direction of rays refracted on plane inclined interface on transition, from second medium to first (the constructions were made for a 30° ray surface). 1—directions of incident rays having azimuths from 0 to 360° at every 10°; 2—directions of refracted rays; 3—direction of normal to interface.

faces required for solving the problem as a whole can be traced in space in a similar way.

The projections of the rays onto the observation plane can be traced on Fig. 10, and the directions (azimuth and angle with the vertical) of the rays at any point on the observation plane determined. This could be used to construct the field of lines of equal azimuthal deviations and the field of lines of equal angles of emergence[3, 4].

One tracing paper can be used to determine the direction of the refracted rays in the given case for all the radial surfaces, since the boundary is a plane boundary and the direction of the normal is the same for all points on the boundary.

It is convenient to determine the direction of the rays after refraction on a separate sheet of tracing paper for each ray surface, since the direction of the normal varies at different points of the interface. From an examination of the constructions for different ray surfaces, it follows that the azimuthal deviations of rays emerging from a source with the same azimuth increase in inverse proportion to the angle φ of inclination with the vertical. When $\varphi = 10°$, for example, rays with azimuths near to 180° suffer azimuthal deviations of very nearly 180° on reflection. This, in particular, explains the fact that the projections of the intersection traces of the 10° radial surface with the reflecting interface and with the refracting boundary intersect after reflection.

Calculating the time field—The time field is constructed by interpolating travel time values for each of the rays under consideration. The travel times along the rays are calculated from their various sections in each layer separately, from the length of the section and the velocity value in the layer. The length of the section is determined from the value of its horizontal projection and from the angle of inclination with the vertical as determined from the Wulff net.

To determine the travel time of a wave along the ray we sum the values for the travel times along its separate links.

The chart of isochrones constructed for our case is shown in Fig. 16. The points of emergence of the ray surfaces which we examined when we were tracing are indicated by small circles. The chart of isochrones is constructed from the values for the travel times at these points. The isochrones are given at 0.05s. intervals.

In this paper we have examined the solution for ray problems in seismic prospecting only for reflected waves. The method is equally applicable to head waves [3].

The accuracy of the solution depends primarily on two factors—accuracy

in determining the direction of the ray by means of the Wulff net and the accuracy of the graphical constructions. The former depends primarily on the size of the Wulff net. After some practice of accurate work with a Wulff net 20 cm in diameter, an accuracy of 0.5° can be obtained in determining the direction of the ray. If a higher degree of accuracy is required, the diameter of the net can be increased and more divisions can be marked on it. The accuracy of the graphical constructions depends on scale, and is limited by an inherent margin of error which experiment has shown to be 0.2 – 0.3 mm. A transverse scale must therefore be used in constructing the graphs. Scales of 1:10,000 and 1:25,000 may be regarded as convenient.

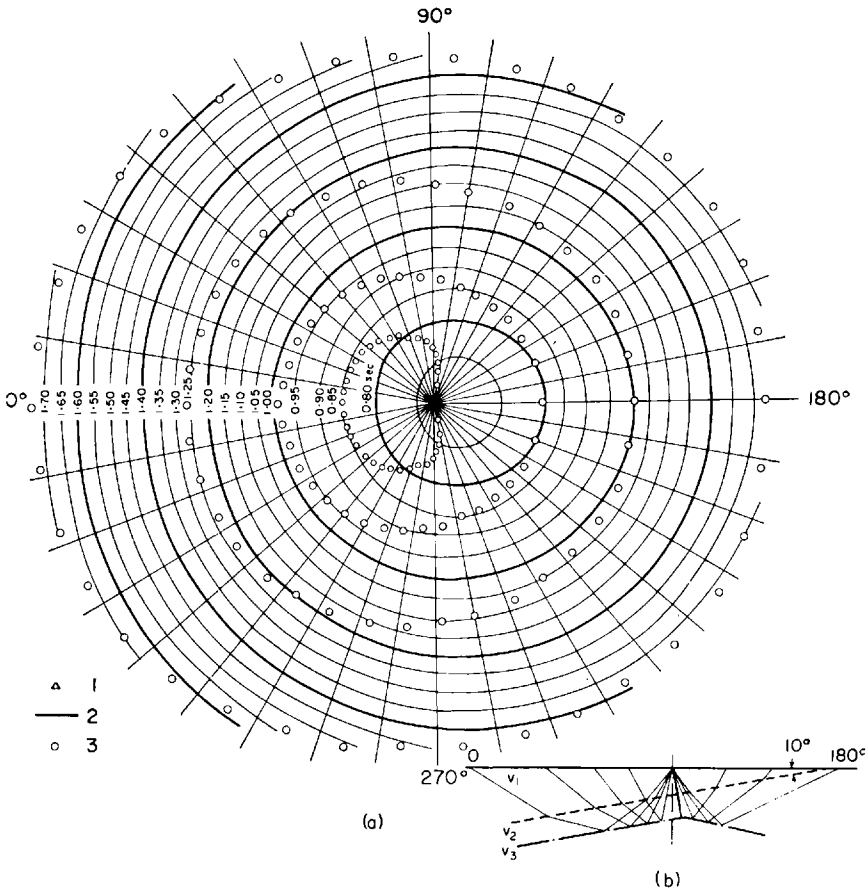

FIG. 16. *a*—Chart of isochrones; *b*—vertical cross section of structure with generators of ray surfaces used in the construction. 1—shot point; 2—isochrones; 3—points of emergence of rays from which the fields were calculated.

SUMMARY

The method we have described for solving three-dimensional linear problems in geometrical seismics of multi-layered media with interfaces of arbitrary shape is based on the use of stereographic projections. Such projections make it possible to follow the seismic rays in space and thereby open up new possibilities for solving problems in geometrical seismics. The method enables us to study the laws governing surface hodographs for various waves whatever the shape and quantity of the interfaces.

REFERENCES

1. I. C. BERSON, The space problem of interpretation of the hodographs of refracted waves. *Publ. Institute Theor. Geophysics*, vol. 2, pt. 2, 1947.
2. G. V. WULFF, On the methods of projection of crystals in relation to theodolite measurements. *Proc. Warsaw Univ.*, 1902.
3. E. I. GAL'PERIN, The solution of direct space problems of geometric seismics for multi-layered media with arbitrary surfaces of separation. *Izv. Akad. Nauk SSSR, ser. geofiz.*, No. 9.
4. E. I. GAL'PERIN, On azimuthal deviations of seismic waves. *Izv. Akad. Nauk SSSR, ser. geofiz.*, No. 9, 1956.
5. V. D. TAV'YALOV, and Yu. V. TIMOSHIN, Hodographs of reflected waves for curved surfaces of separation and their interpretation. *Izv. Akad. Nauk SSSR, ser. geofiz.*, No. 2, 1955.
6. N. N. PUZYREV, On the influence of the curvature of the surfaces of separation and the determination of velocity from hodographs of reflected waves. *Collection "Applied Geophysics"* Issue 13 Gostoptekhizdat, 1955.
7. N. K. RAZUMOVSKII, *Stereographic Projections*, 2nd Ed., 1932.

CHAPTER 3

MULTIPLE REFLECTED WAVES

S. D. SHUSHAKOV

IN seismic prospecting, the separation and tracing of useful waves may be made difficult by interference from multiple reflected waves. These can also be mistaken for single waves and so give rise to errors in interpretation.

Although much has been written on the study of multiple waves the difficulties of recognizing them remained, and in the course of a seismic prospecting operation they are sometimes mistaken for single waves.

The present article describes the results obtained from modelling multiple reflected waves and gives a number of theoretical calculations performed according to the contour integrals method. The main topic is a description of the longitudinal waves which are commonly encountered in seismic prospecting work. Certain features of multiple reflected waves are noted and practical suggestions are put forward.

Multiple reflected waves of one intensity or another probably occur in all, or nearly all regions. In discussing the problems connected with multiple waves the term is frequently applied to those waves which are clearly distinguishable and consequently possess an intensity commensurate with that of single reflected waves with approximately the same transmission times as the multiple waves. Reviewing the seismological conditions which prevail in regions where multiple waves of such intensity are observed, we may conclude that the following special conditions which favour the formation of such waves are found in these regions:

(1) a small number of interfaces characterized by comparatively high reflection coefficients;

(2) comparatively poor damping of the waves between these interfaces.

In the region Leningrad Station of the Krasnodar district, for example, there is a layer of highly wave-resistant Cretaceous deposits which is a reflecting horizon for multiple waves. In the outer zone of the Cis-Carpathian depression, a gypsum-anhydrite horizon from which multiple waves are reflected can be distinguished by its wave resistance. In north-western Germany the lower boundary is formed sometimes by the Cretaceous cover, sometimes by a combination of this with one of the intermediate boundaries which has a high coefficient of reflection[11]. In other regions such bound-

aries are formed by the surfaces of the crystalline basement[14] or by carbonate layers, lava flows and so forth[13, 14, 15].

Some investigators maintain that multiple reflections are found in those regions where surface conditions favour their formation[11, 14] (groundwater level near the surface, this low-velocity zone, level ground surface). This relationship is indeed observed in many areas, but it accounts only for multiple waves reflected from the Earth's surface.

Various answers are given to the question whether the Earth's surface or the base of the low-velocity zone acts as an upper reflecting boundary, but most investigators think that the base of the low-velocity zone plays the main part here [5, 11, 13]. YEPINAT'YEVA [5] explains this on the grounds that a wave reflected from the surface loses a good deal of energy in the process of being reflected by the bottom surface of the low-velocity zone of absorption in this zone. The influence of the conditions of excitation and reception on the intensity of the recorded multiple waves as yet has not been studied. POULTER, however, in a paper on the grouping of aerial explosions, notes that after comparing a large number of seismograms obtained from single well shots and from arrays of aerial explosions he is almost completely convinced that no traces of multiple reflections occur on the film when grouping is used. This can be explained in the case of multiple waves reflected first above the excitation point, and also in the case of interfaces which dip, when the apparent velocities of multiple waves near the source may be less than the apparent velocities of single waves, and the lower these velocities, the greater the number of multiple waves. Conditions which are more favourable to the recording of single rather than multiple waves can therefore be created not merely in grouping the shots but also in grouping the detectors and with other forms of direction finding. This possibility disappears as the angles of gradient of the reflecting boundaries diminishe.

KINEMATIC CHARACTERISTICS

Various types of multiple reflections can be excited in layered geological media. These waves can be subdivided according to the layers in which they are propagated and according to the layers in which they appear as longitudinal or as transverse waves.

The symbols P_i and S_k are used for longitudinal and transverse waves respectively, the subscripts indicating the layers in which these waves are propagated (Fig. 1).

When we are discussing a uniform wave we may confine ourselves to indicating merely the particular boundaries which reflect multiple waves.

These boundaries are usually denoted as follows: the Earth's surface, or the base of the low-velocity zone, by the index zero*, and other boundaries which reflect the multiple wave by the indices 1, 2, ... m, in order from top to bottom. An interbed echo reflected from some boundary denoted by 2, from the base of a weathered zone and from some intermediate boundary 1, is denoted as 201; a fullpath echo reflected n times from a lower boundary 1 and $n-1$ times from the zero boundary is denoted as 10 ... 101.

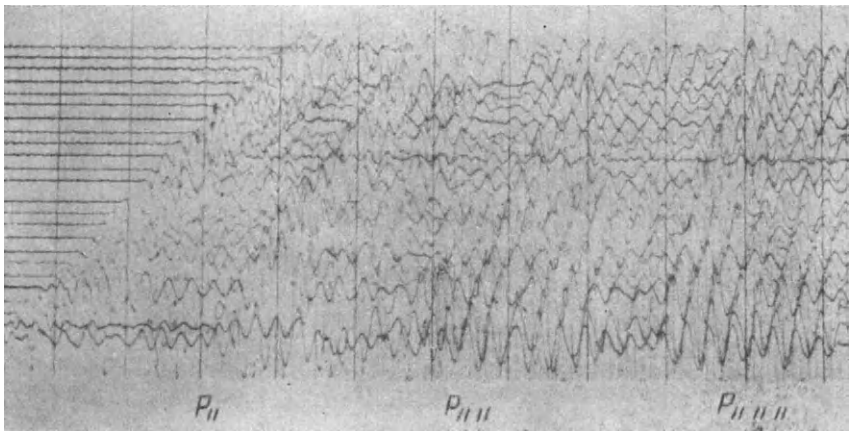

FIG. 1. Records of multiple reflections obtained under natural conditions.

Different types of multiple reflections have certain different kinematic properties. Full-path multiple waves 10 ... 101 appear as single waves reflected from interfaces which lie deeper than the boundary from which they are in fact reflected. Fig. 2 shows a schematic diagram of multiple wave rays, together with the disposition of the actual reflecting boundary and a number of fictitious boundaries which could be constructed if one mistook these waves for single ones. If the real boundary 1_1 is inclined at an angle γ to the zero surface, then a double reflected wave will appear as a single wave reflected from the false boundary 1_2, which acts as a mirror image of the zero boundary in boundary 1_1 and is inclined at an angle of 2_γ.

A boundary 1_n is inclined towards the zero boundary at an angle n_γ. If the depth of the boundary 1_1 along the normal to it below the shot point is equal to H_1, then the depth of a boundary along the normal to it below the same point is given by

$$H_2 = H_1 \frac{\sin 2\gamma}{\sin \gamma} = 2H_1 \cos \gamma.$$

* Henceforth called the zero surface or boundary.

Consequently the depth of the fictitious boundary l_n is given by

$$H_n = H_1 \frac{\sin n\gamma}{\sin \gamma}. \tag{1}$$

The hodograph* for the multiple reflection is given by the equation

$$t = \frac{1}{v_1}\sqrt{4H_1^2 \frac{\sin^2 n\gamma}{\sin^2 \gamma} + 4H_1 x \frac{\sin^2 n\gamma}{\sin \gamma} + x^2}, \tag{2}$$

where n is the number of times the wave is multipled and x is the distance from the source.

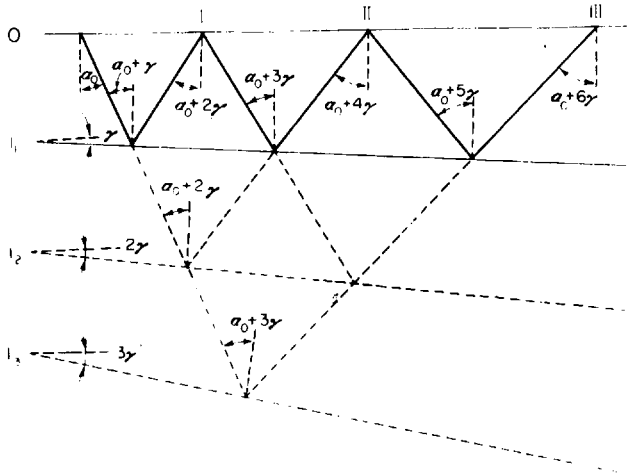

FIG. 2. Diagram of multiple reflection rays.

Near the excitation point, when there is a horizontal reflecting boundary, multiple waves are recorded travelling along a single path normal to this boundary. When the reflecting surface dips, each of these waves is propagated along its own special path (Fig. 3), at the end of which it strikes the zero boundary or boundary I, and after being reflected from this along the same path but in the opposite direction, returns to the detector situated near the point [8, 15]. Odd-number multiples at the end of the path of the incident wave are reflected from the interface I, whereas even-number multiples are reflected from the zero surface.

Full-path echoes have the following kinematic characteristics.

* A Russian term referring to distance—time curves. [Editor's footnote].

1. The travel time is equal to that of a fictitious wave which seems to be reflected from a deeper and more inclined boundary. At short distances from the source and when the dip of the reflecting boundary is slight, the time interval between each arrival of the multiple wave is the same.

2. The effective velocity calculated from the hodograph of a multiple wave which is mistaken for a single one must be near to the effective velocity calculated from the hodograph of a corresponding single wave reflected from the same boundary as that which is reflecting the multiple waves. This effective velocity will generally be lower than the one calculated from

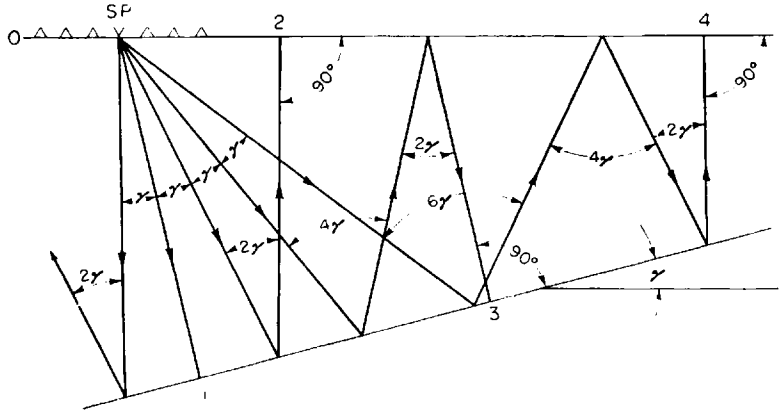

FIG. 3. Diagram of multiple reflection rays recorded near shot-point.

the hodograph of a single wave with a travel time near to that of the multiple wave, and lower than the mean velocity obtained from bore-hole measurement data and corresponding to the travel time of the multiple wave.

3. The angles of gradient of the fictitious interfaces constructed from the hodographs of multiple waves which have been mistaken for single ones increase systematically with depth. The angle of gradient of a fictitious boundary constructed from the hodograph of a wave multiplied n times will be n times greater than the angle of gradient of the real boundary reflecting this wave.

4. The number of multiple reflections with a different number of multiples cannot be more than $n < \pi/2\gamma$, where γ is the angle of gradient of the reflecting boundary, and increases from 1 to ∞ as this angle diminishes to zero.

5. When the reflecting boundary dips, the apparent velocities of multiple waves near the shot point diminish as the number of multiples increases.

Interbed echoes have different travel paths and are correspondingly different in their kinematic properties, which are determined separately in each case.

When the velocity increases monotonically with depth, multiple reflections show the following kinematic properties [2].

1. Depending on the change of type which the multiple wave undergoes as it passes from one hodograph to another with increase of t_0, (when $x = 0$), there may be increase or decrease of the effective velocity calculated from hodographs which have been mistaken for the hodographs of single waves. A decrease but not an increase in effective velocity with growth of t_0 can be used for recognizing multiple waves.

2. As the number of multiples increases, these effective velocities may either increase or decrease, depending on whether the greater part of their journey is through a high-velocity layer or a low-velocity one.

3. As a criterion for recognizing multiple waves, it is possible to use the scatter of the effective velocity values corresponding to identical values of t_0 and determined in different sectors of the operational area from the hodographs of various multiple waves, or on condition that the various multiple waves predominate in the interference vibrations.

A multiple wave of which the first reflection has occurred above the excitation point is distinguished by the fact that the travel time of this wave increases with the increase of the shot depth, whereas the travel time of an ordinary single wave decreases.

DYNAMIC CHARACTERISTICS

Shape oscillation—It is not unusual to find the phase of an oscillation changing through 180° when the number of multiplications of the wave alters to an odd number [13]. The explanation is that in such cases, as the wave passes from top to bottom through a lower boundary and from bottom to top through an upper boundary, there is in the one case an increase and in the other a decrease in wave resistance. Fig. 4 shows traces of multiple reflections obtained by modelling. The phase of the vibration can be seen to vary with the number of multiplications. This effect could not be observed if the wave resistances increased or decreased both when the wave was passing through the lower boundary and when it was passing through the upper one [8]. In general the direction of arrival is reversed if the wave is reflected an odd number of times from boundaries in which the wave resistance diminishes as the wave passes through them. Given some information about the structure of the sector under study, we can get a more accurate idea

of the corresponding properties of the reflecting boundaries by using multiple waves. Conversely, we can determine the arrival direction at the beginning of the path from the arrival directions of waves multiplied an even and an odd number of times. A more complicated phase inversion may occur in the propagation of partially multiplied waves because both the lower and the upper reflecting boundaries may be dissimilar as to the direction

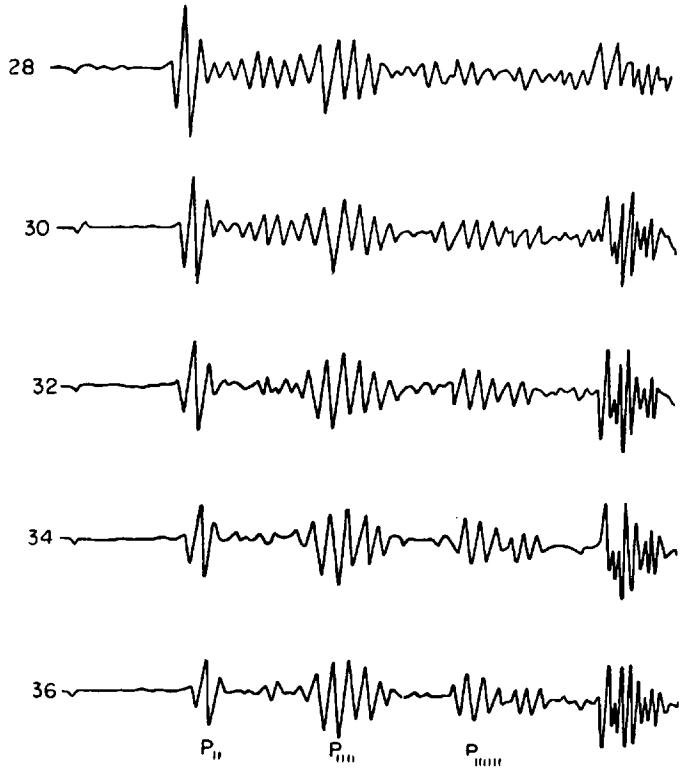

FIG. 4. Records of multiple reflections obtained by modelling.

in which wave resistance alters as the waves pass through them. In such a case one must consider only the number of reflections from boundaries where wave resistance decreases as the wave passes through, and allow for the difference in arrival direction at the beginning and at the end of the path after an odd number of reflections from such boundaries.

Some investigators attribute the change in arrival direction which accompanies a change in the number of multiples to interference reflected from the base and top of a thin layer with a thickness less than half the principal wave length.

In general, multiple waves reflected from a thin layer must be characterized by complex oscillations consisting of vibrations reflected from the base and top of that layer. Reflections from thin layers have been described in works by GURVICH [3] LYAMSHEV [9] and IVAKIN [7]. Fig. 5 shows theoretical hodographs of such waves. At short distances from the source, waves reflected from the top and base of the layer may pile up one upon another. As the

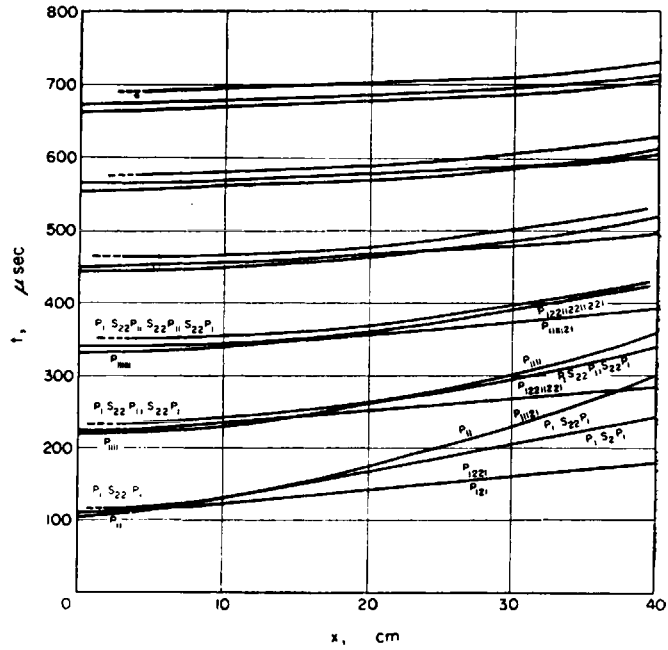

FIG. 5. Theoretical hodographs of multiple reflections.

distance from the source increases, the phase shifts between the component oscillations change, and head waves appear, superimposed on waves reflected from the base of the layer. At great distances from the source the phase shifts between the oscillations of some reflected waves increase with distance, but the phase shifts between the oscillations of the head waves and of the waves reflected from the base of the layer diminish. Many of these phase shifts increase with the number of multiples. As the number of multiples increases, or as distance from the source increases, the complex oscillations resolve into groups of simpler componental oscillations which are separated in time.

Under real conditions it is difficult to distinguish between the multiple and single reflections from the shape of the oscillations. The problem has

been studied by modelling thin reflecting layers, since such layers are often encountered under natural conditions. It has been shown that if the predominant frequency of single reflections in poorly absorbent media increases with distance from the source as the wave divides into its component parts, the predominant frequencies of multiple waves can increase—sometimes after a slight decrease—for the same reasons, but at considerably greater distances from the source. The same thing is observed when the number of multiples increases.

At great distances from the source the subdivision into groups of componental oscillations starts further from the source the greater the number of multiples. At first there is a sharp decline in the predominant frequency, which then rises as soon as the number of multiples increases. In general, the rise in frequency in poorly absorbent media in which the vibrations suffer a change of intensity and shape depending mainly on the divergence of fronts and on interference from these waves is more pronounced when the distance from the source increases at the same time as the number of multiples. This effect becomes negligible as the wave velocity in the reflecting layer increases.

The predominant frequencies of single and multiple waves rise sharply with distance from the source on passing through the points of origin of head waves when the low-frequency components belonging to the head waves separate out from the summed vibrations. JOHNSON, using data obtained in California, shows that when the number of multiples increases at small distances from the point of origin, the traces of multiple reflections from a thin layer of basalt keep their shape. This agrees only with the results obtained from model experiments or with a rigid reflecting layer, (Fig. 4), an inference which is corroborated in other works [13]; but in recording waves at high and medium frequency stations it has been noted that multiple waves are more clearly distinguished when they are recorded at medium frequency stations and when their predominant frequencies are consequently lower than those of the single waves. The explanation may well be that real media are more absorbent than models of them, so that as the wave path becomes longer there is a more noticeable enrichment of the vibrations in low-frequency components at the expense of relatively higher-frequency components.

In the case of certain thin layers [13], which possess comparatively slight wave resistance, we do not always find a strict similarity of form between multiple and single waves.

Figure 6 shows theoretical seismograms calculated according to the method of contour integrals for the case of a liquid layer covering a solid halfspace.

The shape of the multiple wave, like that of the single wave, maintains to a certain distance from the source, but changes as the distance grows further still. The point at which the shape of the oscillations changes from constant to variable is the point of origin of the head waves. Beyond this point the shape of the multiple wave may not be repeated as the number of multiples increases at any one distance from the source. No such change in form is found in certain cases of modelling multiple waves in thin reflecting layers.

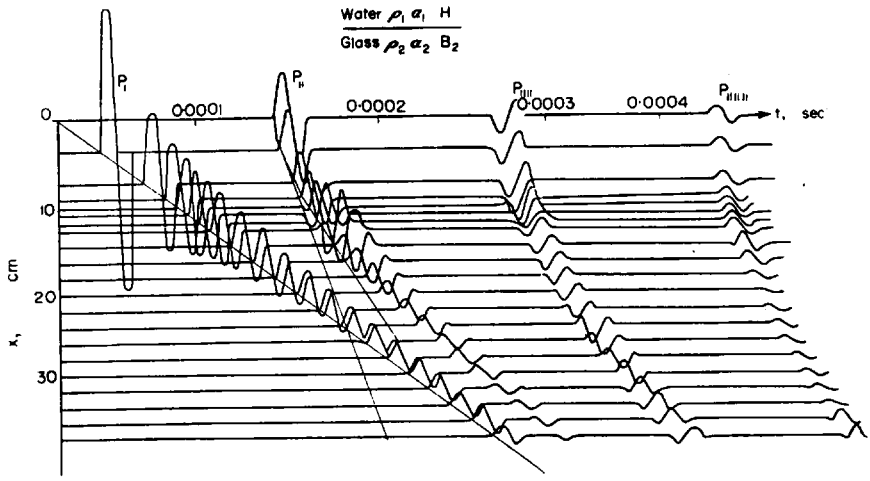

FIG. 6. Theoretical seismograms calculated for large difference between the wave resistances of the media separating the reflecting plane.

$\varrho_1=1.0$, $a_1=1450$ m/sec, $H=10$ cm, $\varrho_2=2{,}47$, $a_2=5490$ n/sec, $B=2700$ m/sec.

This may be because in these cases it is an interference wave consisting of waves reflected from the roof and base of the layer which is recorded. If the wave resistance diminishes as the wave passes through one of these boundaries, there will be no points of origin of head waves and the corresponding component will keep its form at any distance from the source. This component, superimposed on a second component for which there are points of origin of head waves, can cause the changes in its shape to be unnoticeable. Thus, in the case of thin layers it can happen that the changes in shape which are chiefly observed are those caused by wave interference of the kind described above. This may explain the fact that, as the distance from the source increases, the single and multiple reflections from many thin layers are easier to follow than the reflections from thick layers.

The modelling of multiple waves has also shown that the principal frequencies become considerably higher as the thickness of the thin reflecting layer

decreases, as the velocity in this layer increases and as the predominant frequencies of the excited oscillations rise. The fact that the predominant frequencies of multiple waves rise as the thickness of the reflecting layer decreases and the velocity in it increases has been confirmed theoretically [3] and from observations under natural conditions. For example, multiple waves reflected from the gypsum-anhydrite layer in the outer zone of the Cis-Carpathian depression, and waves reflected from a thin basalt layer [18] are of higher frequency than waves reflected from argillaceous sandstone deposits in the same regions.

The duration of the oscillations which is expressed by the number of visible periods, noticeably increases as the number of multiples increases (Fig. 4) and the velocities in the reflecting layer diminish. The reason is that the phase shifts between the componental oscillations increase.

Oscillation intensity — Since the shape of a reflected wave changes shape with distance from the source, the concept of "intensity" in such cases is an arbitrary one, and we shall often take it as meaning a quantity which is a function of the greatest amplitude of the oscillations, irrespectively of the phase to which this amplitude belongs.

In many regions, oscillations caused by multiple reflections are more intensive than many other vibrations. Usually, the multiple waves stand out in sharper relief the greater the wave resistance of the lower reflecting layer and the shallower the depth of absorption. This is particularly noticeable in the outer zone of the Cis-Carpathian depression, where there are sectors close to one another in which multiple waves are found to be reflected from a thin gypsum-anhydrite layer bedded at depths of the order of 500 m and less in some parts and at depths of the order of 1000 m and more in others. In the Ukraine, in the West Siberian plain, in Austria, California and certain other regions [5, 13, 14, 17] where there is a near-surface crystalline basement records of waves possessing distinctive amplitude and reflected singly and repeatedly from the surface of this basement have been obtained. In neighbouring sectors within these regions, where the surface of the crystalline basement is deep-seated, the waves reflected singly or repeatedly from it are lost among the numerous other waves. The portion of wave energy which is lost through reflection from intermediate boundaries increases as the number of these boundaries increases with greater depth of the crystalline basement surface.

HANSEN [14] reports that on apparently good records obtained in the River Salado basin, Argentina, all the distinguishable deep reflections are multiple and so intensive that it is impossible to pick out single reflections among them. Conversely, on seemingly poorer traces, multiple reflections

are not so evident and some singles can be distinguished. BORTFELD [11] observed the same thing in north-western Germany. Under certain conditions then, multiple reflections can be more intensive than single ones.

Some investigators, comparing the intensities of multiple reflections of different types, point out that full-path echoes are the more intensive [13]. Such waves can in fact be distinguished by their records in the Krasnodar country, in the Ukraine and in many other regions. This can be explained to some extent by the fact that such waves are more noticeable owing to the periodic repetition of their records. BORTFELD, however [11], demonstrates

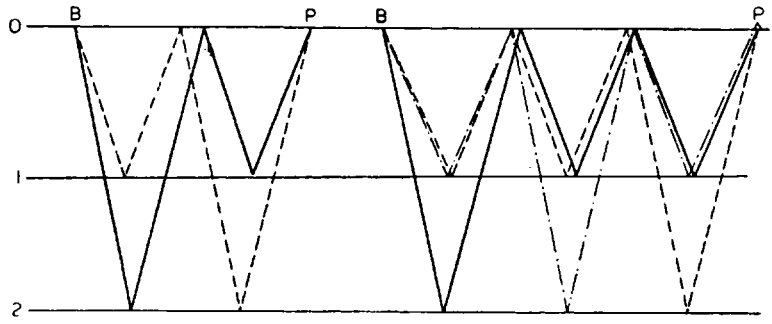

FIG. 7. Asymmetrical paths of wave propagation.

that under certain conditions interbed echoes can be more intensive than full-path ones. The reason is that an interbed echo does not have a single path along which it is propagated, but when the reflecting boundaries are bedded horizontally, simultaneously arrives at the observation point and there causes co-phasally accumulated vibrations (Fig. 7). With increased angles of gradient of the reflecting boundaries or with increased differences between these angles, the phase displacements of the component vibrations increase. As a result of such interference some multiple waves can be distinguished while others are to some extent suppressed.

The intensity of different types of multiple waves and their dependence on seismological conditions can be estimated by using tables compiled according to the method of contour integrals [10]. The complicated relationships obtained by this method have been simplified by K. I. OGURTSOV for the following simple conditions: an excitant force applied to a free surface; a lower reflecting boundary which is the surface of a solid elastic halfspace covered by a medium in which no transverse waves are excited, while the upper reflecting boundary is the surface of this medium parallel to the lower

boundary. We give below formulas to describe the vertical component of displacement W at the front of a double reflected wave.

$$0 \leqslant a < \arcsin \frac{a_1}{a_2},$$

$$W = W_s \frac{E_1}{2}, \tag{3}$$

With angles of incidence

$$E_1 = \frac{B\left(\frac{a_1}{b_2}\right)^4 \frac{\varrho_1}{\varrho_2} - A(D^2 + 4BC \sin\alpha)}{B\left(\frac{a_1}{b_2}\right)^4 \frac{\varrho_1}{\varrho_2} + A(D^2 + 4BC \sin^2\alpha)};$$

$$W_s = \frac{A^3}{2\pi H a_1 \sqrt{\varrho_1}} E_1; \tag{4}$$

Here W_s is the vertical component of displacement at the front of a single reflected wave; a_1, a_2, b_2 are the velocities of longitudinal and transverse waves in the overlying (1) and underlying (2) media; ϱ_1 and ϱ_2 are the densities in these media, and H is the depth of the lower reflecting boundary;

$$A = \sqrt{1 - \sin^2\alpha}; \quad B = \left|\sqrt{\left(\frac{a_1}{a_2}\right)^2 - \sin^2\alpha}\right|;$$

$$C = \left|\sqrt{\left(\frac{a_1}{b_2}\right)^2 - \sin^2\alpha}\right|; \quad D = \left(\frac{a_1}{b_2}\right)^2 - 2\sin^2\alpha.$$

For angles of incidence $\arcsin \frac{a_1}{a_2} < a < \arcsin \frac{a_1}{b_2}$

$$W = \frac{A^3}{4\pi H a_1 \sqrt{\varrho_1}} \sqrt{[R_e(E_2^2)]^2 + [I_m(E_2^2)]^2} F, \tag{5}$$

where

$$E_2 = \frac{B\left(\frac{a_1}{b_2}\right)^4 \frac{\varrho_1}{\varrho_2} i + A(D^2 - 4BCi \sin^2\alpha)}{B\left(\frac{a_1}{b_2}\right)^4 \frac{\varrho_1}{\varrho_2} i - A(D^2 - 4BCi \sin^2\alpha)};$$

$i = \sqrt{-1}$; Re and I_m indicate respectively the real and imaginary parts of the quantity E_2^2; F expresses the form of the oscillation.

For angles of incidence $\arcsin(a_1/b_2) < \alpha \leqslant \pi/2$ the quantity W is expressed by the foregoing formula, in which we must replace E_2 by

$$E_3 = \frac{B\left(\frac{a_1}{b_2}\right)^4 \frac{\varrho_1}{\varrho_2} i + A\,(D^2 - 4BC\sin^2\alpha)}{B\left(\frac{a_1}{b_2}\right)^4 \frac{\varrho_1}{\varrho_2} i - A\,(D^2 - 4BC\sin^2\alpha)}.$$

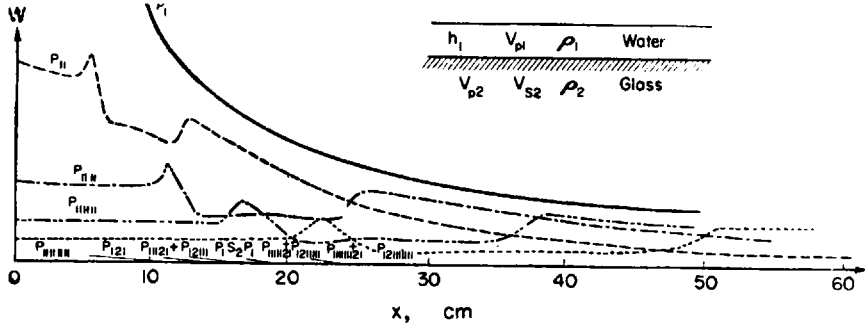

FIG. 8. Graphs of intensities of single and multiple waves as function of distance from source.

Water: $h=10$ cm, $v_p=1450$ cm/sec², $\varrho=1.0$; glass: $S=2.47$, $v_p=5490$ cm/sec², $v_s=2700$ cm/sec².

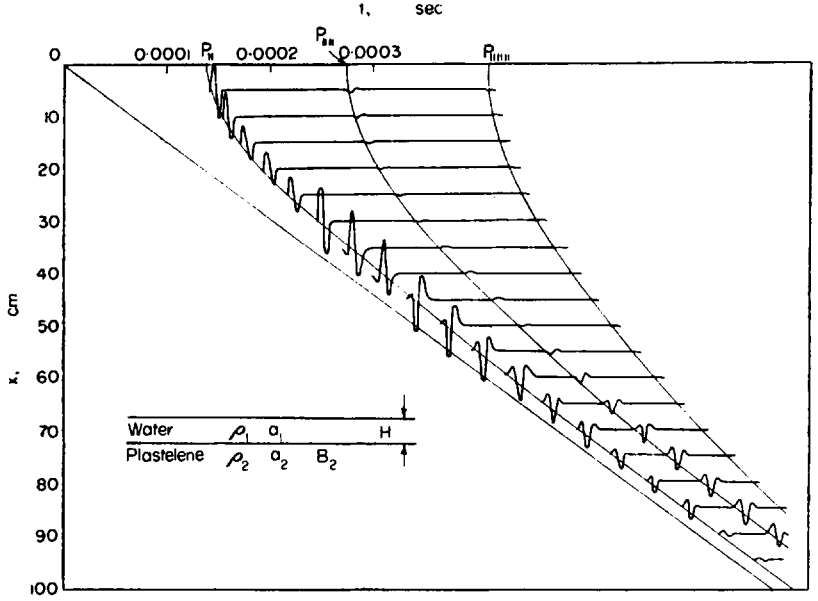

FIG. 9. Theoretical seismograms calculated for small differences in wave resistances of media separating the reflecting plane.

$\varrho=1.0$, $a_i=1450$ m/sec, $H=10$ cm; $\varrho_2=1.46$, $a_2=1710$ n/sec, $B_2=380$ m/sec.

These formulas do not apply to the vicinity of the points of origin of head waves.

Fig. 8 shows graphs representing the dependence of W on distance from the source for various waves, and Figs. 6 and 9 show the corresponding theoretical

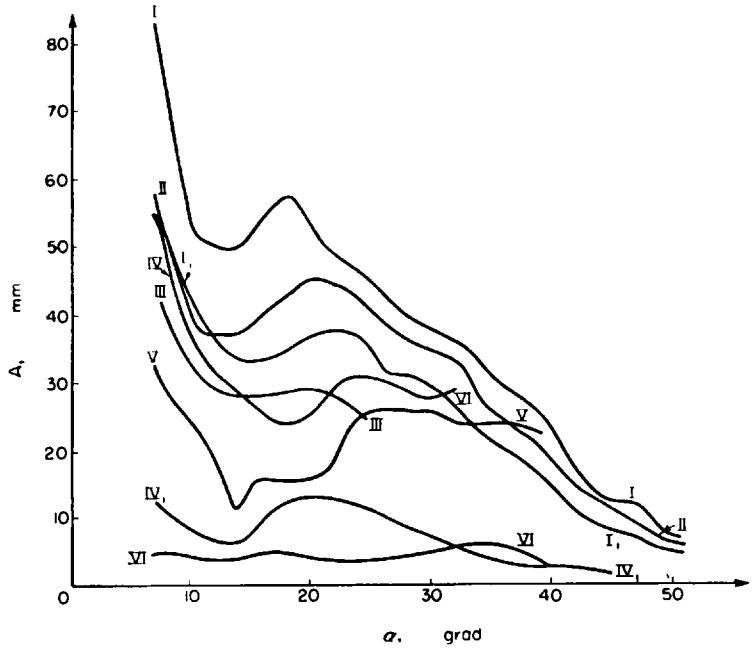

FIG. 10a. Graphs showing intensity of double reflections as function of angle of incidence with different wave resistances of a thin reflecting layer, *a*—predominant frequency of radiated vibrations 60 c/s, *b*—predominant frequency of radiated vibrations 30 c/s.

No.	Material	Thickness of layer, cm	Ratio of wave resistance	Critical angle, degrees
I	Aluminium	0·62	9·32	16°48'
I_1	Aluminium	0·35	9·32	16°48'
II	Glass	0·60	9·10	15°34'
III	Textolite	1·72	3·39	25°55'
IV	Organic glass	1·60	2·26	32°04'
IV	Organic glass	0·50	1·95	38°15'
V	Ebonite	1·10	1·49	42°00'
VI	Rubber	1·0	1·04	

seismograms. In the calculations no allowance was made for absorption of seismic wave energy (the media are regarded as ideally elastic). In the case under consideration, moreover, we are treating the covering medium, for convenience in calculation, as possessing the properties of a liquid (transverse vibrations are not excited in it), and we do not make allowance for the dependence of the coefficients of reflection on the ratio of longitudinal to transverse wave velocities in the medium covering the lower reflecting layer. However, even in this case the formulas obtained express a complicated relationship between the intensity of the multiple waves and the ratio between longitudinal and transverse velocities and wave resistances in the media indicated. Fig. 10 shows graphs obtained by modelling seismic waves. These graphs express the relationship between the intensity of waves reflected twice from various thin layers covered by water, and the angle of incidence.

From theoretical calculations and experimental observations it follows that with small angles of incidence the intensity of the multiple reflections increases as the absolute values of the difference between wave resistances in the reflecting layer and the covering medium increase. In the case of a thin reflecting layer this intensity depends on the thickness of the reflecting layer to a greater extent, the greater the difference between the wave resistances in this layer and in the underlying medium.

Damping—Little work has yet been done on the study of the variation in intensity of multiple reflections as a function of the distance from the source and of the number of multiples. Investigation of this relationship by the modelling method has yielded the following results. The intensity of multiple reflections in the case of thin reflecting layers has a complex relationship with the angle of incidence. Individual intensity peaks stand out against a general background of damping. The greater the differences between the wave resistances in the media separated by the reflecting surfaces, the greater the amount of overall damping and the more strongly do the intensity peaks stand out. A characteristic feature of double reflected waves, for example, is the existence, in many cases, of one extra minimum and one extra maximum at angles of incidence ranging from 10° to 30° (Fig. 10).

When the difference between the wave resistance in the reflecting layer and that in the covering medium is not great, the curve representing the damping of the multiple waves distance from the source is found to have a wavelike form (Fig. 10). This is because of the periodicity of the function which expresses the dependence of the reflection coefficient on the angle of incidence [3] and also because of certain other characteristics of reflections

from thin layers [9]. It is also found that in the case of reflection from a thin layer the damping of multiple waves with distance decreases as the difference between the wave resistance in the reflecting layer and the wave resistance in the underlying medium increases.

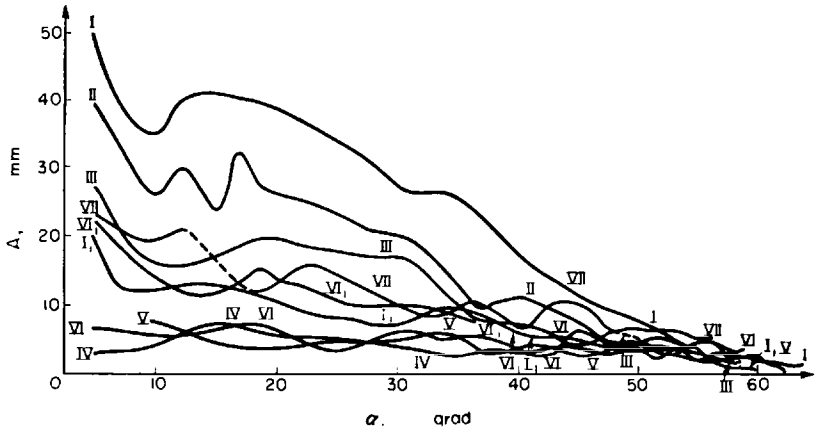

FIG. 10b.

The damping of reflected waves with distance from the source is in inverse ratio to the number of multiples. Fig. 11 shows the results obtained from modelling in the case of a thin reflecting layer. It can be seen that at short distances from the source and when the reflecting boundary is at shallow depths, the intensity of the multiple waves diminishes as the number of multiples increases. Further away from the source double waves become more intensive than single ones (Fig. 4). Still further away, triples are more intensive

No	Material	Thickness of layer, cm	Ratio of wave resistances	Critical angle, degrees
I	Aluminium	0·76	10·18	15° 15'
II	Glass	0·69	9·35	15° 47'
III	Textolite	1·56	3·38	24° 23'
IV	Organic glass	0·52	2·26	32° 25'
V	Ebonite	0·62	1·57	49° 49'
VI_1	Rubber (corrug.)	0·62	—	—
VI	Rubber	0·93	1·31	83° 13'
VII	Plasteline	1·06	1·47	—
I_1	Aluminium	0·35	10·35	15° 00'

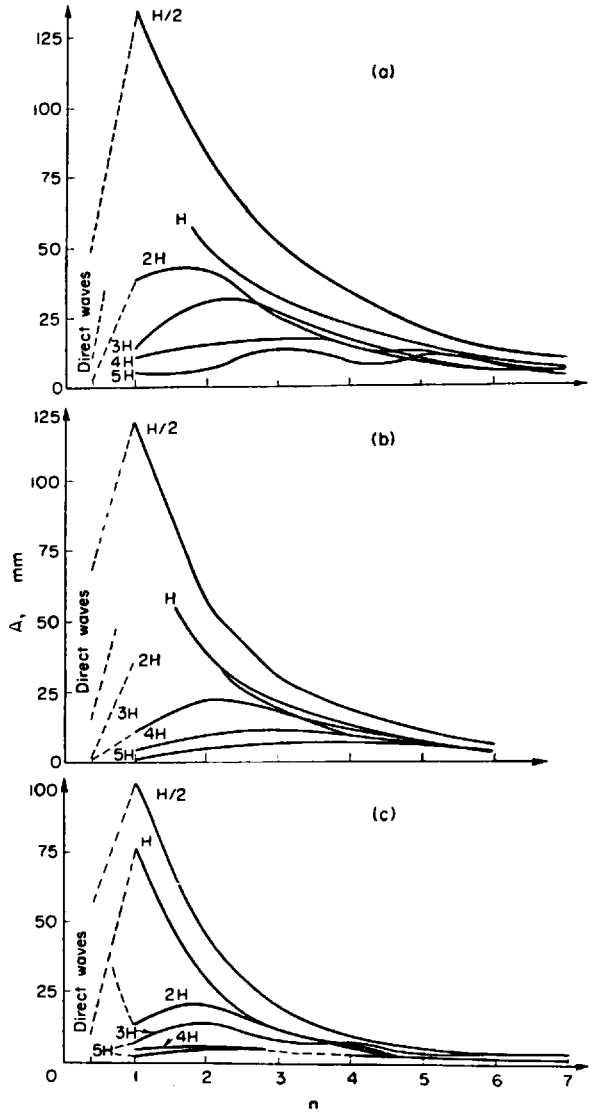

FIG. 11. Graphs showing intensity A of multiple waves as a function of the number of multiples n at various distances from source; predominant frequency 60 c/s; reflecting layers: a—aluminium 0.62 cm, a_{cr} 16° 48′; $(a_2\varrho_2)/(a_1\varrho_1) = 9.32$; b—glass —0.6 cm, $a_{cr} = 15°\ 34'$, $(a_2\varrho_2)/(a_1\varrho_1) = 9.10$; c—organic glass—1.6 cm, $a_{cr} = 32°04'$, $(a_2\varrho_2)/(a_1\varrho_1) = 2.26$

than doubles, and so on. At great distances from the source (for example, four times the depth of the reflecting boundary) there is little difference in intensity between waves repeated a different number of times. In this case the modelling was done with an emitter and a detector which did not possess acute directional qualities.

This is borne out by the theoretical calculations (Figs. 8 and 9) and is explained by the dependence of the reflection coefficient on the angle of incidence, namely, the greater the number of multiples, the slower does the angle of incidence change with distance from the source and the slower does the reflection coefficient change. Modelling multiple waves in a case of a thin reflecting layer shows that when the distance from the source is large, the curve representing the damping of the multiple waves as a function of the number of multiples sometimes has a wavelike form (Fig. 11).

Damping increases as the number of multiples increases, in inverse ratio to the difference between the wave resistance in the reflecting layer and the wave resistance in the covering medium (Fig. 11); and in the case of a thin reflecting layer, also in inverse ratio to the difference in wave resistance between the covering medium and the underlying layer.

In some cases the refraction coefficient first increases with the angle of incidence, reaches some maximum and then decreases. This effect not only reduces the damping of the multiple waves in some sectors of the observation line, but also in certain cases, causes their intensity to increase, with distance from the source. With some slight difference in wave resistance and in the travel velocities of the waves in the media covering and underlying the reflecting boundaries, for example, multiple waves can increase in intensity up to a certain distance from the source. This is implied in the foregoing formulas and is shown in Fig. 9.

The relationships we have indicated are to a considerable extent connected with the absorbent properties of the media lying between the reflecting boundaries. Multiple waves were therefore modelled under conditions in which water, marble, paraffin, plastilene, were used as the covering media, and the absorbent properties of real media must lie within the range of the absorbent properties of these models. Despite the wide range of the latter, qualitative confirmation of the dependence we have indicated was obtained from the modelling, but the quantitative ratios varied.

We may note that the relationship between damping and frequency is connected with the absorbent properties of the media. The damping of multiple waves consequently depends on the prevailing frequency of the vibrations, and in the case of strongly absorbent media must be more pronounced with relatively high prevailing frequencies than with low ones.

In the upper part of Fig. 10 we show the damping of a double wave at higher frequencies than in the lower part of the same figure.

The relationships we have indicated are also connected with the depth of the reflecting boundary. If this depth is reduced the path of a multiple reflection is reduced (the more multiples there are, the smaller it becomes) to a greater extent than the path of a single reflection. At the same time, the angles of incidence increase at shallow depths more rapidly with distance from the source than they do at great depths, and become bigger in proportion to the number of multiples. Therefore the intensity of a reflected wave with a large number of multiples grows as the depth diminishes, to a greater extent than does a reflected wave with a small number of multiples.

The relationships indicated are more pronounced when the angles of incidence at the lower reflecting boundaries are small in comparison with those at the upper reflecting boundaries, and less pronounced when these angles are large. Moreover, the intensity of a multiple reflection in the direction of a rise of the lower reflecting boundary is characterized by having a more distinct peak than the intensity of a single wave; whereas in the direction of a dip in this boundary the intensity is characterized by monotonic and sharper damping. At the same time, the intensity of waves with a large number of multiples becomes greater in the direction of a dip in the lower reflecting boundary, in inverse ratio to the number of multiples, at considerably greater distances from the source than it does in the direction of a rise.

Some Features of Multiple Waves which have their first Reflections above the Excitation point — Records of waves obtained by well-shooting, where the first reflection occurs above the shot point, can be more intensive than records of direct waves. The reflection coefficient from the base of the low-velocity zone is roughly equal to 0.6–0.8 (16,5). The amplitude of the vibrations for a spherical direct wave is.

$$A_d = \frac{A_0}{S_d} e^{-aS_d},$$

where A_0 is some constant, S_d is the path length and a is the absorption coefficient for one unit of path.

For a reflected wave

$$A_r = \frac{A_0 K}{S_r} e^{-aS_r},$$

where K is the reflection coefficient and S_r the length of path. Hence

$$K = \frac{A_r S_r}{A_d S_d} e^{a(S_r - S_d)}. \tag{6}$$

The amplitudes of multiple waves recorded on the surface, when the first reflection occurs above the shot point, can be less than, equal to or greater than the amplitudes of the corresponding single waves [5].

Multiple waves have been found superimposed on single ones. The peak of the combined wave must occur when the shot depth is such that the distance from the excitation point to the upper reflecting boundary is equal to one quarter of the wave length. Furthermore the intensity and shape of the oscillations in a multiple wave depends on the properties of the several boundaries from which it is reflected. This partly explains its greater variability along the observation line than that of a corresponding single wave. This intensity and shape of vibration may be different at reciprocal points owing to different conditions of reflection at these points from the upper boundary.

REMARKS ON THE USE OF MULTIPLE REFLECTIONS

A question which frequently arises in regions where records of multiple reflections predominate in intensity over records of single waves, so that the single waves cannot be distinguished, is whether the multiple reflections can be used.

In these regions the following problems must first be solved:

(1) recognizing multiple reflections (establishing the boundaries from which they are reflected, and determining the types of vibration—longitudinal or transverse—with which they travel between these boundaries);

(2) determining whether it is possible to follow these waves in the region under investigation.

To recognize multiple reflections one must use the kinematic and dynamic characteristics of multiple reflections which have been indicated above, and on the basis of appropriate observations show to which type of waves they belong. The second problem is dealt with by trying to follow these waves under the various conditions which exist in the region concerned.

For regions where both initial problems can be settled satisfactorily, it only remains to decide whether the corollary task of interpretation can be dealt with. This question can be decided in a first approximation by constructing a seismic cross-section with the condition that all the distinguishable waves are regarded as single waves. Then, in the case of full-path reflections, and with a known number of n, one must compute the angle of incidence of the lower reflecting boundary, which is equal to

$$\gamma = \frac{\gamma'}{n},$$

where γ' is a fictitious angle of incidence computed from the section constructed.

After this formula (1) can be used to calculate the depth H_1 along the normal to this boundary and to construct the cross-section for the boundary. For different multiple waves and under different seismic and geological conditions, there may be a different answer to the problem of interpretation. Accuracy may vary and may more or less satisfy practical requirements, just as in the case of single waves.

In elaborating methods for using multiple reflections a problem which may arise is how to use these waves to separate, in the cross-section, the reflecting boundaries which have the highest reflection coefficients, with the result that multiple waves are reflected from these boundaries. The identification of such boundaries can help to improve the geological interpretation of seismic observations.

For this purpose we can use the determination of effective velocities from the hodographs of certain multiple reflections, such as the hodographs of the most distinct full-path echoes. In order to use these velocities we must determine the kind of boundaries these waves are reflected from.

For purposes of geological interpretation, it is possible to use the relationship described in the foregoing sections, between the directivity of vibrations with different numbers of multiples and the combination of properties in the boundaries from which they are reflected; we can also use the shape characteristics of the graphs representing the variation in intensity or form of the record for multiple waves with distance from the source and with increase in the number of multiples.

PRINCIPAL CONCLUSIONS

Multiple reflections can interfere considerably with the recognition and tracing of single reflections and—under certain conditions—refracted waves. This is particularly true when the interfaces from which these waves are reflected are at shallow depths. Moreover, they can be taken for single reflections and so give rise to errors in interpretation.

At the same time, under certain conditions multiple reflections can be used in seismic prospecting, especially in regions where these waves predominate over single waves which have nearly the same travel times as their own.

So far, however, insufficient work has been done on elaborating methods for recognizing multiple reflections. Recognition by kinematic indications

is not sufficiently unambiguous, and must be supplemented by the use of dynamic indications.

The first point to be noted is the variation or lack of variation in the direction of the oscillations when the number of multiples changes to an odd number. This depends on the combination of properties of the interfaces from which the multiples are reflected.

The prevailing oscillation frequencies, caused by multiple waves reflected from thin layers and travelling through poorly absorbent media, can under certain conditions rise when there is a simultaneous increase in the number of multiples and in the distance from the source. The prevailing frequencies of single reflections usually fall, but in certain cases can also rise, with increase in the depth of the reflecting boundary. Consequently, under certain conditions, a frequency analysis of the waves recorded may be an aid to recognizing the multiple waves. Sometimes it may help to compare the duration of the vibrations, expressed by the number of their periods; for multiple reflections from thin layers this increases with the number of multiples.

The damping of multiple reflections with distance from the source is weaker the more multiples there are; at some distances from the source (of the order of the depth of the reflecting boundary) some multiple reflections with a larger number of multiples can be more intensive than multiple reflections with a smaller number of multiples. Consequently, at greater distances from the source in comparison with the depth of the principal reflecting boundary, multiple reflections may predominate over single ones with respect to the amplitudes of the traces. Multiple reflections from thin layers may be characterized by a peculiar shape of the curve representing the relationship between a quantity connected with the amplitude of the vibration on the one hand, and the distance from the source and the number of multiples on the other.

REFERENCES

1. I. S. BERZON, Hodographs of multiple reflected, reflected-refracted and refracted-reflected waves. *Izv. Akad. Nauk SSSR, ser. geogr. i geofiz.* No. 6 (1942).
2. I. S. BERZON, Effective velocities and depths determined from hodographs of multiple reflections. *Izv. Akad. Nauk, SSSR, ser. geofiz.* No. 8 (1956).
3. I. I. GURVICH, Reflections from thin strata in seismic prospecting. *Applied geofiz.* Pt. 9. Gostoptekhizdat (1952).
4. A. M. YEPINAT'YEVA, Some seismic waves with long travel times. *Izv. Akad. Nauk SSSR, ser. geofiz.*, No. 6 (1952).
5. A. M. YEPINAT'YEVA, Some types of multiple seismic waves. *Izv. Akad. Nauk SSSR, ser. geofiz.* No. 8 (1956).
6. N. V. ZVOLINSKII, Multiple reflections of elastic waves in a layer. *Tr. Geofiz. in-ta Akad. Nauk SSSR*, No. 22 (149) (1954).

7. B. N. IVAKIN, Head, forward and other waves in the case of a thin solid layer in a liquid. *Tr. Geofiz. in-ta Acad. Nauk SSSR* No. 35 (162), (1956).
8. I. K. KUPALOV-YAROPOLK, Multiple reflections. *Applied geofiz.* Pt. 6, Gostoptekhizdat (1950).
9. L. M. LYAMSHEV, *The Reflection of Sound by Thin Plates and Films in Liquid.* Izd. Akad. Nauk SSSR (1955).
10. G. I. PETRASHEN', *Problems in the Dynamic Theory of Seismic Wave Propagation.* Coll. papers I, Gostoptekhizdat (1957).
11. R. BORTFELD, Beobachtungen multipler Reflexionen in Nordwestdeutschland. *Erdoel-Leitschrift* Bd. 72, Nr. 9 (1956).
12. C. H. DIX, The existence of multiple reflections. *Geophysics*, **13**, 1 (1948).
13. J. P. ELLSWORTH, Multiple reflections. *Geophysics*, **13**, 1 (1948).
14. R. F. HANSEN, Multiple reflections of seismic energy. *Geophysics*, **13**, 1 (1948).
15. J. SLOAT, Identification of echo reflections. *Geophysics*, **13**, 1 (1948).
16. F. A. VAN MELLER and K. R. WEATHERBURN, Ghost reflections caused by energy initially reflected above the level of the shot. *Geophysics*, **18**, 4 (1953).
17. J. C. WATERMAN, Multiple reflection evidence. *Geophysics*, **13**, 1 (1948).

CHAPTER 4

DIFFRACTED SEISMIC WAVES

T. I. OBLOGINA

INTRODUCTION

IN order to solve the problems which are encountered in seismic prospecting over areas of complex geological structure it is essential to study the dynamic properties of waves, since kinematic indications are often missing when the wave pattern is of a complicated nature.

When waves are diffracted their dynamic properties acquire fundamental importance for determining the different types of waves, and so for a correct geological interpretation of the data obtained in seismic prospecting when tectonic disturbances or steeply dipping and tapering layers are present in the cross-section.

Diffraction is generally understood to mean either the curving of waves round obstacles in their path or the scattering of waves on various irregularities in the medium.

Diffracting objects in seismic prospecting can be divided into three types: diffracting edges, individual diffracting bodies and multiple diffracting bodies.

The first category includes the edges of extended interfaces. Examples of structural features which contain diffracting edges are fault-type dislocations, steeply dipping and tapering strata, the deges of intrusions and salt domes, and so forth.

The second category includes more or less isometrically shaped bodies which are small in comparison with the wave length: ore chutes, caverns and kettle holes. We may note that ore chutes and kettle holes are not objects of study by seismic prospecting methods; at present searches for these are carried out by other geophysical methods.

The third category includes a great number of bodies which are small in comparison with the wave length: small inclusions of rocks which are different in their lithological composition from the enclosing rocks, small reflecting surfaces distributed at random in a fractured zone, small irregularities in interfaces. Small diffracting bodies make the medium texturally nonhomogeneous ("turbid"). In seismic prospecting this interferes with

the isolation of useful waves; the record becomes so difficult to decipher that as a rule the individual waves cannot be distinguished.

Of the three types of diffracting objects we have mentioned, the one which has greatest practical importance is the diffracting edge.

Comparatively little work has been done on problems of diffraction in seismic prospecting. Most of the existing papers deal with particular problems in the kinematics of diffracted waves [1, 2, 3, 6, 8]. Only in certain experimental works do we find any indications of the relationship between the amplitudes of diffracted waves and the amplitudes of reflected and refracted waves: some investigators stress the low intensity of diffracted waves as compared with refracted waves [3], while others on the contrary note that diffracted waves may have the same order of intensity as other types of waves [11, 12]. In essence, however, the dynamic properties of waves in a case of diffraction have yet to be examined.

This paper explains the kinematic basis for distinguishing diffracted waves on seismograms, sets out recent experimental findings on the dynamic properties of these waves and compares these findings with theoretical data.

THE KINEMATIC PROBLEM OF DIFFRACTION FROM THE EDGE OF A VERTICAL CONTACT

Let us imagine a combination of media consisting of a medium with a velocity v_0 filling an upper half-plane, and media with velocities v_1 and v_2 filling respectively the left-hand and right-hand quarters of a lower half-plane (Fig. 1). Let the velocities v_0, v_1 and v_2 be constants, and let $v_0 < v_1 \lesseqgtr v_2$. We shall treat the case of $v_1 < v_2$ separately from the case of $v_1 > v_2$. The v_0 medium is separated from the other two media by a horizontal interface; these two in turn are separated from each other by a vertical boundary.

Let a system consisting of a head and a shear wave move along the horizontal interface from left to right. In Fig. 1 (a) the dashed line shows the fronts of these waves at some moment of time $t < 0$, before diffraction has occurred, and the direction of travel is indicated by arrows. It is required to determine the kinematic pattern of wave propagation after diffraction occurs; that is, we have to find the position of the wave fronts in the plane xy and the form of the wave hodographs* in the plane xt.

We choose a system of co-ordinates xy such that its origin lies on a diffracting edge, with the x-axis running along the horizontal interface and the y-axis upwards towards the observation line (profile). The contact

* A Russian term referring to distance-time curves. [Editor's footnote].

edge—the rectilinear diffracting edge—will then pass through the origin of the co-ordinates O normally to the plane of drawing.

We shall now examine the case when v_1 is greater than v_2; that is, when the shear wave passes from the medium with the higher velocity into the medium with the lower velocity. At a moment of time $t = 0$, let the system consisting of the head wave and the shear wave reach the vertical contact

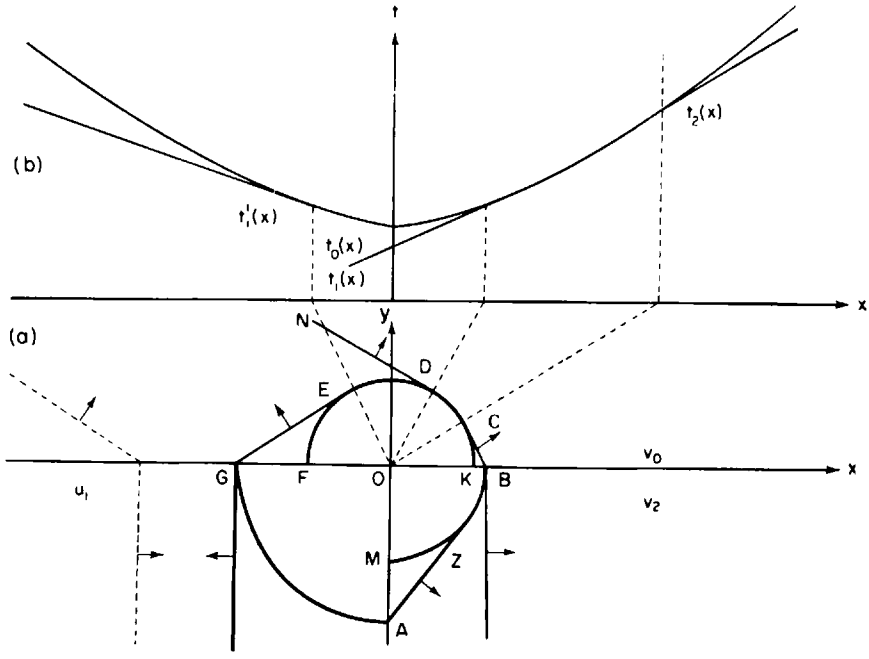

FIG. 1. Fronts and hodographs of a diffracted and a head wave in a case where a shear wave passes from a higher- to a lower-velocity medium.

edge O. According to Huygens's principle, this edge O is, as it were, the source of a diffracted wave travelling in all directions. In Fig. 1, (a) shows the position of the wave fronts at a moment of time $t > 0$, when the wave has already encountered the contact edge. The front of the diffracted wave in the v_0 medium will be the semicircle $KCDEF$ with radius $v_0 t$; in the v_1 medium it will be the quarter circle GA with radius $v_1 t$; and in the v_2 medium it will be the quarter circle MB with radius $v_2 t$.

The shear wave is partly reflected from the vertical contact and partly refracted by it. The reflected shear wave causes a head wave EG on the path FG, while the refracted shear wave will pull the head wave CB on

to the path KB. The fronts of the head waves EG and CB will touch the front of the diffracted wave at E and C respectively. Note that after diffraction there are two head waves for the one head wave before diffraction (dashed line): the wave CB which we have referred to above, and a wave DN, the front of which is parallel to the dashed-line front and touches the front of the diffracted wave at D. We may also note the further wave AL excited on the path MA by the front GA.

Writing down the equations for the wave hodographs along the longitudinal profile $y = H$, we obtain

$$t_0 = \frac{1}{v_0}\sqrt{x^2 + H^2}; \tag{1}$$

for the diffracted wave $KCDEF$;

$$t_1 = \frac{1}{v_1}x + \frac{H}{v_0}\cos\alpha_1; \tag{2}$$

for the head wave DN;

$$t_1' = -\frac{1}{v_1}x + \frac{H}{v_0}\cos\alpha_1; \tag{3}$$

for the head wave EG;

$$t_2 = \frac{1}{v_2}x + \frac{H}{v_0}\cos\alpha_2, \tag{4}$$

for the head wave CB

where $\alpha_1 = \arcsin\frac{v_0}{v_1}$, $\quad \alpha_2 = \arcsin\frac{v_0}{v_2}$ -- the critical angles.

Figure 1, b shows hodographs for t_0, t_1, t_1' and t_2 waves. In the sector of the profile which lies above the contact we observe a diffracted wave t_0, the hyperbolic hodograph of which touches the hodographs of the head waves t_1, t_1' and t_2 (the wave t_1' has a negative apparent velocity). As we see, when v_1 is greater than v_2, the diffracted wave emerges into the first onsets in the sector of the profile

$$\Delta x = H(\tan\alpha_2 - \tan\alpha_1) = Hv_0\left(\frac{1}{\sqrt{v_2^2 - v_0^2}} - \frac{1}{\sqrt{v_1^2 - v_0^2}}\right).$$

We shall now examine a case when v_1 is smaller than v_2 and the system of a head and a shear wave moves as before from left to right; in other

words, the shear wave passes from the lower-velocity medium to the higher-velocity medium.

By a similar process of reasoning we obtain the arrangement of wave fronts for some moment of time $t > 0$ in the plane xy (Fig. 2, *a*) and the position of the wave hodographs in the plane x, t (Fig. 2, *b*).

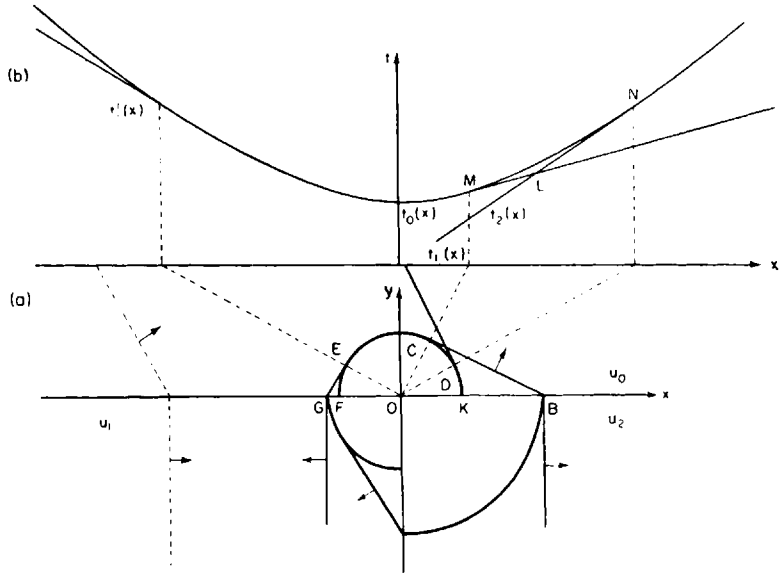

FIG. 2. Fronts and hodographs of a diffracted and a head wave in a case where a shear wave passes from a lower- to a higher-velocity medium.

On the sector of the profile

$$\Delta x = H(\tan \alpha_1 - \tan \alpha_2) = Hv_0 \left(\frac{1}{\sqrt{v_1^2 - v_0^2}} - \frac{1}{\sqrt{v_2^2 - v_0^2}} \right)$$

the hodographs of $t_1(x)$ and $t_2(x)$ intersect, while the hodograph of the diffracted wave $t_0(x)$ touches these hodographs at the points M (the beginning of the hodograph of $t_2(x)$) and M (the end of the hodograph of $t_1(x)$). The hodographs of $t_0(x)$, $t_1(x)$ and $t_2(x)$ form a kind of loop between the points L, M, N. This case differs from the previous one in that the diffracted wave does not emerge into the first onsets.

Combining both the cases we have examined, we conclude that the minimum on the direct and inverse hodographs corresponds to one and the same marker peg on the profile; it lies above the diffracting edge. Here we have a diagnostic

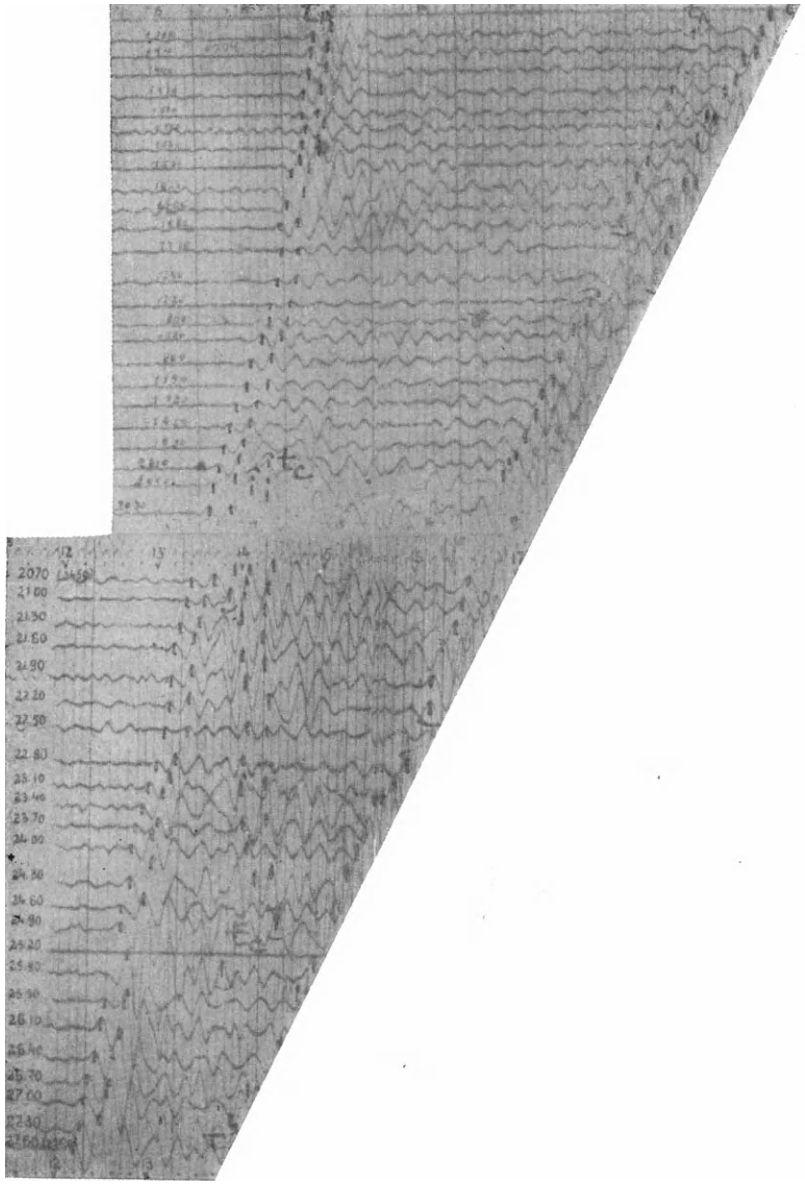

FIG. 3. Example of a diffracted wave trace t_A refracted waves with low apparent velocity; t_B–refracted waves with high apparent velocity; t_C–diffracted wave.

character which is peculiar to a diffracted wave and distinguishes it from all other types of seismic waves.

We may further note that in overtaking systems the tangential points of the hodographs of the diffracted and the head waves also correspond to a single marker peg on the profile.

FIELD OBSERVATIONS

The field observations were made in a region where the geological cross-section included primarily aranaceous and sandstone deposits of Cretaceous, Ternary and Quaternary ages.

The Cretaceous deposits lie directly on a Paleozoic basement at a depth of about 1000 m. The top of this basement contains rocks of different lithological varieties bedded in the form of a block of steeply dipping strata. Diffraction of vertical head waves was observed to occur from the contact edges between these strata, which have different velocities.

The observations were made with a standard detector whose response curve had its maximum at $f_{max} = 37$ c/s.

Kinematic Properties.

Three groups of waves were recorded in the course of seismic observations in the sector mentioned: A, B and C. Group A consisted of refracted waves with low apparent velocities (1200–1600 m/sec); group B of refracted waves with high apparent velocities (5000–6500 m/sec); group C of diffracted waves.

In this paper we shall treat in detail only the characteristics of the diffracted waves. The seismograms given below show diffracted waves recorded after the refracted waves with high apparent velocities. The hodographs of these waves invariably have an almost hyperbolic shape.

On the seismograms in Fig. 3, group A refracted waves, a group B refracted wave and a group C diffracted wave can be distinguished. The diffracted wave t_C, which has a distinctly curvilinear axis of co-phasality, was followed over a distance of 450 m.

Another example of a diffracted wave trace is given in Fig. 4. Here the first waves to arrive are the B group waves t_B^1, t_B^2 and t_B^3. A diffracted wave t_C is recorded behind the wave t_B^3. This can be seen on the seismogram at a distance of 5100 m from the shot point and followed up to a distance of 5520 m, where it is already converging with the wave t_B^3. The diffracted wave has a distinctly curvilinear axis of co-phasality; its intensity is roughly the same as that of the wave t_B^3.

Specific observations showed that minima on the opposing hyperbolic hodographs of the diffracted waves corresponded to one and the same marker peg on the profile. Figure 5 shows two seismograms *a* and *b*, one of which corresponds to the direct hodograph and the other to its inverse. On both seismograms it can be seen that the minimum travel time of the diffracted wave corresponds to the 5100 marker.

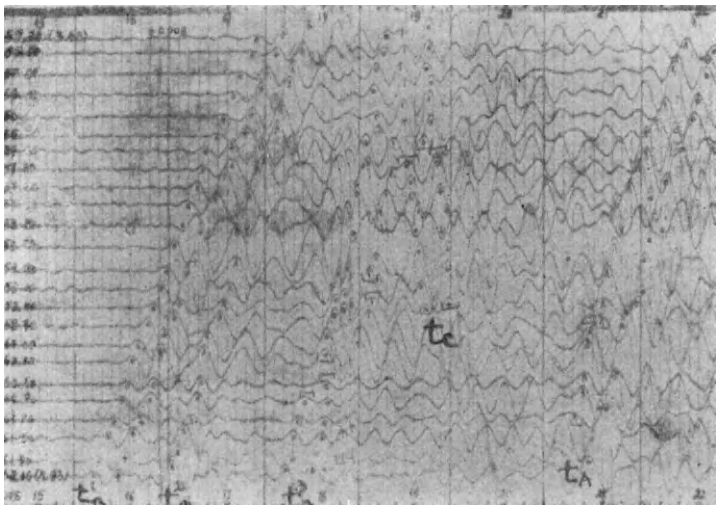

FIG. 4. Example of a diffracted wave trace t_B^1, t_B^2, t_B^3-group *B* refracted waves; t_C–diffracted wave.

Note the following point about the relationship between the intensity of the recorded vertical component of the diffracted wave and the angle at which this wave approaches the detectors. For a distance x along the profile from the projection of the diffracting edge on to the plane of the observations, when x is not greater than the depth H of the diffracting edge ($x \leqslant H$), the angle of approach φ of the diffracted wave (that is, the angle between the diffracted ray and the observation line) is not less than 45° ($\varphi \geqslant 45°$). Within the range of such x distances therefore, depending on the depth H, a fairly intensive vertical component is recorded; whereas for $x > H$ the horizontal component will be greater than the vertical. There is a particularly marked variation in the approach angle when shallow depths are being prospected. The only indication that diffracted waves have been recorded during shallow depth prospecting which is to be found in the literature is in YEPINAT'YEVA's paper [3]. Ordinary seismic apparatus

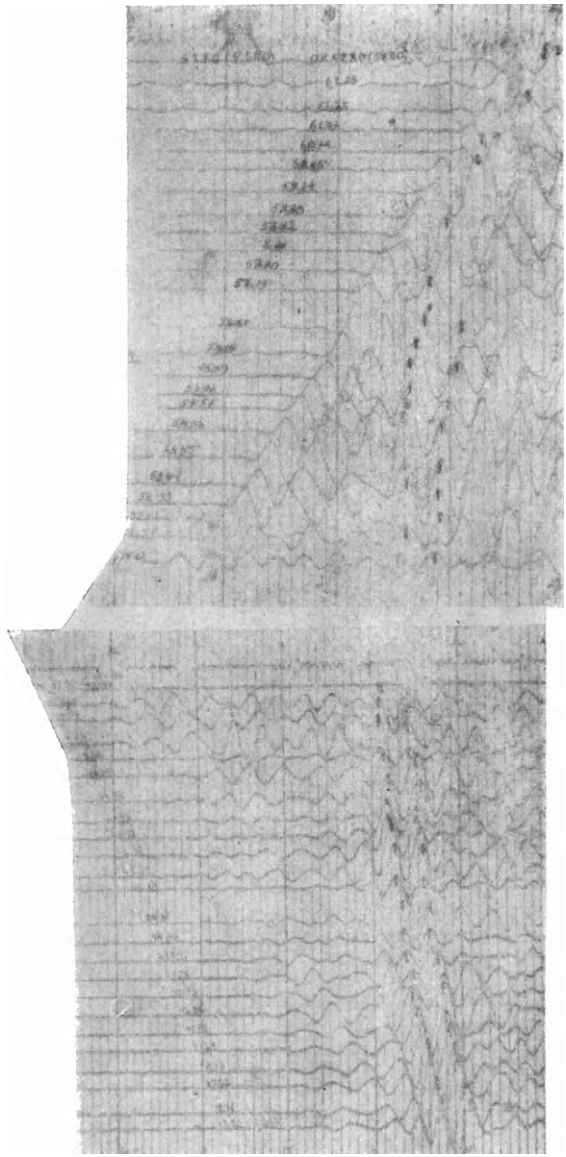

FIG. 5. Seismograms obtained from two opposite shot points, showing that the minimum on the direct and inverse hodographs of the diffracted wave correspond to the same profile marker (marker 5100).

was used in the work and the extremely low intensity of these waves was noted.

We must also emphasize that the dominant frequency of the diffracted waves is lower than that of the head wave. Therefore an apparatus for which the response curves have a steep left-hand slope and which is designed to record high frequencies produces marked distortions in tracing diffracted waves.

Dynamic Characteristics — Examining the diffracted waves on the seismograms we can see that the amplitudes of the vertical component of displacement of a diffracted wave are different at different points on

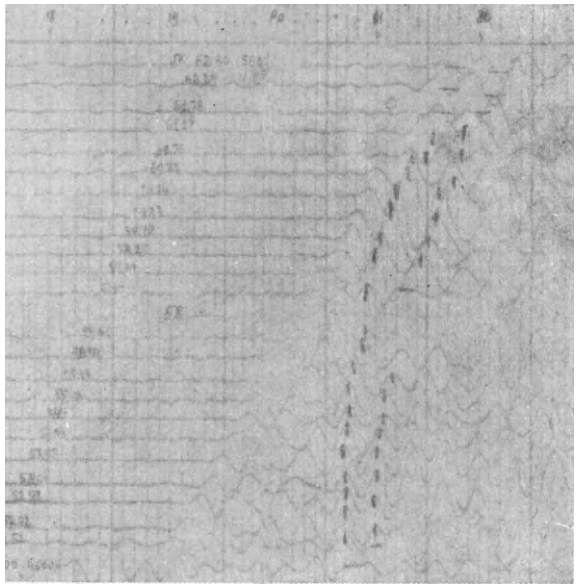

FIG. 6. Seismogram showing growth of diffracted wave amplitude near point of contact with refracted wave.

the profile, and that a diffracted wave has its greatest intensity in the neighbourhood of the point at which is tangential to a refracted wave. Figure 6 shows a seismogram on which a refracted wave is recorded in the first onsets and a diffracted wave in the last onsets. As we see, the amplitudes of the diffracted wave increase along the profile as the wave approaches the point at which it is tangential to touch the refracted wave.

From analysis of the seismograms it follows that in the vicinity of a point of tangentionality the phase of the diffracted wave changes. As a rule this gives

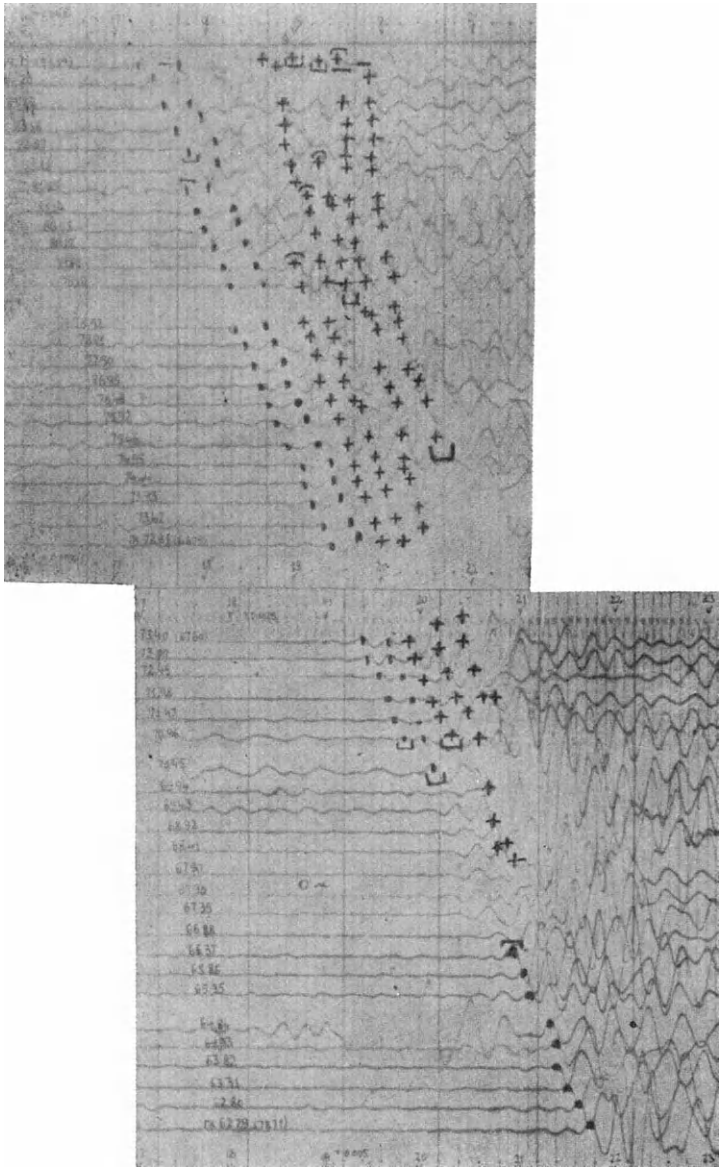

FIG. 7. Seismogram showing phase inversion of diffracted wave near point of contact with refracted wave.

the impression that in the vicinity of this point the detectors are connected to the wrong poles (Fig. 6). In Fig. 7, *a* and *b*, we show a seismogram on which a refracted wave is followed in the first onsets and a diffracted wave in the last. As can be seen, a phase inversion occurs in the region of markers 70.96–70.45. The smaller the spread, the more marked is the phase inversion near the point of tangentionality.

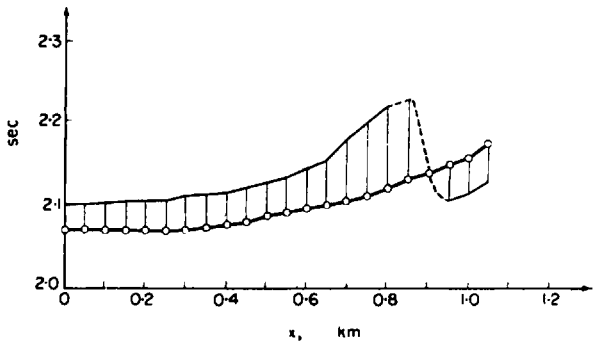

FIG. 8. Observed dynamic hodographs of a diffracted wave along longitudinal profiles.

Dynamic hodographs were constructed for the diffracted waves observed. An example is given in Fig. 8. Here, as usual, distances from the shot point are plotted along the x-axis and time along the y-axis. The amplitudes of the diffracted wave were plotted from the points of the ordinary kinematic hodograph $t = t(x)$. The dynamic hodographs show that the intensity of the diffracted wave increases as the wave approaches the point of tangentionality we have referred to, and that phase inversion occurs in the neighbourhood of this point.

THE DYNAMIC PROBLEM OF DIFFRACTION FROM THE EDGE OF A "TAPERING STRATUM"

Formulation of the Problem — Let us take two media made up of two elastic liquids separated by a plane boundary. The upper medium is characterized by the velocity $1/a_0 = \sqrt{(\lambda_0/\varrho_0)}$, and the lower one by $1/a_0 = \sqrt{(\lambda_1/\varrho_1)}$, where λ_0 and λ_1 are the elastic constants and ϱ_0, ϱ_1 the densities of the media. We shall assume that the velocity in the upper medium is lower than in the medium which is underneath it.

We choose a system of co-ordinates so that the x-axis runs along the interface and the y-axis up towards the upper medium (we are considering the plane problem).

Along the half-line $x > 0$, $y = h$ let a cross-section be taken, the edges of which are firmly attached; that is to say, the displacements on them will be zero. Such a cross-section will be an approximate representation of a thin tapering stratum with high velocity in seismic prospecting.

Let $t < 0$ and let the following wave system

$$\varphi_0 = \gamma_0 f_1(t - a_0 x \sin \alpha_0 - a_0 y \cos \alpha_0), \quad \gamma_0 = \frac{2a_1}{a_0 \cos \alpha_0}, \tag{5}$$

$$\varphi_1 = A f_1(t - a_1 x) - B y f_1'(t - a_1 x), \quad A = \frac{2a_1 \varrho_0}{a_0 \varrho_1 \cos a_0}, \quad B = 2a_1, \tag{6}$$

where $a_0 = \text{arc sin } a_1/a_0$ be propagated along the interface in the direction of increase of x.

The potentials φ_0 and φ_1 satisfy the wave equations in the upper and lower media. As has been shown in [4], formulas (5) and (6) give the local representation of a head and a shear wave near the interface. At a distance from the boundary we can regard (5) as an ordinary plane wave. We shall give the function f_1 in the form

$$f_1(s) = \begin{cases} 0 \text{ when } s < 0, \\ 1 \text{ when } s > 0. \end{cases} \tag{7}$$

Since the components of the displacements are expressed by the displacement potential as partial derivatives of this potential along the corresponding co-ordinates, the boundary condition on the boundaries of the cross-section $x > 0$, $y = h$ is expressed by the equation

$$\frac{\partial \varphi}{\partial y} = 0 \tag{8}$$

Now let the wave (5) meet the edge O_1 of the cross-section at a moment of time $t = 0$. Fig. 9 shows the wave fronts and the values of the displacement potential in front of and behind the wave fronts at some moment of time $t > 0$. It is required to find the diffraction disturbance, at a moment of time $t > 0$, which is concentrated inside the region bounded by the contour ABA_1CA (Fig. 9).

With high values of h, the problem as formulated is in essence the classic problem of the diffraction of an ordinary plane wave from a rectilinear edge

for a single wave equation. This problem has been solved in several works [7,9]. The solutions obtained, however, are unsuitable for studying the dynamic properties of diffracted waves, since the very construction of these solutions makes it difficult to extract an expression for the displacement field near the wave fronts which is suitable for purposes of calculation.

The problem of plane-wave diffraction from the edge of a tapering stratum is solved below by the Smirnov-Sobolev method of functional invariants; the dynamic hodographs and theoretical seismograms for diffracted waves are calculated.

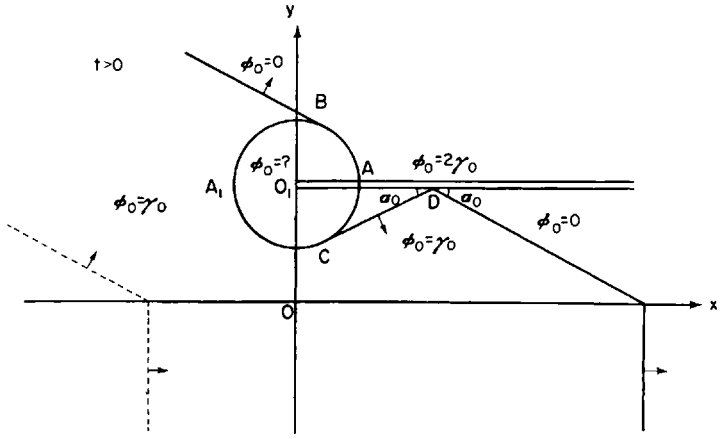

FIG. 9. Diagram to aid formulation of diffraction problem for a plane wave from the edge of a "tapering stratum".

Solution. The function φ_0 depends solely on the ratios $x/t, y/t$. As SOBOLEV shows, by substitution of the variables $\xi = x/t$ $\eta = y/t$ the wave equation

$$a_0^2 \frac{\partial^2 \varphi_0}{\partial t^2} = \frac{\partial^2 \varphi_0}{\partial x^2} + \frac{\partial^2 \varphi_0}{\partial y^2} \tag{9}$$

is converted into an equation of mixed type,

$$\begin{aligned}(a_0^2\xi^2-1)\,\varphi_{0\xi\xi}+2a_0^2\,\xi\eta\varphi_{0\xi\eta}+(a_0^2\,\eta^2-1)\,\varphi_{0\eta\eta}+2a_0^2\,\xi\varphi_{0\xi}+\\ +2a_0^2\,\eta\varphi_{0\eta}=0.\end{aligned} \tag{10}$$

The above equation in the hyperbolic region is reduced by substituting the variables according to the formulas:

$$\sigma = \frac{\xi}{\xi^2 + \eta^2}, \qquad \tau_1 = \frac{\eta\sqrt{a_0^2(\xi^2 + \eta^2) - 1}}{\xi^2 + \eta^2} \tag{11}$$

to the chord equation

$$\frac{\partial^2 \varphi_0}{\partial \sigma^2} - \frac{\partial^2 \varphi_0}{\partial \tau_1^2} = 0. \tag{12}$$

In the elliptical region, by substituting the variables according to the formulas

$$\sigma = \frac{\xi}{\xi^2 + \eta^2}, \qquad \tau_1 = \frac{\eta\sqrt{1 - a_0^2(\xi^2 + \eta^2)}}{\xi^2 + \eta^2} \tag{13}$$

it is reduced to the Laplace differential

$$\frac{\partial^2 \varphi_0}{\partial \sigma^2} + \frac{\partial^2 \varphi_0}{\partial \tau_1^2} = 0. \tag{14}$$

Using this and introducing the complex variable

$$\theta_0 = \frac{tx}{x^2 + (y-h)^2} + i\frac{(y-h)\sqrt{t^2 - a_0^2[x^2 + (y-h)^2]}}{x^2 + (y-h)^2}, \tag{15}$$

we shall seek the solution in the region ABA_1CO_1A (Fig. 9) which is filled with a diffracted wave in the form

$$\varphi_0 = R_e \Phi(\Theta_0), \tag{16}$$

where $\Phi(\theta_0)$ is the analytic function in the region to which the region ABA_1CO_1A passes; and $R_e\Phi(\theta_0)$ is the real part of the function.

Let us see what happens to points on the circumference ABA_1CO_1A after conversion (15).

It can be readily seen that $\Theta_e = a_0$ corresponds to the point A $\{x = t/a_0, y = h\}$; $\Theta_0 = a_1$ to the point B $\{x = (t/a_0) \sin a_0, y = (t/a_0)\cos a_0\}$; $\Theta_0 = -a_1$ to the point A_1 $\{x = -t/a_0, y = h\}$ and $\Theta_0 = \infty$ to the point O_1 $\{x = 0, y = h\}$.

The lower semicircle is converted into a lower plane, while the whole circle $O_1ABA_1CO_1$ passes by means of the conversion indicated into the plane of the complex variable θ_0 with a cross-section along the real axis $\theta_0 > -a_0$.

The boundary condition (8) is written in the form

$$Re\{\sqrt{a_0^2 - \theta_0^2}\,\Phi'(\theta_0)\} = 0. \tag{17}$$

when we use the variable θ_0.

Making use of the fact that in the region ahead of the front of the plane wave (5) $\varphi_0 = 0$, in the region ACD $\varphi_0 = 2\gamma_0$ and in the region to the left of the line NBA_1CDM $\varphi_0 = \gamma_0$, we introduce the boundary conditions for the function $\Phi'(\theta_0)$.

In the interval $a_0 < \theta_0 < \infty$ into which the segment O_1A_1 passes, θ_0 always satisfies the inequality $\theta_0 > a_0$. In the boundary equation (17) the radical $\sqrt{(a_0^2-\theta_0^2)}$ will have an imaginary value, and therefore to fulfil this boundary condition the condition $Im\,\Phi'(\theta_0) = 0$ must be satisfied.

It is sufficient to solve the problem for the upper half-plane. At the point $\theta_0 = a_1$ the function $\Phi'(\theta_0)$ will have a pole with its main part $-[i\gamma_0/\pi(\theta_0-a_1)]$. Let us now construct such a function so that its material part is converted to zero. We multiply the function $\Phi'(\theta_0)$ by the radical $\sqrt{(a_0-\theta_0)}$. For the upper half-plane when $\theta_0 > a_0$ we choose a minus sign; that is, $Im\sqrt{(a_0-\theta_0)} < 0$. It will be seen that $R_e(\Phi'(\theta_0)\sqrt{(a_0-\theta_0)} = 0$ on the entire material axis.

Making use of this, and also of the fact that at the point $\theta_0 = a_1$ there will be a pole with the main part we have indicated, we obtain

$$\Phi'(\theta_0) = \frac{i\gamma_0\sqrt{a_0-a_1}}{\pi(\theta_0-a_1)\sqrt{a_0-\theta_0}}. \tag{18}$$

The components of the function required are equal to

$$\left.\begin{aligned} u &= R_e\left(\Phi'(\theta_0)\frac{\partial\theta_0}{\partial x}\right), \\ v &= R_e\left(\Phi'(\theta_0)\frac{\partial\theta_0}{\partial y}\right). \end{aligned}\right\} \tag{19}$$

Formulas (18) and (19) give the solution to our problem. We thus find the displacements in a region filled with a diffracted wave.

The Dynamic Hodographs — To determine the dynamic hodograph of a diffracted wave we must find an expression for the components of the displacement of this wave near its front. First we find asymptotic formulas for the displacement of the diffracted wave in the vicinity of its front for the case of a Dirac pulse as the shape of the incident wave, then we convert to an alternating smooth pulse for the displacement.

For the region near the front of the diffracted wave when $r \to t/a_0$, we obtain from (15) and (19) the following asymptotic expressions for the hori-

zontal component u_1 and the vertical component v_1 of the displacement:

$$\left.\begin{aligned} u_1(x, y, t) &= \frac{\sqrt{2}a_0^4\, x(y-h)\, Im\, \Phi'(\theta_0')}{t_0^2\sqrt{t_0}} \frac{1}{\sqrt{t-a_0 r}} + \\ &+ O\left(\frac{\sqrt{t^2-a_0^2 r^2}}{t^2}\right), \\ v_1(x, y, t) &= \frac{\sqrt{2}a_0^4\,(y-h)^2\, Im\, \Phi'(\theta_0')}{t_0^2\sqrt{t_0}} \frac{1}{\sqrt{t-a_0 r}} + \\ &+ O\left(\frac{\sqrt{t^2-a_0^2 r^2}}{t^2}\right), \end{aligned}\right\} \tag{20}$$

where

$$\Theta_0' = \frac{a_0^2 x}{t_0}. \tag{21}$$

Here t_0 is the time of the first onsets of the diffracted wave. Formulas (20) are valid in the neighbourhood of its front, except for the vicinity of the singular point B (Fig. 9), where they do not apply.

We can now give the shape of the incident wave in the form of a smooth pulse

$$G'(t) = 4\left(t - \frac{T}{2}\right)(t-T). \tag{22}$$

To obtain the components of displacement u_1 and v_1 for such a pulse, we must, as is known, integrate according to a parameter

$$u_1(t, x, y) = \int_0^T u(t-\tau, x, y)\, dG, \tag{23}$$

where u is the function for the case of a single pulse, which we know already, and τ is the parameter.

Performing the integration, we get

$$\left.\begin{aligned} u_1(x, y, t) &= \frac{a_0^4 x\,(y-h)\, Im\Phi'(\Theta_0')}{t_0^2\sqrt{2t_0}} f(t-a_0 r), \\ v_1(x, y, t) &= \frac{a_0^4\,(y-h)^2\, Im\Phi'(\Theta_0')}{t_0^2\sqrt{2t_0}} f(t-a_0 r), \end{aligned}\right\} \tag{24}$$

where

$$f(t-a_0 r) = 4T^2\left\{\Delta t\left(\sqrt{\Delta t}-\sqrt{\Delta t-T}\right) - \frac{1}{3}\left[\Delta t^{3/2}-(\Delta t-T)^{3/2}\right]\right\} -$$

$$-12\,T\{\Delta t^2(\sqrt{\Delta t}-\sqrt{\Delta t-T})-\frac{2}{3}\Delta t\,[\Delta t^{3/2}-(\Delta t-T)^{3/2}]+$$

$$+\frac{1}{5}[\Delta t^{5/2}-(\Delta t-T)^{5/2}]\}+8\{\Delta t^3(\sqrt{\Delta t}-\sqrt{\Delta t-T})-$$

$$-\Delta t^2[\Delta t^{3/2}-(\Delta t-T)^{3/2}]+\frac{3}{5}\Delta t\,[\Delta t^{5/2}-(\Delta t-T)^{7/2}]-$$

$$-\frac{1}{7}[\Delta t^{7/2}-(\Delta t-T)^{7/2}]\},$$

$$\Delta t = t-a_0 r.$$

To calculate the dynamic hodographs from these formulas we must first find the values of Δt at which the function $f(t-a_0 r)$ has its first extreme value. Assuming $T = 0.03$ sec and calculating values for the function $f(t-a_0 r)$ at a series of points, we find that when $\Delta t = 0.01$ sec it has its first maximum, at a value of 0.857.

We shall further assume that the velocity in the upper medium $1/a_1 = 4$ km/sec, and that the bedding depths of the interface and the tapering stratum are $|y| = 1$ km and $|y|-h = 0.5$ km respectively.

We select observation points on the profile at intervals $\Delta x = 200$ m and calculate the first onset times at these points, using the kinematic hodograph equation.

For each pair of values of x and t_0 we compute values for Θ_0' and $\Phi'(\Theta_0')$ according to formulas (21) and (18). We then calculate the functions u_1 and v_1 according to formula (24) and obtain a value for the wave amplitude at each point on the hodograph.

Figure 10 shows the dynamic hodographs for u_1 and v_1 calculated for twenty-one observation points on the profile. The following regular features can be noticed: the amplitudes of the diffracted wave are different at different points of the profile; and the nearer the observation point is to the point of contact between the hodographs of the diffracted and the head waves, the greater the amplitudes of the diffracted wave. In the example given, the point of contact has an abscissa $x = 0.288$ m. The vector of the displacement (u_1, v_1) changes sign near this point of contact. The horizontal component of displacement u_1 becomes zero at the point on the profile $x = 0$, which is a projection of a point on the diffracting edge on to the profile. This is obvious even physically, without calculation: the displacement vector runs along the radius of a circle which is the front of the diffracted wave; at the point on the profile $x = 0$, $y = 1$ km it is perpendicular to the x-axis, and consequently its horizontal component is nil (Fig. 10).

When the diffracting edge lies on the interface, the following may be noted. As can easily be seen, in order to calculate the dynamic hodographs in such a case, we must assume $h = 0$ and confine ourselves to values of $x \geqslant 0$.

The shape of the diffracted wave in a case where the incident wave has the shape of a smooth alternating pulse (22) can be found from formula (24).

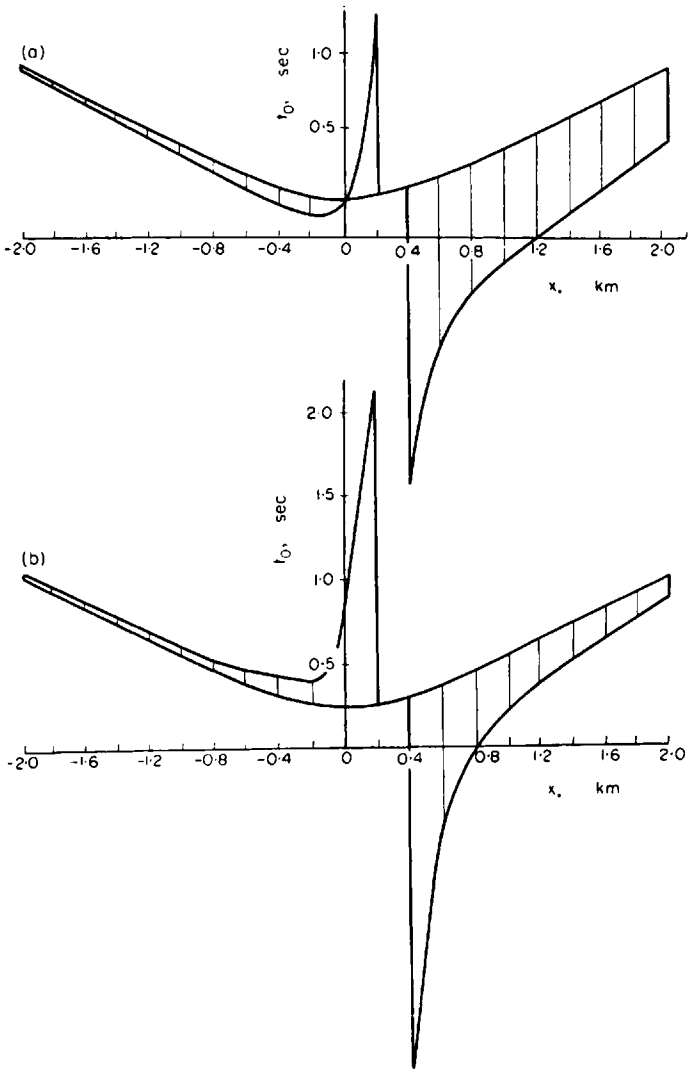

FIG. 10. Calculation dynamic hodographs of a diffracted wave *a*–horizontal component of displacement, u_1; *b*–vertical component of displacement, v_1.

From this formula we can see that the expression for u_1, as well as that for v_1, can be regarded as consisting of two multipliers, one of which is the function $f(t-a_0r)$, and the other all the rest of the expression which goes before this function. The function $f(t-a_0r)$ itself also gives the variation in time of the components of displacement (that is, the shape of the wave), and the multiplier with it gives the change in the shape of the wave as a function of the position of the observation point x on the profile, the first onset time t_0, the velocity values $1/a_0$ and $1/a_1$, the distance on the profile from

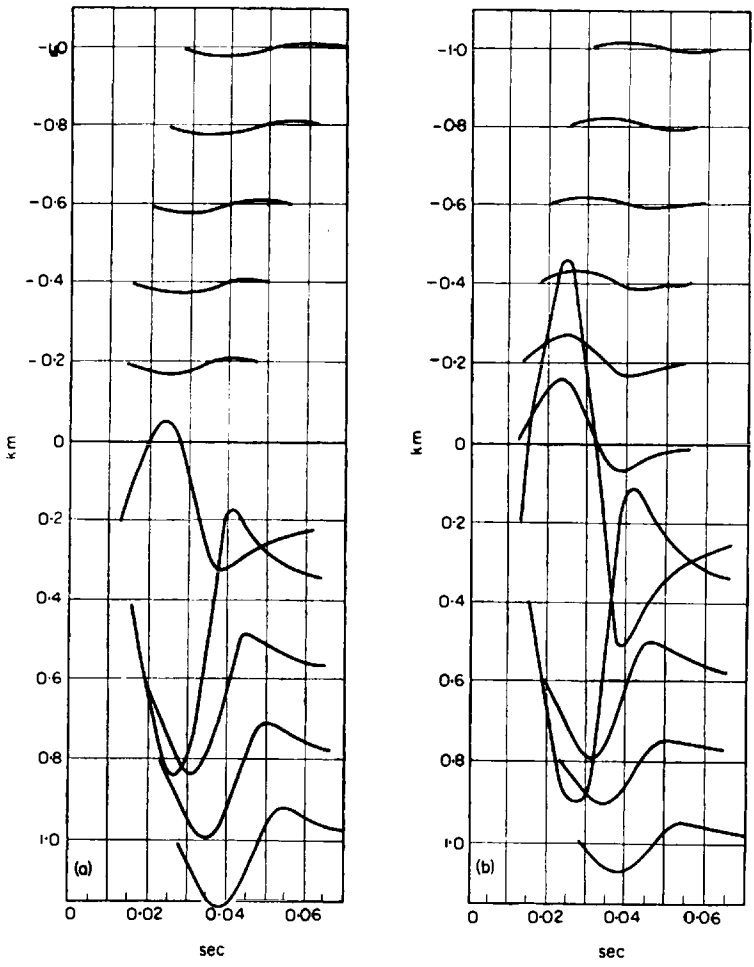

FIG. 11. Theoretical seismograms for a diffracted wave *a*–trace of horizontal component of displacement; *b*–trace of vertical component of displacement.

the interface and the distance h from the "tapering stratum" to the interface.

Figure 11 shows two theoretical seismograms of the horizontal and vertical displacements of a diffracted wave in a case where a wave incident on the edge of a "tapering stratum" has the shape of a smooth alternating pulse. The same values have been taken for all the characteristics of the medium as were taken in calculating the dynamic hodographs. The shape of the diffracted wave can be seen on each trace. The dominant period of this wave ($T_p = 0.04$ sec) is greater than that of the incident wave ($T_p = 0.03$ sec). Moreover, with the given shape of the incident wave, both its extremal values—the first and second—are identical. The value of the first extreme for the diffracted wave, however, is greater than that of the second, so that in the given case this wave is characterized by a less symmetrical vibration shape.

SUMMARY

Comparison of the experimental and theoretical findings set out above yields the following conclusions.

1. Minima on the direct and inverse hodographs of a diffracted wave correspond to one and the same marker on the profile.

2. The amplitudes of the diffracted wave increase along the profile as this wave approaches its point of contact with a refracted wave.

3. The diffracted wave suffers phase inversion in the neighbourhood of this point of contact.

REFERENCES

1. I. S. Berzon, Some problems in the kinematics of propagation of diffracted seismic waves. *Tr. geofiz. in-ta Akad. Nauk SSSR*, No. 9 (1950).
2. G. A. Gamburtsev, *et al. The Refracted Wave Correlation Method.* Izd. Akad. Nauk SSSR (1952).
3. A. M. Yepinat'yeva, Some types of diffracted waves recorded in the course of seismic observations. *Izv. Akad. Nauk SSSR, ser. geogr. i geofiz.*, **14**, 1 (1950).
4. T. I. Oblogina, A local representation of a system consisting of a head wave and a sliding wave. *Vestn. MGU (Univ. Moscow), No. 1*, (1956).
5. V. I. Smirnov and S. L. Sobolev, *Tr. Seismol. in-ta No. 20*, Izd. Akad. Nauk SSSR (1932).
6. P. T. Sokolov, *Physical and Theoretical Foundations for the Seismic Method of Geophysical Prospecting*, GONTI (1933).
7. S. L. Sobolev, *Tr. Seismol. in-ta, No. 41*, Izd. Akad. Nauk SSSR (1934).
8. G. K. Tvaltvadze, Theory of the seismic method of prospecting for vertical interfaces. *Tr. Tbilisskogo geofiz. in-ta*, **2** (1937).

9. A. A. KHARKEVICH, The construction of a qualitative picture of diffraction. *Zh. tekh. fiziki, Pt.* 7 (1949).
10. Q. MILLER, Fault interpretation from seismic data in southwest Texas. *Geophysics.* **13**, 3 (1950).
11. T. KREY, The significance of diffraction in the investigation of faults. *Geophysics*, **17**, 4 (1952).
12. F. RIEBER, A new reflection system with controlled directional sensitivity. *Geophysics* **1**, 2 (1936).
13. W. B. ROBINSON, Refraction waves reflected from a fault zone. *Geophysics*, **10**, 4 (1945).

CHAPTER 5

THE INFLUENCE OF DISTURBING ACCELERATIONS WHEN MEASURING THE FORCE OF GRAVITY AT SEA USING A STATIC GRAVIMETER

K. YE. VESELOV and V. L. PANTELEYEV

GRAVITATIONAL force measurements at sea are of great scientific and practical importance. The perfecting of a method for measuring the force of gravity at sea is therefore a pressing problem.

Up till now the principal method for measuring the force of gravity at sea has been the fictitious pendulum method, the theory of which was put forward by VENING MEINESZ [1] and other authors. It has been established that to obtain satisfactory results at sea with a pendulum device it is absolutely essential to measure the value of the vertical and horizontal accelerations in addition to the inclination of the base.

The static method of measuring gravity at sea has been studied for some few years in the Gravimetric Laboratory of the All-Union Research Institute for Geophysical Methods of Prospecting: in particular, they have constructed prototype instruments and tested them at sea. The results of these tests show that gravity can be measured by marine pendulum devices to an accuracy of the order of a few milligals.

Some of the basic points in the theory of measurements of this type are examined in paper (1). In the present paper the authors have set themselves the further task of making a theoretical examination of certain other points, such as the determination of the equilibrium position of the gravimeter bar from observations taken during its motion, definition of the dynamic coefficient of gravimeters, the effect of inclinations and accelerations on readings, and ways of reducing and compensating these effects.

The essence of the static method for measuring gravity lies in the creation of a very powerful damping – several hundred times greater than the critical—in the moving part of the gravimeter, as a result of which high frequency accelerations are filtered off (accelerations due to the vessel's motion) and low frequency accelerations (change of gravity accelerations) remain unaltered.

The equation of motion for a system of this type is solved in VESELOV'S

paper [2] given that only the vertical disturbing acceleration, which is sinusoidal in character, is acting, that the angles of deviation of the pendulum from the equilibrium position are small and that the damping is proportional to the speed at which the pendulum moves.

In this case the equations for forced and natural motion take the form:

$$\Theta_1 = \frac{\frac{ml}{I} a_z}{\sqrt{(n_0^2 - p^2) - 4\varepsilon^2 p^2}} \sin(pt + \delta), \tag{1}$$

$$\Theta_2 = \frac{\theta_0}{a_1 - a_z} (a_1 e^{-a_2 t} - a_z e^{-a_1 t}) \tag{2}$$

where a_1 and a_2 are the roots of the characteristic equation ($a_1 = -\varepsilon + \sqrt{\varepsilon^2 - n_0^2}$, $a_2 = -\varepsilon - \sqrt{\varepsilon^2 - n_0^2}$); n_0 is the natural oscillatory frequency of the pendulum without damping; I is the moment of inertia of the bar in the system; $mla_z \cos(pt)$ is the moment of the disturbing force, on the assumption that the disturbing acceleration is sinusoidal in character; h is the damping coefficient; K is the torsional rigidity coefficient of the elastic element; p, a_z are the amplitude and frequency of the disturbing acceleration;

$$\frac{K}{I} = n_0^2, \frac{2h}{I} = 2\varepsilon.$$

It follows from formula (1) that, under the influence of sinusoidal disturbing accelerations, the bar will also accomplish sinusoidal forced vibrations.

If the value of the static amplitude $\theta = \frac{ml}{In_0} 2a_z$ be divided by the value for the dynamic amplitude obtained from equation (2), we obtain the dynamic coefficient (in paper (2) a value which is the reciprocal of the dynamic coefficient is named the coefficient of interference suppression).

$$\lambda = \frac{n_0^2}{\sqrt{(n_0^2 - p^2) + 4\varepsilon^2 p^2}}. \tag{3}$$

Where λ, the dynamic coefficient, shows the decrease in the oscillatory amplitude of the gravimeter bar under the influence of sinusoidal acceleration of a given frequency compared with the constant acceleration of the same frequency.

The dynamic coefficient is necessary firstly in order to know the amplitude and frequencies of the disturbing acceleration at which measurements can be made, and secondly to find the amplitude of the vertical component

of the disturbing acceleration from the oscillatory amplitude of the gravimeter pendulum.

In order to be able to calculate the dynamic coefficient one needs to know the damping coefficient ε in addition to the natural frequency of the disturbing oscillations.

Let us examine equation (2) to find the value of ε.

Equation (2) indicates that when the gravimeter pendulum is deflected by an angle θ_0 it will return to a position of equilibrium exponentially.

Let us find approximate values for a_1 and a_2;

$$a_2 = -2\varepsilon + \frac{1}{2}\frac{{n_0}^2}{\varepsilon}, \qquad a_1 = -\frac{1}{2}\frac{{n_0}^2}{\varepsilon}.$$

Substituting in equation (2), we obtain

$$\Theta_2 = \Theta_0 e^{-\frac{1}{2}\frac{n_0^2}{\varepsilon}t}\left(1 - \frac{{n_0}^2}{4\varepsilon^2} - \frac{{n_0}^2}{4\varepsilon^2}e^{-\left(2\varepsilon - \frac{n_0^2}{\varepsilon}\right)t}\right). \tag{4}$$

The term $-\frac{{n_0}^2}{4\varepsilon^2}e^{-\left(2\varepsilon-\frac{n_0^2}{\varepsilon}\right)t}$ is vanishingly small, since in the marine gravimeter the value of ε must be greater than 1000 and the value n_0 not greater than 10:

$$\Theta_2 = \Theta_0 e^{-\frac{1}{2}\frac{n_0^2}{\varepsilon}t}\left(1 - \frac{{n_0}^2}{4\varepsilon^2}\right). \tag{5}$$

Let us write the expression (5) for two moments of time and take their ratio.

$$\frac{\Theta_2'}{\Theta_2''} = e^{-\frac{1}{2}\frac{n_0^2}{\varepsilon}(t_1 - t_2)}. \tag{6}$$

Converting into logarithms we obtain

$$\ln\frac{\Theta_2'}{\Theta_2''} = \frac{1}{2}\frac{{n_0}^2}{\varepsilon}(t_2 - t_1). \tag{7}$$

Let us rewrite formula (6), replacing $\Theta_2{}^1$ in it by $A_1 - A_0$, and Θ_2'' by $A_2 - A_0$, where A_0 is the reading on the gravimeter scale when the bar is in a position of equilibrium, A_1 and A_2 are the readings for moments of time t_1 and t_2.

$$\frac{A_1 - A_0}{A_2 - A_0} = e^{-\frac{1}{2}\frac{n_0^2}{\varepsilon}(t_1 - t_2)}, \tag{8}$$

whence

$$A_0 = \frac{A_1 B e^{(t_2 - t_1)} - A_2}{1 - B e^{(t_2 - t_1)}}, \tag{9}$$

where $B = e^{-\frac{n_0^2}{2}}$.

Let us write the analogous equation for the moments t_3 and t_1:

$$A_0 = \frac{A_1 B e^{(t_3-t_1)} - A_3}{1 - B e^{(t_3-t_1)}}. \tag{10}$$

From equations (9) and (10) we can find

$$B = \frac{A_2 - A_3}{A_1 e^{(t_3-t_1)} + A_2 e^{(t_3-t_1)} - A_1 e^{(t_3-t_1)} - A_3 e^{(t_3-t_1)}}. \tag{11}$$

It is not necessary to wait for complete abatement of the gravimeter system at each point to find A_0. A minimum of three readings must be taken at certain points in time. This enables the time taken in observation at the point to be considerably shortened.

The accuracy of finding A_0 can be raised by increasing the number of readings and averaging the results of the calculations, and also by working out the results of the measurement by the method of least squares.

As will be shown below, the gravimeter readings are influenced by the vertical and horizontal accelerations of the motion of the Cardan suspension in addition to the force of gravity. They must be accurately measured to correct the readings for their influence.

The amplitude value of the vertical accelerations can be found from the very observations made with the instruments for which it is necessary to divide the oscillatory amplitude of the pendulum by the dynamic coefficient. Consequently, in order to find the value of the vertical accelerations, we have to know the value of the dynamic coefficient:

$$\lambda = \frac{n_0^2}{\sqrt{(n_0^2 - p^2)^2 + 4\varepsilon^2 p^2}},$$

or

$$\lambda = \frac{n_0^2}{2\varepsilon p}\left[\frac{(n_0^2 - p^2)^2}{4\varepsilon^2 p^2} + 1\right]^{-\frac{1}{2}}, \tag{12}$$

$$\lambda \approx \frac{n_0^2}{2\varepsilon p}\left(1 - \frac{n_0^2 - p^2}{8\varepsilon^2 p^2}\right).$$

Since in gravimeters n_0^2 is usually less than 100 radian/sec and p^2 is no greater than a few units, formula (12) can be written in the form:

$$\lambda = \lambda_0\left(1 - \frac{1}{2}\lambda_0^2\right), \tag{13}$$

where

$$\lambda_0 = \frac{n_0^2}{2\varepsilon p}.$$

Experience shows that to measure Δg with sufficient accuracy it must be less than 0.01. Proceeding from this, formula (13) can be rewritten with an accuracy of up to 10^{-6} thus:

$$\lambda = \frac{n_0^2}{2\varepsilon p}. \tag{14}$$

Being in possession of the recorded motion of the gravimeter pendulum when deflected from a state of equilibrium, we can find the value $B = e^{-\frac{n_0^2}{2}}$, from which $-\frac{n_0^2}{2} = \ln B$.

The dynamic coefficient can be determined in this manner from the formula

$$\lambda = -\frac{T_b}{2\pi} \ln B, \tag{15}$$

if we know T_b, the period of the vessel's oscillation and are also in possession of the recorded movement of the gravimeter pendulum when deflected from a state of equilibrium.

We are now therefore in a position to find the amplitude of the vertical accelerations as we know the dynamic coefficient λ and have measured the mean oscillatory amplitude of the pendulum.

If it is possible to read off the value A_0, i.e. if the observations close with the pendulum completely at rest, we can obtain from formulas (7) and (14) a formula for calculating the dynamic coefficient of the gravimeter for two readings, A_1 and A_2, on the gravimeter scale at points of time t_1 and t_2 and for the known position of static equilibrium A_0.

$$\lambda = \frac{T_b}{2\pi} \frac{\ln \frac{A_1 - A_0}{A_2 - A_0}}{t_2 - t_1} = 0.3663 \log \frac{A_1 - A_0}{A_2 - A_0} \frac{T_b}{t_2 - t_1}. \tag{16}$$

The values A_0, A_2, A_1 can be read off from the curve of change in the reading shown in Fig. 1.

For example, let the deviation of the system from a position of equilibrium decrease by 10 times in relation to the initial deviation in a period of 10 minutes, i.e.

$$\frac{A_1 - A_0}{A_2 - A_0} = 10.$$

Let $T_b = 10$ sec. Then, by substituting in formula (16) we obtain

$$\lambda = \frac{0.3663 \times 10.1}{10.60} = 0.0061$$

Let us assume that the amplitude of the vertical accelerations is 5 gal, and their oscillatory period 10 sec. In this case the gravimeter pendulum will oscillate with an amplitude of $5 \times 0.0061 = 30$ mgal.

The above gives rise to certain assertions.

Firstly, under conditions of strong damping, small sinusoidal vertical accelerations do not produce systematic changes in the gravimeter reading but only forced sinusoidal oscillations in the pendulum, the amplitude of which is decreased proportionally to the value of λ. The amplitude of the vertical accelerations can be found from the recording of these oscillations.

Secondly, it is not necessary to wait for the system to come completely to rest in order to take readings from the instrument. The reading for a posi-

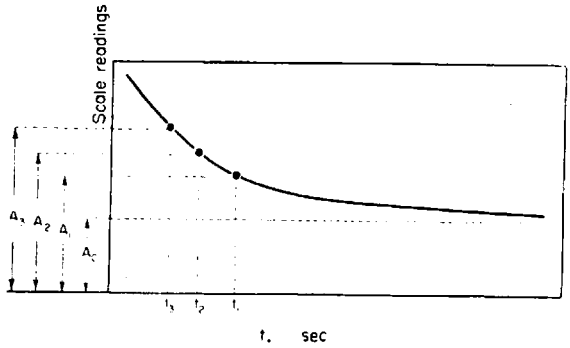

FIG. 1.

tion of static equilibrium of the system may be calculated from the recorded motion of the pendulum, thus considerably reducing the amount of time spent in observations at the point.

Thirdly, the dynamic coefficient which, for a given oscillatory frequency of the vessel, is the basic parameter of the gravimeter can be found from the recorded motion of the gravimeter pendulum when deflected from a state of equilibrium.

Apart from the methods of measurement and the determination of the instrumental parameters, the problem of the combined effect of vertical and horizontal accelerations and inclination on the instrument readings is of considerable relevance to the static method of measuring gravity at sea.

We shall attempt to solve the problem to the first degree of approximation.

It is assumed that the instrument is mounted on a Cardan suspension subjected to vertical and horizontal accelerations so that the suspension

oscillates at natural and induced frequencies. In this case the induced oscillations of the Cardan suspension are mainly due to the horizontal acceleration component of the vessel's motion.

Let us introduce a mobile system of co-ordinates $\xi\zeta$ related to the instrument. In the absence of vertical accelerations the pendulum of the gravimeter is orientated parallel to the axis 0ζ. Let us select a further system of co-ordinates $x0z$ in which the direction of the axes is orientated relative to the fixed horizon.

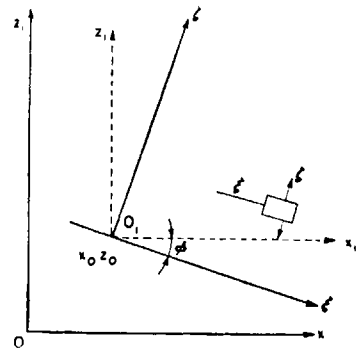

FIG. 2.

The transition from one system to the other can be easily achieved by the following scheme

		x_1	z_1
$x = x_0 + x_1$	ξ	$\cos\varphi$	$\sin\varphi$
$z = z_0 + z_1$	ζ	$\sin\varphi$	$\cos\varphi$

$$\left.\begin{aligned} x &= x_0 + \xi\cos\varphi + \zeta\sin\varphi \\ z &= z_0 - \xi\sin\varphi + \zeta\cos\varphi \end{aligned}\right\} \qquad (17)$$

The system $\xi0\zeta$ moves relative to $x0z$ and rotates.

The variables in formula (17) are x_0, z_0 and φ.

ξ'', ζ'' denote projections of the acceleration of the system of co-ordinates $\xi0\zeta$ translated to the axes ζ and ξ via $\xi_0\zeta_0$, the co-ordinates of the centre of gravity of the pendulum.

It is common knowledge in mechanics that the projection of the acceleration

of a point on a moving body onto a co-ordinate consists of the corresponding components of translated, tangential and centrifugal accelerations, i.e.

$$\zeta'' = \zeta_0'' - \xi_0\varphi'' - \zeta_0(\varphi')^2. \tag{18}$$

In order to evaluate the influence on the readings given by the gravimeter, we need to know the equation of the motion of the instrument itself or the equation of the motion of the Cardan suspension.

The Cardan suspension is a damped or undamped pendulum subjected to the disturbing influence of accelerations.

The Cardan suspension will have natural and induced oscillations, the period of which will equal that of the horizontal accelerations.

Thus, if

$$\ddot{x} = a_x \cos(pt + \delta_x), \tag{19}$$

it follows that

$$\varphi = \varphi_0 + \varphi_1 \cos(n_1 t + \delta_1) + \varphi_2 \cos(pt + \delta_2), \tag{20}$$

where φ_0 is the constant component of the angle of inclination of the instrument's pendulum; φ_1 is the amplitude of the natural oscillations of the Cardan suspension; n_1 is the frequency of the natural oscillations of the Cardan suspension; φ_2 is the amplitude of the induced oscillations; a_x is the amplitude of the horizontal acceleration components; p is the oscillatory frequency of the horizontal component.

Let us now find the values entering equation (18).

The influence of the translated acceleration can be written in accordance with (17) as

$$\ddot{\zeta}_0 = \ddot{x}\sin\varphi + \ddot{z}\cos\varphi = \sqrt{\ddot{x}^2 + \ddot{z}^2}\cos\left(\varphi - \arctan\frac{\ddot{x}}{\ddot{z}}\right). \tag{21}$$

Taking into account that

$$\ddot{z} = g + a_z\cos(pt + \delta_z) = g + \ddot{z}_1,$$

where

$$\ddot{z}_1 = a_z\cos(pt + \delta_z),$$

and also that $\dfrac{\ddot{x}}{g}$ is small, we obtain

$$\sqrt{\ddot{x}^2 + (\ddot{z}_1 + g)^2} = g\sqrt{\left(\frac{\ddot{z}_1}{g} + 1\right)^2 + \frac{\ddot{x}^2}{g^2}} = g\left(1 + \frac{2\ddot{z}_1}{g} + \frac{\ddot{z}_1^2}{g^2} + \frac{\ddot{x}^2}{g^2}\right)^{\frac{1}{2}} =$$

$$= g\left(1 + \frac{\ddot{z}_1}{g} + \frac{\ddot{x}}{2g^2} - \frac{4\ddot{z}_1^2}{8g^2} + \frac{\ddot{z}_1^2}{2g^2} + \ldots\right) \approx$$

$$\approx g\left(1 + \frac{\ddot{z}_1}{g} + \frac{\ddot{x}^2}{2g^2}\right). \tag{22}$$

We transform the second factor of expression (21). Taking into account (20), we obtain

$$\cos\left(\varphi - \arctan\frac{\ddot{x}}{\ddot{z}}\right) \approx 1 - \frac{1}{2}\left(\varphi - \frac{\ddot{x}}{g}\right)^2 =$$

$$= 1 - \frac{1}{2}\left[\varphi_0 + \varphi_1 \cos(n_1 t + \delta_1) + \varphi_2 \cos(pt + \delta_2) - \right.$$

$$\left. - \frac{a_x}{g}\cos(pt + \delta_x)\right]^2. \tag{23}$$

Before proceeding to further transformations we wish to interpolate the following comment which will henceforward apply throughout.

We assume that the amplitude of the accelerations does not exceed 20gal and that the dynamic coefficient is not greater than 0.01. In this case we shall in future disregard all purely sinusoidal components of the second order of smallness by comparison with $\frac{\ddot{z}_1}{g}$ in our calculations since their registration will be reduced by the number of times by which the dynamic coefficient is less than unity. We shall only retain the systematic part of periodic components of the second order of smallness by comparison with $\frac{\ddot{z}_1}{g}$, i.e. their mean value for a large time interval.

Thus we shall write for (21)

$$g\left(1 + \frac{\ddot{z}_1}{g} + \frac{\ddot{x}^2}{2g^2}\right)\cos\left(\varphi - \frac{\ddot{x}}{g}\right) \approx$$

$$\approx g\left\{1 + \frac{a_z}{g}\cos(pt + \delta_z) + \frac{a_x^2}{2g^2}\cos^2(pt + \delta_x)\right\} \times$$

$$\left\{1 - \frac{1}{2}\left[\varphi_0 + \varphi_1 \cos(n_1 t + \delta_1) + \varphi_2 \cos(pt + \delta_2) - \frac{a_x}{g}\cos(pt + \delta_x)\right]^2\right\} =$$

$$= g\left\{1 + \frac{a_z}{g}\cos(pt + \delta_z) + \frac{a_x^2}{2g^2}\cos^2(pt + \delta_x)\right\} \times$$

$$\left\{1 - \frac{1}{2}[\varphi_0 + \varphi_1 \cos(n_1 t + \delta_1) + a]^2\right\}. \tag{24}$$

Here a is the deviation of the Cardan suspension from the direction of the resultant force: the force of gravity plus the inertial force developed by the horizontal acceleration or the deviation of the Cardan suspension from the direction of the instantaneous vertical, i.e.

$$a = \varphi_z \cos(pt + \delta_z) - \frac{a''x}{g} \cos(pt + \delta_x) = a_{\max} \cos(pt + \delta),$$

where δ which depends on δ_x, δ_z is the phase of this deviation; $a_{\max}$ is the amplitude of the deviation of the Cardan suspension from the instantaneous vertical.

In marine pendulum devices this angle is registered by damped short period pendulums.

Bearing in mind what has been said previously, let us find an approximated expression for $\ddot{\zeta}_0$, disregarding sinusoidal terms of the order of $\left(\frac{\ddot{x}}{g}\right)^2$:

$$\ddot{\zeta}_0 = g\left(1 + \frac{\ddot{z}_1}{g} + \frac{\ddot{x}^2}{2g^2}\right) \cos\left(\varphi - \frac{\ddot{x}}{g}\right) \approx$$

$$\approx g\left[1 + \frac{a_z}{g} \cos(pt + \delta_z) + \frac{a_x^2}{4g^2} - \frac{1}{2}\varphi_0^2 - \frac{1}{4}\varphi_1^2 - \frac{1}{4}a_{\max}^2\right]. \quad (25)$$

THE TANGENTIAL ACCELERATION

In accordance with (18) and (20) the tangential acceleration component on the axis is

$$-\xi_0 \ddot{\varphi} = \xi_0[\varphi_1 n^2 \cos(n_1 t + \delta_1) + \varphi_2 p^2 \cos(dt + \delta_2)] \quad (26)$$

It is evident that this acceleration only yields terms the periods of which are equal to the oscillatory periods of the Cardan suspension and the disturbing accelerations. The periodic terms of frequency n_1 can easily be separated from the second term in brackets in expression (26) since the period of the natural oscillations of the Cardan suspension differs from the period of the accelerations. In addition, damping of the Cardan suspension enables one to get rid of the influence of its natural oscillations.

On the basis of the above we can replace (26) by

$$-\xi_0 \ddot{\varphi} \approx \xi_0 \varphi_2 p^2 \cos(pt + \delta_2). \quad (27)$$

THE CENTRIFUGAL ACCELERATION

In accordance with (18) and (20) the centrifugal acceleration component is

$$-\zeta(\varphi')^2 = \zeta_0[\varphi_1 n_1 \sin(n_1 t + \delta_1) + \\ + \varphi_2 p \sin(pt + \delta_2)^2] \approx -\zeta_0 \left(\frac{1}{2}\varphi_1^2 n_1^2 + \frac{1}{2}\varphi_2^2 p^2\right), \tag{28}$$

consequently the centrifugal acceleration introduces a systematic error.

Thus, for the full component of acceleration in the direction of the axis one can write an approximate equation

$$\zeta'' \approx \zeta'' - \xi_0\varphi'' - \zeta\varphi^{12} = g\left[1 - \frac{1}{2}\varphi_0^2 - \frac{1}{4}\varphi_1^2 + \right. \\ \left. + \frac{a_{x^3}}{4g^2} - \frac{a^2_{\max}}{4}\right] + a_z \cos(pt + \delta_z) + \\ + \xi_0\varphi_2 p^2 \cos(pt + \delta_2) - \zeta_0 \times \\ \times \left(\frac{1}{2}\varphi_1^2 n_1^2 + \frac{1}{2}\varphi_2^2 p^2\right). \tag{29}$$

The equation for the motion of the gravimeter pendulum can be written down (taking into consideration that $I\ddot{\varphi}$, the moment of inertia, is small by comparison with the remaining terms making up the equation) in the form:

$$I\Theta_1'' + 2h\Theta_1' + K\Theta_1 = m\zeta'' l. \tag{30}$$

Let us divide by I. Taking into consideration the notations in formulas (1) and (2) we obtain

$$\Theta_1'' + 2\varepsilon\Theta_1' + n^2\Theta = \frac{ml}{I}\zeta = \frac{ml}{I}g + \\ + \frac{ml}{I}\left\{\frac{a_x^2}{4g} - \frac{1}{4}a^2_{\max}g - \frac{1}{2}\varphi_0^2 g - \frac{1}{4}\varphi_1^2 g - \right. \\ - \zeta_0\left(\frac{1}{2}\varphi_1^2 n_1^2 + \frac{1}{2}\varphi_2^2 p^2\right) + a_z \cos(pt + \delta_z) + \\ \left. + \xi_0\varphi_2 p^2 \cos(pt + \delta_2)\right\}. \tag{31}$$

Equation 31 contains two periodic terms on the right hand. Let us estimate the value of the second of these terms.

Let us assume that $a_x = 10\,\text{gal}$, $\varphi_2 = \frac{a_x}{g}, p = \frac{2\pi}{T_n} = \frac{6.28}{10\,\text{sec}} = 0.63, p^2 = 0.40$.

If the distance between the axis of rotation of the Cardan suspension and the axis of rotation of the pendulum does not exceed 1 cm then the last term in formula (31)

$$\xi_0 \frac{a_x}{g} p^2 = \xi_0\, 0.004$$

is very small by comparison with a_z and can therefore be discarded.

The periodic term $a_z \cos(pt + \delta_z)$ causes the forced oscillations of the system.

This phenomenon was analysed in detail in paper (2). If we analyse equation (31) we see that when horizontal accelerations are present the reading of the instrument will not correspond to the true value for gravity but to a certain value of G and that we shall have to introduce the necessary corrections to obtain a true reading.

Thus we have

$$g = G - \frac{a_x^2}{4g} + \frac{1}{2}\left[\varphi_0^2 g + \frac{\varphi_1^2}{2} g + \zeta_0(\varphi_1^2 n_1^2 + \varphi_2^2 p^2) + \frac{1}{4} a^2_{\max} g\right] \quad (32)$$

and further

$$g = G - \frac{a_x^2}{4g} + \frac{g}{2}\left[\varphi_0^2 + \frac{a^2_{\max} + \varphi_1^2}{2} + \frac{\zeta_0}{g}(\varphi_1^2 n_1^2 + \varphi_2^2 p^2)\right]. \quad (33)$$

Here $\frac{a_x^2}{4g}$ is simply a Brown term, and the expression in square brackets a correction for inclination (deviation from the instantaneous vertical).

Formula (33) can also be written

$$g = G - \frac{a_x^2}{4g} + \frac{g}{2}\left[\varphi_0^2 + \frac{a^2_{\max} + \varphi_1^2}{2} + \frac{4\pi^2 \zeta_0}{g}\left(\frac{\varphi_1^2}{T_k^2} + \frac{\varphi_2^2}{T_b^2}\right)\right].$$

where T_k and T_b are the oscillatory periods of the vessel and the Cardan suspension respectively.

For a short period Cardan suspension φ_2 is normally close to $\frac{a_x}{g}$, and therefore

$$g = G - \frac{a_x^2}{4g} + \frac{g}{2}\left[\varphi_0^2 + \frac{a^2_{\max} + \varphi_1^2}{2} + \frac{4\pi^2 \zeta_0}{g}\left(\frac{\varphi_1^2}{T_k^2} + \frac{a_x^2}{g^2}\frac{1}{T_b^2}\right)\right]. \quad (34)$$

To assess the influence of the acceleration on an instrument mounted on a Cardan suspension with natural oscillations of large period, such as a stabilized gyroscopic device, we must return again to expression (26).

Here

$$a = \varphi_2 \cos(pt + \delta_2) - \frac{a_x}{g} \cos(pt + \delta_x).$$

Taking into consideration that for the given case the phase difference $(\delta_2 - \delta_x)$ is close to π, we find

$$\begin{aligned} a &\approx -\left(\frac{a_x}{g} + \varphi_2\right) \cos(pt + \delta_x), \\ \frac{a^2_{\max}}{2} &= \frac{a_x^2}{2g^2} + \frac{a_x}{g}\varphi_2 + \frac{\varphi_2^2}{2}. \end{aligned} \tag{34a}$$

Introducing this expression into formula (33) we obtain

$$g = G + \frac{g}{2}\left[\varphi_0^2 + \frac{\varphi_1^2 + \varphi_2^2}{2} + \frac{a_x}{g}\varphi_2 + \frac{4\pi^2}{g}\zeta\left(\frac{\varphi_1^2}{T_k^2} + \frac{\varphi_2^2}{T_b^2}\right)\right]. \tag{35}$$

More exactly

$$g = G + \frac{g}{2}\left[\varphi_0^2 + \frac{\varphi_1^2 + \varphi_2^2}{2} - \frac{a_x}{g}\varphi_2 \cos(\delta_2 - \delta_x) + \frac{4\pi}{g}\zeta_0\left(\frac{\varphi_1^2}{T_k^2} + \frac{\varphi_2^2}{T_b^2}\right)\right],$$

where $(\delta_2 - \delta_x)$ is the phase difference of the forced oscillation of the Cardan suspension and the disturbing acceleration.

Let us examine a few examples:

(a) the instrument is mounted on a short period Cardan suspension.

$$\varphi_2 \approx \frac{a_x}{g},\ \zeta = 0,\ \varphi_1 = 0,\ \varphi_0 = 0,\ a_{\max} = 0,\ a_x = 20\,\text{gal}$$

(b) the instrument is mounted on a stabilized gyroscopic device working with an accuracy of $\pm 2'$;

$$\varphi_2 = 2',\ \zeta_0 = 0,\ \varphi_1 = 0,\ \varphi_0 = 0,$$

$$a_{\max} = \frac{a_x}{g}, a_x = 20\,\text{gal}$$

Then for case (a) we have

$$\Delta g = \frac{a_x^2}{4g} \approx 105\,\text{ngal}$$

and for case (b)

$$\Delta g = \frac{g}{2}\left[\varphi_2\left(\frac{\varphi_2}{2} + \frac{a_x}{g}\right)\right] = 6\,\text{ngal}$$

Therefore the gyroscopic stabilization decreases the correction for the influence of accelerations on the pendulum of the instrument.

All the previous conclusions have assumed a single degree of freedom of the Cardan suspension and the presence of a single horizontal component. In actual fact we have to deal with the two horizontal components and two degrees of freedom of the Cardan suspension. Repeating an analogous conclusion for the second degree of freedom we obtain thereby formulas for long and short period Cardan suspensions analogous to formulas (34) and (35)

$$g = G - \frac{a_x^2}{4g} + \frac{g}{2}\left[\varphi_{0x}^2 + \frac{(a_x^2+\varphi_{1x}^2)}{2} + \frac{4\pi^2\zeta_0}{gT_{kx}^2}\left(\varphi_{1x}^2 + \frac{a_x^2}{g^2}\frac{T_{kx}^2}{T_{bx}^2}\right)\right] +$$

$$+ \frac{-a_y^2}{4g} + \frac{g}{2}\left[\varphi_{0y}^2 + \frac{a_y^2+\varphi_{1y}^2}{2} + \frac{4\pi^2\zeta_0}{gT_{ky}^2}\left(\varphi_{1y}^2 + \frac{a_y^2}{g^2}\frac{T_{ky}^2}{T_b^2}\right)\right], \qquad (36)$$

$$g = G + \frac{g}{2}\left[\varphi_{0x}^2 + \frac{\varphi_{1x}^2+\varphi_{2x}^2}{2} - \frac{a_x}{g}\varphi_{2x}\cos(\delta_{2x}-\delta_x) +\right.$$

$$\left. + \frac{4\pi}{g}\zeta_0\left(\frac{\varphi_{1x}^2}{T_k^2} + \frac{\varphi_{2x}^2}{T_b^2}\right)\right] + \frac{g}{2}\left[\varphi_{0y}^2 + \frac{\varphi_{1y}^2+\varphi_{2y}^2}{2} -\right.$$

$$\left. - \frac{a_y}{g}\varphi_{2y}\cos(\delta_{0y}-\delta_y) + \frac{4\pi}{g}\zeta_0\left(\frac{\varphi_{1y}^2}{T_k^2} + \frac{\varphi_{2y}^2}{T_b^2}\right)\right]. \qquad (37)$$

The quantities denoted by subscript x relate to the degree of freedom of movement of the instrument's pendulum in a plane; the quantities denoted by subscripts relate to the degree of freedom perpendicular to the above.

The principal correction term in formula (36) is the Brown term

$$\frac{-a_{x^2}+a_{y^2}}{4g}$$

When the horizontal accelerations are small and the instrument is well adjusted the remaining terms are negligible. In such a case one can proceed to calculate the accelerations without having recourse to accelerographic devices. One can assume from the theory of trochoidal waves that

$$a_z^2 = a_x^2 + a_y^2,$$

given that there is a certain degree of approximation in the satisfaction of this equation.

It is clear that the Brown correction will equal

$$\delta_g = -\frac{a_x^2 + a_y^2}{4g} = -\frac{a_z^2}{4g}. \tag{38}$$

As was shown above a_z may be recorded by taking readings of the instrument which register the amplitude of its forced oscillations.

The special reservation should, however, be made that in practice the horizontal and vertical acceleration components on vessels are far from being identical. If the influence of the accelerations on the gravimeter readings is to be more strictly accounted for, an especial measurement of the horizontal accelerations by one of the methods currently in use in pendulum observations becomes necessary.

CONCLUSIONS

In closing, the main conclusions can be briefly formulated.

1. It is not necessary to wait for total abatement of the instrument's beam when taking readings with a damped marine gravimeter. The reading for a position of static equilibrium can be calculated from the record of the gravimeter pendulum and this considerably curtails the time required for observations at the point.

2. The basic parameter of the gravimeter (for a given oscillatory frequency of the vessel)—the dynamic coefficient—can be derived from the recorded motion of the instrument's pendulum.

3. When the instrument's pendulum is strongly damped small sinusoidal vertical accelerations only evoke sinusoidal forced oscillations in the pendulum, the amplitude of which is proportional to the value of the dynamic coefficient.

The amplitude of the vertical accelerations is arrived at from the record of the oscillations of the gravimeter pendulum. Having allowed for the existence of the relation $a_z^2 = a_x^2 + a_y^2$ we can find the value of the Brown correction from the recorded oscillations of the gravimeter alone.

The accelerations and rotatinal movements of the Cardan suspension must be registered if there is uncertainty as to the satisfaction of the equality $a_z^2 = a_x^2 + a_y^2$.

4. A period of natural oscillation of the Cardan suspension considerably greater than the period of the vessel's oscillations is selected in order to diminish the influence of the horizontal accelerations.

In this connection it is undoubtedly advantageous to use gyroscopic stabilization for the position of the gravimeter.

The gyroscopically stabilized Cardan suspension is treated in this case as a Cardan suspension with a very large period of natural oscillation. It is

obvious that the use of sufficiently accurate gyroscopic stabilization for a damped gravity measuring device with a horizontal torsion thread makes highly accurate observations possible even for amplitudes of the accelerations of 10–20 gal. This, at the same time, leads to the introduction of a minimum number of corrections arising from the measurements.

REFERENCES

1. F. L. VENING MEINESZ, *Gravimetric observations at sea.* Theory and practice. Geodezizdat, 1940.
2. K. Ye. VESELOV, The static method of measuring the force of gravity at sea. *Prikladnaia geofizika, fasc.* 15 Gostoptekhizdat (1956).
3. L. V. SOROKIN, *Gravimetry and gravimetric prospecting.* Gostoptekhizdat, 1951.

CHAPTER 6

EVALUATING THE ACCURACY OF A GRAVIMETRIC SURVEY, SELECTING THE RATIONAL DENSITY OF THE OBSERVATION NETWORK AND CROSS-SECTIONS OF ISOANOMALIES OF THE FORCE OF GRAVITY

B. V. KOTLIAREVSKII

IN PLANNING gravimetric work, the density of the network of observations is selected with regard to the geological problems and the expected character of the gravimetric field. Normally no calculations are carried out and the selection of the network is mainly based on previous experience.

The cross-section of isoanomalies planned in areal surveys is determined as the function of the expected mean square error for the values of the force of gravity at consecutive points. The actual value of this error obtained after carrying out field work is considered as a measure of the accuracy of the survey.

Methods of selecting the observation network and evaluating the accuracy of the survey are of course imperfect. They do not make it possible to solve the basic problem, arising in the planning of the work, which is to find the optimal technical and economic solution of the geological problem in the gravimetric survey. The problem consists in predicting the density of the network and the accuracy of the observations, which will ensure the detection of the features of the field with the required accuracy.

It is therefore not by accident that the accuracy of the survey and the choice of a rational network of observations have been studied both in this country and abroad. We mention in particular the work of ANDREEV [1] and LUKAVCHENKO [5], who determined the density of the network as a function of the value and extent of the anomalies, caused by certain geometrically regular bodies; the work of BULANZHE [2], devoted to the problems of accuracy of survey, selection of the rational section of isoanomalies and the scale of the geophysical map under conditions which permit linear interpolations between the points of observations; finally, a number of recent articles by VOLODARSKII [3], GRUSHINSKII [4], MALOVICHKO [6] and PUZYREV [7] who consider from another point of view the various facets of the problem of the density of the network, the accuracy of constructing from isolines, etc.

In the present article, an attempt is made to solve these problems in a sufficiently general from, taking into account the errors in observation and interpolation. The proposed method of evaluating the accuracy of a gravimetric survey, of the determining the rational density of the network and of selecting the cross-section of isoanomalies is basically suitable for any type of survey. However, it has been mainly developed for the commonest types of regional and exploratory surveys. With regard to detailed surveys, another and somewhat different method can be recommended, which owing to the lack of space is not given here.

SELECTING THE CRITERIA FOR EVALUATING THE ACCURACY OF A GRAVIMETRIC SURVEY

The accuracy of the observed gravity field depends on the accuracy of determining the values of gravity at the observation points, on the density of the network and on the character of the field itself. Furthermore, it depends on the method of interpolating the gravity values in the intervals between the observation points. We have accepted the idea of linear interpolation since it is universally used in gravimetric work.

Before proceeding to the development of a method for evaluating the accuracy of a gravimetric survey, it is necessary to select the basic criteria for this evaluation.

The main type of gravimetric work is areal survey the results of which are represented by a map of isoanomalies of gravity. The accuracy of the map can be determined from its various features. It is also possible to evaluate the value for the error in the observed field; this value being the mean square error in the value for gravity at a certain arbitrarily selected point on the map.

This error does not depend on the cross-section of the isoanomaly and is a function of the errors of the values of gravity at the observation point, the density of the network and the character of the gravity field. For a field along a profile, this error (we will call it ε_m) is determined by the following integral equation:

$$\varepsilon_m^2 = \frac{1}{l}\int_l [\bar{g}(x) - g(\sigma, a, \bar{g})]^2 \, dx, \tag{1}$$

where $\bar{g}$ is the true gravity field (unknown); g is the observed field, which depends on the mean square error σ in determining the force of gravity at the observation points, on the average distance a between these points and

on the character of the true field $\bar{g}$; l is the range of integration on the profile.

However, one of the basic problems of a gravimetric survey (if it is carried out for geological purposes) is the study of the changes in the gravity anomaly field from point to point. The pattern of these changes is given by the gravity isoanomalies. It is important to evaluate the accuracy with which these changes are determined by means of the isoanomalies. For this purpose it is necessary to find the mean square value of the error in determining the gravity increment between two neighbouring isoanomalies. Let us find the mathematical expression for this error.

Along the profile let there be a curve for the true value of gravity $\bar{g}(x)$ and at the points x_1, x_2 and x_3 the obtained gravity values g_1, g_2, g_3 (Fig. 1). As a result of linear interpolation, we obtain an approximate expression of the function $g(x)$ in the interval (x_1, x_3) of the profile in the form of a broken LMN. On the profile let us select the points A and B, to which correspond the true values for the force of gravity $\bar{g}_A$ and $\bar{g}_B$ and the observed (taken with the broken LMN) values g_A and g_B.

Let the points A and B be selected so that $g_B - g_A = p$, where p is the cross-section of the isoanomalies. Then the expression

$$\delta = (g_B - g_A) - (\bar{g}_B - \bar{g}_A) \tag{2}$$

will give the value for the absolute error in determining the increase in the force of gravity within the limits of two neighbouring isoanomalies. This value is a function of σ, a, g and p. The mean square value (we will call it δ_m) of this function, determined for a certain section l of the profile, can be represented by the following integral expression:

$$\delta_m^2 = \frac{1}{l}\int_l \delta^2 [\sigma, a, \bar{g}(x), p]\, dx. \tag{3}$$

As will be shown, the two criteria proposed for evaluating the accuracy of a gravimetric map—from the mean square error in the value of gravity at an arbitrary point of the map (ε_m) and from the value of the mean square error in determining the gravity increment between limits of two neighbouring isoanomalies (δ_m) are in practice sufficient for solving all basic problems connected with an evaluation of the quality of work carried out and for the determination of the necessary parameters of the survey at the planning stage.

The indices of accuracy ε_m and δ_m give the absolute value of the errors. However, in practice, anomaly fields with differing intensities are encoun-

tered. Therefore, in order to make comparisons of the surveys of such different types of fields, it is necessary to give the field error ε_m not in absolute, but in relative magnitudes, for example, in fractions of the mean value of gravity for one gravimetric anomaly (of one extremum*). We will call this value g_m. In this way, the results of different surveys can be represented by maps with differing cross-section of the isoanomalies. In order to compare the accuracy of these maps, it is necessary to determine the error in the gravity increment between two isoanomalies δ_m in fractions of the cross-section of the isoanomalies (p). For the objective quantity indices of map accuracy, it is convenient to adopt the following expressions:

$$E_m(\sigma, a, \bar{g}) = \frac{\varepsilon_m}{g_m}, \tag{4}$$

$$D_m(\sigma, a, \bar{g}, p) = \frac{\delta_m}{p}, \tag{5}$$

where E_m is the mean square error of the value of gravity at an arbitrary point of the field, expressed as fractions of the mean value of gravity within the limits of one extreme point;

D_m is the mean square error in determining the gravity increment between the limits of one cross-section of the isoanomalies, given in fractions of this cross-section.

BASIC FORMULAE

The study of the expressions (4) and (5) should, strictly speaking, be carried out for the planar field $\bar{g}(x, y)$, since we are mainly concerned with areal surveys. To facilitate the task, we will be limited to a study of these expressions for the field $\bar{g}(x)$, given along the profile. It can be shown that as a result of this replacement, the values of the E_m and D_m in which we are interested are a little higher.

Let us consider the interval x_2, x_3 on the profile (Fig. 1). The observed values of gravity are determined within the limits of this range by a section of the straight line MN. If the observations at the points x_2 and x_3 were absolutely accurate, instead of the section MN it would have been necessary to consider the section $M'N'$. Let us choose a certain point C in the same interval. The true value of gravity at this point is $\bar{g}_c$ and is obtained from the observations (with subsequent linear interpolation) $-g_c$. Provided that observations were absolutely accurate, the interpolated value of the force

* A Russian word signifying either a maximum or a minimum. Elsewhere throughout this paper the word *extreme point* is used [Editor's footnote].

of gravity at this point would be equal to g_c'. It can readily be seen that the error in ε of the observed (more accurately, interpolated) value for gravity at the point C is composed of the following two errors:

$$\varepsilon = (g_c - \bar{g}_c) = (g_c - g_c') + (g_c' - \bar{g}_c) = \varepsilon_0 + \varepsilon_i,$$

where ε_0 is the error due to observation errors;

ε_i is the error due to the non-linearity of the field.

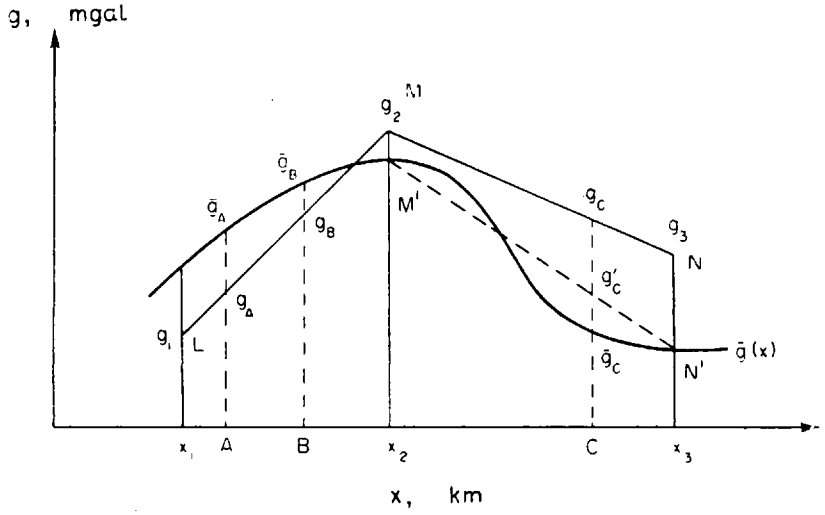

FIG. 1.

This equation will be justified for any point on the profile Moreover, owing to the independence of the signs and the absolute values of the components ε_0 and ε_i for a multitude of n points on the profile, the following equation will hold

$$\sum_n \varepsilon^2 = \sum_n (\varepsilon_0 + \varepsilon_i)^2 = \sum_n \varepsilon_0^2 + \sum_n \varepsilon_i^2$$

or

$$\varepsilon_m^2 = \varepsilon_{0m}^2 + \varepsilon_{im}^2, \tag{6}$$

where ε_{0m} and ε_{im} are the mean square errors in the values of gravity at a profile, caused by the corresponding error in the observations and the non-linearity of the field.

Similar relationships can readily be established for the value δ_m:

$$\delta_m^2 = \delta_{0m}^2 + \delta_{im}^2, \tag{7}$$

where δ_{0m} and δ_{im} are the mean square errors in determining the increment in gravity between two isoanomalies, caused by the error in observations and non-linearity of the field respectively.

Comparing the relationships (6) and (7) with (4) and (5), it can be seen that the required indices of accuracy E_m and D_m also split up into two independent terms:

$$E_m^2 = E_{0m}^2 + E_{im}^2, \tag{8}$$

$$D_m^2 = D_{0m}^2 + D_{im}^2, \tag{9}$$

where

$$E_{0m} = \frac{\varepsilon_{0m}}{g_m}, \quad E_{im} = \frac{\varepsilon_{im}}{g_m}, \quad D_{0m} = \frac{\delta_{0m}}{p}, \quad D_{im} = \frac{\delta_{im}}{p}.$$

Thus, the problem of finding indices of absolute accuracy (ε_m and δ_m) and the relative accuracy (E_m and D_m) of a gravimetric map is divided into two independent problems of finding the absolute (ε_{0m}, δ_{0m}) and the relative $\left(\frac{\varepsilon_{0m}}{g_m}, \frac{\delta_{0m}}{p}\right)$errors due to the error in observations, and finding the absolute (ε_{im}, δ_{im}) and the relative$\left(\frac{\varepsilon_{im}}{g_m}, \frac{\delta_{lm}}{p}\right)$errors, caused by non-linearity of the field.

Errors Due to Inaccuracies of the Observations (ε_{0m}, δ_{0m})

1. The derivation of the relationship $\varepsilon_{0m} = \varepsilon_{0m}(a, \sigma)$.

At the points x_1 and x_2 let $\bar{g}_1$ and $\bar{g}_2$ be the true values of gravity, and g_1 and g_2 the observed values, and σ_1 and σ_2 (Fig. 2) be the errors.

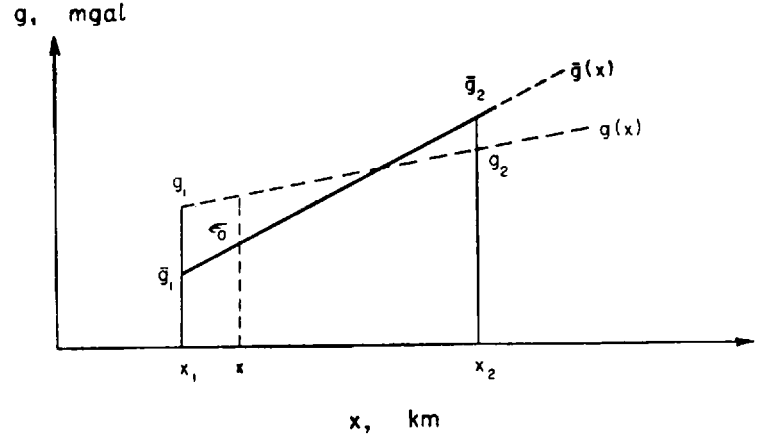

FIG. 2.

Within the range $x_2-x_1 = a$, we consider that the true values of gravity vary in a linear manner.
Hence we have

$$\bar{g}(x) = \bar{g}_1 + \frac{\bar{g}_2-\bar{g}_1}{a}(x-x_1),$$

$$g(x) = g_1 + \frac{g_2-g_1}{a}(x-x_1).$$

For a certain point x, within the range (x_1, x_2) the following relationship will hold

$$\bar{g}(x)-\bar{g}(x) = \varepsilon_0 = \sigma_1 + \frac{\sigma_2-\sigma_1}{a}(x-x_1)$$

or

$$\varepsilon_0 = \left(1-\frac{x-x_1}{a}\right)\sigma_1 + \frac{x-x_1}{a}\sigma_2.$$

Assuming that $x_1 = 0$ and bearing in mind that the observational errors σ_1 and σ_2 are independent and random, after squaring we obtain

$$\varepsilon_0^2 = \frac{\sigma^2}{a^2}(a^2-2ax+2x^2).$$

The integral mean of this value within the range $0 \leqslant x \leqslant a$ has the form:

$$\varepsilon_{0m}^2 = \frac{1}{a}\int_0^a \varepsilon_0^2\, dx.$$

Integrating, we obtain

$$\varepsilon_{0m}^2 = \frac{2}{3}\sigma^2.$$

Thus, ε_{0m} depends only on the mean square error in the values of gravity at the observation points.

2. The derivation of the relationship $\delta_{0m} = \delta_{0m}(a, \sigma, p)$.

As the points x_1, x_2, x_3 let there be true values of gravity $\bar{g}_1$, $\bar{g}_2$, $\bar{g}_3$ and the observed values g_1, g_2, g_3 with errors σ_1, σ_2, σ_3 (Fig. 3). Within the ranges $x_3-x_2 = x_2-x_1 = a$, the change in the force of gravity will be considered linear. Let us select in the range (x_1, x_3) two such points x_4 and x_5 for which the difference in the interpolated values of gravity g_4 and g_5 is equal to the cross-section of the isoanomalies p, i. e. $g_5-g_4 = p$.

Assuming $x_5-x_4 = d \leqslant a$, we find the expression

$$\delta_0 = (\bar{g}_5-\bar{g}_4)-(\bar{g}_5-\bar{g}_4).$$

There can be two cases for both points (x_4 and x_5) lying in the range (x_1, x_2); the point x_4 is in the range (x_1, x_2) and the point x_5 in the range (x_2, x_3). The values of δ_0 will be different for these cases. Let us designate these values by $(\delta_0)_1$ and $(\delta_0)_2$ respectively. Dispensing with intermediate calculations, we find the expression

$$(\sigma^2_{0m})_1 = \frac{2d^2}{a^2}\sigma^2,$$

which does not depend on the abscissa x_4 and holds within the range $0 \leqslant x_4 \leqslant a-d$ (the index m for δ_0 is added so that δ_0 does not depend on x_4, and, consequently, is equal to δ_{0m}).

$$(\delta_0{}^2)_2 = \frac{2}{a^2}\sigma^2\left[(3a^2-3ad+d^2)+(3d-6a)x_4+3x_4{}^2\right]$$

the expression holds in the range $(a-d) \leqslant x_4 \leqslant a$.

Integrating over x_4 in the range, we obtain

$$(\delta^2_{0m})_2 = \frac{d^2}{a^2}\sigma^2.$$

The mean integral value for the required value δ^2_{0m} will be equal to

$$\delta^2_{0m} = \frac{1}{a}\left[(a-d)(\delta^2_{0m})_1 + d(\delta^2_{0m})_2\right].$$

Substituting for $(\delta^2_{0m})_1$ and $(\delta^2_{0m})_2$ the values found for them, we finally obtain

$$\delta^2_{0m} = \frac{d^2}{a^2}\left(2-\frac{d}{a}\right)\sigma^2. \tag{11}$$

The relationship (11) is derived for the case $d \leqslant a$; the inequality meaning that between two points of the observations there are not less than two isoanomalies. In practice, there may be other cases, for example, when between two points of observations there are not less than one and not more than two anomalies, which is expressed by the inequality $a \leqslant d \leqslant 2a$.
Without carrying out intermediate calculations, we will write for this case the final expression for δ^2_{0m}:

$$\delta^2_{0m} = \frac{\sigma^2}{3}\left[4-\left(2-\frac{d}{a}\right)^3\right]. \tag{12}$$

Formulae (11) and (12) enhance the majority of cases encountered in practice when the isoanomalies (on the average for the whole field) are situated between the observation points.

Errors Due to Non-Linearity of the Field (ε_{im}, δ_{im})

The values ε_{im} and δ_{im} are functions of $\bar{g}$, a and p. However, we do not know an exact form of the function $\bar{g} = \bar{g}(x)$ (to simplify we will consider a field along the profile). It remains, therefore, to approximate the field $\bar{g}(x)$ from its discreet values at the observation points. A check of the various methods of approximation showed that the simplest and most convenient is the parabolic interpolation.

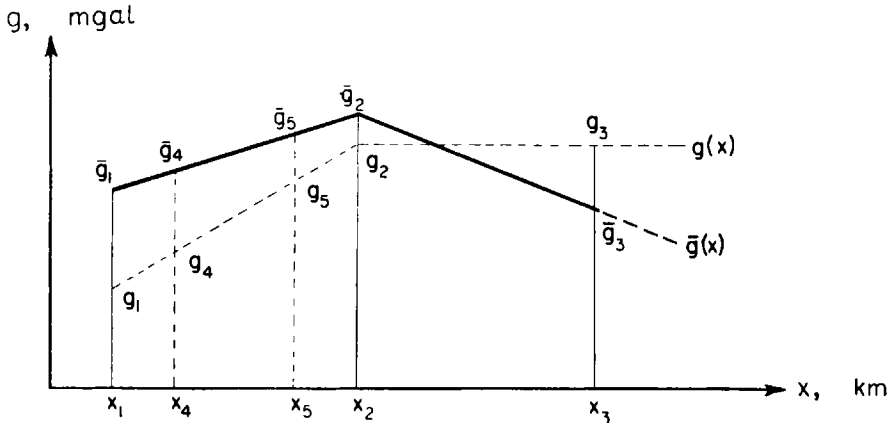

FIG. 3.

The parabolic interpolation can be carried out by various methods. The most obvious way is to draw a parabola through three observation points. This method leads to very simple expressions for ε_{im} and δ_{im}. However, it necessitates finding the mean square values of the differences of the first and second order for the observed field.

$$\Delta_{10} = (\bar{g}_2 - \bar{g}_1) \text{ and } \Delta_2 = (\bar{g}_3 - \bar{g}_2) - (\bar{g}_2 - \bar{g}_1).$$

This involves considerable expense in time. For detailed surveys this method is probably the best. As regards the surveys of a regional and exploratory nature, a much simpler method of parabolic interpretation can be used.

The usually observed field consists of a succession of maxima and minima of gravity. Let us assume that by measurements the mean arithmetical values g_0 and l_0 have been found, so that $2g_0$ is the mean value for the differences in gravity of the neighbouring maxima and minima and $2l_0$ is the mean distance between them. Given a parabolic law for the change in

gravity within the limits of one extreme point, it is possible from the found values of g_0 and l_0 to reconstruct (on the average) the investigated field.

Depending on the number of points used in constructing the parabola, the rule for the change in the force of gravity will be different. We have tested several methods, of which the method of parabolic interpretation with three points would seem to be the best.

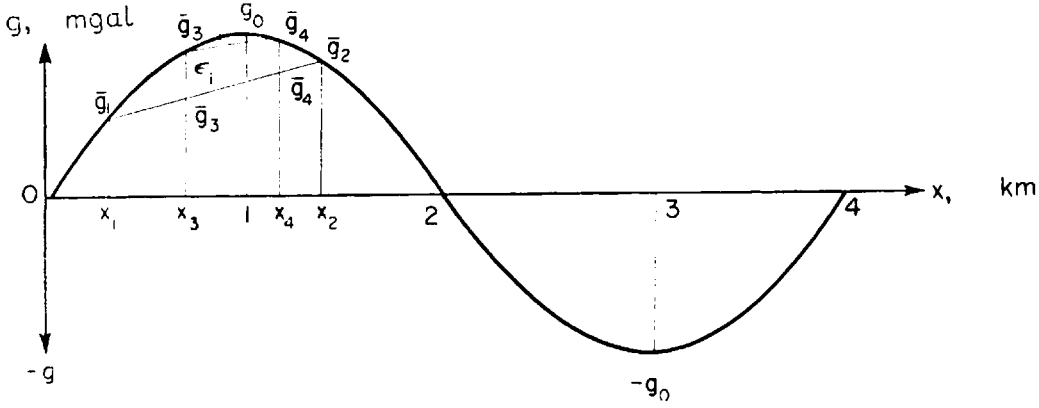

FIG. 4.

Let us construct a parabola through three points (0,0), (l_0, g_0) and $(2l_0, 0)$. Putting for the sake of simplicity $l_0 = 1$, we obtain an equation for a parabola of the second power:

$$\bar{g} = g_0(2x - x^2). \tag{13}$$

From this equation we construct the curve of the gravity maximum (Fig. 4).

We then draw a parabola through the points $(2l_0, 0)$, $(3l_0, -g_0)$ $(4l_0, 0)$, determining the curve for the gravity minimum. Its equation will have the following form:

$$\bar{g} = g_0(8 - 6x + x^2). \tag{14}$$

For the gravity curve so constructed we now find the values ε_{im} and δ_{im}.

1. *Deriving The Relationship* $\varepsilon_{im} = \varepsilon_{im}(\bar{g}, a)$—Let the observations be carried out at the points x_1 and $x_2 = x_1 + a$, representing two values of gravity $\bar{g}_1$ and $\bar{g}_2$ (remembering that when determining errors due to non-linearity of the field, we assume the observational error to be nil). Let us take within the range (x_1, x_2) a certain point x_3, for which the true gravity value will be $\bar{g}_3$ and the interpolated value g_3 (Fig. 4). To find $\varepsilon_i = g_3 - \bar{g}_3$

it is necessary to derive an equation for the secant passing through the points $(x_1, \bar{g}_1)$ and $(x_2, \bar{g}_2)$, and to determine g_3 from this equation. Then, using the parabolic equation (13), we substitute in the expression for ε_i the magnitudes $\bar{g}_1$, g_2, g_3 by g_0 and l_0. As a result we obtain

$$\varepsilon_i = g_0[(ax_1 + x_1^2) - (a + 2x_1)x_3 + x_3^2].$$

In this expression the variables are the arbitrarily selected points x_1 in the range (0,2) and the point x_3, in the range (x_1, x_2). In order to obtain the value ε_{im}, it is necessary first of all to find the mean integral value ε_i^2 in the range $x_1 \leqslant x_3 \leqslant x_1 + a$. Dispensing with laborious calculations, we give the final result

$$\varepsilon_{im}^2 = \frac{1}{30} g_0^2 a^4, \tag{15}$$

where a should be measured in fractions of l_0, since in deriving the parabolic equation (13) it was assumed that $l_0 = 1$.

In view of the fact that the results of integration along x_3 were not dependent on x_1, the relationship (15) will also determine the required value of ε_{im}.

2. *Deriving the Relationship* $\delta_{im} = \delta_{im}(\bar{g}, a, p)$ — Let two neighbouring isoanomalies of gravity have abscissae x_3 and $x_4 = x_3 + d$ (Fig. 4). We find the expression

$$\delta_i = (g_4 - g_3) - (\bar{g}_4 - \bar{g}_3),$$

where $(g_4 - g_3)$ is the cross-section of the isoanomalies;

$(\bar{g}_4 - \bar{g}_3)$ is the actual difference in the values of gravity at the points with abscissae corresponding to the two adjacent isoanomalies.

Here (as in the derivation of the value δ_{0m}) there can be two cases; both points (x_3 and x_4) lie in the range (x_1, x_2); the point x_3 lies in the range (x_1, x_2) and the point x_4 outside this range. The values of δ_i will be different for these cases.

The position of the points x_3 and x_4 for the first case supposes that $0 \leqslant d \leqslant a$; this position is represented in Fig. 4. For this case

$$\delta_i = g_0 d[(d - a - 2x_1) + 2x_3].$$

Squaring both sides of this expression and integrating for x_3 in the limits $x_1 \leqslant x_3 \leqslant x_1 + a - d$, we obtain

$$\delta_{im}^2 = \frac{1}{3} g_0^2 d^2 (a - d)^2. \tag{16}$$

Here also, the result of integrating for x_3 was not dependent on x_1; therefore it is the required value δ_{im}.

The position of the points for the second case, which is not given in Fig. 4, presupposes that $a \leqslant d \leqslant 2a$. For this case the following expression can be obtained for δ_{im}:

$$\delta_{im}^2 = \frac{1}{3} g_0^2 (a-d)^2 (2a-d)^2 \tag{17}$$

On the right-hand sides of formulae (11), (12), (16) and (17) there is the value d. It can easily be seen that

$$\frac{d}{a} = \frac{p}{\Delta_{10}}, \tag{18}$$

where Δ_{10} is the increase in gravity between two neighbouring points of observations. We determine $\Delta_{10} = \Delta_{10}(\bar{g}, a)$.

As above, we will seek this expression for the gravity curve in an approximate parabola passing through three points. Since the positive branch of the curve $\bar{g}(x)$, shown in Fig. 4, is identical in form to its negative branch, to find the mean integral value of $\Delta_{10}^2 = (\bar{g}_2 - \bar{g}_1)^2$ it is sufficient to take the range of integration from 0 to 2 (remembering that l_0 is taken equal to unity).

Here there can be two cases: (a) both points of observation (x_1 and x_2) lie within the limits of the positive branch of the curve $\bar{g}(x)$; (b) the point x_1 is within the limits of the positive branch while the point x_2 is in the limits of the negative branch (this case is not shown on Fig. 4). The values of Δ_{10} will be different for these cases. We will designate these values by $(\Delta_{10})_1$ and $(\Delta_{10})_2$, respectively. Dispensing with the intermediate calculations, we obtain:

for $0 \leqslant x_1 \leqslant 2-a$

$$(\Delta_{10}^2)_1 = g_0^2 a^2 [(2-a) - 2x_1]^2,$$

for $2-a \leqslant x_1 \leqslant 2$

$$(\Delta_{10}^2)_2 = g_0^2 [(8-6a+a^2) + 2(a-4)x_1 + 2x_1^2]^2.$$

The required average integral value of the form Δ_{10}^2 in the range $0 \leqslant x_1 \leqslant 2$ will be equal to half the sum of the following integrals:

$$\Delta_{10}^2 = \frac{1}{2}\left[\int_0^{2-a} (\Delta_{10}^2)_1 \, dx_1 + \int_{2-a}^{2} (\Delta_{10}^2)_2 \, dx_1\right].$$

Omitting the laborious calculations, we give the final result:

$$\Delta_{10}^2 = \frac{1}{15} g_0^2 a^2 (20 - 5a^2 + a^3), \tag{19}$$

where a is given in fractions of l_0.

In formula (18), replacing the value of Δ_{10} by its mean square value from equation (19), we obtain

$$\frac{d}{a} = \frac{p}{\Delta_{10}} = \frac{p\sqrt{15}}{g_0 a\sqrt{20 - 5a^2 + a^3}}. \tag{20}$$

We now find the value g_m—which is the average value of gravity for one extreme point. Using the parabolic equation (13), we obtain

$$g_m = \frac{g_0}{2} \int_0^2 (2x - x^2)\, dx = \frac{2}{3} g_0. \tag{21}$$

From formulae (10) and (21) we find

$$E_{0m}^2 = \frac{\varepsilon_{0m}^2}{g_m^2} = 1.5 \frac{\sigma^2}{g_0^2}. \tag{22}$$

From formulae (15) and (21) we find

$$E_{lm}^2 = \frac{\varepsilon_{lm}^2}{g_m^2} = 0.075\, a^4. \tag{23}$$

For the error in determining the gravity increments there will be two groups of formulae:

(1) $0 \leqslant d \leqslant a$ or on the basis of formula (18) $0 \leqslant p \leqslant \Delta_{10}$.

From the equations (11) and (20)

$$D_{0m}^2 = \frac{\delta_{0m}^2}{p^2} = \frac{\sigma^2}{\Delta_{10}^2} \left(2 - \frac{p}{\Delta_{10}}\right). \tag{24}$$

From the equations (16) and (20)

$$D_{lm}^2 = \frac{\delta_{lm}^2}{p^2} = \frac{g_0^2 a^4}{3\Delta_{10}^2} \left(1 - \frac{p}{\Delta_{10}}\right)^2. \tag{25}$$

(2) $\Delta_{10} \leqslant p \leqslant 2\Delta_{10}$.

From the equations (12) and (20)

$$D_{0m}^2 = \frac{\sigma^2}{3p^2} \left[4 - \left(2 - \frac{p}{\Delta_{10}}\right)^3\right]. \tag{26}$$

The relationship (26) can be represented approximately (with an error $\leqslant 8\%$) also in the following form:

$$D_{0m}^2 = 1.167 \frac{\sigma^2}{p^2}.$$

From formulae (17) and (20)

$$D_{im}^2 = \frac{g_0{}^2 a^4}{3\Delta_{10}^2} \left(\frac{\Delta_{10}}{p} - 1 \right)^2 \left(2 - \frac{p}{\Delta_{10}} \right)^2.$$

Finally, substituting in the equation (8) the values E_{0m} and E_{im} from formulae (22) and (23), we obtain

$$E_m^2 = 0.075 a^4 + 1.5 \frac{\sigma^2}{g_0{}^2}.$$

In the same way, substituting in equation (9) the values D_{0m} and D_{im} from the formulae (24) and (25) or (26) and (28), we obtain:
for the case $0 \leqslant p \leqslant \Delta_{10}$

$$D_m^2 = \frac{g_0{}^2 a^4}{3\Delta_{10}^2} \left(1 - \frac{p}{\Delta_{10}} \right)^2 + \frac{\sigma^2}{\Delta_{10}^2} \left(2 - \frac{p}{\Delta_{10}} \right); \tag{30}$$

for the case $\Delta_{10} \leqslant p \leqslant 2\Delta_{10}$

$$D_m^2 = \frac{g_0{}^2 a^4}{3\Delta_{10}^2} \left(\frac{\Delta_{10}}{p} - 1 \right)^2 \left(2 - \frac{p}{\Delta_{10}} \right)^2 + \frac{\sigma^2}{3p^2} \left[4 - \left(2 - \frac{p}{\Delta_{10}} \right)^3 \right]. \tag{31}$$

In all the formulae, a is given in fractions of l_0.

The formulae (29) and (30) or (31) are the most general. They establish the dependence between the seven variable values: the elements of the field (g_0, l_0), the parameters of the survey (a, σ, p) and the indices of the relative accuracy of the map (E_m, D_m). Knowing any five of them, it is possible to find the other two. The most typical in practice can be the following cases.

1. The elements of the field (g_0, l_0) and all the parameters of the survey (a, σ, p) are given. It is required to find the indices of accuracy (E_m and D_m) of the survey.

2. The elements of the field (g_0, l_0), the indices of accuracy of the work (E_m, D_m) and the value σ are given. It is required to find the network density a and the cross-section of the isoanomalies p of the planned survey.

3. The values g_0, l_0, E_m, D_m and p are given. It is required to determine the network density a of the planned investigation and the accuracy of the values of gravity at the consecutive points of observation σ.

To speed up the calculations, graphs and nomograms can be compiled. Some of them are given in this arcticle. We will give a brief description of them.

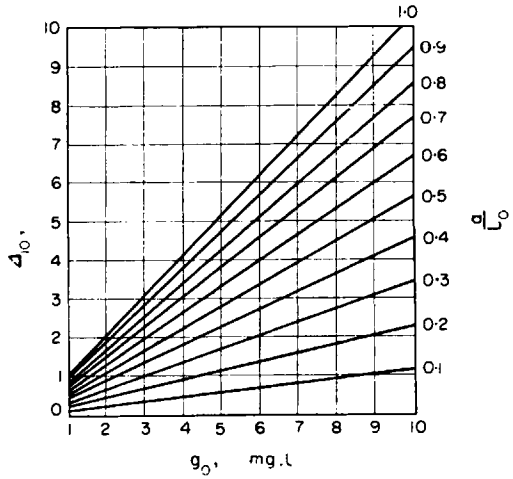

FIG. 5.

The nomogram for the relationship (19) serves to determine Δ_{10} as a function of g_0 and the ratio $\frac{a}{l_0}$, which is a variable parameter (Fig. 5).

The nomogram for the relationship (22) serves to determine E_{0m} as a function of σ and g_0, which is a parameter (Fig. 6).

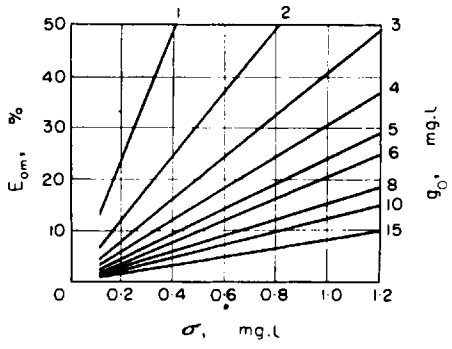

FIG. 6.

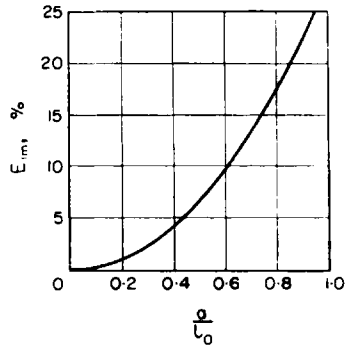

FIG. 7.

The graph for the relationship (23) makes it possible to determine the value E_{im} as a function of $\frac{a}{l_0}$ (Fig. 7).

The nomograms for the relationship (24) establishes the connection between D_{0m} and $\frac{\sigma}{p}$ for the variable parameter $\frac{\Delta_{10}}{p}$ (Fig. 8). In order to obtain

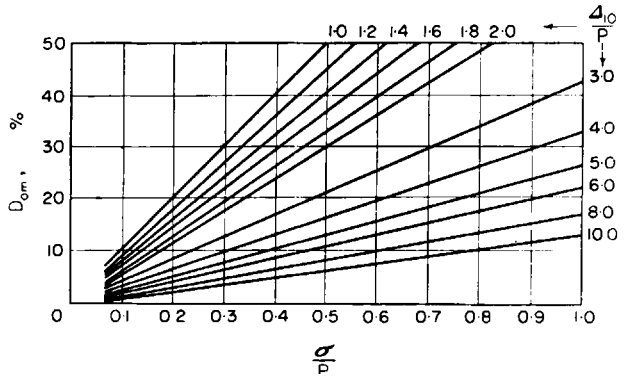

FIG. 8.

this relationship, the right-hand side of the relationship (24) must be multiplied and divided by p^2.

The nomograms for the dependences (25) and (28) serve to determine D_{im}, as a function of $\frac{\Delta_{10}}{p}$, for the variable parameter $\frac{a}{l_0}$ (Figs. 9 and 10).

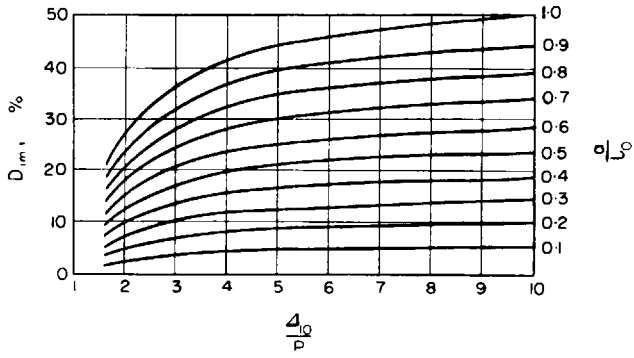

FIG. 9.

To derive these relationships in the right-hand sides of formulae (25) and (28), Δ_{10}^2 must be replaced by its value from formula (19). The nomogram (Fig. 9) is used for $0 \leqslant p \leqslant \Delta_{10}$, the nomogram (Fig. 10). – for $\Delta_{10} \leqslant p \leqslant 2\Delta_{10}$.

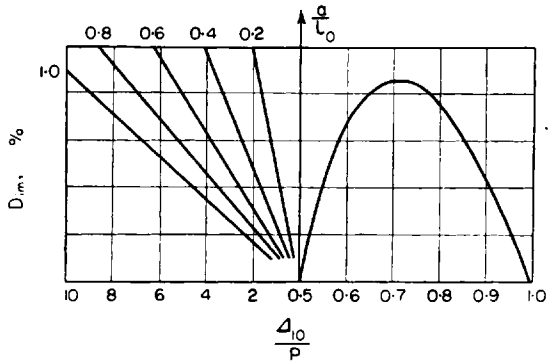

FIG. 10.

To determine the total error E_m as a function of $\frac{a}{l_0}$ and $\frac{\sigma}{g_0}$ according to formula (29) the nomogram of Fig. 11 is used.

To determine the total error D_m for the condition $0 \leqslant p \leqslant \Delta_{10}$ according to formula (30) two nomograms are given (Figs. 12 and 13): the first for

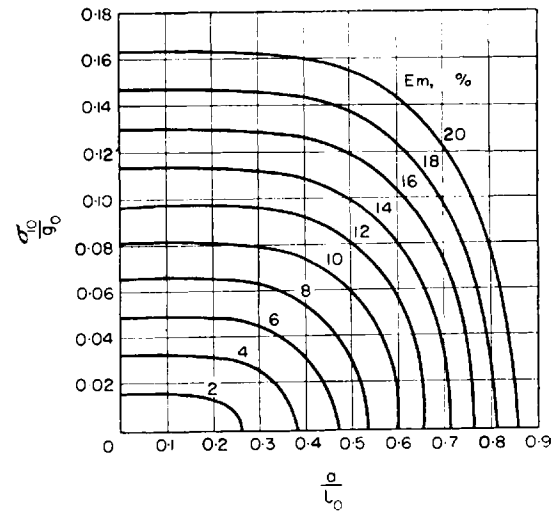

FIG. 11.

$E_m = 10\%$ and the second for $E_m = 15\%$. To compare these nomograms in formula (30), σ should be replaced by its value from formula (29).

All the nomograms are drawn for the case $\frac{a}{l_0} \leqslant 1$, i.e. supposing that within the limits of one extreme point of gravity there are not less than two points of observation. It was also supposed that $\frac{g_0}{p} \geqslant 2$; observations of this inequality require that each extreme point is mapped by not less than two isoanomalies.

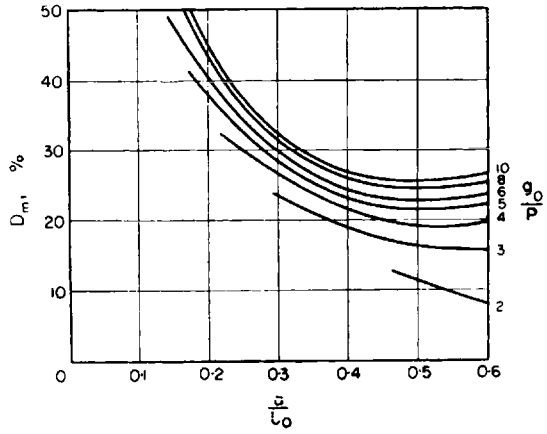

FIG. 12.

It is difficult to find from the nomogram (Fig. 11), for a given E_m, values of $\frac{\sigma}{g_0}$ for large values of $\frac{a}{l_0}$ or small values of $\frac{a}{l_0}$ for any values of $\frac{\sigma}{g_0}$. It is also difficult to find from given values of D_m and $\frac{g_0}{p}$ a value of $\frac{a}{l_0}$ from the nomograms (Fig. 12) for $\frac{a}{l_0} > 0.4$ and from the nomogram (Fig. 13) for $\frac{a}{l_0} > 0.5$.

The reason lies not in any defects of the nomogram or formulae, from which they were calculated, but in the very nature of the formation of total errors of the field and errors of the increment of gravity between two isoanomalies. Since the errors E_m and D_m are made up of errors in the observations and interpolations for certain relationships between the elements of the field and the parameters of the surveys, the values of the separate parameters

become variable. For example, with increase in the network density (i.e. with decrease in the ratio $\frac{a}{l_0}$) the value of D_{0m} increases, at the same time the value D_{im} decreases, as a result of which the total error D_m can remain unchanged. The value E_{0m} with decrease in $\frac{a}{l_0}$ does not change, and E_{im} decreases. By increasing the value of σ, which causes an increase in E_{0m}, it

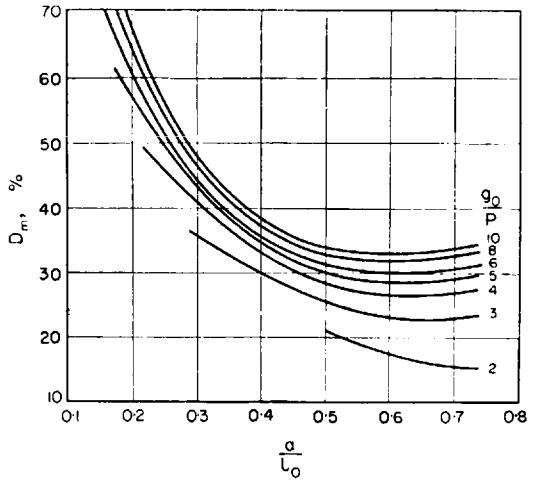

FIG. 13.

is possible to keep the total error E_m at the previous level. Thus, for certain relationships between the parameters it is possible to find a number of pairs of values for σ and $\frac{a}{l_0}$, for which the values of the total errors E_m and D_m are maintained practically unchanged. Larger values of $\frac{a}{l_0}$ will correspond to the smaller values of σ, and vice versa. The corresponding pair of values of σ and $\frac{a}{l_0}$ is selected in accordance with technical and economic considerations.

EXPERIMENTAL CHECKS OF FORMULAE

The obtained relationships were checked in a number of theoretical examples. We will give the results of checking one of the more complicated examples.

The field $\bar{g}(x)$ was given along the profile in the form of a smooth curve having maxima and minima. The absolute values of gravity at the maxima and minima, and also the linear dimensions of the latter varied considerably. The length of the profile was 195 km, the total number of extreme points—50. The obtained values $g_0 = 4.5$ mgal, $l_0 = 1.95$ km.

Later, on the profile were fixed the "observation points" with 2 km interval (i.e. for each extreme point there was an average of two observations). A certain error was ascribed to each observation. The values of the errors obeyed the normal law, their distribution between the observation

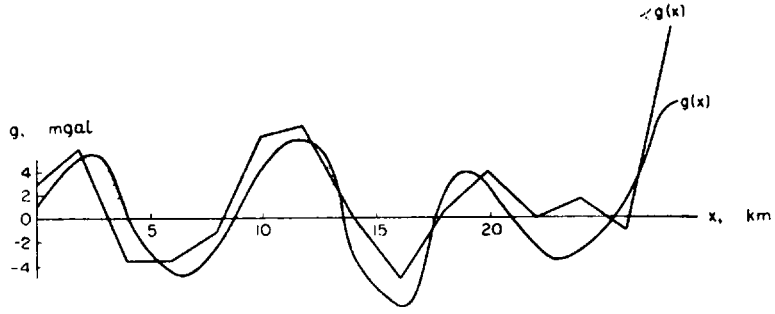

FIG. 14.

points being random. The mean square error in the values of gravity at the observation points was $\sigma = \pm 2.58$ mgal. A linear interpolation was caried out between the observation points and the errors were calculated. The errors in the gravity increment between two isoanomalies were calculated for the case $p = 2$. The results of the comparison of the measured values of the errors with their theoretical values, obtained from the formulae, are given in Tables 1 and 2. By way of illustration, Fig. 14 gives a part of the experimental profile.

A check was also made of formula (19). Measurements were made along the profile of the first differences Δ_{10} for different values of a and the

TABLE 1. MEAN SQUARE ERROR IN VALUES OF THE FORCE OF GRAVITY

Mean quadratic value	Number of measurements	Actual mgal	Theoretical		Error %
			Actual mgal	Formula	
ε_{0m}	297	$\pm$ 2.19	$\pm$ 2.11	(10)	4
ε_{im}	297	$\pm$ 0.81	$\pm$ 0.86	(15)	6
ε_m	297	$\pm$ 2.22	$\pm$ 2.27	(6)	2

TABLE 2. MEAN SQUARE ERROR OF THE INCREASE IN THE FORCE OF GRAVITY BETWEEN NEIGHBOURING ISOANOMALIES (SECTION OF THE ISOANOMALIES 2 mgal)

Mean quadratic value	Number of measurements	Actual mgal	Theoretical		Error %
			Actual mgal	Formula	
δ_{0m}	—	—	± 1.36	(11)	—
δ_{im}	177	± 0.79	± 0.66	(16)	16
δ_m	177	± 1.38	± 1.51	(7)	9

mean square values Δ_{10} were determined. The results obtained in comparison with the theoretical values of Δ_{10}, found from formula (19), are given in Table 3.

The example considered is extremely unfavourable, since the "observed" field was obtained with a very sparse network and the adopted mean square observational error very large.

TABLE 3. THE MEAN SQUARE VALUES OF THE FIRST DIFFERENCES IN Δ_{10} FOR VARIOUS DISTANCES BETWEEN THE OBSERVATION POINTS

a, (km)	Number of observations	Mean quadratic values		Error
		Actual	Theoretical	
0.5	207	1.37	1.30	5
1.0	180	2.80	2.60	8
1.5	117	4.00	3.70	8
2.0	90	5.00	4.75	5

Despite this, as shown by the data of the sixth columns of Tables 1 and 2 and the fifth column of Table 3, the results of checking the theoretical relationships were very good. For a field with a denser network of observations and with a smaller value of the mean square error in the force of gravity for consecutive points, the comparison between theory and practice should give results which, given a sufficient number of tests, will agree still more closely.

On the whole, the experimental check showed that the proposed method for determining the errors in the gravity field, from the point of view of the obtained accuracy, is suitable for use in practice.

SOME EXAMPLES

We give several examples of the use of the derived relationships for determining the accuracy of gravimetric surveys made by production concerns.

1. The gravimetric survey of the Shar'insk party No. 23/53 in the north-eastern part of the Moscow synclinal basin in 1953 (R. F. VOLODARSKII).

The aim of the work was to study regional tectonics. The area of the survey was 7200 km², the number of the coordinate points was 674. The points were distributed sufficiently evenly within the limits of the area of work. From the value of the area S and the number of points N, using the formula

$$a = 1.138 \frac{\sqrt{S}}{\sqrt{N-1}}, \tag{32}$$

which we give without derivation*, we will determine the mean distance between the observation points. It is equal to 3.9 km. The mean square error in the observation $\sigma = \pm 0.62$ mgal.

The map with a cross-section of isoanomalies every 2 mgal was drawn to a scale of 1:200,000. Furthermore, in the calculation use was made of a compound map of the area of work by the 20/53, 21/53, and 23/53 parties with the same cross-section of isoanomalies to a scale of 1:500,000. Using this map, which covered a much larger area than the calculation map, we find the average amplitude and the linear dimensions of the anomaly: $g_0 = 9.5$ mgal and $l_0 = 15.5$ km. All further calculations will be made on the assumption that the error in calculation of ± 0.62 mgal characterizes the error in the value of gravity at a consecutive point, since for the survey under consideration the remaining errors are small.

The results of the calculations are given in Table 4, which also gives calculations for a less dense network of observations: in the second line for a, it is doubled, and in the third line, it is trebled in comparison with its actual value.

With increase in a the value E_{0m} remains constant, as it should do. The values of E_{im} and E_m increase with increase in a. The value D_{0m} with increase

TABLE 4. ACCURACY OF GRAVIMETRIC SURVEY SHAR'INSK PARTY NO. 23/53

Given					Calculated						
g_0	l_0	a	σ	p	Δ_{10}	E_{0m}	E_{im}	E_m	D_{0m}	D_{im}	D_m
9.5	15.5	3.9	$\pm$ 0.62	2	2.7	8	2	8	25	4	25
9.5	15.5	7.8	$\pm$ 0.62	2	5.3	8	7	11	16	17	23
9.5	15.5	11.7	$\pm$ 0.62	2	7.7	8	16	18	11	31	33

* The formula is derived with the assumption that the points are distributed over a square network. When the points are not on a square network, this formula gives results with an error not greater than 5–6%.

in a decreases rather significantly (from 25 to 11%), the value D_{im} increases sharply (from 4 to 31%). As a result, the value of the total mean square error for gravity increment between neighbouring isoanomalies D_m varies very little. It appears that with reduction in the network density by a half the value of E_m increases only by 3% of the actual, and the value D_m becomes even less than the actual. In other words, this reduction in the network had practically no effect on the accuracy of the survey (of the determined value E_m) and would somewhat increase the accuracy of the map of the gravity isoanomalies. R. F. VOLODARSKII, the author of the report considered, also came to the conclusion of the desirability for reducing the network density for this type of survey. He showed this conclusively by reducing the density network of a survey which had already been carried out and by reconstructing the map for the gravity isoanomalies with the new smaller density network.

2. The gravimetric survey of the Atlymsk party No. 7 (55–32) 55–56 in the region of Western Siberia in 1955–1956 (A. A. SERZHANT).

The aim of this work was to carry out geotectonic mapping of the area and to find local gravitational anomalies within its limits. The author observes that this was the first gravimetric survey to be carried out in this region, there was, therefore, no information on possible dimensions and intensity of local anomalies.

The area of the survey was 7100 km^2, and there were 1849 coordinate points. Consecutive observation points were placed on profiles, the point-intervals being 1 km. and the profile-intervals 4 km. The mean square error in the values of gravity at the consecutive points was ± 0.50 mgal. The map with a cross-section of isoanomalies for every 2 mgal was drawn to a scale of 1:200,000. On the map there were several large anomalies of the force of gravity with value $g_0 = 5$ mgal and $l_0 = 10$ km. Furthermore, there are doubtful indications of the anomalies of smaller dimensions and amplitudes for which it can be assumed that $g_0 = 2$–2.5 mgal and $l_0 = 5$ km (values of g_0 and l_0 in both cases are determined from a very small number of anomalies).

Since the point-intervals differ considerably from the profile-intervals, it is desirable to calculate the accuracy of the survey individually for different values of a. In the first line of Table 5 there are the actual values for the relative errors for large anomalies in a direction perpendicular to the profiles, i.e. for a equal to 4 km. In the second and third lines there are the errors for a equal to 2 and 6 km.

The data of Table 5 show that with decrease in the point-intervals from 4 to 2 km, the error in the observed field E_m decreases by about 1%. This is

explained by the fact that for the considered field with $a = 4$ km, the error in the linear interpolation E_{im} is very small. As regards the error E_{0m}, connected with the observational errors, it does not depend on the point-intervals. As a result, the decrease in the value of a has practically no effect on the value of the total error in the field E_m. The position is different with errors in the gravity increments. Here, as a result of a certain increase in the error D_{0m}, there was also an increase in the total error D_m (from 24 to 27%). With further decrease in the point-intervals, value of E_m is maintained at practically the same level, and the value of D_m can only increase.

TABLE 5. ACCURACY OF GRAVIMETRIC SURVEY ATLYMSK PARTY No. 7 (55—32) 55—56

Given					Calculated						
g_0	l_0	a	σ	p	Δ_{10}	E_{0m}	E_{im}	E_m	D_{0m}	D_{im}	D_m
5	10	4	± 0.50	2	2.3	12	4	13	24	1	24
5	10	2	± 0.50	2	1.1	12	1	12	27	1	27
5	10	6	± 0.50	2	3.4	12	10	16	17	12	21

In the third line (for $a = 6$ km) the value of E_m increases very little, and D_m decreases. A comparison of the figures in the second and third lines shows that to determine the anomalies characterized by the parameters $g_0 = 5$ and $l_0 = 10$ km, the value $a = 6$, and not 2 km is the most favourable. The network of observations taken is therefore extremely dense, and this increased density had very little effect on increasing the accuracy of the observed field and at the same time somewhat reduced the accuracy of the determination for the increase in the force of gravity between the neighbouring isoanomalies. In practice, of course, this decrease in accuracy need not happen, since in tracing the isoanomalies it is usual to carry out a certain smoothing of the values for the force of gravity at the points of the observations, as a result of which the effect of random errors is reduced. However, this smoothing cannot be represented numerically, and therefore we do not take it into account.

TABLE 6. DETERMINING THE PARAMETERS OF THE SURVEY AS FUNCTIONS OF THE ELEMENTS OF THE FIELD AND ACCURACY OF THE SURVEY

Given					Calculated	
g_0	l_0	p	E_m	D_m	a(km)	σ(mgal)
2.5	5	0.5	15	29	2.6	±0.26
2.5	5	0.5	15	29	3.6	±0.12

In the report it is mentioned that the anomalies which were very small in their dimensions and amplitudes and which are unreliably indicated on the map, are also of geological interest. Table 6 gives values for a and σ, ensuring a reliable determination of this type of anomaly with parameters $g_0 = 2.5$ mgal and $l_0 = 5$ km with the condition that the isoanomalies are carried out every 0.5 mgal and the relative errors in the gravity field and gravity increments between the neighbouring isoanomalies are equal to 15 and 29% respectively. Table 6 gives two pairs of extreme values of a and σ, each of which satisfies the requirements. This example shows that the same problem of determining anomalies with a given accuracy and a given cross-section of anomalies in some cases can have a different technical and economic solution.

The values of a and σ in Table 6 are found from the nomograms (Figs. 11 and 13).

Table 7 gives separately the observational and interpolational errors for this case, as found on the appropriate graphs.

It follows from the preceding that the proposed method of finding errors from the parameters of an accomplished survey, or of determining the parameters of a planned survey from adopted errors, requires in both cases a knowledge of the field g_0 and l_0. At the planning stage of an investigation, this requirement can always be fulfilled, since the main problem of gravimetric exploration is to determine the anomalies. Consequently, their

TABLE 7.

Given					Calculated				
g_0	l_0	a	σ	p	Δ_{10}	E_{0m}	E_{im}	D_{0m}	D_{im}
2.5	5	2.6	$\pm$ 0.26	0.5	1.5	13	7	23	18
2.5	5	3.6	$\pm$ 0.12	0.5	2.0	6	14	8	28

parameters can be given at the beginning. In the majority of cases, this method can be used to determine the accuracy of the finished work, since the observed field is usually non-linear. Frequently, in regional surveys the field does not have closed anomalies. However, if the curves for the change in the force of gravity along arbitrary profiles cutting the map have even only relative extreme points, this is sufficient for determining g_0 and l_0. In connection with this it should be stated that the field factors should be determined along the profiles of the arbitrary directions in those cases where the field is represented by clearly mapped maxima and minima of gravity.

Much less frequently there are cases of linear or near-linear fields, having points of inflection but no extreme points. For these fields, g_0 and l_0 cannot be determined. In these cases, keeping to the framework of the proposed method, only negative conclusions can be drawn from the results. Let us assume that the parameters of the survey under consideration. $\sigma = 0.6$ mgal, $a = 6$ km and $p = 2$ mgal from the nomograms (Figs. 11 and 13) we find that such a survey makes it possible to determine anomalies characterized by the values $g_0 = 11.8$ mgal and $l_0 = 8.5$ km with an accuracy of $E_m = 15\%$ and $D_m = 30\%$. However, there are no such anomalies on the map, consequently they do not exist in actual fact. Given other indices of accuracy, we find the new values of g_0 and l_0, etc. With regard to the actual accuracy of this survey, another method of determination should be used. This method is based on the use of the first and second order differences Δ_{10} and Δ_2 as gravity field characteristics.

SUMMARY

In planning the work, a considerable problem is the selection of the values of E_m and D_m since they determine the parameters of the survey. These values should obviously be different for detailed and regional or exploratory surveys. It is difficult, however, to give actual figures for any of these forms of survey. After studying certain production data, the author came to a preliminary conclusion that for regional and exploratory surveys, the values $E_m = 15\%$ and $D_m = 25 + 30\%$ give quite reliable results. However, with respect to the regional and exploratory surveys, these requirements are too high. Let us consider in particular, the data of the experimental example. The survey parameters in this example are exceptionally unfavourable. As a result, the relative errors are very large, being $E_m = 50\%$ and $D_m = 69\%$. Despite this, of the 50 extreme points of the true field, only 5 points were not noticed in the observed field. All the remaining extreme points, although distorted in their shape and amplitude, are reliably differentiated on the observed curve. Consequently, if the survey is only required to give localization of anomalies, at the planning stage the values of E_m and D_m can be considerably increased. To solve this problem finally, it is necessary to analyse a large amount of the actual material, as was done by the author.

At the start of the article, a mention was made of the method of evaluating the accuracy of the survey according to the value of the mean square error in the force of gravity at the observation points, and on the method for determining the cross-sections of the isoanomalies according

to the value of this error. After analysing the errors, it is useful to consider the errors introduced by the classical criteria and to compare them with the criteria E_m and D_m suggested by the author.

The value σ gives the objective error in accuracy for the whole run of a survey, including both the gravimetric and geodesic measurements, the processing of the observations, the introduction of corrections, etc. However, the value of this error does not make it possible to draw conclusions on the accuracy of the observed field ε_m which, depending on the network density and the character of the field, can have higher or lower values than σ. Thus, the "σ criterion" is essential but not sufficient to evaluate the quality of the observed gravity field.

It follows from the preceding that the evaluation of the accuracy of the field from the value σ is replaced by the evaluation from the value ε_m or E_m, thus bearing in mind the parameters of the survey σ and a, and also the character of the field g_0 and l_0.

The second criterion, which is determined by the inequality $p \geqslant 2.5\ \sigma$, does not take into account either the network density or the character of the field, and is not adequate for either of these reasons. We have replaced it by the criterion $\delta_m = D_m p$. In particular, for the recommended value $D_m = 30\%$, we obtain $p = 3.3\ \delta_m$. This condition means that the map of the gravity isoanomalies will have practically no sections where the error in the gravity increment between two neighbouring isoanomalies would be equal to the cross-section of the isoanomalies.

Although a preliminary test of the proposed method with theoretical examples and with actual material gave sufficiently reliable results, in later practical use of this method, in some cases difficulties might be encountered and individual faults discovered, which have not been mentioned by the author. The future problems will be to check this method and for this purpose the cooperation of production workers will be required.

The author thanks K. E. VESELOV, A. M. LOZINSKII, L. V. PETROV and N. N. PUZYREV for valuable advice and comments made during a discussion of the present article.

REFERENCES

1. B. A. ANDREEV, *Calculation of a Network of Observations in Gravimetric Work.* Documents of Ts. NIGRI. Geofizika, Collection 5, ONTI NKTP SSSR, (1938).
2. YU. D. BULANZHE, Some problems in the method of gravimetric work. *Appl. Geophysics*, No. 1, Gostoptekhizdat, (1945).
3. R. F. VOLODARSKII, Some problems of a gravimetric survey. *Survey and Industrial Geophysics*, No. 11. Gostoptekhizdat, (1954).

4. N.P. GRUSHINSKI, Establishing a rational density of points and the required accuracy in determining the anomalies of the force of gravity in gravimetric surveys. *Survey and Industrial Geophysics*, No. 15. Gostoptekhizdat, (1956).
5. P. I. LUKAVCHENKO, Determining the density of a survey network in gravimetric and magnetic survey. *Survey and Industrial Geophysics*, No. 4, Gostoptekhizdat, (1952).
6. A. K. MALOVICHKO, The density and form of the network in an area survey with gravimetry. *Survey and Industrial Geophysics*, No. 15. Gostoptekhizdat, (1957).
7. N. N. PUZYREV, The connection between the density of the observation network and the cross-section of the geophysical maps. *Applied Geophysics*, No. 18. Gostoptekhizdat, (1957).

CHAPTER 7

THEORETICAL BASES OF ELECTRICAL PROBING WITH AN APPARATUS IMMERSED IN WATER

E. I. TEREKHIN

MARKED successes have been achieved recently in the development of electrical prospecting at sea. A method has been developed for the production of continuous two-way dipole axial probes with a distance between the centres of the dipoles of up to 6–8 km, with sea depths of up to 50–60 m (O. V. NAZARENKO).

In this method, during measurements the feeding and measuring dipoles are situated at the bottom of the sea, i.e. at the lower boundary of the first layer. With the same geoelectrical cross-section, the values of the apparent resistance measured with the sea-bottom apparatus differ from the values of apparent resistance measured with the same apparatus on the surface of the water. The solution of the problem of distribution of the field of a point source, within the limits of the first layer, and in particular at its lower boundary, is therefore of practical interest.

The problem of the distribution of potential for a point source of current at the lower boundary of the first layer of a three-layer horizontally homogeneous medium was first solved in 1934 by M. YA. SAMOILOV. Based on this solution, in the same period in the Geophysical Section of the AzNII certain theoretical curves were calculated and published later, without a derivation of formulae, in a book by S. YA. LITVINOV [6]. These include the two-layer curves with $\varrho_2/\varrho_1 = 1, 2, 5, 10, 40\ \infty$, three-layer curves for the case $\varrho_3/\varrho_1 = 1.5$, $\varrho_2/\varrho_1 = 1, 2, 5, 10, 40, \infty$ and $h_2/h_1 = 2, 5, 10, 40$.

In the general case of a horizontally homogeneous stratified medium, the problem of the distribution of the field of a point source at the boundary of separation of the first and second layers, was solved by L. L. VAN'YAN [3].

In this paper two-layer curves are given for the AMNB apparatus and the dipole axial apparatus and three-layer curves for the AMNB apparatus for the case $\varrho_3 = \infty$, $h_2 = h_1$ and various values of ϱ_2/ϱ_1.

In the article by V. V. BURGSDORF [2], a solution of the problem of distribution of a field for the most general case, with an arbitrary placing of the electrode in a horizontally stratified medium is given in an integral form.

Of practical interest for electrical prospecting at sea and in other expanses of water, is the case where the source of current and the measuring apparatus are placed at a certain depth within the limits of the water layer or, in a special case, at the bottom of the water.

The present paper gives a developed solution of the problem of distribution of the field of a point source situated within the limits of the first layer of a horizontally stratified medium and, as a special case, a point source situated at the lower boundary of the first layer.

The paper gives expressions for the apparent resistance for a number of instruments placed at the bottom of the water. From these formulae, calculations of the theoretical curve for electrical probing at sea were made. In one of the sections details are given of methods of calculation used for the theoretical curves of probing at sea, and also an evaluation of the accuracy of the calculations.

THE FIELD OF A POINT SOURCE AT THE BOUNDARY OF SEPARATION OF THE FIRST AND SECOND LAYERS

The main problem in electrical probing is to determine the depth of various layers of the section differing in resistance.

One of the main methods of interpreting probe curves is to compare them with specially calculated theoretical curves. To calculate these curves, the character of distribution of the field created by the point source of current should be known.

Let us assume a horizontally homogeneous stratified medium. Let 0, 1, 2, 3, ..., n be the orders of the layers (from the top downwards) h_0, h_1, h_2, ..., h_{n-1} be the thicknesses of the layers covering the supporting level and ϱ_0, ϱ_1, ϱ_2, ..., ϱ_n be the specific electrical resistances of the various layers.

Thus, the upper layer (in this case the water layer) has a zero number and thickness h_0 and specific resistance ϱ_0 respectively.

The current source A of strength I is placed in the upper layer at a certain depth $z_0 < h_0$ from the surface.

The potential at the point M, arbitrarily placed in the conducting semispace at a distance R from the current source, is expressed by the following

functions:

$$U_0 = \frac{I\varrho_0}{4\pi}\frac{1}{R} + U_0', U_1 = U_1', U_2 = U_2', \ldots, U_n = U_n'. \quad (1)$$

These functions are partial integrals of the Laplace equation

$$\Delta^2 U = 0.$$

To solve the problem we use the Laplace equation in a cylindrical system of coordinates. The origin of this system we put at the point A, the axis z is put vertically downwards.

The problem has axial symmetry with respect to the z axis, the Laplace differential equation in this case, does not therefore depend on the angle φ, placed in a horizontal plane, and has the following form:

$$\frac{\partial^2 U}{\partial r^2} + \frac{1}{r}\frac{\partial U}{\partial r} + \frac{\partial^2 U}{\partial z^2} = 0.$$

The potential functions U_0, U_1, U_2, ..., U_n, apart from the fact that they should be integrals of the Laplace equation, should satisfy the following conditions.

1. The functions U_0', U_1, U_2, U_3, ..., U_n should be finite at the points situated at a finite distance from the source of the current and change to zero for points an infinite distance away.

2. When $R \to 0$

$$U_0 \to \frac{I\varrho_0}{4\pi}\frac{1}{R}.$$

3. For each boundary of separation there should not be jumps in the potential and the normal components of current density should be equal, i.e.

$$U_i = U_{i+1} \text{ and } \frac{1}{\varrho_i}\frac{\partial U_i}{\partial z} = \frac{1}{\varrho_{i+1}}\frac{\partial U_{i+1}}{\partial z}.$$

4. At the boundary of separation of water—air, the normal component of the current density should be zero, i.e.

$$\frac{1}{\varrho_0}\frac{\partial U_0}{\partial z}\bigg|_{z=-z_0} = 0.$$

The solution of the Laplace differential equation is obtained by the known method of dividing variables. A general integral of the equation is the expression

$$U = \int_0^\infty [\bar{B}e^{mz} I_0(mr) + \bar{A}e^{-mz} I_0(mr)]\, dm. \quad (2)$$

Representing $\frac{I\varrho_0}{2\pi}$ by q, the potential at any point of the upper layer can be expressed thus:

$$U_0 = \frac{q}{2\sqrt{r^2+z^2}} + \int_0^\infty \bar{B}_0 e^{mz} I_0(mr)\,dm + \int_0^\infty \bar{A}_0 e^{-mz} I_0(mr)\,dm \qquad (3)$$

or, using the Weber-Lipshitz formula for negative values of z

$$\frac{1}{\sqrt{r^2+z^2}} = \int_0^\infty e^{mz} I_0(mr)\,dm,$$

at points in the upper layer above the electrode A, i.e. at points for which $z < 0$, we obtain

$$U_0\Big|_{z<0} = \frac{1}{2}\int_0^\infty e^{mz} I_0(mr)\,dm + \int_0^\infty \bar{B}_0 e^{mz} I_0(mr)\,dm +$$

$$+ \int_0^\infty \bar{A}_0 e^{-mz} I_0(mr)\,dm, \qquad (4)$$

and

$$\frac{\partial U_0}{\partial z}\Big|_{z<0} = \frac{1}{2} q \int_0^\infty m e^{mz} I_0(mr)\,dm + \int_0^\infty m\bar{B}_0 e^{mz} I_0(mr)\,dm -$$

$$- \int_0^\infty m\bar{A}_0 e^{-mz} I_0(mr)\,dm.$$

According to the condition (4) $\frac{\partial U_0}{\partial z}\Big|_{z=z_0} = 0$, since in general $\varrho_0 \neq 0$ and $\varrho_0 \neq \infty$.

Consequently, for all values of r

$$\int_0^\infty \left[\frac{1}{2} q e^{-mz_0} + \bar{B}_0 e^{-mz_0} - \bar{A}_0 e^{mz_0}\right] m I_0(mr)\,dm = 0.$$

Since $m \neq 0$, then

$$\frac{1}{2} q e^{-mz_0} + \bar{B}_0 e^{-mz_0} - \bar{A}_0 e^{mz_0} = 0,$$

hence

$$\bar{A}_0 = \left(\bar{B}_0 + \frac{1}{2} q\right) e^{-2mz_0}. \tag{6}$$

Considering the value of the coefficient $\bar{A}_0$, we write the expression for the potential in the upper medium

$$U_0 = \frac{1}{2} q \frac{1}{\sqrt{r^2 + z^2}} +$$

$$+ \frac{1}{2} q \int_0^\infty [e^{-m(2z_0+z)} + \bar{B}_0 (1 + e^{-2m(z_0+z)}) e^{mz}] I_0(mr)\, dm. \tag{7}$$

At any point lying below the origin of the coordinates, i.e. at any point with $z \geqslant 0$, to express the potential we have the following formulae:

$$U_0 = \int_0^\infty \left[\frac{1}{2} q(1 + e^{-2mz_0}) e^{-mz} + \bar{B}_0 (1 + e^{-2m(z_0+z)}) e^{mz}\right] I_0$$

$$U_1 = \int_0^\infty (\bar{B}_1 e^{mz} + \bar{A}_1 e^{-mz}) I_0(mr) dm; \tag{7'}$$

$$U_2 = \int_0^\infty (\bar{B}_2 e^{mz} + \bar{A}_2 e^{-mz}) I_0(mr) dm;$$

. . . . . .

$$U_{n-1} = \int_0^\infty (\bar{B}_{n-1} e^{mz} + \bar{A}_{n-1} e^{-mz}) I_0(mr) dm;$$

$$U_n = \int_0^\infty \bar{A}_n e^{-mz} I_0(mr) dm.$$

Where $\bar{B}_n = 0$, since when $z \to \infty$ $e^{mz} \to \infty$, which contradicts the first condition of the problem.

To find the values of the fuctions $U_0, U_1, U_2, \ldots, U_n$, it is necessary to determine the coefficients $\bar{A}_i$ and $\bar{B}_i$.

Using the boundary conditions we write the system of equations:

$$
\begin{aligned}
&\bar{B}_0(1+e^{-2mh_0})-\bar{B}_1-\bar{A}_1 e^{-2m(h_0-z_0)} = \\
&\quad = -\frac{1}{2} q(1+e^{-2mz_0}) e^{-2m(h_0-z_0)} \\
&\frac{1}{\varrho_0}\bar{B}_0(1-e^{-2mh_0})-\frac{1}{\varrho_1}\bar{B}_1+\frac{1}{\varrho_1}\bar{A}_1 e^{-2m(h_0-z_0)} = \\
&\quad = \frac{q}{2\varrho_0}(1+e^{-2mz_0}) e^{-2m(h_0-z_0)} \\
&\bar{B}_1+\bar{A}_1 e^{-2m(h_0+h_1-z_0)}-\bar{B}_2-\bar{A}_2 e^{-2m(h_0+h_1-z_0)} = 0 \\
&\frac{1}{\varrho_1}\bar{B}_1-\frac{1}{\varrho_1}\bar{A}_1 e^{-2m(h_0+h_1-z_0)}-\frac{1}{\varrho_2}\bar{B}_2+ \\
&\quad +\frac{1}{\varrho_2}\bar{A}_2 e^{-2m(h_0+h_1-z_0)} = 0 \\
&\bar{B}_2+\bar{A}_2 e^{-2m(h_0+h_1+h_2-z_0)}-\bar{B}_3-\bar{A}_3 e^{-2m(h_0+h_1+h_2-z_0)} = 0 \\
&\quad \cdots\cdots\cdots\cdots\cdots\cdots\cdots\cdots \\
&\bar{B}_{n-1}+\bar{A}_{n-1} e^{-2m\left(\sum_{i=0}^{n-1} h_i-z_0\right)}-\bar{A}_n e^{-2m\left(\sum_{i=0}^{n-1} h_i-z_0\right)} = 0 \\
&\frac{1}{\varrho_{n-1}}\bar{B}_{n-1}-\frac{1}{\varrho_{n-1}}\bar{A}_{n-1} e^{-2m\left(\sum_{i=0}^{n-1} h_i-z_0\right)}+ \\
&\quad +\frac{1}{\varrho_n}\bar{A}_n e^{-2m\left(\sum_{i=0}^{n-1} h_i-z_0\right)} = 0
\end{aligned}
\qquad (8)
$$

These expressions form a system of linear heterogeneous equations. The solution of this system of equations with respect to $\bar{A}_i$ and $\bar{B}_i$ makes it possible to determine the final expressions for the potential functions.

In practice we are interested in the distribution of potential only in the upper medium; it is therefore quite sufficient to find the value of only one coefficient B_0. This system of equations can be solved by the Kramer formulae. In a general form we have

$$\bar{B}_0 = q\frac{\bar{M}}{\bar{\Delta}}, \qquad (9)$$

where $\bar{\Delta}$ is the determinant composed of coefficients for unknowns $(\bar{B}_i, \bar{A}_i)$, of a system of equations, and $\bar{M}$ is a determinant obtained from $\bar{\Delta}$ by replacing

the numbers of the first column by terms in the right hand side of the equations.

(9a)

$$\Delta = \begin{vmatrix} 1+e^{D} & -1 & -e^{F} & 0 & 0 & \dots & 0 & 0 & 0 \\ \frac{1}{\varrho_0}(1-e^{D}) & -\frac{1}{\varrho_1} & \frac{1}{\varrho_1}e^{F} & 0 & 0 & \dots & 0 & 0 & 0 \\ 0 & 1 & e^{L} & -1 & -e^{L} & \dots & 0 & 0 & 0 \\ 0 & +\frac{1}{\varrho_1} & \frac{1}{\varrho_1}e^{L} & -\frac{1}{\varrho_2} & \frac{1}{\varrho_2}e^{L} & \dots & 0 & 0 & 0 \\ \dots & \dots & \dots & \dots & \dots & \dots & \dots & \dots & \dots \\ 0 & 0 & 0 & 0 & 0 & \dots & 1 & e^{Q} & -e^{Q} \\ 0 & 0 & 0 & 0 & 0 & \dots & \frac{1}{\varrho_{n-1}} & \frac{1}{\varrho_{n-1}}e^{Q} & \frac{1}{\varrho_n}e^{Q} \end{vmatrix}$$

where $D = -2mh_0$;

$$F = -2m(h_0 - z_0);$$

$$L = -2m(h_0 + h_1 - z_0);$$

$$Q = -2m\left(\sum_{i=0}^{n-1} h_i - z_0\right).$$

Removing from the sign of the determinant Δ the general factor e^{2mz_0}, we obtain:

$$\Delta = e^{-2mnz_0}\Delta, \tag{10}$$

where

$$\Delta = \begin{vmatrix} 1+e^{D} & -1 & -e^{D} & 0 & 0 & \dots & 0 & 0 & 0 \\ \frac{1}{\varrho_0}(1-e^{D}) & -\frac{1}{\varrho_1} & \frac{1}{\varrho_1}e^{D} & 0 & 0 & \dots & 0 & 0 & 0 \\ 0 & 1 & e^{R} & -1 & -e^{R} & \dots & 0 & 0 & 0 \\ 0 & \frac{1}{\varrho_1} & \frac{1}{\varrho_1}e^{R} & -\frac{1}{\varrho_2} & \frac{1}{\varrho_2}e^{R} & \dots & 0 & 0 & 0 \\ \dots & \dots & \dots & \dots & \dots & \dots & \dots & \dots & \dots \\ 0 & 0 & 0 & 0 & 0 & \dots & 1 & e^{U} & -e^{U} \\ 0 & 0 & 0 & 0 & 0 & \dots & \frac{1}{\varrho_{n-1}} & \frac{1}{\varrho_{n-1}}e^{U} & \frac{1}{\varrho_n}e^{U} \end{vmatrix}$$

Similarly, for $\bar{M}$ we obtain:

$$\bar{M} = \frac{1}{2}(1 + e^{-2mz_0})\, e^{2m(n+1)z_0} M, \tag{11}$$

where $M =$

$$\begin{vmatrix} -qe^D, -1, & -e^D, & 0, 0, \ldots, 0, & 0, \\ -\frac{1}{\varrho_0} e^D, \frac{1}{\varrho_1}, & \frac{1}{\varrho_1} e^D, & 0, 0, \ldots, 0, & 0, \\ 0, 1, & e^R, & -1, -e, \ldots, 0, & 0, \\ , \frac{1}{\varrho_1}, & \frac{1}{\varrho_1} e^R, & -\frac{1}{\varrho_2}, \frac{1}{\varrho_2} e^R, \ldots, 0, & 0, \\ \cdots\cdots\cdots\cdots & \cdots\cdots & \cdots\cdots\cdots & \cdots\cdots \\ 0, 0, 0, & 0, 0, & \ldots, 1, & e^U, \\ 0, 0, 0, & 0, 0, & \ldots, \frac{1}{\varrho_{n-1}}, & \frac{1}{\varrho_{n-1}} e^U, \end{vmatrix} \quad \begin{matrix} 0 \\ 0 \\ 0 \\ 0 \\ \cdots \\ -e^U \\ \frac{1}{\varrho_n} e^U \end{matrix}$$

where $\begin{cases} D = -2_{mh_0}; \\ R = -2m(h_0 + h_1); \\ U = -2m \sum_{i=0}^{n-1} h_i. \end{cases}$

It is known that $B_1 = \frac{M}{\Delta}$ is a coefficient which enters the expression for the potential function when the current source is at the earth—air boundary [5]. Therefore, the desired coefficient, corresponding to an arbitrary placing of the current source within the limits of the first stratum, can be expressed by the expressions for the coefficient B_1 [8] which we know for any number of layers:

$$\bar{B}_0 = \frac{q}{2}(1 + e^{2mz_0}) B_1, \tag{12}$$

where $B_1 = \frac{P_n(e^{-2mh})}{Q_n(e^{-2mh})}$ is a fraction, in the numerator and denominator of which are the polynomials of the power p_{n-1} from the variable e^{-2mh}.

Substituting the expression $\bar{B}_0$ in the formula for the potential with an arbitrary placing of the source and the point of measurement in the upper layer (7), we have

$$U_0 = \frac{1}{2} q \frac{1}{\sqrt{r^2 + z^2}} + \frac{1}{2} q \int_0^\infty [e^{-m(2z_0 + z)} + B_1(e^{mz} + e^{-mz}) + \\ + B_1(e^{m(2z_0 + z)} + e^{-m(2z_0 + z)})]\, I_0(mr)\, dm. \tag{13}$$

The obtained expression is basic, being the most general integral expression of potential for an arbitrary position of the current source and the point of observation within the limits of the upper layer.

When working with the method of electrical sonde, the apparatus is always placed horizontally, consequently in formula (13) we can put $z = 0$:

$$U_0 = \frac{q}{2r} + \frac{1}{2} q \int_0^\infty [e^{-2mz_0} + 2B_1 + B_1 (e^{2mz_0} + e^{-2mz_0})] I_0 (mrd)\, m. \quad (14)$$

Let us suppose that the thicknesses of the individual layers h_0, h_1, h_2, ..., h_{n-1} have a general measurement, which we can represent by h such that

$$h_0 = p_0 h,\ h_0 + h_1 = p_1 h,\ h_0 + h_1 + h_2 = p_2 h,\ \ldots,\ \sum_{i=0}^{n-1} h_i = p_{n-1} h,$$

where $p_0, p_1, p_2, \ldots, p_{n-1}$ are whole numbers.

The function

$$B_1 = \frac{P_n (g)}{Q_n (g)},$$

where $g = e^{-2mh}$ is a rational fraction which can be split up into a series in increasing powers of g by dividing the polynomial in the numerator by the polynomial in the denominator. In a general form we have

$$B_1 = \sum_{n=1}^{\infty} q_n e^{-2mnh},$$

where q_n = the coefficients of emission.

Substituting the expression for the coefficient B_1 in formula (14) we obtain

$$U_0 = \frac{q}{2r} + \frac{1}{2} q \int_0^\infty e^{-2mz_0} I_0(mr)\, dm + q \sum_{n=1}^{\infty} q_n \int_0^\infty e^{-2mnh} I_0(mr)\, dm +$$

$$+ \frac{1}{2} q \sum_{n=1}^{\infty} q_n \int_0^\infty e^{-2mnh} (e^{2mz_0} + e^{-2mz_0}) I_0(mr)\, dm, \quad (15)$$

Using the Weber–Lipshitz formula, we obtain an expression with which it is possible to calculate directly the potential at points on one level with

the source of the field within the limits of the first layer:

$$U_0 = \frac{I\varrho_0}{4\pi}\left[\frac{1}{r} + \frac{1}{\sqrt{r^2+4z_0^2}} + 2\sum_{n=1}^{\infty}\frac{q_n}{\sqrt{r^2+(2nh)}} + \right.$$

$$\left. + \sum_{n=1}^{\infty} q_n\left(\frac{1}{\sqrt{r^2+4(nh-z_0)^2}} + \frac{1}{\sqrt{r^2+4(nh+z_0)^2}}\right)\right]. \qquad (16)$$

In a special case for an apparatus placed at the bottom of the water we have

$$z_0 = h_0$$

and

$$U_0 = \frac{I\varrho_0}{4\pi}\left[\frac{1}{r} + \frac{1}{\sqrt{r^2+4h_0^2}} + 2\sum_{n=1}^{\infty}\frac{q_n}{\sqrt{r^2+(2nh)^2}} + \right.$$

$$\left. + \sum_{n=1}^{\infty} q_n\left(\frac{1}{\sqrt{r^2+4(nh-h_0)^2}} + \frac{1}{\sqrt{r^2+4(nh+h_0)^2}}\right)\right]. \qquad (17)$$

If we consider the obtained formula from the point of view of the theory of reflection, then it can be readily seen that when the source of the field is at the boundary of the first and second conducting layers, the distribution of the fictitious reflected sources is complicated in comparison with the case where the source is at the surface of the conducting semispace.

When the source of the field is at a certain depth, the symmetry is lost in the location of the fictitious sources with respect to the real source, reflected sources of equal power appear at different distances ($\sqrt{r^2+(2nz_0)^2}$, $\sqrt{r^2+4(nh-z)^2}$ and $\sqrt{r^2+4(nh+z_0)^2}$ from the point of measurement of the potential. The formation of these fictitious sources is connected with the presence of a boundary of separation with a coefficient of reflection $K = 1$ (the water–air boundary), which does not pass through the actual current source.

AN EXPRESSION FOR THE APPARENT SPECIFIC RESISTANCE FOR AN APPARATUS AT THE BOTTOM OF THE WATER

The apparent resistance is a complex function, depending both on the parameters of the geoelectrical cross-section and on the mutual disposition of the feeding and receiving electrodes of the apparatus. It is calculated from the formula

$$\bar{\varrho} = K\frac{\Delta U}{I}, \qquad (17a)$$

where K is an instrumental coefficient (the apparatus placed at the water surface) determined for the condition that in a homogeneous medium, the value of $\bar{\varrho}$ is equal to the true specific resistance of this medium.

If this condition is also taken as a basis of determining the coefficient for instrument at the bottom, then the coefficient of the bottom apparatus will depend not only on the geometrical dimensions of the latter but also on the relative depth of its immersion.

It can readily be shown that in the general case of 4-electrode symmetry of the apparatus, immersed to a depth h, the coefficient K_M can be expressed in the following way:

$$K_M = K \frac{2\left[\left(\frac{r}{h}\right)^2 + 4\right]}{2\left(\frac{r}{h}\right)^2 + 4}.$$

Since $K_M = MK$, where

$$M = \frac{2\left[\left(\frac{r}{h}\right)^2 + 4\right]}{2\left(\frac{r}{h}\right)^2 + 4},$$

depends only on $\frac{r}{h}$, the shape of the curves obtained experimentally and theoretically changes in exactly the same way if, for these and others, the coefficient K is used instead of K_M.

Under working conditions it is more convenient to use the coefficient K instead of K_M, since the values of K for various types of apparatus are calculated and given in nomograms. In calculating the theoretical curves for sea probing with an apparatus at the bottom, the change in the coefficient of the apparatus on being immersed to the bottom was therefore not taken into consideration.

We represent the apparent resistance, measured by the bottom apparatus, as $\bar{\varrho}_M$ (without correcting the coefficient of the immersed apparatus). The apparent specific resistance of the $AMNB$ apparatus for $MN \to 0$ is determined from the formula

$$\bar{\varrho} = 2\pi r^2 \frac{E}{I}.$$

We find

$$E = -\frac{\partial U}{\partial r} = \frac{I\varrho_0}{4\pi}\left[\frac{1}{r^2} + \frac{r}{(r^2+4h_0^2)^{3/2}} + 2\sum_{n=1}^{\infty} q_n \frac{r}{[r^2+(2nh)^2]^{3/2}}\right] +$$

$$+ \sum_{n=1}^{\infty} q_n \left[\frac{r}{[r^2+4(nh+h_0)^2]^{3/2}} + \frac{r}{[r^2+4(nh-h_0)^2]^{3/2}}\right], \tag{18}$$

hence

$$\bar{\varrho}_M = \frac{1}{2}\varrho_0\left[1 + \frac{r^3}{(r^2+4h_0^2)^{3/2}} + 2\sum_{n=1}^{\infty} q_n \frac{r^3}{[r^2+(2nh)^2]^{3/2}} +\right.$$

$$\left. + \sum_{n=1}^{\infty} q_n \left(\frac{r^3}{[r^2+4(nh+h_0)^2]^{3/2}} + \frac{r^3}{[r^2+4(nh-h_0)^2]^{3/2}}\right)\right]. \tag{19}$$

Representing $\dfrac{\left(\dfrac{r}{h}\right)^3}{\left[\left(\dfrac{r}{h}\right)^2 + 4_i^2\right]^{3/2}}$, the so-called coefficient of recession of the symmetrical apparatus $AMNB$, by l_i^c, we finally obtain

$$\bar{\varrho}_M = \frac{1}{2}\varrho_0\left(1 + 2\sum_{n=1}^{\infty} q_n l_n{}^c\right) +$$

$$+ \frac{1}{2}\varrho_0\left[l_{p_0}{}^c + \sum_{n=1} q_n (l_{n+p_0}^c + l_{n-p_0}^c)\right]. \tag{20}$$

To obtain an expression for the apparent specific resistance for a bottom radial apparatus, we use the known relationship [1]

$$\varrho_r = \bar{\varrho} - \frac{r}{2}\frac{\partial \varrho}{\partial r}.$$

Representing by $\bar{\varrho}_{rM}$ the apparent specific resistance of a radial apparatus at the bottom of the water, without considering the change in the coefficient of the apparatus during immersion, we obtain

$$\bar{\varrho}_{rM} = \bar{\varrho}_M - \frac{r}{2}\cdot\frac{\partial \bar{\varrho}_M}{\partial r}. \tag{21}$$

After substituting and simple conversions we have

$$\bar{\varrho}_{r_M} = \frac{1}{2}\varrho_0\left[1+2\sum_{n=1}^{\infty} q_n \frac{r^3(r^2-2n^2h^2)}{[r^2+4n^2h^2]^{5/2}}\right] + \frac{1}{2}\varrho_0\left\{\frac{r^3(r^2-2h^2_0)}{[r^2+4h_0^2]^{5/2}} + \right.$$

$$\left. + \sum_{n=1}^{\infty} q_n\left[\frac{r^3[r^2-2(nh+h_0)^2]}{[r^2+4(nh+h_0)^2]^{5/2}} + \frac{r^3[r^2-2(nh-h_0)^2]}{[r^2+4(nh-h_0)^2]^{5/2}}\right]\right\} \tag{22}$$

Representing here $\dfrac{\left(\dfrac{r}{2h}\right)^3\left[\left(\dfrac{r}{2h}\right)^2-\dfrac{i^2}{2}\right]}{\left[\left(\dfrac{r}{2h}\right)^2+i^2\right]^{5/2}} = l_i^r$ as the coefficient of recession of the radial apparatus, we obtain a formula similar to the formula for the symmetrical $AMNB$ apparatus:

$$\bar{\varrho}_{r_M} = \frac{1}{2}\varrho_0\left[1+2\sum_{n=1}^{\infty} q_n l_n^r\right] + \frac{1}{2}\varrho_0\left[l^r_{p_0} + \sum_{n=1}^{\infty} q_n(l^r_{n-p_0} + l^r_{n+p_0})\right]. \tag{23}$$

It can be readily shown that for any other arrangement (quadrilateral, perpendicular, etc.) at the bottom of the water, the general form of the formula for the apparent specific resistance will not differ from the expressions obtained, but only the coefficients of recession will change. Thus, in general we have

$$\bar{\varrho}_M = \frac{1}{2}\varrho_0\left(1+2\sum_{n=1}^{\infty} q_n l_n\right) + \frac{1}{2}\varrho_0\left[l_{p_0} + \sum_{n=1}^{\infty} q_n(l_{n-p_0} + l_{n+p_0})\right]. \tag{24}$$

Let us consider the asymptotic values of $\bar{\varrho}_M$. For this we suppose that $\frac{r}{h_0} \to \infty$, and since $h_0 \geqslant h$, then $\frac{r}{h} \to \infty$, in this case $(l_{n-p_0} + l_{n+p_0}) \to 2l_n$, and $l_{p_0} \to 1$, and consequently, $\bar{\varrho}_M \to \varrho_0\,(1+2\sum_{n=1}^{\infty} q_n l_n) = \bar{\varrho}$, i.e. with sufficiently large operating distances r in comparison with the depth of immersion, the apparent resistance measured with this apparatus will not differ from the value of the apparent resistance which would be obtained if a similar apparatus of these dimensions were placed at the water surface.

Assuming that $\frac{r}{h} \to 0$ and also $\frac{r}{h_0} \to 0$, we find that all coefficients of

recession tend to zero; except l_{n-p_0}, which is 1 when $n = p_0$. Therefore in this case

$$\bar{\varrho}_M \to \frac{1}{2}\varrho_0 + \frac{1}{2}\varrho_0 q_{p0}.$$

From [7] it is known that

$$q_{p0} = k_0,$$

where k_0 is the coefficient of reflection at the first boundary of separation:

$$k_0 = \frac{\varrho_1 - \varrho_0}{\varrho_1 + \varrho_0}.$$

Substituting the value of q_{p0} in expression $\bar{\varrho}_M$ for $\frac{r}{h} \to 0$, we find that

$$\bar{\varrho}_M \to \frac{1}{2}\varrho_0(1 + k_0) = \frac{\varrho_0\varrho_1}{\varrho_0 + \varrho_1}.$$

Thus, on the left part, the probe curves obtained by the apparatus at the bottom have a horizontal asymptote $\bar{\varrho} = \frac{\varrho_0\varrho_1}{\varrho_0 + \varrho_1}$, since the curves obtained by an apparatus at the surface would have an asymptote ϱ_0.

Let us consider certain special cases of geoelectrical sections.

(a) Under the water layer let there be an electrically homogeneous medium stretching to an infinite depth. In this case $p_0 = 1$ and $q_n = k^n$ where k is the coefficient of reflection.

The general formula for apparent resistance obtained by an apparatus at the bottom of the water becomes

$$\bar{\varrho}_M = \frac{1}{2}\varrho_0\left(1 + 2\sum_{n=1}^{\infty} k^n l_n\right) + \frac{1}{2}\varrho_0\left(l_1 + \sum_{n=1}^{\infty} k^n l_{n-1} + \sum_{n=1}^{\infty} k^n l_{n+1}\right).$$

After certain simple conversions we finally obtain for a two-layer medium

$$\bar{\varrho}_M = \frac{1}{2}\varrho_0(1 + k)\left[1 + \frac{1 + k}{k}\sum_{n=1}^{\infty} k^n l_n\right]. \tag{25}$$

In practice (from the point of view of interpreting field material) this case is not of particular interest although this expression is undoubtedly of theoretical interest.

(b) In the case of a multi-layered medium, when the thickness of the layer of water is a general measure of the thicknesses of the underlying

layers ($p_0 = 1$), the expression (24) for the apparent resistance for an apparatus at the bottom becomes:

$$\varrho_M = \frac{1}{2}\varrho_0\left(1+2\sum_{n=1}^{\infty} q_n l_n\right) + \frac{1}{2}\varrho_0\left[l_1+\sum_{n=1}^{\infty} q_n(l_{n-1}+l_{n+1})\right]. \quad (26)$$

CALCULATIONS OF THE THEORETICAL CURVES OF SEA PROBING

With the formulae obtained, a calculation was made for two-layer and three-layer theoretical probe curves with an apparatus at the bottom of the water.

The theoretical curves for probing with an apparatus both at the surface and at the bottom of the water correspond to the equation

$$\frac{\bar{\varrho}}{\varrho_0} = f\left(\frac{\varrho_1}{\varrho_0}, \frac{\varrho_2}{\varrho_0}, \ldots, \frac{h_1}{h_0}, \frac{h_2}{h_0}, \ldots, \frac{r}{h_0}\right),$$

where r is the operating distance of the apparatus;

$$\frac{\varrho_1}{\varrho_0} = \mu_1, \frac{\varrho_2}{\varrho_0} = \mu_2, \ldots, \frac{h_1}{h_0} = \nu_1, \frac{h_2}{h_0} = \nu_2 \ldots$$

are the parameters of the geoelectrical section.

The theoretical probing curves are drawn on a double logarithmic scale as the values for the dependence of $\frac{\bar{\varrho}}{\varrho_0}$ on $\frac{r}{h_0}$, the remaining parameters ($\mu_1, \mu_2, \ldots, \nu_1, \nu_2 - \ldots$) for each curve are constant values. The parameters of the calculated curves were selected to correspond with the parameters of three-layer theoretical curves of the Schlumberger charts and curves calculated at the GSGT, taking into account the features of the section, the upper layer of which is the sea-water.

For a two-layer section the following values were selected for μ_1: 11/9, 3/2, 13/7, 7/3, 3, 4, 17/3, 7, 9, 19, 39, 99 and ∞. The curves with $\mu < 1$ were not calculated since in practice the water always has a lower resistance than that of the underlying medium.

For the three-layer section the following parameters were chosen:

$$\frac{\varrho_2}{\varrho_0} = \infty, \left(\frac{\varrho_1}{\varrho_0}\right)^2, \left(\frac{\varrho_1}{\varrho_0}\right)^{3/2}, \left(\frac{\varrho_1}{\varrho_0}\right)^{1/2}, 1;$$

$$\frac{\varrho_1}{\varrho_0} = {}^3/_2, {}^7/_3, 4, 9, 19, 39;$$

$$\frac{h_1}{h_0} = 1, 2, 3, 5, 9, 24.$$

Furthermore, for $\frac{\varrho_2}{\varrho_0} = \infty$ curves were calculated with $\frac{h_1}{h_0} = 1/5$, 1/3, and 1/2. The curves with $\frac{\varrho_2}{\varrho_0} = 0$ were not calculated for a three-layer section since this case is not of practical interest for geoelectrical sections with an upper layer of high conductivity. All curves were calculated both for the symmetrical *AMNB* apparatus and for the dipole axial apparatus. Thus, the total volume of calculated material was 420 curves combined according to the variable parameter $\frac{\varrho_1}{\varrho_0}$ into 68 graphs.

All these graphs were published in 1956 by the All-Union Research Institute for Geophysical Methods of Prospecting (VNII Geofizika), as a collection of theoretical curves for sea probing.

According to the new notation of theoretical probing curves adopted in the NIGGR in 1956, all curves corresponding to the bottom position of the apparatus are given the letter *M* ("morskie" — sea), at the beginning of the number, and the number of curves calculated for a radial (dipole axial) apparatus have the letter *P*. The variable parameter for which the graph is prepared is designated by the letter *c* ("Soprotivlenie" — the resistance, of the upper layer under the water) or *m* ("moshchnost" — the thickness, of this layer), and the relative values of the attached parameters of the section are shown by numbers. Thus, the graph $M-c-1/5-c^2$ means that it contains the theoretical curves of probing with the symmetrical *AMNB* apparatus at the boundary of the first and second layers; the resistance of the second stratum $\frac{\varrho_1}{\varrho_0}$ being different for different curves (it is named for each curve), its thickness constituting 1/5 of the thickness of the upper layer, and finally, the resistance of the underlying medium being $\left(\frac{\varrho_1}{\varrho_0}\right)^2$.

As is known [7], the theoretical probe curves in a general form are calculated from the formula

$$\frac{\bar{\varrho}}{\varrho_0} = 1 + 2\sum_{n=1}^{\infty} q_n l_n, \tag{27}$$

where q_n is a function depending only on the ratios of the resistances and the thicknesses of the various levels and the serial number n;

l_n is a function depending only on the size of the apparatus and the serial number n.

For instruments at the boundary of separation of the first and second layers, this formula becomes somewhat complex.

Let us consider first a two-layered medium. In this case the problem of the calculation of the theoretical curves is solved most simply. From equation (27) we obtain

$$\sum_{n=1}^{\infty} q_n l_n = \frac{1}{2}\left(\frac{\bar{\varrho}}{\varrho_0} - 1\right).$$

Having substituted the value for the series $\sum_{n=1}^{\infty} q_n l_n$ in the expression (25). we obtain the following after simple conversions:

$$\bar{\varrho}_M = \varrho_0 \left[\frac{\mu}{\mu+1} + \frac{\mu^2}{\mu^2-1}\left(\frac{\bar{\varrho}}{\varrho_0} - 1\right)\right], \tag{28}$$

bearing in mind that $k = \dfrac{\mu-1}{\mu+1}$.

From this formula, which has the coordinates of the two-layer curves for an apparatus at the surface, it is easy, without additional summation, to calculate the coordinates of the corresponding two-layer curves for an apparatus at the bottom of the water.

For a three-layer section, the formulae for the apparent resistance of a bottom apparatus cannot be brought to a form suitable for simple conversion and the calculation of the three-layer curves for a bottom apparatus requires an additional summation of infinite series.

A certain part of the curves, i.e. the curves with $\dfrac{\varrho_2}{\varrho_0} = \infty$ and $\dfrac{h_1}{h_0} = 1/5$, 1/3, 1/2, 1, 2, 3, 5 were calculated by the method of splitting up the function B into simple fractions. This method was proposed by S. STEFANESKO and has been further developed in a number of papers [5, 7, 8, 9].

The essence of this method is as follows. If the underlying medium has a very high ($\varrho_n = \infty$) or a very low ($\varrho_n = 0$) specific electrical resistance, then the function

$$B_1 = \frac{P_n(e^{-2mh})}{Q_n(e^{-2mh})}$$

for such sections can be represented in the form of the sum of elementary fractions.

Thus, for $\varrho_n = \infty$

$$B_1 = b_1 \frac{e^{-2mh}}{1-e^{-2mh}} + b_2 \frac{-e^{-2mh}}{1+e^{-2mh}} + \\ + \sum_{j=3}^{\frac{1}{2}(p_{n-1}+2)} b_j \frac{k_j' e^{-2mh} - e^{-4mh}}{1-2k_j' e^{-2mh} + e^{-4mh}}, \tag{29}$$

if p_{n-1} is an even number.

If p_{n-1} is an odd number, then

$$B_1 = b_1 \frac{e^{-2mh}}{1-e^{-2mh}} + \sum_{j=3}^{\frac{1}{2}(p_{n-1}+3)} b_j \frac{k_j' e^{-2mh} - e^{-4mh}}{1-2k_j' e^{-2mh} + e^{-4mh}}. \tag{30}$$

In these expressions the functions $\frac{e^{-2mh}}{1-e^{-2mh}}$ and $\frac{-e^{-2mh}}{1+e^{-2mh}}$ correspond to a two-layer section with $\varrho_2 = \infty$ and $\varrho_2 = 0$, and the functions of the form $\frac{k_j' e^{-2mh} - e^{-4mh}}{1-2k_j' e^{-2mh} + e^{-4mh}}$ correspond to a three-layer section, when the two layers of equal thickness with resistances ϱ_j^1 and ϱ_{j-1}^1 (the coefficient of reflection k_j') lie on the underlying medium of infinite conductivity ($\varrho_3 = 0$).

From (8) it is known that the function $\frac{k_j' e^{-2mh} - e^{-4mh}}{1-2k_j' e^{-2mh} + e^{-4mh}}$ can be represented in the form of the series $\sum_{n=1}^{\infty} e^{-2mh} \cos n\varphi$, where $\varphi = \arccos k_j'$.

The functions $\frac{e^{-2mh}}{1-e^{-2mh}}$ and $\frac{-e^{-2mh}}{1+e^{-2mh}}$ can also be represented in the form of the series:

$$\frac{e^{-2mh}}{1-e^{-2mh}} = \sum_{n=1}^{\infty} e^{-2mh},$$

$$\frac{-e^{-2mh}}{1+e^{-2mh}} = \sum_{n=1}^{\infty} (-1)^n e^{-2mh}.$$

Let there be a geoelectrical n-layer cross-section, where at a relative depth p_{n-1} there is a medium with zero conductivity ($\varrho_n = \infty$).

If we consider the potential of a point source of current at the boundary of intersection of the first and second layers, then for this boundary of

intersection, according to formula (14), we obtain

$$U_0 = \frac{I\varrho_0}{4\pi}\left[\frac{1}{r} + \int_0^\infty e^{-2mh_0} I_0(mr)\,dm + 2\int_0^\infty B_1 I_0(mr)\,dm + \right.$$

$$\left. + \int_0^\infty B_1(e^{-2mh_0} + e^{2mh_0})\, I_0(mr)\,dm\right].$$

Let p_{n-1} be an even number. Then, using formula (31) and the corresponding expressions for elemental fractions as a series, we obtain:

$$U_0 = \frac{I\varrho_0}{4\pi}\left\{\frac{1}{r} + 2\int_0^\infty \left(b_1 \sum_{n=1}^\infty e^{-2mnh} + b_2 \sum_{n-1}^\infty (-1)^n e^{-2mnh} + \right.\right.$$

$$+ \sum_{j=3}^{\frac{1}{2}(p_{n-1}+2)} b_j \sum_{n=1}^\infty e^{-2mnh}\cos n\varphi\Big) I_0(mr)\,dm + \int_0^\infty e^{-2mh_0} I_0(mr)\,dm +$$

$$+ \int_0^\infty \left[b_1 \sum_{n=1}^\infty e^{-2mnh}(e^{-2mh_0} + e^{2mh_0}) + \right.$$

$$+ b_2 \sum_{n=1}^\infty (-1)^n e^{-2mnh}(e^{-2mh_0} + e^{2mh_0}) +$$

$$\left.\left. + \sum_{j=3}^{\frac{1}{2}(p_{n-1}+2)} b_j \sum_{n=1}^\infty e^{-2mnh}\cos n\varphi\,(e^{-2mh_0} + e^{2mh_0})\right] I_0(mr)\,dm\right\}.$$

Using the Weber–Lipshitz formula, we obtain

$$U_0 = \frac{I\varrho_0}{4\pi}\left[\frac{1}{r} + 2\left(b_1 \sum_{n=1}^\infty \frac{1}{\sqrt{r^2 + (2nh)^2}} + b_2 \sum_{n=1}^\infty \frac{(-1)^n}{\sqrt{r^2 + (2nh)^2}} + \right.\right.$$

$$+ \sum_{j=3}^{\frac{1}{2}(p_{n-1}+2)} b_j \sum_{n=1}^\infty \frac{\cos n\varphi_j'}{\sqrt{r^2 + (2nh)^2}}\Big) + \frac{1}{\sqrt{r^2 + (2h_0)^2}} +$$

$$+ b_1 \sum_{n=1}^\infty \left(\frac{1}{\sqrt{r^2 + (2nh - 2h_0)^2}} + \frac{1}{\sqrt{r^2 + (2nh + 2h_0)^2}}\right) +$$

$$+b_2\sum_{n=1}^{\infty}(-1)^n\left(\frac{1}{\sqrt{r^2+(2nh-2h_0)^2}}+\frac{1}{\sqrt{r^2+(2nh+2h_0)^2}}\right)+$$

$$+\sum_{j=3}^{\frac{1}{2}(p_{n-1}+2)}b_j\sum_{n=1}^{\infty}\left(\frac{\cos n\varphi_j'}{\sqrt{r^2+(2nh-2h_0)^2}}+\frac{\cos n\varphi_j'}{\sqrt{r^2+2nh+2h_0)^2}}\right)\Bigg].$$

In agreement with the obtained expression for the potential, we find an expression for apparent resistance for a symmetrical 4-electrode $AMNB$ or a 3-electrode AMN apparatus, at the bottom of the water:

$$\bar{\varrho}_M=\frac{1}{2}\varrho_0\Bigg[1+2\Bigg(b_1\sum_{n=1}^{\infty}\frac{r^3}{[r^2+(2nh)^2]^{3/2}}+b_2\sum_{n=1}^{\infty}\frac{(-1)^n r^3}{[r^2+(2nh)^2]^{3/2}}+$$

$$+\sum_{j=3}^{\frac{1}{2}(p_{n-1}+2)}b_j\sum_{n=1}^{\infty}\frac{r^3\cos n\varphi_j'}{[r^2+(2nh)^2]^{3/2}}\Bigg)+\frac{r^3}{[r^2+(2h_0)^2]^{3/2}}+$$

$$+b_1\sum_{n=1}^{\infty}\left(\frac{r^3}{[r^2+(2nh-2h_0)^2]^{3/2}}+\frac{r^3}{[r^2+(2nh+2h_0)^2]^{3/2}}\right)+$$

$$+b_2\sum_{n=1}^{\infty}\left(\frac{(-1)^n r^3}{[r^2+(2nh-2h_0)^2]^{3/2}}+\frac{(-1)^n r^3}{[r^2+(2nh+2h_0)^2]^{3/2}}\right)+$$

$$+\sum_{j=3}^{\frac{1}{2}(p_{n-1}+2)}b_j\sum_{n=1}^{\infty}\left(\frac{r^3\cos n\varphi_j'}{[r^2+(2nh-2h_0)^2]^{3/2}}+\frac{r^3\cos n\varphi_j'}{[r^2+(2nh+2h_0)^2]^{3/2}}\right)\Bigg].$$

Since $\sum_{j=1}^{\frac{1}{2}(p_{n-1}+2)}b_j=1$, then, introducing symbols for the coefficients of recession, we have

$$\varrho_M=\frac{1}{2}\varrho_0\Bigg[b_1\left(1+2\sum_{n=1}^{\infty}l_n\right)+b_2\left(1+2\sum_{n=1}^{\infty}(-1)^n l_n\right)+$$

$$+\sum_{j=3}^{\frac{1}{2}(p_{n-1}+2)}b_j\left(1+2\sum_{n=1}^{\infty}l_n\cos n\varphi_j'\right)+b_1\left(l_{p_0}+\sum_{n=1}^{\infty}(l_{n-p_0}+l_{n+p_0})\right)+$$

$$+b_2\left(l_{p_0}+\sum_{n=1}^{\infty}(-1)^n(l_{n-p_0}+l_{n+p_0})\right)+$$

$$+\sum_{j=3}^{\frac{1}{2}(p_{n-1}+2)}b_j\left(l_{p_0}+\sum_{n=1}^{\infty}\cos n\varphi_j'(l_{n-p_0}+l_{n+p_0})\right)\Bigg]. \qquad (31)$$

In a more general form we can write

$$\varrho_M = \frac{1}{2}\varrho_0 \left\{ \sum_{j=1}^{\frac{1}{2}(p_{n-1}+2)} b_j \left(1 + 2 \sum_{n=1}^{\infty} l_n \cos n\varphi_j' \right) + \right.$$

$$\left. + \sum_{j=1}^{\frac{1}{2}(p_{n-1}+2)} b_j \left[p_0 + \sum_{n=1}^{\infty} (l_{n-p_0} + l_{n+p_0}) \cos n\varphi_j' \right] \right\}, \tag{32}$$

since the terms $b_1 \left(1 + 2 \sum_{n=1}^{\infty} l_n \right)$ and $b_2 \left(1 + 2 \sum_{n=1}^{\infty} (-1)^n l_n \right)$ are partial forms for $k_j' = +1$ and $k_j' = -1$. The same can be said for the terms

$$b_1 \left[l_{p_0} + \sum_{n=1}^{\infty} (l_{n-p_0} + l_{n+p_0}) \right] \text{ and } b_2 \left[l_{p_0} + \sum_{n=1}^{\infty} (-1)^n (l_{n-p_0} + l_{n+p_0}) \right].$$

We will consider in a general form one of the terms in the second sum of the expression (32):

$$\left[l_{p_0} + \sum_{n=1}^{\infty} (l_{n-p_0} + l_{n+p_0}) \cos n\varphi \right] = l_{p_0} + (l_{-(p_0-1)} + l_{(1+p_0)}) \cos \varphi +$$

$$+ (l_{-(p_0-2)} + l_{2+p_0}) \cos 2\varphi + \ldots + (l_{-1} + l_{2p_0-1}) \cos (p_0 - 1)\varphi +$$

$$+ (l_0 + l_{2p_0}) \cos p_0\varphi + (l_1 + l_{2p_0+1}) \cos (p_0 + 1)\varphi + \ldots$$

Since the function l_i is an even function with respect to i, then assuming that $l_i = l_{-i}$, we find

$$\left[l_{p_0} + \sum_{n=1}^{\infty} l_{n-p_0} + l_{n+p_0}) \cos n\varphi \right] = l_0 \cos p_0\varphi + l_1 [\cos (p_0 + 1)\varphi +$$

$$+ \cos (p_0 - 1)\varphi] + l_2 [\cos (p_0 + 2)\varphi + \cos (p_0 - 2)\varphi] + \ldots +$$

$$+ l_{p_0} [\cos 2p_0\varphi + 1] + l_{p_0+1} [\cos (2p_0 + 1)\varphi + \cos \varphi] + \ldots =$$

$$= \cos p_0\varphi + 2l_1 \cos p_0\varphi \cos \varphi + 2l_2 \cos p_0\varphi \cos 2\varphi + 3l_3 \cos p_0\varphi \cos 3\varphi +$$

$$+ \ldots + 2l_{p_0} \cos p_0\varphi \cos p_0\varphi + 2l_{p_0+1} \cos p_0\varphi \cos (p_0 + 1)\varphi + \ldots =$$

$$= \cos p_0\varphi [1 + 2(l_1 \cos \varphi + l_2 \cos 2\varphi + l_3 \cos 3\varphi + \ldots)].$$

Thus we find that

$$\left[l_{p_0} + \sum_{n=1}^{\infty} (l_{n-p_0} + l_{n+p_0}) \cos n\varphi \right] = \cos p_0\varphi \left[1 + 2 \sum_{n=1}^{\infty} l_n \cos n\varphi \right]. \tag{33}$$

Substituting the obtained value in the expression (32) we obtain

$$\bar{\varrho}_M = \varrho_0 \sum_{j=1}^{\frac{1}{2}(p_{n-1}+2)} b_j \frac{1+\cos p_0 \varphi_j'}{2} \left(1 + 2\sum_{n=1}^{\infty} l_n \cos n\varphi\right).$$

The first two terms of this sum represent a two-layer medium $p_0 = 1$ with $k_j' = +1$ and $k_j' = -1$ and, consequently, $\cos p_0 \varphi_j'$ for these cases is equal to $+1$ and -1 respectively. Taking this into account and adopting the symbols for apparent resistance according to A. I. ZABOROVSKII, we finally obtain

$$\bar{\varrho}_M = \varrho_0 \left[b_1 \bar{\varrho}^+ + \sum_{j=3}^{\frac{1}{2}(p_{n-1}+2)} b_j \frac{1+\cos p_0 \varphi_j'}{2} \bar{\varrho}_j' \right]. \tag{34}$$

By similar reasoning it can readily be shown that for an odd p_{n-1} the expression for the apparent resistance for an apparatus at the bottom of the water has the form of

$$\bar{\varrho}_M = \varrho_0 \left[b_1 \bar{\varrho}^+ + \sum_{j=3}^{\frac{1}{2}(p_{n-1}+3)} b_j \frac{1+\cos p_0 \varphi_j'}{2} \bar{\varrho}_j' \right]. \tag{34'}$$

Thus, splitting up the coefficient B_1 into simple fractions does not depend only on the type of the apparatus [9], but also on its position relative to the section.

The coefficients of serial expression b_1, b_3, b_4, ... and the coefficients of reflection k_j' were found from formulae given by G. D. TSEKOV [8]. All calculations were carried out with a projected accuracy of obtaining the coordinates within $\pm 0.5\%$.

Most of the curves were calculated by the method of summation of series. From formula (24), assuming that

$$\bar{\varrho} = \varrho_0 \left(1 + 2\sum_{n=1}^{\infty} q_n l_n\right),$$

we have

$$\bar{\varrho}_M = \bar{\varrho} + \frac{1}{2}\varrho_0 \left[(l_{p_0} - 1) + \sum_{n=1}^{\infty} q_n (l_{n-p_0} + l_{n+p_0} - 2l_n) \right]. \tag{35}$$

In this expression the apparent resistance measured by an apparatus at the bottom of the water, is represented as the sum of the apparent resistance, measured by a similar apparatus at the surface of the water, and a certain correction. Since the values of $\bar{\varrho}$ have been calculated for

a large number of different three-layer geoelectrical sections and are given in tables of coordinates of three-layer probing curves for various types of instruments, only the correction of the expression which is in square brackets is subject to calculations. In calculations an important element included in this expression is the series:

$$s_1 = \frac{1}{2}\sum_{n=1}^{\infty} q_n(l_{n-p_0} + l_{n+p_0} - 2l_n).$$

Naturally, in practice, only a certain series

$$s_2 = \frac{1}{2}\sum_{n=1}^{m} q_n(l_{n-p_0} + l_{n+p_0} - 2l_n)$$

can be calculated. the value of which, depending on the value of the number m for which the summation was completed, approximates, with a certain degree of accuracy, to the value of the series s_1.

The evaluation of the accuracy of approximation and, consequently, the determination of the necessary number of summation terms m to attain the projected accuracy were carried out according to the method proposed by L. L. VAN'YAN.

In calculating the apparent specific resistance, measured by an instrument at the sea-bottom, with the aid of formula (37), as a result of shortening the summation of the series at the m-th term an error is introduced into the calculated value. This error can be expressed by the value

$$\Delta s = |s_1 - s_2| = \left|\frac{1}{2}\sum_{n-m+1}^{\infty} q_n(l_{n-p_0} + l_{n+p_0} - 2l_n)\right|.$$

To evaluate the obtained value, we carry out a series of conversions:

$$\Delta s = \left|\frac{1}{2}\sum_{n=m+1}^{\infty} q_n(l_{n-p_0} + l_{n+p_0} - 2l_n) \leqslant\right.$$

$$\leqslant \frac{1}{2}\sum_{n=m+1}^{\infty} \left| \times q_n(l_{n-p_0} + l_{n+p_0} - 2l_n)\right| \leqslant$$

$$\leqslant \frac{1}{2}\sum_{n=m+1}^{\infty} \left| q_n \right| l_{n-p_0} + l_{n+p_0} - 2l_n |, \qquad (36)$$

therefore,

$$\Delta s \leqslant \frac{1}{2}|q_{\max}| \sum_{n=m+1}^{\infty} |l_{n-p_0} + l_{n+p_0} - 2l_n|.$$

Here $q_{\max}$ is the greatest numerical coefficient of emission in the residual series Δs from $n = m + 1$ to ∞.

To study the character of the functions

$$\sum_{n=m+1}^{\infty} (l_{n-p_0} + l_{n+p_0} - 2l_n) \text{ and } (l_{n-p_0} + l_{n+p_0} - 2l_n)$$

with change in n, we present the second of them as the second derivative of the coefficient of recession l_n for n:

$$(l_{n-p_0} + l_{n+p_0} - 2l_n) = (l_{n-p_0} - l_n) - (l_n - l_{n+p_0}) \approx \frac{d^2 l_n}{dn^2} (\Delta n)^2.$$

Putting $\Delta n = 1$, we have

$$(l_{n-p_0} + l_{n+p_0} - 2l_n) \approx \frac{d^2 l_n}{dn^2}$$

and, consequently,

$$\sum_{n=m+1}^{\infty} (l_{n-p_0} + l_{n+p_0} - 2l_n) \approx - \frac{dl_n}{dn}.$$

For the symmetrical $AMNB$ apparatus $l_n = \dfrac{x^3}{(x^2 + 4n^2)^{3/2}}$. After differentiation we obtain

$$\frac{dl_n}{dn} = - 12x^3 \frac{n}{(x^2 + 4n^2)^{5/2}}$$

$$\frac{d^2 l_n}{dn^2} = 12x^2 \frac{16n^2 - x^2}{(x^2 + 4n^2)^{7/2}}.$$

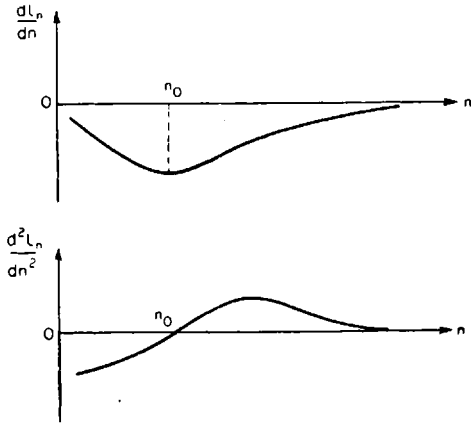

FIG. 1.

The function $\frac{dl_n}{dn}$ has one extreme value for $n_0 = 0.25x$; for $n \to 0$ and $n \to \infty$ the function $\frac{dl_n}{dn} \to 0$, i.e. $\lim_{n \to 0,\infty} \frac{dl_n}{dn} = 0$.

Figure 1 shows graphs for the functions $\frac{dl_n}{dn}$ and $\frac{d^2 l_n}{dn^2}$.

A study of these functions shows that in the summation sign in expression (36) in straight brackets, the components can be positive for $n > n_0$, and negative for $n < n_0$. To evaluate the error, these terms should be summed to the absolute value. We will consider two cases.

(a) Let $m > n_0$. In this case, all the components in the summation sign of expression (36) are positive and the error can be evaluated by the inequality

$$\Delta s \leqslant \frac{1}{2} \left| q_{\max} \right| \sum_{n=m+1}^{\infty} (l_{n-p_0} + l_{n+p_0} - 2l_n).$$

We will consider the series:

$$\sum_{n=m+1}^{\infty} (l_{n-p_0} + l_{n+p_0} - 2l_n) = \sum_{n=m+1}^{\infty} (l_{n-p_0} - l_n) - \sum_{n=m+1}^{\infty} (l_n - l_{n+p_0}) =$$

$$= (l_{m+1-p_0} - l_{m+1}) + (l_{m+2-p_0} - l_{m+2}) + (l_{m+3-p_0} - l_{m+3}) + \ldots +$$

$$+ (l_{m+1} - l_{m+1+p_0}) + (l_{m+2} - l_{m+2+p_0}) + (l_{m+3} - l_{m+3+p_0}) + \ldots -$$

$$- (l_{m+1} - l_{m+1+p_0}) - (l_{m+2} - l_{m+2+p_0}) - (l_{m+3} - l_{m+3+p_0}) - \ldots =$$

$$= (l_{m+1-p_0} + l_{m+1}) + (l_{m+2-p_0} + l_{m+2}) + \ldots + (l_m - l_{m+p_0}) =$$

$$= \sum_{i=1}^{p_0} (l_{m-p_0+i} - l_{m+i}).$$

The magnitude of the error is therefore expressed in this case by the inequality

$$\Delta s_1 \leqslant \frac{1}{2} \left| q_{\max} \right| \sum_{i=1}^{p_0} (l_{m-p_0+i} - l_{m+i}). \tag{37}$$

(b) We will now put $m < n_0$. In this case, the values in the summation sign of expression (36) in straight brackets are both positive and negative; thus it can be written

$$\sum_{n=m+1}^{\infty} \left| l_{n-p_0} + l_{n+p_0} - 2l_n \right| = \sum_{n=n_0+1}^{\infty} (l_{n-p_0} + l_{n+p_0} - 2l_n) -$$

$$- \sum_{n=m+1}^{n_0} (l_{n-p_0} + l_{n+p_0} - 2l_n)$$

or, representing the second term of the equation as the difference between the two sums,

$$\sum_{n=m+1}^{\infty} \left| l_{n-p_0} + l_{n+p_0} - 2l_n \right| = \sum_{n=n_0+1}^{\infty} (l_{n-p_0} + l_{n+p_0} - 2l_n) -$$

$$- \left[\sum_{n=m+1}^{\infty} (l_{n-p_0} + l_{n+p_0} - 2l_n) - \sum_{n=n_0+1}^{\infty} (l_{n+p_0} + l_{n-p_0} - 2l_n) \right] =$$

$$= 2 \sum_{n=n_0+1}^{\infty} (l_{n-p_0} + l_{n+p_0} - 2l_n) - \sum_{n=m+1}^{\infty} (l_{n-p_0} + l_{n+p_0} - 2l_n).$$

Treating the obtained series exactly the same as for case (*a*), we obtain

$$\sum_{n=m+1}^{\infty} \left| l_{n-p_0} + l_{n+p_0} - 2l_n \right| = 2 \sum_{i=1}^{p_0} (l_{n_0-p_0+i} - l_{n_0+i}) -$$

$$- \sum_{i=1}^{p_0} (l_{m-p_0+i} - l_{m+i}).$$

The error in this case is determined by the inequality

$$\Delta s_2 \leqslant \frac{1}{2} |q_{\max}| \left[2 \sum_{i=1}^{p_0} (l_{n_0-p_0+i} - l_{n_0+i}) - \sum_{i=1}^{p_0} (l_{m-p_0+i} - l_{m+i}) \right]. \quad (38)$$

The relative value of the error can then be found

$$\delta = \frac{\Delta s}{\varrho_M} \leqslant \frac{\Delta s}{\bar{\varrho} \dfrac{\mu}{1+\mu}}.$$

All geoelectrical sections, for which the curves of apparent resistance were calculated by the shortened method, for a sea-bottom apparatus, had $p_0 = 1$ (the layer lying directly under the water, greater than or equal to the thickness of the water layer) the expressions for the errors were therefore considerably simplified:

$$\Delta s_1 \leqslant \frac{1}{2} |q_{\max}| (l_m - l_{m+1}),$$

$$\Delta s_2 \leqslant \frac{1}{2} |q_{\max}| [2 (l_{n_0} - l_{n_0+1}) - (l_m - l_{m+1})].$$

Replacing $(l_m - l_{m+1})$ by Δl_m, and $(l_{n_0} - l_{n_0+1})$ by $\Delta l_{\max}$ we find the expression for the relative error:

for $m > n_0$

$$\delta = \frac{\Delta s_1}{\bar{\varrho}_M} \leqslant \frac{|q_{\max}|\,\Delta l_m}{2\bar{\varrho}\,\dfrac{\mu}{1+\mu}} \tag{39}$$

and for $m < n_0$

$$\delta = \frac{\Delta s_2}{\bar{\varrho}_M} \leqslant \frac{|q_{\max}|\,(2\Delta l_{\max} - \Delta l_m)}{2\bar{\varrho}\,\dfrac{\mu}{1+\mu}} \tag{39'}$$

Given a certain degree of accuracy (in our case the accuracy taken was $\delta = 0.005$, or 0.5%), it is possible to select such a number m of terms of the sum, to satisfy the inequality

$$\Delta l_m \leqslant \frac{2\delta\mu}{100\,(1+\mu)}\,\frac{\bar{\varrho}}{|q_{\max}|} \quad \text{for} \quad m > n_0 \tag{40}$$

or

$$(2\Delta l_{\max} - \Delta l_m) \leqslant \frac{2\delta\mu}{100\,(1+\mu)}\,\frac{\bar{\varrho}}{|q_{\max}|} \quad \text{for} \quad m < n_0, \tag{40'}$$

which ensures the given accuracy δ.

This operation is readily carried out by means of a slide rule and an appropriate table for the function l_n. For most of the probe curves for any value of $\frac{r}{h}$ the value m for an accuracy $\delta = 0.5\%$ lies within the limits of 1–15 and does not exceed 35.

REFERENCES

1. L. M. Al'pin, *The Theory of Dipole Probes.* Gostoptekhizdat, (1950).
2. V. V. Burgsdorf, Calculation of earthings in heterogeneous grounds. *Elektrichestvo* No. 1. (1954).
3. L. L. Van'yan, Theoretical Curves for Electrical Sea probing with a sea-bottom apparatus. *Applied Geophysics* No. 50. Gostoptekhizdat, (1956).
4. V. N. Dakhnov, *Electrical Prospecting of Petroleum and Gaseous Deposits.* Gostoptekhizdat, (1953).
5. A. I. Zaborovskii, *Electrical Prospecting.* Gostoptekhizdat, (1943).
6. S. Ya. Litvinov, *Electrical Sea Prospecting.* Gostoptekhizdat, (1941).
7. R. Maie, *Mathematical Bases for Electrical Prospecting with a Direct Current.* ONTI. (1935).
8. G. D. Tsekov, *A Method for Calculating Multilayer Curves of Vertical Electrical Probing for a Case where the Underlying Medium is in the Form of Rocks of Very High or Very Low Resistance.* Thesis. Documents VNII Geofizika.
9. K. Flathe, A practical method of calculating geoelectrical model graphs for horizontally stratified media. *Geophysical Prospecting,* vol. 3. (1955).

CHAPTER 8

THE USE OF NEW METHODS OF ELECTRICAL EXPLORATION IN SIBERIA

A. M. ALEKSEEV, M. N. BERDICHEVSKII and A. M. ZAGARMISTR

THE effectiveness of using the method of vertical electrical probing in a number of regions of Siberia and the Far East was shown in the 1930s and 1940's. Electrical studies of the territory of the Western Siberian lowlands, in the regions of Eastern Siberia (especially at Lake Baikal), and on Sakhalin made it possible to obtain valuable geological results. Since then however, electro-prospecting work in Siberia has not received much development, since swampy conditions and wooded nature of the territory have presented considerable difficulties in carrying out vertical electrical probing. The necessity of using long feed lines (12–20 km), and power generators, (10–20 kW) have considerably limited the possibilities of using vertical electrical probing in accessible places. Because of this, in some geophysical institutes in Siberia, electrical exploration has been excluded entirely from the exploratory work for oil and gas. The exclusion of electrical exploration from the geophysical studies has necessitated the solution of prospecting and detailed problems of surveying almost exclusively by seismological methods, which are more difficult and expensive in comparison with other methods of petroleum geophysics.

The development in the VNII Geofizika of new methods (the method of two-way electrical probing and the method of telluric currents), which considerably extend the possibilities of electrical exploration, led to the organization in 1955–56 of widespread experimental electrical exploration in Siberia. The aim of this work was to determine the geological effectiveness of new methods under geoelectrical conditions of the Western Siberian lowlands and to develop a method of measurement in inaccessible regions.

Experimental work was carried out by parties from the VNII Geofizika (under the direction of V. P. Bordovskii and Yu. N. Popov) on the North West depression of the Kolyvan-Tomsk fold belt and within the limits of the Tobol'sk and the Vagai-Ishim tectonic zones, and also in the region of the Berezovka gas deposits. This work showed the desirability for carrying

out a considerable extension of electrical exploration in the rather inaccessible regions of Siberia.

The present article deals with the basic results of the studies.

THE METHOD OF TWO-WAY ELECTRICAL PROBING

The theory of two-way electrical probing by dipole instruments was developed by L. M. AL'PIN between 1948 and 1950 [1]. In subsequent years, in the VNII Geofizika a method was developed for the practical use of two-way probes with quadrilateral* arrangements. This has now been put into practice in geophysical studies over the territory of the European part of the USSR [3].

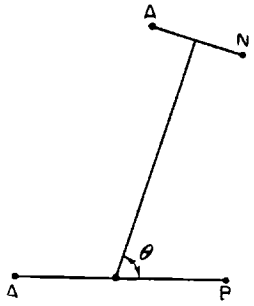

FIG. 1. Azimuthal arrangement.

This method has a number of advantages over the vertical electrical probing carried out with the symmetrical four-pole AMNB apparatus. Apart from the possibility of producing deep probings by using small spacings of electrodes (1–2 km) and the improved quality of the measurements due to decrease in the harmful effect of leaks, the quadrilateral probings have increased resolving capacity with respect to the inclination of the reflecting electrical horizon.† However, under conditions involving swamps and forests, the method of quadrilateral probings, which requires movements over long straight routes, is of limited application.

In this respect, much better possibilities are shown by the method of two-way probings with an azimuthal arrangement (Fig. 1), a special case of

* The word equatorial is used in Russian, which however would be misleading in English. [Editor's footnote].

† Electrically reflecting horizon is a horizon of high resistance. This translation is necessary since the same term is used by the Russian geophysicists for a seismically reflecting horizon.

which are the quadrilateral probings. When carrying out azimuthal probing, it is by no means necessary to place the centres of the measuring lines on a straight line, directed along the axis of probing.

For a number of dipole arrangements including the azimuthal, in a horizontally homogeneous medium, the values of *KS** do not depend on the angle Θ which makes it possible to use these arrangements in studies on the roads and other curved routes. The curved azimuthal probings† have all the advantages of the quadrilateral probes but are much more readily applied to the region.

The possibility of practical curved azimuthal probes was first shown by the electro-prospectors of VNII Geofizika working (1954) in the Cis-Baltic depression. Three azimuthal probes were carried out with working distances of up to 12 km. The probes were carried out by means of the EPS-23, mobile electrical prospecting station, with the limiting deviations of angle Θ from 90° not exceeding $\pm 30°$.

The curves obtained show sufficiently well the geoelectrical cross-section of the Cis-Baltic depression. The results showed the suitability of a similar arrangement of work for carrying out deep electrical probes and made it possible to plan a programme of further studies on the method of measurements with the azimuthal arrangement. The development of the method of curved azimuthal probes was continued in 1955–1956 in the Western Siberian Lowlands.

An experimental party from VNII Geofizika carried out 40 two-way curved azimuthal probings in the Kochanevsk region of the Novosibirsk region (1955), where the supporting electrical levels lie at depths of from 200 to 1000 m. The measurements were made along winding roads, running through swampy and wooded territory. The maximum working distance achieved in the majority of cases was 6 km with a length of feed line up to 1 km. As a rule, the length of the measuring line did not exceed 400 m. The topographic basis for the azimuthal probes was worked out by means of a plane table. Numerous control measurements showed the good reproducibility of the azimuthal probing results within the limits of 5–6% providing that the angle Θ did not differ from 90° by more than $\pm 20°$. This condition does not seriously limit the possibilities of curved probings, since if necessary it is possible to use 2 feed lines in different directions.

In the southern part of the surveyed area, where it was easier to move,

* *KS*-Koeffitsient soprotivleniya — Coefficient of resistance-resistivity [Editor's note].

† The article by Berdichevskii "The method of curved azimuthal probes" is in the present collection.

several quadrilateral and azimuthal probes were carried out with coincident centres. The results obtained were sufficiently close to one another.

In 1956, curved azimuthal probings were carried out in the Tobol'sk and Vagai'-Ishim tectonic zones (Tyumensk region) in localities characterized by a depth of the reflecting level of 1200 to 2500 m. The studies were carried out over a route about 250 km long. The maximum distances between the dipoles of the azimuthal arrangements were between 8 and 10 km. The field laboratories moved along winding roads. Despitc the fact that owing to the frequent rains, the road conditions in a number of regions were bad, the party was able to carry out more or less regularly one two-way probing in one working day equivalent to two AMNB probings with maximum spacings of AB = 16–20 km. The curves of the azimuthal probing agree sufficiently well with the curves for quadrilateral probing. The oscillograms referring to the large dispersions of the azimuthal probing were worked out with a sufficient degree of accuracy.

As well as with the azimuthal arrangement tests were made using a radial arrangement and a parallel arrangement, with small angle Θ, making it possible to obtain results which practically coincided with the results of the radial probes. These studies were also carried out over curved routes. With radial and especially with parallel probes, it was much easier to unreel the wire. However, due to the reduced depth of the study, these methods under conditions involving an electrically reflecting level at a great depth were used in an auxiliary capacity.

The work showed the effectiveness of using the method of two-way electrical probes for surveying upfolds in the top surface of the marker horizon, which in a number of sections of the Western Siberian Lowlands represents the top surface of the Paleozoic deposits. It was also shown that in zones of sedimentary and volcanic layers of the second structural level the stratigraphic position of the electrical marker horizons can change depending on the degree of metamorphism of the sedimentary rocks, and the presence of volcanic formations in them. In this case, the data of the electrical survey reflect the changes in the thickness of the conducting part of the section, which is represented by friable, weakly-metamorphized aranaceous argillaceous deposits, devoid of widespread intrusive sills.

The curves of two-way electrical probing can be interpreted more reliably than the curves of the vertical electrical probe and give fuller information about the nature of disposition of rocks. The methods of qualitative and quantitative interpretations of electrical probe curves in two-way measurements are supplemented by an analysis of the divergence of positive and negative *KS* curves. This divergence is caused by the dip of the

electrical curves by responsive horizons and by the change in their specific resistance in the region adjoining the probe apparatus.

The qualitative analysis of curves for two-way probing consists in following the character of the relationships of the positive and negative *KS* curves in the profiles (especially their right-hand branches), and also in constructing and studying: graphs of positive and negative *KS* values (*KS* lines) for a given dispersion; graphs of positive and negative values of *S* (*S* lines); vectors maps for difference in plus and minus *KS* values (vectors $\Delta\varrho$).

In the quantitative interpretation of curves of two-way probing, not only were the average *KS* curves processed, being largely similar to the curves for vertical electrical probing, but also the plus and minus *KS* curves, and also the derived *KS* curves given by the method of O. V. NAZARENKO, V. A. LIPILIN, *et al.* The geoelectrical sections were constructed both by using a handbook of theoretical curves, calculated for the AMN arrange-

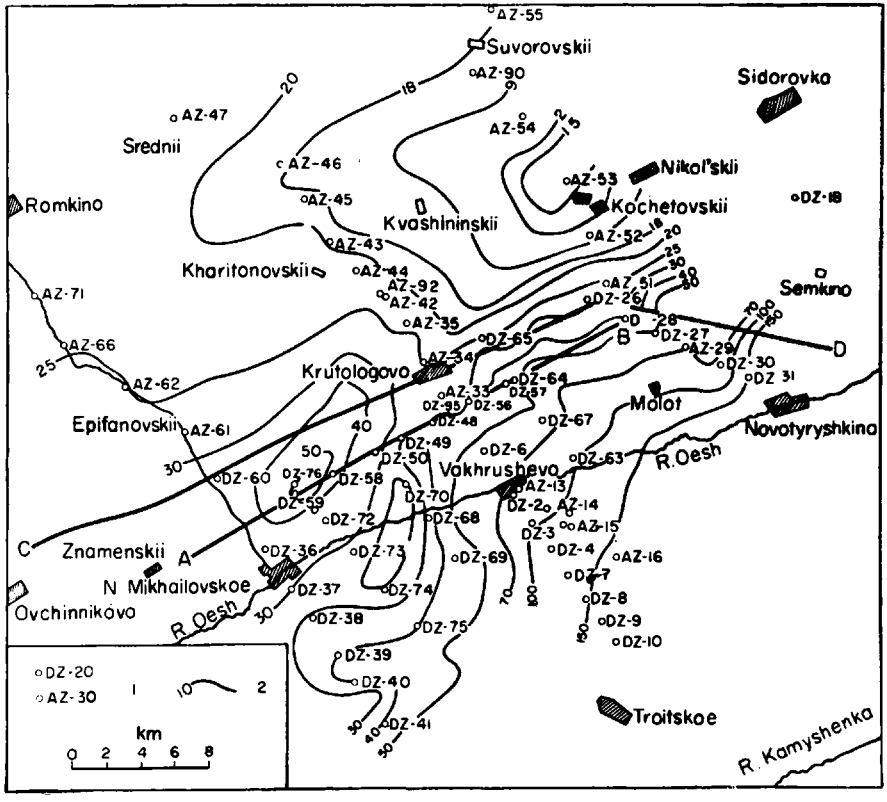

FIG. 2. KS map for operating distance $\bar{R}$=3000 m. 1—centres of two-way equatorial and azimuthal probes; 2—KS isolines.

ment, and by a number of specially developed methods (method S, the method of giving the value ϱ_l, the method for transforming curves of quadrilateral azimuthal probing into curves of axial probing).

As an example, results are given for studies in two different regions of the Western Siberian Lowlands.

First of all, we will deal with the material of the qualitative and quantitative interpretations of two-way probing on the north-west ends of the Kolyvan'-Tomsk fold belt (the work of 1955). The surveyed area includes the pre-Jurassic foundation, covered by Meso-Cenezoic aranaceous argillaceous deposits, and dipping in a north-westerly direction to depths of the order of 1000 m. The problem of the electrical survey was to study the relief of the surface of the pre-Jurassic foundation.

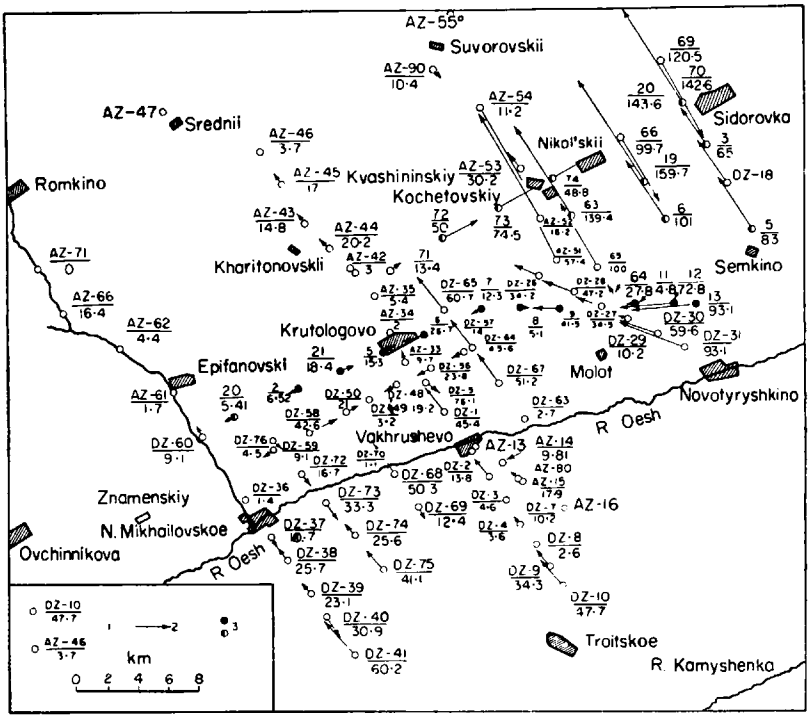

FIG. 3. Map for $\Delta\bar{\varrho}$ vectors for an operating distance $\bar{R} = 3000$ m. 1—centres of 2-sided equatorial and azimuthal probes by the VNIIGeofizika party; 2—vector of $\Delta\bar{\varrho}$; 3—centres of two-way quadrilateral probes by the Sibneftegeofizika Department. The numerator represents the number of the probe; the denominator represents the value for the vector $\Delta\bar{\varrho} = 100\,\dfrac{\varrho + \varrho'}{\varrho_{av}}$.

Figure 2 shows a *KS* map drawn from the average *KS* curves for a working distance $\bar{R}$ = 3,000 m. There is a regular decrease in the *KS* values in a north-westerly direction, corresponding to increase in the thickness of the friable Meso-Cenezoic formations. On this background to the north of L. Mikhailovskoe a local maximum of *KS* values is identifiable which is an indication that the Paleozoic foundation is lifted up between the points L. Mikhailovskoe and Epifanovskii. This interpretation of the structure of the Paleozoic rocks is supported by the vectors $\Delta\varrho$ (Fig. 3) for the same working distance.

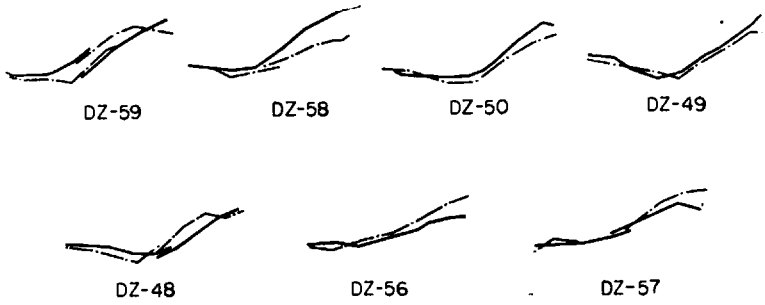

FIG. 4. Curves for two-way probes along AB profile.

As can be seen, the directions of the vectors $\Delta\varrho$ clearly characterize the basic features of the surface of the Paleozoic foundations (remembering that the vectors $\Delta\varrho$ indicate the direction in which the *KS* values decrease). The presence of elevations in the top surface of the foundation are particularly well observed on comparing the plus and minus *KS* curves (Fig. 4). Thus, on the *AB* profile, which intersects the zone of increased *KS* value, there is a reversal of the plus and minus *KS* curves (DZ–58, DZ–59), characteristic of a passage across the crest of the structure. On the DZ-58 the right-hand branch of the positive (south-west) curve, represented by a continuous line, is placed above the right-hand branch of the negative (north-east) curve, shown by a dotted line, which indicates a rise in the foundation in a south-westerly direction.

On the DZ–59, reverse relationships were observed, which indicate the change in direction of dip of the foundation. Very characteristic are the relationships of the right-hand branches of the curves DZ–48, DZ–49, DZ–50, showing the presence of a depression in the surface of the foundation with deepest part in the DZ–49 zone, where the right-hand branches of the positive and negative curves coincide almost completely.

On the north-east section of the profile, the relationships of the right-hand branches of the two-way probe reflect the rise of the pre-Jurassic rocks in a north-eastern direction (DZ–56, DZ–57).

The results of the qualitative interpretation facilitate the selection of parameters for subsequent quantitative calculations and improve their reliability.

Figure 5 gives a geoelectrical cross-section through the profile considered above. As can be seen, the quantitative treatment agrees well with the qualitative impressions of the surface relief of the Paleozoic foundation at the

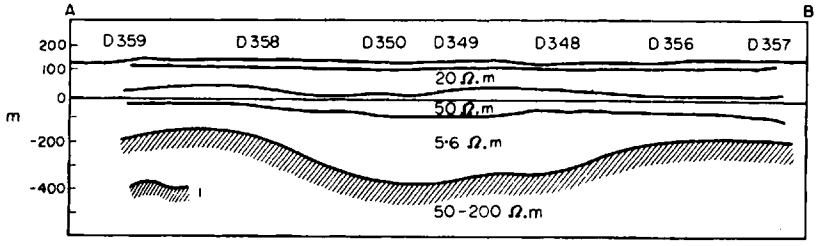

FIG. 5. Geoelectrical cross-section along AB profile. 1—top surface of the Paleozoic rocks according to data of layer processing of average curves of quadrilateral and azimuthal probes.

investigated section and, furthermore, indicate the structure of the sedimentary succession. As well as the layer interpretation with the aid of theoretical graphs, the average *KS* curves were also processed by the method of transformation into curves of axial probing [5]. Fig. 6 compares the results of the quantitative interpretation by both methods along 40 km of the *CD* profile.

The second example refers to results of the application of two-way azimuthal probes in 1956 at one of the sections of the Vagai-Ishim tectonic zone, where the rocks of the pre-Jurassic foundation lie at depths greater than 1600 m. The curves of the azimuthal probe clearly subdivide the geoelectrical cross-section. They differentiate a thick succession of conducting friable deposits, underlain by the highly resistant rocks which form the electrically reflecting horizon.

As shown above, the stratigraphic continuity of the high resistance, electrical marker horizon is apparently not maintained in the zones of development of effusively deposited rocks of the second structural stage. At the present time, due to the absence of geological data, this problem has been insufficiently studied. It can only be supposed that, depending

on the degree of metamorphism of the rocks of this stage and the development in them of layers of lava, the surface of the high-resistance electrical marker horizon may be displaced within the limits of the whole volcano-sedimentary succession.

However, this fact does not prevent the application of electric-prospecting to surveys of elevations in the relief of the bottom of the platform-Mesozoic. The results of electrical well-logging show that volcano-sedimentary strata have a higher resistance, due to which the values of total longitudinal conductivity (S), obtained during probing, are mainly determined from the parameters

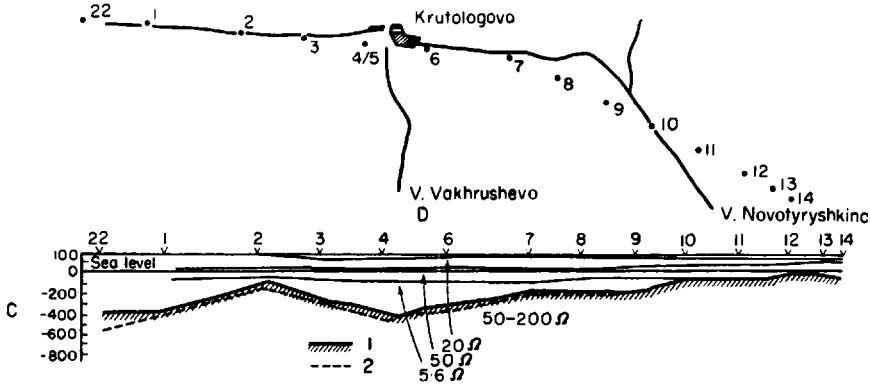

FIG. 6. Geoelectrical cross-section along CD profile. 1—top surface of the Paleozoic rocks from data of layer processing of average curves of equatorial and azimuthal probes; 2—top surface of the Paleozoic rocks from results of transforming average curves of equatorial and azimuthal probes into curves of axial probes.

of the Meso-Cenezoic deposits. The small change in the specific electrical resistance of the rocks of the Meso-Cenezoic over a wide range of territory provides favourable conditions for tracking the relative changes in thickness of the friable Meso-Cenezoic succession by the changes in S. This conclusion is confirmed by the results of observations on areas studied by seismic methods. Figure 7 gives a graph of S compared with the seismic data on the reflecting horizon in the Lower Cretaceous (Valanginian) deposits. The graph of S differentiates two zones of reduced values, associated with the crests of the Viatkinskaia and Krotovskaia structures, which were surveyed by the method of reflected waves.

Of interest is the identical behaviour of the graph S and the seismic marker horizon which makes it possible to use the S method with a constant parameter ϱ_l selected from the drilling data of the Vyatkinsk area as one of the methods for the quantitative interpretation.

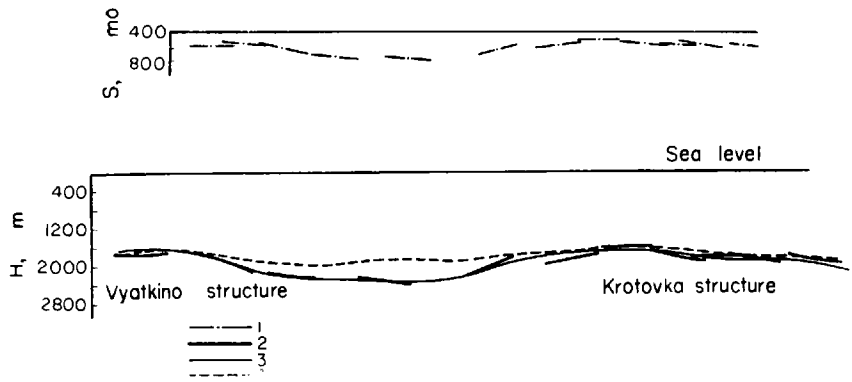

FIG. 7. Results of geophysical studies along the profile Viatkino-Krotovka. 1—*S* lines; 2—depth lines; 3—supposed surface of supporting electrical high-resistance level; 4—surface of seismical supporting levels.

The geoelectrical section, denoting the behaviour of the electrically highly resistant horizon level is given in the lower part of the drawing. It follows from the data given that the results of the interpretation of electrical probes make it possible to decide on the tectonics of the Mesozoic deposits.

Similar results were obtained on other structures revealed by seismical work in the region between the townships Viatkino and Vikulovo (Dmitrievskaia and Krutikhinskaia structures) and also on certain areas of the Tobolsk

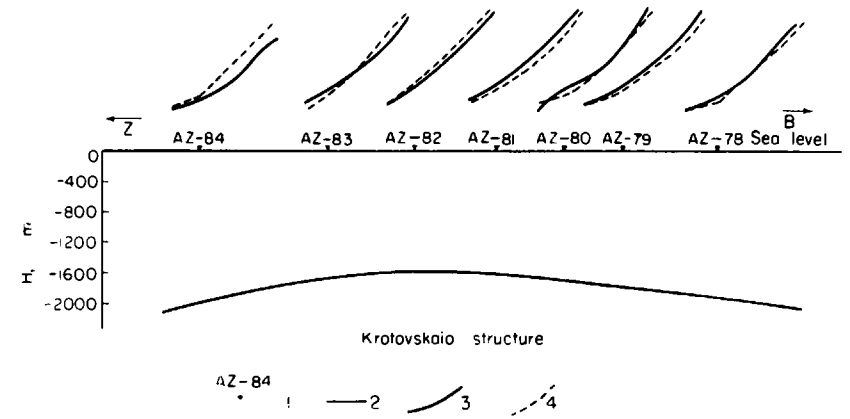

FIG. 8. Two-way curves of an azimuthal probe over an upheaval of a support high-resistance level. 1—centres of two-way electrical probes; 2—supposed surface of highly resistant reflecting horizons; 3—right-hand branches of AZ Western curves; 4—right-hand branches of Eastern AZ curves.

tectonic zone (Zavodoukovskaia, Komissarovskaia and Kapralikhskaia structures). However, in one case at the section between the township's Bol'shoe Sorokino and Vikulovo an elevation of the electrical marking horizon was observed. The elevation was not reflected in the seismic profile. This fact requires further study.

Despite the considerable depths of the electrical marking horizon in the Tobol'sk and Vagai-Ishim tectonic zones, the curves of two-way probing have very well defined qualitative features, associated with the non-horizontal nature of the studied surface. Fig. 8 gives as an example of two-way curves for the azimuthal probing along the profile intersecting the Krotovskaia structure. It can easily be seen that here the above-described regularities are maintained in the mutual positions of the right-hand branches of the plus and minus curves. It is obvious that such clear indications are possible under conditions of comparative constancy of the geoelectrical section with regard to the distances, which is characteristic for the territory being studied.

THE METHOD OF TELLURIC CURRENTS

The idea of the method of telluric currents was proposed by K. SCHLUMBERGER in the thirties. However, owing to the intensive development in the resistance method, observations on the telluric currents were rarely conducted. After the war the systematic development of the telluric current method in the USSR was started by the staff of the VNII Geofizika working initially under S. M. SHEINMAN, and then ALEKSEEV and BERDICHEVSKII [2]. Experimental work conducted by parties from VNII Geofizika in the Saratovsk Zavolzh'e (1949), the Dneprovsko-Donetsk depression (1952) and the Cis-Baltic depression (1954), gave favourable results and made it possible to change over to the large-scale use of this method. Abroad [6] the method of telluric currents also finds industrial application.

The use of the telluric current method involves studies of the average periodic variations of the natural non-stationary electrical field of the earth (field of telluric currents) associated with a certain electrical phenomenon in the ionosphere. Telluric currents, embrace the whole of the globe, forming on its surface regional current whirlpools, and have a pulsating character, changing in time, in value and direction. The maximum intensity of variation of the field of telluric currents is usually observed in the period from 1–12 hr (Greenwich Mean Time) [7].

The theory of the telluric current method proposes that within the limits of small areas of the earth's surface, the field of telluric currents at any given instant of time can be considered as the field of a constant current, caused

by an infinitely long supply line AB. If the medium under investigation is horizontally homogeneous, then this field is always constant in value and direction. On the other hand, on the surface of a horizontally heterogeneous medium, the field shows variations both in value and in direction. These anomalies are associated with features of the geological structure of the medium under investigation, especially with the change in the total longitudinal conductivity of the sedimentary succession lying on a non-conducting foundation.

Thus, the field of telluric currents, as distinct from gravitational and magnetic fields of the earth, does not depend on the structure and petrographic composition of the rocks underlying the friable deposits, and under favourable conditions reflects the basic, features of the relief of the reflecting highly resistant level.

Exploratory observations of telluric currents are made at various points of the studied area at the same time as observations at the stationary base point. The distance between the base and field stations does not usually exceed 30–35 km.

The dimensions of the measuring devices are selected independently of the depth of the electrically reflecting horizon and in most cases are limited to 500–1000 m. This offers possibilities for using the method of telluric current in deep surveys, especially in difficultly accessible locations.

By processing the tellurograms obtained simultaneously at the base and field stations, the so-called parameter K associated in a simple way with the ratio of the areas of synchronized closed hodographs* of the field of telluric currents at the base and field points. The parameter K is the ratio of the average field intensities of the telluric currents at the points of observation. Using the value of the parameter K and taking the average intensity E of the field of the telluric current at the base point as being equal to any arbitrary value, it is possible to calculate the value of E at a number of field points and construct a map of E (a map of the average intensity of the field of the telluric currents) which represents the main results. In large-scale surveys, in addition to the E map, maps are drawn for other values, of auxiliary importance.

The geological interpretation of the E map is based on the idea that the decrease in E values is caused by an increase in the total longitudinal conductivity of the layer above the marker horizon and, consequently, under conditions of a constant geoelectrical cross-section by the downward dip of the high-resistance marker horizon. The regions of increased valwes of E

* Distance–time curves.

are interpreted as zones of reduced total longitudinal conductivity of the succession above the marker horizon and as the zone of elevation of the highly resistant marker horigon.

The method of telluric currents doesn ot involve a subdivision of the studied cross-section based on resistance, but gives results somewhat dependent on the influence of the horizontal electrical heterogeneity of the conducting sequence. In this connection, it would be desirable to combine the method of telluric currents with electrical resistance probings at various sections of the studied area. A combination of the observations on telluric currents with electrical probes not only increases the reliability of the qualitative conclusions on the geological structure of the region, but also makes it possible to carry out approximate quantitative calculations, necessary for conversion from the map of average field intensity of the telluric currents to a schematic structural map of the reflecting highly resistant horizon. With an equally-spaced network of resistance probes, the quantitative interpretation of the data of the telluric current method is made by using the empirical formula $H = FE^{\alpha}$, in which the values of F, α for the whole area of the survey are determined by comparing the average field intensity E of the telluric currents with the thickness H of the conducting sequence at the reflection points (from the data of electrical probes).

Depending on the character of the territorial distribution of the obtained coefficients, they are either averaged or interpolated. In the case of an extremely sparse network of resistance probes, use is made of the simpler formula $H = F/E$, which, as shown experimentally, gives less accurate results.

It should be mentioned that the quantitative interpretation of data of telluric currents can also be based on the use of values of depths of reflection from the results of seismic exploration under conditions where the seismic and electrical reflecting horizons correspond to the same formation.

In 1955, exploratory observations of telluric currents were carried out by an experimental party of the Siberian Aerogeophysical Expedition of VNII Geofizika in the Tomsk region in the closed polygon Tomsk – Bakchar – Podgornoe – Chezhemto – Mogochin – Shegarskoe of total length 750 km. The observation points were placed at a distance of 10 km from one another. The transport was provided by vehicles which were particularly suitable for rough ground, and when there was no road at all a helicopter was used for the first time, in electrical exploration work. During the survey, the position of the base station was changed after every 30 km. The values of E at the base points were equated by the correlation method and then reduced to

the original base station which made it possible to construct a combined map of the average intensity of the field of the telluric currents.

The field of telluric currents in Western Siberia in the summer of 1955 was characterized by a more or less intense variation with a period of 10–40 sec and an amplitude of the order of 1–2 mV/km. The maximum variation as a rule was observed in the daylight hours (9–15 hr). A periodic weakening was observed in the variations of the field of the telluric currents up to complete extinction (during August, September and October there were 10 such days).

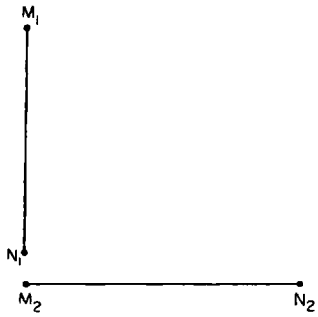

FIG. 9. L-shape arrangement.

The measurements were carried out with L-shape arrangements with measuring lines between 300–500 m long (Fig. 9). For synchronization of the observations a specially developed interference-free TB-6 Tele-switch was used in circuit with an RPMS radio station [8]. EPO-4 oscillographs were used to record the variations in the telluric current fields.

Fig. 10 shows the graph for the average field intensity of the telluric currents on the Tomsk-Bakchar profile, constructed on the assumption that the value E at point 24 is equal to one arbitrary unit. The values of E along the profile decrease regularly from Tomsk to Bakchar, changing more than four times. The character of the decrease in the average field intensity of the telluric current agrees well with known geological data and corresponds to a rapid increase in thickness of the sequence at the north-west limb of the Kolyvan'—Tomsk upfold, there being a clearly defined steplike lowering of the Paleozoic foundation in the immediate vicinity of Tomsk, and also between the villages Markelevo and Plotnikovo.

There is an interesting local maximum of average field intensity in the region of the points 15, 16, showing the possible presence here of an elevation of the Paleozoic foundation. It is interesting to notice that in this region,

seismological survey had shown an upfold in the Mesozoic deposits (Krasno-Bakcharskaia structure).

In view of the lack of a sufficient number of electrical resistance probes over this territory in the process of the geological interpretation of the observations on telluric current it was necessary to deal only with information on the depths of the current of Paleozoic rocks in the region of Kolpashevo (from drilling data) and in the region of Shegarskoe (from the data of vertical electrical probing). On the basis of these data and using the above formula, a schematic map was drawn for the thickness of friable deposits, lying on the

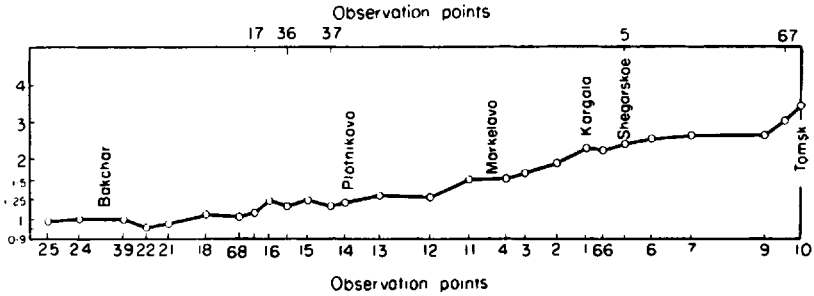

FIG. 10. Graph of average intensities of the field of telluric currents along the Tomsk-Bakchar profile (the vertical scale is logarithmic).

pre-Jurassic foundation (Fig. 11). Despite the rough diagrammatic constructions occasioned by sparse network of observations, and the absence of data on the parameters of the cross-section, this map shows how pre-Jurassic rocks dip towards the central regions of the western Siberian Lowlands. To the south of Kolpashevo, there is a zone of upfolded pre-Jurassic rocks, which are of interest for further study.

In 1956 in the Western part of the Lowlands the experimental work of the VNII Geofizika was continued in order to decide on the applicability of the telluric current method for solving regional and survey problems in the zones of development of volcano-sedimentary deposits of the second structural level, and also in the selling of the Berezovka gas deposits. Within the limits of the Tobol'sk and Vagai-Ishimsk tectonic zones, the party together with the department Zapsibneftegeofizika (led by YU. S. KOPELEV) carried out a large scale structural survey of the Zavodoukovsk area and also a route survey along the profile Zavodoukovsk–Vyatkino–Vikulovo. On the Berezovka area studies were made in the region of the group of Berezovka upfolds and along a 280 km regional route along the river Severnaya Sos'va.

In 1956 in Western Siberia the periods of intensive variation alternated with periods of weakening in the field intensity.

For example, if in the second half of August the variations with amplitude up to 3 mV/km were continued almost uninterruptedly for a period of 10–12hr,

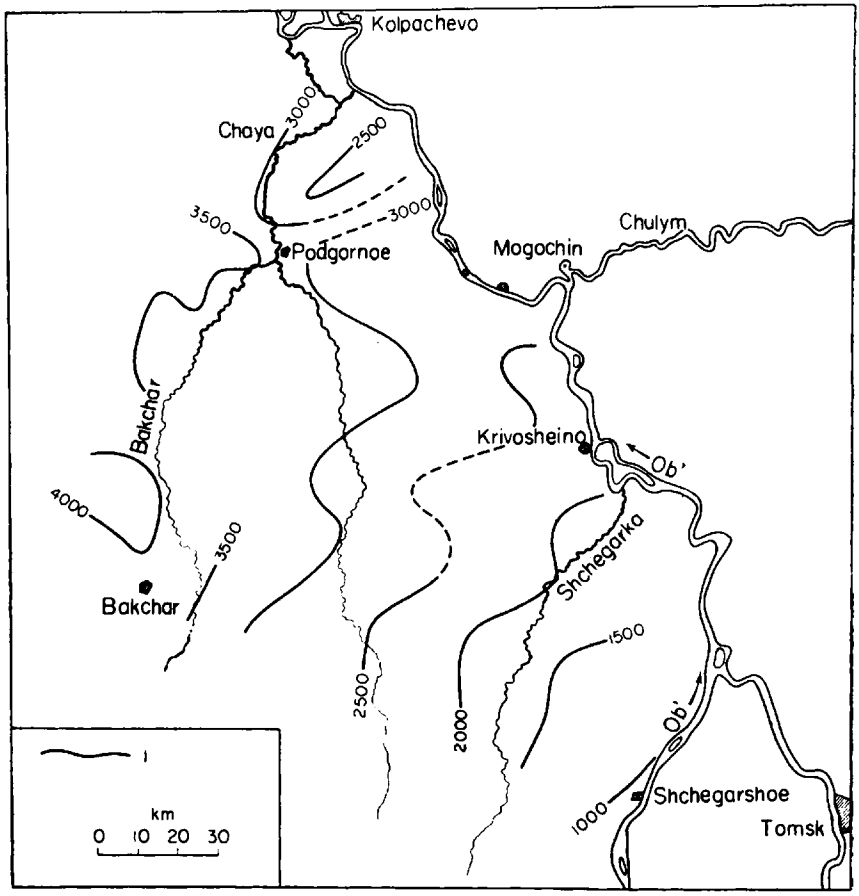

FIG. 11. Map of thickness of friable deposits. 1—Equal thickness line for the friable deposits.

then in September, the amplitude of the variations was reduced to 0.5–1mV/km, and the duration of variations to 5–6 hr. For each month of the field season of 1956 there were 2 to 6 days when there were no measurable variations. The average rate of production using the telluric current method was 1 point per instrument change in route surveys with a 10–30 km step and 2 points in an areal survey with a 3–5 km step.

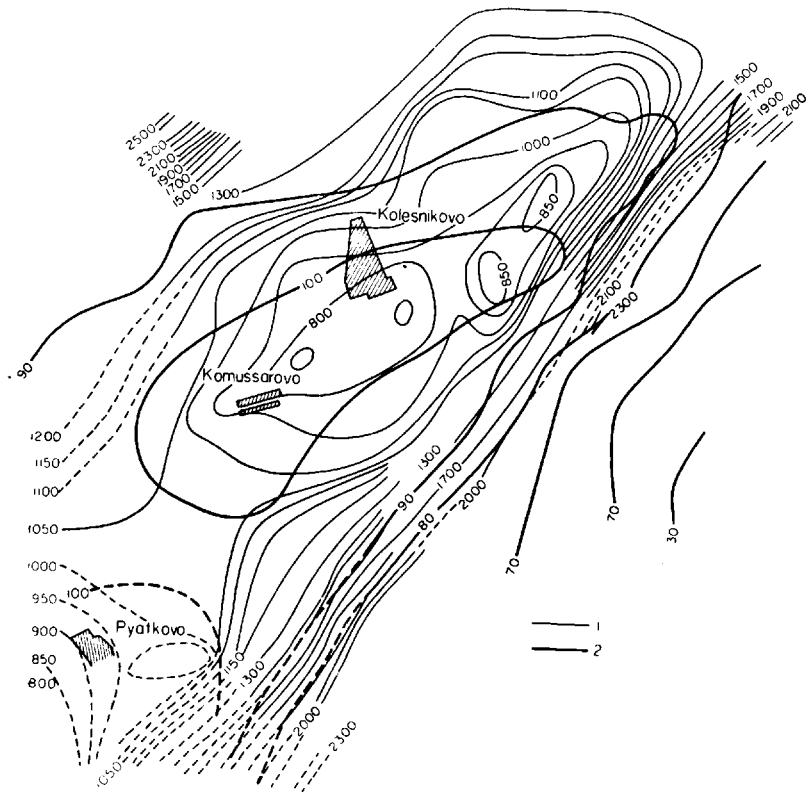

FIG. 12. Map of the average intensity of the field of telluric currents (from material of VNII Geofizika and Zapsibenftegeofizika). The value of E at the base point is taken as 100 arbitrary units. 1—structure contours of the seismical reflecting horizon; 2—isolines of average field intensity.

In the wooded and swampy Berezovka region, work was conducted along the rivers, with sections being landed on the banks and the lines unreeled in the zone near the banks.

Fig. 12 shows the results for the study of telluric currents at the Komissarovskaya structure in comparison with the data of seismical surveys. It can be seen that the known Komissarovskaya structure appears clearly on the map of the average field intensity of the telluric currents; the telluric current method can therefore be recommended for surveys of similar upfolds.

Good results were also obtained in the regional studies. Fig. 13 gives a geoelectrical cross-section constructed on the resistance observations of telluric currents, made for a determination of resistance values of the average field intensity at the base points (step of resistance network 30 km).

Quantitative calculations were made using the seismic exploration results at the Komissarovskaia structure (65 km to the south-west of the start of the profile) as initial data. A zone of upfolding is observed in the high-resistance level to the west of the Vyatkino well and in the region of the Krotovsk structure. The behaviour of the electrical marker horizon agrees well with the tectonics of the Mesozoic deposits deduced from the data of seismic explorations. The absolute values of stratum thicknesses of the friable deposits, calculated from the telluric current are close to the bore-hole data in the region of Vyatkino and Vikulovo.

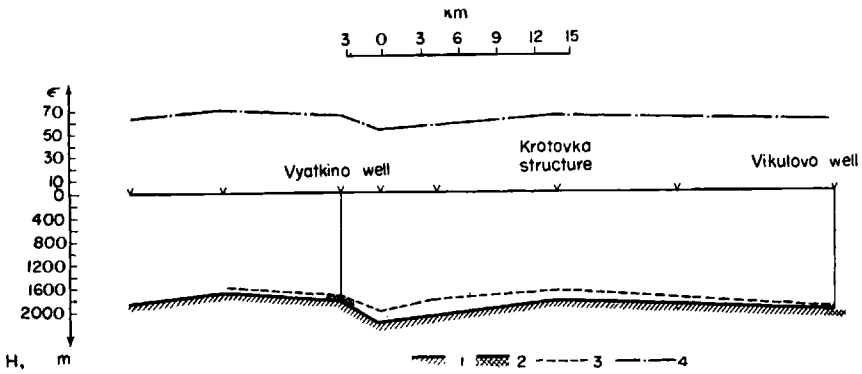

FIG. 13. Geoelectrical section along the Vyatkino–Vikulovo profile. 1—surface of electrically reflecting horizon; 2—bottom of the friable Mesozoic deposits; 3—surface of the seismical reflecting horizon at the bottoms of the Mesozoic; 4—average field intensity of telluric currents.

Also effective was the use of the telluric current method in the Berezov region, where the results of a study by telluric currents make it possible to formulate a general idea of the relief of the Paleozoic foundations.

A NEW ELECTRICAL EXPLORATION APPARATUS FOR WORK IN SIBERIA

The standard electrical exploration equipment used by the MNP geophysical parties is not very suitable for working in inaccessible localities. A modern electrical exploration station can be used only in regions with a well developed road system, even when the station is mounted on the GAZ-63 vehicles. The apparatus for the method of telluric currents is in the form of the EPO-4 oscillograph and its power supply is too large for forest parties. For this reason, a number of new designs have been developed in VNII Geofizika to be employed in Siberian settings.

In 1956, at the laboratory of electrical exploration and the design bureau

of VNII Geofizika, A. M. ALEXEEV, N. A. BULANOV and others, designed two new electrical exploration stations, one of which—ERST-23-56—is intended for working in inaccessible country and also in the winter (the so-called tractor variant); the second—the EPS-16-56—a cross-country dismountable, is only for dipole probing in inaccessible country.

The following are the basic features of the new stations which will indicate the possibilities of their use in other problems of surveying under various conditions.

The ERST-23-56 station is mounted on a trailer and its two PN-100 generators are powered by a special gasoline engine ZIS-120, the gear box shaft of which is connected by a universal joint to the shaft of the first generator (Fig. 14). The engine and generators are mounted on shock absorbers and since they are connected by a universal joint during operations the power unit does not cause vibration in the body or measuring apparatus.

To control the engine, on the control desk there is a special panel which has: a gasoline level indicator, an ammeter to check the operation of the charging generator, an oil manometer included in the lubrication system of the engine, a thermometer to check the cooling system of the engine. Also on the control desk there are buttons for controlling the gas and the air intake, a starter button, and also a clutch pedal and gear shift.

With a booster arrangement, the voltage of the two connected generators can be increased to 1000 V providing the resistance of the insulation of the current leads is not less than 5 MΩ.

The new station has benefited from the experience of the ERS-23-53 stations which are used by the electrical exploration parties. In the station there is a fixed loading resistance, which can be used as a ballast loading to use when operating with the usual arrangement, since in a number of regions in measurements with the doubling arrangement there is distortion in the rectangular nature of the current impulses.

Apart from the EPO-5 oscillograph, an extra apparatus is provided to measure ΔU. Under winter conditions, considerable difficulties are experienced in earthing; the station therefore has a d.c. amplifier with an input resistance of the order of several megohms; this makes it possible to carry out measurements of ΔU in regions with poor earthing conditions of MN, where the intermediate resistance can reach very high values (of the order of $50–100 \times 10^3 \Omega$).

In the tractor variant of the station, the generator group and all the measuring apparatus are placed on a trailer with caterpillars, which is drawn by an S-80 tractor. On the trailer there is a metal body suitable for operation under winter conditions. Between the two walls of the body there is a heat

insulating lining, there are double window-frames and to protect the body from cold air there is a tambour. Inside the body there is a stove; for further heating, use can be made of the ballast resistance, the main function of which is to load the generators during the time when their insulation is being dried. The body is divided into two parts: in the first there is the operator's section, in the second, the motor section. In the operator's section there is a desk which carries the engine controls, the generators and the measuring apparatus.

There is also dark-room for developing the oscillograms. This part is suitable for use as temporary living quarters for technical personnel working at the station.

Combining the generator and measuring apparatus in one body makes it possible to use the ERST-23-56 station for probing with the AMNB arrangement with only one operator.

The pressure exerted by the tracks of the trailer with the station does not exceed 0.2 kg/cm^2.

The S-80 tractor intended for operation with the station is equipped with a heated body, in which there is a table for the measuring apparatus, if it becomes necessary to carry out dipole probes, and a winch to reel and unreel the supply line when working with the AMNB arrangement.

The winch is driven by a shaft from the tractor and is provided with an automatic cable-laying device, designed for a PUM grade cable. The winch can hold 6–8 km of this cable. During reeling and unreeling of the lines, the tractor moves at speeds up to 9 km/hr.

The dismountable electro-prospecting station is mounted on the GAZ-69 vehicle which can move cross-country. If the station cannot be moved independently, the generator group can be taken to the place of work on an MI-4 helicopter or on a small barge on the river. The overall layout of the generator group is given in Fig. 15. If necessary, the generator (PN-145) can be removed from the generator group together with the plug board and certain other auxiliary parts.

The generator is mounted on a special sledge which guides it onto the platform of the vehicle. To ease the assembly of the detachable parts there is a special small winch on the vehicle and also screw clamps with which one person without using tools can secure the generator to the vehicle. At the same time as the generator is installed its shaft is connected to the shaft from the gearbox. To reduce the length of the generator group, certain units and components of the motor car body are removed, and the electrical arrangement is simplified as much as possible, even to the exclusion from it of an excitation rheostat.

The rated power of the generator group is 16.5 kW, but as is usual in electrical exploration stations, the power developed can be boosted to 18 kW with a current strength of up to 40 A, which is sufficient in most cases for carrying out dipole probes. The voltage and the power developed by the generator group are controlled by changing the number of revolutions in the engine, since the impulse windings are connected directly to the circuit of the generator's armature.

Since the ERS-16-56 station is mainly intended for dipole probes in

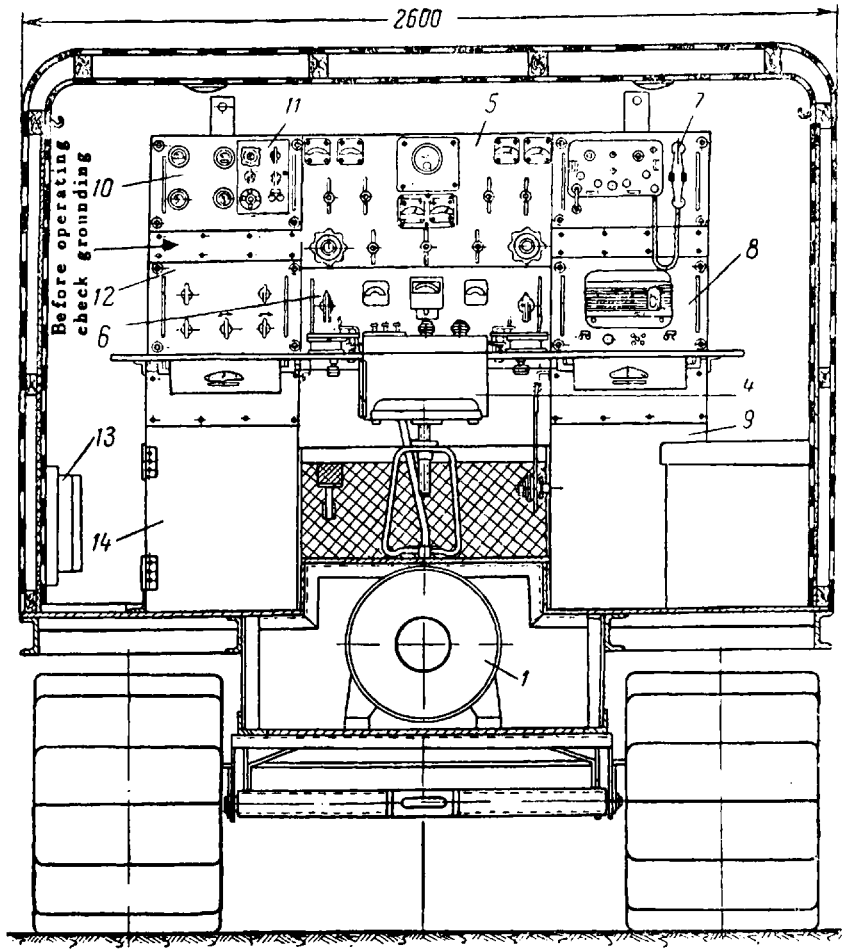

FIG. 14. Position of ERST-23-56 apparatus and equipment in the body of the trailer. 1—generators; 2—ZIS-120 engine; 3—control panel; 4—EPO-5 oscillograph; 5—high voltage panel; 6—low voltage panel; 7—receiving and transmitting radio

[*continued opposite*

inaccessible regions, to measure ΔU there are two portable EShO-56 electron loop oscillographs with cinefilm recording.

The EShO-56 electrical exploration loop oscillograph (Fig. 16) was developed in 1956 at the L'vov Institute of Machines and Automatics at the request of the Electrical Prospecting Laboratory of VNII Geofizika especially for dipole probing in inaccessible country. The oscillograph has an a.c. amplifier with converter, in the form of a VT vibro-converter (Fig. 17). The vibroconverter converts the input current into an alternating current with a frequency of about 180 c/s and, at the same time, acts as a mechanical rectifier for the output of the amplifier.

In the output stage of the amplifier there is a Tr-2 transformer, in the secondary winding of which there are connected in series a micro-ammeter, a resistance R_{26}, one of the resistances R_{19}–R_{25}, (depending on the limit of measurement) and the left contact of the P vibro-converter.

When the armature of the vibro-converter is moved to the left, the secondary winding of the output transformer is loaded and current flows in it, moving the pointer of the micro-ammeter and the mirror of the galvanometer G. At the same time the voltage of the feedback input of the amplifier, with a polarity opposite to that fed to the input signal, is taken from one of the resistances R_a–R_{25}, i.e. in the instrument there is a deep (close to 100%) negative feedback with direct current, and the arrangement as a whole

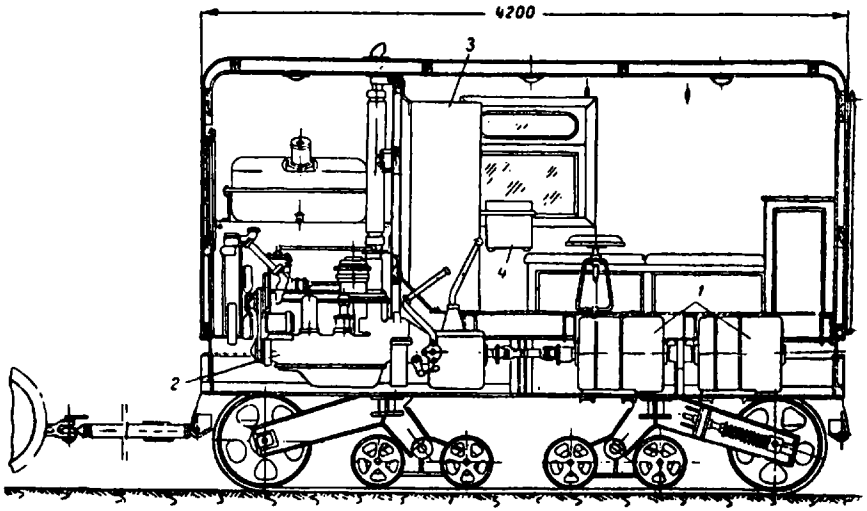

station; 8—calling device; 9—block of contactors; 10—control panel for engine operation; 11—D. C. amplifier; 12—measurement panel; 13—output panel; 14—loading resistance.

is self-compensating. The instrument readings do not, therefore, depend on the state of the feeding sources, and there is practically no drifting of the zero point.

At the instant when the armature of the vibro-converter is moved to the right contact, the input of the amplifier is shorted and simultaneously the circuit of the secondary winding of the Tr-2 transformer is disconnected. In other words, the instrument produces a half-period rectification.

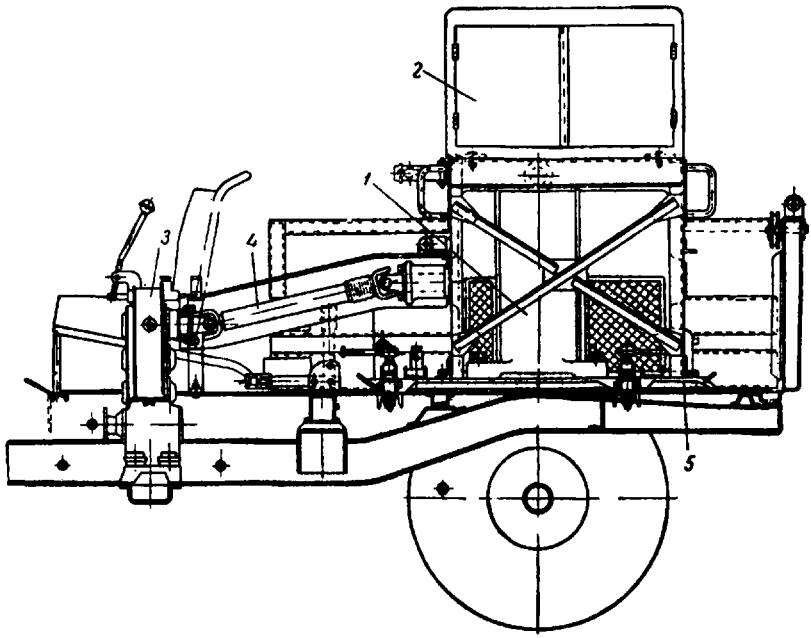

FIG. 15. The body of the GAZ-69 vehicle with the PN-145 generator. 1—PN-145 generator; 2—block of contactors; 3—gearbox; 4—propeller shaft; 5—slides.

The main features of the instrument are as follows:

1. The high sensitivity of the instrument, corresponding to 1.0 mV over the whole width of the film, can be further increased.

2. The record is made on a standard low sensitivity cinefilm.

3. When processing the results of the record, a photomultiplier is used which magnifies the record of up to 10 times linear.

4. The film is moved by a spring motor with a speed of 0.25 mm/sec.

5. The instrument has its own power supply from five 2S-KU and two GB-225 dry batteries which ensure normal operation of the instrument for 40–50 hours.

6. The temperature range over which the instrument operates is determined by the capacity of the supply sources.

7. The relative error in the camera measurements on the film does not exceed 2%.

8. The input resistance of the instrument at the highest sensitivity is 2–3 MΩ.

9. During recording visual readings can be taken of a pointer.

10. The instrument measures 340 × 220 × 240 mm.

11. The instrument, together with supply sources, does not weigh more than 14 kg.

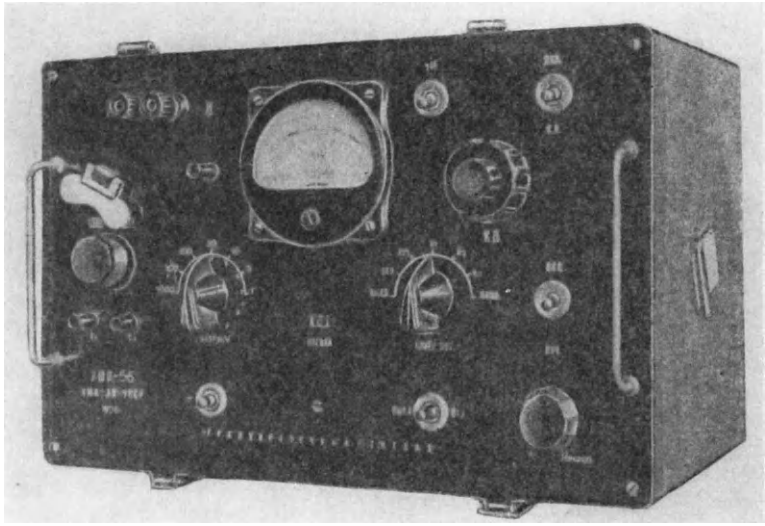

FIG. 16. The EShO–56 oscillograph.

Thus, if the generator group is brought to the field location, then measurements can be made in every case, since all the parts of the measuring devices are portable. The device can be used under all earthing conditions of the MN electrodes (sand, frozen earth), and its readings in practice do not depend on the state of the supply sources.

Still greater advantages are given by a new electronic measuring apparatus which operates with the telluric current method. A field station which is now being built for the telluric current method is placed on the GAZ-69 motorcar and includes:

1. A 2-channel electron amplifier (weighing about 10 kg together with

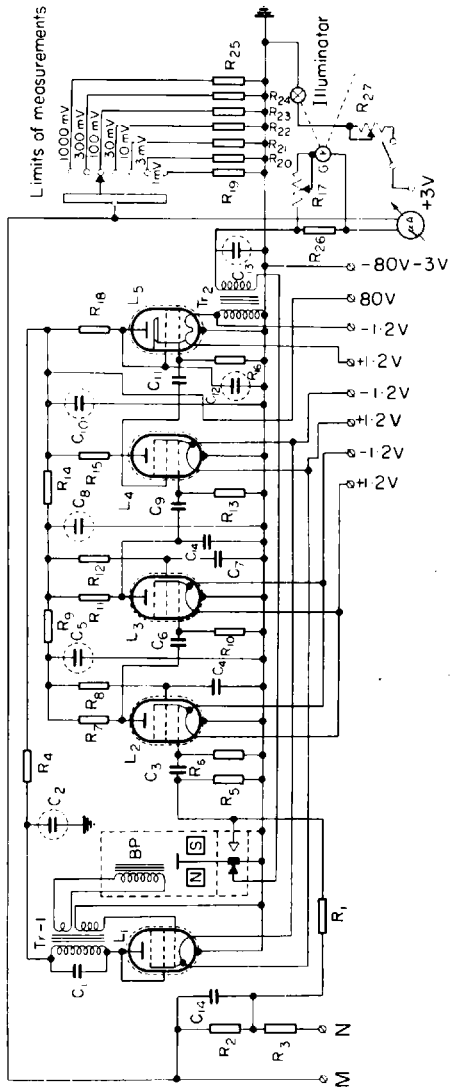

FIG. 17. Arrangement of electron loop oscillograph ESh O-56, developed by K. B. KARANDEEV L. YA. MIZYNK and V. N. GONCHARSKII. G—galvanometer ($S = 1.10^{-7}$ a/milliradian); T_1, T_2, T_3, T_4 are 1 B 1P* tubes, T_5 is a 2P 1 P† tube. Resistances: R_1—470 K; R_2—8.2 meg; R_3—5 K; R_4—30 K; R_5—2.2 M; R_6—8.2 M; R_7—1 M; R_8—6.8 M; R_9—51 K;R_{10}—7.5 M; R_{11}—1 M; R_{12}—6.8 M; R_{13}—7.5 M; R_{14}—51 K; R_{15}—240 K; R_{16}—1 M; R_{17}—400; R_{18}—10 K; R_{19}—10; R_{20}—30; R_{21}—100; R_{22}—300; R_{23}—1000; R_{24}—3 K; R_{25}—10 K; R_{26}—200; R_{27}—30. Condensers: C_1—0.1 F; C_2—10 F; C_3—5100 pF; C_4—10 F; C_5—30 F; C_6—5100 pF; C_7—0.1 F; C_8—30 F; C_9—5100 pF; C_{10}—30 F; C_{11}—0.02 F; C_{12}—0.30 F; C_{13}—2000 F; C_{14}— F;

* Translator's note: equivalent to U. S. tube 1 U5.

† Translator's note: no equivalent given in literature; a beam power tube.

the supply sources) with a high-voltage input, its circuit being similar to that of the EShO-56 oscillograph.

2. An oscillograph with a spring motor (weighing not more than 8 kg together with the filament batteries of the illuminator lamp.

3. An RPMS radio station with a power pack, into which is also assembled the TV-6 tele-switch used in transmitting and receiving the time signals by radio (two units weighing 11 kg each). In the tele-switch there is introduced an interference stable system, which limits the interference level. Consequently, even with a high level of interference, the TV-6 does not give false time signals.

4. Non-polarizing portable electrodes;

5. Two cable reels (weighing 2 kg each).

The use of the amplifier makes it possible to record also telluric current variations, which due to the insufficient amplitude would be considered unworkable when using an EPO-4 oscillograph.

The whole of the apparatus is fixed in the body of the station but if the vehicle is unable to continue, since the arrangement is sufficiently portable the apparatus can be removed in 2–3 min and carried by three of the field-party members to the observation point.

CONCLUSIONS

The work of the VNII Geofizika has shown the effectiveness of new electrical survey methods under conditions prevalent in the Western Siberian Lowlands.

These methods should find applications in solving regional and survey problems of geophysical investigations for petroleum and gas.

At the present stage the exploratory observations on telluric currents are best used to solve problems of a regional character (separating out large depressions and culminations, and also detecting upfolds of the second order) in conjunction with gravimetric and aeromagnetic work in tectonic surveys of the Western Siberian territory.

The most effective results can be obtained on a scale of 1:1,000,000 with a net work density of 1 point per 100 km^2. It is desirable also to carry out separate length profiles along rivers. With a favourable geoelectrical cross-section the telluric current method can also be used to survey local upfolds.

The two-way electrical probing should preferably be directed towards the solution of survey and exploration problems, and also for setting up a basic network for the telluric current method in regional studies.

The results of experimental work carried out in the Western Siberian Lowlands open up possibilities for a more extensive use of electrical prospect-

ing in Siberia. To introduce electrical prospecting into the geophysical investigations in Siberia, it is essential to speed up the serial production of new equipment.

Serious attention should be paid to the further development and improvement of electrical prospecting methods, the possibilities of which have not been exhausted by work done up to the present. In particular, the energy of research workers should be concentrated on the creation of methods using natural and artificial variable electromagnet fields. These methods can be used to increase the efficiency of electrical prospecting work and also to extend the sphere of application (studies in the regions of permanent frost) of electrical prospecting.

REFERENCES

1. L. M. AL'PIN, *The Theory of Dipole Probes*, Gostoptekhizdat (1950.)
2. A. M. ALEKSEEV, and M. N. BERDICHEVSKII, Electrical prospecting by the telluric current method. *Applied Geophysics*, No. 8, Gostoptekhizdat (1950).
3. M. N. BERDICHEVSKII, and A. D. PETROVSKII, The method of two-way equatorial probes. *Applied Geophysics*, No. 14, Gostoptekhizdat (1955).
4. M. N. BERDICHEVSKII, *Instructions for Processing Electrical Probe Oscillograms*. VNII Geofizika (1954).
5. A. M. ZAGARMISTR, Using the Increased Resolving Power of Axial Probe Curves. *Applied Geophysics*, No. 16, Gostoptekhizdat (1957).
6. L. MIGO, and G. KUZNETS, *Electrical Prospecting for Petroleum*. IVth International Petroleum Congress. Geophysical prospecting methods. Gostoptekhizdat (1956).
7. V. A. TROITSKAYA, The Earth's currents. *Priroda*, No. 5 (1955).
8. YU. V. KHOMENYK, The TV-6 tele-switch. *Exploratory and Industrial Geophysics*, No. 17, Gostoptekhizdat (1957).

CHAPTER 9

THE METHOD OF CURVED ELECTRICAL PROBES

M. N. BERDICHEVSKII

THE method of two-way quadrilateral probes* has been widely accepted by electrical exploration workers carrying out electrometric studies in regions where field sections can travel along long straight profiles [2]. However, when working in country where conditions are difficult, the use of quadrilateral probes is often impossible since the swampy or wooded sections of the surveyed area hinder movement of field parties along a straight line. In this case, it is desirable to change from measurements with a quadrilateral setting to those with an azimuthal arrangement, which would make it possible to use the so-called curved probe, i.e. probes with the observation points on curved routes. The curved probes can also be carried out with a radial arrangement and an arbitrary two-component arrangement by means of which measurements are made of the mutually perpendicular components of the field.

The properties of an azimuthal arrangement and the method for carrying out curved azimuthal probes (from the results of studies made in the VNII-Geofizika in 1954–1956 by the author together with T. N. ZAVADSKAYA and V. P. BORDOVSKII) are given below.

AZIMUTHAL ARRANGEMENT

The azimuthal arrangement is shown in Fig. 1. Here AB is the supply line, MN the measuring line, R the distance between centres O and Q of the feed and measuring lines, θ is the angle formed by the feed line AB and the line OQ.

A basic condition of the azimuthal arrangement is the perpendicularity of the measuring line MN to the section OQ, connecting the centers O and Q of the feed and measuring lines. It is apparent that the quadrilateral ar-

* The quadrilateral [literally equatorial in the Russian edition] probe is one of the modifications of the dipole probes proposed by L. M. Al'pin. He has developed the whole theory of dipole probes [1].

rangement is a particular case of an azimuthal arrangement. L. N. AL'PIN has shown that the KS value of an azimuthal dipole arrangement* in a horizontally homogeneous medium does not depend on the angle Θ and for the same distances R between the centres of the feed and measuring dipoles coincides with the KS value of the quadrilateral dipole arrangement and consequently with the KS value of the limiting AMN arrangement the

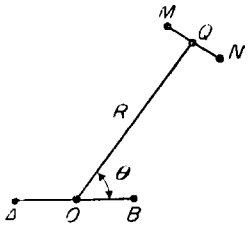

FIG. 1.

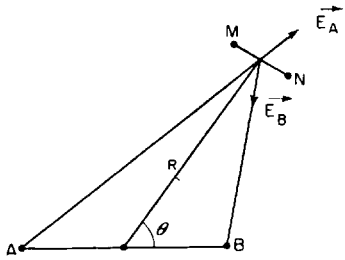

FIG. 2.

length of which is equal to the distance R. This property of an azimuthal dipole arrangement also creates possibilities for carrying out curved probes, since in the transfer from one spacing of azimuthal probing to another it is not necessary to keep the angle Θ unchanged.

THE COEFFICIENT OF THE AZIMUTHAL ARRANGEMENT

The coefficient of the azimuthal arrangement will be calculated from an approximate formula, the derivation of which is based on the assumption that the length of the measuring line is sufficiently small, and to a sufficient approximation the value of the difference in potential between the poles of the measuring line can be taken as equal to

$$\Delta U^{AB}_{MN} = E^{AB}_{MN}\,\overline{MN} \tag{1}$$

where: E^{AB}_{MN} is the component of the field of the feed line AB along the direction MN.

It is obvious that (Fig. 2)

$$E^{AB}_{MN} = E^{A}_{MN} + E^{B}_{MN} = E^{A}\cos(\vec{E}^{A}, MN) + E^{B}\cos(\vec{E}^{B}, MN).$$

The values E^A and E^B for a homogeneous medium with a specific resist-

* We will call a dipole arrangement that in which the feed and measuring lines have an infinitely small value.

ance ϱ are determined by the expression:

$$E^A = \frac{I\varrho}{2\pi\left(R^2 + \frac{\overline{AB}^2}{4} + R\overline{AB}\cos\Theta\right)},$$

$$E^B = \frac{I\varrho}{2\pi\left(R^2 + \frac{\overline{AB}^2}{4} - R\overline{AB}\cos\Theta\right)}.$$

Bearing in mind that

$$\cos(\vec{E}^A, MN) = \frac{\overline{AB}\sin\theta}{2\sqrt{R^2 + \frac{\overline{AB}^2}{4} + R\overline{AB}\cos\Theta}},$$

$$\cos(\vec{E}^B, MN) = \frac{\overline{AB}\sin\Theta}{2\sqrt{R^2 + \frac{\overline{AB}^2}{4} - R\overline{AB}\cos\Theta}},$$

we obtain according to (1)

$$\Delta U^{AB}_{MN} = \frac{I\varrho\,\overline{AB}\,\overline{MN}\sin\Theta}{4\pi}\left\{\left[R^2 + \frac{\overline{AB}^2}{4} + R\overline{AB}\cos\Theta\right]^{-3/2} + \right.$$

$$\left. + \left[R^2 + \frac{\overline{AB}^2}{4} - R\overline{AB}\cos\Theta\right]^{-3/2}\right\}.$$

From the expressions for the difference in potentials we transfer to an expression for the coefficient of the arrangement, representing the latter in the form of the product of two factors

$$K = K^* A. \tag{2}$$

The factor K^* is calculated from the formula*

$$K^* = \frac{R^3}{\overline{AB}\,\overline{MN}}\,10^{-3}, \tag{3}$$

and the factor A from the formula

$$A = \frac{4\pi}{\sin\Theta}\,\frac{1}{\left(1 + \frac{\overline{AB}^2}{4R^2} + \frac{\overline{AB}}{R}\cos\Theta\right)^{-3/2} + \left(1 + \frac{\overline{AB}^2}{4R^2} - \frac{\overline{AB}}{R}\cos\Theta\right)^{-3/2}}. \tag{4}$$

To facilitate the calculations we will use a special nomogram for the factor A, shown in Fig. 3.

* The formula is given for the case where the current is determined in amperes and the potential difference in millivolts.

On the nomogram values $\frac{\overline{AB}}{2R}$ are plotted along the ordinate and the values for the angle Θ along the abscissa. The required value for the factor A should be determined by interpolating between the lines of identical values of the factor A.

Example—We will calculate the coefficient for an azimuthal arrangement, characterized by the following dimensions: $\overline{AB} = 1000$ m, $MN = 200$ m, $R = 3000$ m, $\Theta = 75°$. From formula (3) we find the value of the factor

$$K^* = \frac{3000^3 \cdot 10^{-3}}{1000 \cdot 200} = 135.$$

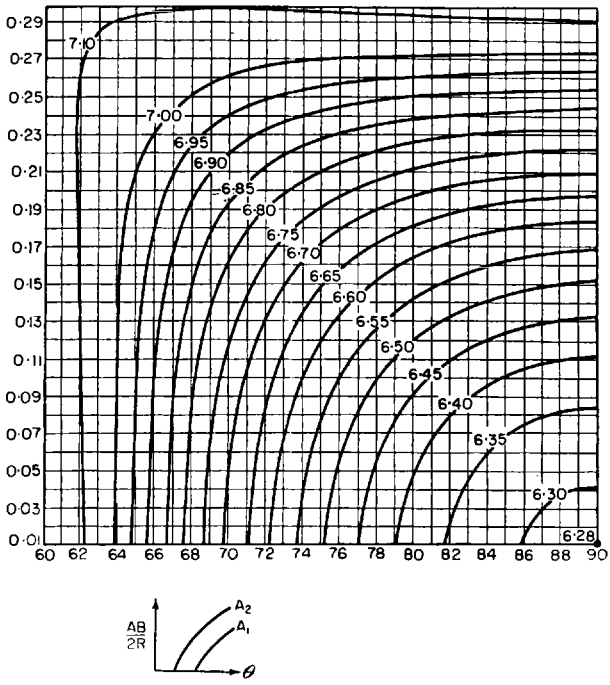

FIG. 3. Nomogram of factor A.

From the nomogram (see Fig. 3) we determine the value of the factor A for the coordinates $\frac{\overline{AB}}{2R} = 0.167$, $\Theta = 75°$. Interpolating between the isolines 6.65 and 6.70, we obtain $A = 6.68$.

Thus, the required value for the coefficient K is

$$K = 135 \cdot 6.68 = 902.$$

OPERATIONAL DISTANCE AND DIMENSIONS OF THE AZIMUTHAL ARRANGEMENT

The operational distance $\bar{R}$ of the azimuthal arrangement is taken as equal to the length of the three-electrode limiting AMN arrangement which on the surface of a horizontally homogeneous medium gives a KS value, coinciding with that for an azimuthal arrangement.

The KS value for an azimuthal arrangement is determined from the formula

$$\varrho_a = K\frac{\Delta U_{MN}^{AB}}{I}, \tag{5}$$

where: K is the coefficient of the azimuthal arrangement.

For a limiting 3-electrode AMN arrangement, the KS value will be

$$\varrho = 2\pi\bar{R}^2\frac{E}{I}, \tag{6}$$

where: E is the intensity of the field of the point source;

$\bar{R}$ is the length of the 3-electrode arrangement (the distance from the point source to the center of the measuring dipole).

Let $\bar{R}$ be the operating distance of the azimuthal arrangement. Hence

$$\varrho_a = \varrho. \tag{7}$$

Starting from equation (7) we will attempt to show the connection between the operating distance of the azimuthal arrangement and its dimensions.

According to the principle of reciprocity

$$\Delta U_{MN}^{AB} = U_M^{AB} - U_N^{AB} = \Delta U_{AB}^{M} - \Delta U_{AB}^{N}. \tag{8}$$

Here the lower indices indicate the points and arrangements of the observation, the upper indices the points and arrangements of supply.

It is obvious that:

$$\begin{aligned} \Delta U_{AB}^{M} &= \int_A^B E_{AB}^{M}\,dl, \\ \Delta U_{AB}^{N} &= \int_A^B E_{AB}^{N}\,dl, \end{aligned} \tag{9}$$

where: E_{AB}^{M}, E_{AB}^{N} are the components of the field of the point sources M and N along the direction AB.

To determine the values of the field E of the point source we return to

the theoretical curve of ϱ for a limiting 3-electrode apparatus and we mark out on this curve a certain small section, in the limits of which the dependence of the ordinate $\log \varrho$ on the abscissa $\log \bar{R}$ can, with sufficient accuracy, be expressed by a linear equation

$$\log \varrho = t \log \bar{R} + \log T, \tag{10}$$

where: t and T are certain parameters, which depend on the dimensions of the arrangement and the geoelectrical cross-section, t being an angular coefficient of the tangent to the KS curve (in a bi-logarithmic form).

Using expression (10) and considering formula (6), we write

$$E = \frac{IT}{2\pi} \bar{R}^{t-2}$$

We use this expression to determine the components E_{AB}^{M} and E_{AB}^{N} of the field of the point sources M and N along the direction AB (on the surface of a horizontally homogeneous medium).

Then integrating (9), we obtain:

$$\Delta U_{AB}^{M} = \frac{IT}{2\pi} \frac{\overline{MB}^{t-1} - \overline{MA}^{t-1}}{t-1},$$

$$\Delta U_{AB}^{N} = \frac{IT}{2\pi} \frac{\overline{NB}^{t-1} - \overline{NA}^{t-1}}{t-1}$$

Thus,

$$\Delta U_{MN}^{AB} = \frac{IT}{2\pi(t-1)} [\overline{MB}^{t-1} - \overline{MA}^{t-1} - \overline{NB}^{t-1} + \overline{NA}^{t-1}]. \tag{12}$$

Using expressions (11) and (12), we obtain from condition (7)

$$2\pi \bar{R}^{t} = \frac{K}{t-1} [\overline{MB}^{t-1} - \overline{MA}^{t-1} - \overline{NB}^{t-1} + \overline{NA}^{t-1}]. \tag{13}$$

We express the operating distance $\bar{R}$ by the product of two factors

$$\bar{R} = pR, \tag{14}$$

where: p is a correction coefficient;

R is the distance between the centres of the feed and measuring lines of the azimuthal arrangement.

According to (13) and (14), the coefficient p will be equal to

$$p = \sqrt{\frac{K}{2\pi R^{t}(t-1)} [\overline{MB}^{t-1} - \overline{MA}^{t-1} - \overline{NB}^{t-1} + \overline{NA}^{t-1}]}. \tag{15}$$

TABLE 1. VALUES OF THE COEFFICIENT p

t	Θ / $\overline{AB}/2R$ / $\overline{N}/2R$	90°				80°				70°				60°			
		0.1	0.15	0.2	0.3	0.1	0.15	0.2	0.3	0.1	0.15	0.2	0.3	0.1	0.15	0.2	0.3
+1	0.1	0.9950	1.0018	1.0105	1.0354	0.9956	0.9993	1.0064	1.0255	0.9913	0.9926	0.9951	1.0024	0.9864	0.9826	0.9774	0.9667
	0.05	1.0027	1.0084	1.0169	1.0417	1.0030	1.0064	1.0135	1.0318	0.9986	0.9985	1.0024	1.0097	0.9939	0.9896	0.9846	0.9736
	0.02	1.0048	1.0113	1.0194	1.0433	1.0049	1.0077	1.0155	1.0357	1.00071	1.00158	1.0043	1.0112	0.9963	0.9920	0.9866	0.9754
−1	0.1	1.0246	1.0302	1.0380	1.0601	1.0216	1.0274	1.0331	1.0514	1.0196	1.0194	1.0188	1.0214	1.01302	1.0700	0.9982	0.9771
	0.05	1.0099	1.0161	1.0243	1.0480	1.0069	1.0130	1.0193	1.0393	1.0049	1.0048	1.0046	1.0073	0.9990	0.9921	0.9834	0.9632
	0.02	1.0054	1.0120	1.0205	1.0447	1.0027	1.0091	1.0154	1.0339	1.0071	1.00052	1.0059	1.0043	0.9950	0.9879	0.9793	0.9605
−2	0.1	1.0172	1.0230	1.0310	1.0537	1.0149	1.0198	1.0256	1.0430	1.0115	1.0106	1.0097	1.0102	1.0053	0.9969	0.9867	0.9638
	0.05	1.0080	1.0146	1.0277	1.0464	1.0056	1.0110	1.0169	1.0356	1.0024	1.0016	1.0075	1.0020	0.9957	0.9878	0.9776	0.9555
	0.02	1.0053	1.0115	1.0199	1.0444	1.0030	1.0083	1.0145	1.0325	0.9998	0.9993	0.9986	0.9999	0.9938	0.9851	0.9752	0.9533
−3	0.1	1.0146	1.0205	1.0285	1.0514	1.0126	1.0170	1.0228	1.0394	1.0085	1.0070	1.0053	1.0040	1.0017	0.9921	0.9811	0.9549
	0.05	1.0076	1.0135	1.0219	1.0459	1.0052	1.0098	1.0158	1.0336	1.0095	0.9996	0.9986	0.9979	0.9939	0.9842	0.9731	0.9485
	0.02	1.0052	1.0017	1.0201	1.0442	1.0032	1.0078	1.0140	1.0312	0.9992	0.9979	0.9965	0.9962	0.9925	0.9826	0.9703	0.9467
	$\bar{p}$	1.0084	1.0146	1.0224	1.0466	1.0066	1.0114	1.0177	1.0360	1.0032	1.0028	1.0029	1.0055	0.9972	0.9899	0.9811	0.9616

We will study the dependence of the correction coefficient p on the dimensions of the azimuthal arrangement and the parameter t (Table 1).

As can be seen from the Table, the values of p oscillate around unity and for fixed $\frac{\overline{AB}}{2R}$ and Θ vary within the limits of 3%. In connection with this, it can be concluded that when the conditions are satisfied:

$$\frac{\overline{AB}}{2R} \leqslant 0.3, \frac{\overline{MN}}{2R} \leqslant 0.1, 120° \leqslant \Theta \leqslant 60°.$$

the values of the coefficient p do not depend to any great extent on the shape of the KS curve (on the parameter t).

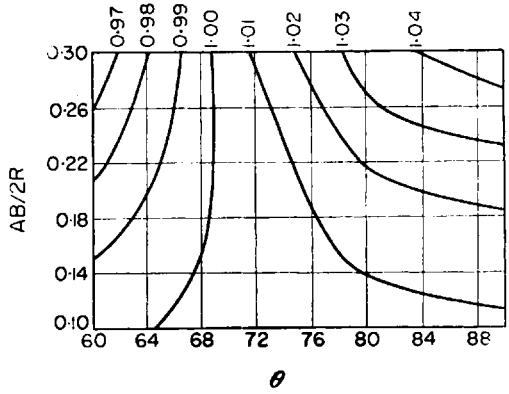

FIG. 4. Nomogram of coefficient p.

Let us determine the average arithmetic means of $\bar{p}$ for each vertical column of the table. It can readily be seen that the individual values of p differ from the arithmetic means of $\bar{p}$ by not more than 1.6%. Let us use the obtained arithmetic means of $\bar{p}$ to construct a nomogram of the correction coefficient of $\bar{p}$ shown in Fig. 4. This nomogram gives the required value of the coefficient of p with errors not exceeding 2%.

To find the operating distance of the azimuthal arrangement it is necessary to determine from its given dimensions—using the above-described nomogram—the value of the correction coefficient p and to calculate the operating distance of the azimuthal arrangement from formula (14).

If $\Theta = 90°$, the azimuthal arrangement becomes equatorial, and the operating distance $\bar{R}$ of such an arrangement can be obtained either by the above-described method or from formulae and nomograms used for quad-

rilateral probes. The difference in the values of the operating distances obtained by this and other methods does not exceed 2%.

Example—We will calculate the operating distance of an azimuthal arrangement with dimensions $\overline{AB} = 1000$ m, $MN = 200$ m, $R = 3000$ m, $\Theta = 75°$.

From the nomogram (see Fig. 4) we determine that the value of the coefficient p for the coordinates $\frac{\overline{AB}}{2R} = 0.157$ and $\Theta = 75°$. Interpolating between the isolines 1.00 and 1.01, we obtain

$$p = 1.005.$$

Therefore, $R = 1.005 \cdot 1000$ m $= 1.05$ m.

THE EFFECT OF INACCURACY IN PLACING THE FEED AND MEASURING LINES ON THE RESULTS OF AN AZIMUTHAL PROBE

To simplify the calculations we will consider an azimuthal arrangement with a feed line AB of finite dimensions and with a limiting small measuring line MN. Since in practice the measuring lines are sufficiently short $\left(MN \leqslant \frac{1}{5} R\right)$, it should therefore be expected that with an inaccurate sighting of the lines of the azimuthal arrangement the results obtained here will make it possible to evaluate the order of errors introduced into the KS value.

(a) *The effect of inaccuracy in position of the measuring line on the KS value*—Let us suppose that the measuring line MN forms with the tangential direction (here tangential is the direction perpendicular to the radial direction) a certain angle Δ, measured clockwise and being an angular error in sighting of the measuring line (Fig. 5).

The effect of the sighting inaccuracy of the measuring line on the KS value will be represented by the value

$$\mu = \frac{\varrho_a' - \varrho_a}{\varrho_a} 100\% = \left(\frac{\varrho_a'}{\varrho_a} - 1\right) 100\%, \tag{16}$$

where ϱ_a' is the KS value for an azimuthal arrangement—obtained with an inaccurate sighting of the measuring lines; ϱ_a is the KS value for the azimuthal arrangement—obtained with an accurate sighting of the measuring line (along the tangential direction).

To determine the value $\frac{\varrho_a'}{\varrho_a}$ we find the component of the field of the feed line AB along the tangential direction Θ, the radial direction R and the direction of the measuring line MN (E_Θ, E_R and E_{MN}).

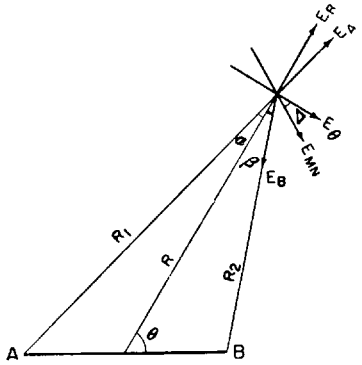

FIG. 5.

Since in the calculation of ϱ_a' and ϱ_a the coefficient of the azimuthal arrangement is taken equal to the same value, then it is obvious that:

$$\frac{\varrho_a'}{\varrho_a} = \frac{E_{MN}}{E_\Theta},$$

i.e.

$$\mu = \left(\frac{E_{MN}}{E_\Theta} - 1\right) 100\%. \tag{17}$$

From the formula for conversion of coordinates we obtain:

$$E_{MN} = E_\Theta \cos \Delta - E_R \sin \Delta,$$

Consequently

$$\frac{E_{MN}}{E_\Theta} = \cos \Delta - \frac{E_R'}{E_\Theta} \sin \Delta.$$

Let us derive expressions for the radial and tangential components E_R and E_Θ of the field of the feed line AB at the observation point:

$$E_R = E_R^A - E_R^B = E^A \cos \alpha - E^B \cos \beta =$$

$$E^A \frac{R + \frac{\overline{AB}}{2} \cos \Theta}{R_1} - E^B \frac{R - \frac{\overline{AB}}{2} \cos \Theta}{R_2},$$

$$E_\Theta = E_\Theta^A + E_\Theta^B = E^A \sin\alpha + E^B \sin\beta =$$

$$E^A \frac{\frac{\overline{AB}}{2}\sin\Theta}{R_1} + E^B \frac{\frac{\overline{AB}}{2}\sin\Theta}{R_2}.$$

Here: E^A, E^B are the field intensitites of the field line AB at the observation point;

R is the distance from the points of observation to the centre of the feed line AB;

R_1 and R_2 are the distances from the point of observation to the poles of the feed line AB;

Θ is the angle formed by the feed line AB and the section connecting the middle of the feed line with the observation point.

By analogy with the calculations for the previous section we find that

$$E^A = \frac{IT}{2\pi} R_1^{t-2},$$

$$E^B = \frac{IT}{2\pi} R_2^{t-2}.$$

Hence

$$\frac{E_{MN}}{E_\Theta} = \cos\Delta - \sin\Delta \times$$

$$\frac{\left[\left(\frac{\overline{AB}}{2R}\right)^2 + 1 + \frac{\overline{AB}}{R}\cos\Theta\right]^{\frac{t-3}{2}}\left(1 + \frac{\overline{AB}}{2R}\cos\Theta\right) -}{\frac{\overline{AB}}{2R}\sin\Theta\left\{\left[\left(\frac{\overline{AB}}{2R}\right)^2 + 1 + \frac{\overline{AB}}{R}\cos\Theta\right]^{\frac{t-3}{2}} + \left[\left(\frac{\overline{AB}}{2R}\right)^2 + 1 - \frac{\overline{AB}}{R}\cos\Theta\right]^{\frac{t-3}{2}}\right\}}$$

$$\frac{-\left[\left(\frac{\overline{AB}}{2R}\right)^2 + 1 - \frac{\overline{AB}}{R}\cos\Theta\right]^{\frac{t-3}{2}}\left(1 - \frac{\overline{AB}}{2R}\cos\Theta\right)}{\frac{\overline{AB}}{2R}\sin\Theta\left\{\left[\left(\frac{\overline{AB}}{2R}\right)^2 + 1 + \frac{\overline{AB}}{R}\cos\Theta\right]^{\frac{t-3}{2}} + \left[\left(\frac{\overline{AB}}{2R}\right)^2 + 1 - \frac{\overline{AB}}{R}\cos\Theta\right]^{\frac{t-3}{2}}\right\}}. \quad (18)$$

The results of the calculations using formulae (17) and (18), are given in Table 2.

As can be seen from this table, the limiting relative error μ for determining the value ϱ_a, caused by angular errors Δ of the order of 1–1.5°, varies

for $70° \leqslant \Theta \leqslant 110°$ from tenths of a percent to 2–3 per cent. For angles Θ of the order of 60° (120°) or 50° (130°) the error in determining ϱ_a becomes 5–8% as shown by calculations.

It follows that when carrying out azimuthal probes, it is generally desirable to use an arrangement with angles Θ from 70 to 110°, and the unreeling of the measuring lines should have an accuracy of 1–1.5°. Measurements within the limits of the rising branch of the *KS* curves, inclined to the axis of the distances at an angle close to 45°, can be conducted with angular errors in the direction of the measuring line, reaching 3–4°, without much effect on the *KS* values.

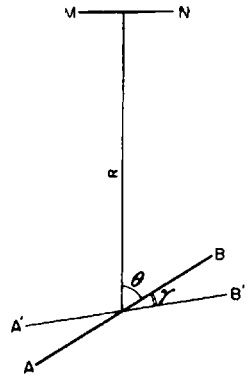

FIG. 6.

(b) *The effect of inaccuracy of sighting the feed line on the KS values*— We will consider an azimuthal arrangement of which the feed line $A'B'$ is laid with a certain angular error γ with respect to the given direction AB (Fig. 6).

The error in the *KS* value, connected with the angular error γ will be characterized by the value

$$\nu = \frac{\varrho_a' - \varrho_a}{\varrho_a} 100\% = \left(\frac{\varrho_a'}{\varrho_a} - 1 \right) 100\%, \tag{19}$$

where: ϱ_a' is the *KS* value obtained with an inaccurate sighting of the feed line;

ϱ_a is the *KS* value obtained with an accurate sighting of the feed line.

It is apparent that

$$\frac{\varrho_a'}{\varrho_a} = \frac{E_{\Theta'}}{E_\Theta},$$

TABLE 2. VALUES OF THE COEFFICIENT μ

t	0 / Δ / $\overline{AB}/2R$	90°								80°						70°					
		+1°	+2°	+3°	+5°	−1°	−2°	−3°	−5°	+1°	+2°	+3°	−1°	−2°	−3°	+1°	+2°	+3°	−1°	−2°	−3°
+1	0.1	0.015	0.061	0.137	0.381	0.015	0.061	0.137	0.381	0.29	0.54	0.77	0.32	0.66	1.04	0.61	1.18	1.73	0.64	1.31	2.00
	0.2	0.015	0.061	0.137	0.381	0.015	0.061	0.137	0.381	0.27	0.51	0.72	0.30	0.63	0.99	0.57	1.11	1.62	0.60	1.23	1.90
	0.3	0.015	0.061	0.137	0.381	0.015	0.061	0.137	0.381	0.24	0.45	0.63	0.27	0.58	0.91	0.52	1.00	1.45	0.55	1.12	1.73
−1	0.1	0.015	0.061	0.137	0.381	0.015	0.061	0.137	0.381	0.89	1.70	2.50	0.92	1.88	2.86	1.85	3.68	5.47	1.88	2.80	5.74
	0.2	0.015	0.061	0.137	0.381	0.015	0.061	0.137	0.381	0.86	1.68	2.47	0.89	1.80	2.75	1.75	3.47	5.16	1.78	2.59	5.43
	0.3	0.015	0.061	0.137	0.381	0.015	0.061	0.137	0.381	0.80	1.56	2.30	0.83	1.68	2.57	1.60	3.17	4.71	1.63	2.29	4.98
−2	0.1	0.015	0.061	0.137	0.381	0.015	0.061	0.137	0.381	1.21	2.38	3.52	1.24	2.50	2.80	2.47	4.91	7.31	2.50	5.03	7.59
	0.2	0.015	0.061	0.137	0.381	0.015	0.061	0.137	0.381	1.15	2.26	3.34	1.18	2.38	2.62	2.31	4.60	6.85	2.34	4.63	7.12
	0.3	0.015	0.061	0.137	0.381	0.015	0.061	0.137	0.381	1.07	2.10	3.11	1.10	2.22	2.38	2.09	4.16	6.19	2.12	4.28	6.46

TABLE 3. VALUES OF THE QUANTITY ν

t	0 / γ / $\overline{AB}/2R$	90°				80°				70°			
		−2°	−3°	+2°	+3°	−2°	−3°	+2°	+3°	−2°	−3°	+2°	+3°
+1	0.1	−0.11	−0.18	0.11	0.18	0.62	−0.98	0.51	0.72	−1.24	−1.9	1.12	1.64
	0.2	−0.04	−0.1	0.04	0.1	−0.48	−0.76	0.39	0.56	−0.98	−1.51	0.88	1.29
	0.3	−0.02	−0.05	0.02	0.05	−0.28	−0.44	0.22	0.32	−0.60	−0.93	0.53	0.77
−1	0.1	−0.05	−0.11	0.05	0.11	−0.52	−0.82	0.43	0.60	−1.05	−1.62	0.96	1.40
	0.2	−0.01	−0.02	0.01	0.02	−0.09	−0.16	0.07	0.10	−0.30	−0.47	0.24	0.35
	0.3	0.05	0.11	−0.05	−0.11	0.52	0.80	−0.43	−0.61	0.82	1.24	−0.77	−1.14
−2	0.1	−0.09	−0.09	0.09	0.09	−0.50	−0.76	0.32	0.47	−1.27	−1.44	0.84	1.22
	0.2	0.02	0.04	−0.02	−0.04	0.17	0.26	−0.15	−0.20	0.17	0.24	−0.18	−0.28
	0.3	0.10	0.23	−0.10	−0.23	1.06	1.65	−0.87	−1.24	1.75	2.68	−1.61	−2.37

where: $E_{\Theta'}$ is the tangential component of the field of the feed line $A'B'$;
E_{Θ} is the tangential component of the field of the feed line AB.

Thus,

$$\nu = \left(\frac{E_{\Theta'}}{E_{\Theta}} - 1\right) 100\%. \tag{20}$$

In agreement with the previously derived formulae we obtain

$$\frac{E_{\Theta'}}{E_{\Theta}} = \frac{\sin(\Theta+\gamma)\left\{\left[\left(\frac{\overline{AB}}{2R}\right)^2 + 1 + \frac{\overline{AB}}{R}\cos(\Theta+\gamma)\right]^{\frac{l-3}{2}} + \left[\left(\frac{\overline{AB}}{2R}\right)^2 + 1 - \frac{\overline{AB}}{R}\cos(\Theta+\gamma)\right]^{\frac{l-3}{2}}\right\}}{\sin\Theta\left\{\left[\left(\frac{\overline{AB}}{2R}\right)^2 + 1 + \frac{\overline{AB}}{R}\cos\Theta\right]^{\frac{l-3}{2}} + \left[\left(\frac{\overline{AB}}{2R}\right)^2 + 1 - \frac{\overline{AB}}{R}\cos\Theta\right]^{\frac{l-3}{2}}\right\}}$$

$$\frac{\left[\left(\frac{\overline{AB}}{3R}\right)^2 + 1 - \frac{\overline{AB}}{R}\cos\Theta\right]^{\frac{l-3}{2}}\right\}}{\sin\Theta\left\{\left[\left(\frac{\overline{AB}}{2R}\right)^2 + 1 + \frac{\overline{AB}}{R}\cos\Theta\right]^{\frac{l-3}{2}} + \left[\left(\frac{\overline{AB}}{3R}\right)^2 + 1 - \frac{\overline{AB}}{R}\cos\Theta\right]^{\frac{l-3}{2}}\right\}}. \tag{21}$$

The results of the calculations for ν, obtained from formulae (20) and (21), are given in Table 3. As can be seen, with an angle Θ, within the range from 70 to 110°, and a length of feed line up to 0.6 R the angular errors γ, reaching 2°, lead to errors in KS not exceeding 2%.

THE PRACTICAL PROCEDURE FOR AZIMUTHAL PROBING

The work of experimental parties of VNII Geofizika made it possible to develop with sufficient completeness a method for azimuthal probes and showed the effectiveness of the described method for measurements under conditions involving difficult transport.

The azimuthal probes were conducted with the ERS-23 electrical survey station, which included two field laboratories, mounted on the GAZ-63 vehicle. The probing profiles were curved roads, not particularly suitable for vehicles. Initially, the topographical surveyers marked out the curb of the road into 100 m spacings. The plan of the markings was entered on to a plane-table grid on a scale 1 : 25,000. The markings were fastened with standard pegs carrying the number of the profile and the peg number. Near the pegs there were high mounds which were easily recognizable in the

area. The plane-table grid also had the outlines of the road, diagnostic orientation features, trigonometrical points situated within the limits of visibility, etc.

At the edges, the plane table grids overlapped by not more than 2 points, with a spacing of over 1000 m.

The profiles were connected in accordance with the "Directions for geodesical work in geophysical surveys in the petroleum industry".

The centres of the azimuthal probes were placed directly on the road. The generator group was placed near the probe centre. To obtain the left branches of the *KS* curves, an AMNB arrangement was used with feed electrodes placed along the road, and also in quadrilateral arrangement. Measurements with the AMNB arrangement were set up to half-spacing of the feed electrodes equal to 200–600 m, and were usually carried out with an electrical prospecting potentiometer. The quadrilateral measurements (under favourable conditions) were made in the range of working distances from 200 to 1000 m.

Measurements with the azimuthal arrangement were commenced with a distance between the centres of the feed and measuring lines of 500–1000 m. When transferring from the AMNB arrangement to the quadrilateral or azimuthal arrangements, the measurements were repeated at 1–2 points. When carrying out azimuthal probes, the field laboratories were placed along the road and measurements were made of the difference in potentials at various distances from the probe centres (Fig. 7). These distances were selected the same as with the usual probes (500, 700, 1000, 1300, 1800, 2500 m. etc.).

Observations with the azimuthal arrangement were made according to a special procedure, which involved all the necessary information on the direction of the feed and measuring lines, and was arranged as follows:

Az. No. Azimuth AB = Marking at the centre

No. II/II	No. mark	R	Θ	Azimuth MN	Remarks
1	2	3	4	5	6

Here the 2nd column gives the number of the pegs for which the measuring lines should be unreeled. The 3rd and 4th columns give the distances R between the centre of the feed line and the centre of the measuring line and angle Θ between the feed line and the section connecting the centres of the feed and measuring lines. The distances and angles were measured

graphically on the plane-table by means of a scale rule and a geodesical protractor.

The 5th column has the magnetic azimuth of the measuring line calculated from the formula $A_{MN}\ A_{\overline{OQ}}\ 90^\circ$ where A_{MN} is the magnetic azimuth of the measuring line;

$A_{\overline{OQ}}$ is the magnetic azimuth of the section OQ connecting the centres of the feed and measuring lines.

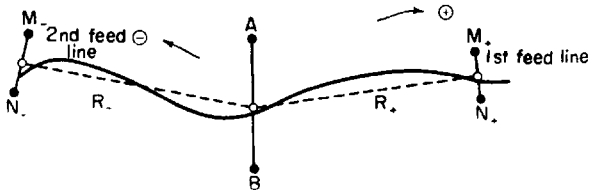

FIG. 7.

In setting up the program of measurements, the azimuth of the feed line was selected so that the angle Θ was between the values 70–110°. Depending on the configuration of the road, the azimuthal probe was carried out with one or several azimuths of the feed line. For example, measurements at the points within the limits of the section 1–2 of the road shown in Fig. 8, were carried out with the direction of the feed line being $A_1 B_1$. To carry out measurements at the section 2–3, a second feed line $A_2 B_2$ was used. On changing from one direction of the feed line to another, the measurements at one of the points placed near the point 2 were doubled so that the sections of the KS curve obtained with different directions of feed line touched one another at one of the spacings.

The dimensions of the measuring and feed lines satisfied the conditions

$$MN \leqslant \frac{1}{5} R,\ AB \leqslant 0.6\, R.$$

The maximum length of the feed lines was 500–1500 m depending on the conditions of the measurements.

In the probe process the length of the feed line changed several times, an attempt being made to keep this number of changes to a minimum. When changing from one feed line to another, the measurements were doubled, which made it possible to combine the sections of the KS curve obtained with different feed lines.

A compass was used when unreeling the cable of the feed line, the max-

imum permissible angular error being about 2°. The wires of the measuring line were unreeled with an accuracy of up to 1–1.5°. However, when obtaining the rising right-hand branch of the *KS* curves, inclined to the

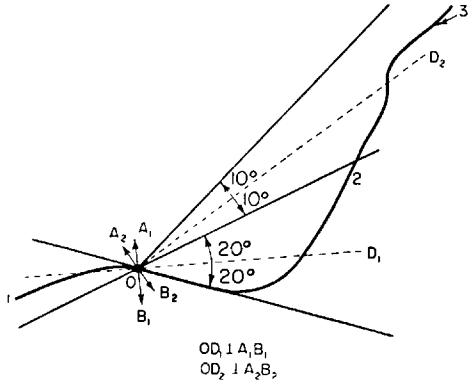

FIG. 8.

axis of distances at an angle close to 45°, the accuracy of unreeling of the measuring line cable was sometimes reduced to 3–4°, which was caused by the complex conditions of unreeling in wooded and swampy country.

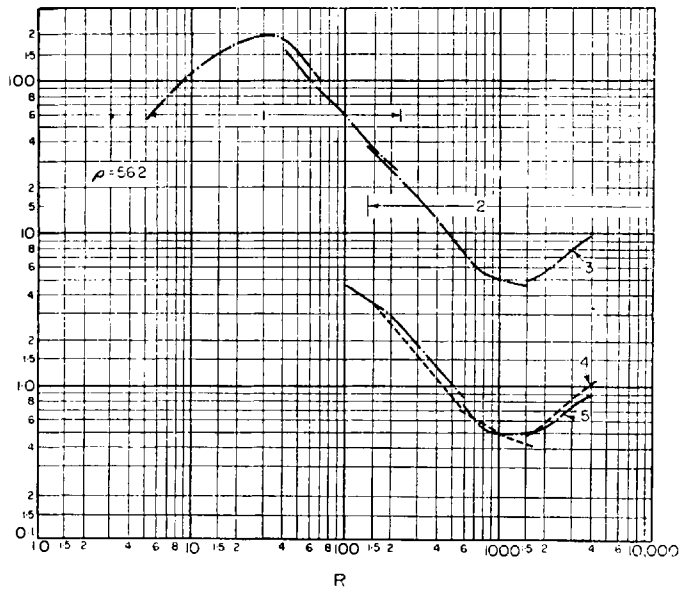

FIG. 9. Two-way curves of azimuthal probes. 1—*AMNB* arrangement; 2—azimuthal arrangement; 3—middle curve; 4—western curve; 5—eastern curve.

The KS values were calculated from formula (5) and in the construction of the KS curves were referred to the working distances $\bar{R}$, determined according to (14).

To find the coefficient of the azimuthal arrangement and the correction factor p, nomograms were used. In other respects, the method of two-way curved azimuthal probes did not differ from the method of two-way quadrilateral probes.

The characteristic curves of two-way curved azimuthal probes are given in Fig. 9. As shown by control measurements, the KS values in azimuthal probing are reproduced with an accuracy up to 5–6%. Under the conditions of a stable geoelectrical cross-section and the more or less gentle slope of the rocks, the curves of the azimuthal probe agree well with curves for the quadrilateral probe carried out in approximately the same direction in which the field laboratory travelled during the azimuthal probing.

In the method of interpreting two-way curved azimuthal probes, there is nothing which is in principle different from the method of interpreting two-way quadrilateral probes.

When constructing the profiles of the resulting values, the points of the record lay on a straight line by the side of the curved profile of the probe.

REFERENCES

1. L. M. AL'PIN, *The Theory of Dipole Probes.* Gostoptekhizdat (1950).
2. M. N. BERDICHEVSKII, and A. D. PETROVSKII, The method of quadrilateral probes. *Applied Geophysics*, No. 14, Gostoptekhizdat (1955).

CHAPTER 10

THE USE OF THE LOOP METHOD (SPIR) IN EXPLORING BURIED STRUCTURES

I. I. KROLENKO

THE loop method refers to a group of inductive methods of electrical surveying. The first work with this method was carried out in 1930–1932 on the Grozneft regions (by V. N. DAKHNOV and then by S. G. MOROZOV and I. G. DIDURA). This work was experimental and showed the possibilities of the method and the optimum conditions for using it [9].

From 1937 to 1941 and from 1945 to 1950, work with the loop method was conducted on the Kerch peninsula (I. I. KROLENKO), where the physico-geological conditions favoured its extensive use.

As a result of this work and the improvements made in 1947 in the techniques of field observations, the loop method became an effective, widely reproducible and relatively cheap method. The method was used to study the tectonics of the upper levels of the geological section.

Apart from the work on the Kerch peninsula, the loop method was successfully used on the Caspian shore to the south of Makhach-Kala (1942), on Taman' (1950–1951), in the Turkmenia (1941–1943 and 1952–1953), and was also tried under the conditions prevalent in Western Siberia (1954–1955) and Ust-Urta (1955).

In the present article we will consider the basic principles of the method and will not deal with the physical nature and the mathematic basis of the loop method, which are given by DAKHNOV [9,10], who worked out the theory of this method, and also in the papers of A. I. ZABOROVSKII, E. N. KALENOV, *et al.*

The loop method is based on the good electrical conductivity of anisotropic (banded) deposits along the layers in comparison with the direction normal to the layer.

This phenomenon in the case of dipping anisotropic deposits causes an asymmetric magnetic field of the earthed feed loop AB, which for variable fields can easily be set up by means of a closed receiving loop, placed symmetrically with respect to AB.

The e.m.f. values arising in the receiving loop are functions of the

coefficient of anisotropy of the rocks $\lambda = \sqrt{\frac{\varrho_n}{\varrho_t}}$ and the angle of inclination α of the studied deposits. In the case of sufficiently homogeneous deposits (λ = const.) the observed values, proportional to the e.m.f. with respect to the modulus and direction, characterize the change in α along a certain profile, i.e. the tectonics of the studied deposits.

The coefficient of mutual induction between the feed and receiving loops can be changed either by deformation of the wire AB or by means of an induction coil.

The value of deformation of the wire, i.e. the area of the constructed triangle of compensation ω, in relation to the area of the whole receiving loop Ω, gives a component of the vector of the loop measured for a given position AB. The ratio $\frac{\omega}{\Omega}$ is usually small; it is therefore multiplied by 1000 and designated by $f = \frac{\omega}{\Omega} 1000$.

Thus with observations employing two mutually perpendicular lines AB, the vector loop is measured. The position of this vector which shows the direction of propagation of the current at a given point, i.e. the dip direction of the rocks being studied. By analysing the vector distribution, it is easy to indicate the position of the anticlinal and synclinal hinges. Thus in terms of the isolines, drawn perpendicular to vectors, the upfolds, their sub-divisions, regions of depression, etc. can be mapped.

This method of interpreting observations, made with the aid of a loop, gives a general idea of the structure of the studied area. The method should, therefore, be recommended in reconnaissance or semi-qualitative surveys, and also in the preliminary processing of data.

The observations made in order to obtain details of the structure of a studied feature, should be processed by the integration method. For this purpose, sections intended for detailing should have connecting profiles of the vectors intersecting the basic profiles. This system of profiles forms a closed polygon, in which the integration of vectors can be carried out by the generally known method.

The advantages of the mathematical construction of isolines was shown at a number of areas of the Kerch peninsula, Stepnyi Krym* and Turkmenia, where considerable details of their structure were shown. This makes it possible to recommend this form of interpretation for wider use when processing observations by the loop method. An example of comparison of both methods of interpretation is given in Fig. 1. To indicate the importance

* The Crimean Steppes [Editor's note].

of the loop method in the systems of geological and geophysical surveys of buried structures, one should deal with the geological-geophysical conditions necessary for its use, and consider briefly the results of work carried out with this method.

The most favourable objects for surveying by the loop method are structures made up of sufficiently homogeneous shales or banded sand-clay or clay-marl

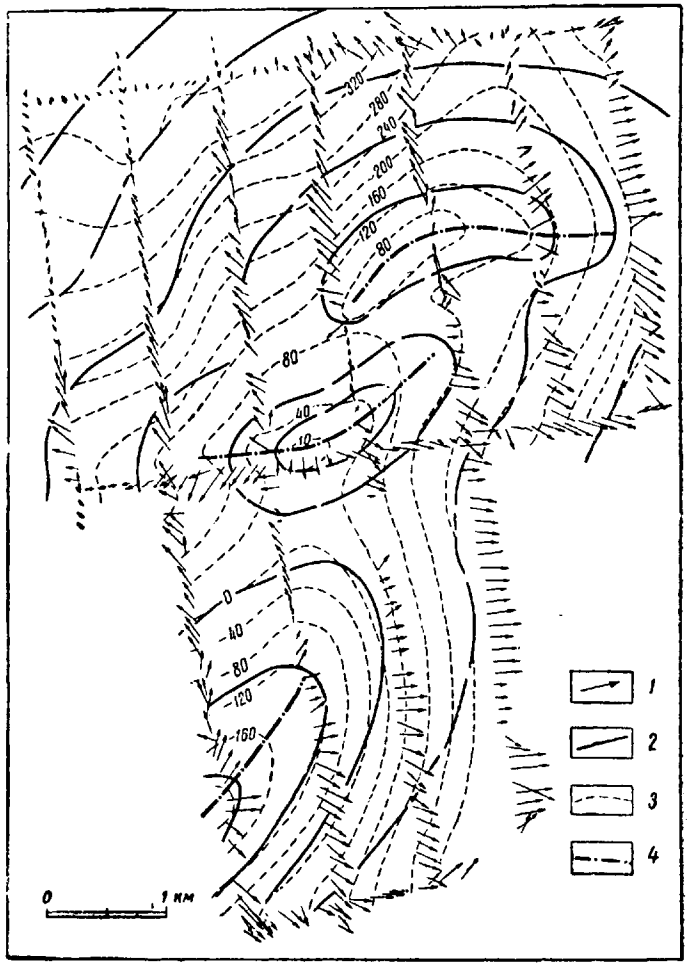

FIG. 1. The tectonic structure of the Marfov section according to data of integration of the loop vectors and the method of constructing isonormals.

1—loop vectors; 2—isonormals to the loop vectors; 3—isolines from the data of integration of loop vectors; 4—the axis of the fold according to the data of the loop method.

deposits, covered with shallow alluvia. The value of the anisotropy coefficient of such deposits varied between 1.2 and 2.5. The electrical homogeneity over the area is established by parametric profiles of resistances with spacings equal to the length of the *AB* line adopted for working with the loop method in the given region. The loop method can also be used to determine the direction of dip of the reflecting highly-resistant horizon, covered with electrically homogeneous rocks. The accuracy of the results of surveying by the loop method is also ensured by the accurately defined forms of the buried fold (angle of dip of the studied rocks from 8 to 80°) and the gentle relief of the surface.

The presence of these favourable conditions on the areas of the Kerch peninsula determined the possibility of extensive work with the loop method and the effectiveness of the results.

The first investigation was carried out in 1937 at the Priozernoe (Chongelekskoe) petroleum deposits and then at the Pogranichnaia* (Chorelekskaia) and Malo-Babchikskaia anticlines for determining the tectonic structure of these areas. This work showed the position of the axes of the structures and marked the regions of greatest amplitude. At the Priozernyi deposit the loop method combined with electrical profiling (mapping the strip of the Middle Sarmatian limestone on the flanks of the structure) revealed a number of cross-cutting disturbances.

The nature of the relationship between the Chorelekskoe and Opukskoe upfolds and the Malaia Babchikskaia structure with the Katerlezskii dome [13, 14]. In 1950, this work extended the knowledge of the Chongeleksko-Chorelekskaia anticlinal zone. This zone, in the limits of the Kerch peninsula, according to the data of the loop method begins at the south-west of the Koyashskoe lake in two small anticlines – Chokur–Koyashskaia and Opukskaia, separated by a small saddle, and ends at the north-east of the Zaozernaia (Tobechikskaia) fold, a considerable part of which is under the water of the Kerch Straits (Fig. 2).

Significant corrections were introduced on the basis of the work carried out by the loop method and core drilling in 1950 in the zone of the Malaia Babchikskaya structure, which was coordinated with the deposition of petroleum. As well as the data on this fold and the Katerlezskii dome adjoining it from the south-west, to the south of the Malaia Babchikskaya anticline was mapped the Yuzhno–Babchikskaia fold with a very narrow closure, bent in the form of a crescent [21, 26]. In between the three upfolds there

* In order to avoid errors the Russian adjectival form is used for the structures unless the correct place name is well known. [Editor's footnote].

is a funnel-shaped depression filled with volcanic deposits interstratified with marine sediments [3]. All three folds are represented in the form of periclines, surrounding a large depression, in which many deposits of the Kerch peninsula are found. By means of the geological survey and the loop method, hinges were traced for a number of anticlines of the Zaparpachskian part of the peninsula [19], [25].

Interesting work was carried out by the loop method in connection with electrical profiling on the Borzovskaia area. This work showed the course of the structure and established the lines of faulting, which conditioned subsequent exploratory drilling.

The work carried out on the neighboring area mapped the Glazovskaia structure and established its connection with the Western periclinal closure of the Mayakskaia structure [19].

On the Glazovskaia structure its asymmetry was confirmed (wide and gentle southern limb and a steep northern) and the zone crumpling was shown on the northern limb near the hinge. The latter is apparently the consequence of mud volcanism and diapiric processes [2].

The most effective was the work with the loop method in the flat southwestern part of the Kerch peninsula, made up of homogeneous muddy Maikop formation. The lithologically homogeneous sections, devoid of distinct marker horizons and the poor exposure of autochthonous rocks considerably hindered the geological survey of this region and the tectonics of the plain were known only in a very general form [1], and only a few anticlines were traced in this area.

With the loop method in a short period (4 field seasons) on the territory of the south-western plain, 24 structures were mapped of which 6 [Yuzhno-Andreevskaia, (Karachskaia) Zhuralevskaia (Chaltemirskaia), Kol-Alchinskaia, Ul'yanovskaia (Mangutskaia) Yuzhno-Marfovskaia and Mar'inskaia] were demonstrated by this type of investigation. Furthermore there were considerable corrections for the majority of the other structures [19].

According to geophysical data, the Moshkarevskaia (Kerleutskaia) structure is a small fold in the southern part of the western depression of the large Shirokovskaia (Uzun-Ayakskaia) structure, whereas, according to geological ideas, its axis continues further to the east [23]. The Shirokovskaia structure owing to the axial variation of plunge is subdivided into 3 culminations. Furthermore, it is genetically connected with the Kuibyshevskaia fold, which complicates its northern limb. As well as the convergence of the Moshkarevsk and Shirokovsk anticlines, which localizes the petroleum deposit, other similar convergences of the Zhuravlevskaia (Chaltemirskaia) and Seleznevskaia (Mamatskaia), on one hand and of Ul'yanovskaia (Mangu-

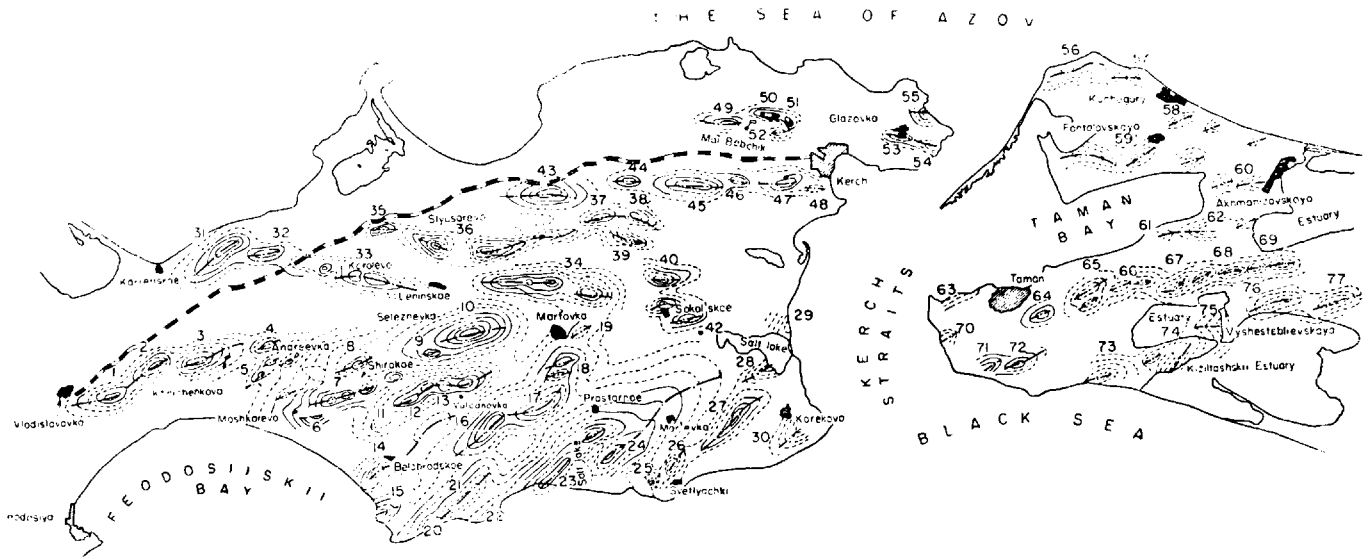

FIG. 2. The tectonic structure of the Kerch and Taman peninsulas according to the data of the loop method.

Structures: 1—Vladislavovskaia; 2—Frontovskaia; 3—Kharchenkovskaia (Arma-Elinskaia); 4—Andreevskaia (Koshaiskaia); 5—Yuzhno-Andreevskaia; 6—Moshkarevskaia (Kerleatskaia); 7—Shirokovskaia (Uzun-Ayakskaia); 8—Kuibyshevskaia; 9—Zhuravlevskaia (Chaltemirskaia); 10—Seleznevskaia (Mamatskaia); 11—Ul'yanovskaia (Mangutskaia); 12—Yarkovskaia (Bash-Kirgizskaia); 13—Vulkanovskaia (Dzhau-Tepinskaia); 14—Northern Belobrodskaia (Sarylarskaia); 15—Southern Belobrodskaia (anticline of the Sarylar Cape); 16—Borukhobinskaia; 17—Aktyuhinskaia; 18—Southern Marfovskaia 19—Northern Marfovskaia; 20—Chaudinskaia; 21—Dyurmenskaia; 22—Karangatskaia; 23—Dal'nyaya (Atan-Alchinskaia); 24—Mar'evskaia; 25—Koyashskaia; 26—Opukskaia; 27—Pogranichnaia (Cherlekskaia); 28—Priozernaia (Chongelekskaia); 29—Zaozernaia (Tobechikskaia); 30—Korenkovskaia (Kop-Takilskaia); 31—Kamenskaia (Akmonaiskaia); 32—Naberezhnaia (Nasyrskaia); 33—Korolevskaia (Kodzhalarskaia); 34—Novoselovaia (Sartskaia); 35—Sergeevskaia; 36—Slyusarevskaia (Karmysh-Kelechinskaia); 37—Alekseevskaia (Chumash-Takil'skaia); 38—Tasunovskaia (Sait-Elinskaia); 39—Chernyakovskaia (Sultanovskaia); 40—Rep'evskaia (Aiman-Kuinskaia); 41—Sokolskaia (Saraiminskaia); 42—Alagolskaia; 43—Novo-Nikolaevskaia (Togonashskaia); 44—Chestopolskaia (Kitaiskaia); 45—Andrevskaia (Chanlugarskaia); 46—Oktyabrskaia (Koshai-Rissinskaia); 47—Voskhodovskaia (Dzhardzhavskaia); 48—anticline Soldatskaia Svoboda; 49—Burashskaia; 50—Malo-Babchinsku; 51—Katerlezsku dome; 52—Southern Malo-Babchinskaia; 53—Glazovskaia (Baksinskaia); 54—Mayakskaia; 55—Borzovskaia; 56—Kamennyi Cape fold; 57—Peklo Cape fold; 58—Kuchugurskaia; Fontalovskaia; 60—Mt. Tsimbala fold; 61—Semenikovskaia; 62—Sennaia; 63—Taman; 64—Mt. Karabetovskaia fold; 65—Mt. Komendantskaia fold; 66—Mt. Vasyurinskaia fold; 67—Blizretsa Hill fold; 68—Cirka fold; 69—Kopantsa fold; 70—Korotkovskaia; 71—Zelenskaia fold; 72—Hill of Kostenkov's Grave fold; 73—Mt. Yuzhnoe Pekole fold; 74—Polivadinskaia; 75—Tsokur estuary fold; 76—Kapustin valley fold; 77—Southern Neftianaia.

tskaia) and Yarkovskaia (Bash-Kirgizkaia) [19] on the other have also been discovered by the loop method.

At the Kharchenkov (Arma-Elin) area instead of two parallel structures, the loop method showed the presence of one structure of considerable dimensions with a small bulge on the northern limb.

The long Vladislavovskaia fold is divided owing to the axial variation of its plunge into two anticlines—Vladislavovskaia and Frontovskaia (Koi-Asanskaia), which is of interest from the point of view of its possible petroleum content [14]. This work in the south-west plain showed the continuation of a number of tectonic zones (Yarkovskaia, Severnaia Belobrodskaia, Dyurmenskaia, Dal'nii, etc.)

Work carried out by the loop method on the Uzunlar area was very revealing. The Uzunlar dome is placed in the south-east part of the south-west plain. Before work with the loop method (1949) the Uzunlar dome was an undefined large bulge of Maikop clay.

The loop method has been used to study the tectonics of the Maikop core within the limits of which a large Mar'inskaia anticline, which lies to the south-west of the Uzunlar lake, was depicted and parallel to it a small upfold related to the distant (Atan-Alchinskaia anticline zone [19] was found.

The Dal'naia zone contains the structure of the same name and the geologically known Karangat anticline [1] which is situated on the Karangat cape. The existence of the Mar'inskaia anticline was shown first by A. D. ARKHANGEL'SKAIA in the section on the western shore of the Uzunlar lake. The northern side of the Karangat structure and the previously accepted schemes of the tectonic structure of the Kerch peninsula referred to the most southerly anticlinal zone, the remaining parts of which were assumed to be covered by the Black Sea.

Geophysical work has shown the course of the Karangat and Dal'naia structures and has produced a more firmly based scheme of tectonics of the southern part of the south-western plain of the Kerch peninsula. The schematic structure of the Uzunlar dome is also supported by the results of a detailed geological survey carried out on this area in 1950 [30].

In 1949–1950, using the loop method, studies were made of an area adjoining the south-west plain from the north and north-east (Zaparpachskaia part). The structure of this part of the peninsula is represented by core of Maikop clays, which lie in depressions and are surrounded by the deposits of Mediterranean age. They differ in the high complexity of the tectonic structure (Fig. 3). However, under these conditions, the loop method clearly shows the tectonic features of the Maikop cores of the structures (position of the axis, the presence of axial variations of plunge and possible faults),

which appear most distinctly if the obsevations are processed by the integration method [19].

As a result of a correlation of the above-described investigations, carried out in 1950, a map of the tectonic structure of the south-west plain of the Kerch peninsula (see Fig. 2) was constructed.

This map shows a regular pattern of structures, arranged along tectonic lines, and also the region of a sharp change in direction of these lines from close to east-west in the northern and central parts of the plain, to the north-east in the southern and eastern parts [19, 31].

The change in direction of the structural units of the south-eastern part of the Kerch peninsula in comparison with the central, is of interest since it can provide favourable conditions for accumulating sand facies in the geological section [28].

About 90% of the structures recorded in the Zaparpachskaia part, by the loop method and up to 60% in the south-western plain of the Kerch pensinsula, have been covered in the post-war years by geological surveying. In the case of many of the structures, core and deep drilling were carried out. On the basis of the materials obtained, composite structural maps were compiled of both the south-west plain and of the Zaparpachskaia part of the Kerch peninsula.

A comparison of these maps with similar maps based on the loop method indicates the correctness of the loop method for both the general pattern of the tectonics in the Kerch peninsula and of the components of structure of the tectonic zones and individual structures. Geophysical data on many areas not only support the geological survey but in a number of cases considerably improve it with additions and corrections.

Oil prospectors on the Kerch peninsula are faced with the problem of finding the relationship between the tectonics of the upper levels, studied by the loop method, and the structure of the lower parts of the Tertiary and Cretaceous systems. To solve this problem use was made of magnetometry, gravimetry and seismic exploration.

The gravitation field of the Kerch peninsula is characterized by a continuous increase in gravity towards the south. Apparently, owing to the presence of a large gravity gradient, local anomalies in the gravitational field appear only in the form of deflections in the isoanomalies. This can be illustrated by the coincidence of the zone of disturbance with a region of gravitational minima, shown on the map by distinct deflections in the isoanomalies.

The magnetometric surveys carried out on the Kerch peninsula in 1948 showed an increase in the intensity of the geomagnetic field to the north, which is apparently connected with an increase in this direction of the thickness of deposited formations [24].

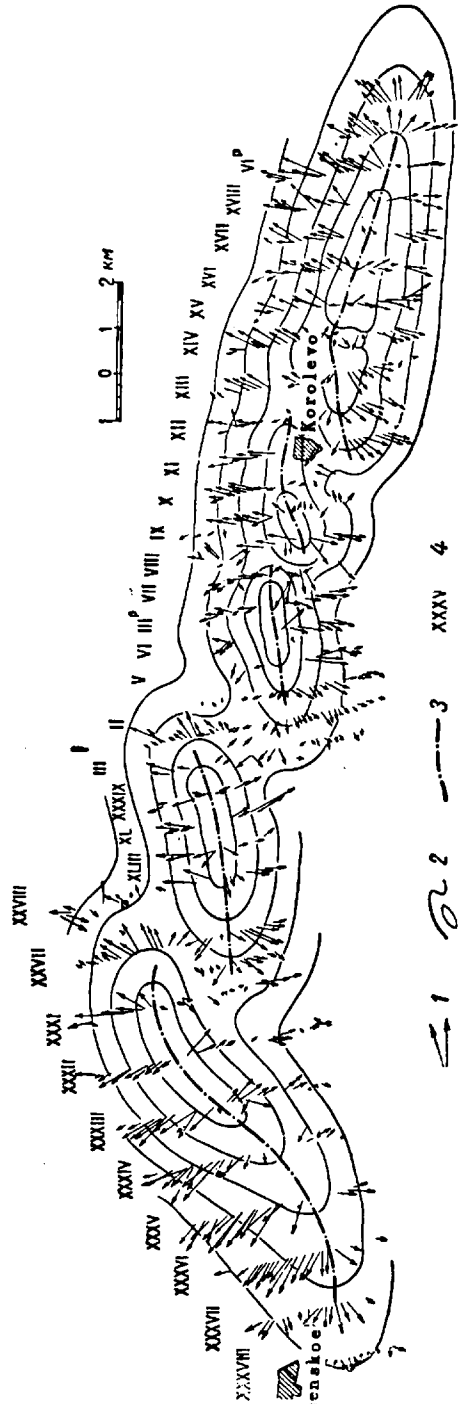

FIG. 3. The tectonic structure of the Tamensk–Korolevsk section (Kerch Peninsula) according to the data of the loop method. Compiled by I. I. Krolenko. 1—loop vectors; 2—lines normal to the vectors; 3—axis of fold according to loop data; 4—numbers of profiles.

Experimental seismic studies by the reflected methods were carried out on a small scale in 1950–1952 in the western part of the Kerch peninsula and in territory adjoining from the west to Feodosiya. This work showed that where the anticline crests produced by diapiric and crypto diapiric structures are separated by narrow and deep synclinal depressions, the use of seismic exploration involves considerable difficulties in correlating these reflections. In many profiles the crestal sections are characterized by irregular readings, by different orientation of the co-phasal axes and by the so-called "blind zones" with almost complete absence of reflecting horizons. In the peripheral parts of the structures on the limbs and in the synclines, where the layers slope relatively gently, the record of reflections is perfectly satisfactory.

As a result of processing the method of seismic exploration of the western part of the Kerch peninsula in 1954, considerable improvements were obtained in the quality of the recorded seismograms. The work showed a certain lack of correspondence of the structural plan of the Tertiary and Mesozoic deposits and an increase in the angle of dip of rocks with depth. Due to the absence of continuous, correlatable horizons, the constructions were made by using two arbitrary seismic horizons: M (stratigraphically related to the top of the upper Kerleutskian horizon) and C_2 (corresponding to the Upper Cretaceous sediments [23]). The accuracy of the constructions was conditioned mainly by the quality in the initial data. It was, therefore, at its least in the hinges of the anticlines, found by the strongly folded rocks with large angles of dip (up to 70–80°).

The seismic profiles showed all the culminations including those which were known previously, and those shown by the loop method: Ul'yanovskaia, Shirokovskaia and Yuzhno Andreevskaia [23]. The closures of the structures formed by the arbitrary seismic horizon M in the overwhelming majority of cases coincide with the closures mapped by the loop method or are slightly displaced. Thus, under the conditions existing on the Kerch peninsula on the limbs of the folds there is a correspondence between the structure contours of the seismic exploration and the isonormals of the loop method. The absence of reflecting areas in the closures of the intensively dislocated folds is easily made up by the data of electrical explorations, i.e. the methods are complimentary to one another, giving a continuous section of observation without "blind zones". This is very important in interpreting geophysical material and should be remembered when planning and carrying out field work.

The loop method, as shown above, successfully depicts local culminations of axial plunge and secondary complications on the limbs. It explains the

nature of merging structures and the relationship between the tectonic zones.

This material should be used for a rational distribution of seismic profiles. If this is not fully appreciated, errors can be introduced when planning work and eventually errors can arise in the deductions about the structure of the area, as was the case in the Vladislavov–Kharchenkovskaia tectonic zone and in the zone of merging of the Moshkarevskaia and Shirokovskaia structures.

Seismical studies on these areas, which have no interesting petroleum-bearing aspect (although complex in their structure), were carried out by a sparse network of profiles ignoring the details [23]. As a result, the Frontovaia and Kharchenkovskaia structures represented by data of the loop method, of the geological survey and by the subsequent exploratory drilling, as two independent connected folds, were united by seismic exploration into one wide structure (Fig. 4). A well drilled in the crest of the fold to the south of Lake Parpach gave an oil gusher of several tens of tons. This fact demanded final solution of the problem of the structural position of the well. For this purpose, in the summer of 1956 detailed seismic profiles were made, confirming that at that section the two structures merged. The gushing well was situated at a deep western depression of the Kharchenkovskaia brachyanticline, in connection with which further exploratory drilling was transferred to the Kharchenkovka region.

In the light of the preceding, it is necessary to reconsider the schematic structural map of the Moshkarevka area, compiled for the arbitrary seismic horizon M. Surveying by the loop method shows the complex merging of the small, intensively dislocated, Moshkarevskaia fold into the relatively large Shirokovskaia fold. Despite the fact that on the western depression of the Shirokovskaia structure and on the Moshkarevskaia upfold more than 100 wells were drilled, up to the present time opinions about the structure of this region to which the location of petroleum is related vary.

From the seismic data on the arbitrary level M, the anticlinal upfold is drawn on an area 8×4 km^2 with an axis striking north-east course [23]. On comparing contours of structures for various data (Fig. 5) it becomes apparent that the whole eastern periclinal part of the fold according to the data of seismical survey is placed within the limits of the western crest of the Shirokovskaia structure. Confirmation of the fact that the structure contours united two different upfolds is provided by the data of the seismic profiles XVIII, XX and XXI, intersecting the Moshkarevskaia anticline, and the XXII profile, cutting the Shirokovskaia structure. The first of them

characterizes the Moshkarevskaia fold with a steep northern limb and a rather steep south limb, since on the profile of the XXII closure (Shirokovskaia) of the structure is characterized by small angles of dip on either limb. Apparently under complex seismogeological and structural conditions of this section in the absence of detailed profiles (especially longitudinal) it is difficult to represent the structure of this area correctly.

According to the data of the loop method, the main bulk of the drilling was apparently related not to the Moshkarevskaia fold, but to a wide periclinal nose of the Shirokovskaia structure.

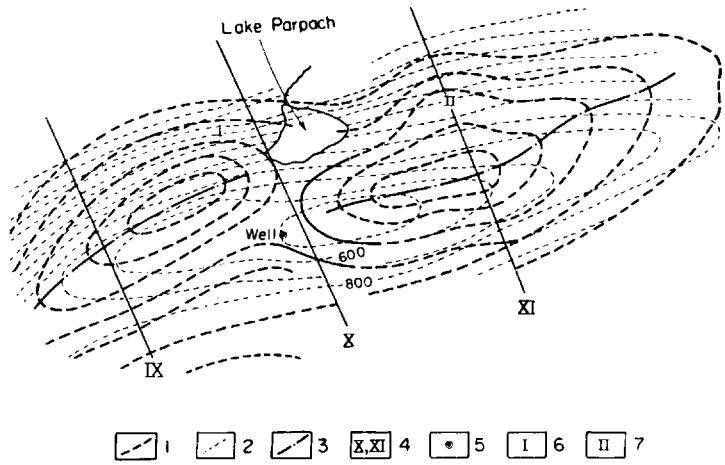

FIG. 4. The structure of the Kharchenkov area from the data of seismic prospecting and the loop method. 1—isonormals to the loop vectors; 2—structure contours; 3—axis of the fold determined from the data of electrical prospecting; 4— seismic profiles; 5—well; 6—Frontovaia structure; 7—Kharchenkovskaia structure.

Similar peculiar linkages of two structures were often observed within the limits of the south-west plain by surveys with the loop method. The presence of a petroleum deposit on the Moshkarev area may be connected with that type of linkage. Therefore a detailed complex geological geophysical survey of the Moshkarev area can give valuable data for solving the problem of finding oil in a number of other areas of the Kerch peninsula both from the point of view of the method and of the practice.

Between 1945 and 1947 the loop method was used in the Crimean Steppes. As a result of these observations, it was found that the physico-geological conditions of this region are unfavourable for the loop method. The considerable electrical differences of the surface deposits, their weak

anisotropy, the considerable thicknesses of the alluvia and the extremely gentle angle of dip of the investigated rock led to an irregular distribution of the vectors. However, on the background of even such a vector field it was nevertheless possible to distinguish a number of sections, on which, owing to a more regular disposition of the vectors, a probable presence of anticlinal upfolds [15] was proposed. To determine the actual nature of the electrical anomaly on three of them, Annovskaia, Severnaia and Yuzhnaia Tshun'skaia between 1948 and 1949, observations were carried out with the vertical electrical probe method, confirming the data of the loop method.

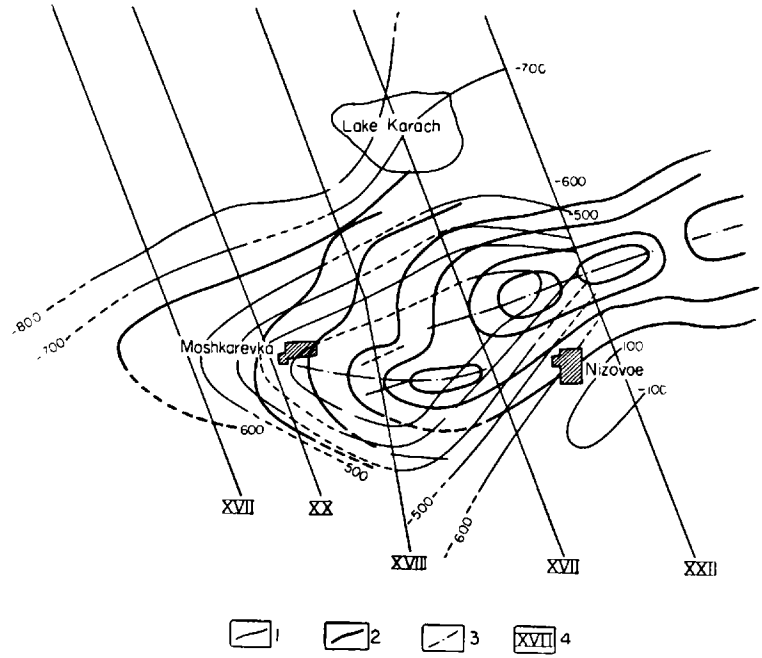

FIG. 5. Comparison of the structures of the Moshkarevka area according to the data of seismic prospecting and the loop method. 1—structure contours; 2—isonormals to the loop vectors; 3—axis of folds determined from the electrical prospecting data; 4—number of seismic profiles.

The Annovskaia and Gor'kovskaia upfolds were also proved by the geological survey.

On the southern edge of the Priazovskaia depression the variometric survey and the loop method showed the Goncharovskaia (Karagozskaia) structure, confirmed later by geological surveying by deep drilling and by seismic explorations.

After completing the surveys of the Kerch peninsula by the loop method and compiling the tectonic pattern of its structure, a natural continuation was the survey by the loop method of the Taman' pensinsula [20, 21].

The geological interpretation of the data of the Taman' peninsula surveyed by the loop method (1950–1951) showed that within the limits of the studied area, there was no north-west (Caucasian) trend of the structures. The extreme northern tectonic line of the Taman' peninsula (anticline folds of the Kamennii Cape and the Peklo Cape) in contrast to the geological ideas [6] was characterized by a nearly east-west trend, i.e. corresponding to a trend of the northern tectonic lines of the Kerch peninsula*. This work (see Fig. 2) considerably amplifies the details of a number of structures and their linkages (Fontalov folds, folds of the Mt. Tsimbala, Karbetovka, Bliznets'a Hill, etc.). The structure of the intervening synclines, formed in the weakly anisotropic Pliocene deposits and alluvia of considerable thickness, was not revealed by the loop method.

During 1952 the Taman peninsula, except for its western part, was seismically surveyed with the aid of the reflection method [22]. In the central part of the peninsula, this work covers the areas which have been surveyed by the loop method. A similarity was observed between the isonormals of the loop method with the structure contours of the arbitrary horizons M (the Upper Paleogene deposits) and B (the Upper Neogene deposits) of the seismic survey on the limbs of the fold. The core, composed of intensively faulted Maikop formation, could be studied in detail only with the loop method. These regions on the seismic cross-sections are expressed in the form of zones of almost complete absence of reflecting areas.

Thus, on the Taman' peninsula, as on the Kerch peninsula as shown on Fig. 6, both methods successfully complement one another in the preparation of structures for Krelius† drilling.

During the second world war, when the prospecting in the Kerch peninsula was temporarily interrupted, the loop method work was transferred to the more eastern regions of the southern USSR. In 1942, a survey was made of a 250 km^2 area between the western shore of the Caspian Sea and the Narat-Tyubinskii range of mountains to the west and south of Makhach-Kala up to the Monas River. On the north-west of this area there was the known Makhachkalinskian brachy-anticline, the crestal part of which was proposed for detailed loop studies. To the south of it was a plain covered

* This conclusion is confirmed by the most recent data of structural core drilling on Taman [35].

† Krelius drilling implies the drilling carried out after the preliminary geophysical survey.

by Quaternary deposits of 8–12 m thickness and descending gently to the sea. For exploratory drilling it was necessary to obtain reconnaissance information on the structure of this area.

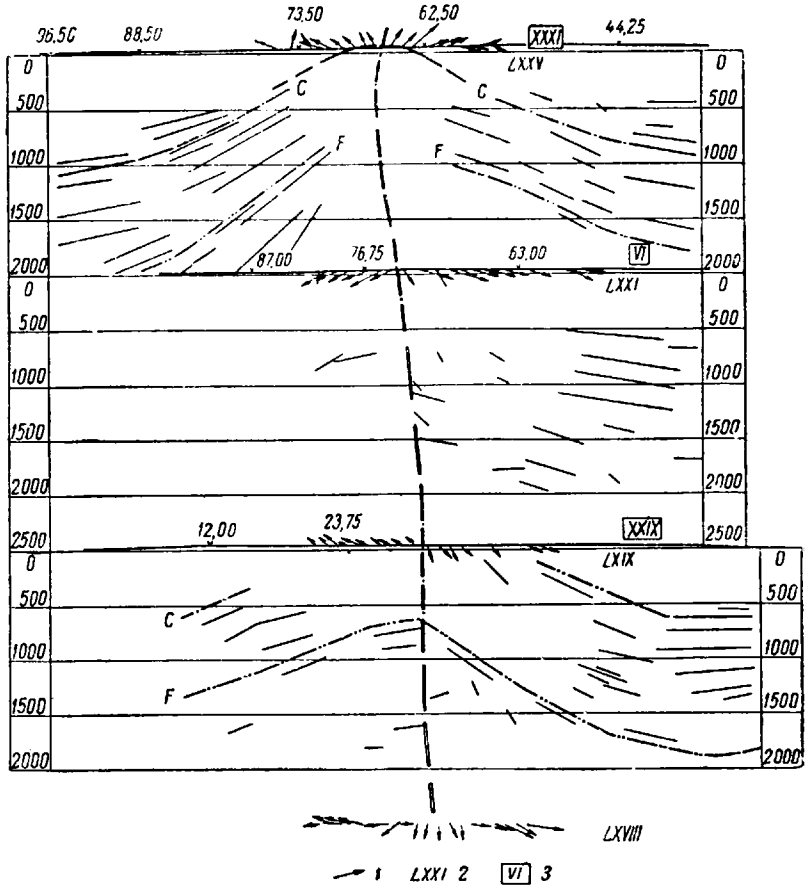

FIG. 6. A comparison of electrical prospecting and seismic profiles on the upfold of Mt. Yuzhnaya Neftianaia (Taman peninsula). 1—loop vectors; 2—number of loop profiles; 3—number of seismic profiles.

Surveying by the loop method gave an accurate structure of the northwestern pericline of the Makhachkalinskian fold and determined the position of the axis in the crestal part [16]. The nature of the connection of the southeastern periclinal nose of the fold with the monoclinally dipping layers which form the coastal plain was established. According to the data of the

reconnaissance surveys of the area to the south of Makhach-Kala the strike of the investigated rocks was shown to be uncomplicated by the presence of any new upfolds (Fig. 7).

Well drilling, using the results of the loop method, showed the petroleum deposits of the Makhach-Kakhachkalinskian brachy-anticline and the deposit was exploited.

Between 1941 and 1943 the loop method was used to map the structures on the upper levels of the section in the western Turkmenia.

In the investigated area, the geological structure of which has not been established by the previously conducted gravimetric survey, geological mapping and Krelius drilling, the Bolshaia Tuzluchaiskaia brachy-anticline, complicated by secondary upfolds, was shown by the loop method first in trials [38] and then in production [11] work. The results of the observations showed the reason for the lack of success in the preceeding Krelius drilling, determined the further course of investigation and confirmed the possibility of the successful use of the loop method to study structures in the western Turkmenia.

Work by the loop method in the western Turkmenia was recommenced in 1952–1955. The survey led to a detailed study of the structure of the Kobek fold, the position of the northern limb being detected as well as the periclinal closures of the structure. On the basis of the studies, further course of development was recommended. By this work, and also by the results of the loop survey of the Chelekenskaia structure, the tracing of faults with the aid of electrical profiling [7, 8] was shown to be possible. The same was found at a number of structures of the Kerch peninsula.

In 1954–1955 experimental work was carried out in Western Siberia. The observations were made within the limits of the Chelyabinskii graben, filled with Trias-Jurassic deposits. The Sineglazov area [17] was the most favourable for the application of the loop method. Here, the investigations established the basic elements of the tectonics of the studied sediments. The insufficient volume of experimental work did not permit reliable correction of the results of geological surveying. However, on the resultant map a possible variant of the structure of the Sineglazov area, as deduced from the data of the loop method (Fig. 8), was presented.

It is certainly possible to survey by the loop method areas which in their physico-geological characteristics are similar to the Sineglazov region. However, this could not be said of the Miass and Sugovak sections, also situated within the limits of the Chelyabinsk graben. In these areas a clear interpretation of the map of loop vectors was difficult and required the use of geological data [37].

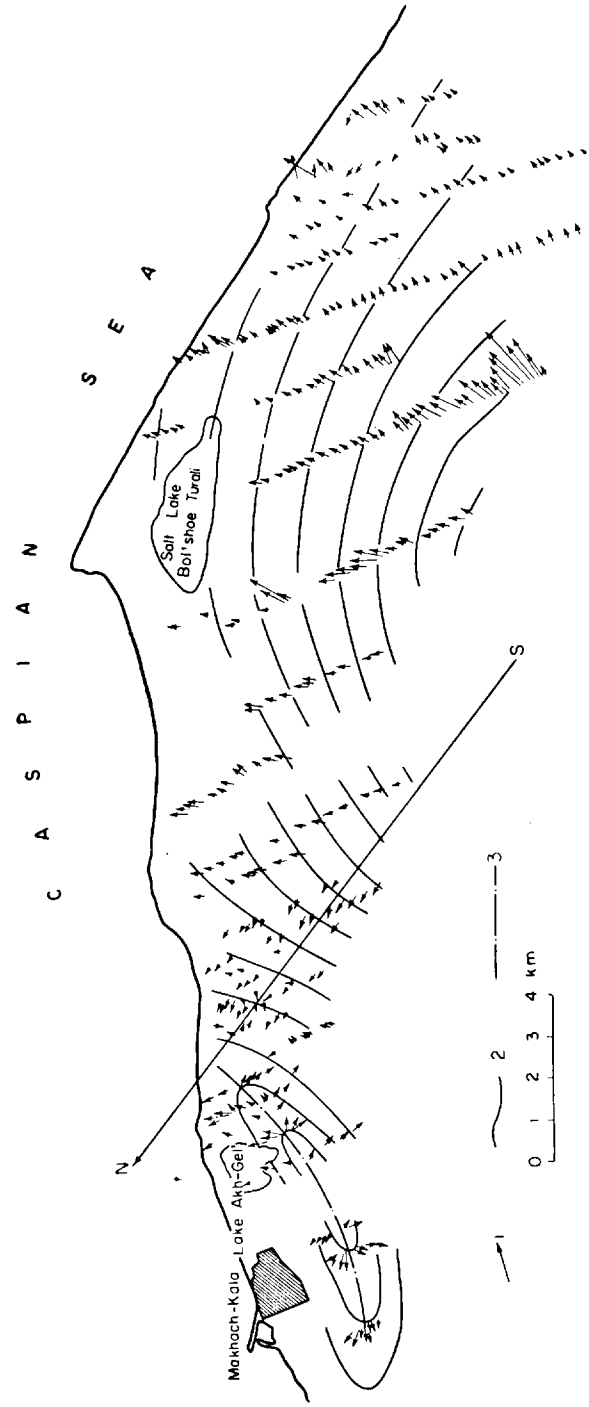

FIG. 7. The tectonic structure of the Turali section (Northern Dagestan) according to the data of the loop vectors. Compiled by I. I. KROLENKO.
1—loop vector; 2—lines normal to the loop vectors; 3—axis of fold according to data of electrical prospecting.

In 1955 small scale trials with the loop method were also carried out on the Ust'-Urt plateau within the limits of the positive gravitation anomaly of the force of gravity, depicted in 1954. Parametric observations showed that the geoelectrical characteristics of the upper part of the section, owing to its electrical heterogeneity, are not favourable for the use of the loop method.

However, the existence of large-scale anisotropism of a sedimentary formation is a factor which makes it possible to recommend working with the loop method provided that the angle of dip of the sediments is sufficient.

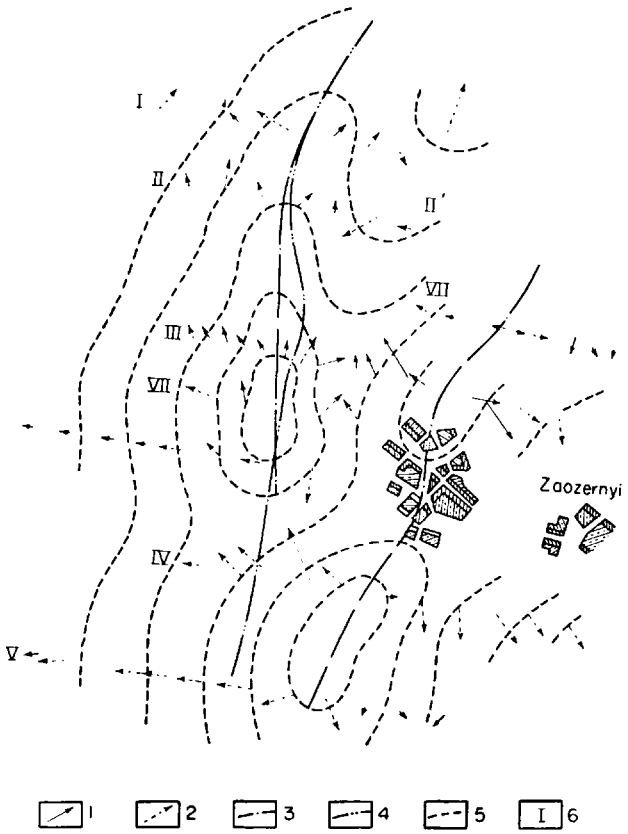

FIG. 8. The structure of the Sineglazovskii area according to the data of the loop method (Chelyabinsk region). Compiled by I. I. KROLENKO. 1—loop vectors (d = 100 m); 2—loop vectors (d = 200 m); 3—axis of fold according to the data of electrical prospecting; 4—axis of fold according to geological data; 5—lines normal to the vectors; 6—number of loop profiles.

This is confirmed by the results of a reconnaissance profile, carried out by the loop method. Within the limits of the gravitation anomaly, the profile indicated the folding of the strata, which is of practical interest in correlating the surface and the deep structure. The intersecting of the gravitation anomaly by a number of reconnaissance profiles at distances of 1–2 km from one another would probably facilitate surveys of the second order folding on the background of the large structure of the Ust-Urt. An example of a similar detailed study is the section covered by the loop method in the southern part of the gravitation anomaly (Fig. 9).

In 1953 the NIIGR electrical prospecting laboratory carried out experimental work to test the possibility of increasing the depth of investigation by the loop method and to increase its efficiency.

To solve the first problem observations were made of the final stage of stabilization of an electromagnetic field in the earth, which characterizes the

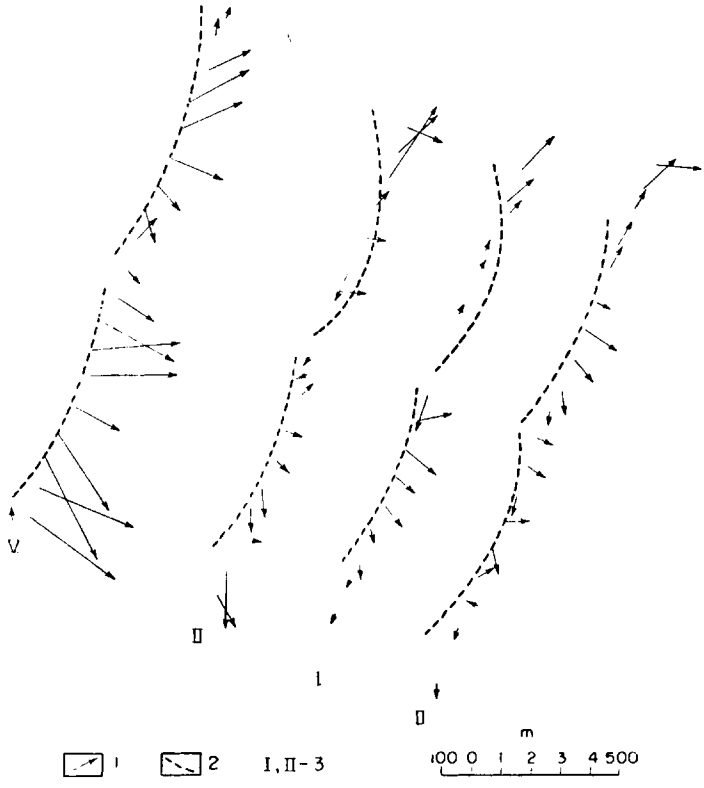

FIG. 9. The arrangement of loop profiles on the Il'todzhe section (Ust'-Urt). 1—loop vectors; 2—lines normal to the loop vectors; 3—number of profiles.

relatively deeply lying deposits. To solve the second problem use was made of the receiving frame circuit.

With the usual loop method, the e.m.f. is measured with a field potentiometer having a high-inertia galvanometer. In practice, this permits the measurement of only a certain average e.m.f. The value of the measured e.m.f. apparently depends to a considerable extent on its initial value, determined by stabilizing the field in the upper layers of the section. Corresponding to this, the arrangement for the commutation of the AB and MN circuits with the old method of working on the PU pulsator (in future it will be referred to as the No. 1 pulsator) provided an observation mainly in the initial stage of stabilization only (Fig. 10).

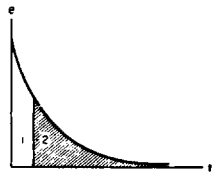

FIG. 10. 1—Observed stabilizing phase of field; 2—stabilizing phase excluded by pulsator.

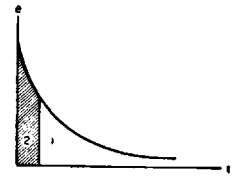

FIG. 11. 1—recorded phase; 2—stabilizing phase excluded by pulsator.

For experimental work a No. 2 pulsator, suggested by YU. A. DIKGOF, was made and tested; this pulsator did not transmit the initial phase into the receiving channel, which made it possible to take the e.m.f. characteristic of the structure of the deeper layers (Fig. 11). For this purpose the connection and disconnection of the MN line somewhat lagged behind those of the AB line.

The quantity characterizing the order of such a shift of collector rings of the No. 2 pulsator will later be referred to by the letter a with positive or negative signs depending on whether the connection of the MN line lags behind or precedes the connection of the AB line. One of the cases of displacement of the collector rings of the No. 2 pulsator is shown in Fig. 12.

The receiving frame circuit is a 2 m square frame with 2500 turns. The frame is tapped off at certain points (500, 600 and 1400 turns). The effective area of this frame is 10,000 m^2. Thus, the frame is equivalent to a square loop of 100 m aside.

The frame was mounted on a 0.5 m high support; the AB cable was folded on top of the frame and divided it into two symmetrical halves. The position did not change very much when the frame was set up on a two-

axle trailer, which made it possible to speed up the whole cycle of observations.

The increase in the length of the AB line and decrease in the effective value of the e.m.f. received, except for the initial stage of the stabilizing process, made it essential to increase the sensitivity of the measuring instrument and to preamplify the e.m.f. received.

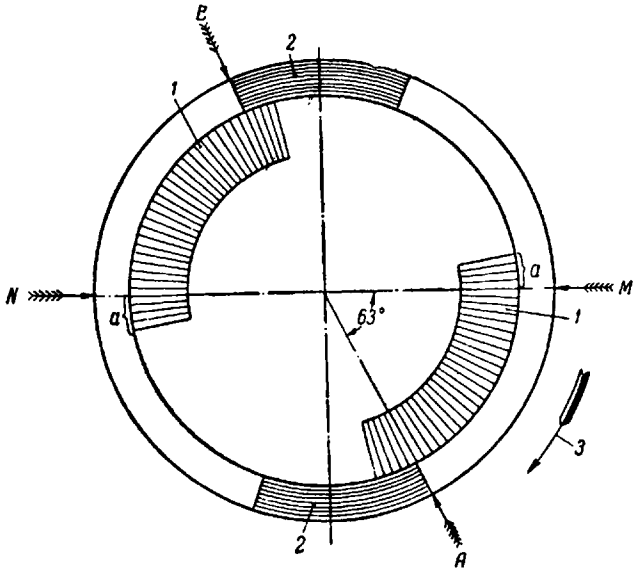

FIG. 12. The mutual disposition of the current and receiving collectors of the No. 2 pulsator with lagging of the start of the e.m.f. record with respect to switching-on of the current ($a > 0$). 1—insulating space of the collector MN (receiving); 2—insulating space of the AB collector (feed); 3—direction of rotation of the pulsator.

With increase in the AB line from 200 to 4000 m, shifts were observed in the phase of the electromagnetic field in the earth with respect to the E and H fields of the feed current in the AB cable. This fact necessitated the use of different methods for cancelling the mutual inductance between both circuits.

Compensation of the e.m.f. induced in the receiving circuit was obtained either by moving electrodes perpendicularly to the AB line or by inclination of the frame circuit. The results of field observations (Fig. 13) were recorded on cine-film by means of the MPO-2 oscillograph.

Visual observations were made with the same arrangement, but in this case, instead of the oscillograph, the EP-1 potentiometer was connected.

An analysis of the extensive experimental data led to a number of interesting conclusions on the dependence of the induced e.m.f. on the number of turns of the receiving circuit, on the AB dimensions, frequency of the pulsating current, the mutual disposition of the collector rings of the pulsator, etc.

To study the depth of reach of the method of e.m.f. corresponding to the final stabilizing stage of the field in the earth, tables were compiled giving the ranges of observations for various values of delay time of the start of e.m.f. reception relative to the time of connecting the current for the 1st and 2nd pulsators and also tables of the time for stabilizing the electromagnetic field according to the dimensions of the AB line were employed.

On the basis of these tables a graph was drawn showing the disposition of the intervals of the record on the curves for stabilizing the electrical and magnetic fields for various values of a and AB (Fig. 14).

On the graph along the ordinate are plotted the relative deviations of the stabilizing field $(\tilde{E}, \tilde{H})$ from the field which is stabilized (E_∞, H_∞), i.e.

$$\frac{E_t}{E_\infty} = \frac{\tilde{E} - E_\infty}{E_\infty}, \quad \frac{H_t}{H_\infty} = \frac{\tilde{H} - H_\infty}{H_\infty},$$

and along the abscissa axis the ratio of the time of observation t to the so-called constant of time

$$\tau_t = \frac{\left(\frac{AB}{2}\right)^2 \pi}{C^2 \varrho},$$

where C is the speed of light;

ϱ is the specific resistance of the investigated rocks.

A comparison of the time for stabilizing the field for various values of AB with the time for recording the e. m. f. when working with the No 2. pulsator led to the conclusion that with the existing design of pulsator, only

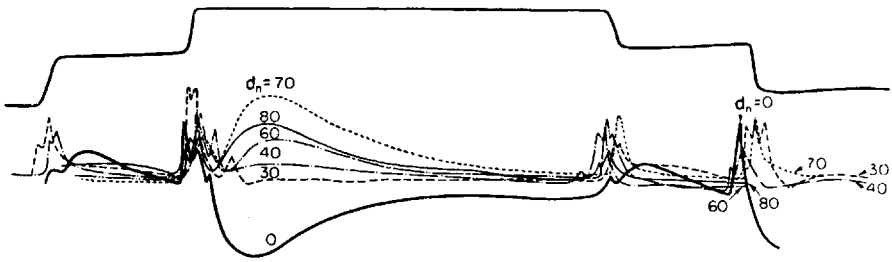

FIG. 13. A comparison of the e.m.f. curves with various values of d_n (single turn contours); AB=200 m; $I=2a$; N_p=600 rev/min; a=+3 mm; d_n is the distance of earthing from the AB line.

for $AB \leqslant 400$ m is the e.m.f. received, corresponding to the final stage of stabilization of the electromagnetic field in the earth.

With further increase in AB, the intervals of the observations referred to the initial stage of stabilizing, i.e. the measured e.m.f.s characterized only the upper deposits of the section.

Calculation showed the possibility for receiving e.m.f.s corresponding to the final stage of field stabilization for any values of AB and other fixed observational conditions by means of the corresponding change in the pulsator collector.

Observations with the frame receiving frame circuit are worthy of attention and are of practical interest.

The e.m.f. induced in the receiving frame for each of the two mutually perpendicular positions of the AB line, fed by a low frequency alternating current, are compensated by inclining the frame or can be measured by an appropriate measuring apparatus.

The two-component vectors of the loop obtained in this way make it possible to construct a vector at each observation point oriented in the direction of preferential propagation of the current, i.e. along the dip of the rocks. The field of the loop method vectors should characterize the tectonics of the studied deposits to a depth corresponding to the depth of penetration of the magnetic field of a given frequency for a known value of AB.

The observations made with a receiving frame circuit even under complex physico-geological conditions, always led to results agreeing with the geological data.

A number of problems arising during the trials on the modernization of the loop method could not be solved due to the low technical level on which they were carried out in 1953. However, this work established the possibility of such a modernization and indicated the future course of development.

From this brief review of work carried out by the loop method it can be seen that under favourable physico-geological conditions, the results of the method are not only supported by geological surveying but in a number of cases they add to it and correct it [32, 33, 34].

For example, by comparing the character of the field of loop vectors for a number of areas in the Kerch peninsula with the seismic results and electric logging of wells, drilled in these areas, it can be concluded that the structure of the upper 40–50 m of the section (observations by the loop method were carried out mainly with $d = 100$ m, $AB = 200$ m) reflects the structure down to a depth of about 500 m. Consequently, in this region the results of surveying by the loop method can orientate the cartographic

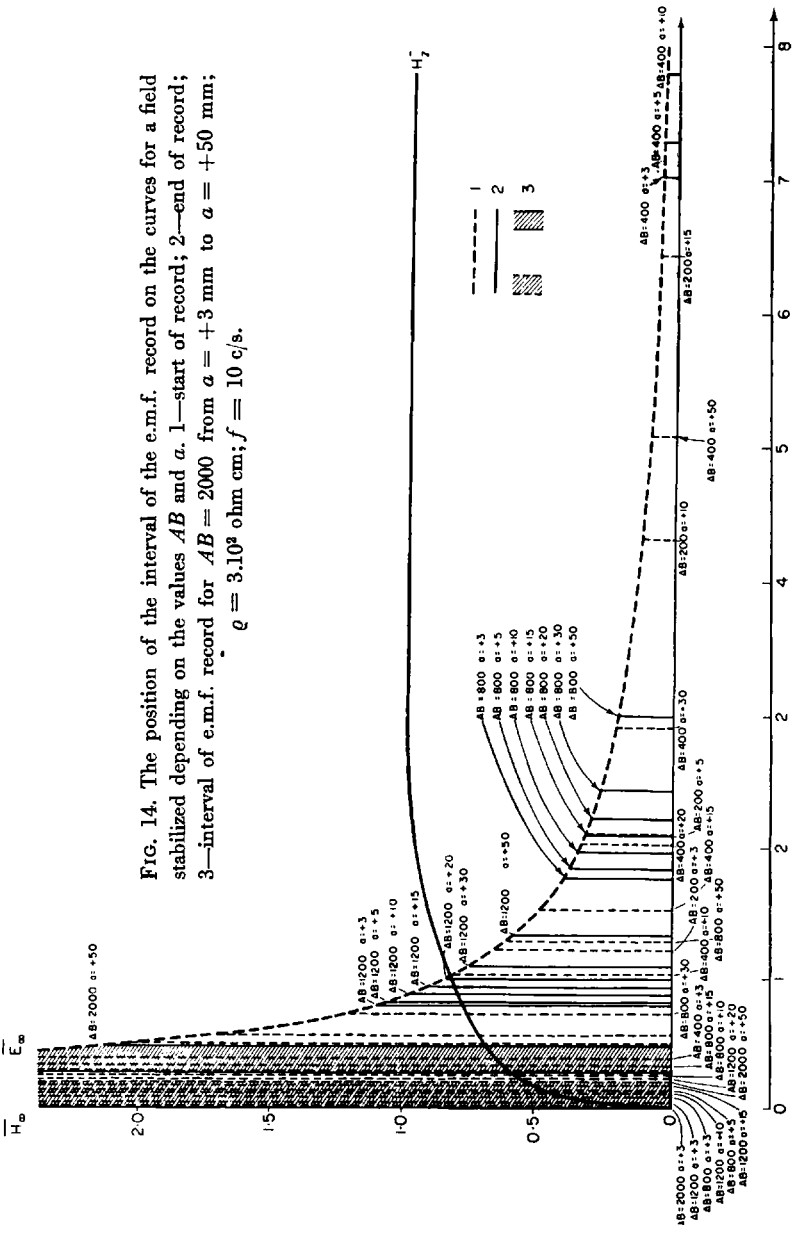

FIG. 14. The position of the interval of the e.m.f. record on the curves for a field stabilized depending on the values AB and a. 1—start of record; 2—end of record; 3—interval of e.m.f. record for $AB = 2000$ from $a = +3$ mm to $a = +50$ mm; $\varrho = 3.10^3$ ohm cm; $f = 10$ c/s.

drilling and, with the established correspondence of deep tectonics to the structure of the upper levels of the section, provide a basis for the laying of deep exploratory wells. By showing the tectonics of the studied area, the results of the loop investigations condition the further geological work, which ensures rational use of materials and time in surveys and explorations of petroleum deposits.

However, the underestimation of the possibilities of this method, and sometimes the simple lack of inclination to sort out the results of previous studies meant that areas covered by detailed surveys by the loop method were overlapped by detailed geological surveys and cartographic drilling which increased the expense of the exploration, especially bearing in mind the difficulties of the geological survey under the conditions of the muddy Maikop formations.

For example, at the Uzunlar dome of the Kerch peninsula a satisfactory solution of the problems facing the geological survey party was achieved by carrying out a large volume of work. On the surveyed area of 150 km^2, 606 prospecting pits were dug to an average depth of 3.4 m, 384 wells were drilled by hand to an average depth of 12.2 m, 36 ditches were dug and 270 exposures were described. The field work took 9 months [30].

The survey of this area by the loop method took 30 days. During this time, about 1300 loop vectors were measured with an octagonal arrangement of diameter $d = 100$ m.

As already mentioned, the results of all these investigations provided the same structural pattern of the studied area. However, owing to the dense network of the observations the pattern is more firmly based on the data of the loop method.

To compare the economic and production effectiveness of geological surveying and geophysical work by the loop method another example can be chosen by quoting the survey on the Marforov area (the south-western plain of the Kerch peninsula). To study the structure of this area of 56 m^2, 133 prospecting pits were dug to an average depth of 3.5 m, 216 wells were hand-drilled with an average depth of 15 m, and 150 natural exposures were described. The field period lasted 10 months [29] and the work cost 183,000 roubles.

The survey of this region with the loop method lasted 12 days, 450 loop vectors being measured. The cost of the work was about 30,000 roubles. The results of the surveys are identical. To illustrate the efficiency of a field group using the loop method we give certain figures from the accounts of the group 13/50 of the department Krasnodarneftegeofizika working in 1950 in the Kerch and Taman peninsulas [21].

A single section group in the course of a field period (lasting 180 working days) surveyed quantitatively an area of 776 km^2 (the distance between the profiles from 600 to 1000 m). Ten structures were mapped in the Kerch and three on the Taman peninsula. 6000 loop vectors were measured with an octagonal arrangement, $d = 100$ m, $AB = 200$ m. The work cost 350,000 roubles.

In conclusion, we will consider which production problems confront the loop method at the present time and the possibilities for its development in surveying.

The results of studies by the loop method under complex conditions of dislocated, homogeneous and anisotropic deposits, covered by alluvia, were confirmed in most cases by geological surveying, by cartographic drilling and partially by seismic exploration. This means that the method can be considered as the first stage in a semi-quantitative co-ordinated exploration of buried structures under the conditions mentioned above.

The first objects of exploration by the loop method should be regions which are unfavourable for other methods. In other words, lithologically homogeneous sections, which do not have clear marker horizons and are poorly exposed. When planning subsequent geological surveying and drilling in these areas, there should be a sparse network of trial shafts and cartographic bore-holes, and the investigation should be concentrated in the zones of local upfolds, variations of axial plunge, secondary complications and in zones of merging of the structures, all of which are indicated on the map with the aid of the loop method.

If the surface and deep tectonics correspond, a similar method also applies to problems of planning seismic exploration and deep drilling. An important role is then played by the combined use of the loop method and seismic exploration. Carrying out these measures makes it possible to reduce the bulk of expensive geological surveying and seismic exploration, and to improve the extent to which the deposit is studied.

A successful application of the loop method in the Crimea, Dagestan, the Taman' peninsula and in the Turkmenia indicate that it was essential to continue this work in these regions. Thus, in the Taman' the loop method only covered the western and central part of the peninsula, in the eastern part and further along the southern edge of the Kuban depression, surveying was not carried out, although in combination with seismic exploration this work would be of practical interest.

In Turkmenia and to the south of Kazakhstan, the loop method could be used for surveying and mapping of buried structures on the western depression of Kopetdag and in north-western Tudakyr and Kaplankyr.

In this respect also the region of Bukhara and Khiva on the right bank of the Armu-Dar'ia is not without interest.

Of considerable help would be the use of the loop method on the extensive, but little studied, Ust'-Urt plateau, where the loop method gave favourable results with deposits showing large-scale anisotropism.

The loop method should also be used to a greater extent in tracing faults in disturbed zones. When carrying out experimental work it would be possible to recommend for this purpose objectives such as the Emba salt domes.

In connection with the proposed modernization of the method, in particular for extending its depth and effectiveness of study and the use of a small dimension frame instead of a large diameter loop, the loop method can be very helpful in a number of wooded regions in Western Siberia; for example, regions to the east of the Chelyabinsk graben.

For the further development of modifications of the loop method, we can also recommend observations at a fixed frequency with increase in the dispersions of the feed electrodes A and B, for work on a fixed length of AB line with changing frequency of the feed current (1, 2, 3 c/s etc.). This would make it possible to follow the change in vectors of the loops with increase (or decrease) in the depth of the study.

At the present time, in view of the absence of a theory for alternating electromagnetic fields in inclined anisotropic media, this suggestion can only be based on an evaluation of the depth of penetration of electromagnetic oscillations at various frequencies in a homogeneous, isotropic unbounded medium.

If we assume the resistance of such an idealized medium to be equal to the resistance of the clays of the Maikop formation ($\varrho = 3 \cdot 10^2\ \Omega \cdot$ cm), then the depth of penetration of the oscillation with a frequency 1 c/s is about 2 km, and for an oscillation with frequency 10 times greater about 640 m. Consequently, the range of depths with change in the frequency from 1 to 10 c/s is sufficiently great to serve as an indication of the possibility of increasing the depth of investigation by reducing the frequency of the feed current, as suggested above.

However, to interpret field observations it is necessary to have a developed theory for an alternating electromagnetic field in anisotropic media, and in particular a calculation of the actual depth of penetration of the alternating magnetic field of a given (low) frequency in inclined anisotropic deposits. This makes it possible to evaluate in the first place the depth of the proposed modification of the loop method and to calculate the range of depths with change in frequency of the feed current, and in the second place, to establish the resolving power of the method in the presence of a hetero-

geneous section. For this it is necessary to check the influence of the heterogeneity of the section and the surface heterogeneity on the results of the observations. It is possible that these calculations will make it possible to extend the area of application of the loop method, using it to determine the angle of inclination of the deposits which are anistropic on a large scale.

To interpret the results of observations obtained with change in the coefficient of mutual induction between the circuits by the method of inclination of the frame, it is necessary to know the effect of the angle of inclination of the anisotropic deposits (α) on the observed angle of inclination of the magnetic field on the earth's surface (ϱ). This effect is given in a general form by DAKHNOV[10]; however, the solution of the integral in the expression for angle β through α and the coefficient of anisotropy λ is given only for two special cases: for points of the observation placed along the dip and for points placed along the strike of the rocks, i.e. along the axes OX and OY. A general solution should be obtained by deriving formulae for calculations and establishing graphs from which it would be possible to interpret field observations.

Experimental work on the modernization of the loop method showed the way for increasing the efficiency of this method, and also the depth of the study which should extend the region of its application. A number of problems should be solved by field experiment; however, further development and improvement in the loop method is possible only on the basis of more extensive production use, as a cheap and highly efficient method for geophysical prospecting.

REFERENCES

1. A. D. ARKHANGEL'SKII, *et al.*, A Brief Report on the Geological Structure and Oil Bearing Deposits of the Kerch Peninsula. *Tr. GGRU*, No. 13, Gosgeolizdat (1930).
2. P. K. ALEINIKOVA, *The Geological Structure of the Glazovsk and Yurkinsk upfolds.* Documents of the Krymneftegeologiya Department (1948).
3. P. K. ALEINIKOVA, *Report on the Structural Geological Survey of the Malo-Babchinsk Area.* Documents of the Krymneftegeologiya Department (1951).
4. V. R. BURSIAN, *The Theory of Electromagnetic Fields used in Electrical Prospecting.* Zhdanov Leningrad Gos. University.
5. V. N. VASLIL'EV, *Report of the Work of the Feodosiisk Seismical Party 10–53 on the Territory of the Staro-Krymsk Region of the Crimea.* Documents of the Krasnodarsk GSGT Glavneftegeofizika MNP, SSSR (1954).
6. I. M. GUBKIN, M. I. VARENTSOV, *The Geology of Petroleum and Gas Deposits of the Taman Peninsula.* Azneftetekhizdat (1934).
7. K. S. GUMAROV, *Report of the Work of the Pribalkhansk Electrical Prospecting Party 10/52 in the Pribalkhansk Region in 1952.* Documents of the Sredneaz. geofiz. tr. Glavneftegeofizika MNP SSSR, (1953).

8. K. S. GUMAROV, *The Results of Work of the Electrical Prospecting Party 7/53 in the South-Western Turkmenia.* Documents of the Sredneaz. geofiz. tr. Glavneftegeofizika MNP SSSR (1954).
9. V. N. DAKHNOV, The Loop Method. *Proceedings of the All-Union Office for Geophysical Prospecting of the main control of the petroleum industry*, No. 4, ONTI (1935).
10. V. N. DAKHNOV, *Electrical Prospecting by the Loop Method.* Gostoptekhizdat (1947).
11. YU. A. DIKGOF, *Report on the Electrical Prospecting Work on the Tuzluchan and Kobek Sections of the Western Turkmenia.* Document of GSGT Glavneftegeofizika MNP SSSR, (1944).
12. N. P. D'YACKHOV, *The Work of the 1950 Kerch Seismical Party 11/50 in the Crimea.* Documents of the Krasnordarsk GSGT Glavneftegeofizika MNP SSSR, (1951).
13. I. I. KROLENKO, *The Electrical Prospecting Work on the Areas of the Krymgazneft Trust in 1938.* Documents of the Union Office for Geophysical Prospecting. The Central Administration of the Petroleum Industry (1939).
14. I. I. KROLENKO, *Work by the Loop Method on the Kerch Peninsula in 1939.* Documents of the GSGT Central Geological Administration of the NKNP SSSR.
15. I. I. KROLENKO, *The Work of the Feodosiisk Electrical Prospecting Party 7/46 in the Crimea in 1946.* Documents of the TsO GSGT, MNP SSSR.
16. I. I. KROLENKO, *Electrical Prospecting by the Loop Method on the Turalin Section (Northern Dagestan).* Documents of the GSGT Central geological Administration of the NKNP, SSSR (1943).
17. I. I. KROLENKO, ANUROV, B. A., *The Results of Trials of the Electrical Prospecting Party 13/14 in the Krasnoarmeisk and Etkul'sk Regions of the Chelyabinsk Province in 1954.* Documents, Zap.-Sib. Geofiz. tr. Glavneftegeofizika MNP, SSSR, (1955).
18. I. I. KROLENKO, *The Work of the Experimental Crimean Electrical Prospecting Party 26/53.* Documents of the NIIGR MNP SSSR (1954).
19. N. G. KROLENKO-GORSHKOVA, *The Subject of the 15/48 Correlation of Geophysical Data for the Crimea.* Documents of the Krasnodar Geophysical Department of the Glavneftegeofizika MNP SSSR, (1950).
20. I. I. KROLENKO, *The Work of the Electrical Prospecting Party 9/51 GSKGT on the Taman Peninsula in 1951.* Documents of the Krasnodarsk GSGT Glavneftegeofizika MNP SSSR, (1952).
21. N. G. KROLENKO-GORSHKOVA, *The Work of the Kerch Electrical Prospecting Party 13/50 KGK on the Kerch Peninsula and the Western Part of the Taman Peninsula in 1950.* Documents of the Krasnodar Geophysical Department of the Glavneftegeofizika MNP SSSR, (1951).
22. A. A. KLIMAREV, YA. M. RYABKIN, *The Work of the 1952 Taman' Seismic Party 1/52.* Documents of the Krasnodar GSGT Glavneftegeofizika MNP, SSSR, (1953).
23. A. A. KLIMAREV, *The Work of the 1954 Aivazovsko-Moshkarevsk Seismic Party 9–10/54 in the Crimean Area of the Ukraine SSR.* Documents of the Krasnodar GSGT Glavneftegeofizika MNP, SSSR, (1955).
24. A. G. KURNYSHEV, *The Work of the 1948 Magnetometry Party 14/48 on the Territory of the Crimea.* Documents of the Krasnodar Geophysical Department of the Glavneftegeofizika MNP, SSSR (1949).
25. G. A. LYCHAGIN, *The Conclusions and Possibilities of Petroleum Prospecting in the Crimea.* Documents of the Drilling Department of the Krymgaznefterazvedka (1956).
26. G. A. LYCHAGIN, N. V. FURASOV, *The Structural Mapping Column Drilling at the*

Malo-Babchik area in 1941. Documents of the Drilling Department of the Krymgaznefterazvedka (1952).

27. Z. L. MAIMIN, *Materials for the study of Maikop deposits of the Kerch Peninsula.* VNIGRI, series A, No. 117 GONTI (1939).
28. Z. L. MAIMIN, *The Tertiary Deposits of the Crimea.* Tr. VNIGRI, otd. seriya, No. 1 ONTI (1951).
29. G. L. MISHCHENKO, *The Geological Structure of the Marfovsk Area (Kerch Peninsula).* Documents of the Krymneftegeologia Department (1951).
30. G. L. MISHCHENKO, *The Structural Geological Survey of the Uzunlarsk area (Kerch Peninsula).* Documents of the Krymneftegeologia Department (1952).
31. M. V. MURATOV, The Tectonics and History of Development of the Alpine Geosyncline area of the Southern European area of the USSR. *Tr. Inst. Geol. Nauk SSSR,* volume II. Izd. Akad. Nauk SSSR (1949).
32. A. N. OSLOPOVSKII, *The Correlation of Data Materials of the Geological Investigations in the Crimea.* Documents of the Krymneftegeologia Department (1951).
33. M. F. OSIPOV, *The Results of Deep Drilling at the Vladislav area (Kerch Peninsula).* Documents of the Drilling Section of the Krymneftegazrazvedka (1953).
34. E. G. SAFONTSEV, *The Geological Report on the Results of Core Drilling at the Akhtanizovsk and Severoakhtanizovsk Area of the Temryukskii Region of the Krasnodar Border.* Documents of the GTK Krasnodarnefterazvedka Department (1952).
35. E. G. SAFONTSEV, *The Geological Report on Results of Column Drilling at the Fontalovsk Area of the Temryukskii Region of the Krasnodar Border.* Documents of the GTK Krasnodarnefterazvedka Department (1955).
36. A. N. TIKHONOV, Stabilizing the Electrical Field in a Homogeneous Conducting Semispace. *Izv. Akad. Nauk SSSR. ser. geograo-geofizich* 7, No. 3 (1946).
37. D. P. FEDOROVA, Yu. S. KOPELEV, *The Work of the Electrical Prospecting Party 11/55 in the Krasnoarmeiskii Region of the Chelyabinsk area.* Documents of the Zap.-Sib. Geofiz Glavnefttegeofizika Department MNP SSSR (1955).
38. V. I. KHOLMIN, *Electrical Prospecting Work in the Turkmen in 1941–1942.* Documents of the Sredneaz. Section of the GSGT of the Central Geological Administration of the NKNP, (1943).
39. S. M. SHEINMAN, Establishing Electromagnetic Fields in the Earth. The collection *"Applied Geophysics",* No. 3. Gostoptekhizdat (1947).
40. D. P. CHETAEV, *The Study of Non-Stabilizing Systems of Electrical Prospecting Fields in Non-Homogeneous Media.* The Documents of the Geophysical Institute, Akad. Nauk SSSR (1953).

CHAPTER 11

ALLOWANCE FOR THE INFLUENCE OF VERTICAL AND INCLINED SURFACES OF SEPARATION WHEN INTERPRETING ELECTRIC PROBINGS

V. I. FOMINA

WHEN interpreting VEP [VES or vertical electrical sonde in Russian; Editor's remark] curves it is assumed that the surface of separation between layers can, in a first approximation, be considered to be horizontal within the limits of each probe point taken separately*. In practice such conditions are encountered very infrequently, especially when the dimensions of the probe feed lines are great (25–30 km). A structure consisting of two or more tectonic blocks, within each of which the condition of horizontal homogeneity of the medium is observed within certain limits, is often the subject of electro-geophysical prospecting. The boundaries of each component of such a structure (as a result of tectonic disturbances) are zones of vertical or inclined contacts between rocks of different specific resistance. In what follows we shall call these zones "zones of vertical or inclined contacts".

In this connection it is extremely important to explain the character and magnitude of the distortions introduced into VEP curves by tectonic disturbances in order to be able to establish with greater accuracy the electric cross-section, the depth at which the electrical marker† horizon lies, and the position of the contacts in each component.

If the distance from the VEP point to the zone of vertical or inclined contact is sufficiently great by comparison with the maximum spacings of AB, the VEP curve will reflect changes in the electric cross-section at the point under examination with sufficient accuracy and may therefore be interpreted by the ordinary method.

If the distance from the VEP point to the contact zone is small, the observed VEP curve will deviate from the curve for a horizontally homogeneous medium.

* The use of ordinary comparison curves is permitted if the marker horizon falls within angles that do not exceed 15–20° (sides of the folds). It is assumed that the diurnal surface is also horizontal.

† An electrically resistant horizon, through which the current does not penetrate easily. [Editor's footnote].

It is known that the nature and degree of the observed distortions depend on:

(1) the size of the ratio $\frac{d}{H}$, where d is the distance from the contact to the VES point; H is the depth at which the reflecting horizon lies;

(2) the correlation $\frac{\varrho_2}{\varrho_1}$ between the specific resistances of the media on both sides of the contact;

(3) the angle of inclination of the contact surface.

CV–2S and CV–3S reference graphs, which are mentioned in some instruction manuals of electro-geophysical prospecting, had been calculated to evaluate the influence of the vertical contact as long ago as 1938 [1, 2, 3].

An examination of these reference graphs shows that the vertical contact of two media (given that the electrodes MN do not pass through it) brings about specific alterations in the values of ϱ_k. Thus, if the spacings of AB are orientated perpendicular to the vertical contact, the VEP curve at spacings of $\frac{AB}{2}$ close to d will show a sharp deflection of the value of ϱ_k from ϱ_1, dependent on the ratio $\frac{\varrho_2}{\varrho_1}$ (increase for $\varrho_2 > \varrho_1$, decrease for $\varrho_2 < \varrho_1$).

The beginning of these deflections is observed with spacings $\frac{AB}{2}$ of an order of $\frac{d}{2}$. They attain their maximum value at $\frac{AB}{2} = d$; at $\frac{AB}{2} > d$ the deflections are gradually decreasing and at $\frac{AB}{2} > 10d$ they are practically imperceptible (CV–3S reference graph).

In the case of spacings of AB being orientated parallel to the vertical contact, the VEP curve will, as is known, show an even deflection beginning with separations of $\frac{AB}{2} \cong 0.8-1.0\,d$ (increase for $\varrho_2 > \varrho_1$ or decrease for $\varrho_2 < \varrho_1$) in the value of ϱ_k from ϱ_1, to an asymptotic value determined by the formula

$$\left(\frac{\varrho_k}{\varrho_1}\right)_{\frac{AB}{2}\to\infty} = \frac{2\varrho_2}{\varrho_1+\varrho_2}\varrho_1. \tag{1}$$

For $\frac{\varrho_2}{\varrho_1} = \infty$, the asymptotic value $\varrho_k = 2\varrho_1$; for $\frac{AB}{2} < d$ distortions in the curve are insignificant (CV–2S reference graph).

In the case of a vertical contact covered by a medium of high specific resistance the thickness of which is small by comparison with the dimensions of the apparatus it is assumed that the nature of the distortions described above will not be changed.

Complex combinations of vertical and horizontal contacts, which are often hidden, are frequently encountered in practice in geophysical investigations, and the influence of the layer which covers the contact can often not be neglected because of its considerable thickness. In certain of the most simple cases an explanation of the nature of the distortions in the VEP curves can be reduced to solution of a known problem concerning the vertical surface of separation between two separate homogeneous media.

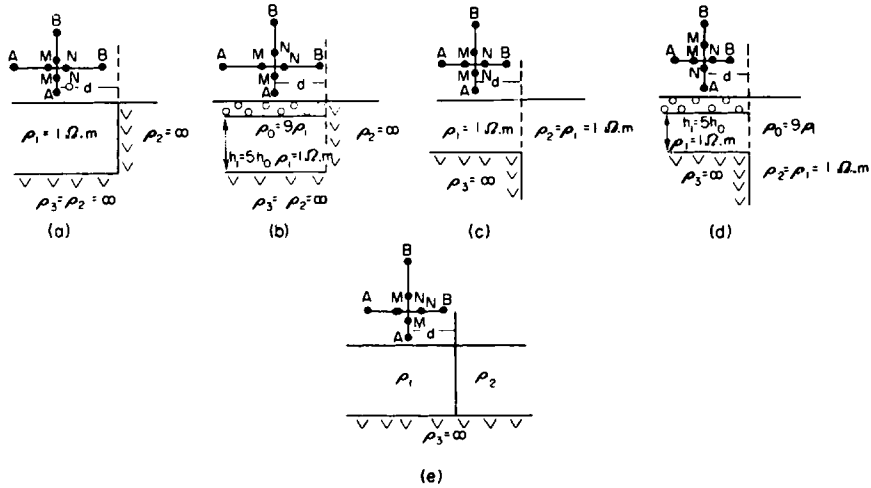

FIG. 1.

Let us consider the case (Fig. 1, *a*) in which the cross section on one side of a vertical contact (at the VEP points) is represented by a double-layered medium and on the other side by homogeneous deposits.

Let us proceed from the hypothesis that a double-layered medium with specific resistivities ϱ_1 and ϱ_3 can be treated for each VEP cross-section as a homogeneous medium the specific resistivity of which is equal to the apparent resistivity $(\varrho_{1k})_L$*. This hypothesis is not open to doubt for the

* That this substitution might be possible was also suggested by D. M. Srebrodol'skii in a thesis in 1936. Documents of the Leningrad State University.

asymptotic portion of the VEP curve, since for sufficiently large spacings over a double-layered medium

$$(\varrho_{1,k})L \to \varrho_3.$$

The approximate construction of VEP curves under these conditions is achieved by graphic summation of the ordinates of two theoretical probe curves, the first of which corresponds to a horizontally layered medium, and the second to cases with a single vertical surface of separation for which CV–2S or CV–3S reference graphs have been calculated.

A curve is selected from a CV–2S or CV–3S reference graph which depends on the direction of the probe spacings and in which the modulus $\mu = \frac{\varrho_2}{\varrho_1}$ is equal to the ratio $\frac{\varrho_2}{(\varrho_{1k,})_L}$ and takes account of various values for the required spacings of AB.

This approach to the construction of the curves follows from a consideration of known formulas used in electric profiling for calculating ϱ_k for the case of the vertical contact of two separately homogeneous media:

(a) If the electrodes are placed perpendicularly to the contact then

$$\varrho_k = \varrho_1\left\{1 + \frac{k}{2}(L^2 - l^2)\left[\frac{1}{(4x-L)^2 - l^2} - \frac{1}{(4x+L)^2 - l^2}\right]\right\}, \tag{2}$$

when all the electrodes are on one side of the contact in a medium with specific resistivity ϱ_1, and

$$\varrho_k = \varrho_1\left\{1 + \frac{k}{2}\left[1 - \frac{L^2 - l^2}{(4x+L)^2 - l^2}\right]\right\}, \tag{3}$$

if the electrode B is in a medium with specific resistivity ϱ_2, and the electrodes AM and N are in a medium with specific resistivity ϱ_1.

(b) If the electrodes are placed parallel to the contact then

$$\varrho_k = \varrho_1\left\{1 + k\frac{y(y+l)}{l}\left[\frac{1}{\sqrt{4d^2 + y^2}} - \frac{1}{\sqrt{4d^2 + (y+l)^2}}\right]\right\}. \tag{4}$$

If the expression in braces is denoted by ϱ_k^V and if we take the above hypothesis into consideration, the value of ϱ_k for each of the formulas given above can be expressed as the product

$$\varrho_k = (\varrho_{1,k})_L \, \varrho_k^V. \tag{5}$$

$(\varrho_{1,k})_L$ for a double-layered medium is expressed in its turn by the known formula

$$(\varrho_{1,k})_L = \varrho_1 \left\{ 1 + 2 \sum_{n=1}^{n=\infty} \frac{k_{1,2}^n r^3}{[r^2 + (2nh_1)^2]^{3/2}} \right\}. \tag{6}$$

If the expression in braces is denoted by ϱ_k^H and the value $(\varrho_{1,k})_L$ is substituted in equation (5) we obtain

$$\varrho_k = (\varrho_{1,k})_L \varrho_k^V = \varrho_1 \varrho_k^H \varrho_k^V$$

or

$$\frac{\varrho_k}{\varrho_1} = \varrho_k^H \varrho_k^V, \tag{7}$$

where ϱ_k^H is the value of the ordinate of the curve on an SN–1 reference graph for each spacing of the probes; ϱ_k^V is the corresponding value of the ordinate of the curve on a CV–2S or CV–3S reference graph.

Taking logs of expression (7) we obtain

$$L_g \left(\frac{\varrho_k}{\varrho_1} \right) = L_g \varrho_k^H + L_g \varrho_k^V.$$

When, therefore, we are constructing a desired curve on a bilogarithmic paper we sum the ordinates of the curves given above graphically.

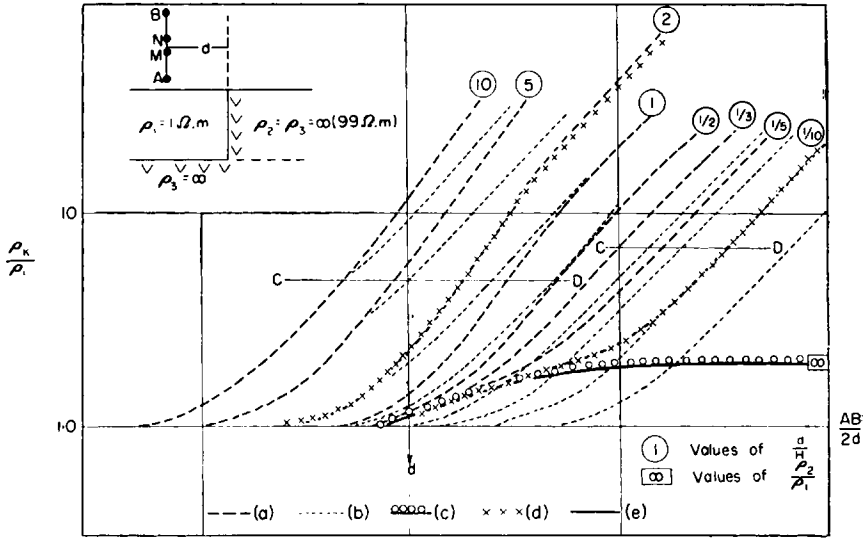

FIG. 2. *a*—approximately constructed VEP curves; *b*—VEP curves for a horizontally homogeneous medium; *c*—curves of the CV–2S reference graph; *d*—curves of the HVC reference graph; *e*—line connecting the points on VEP curves for the maximum separations of AB used in practical work.

Figure 2 shows curves which have been constructed in the manner described above for case 1, *a*, in which the direction of the separations is parallel to the surface of the vertical contact for various values of the ratio $\frac{d}{H}$. It also shows curves for a double-layered medium at the VEP point and a curve on the reference graph CV–25.

As may be seen from Fig. 2, approximately constructed curves only give satisfactory results for true transverse conductivities S when $d \geqslant 2H^*$.

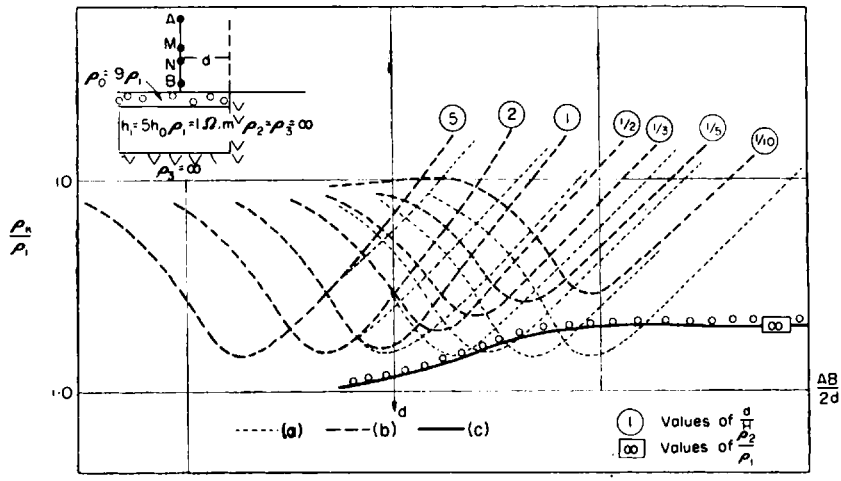

FIG. 3. *a*—VEP curves for a horizontally homogeneous medium: *b*—approximately constructed VEP curves; *c*—curves of the CV–3S reference graph.

When $d \leqslant \frac{H}{2}$ the value of S obtained is half the true value, and when $2H > d > \frac{1}{2}H$, S takes on a value intermediate between S and $\frac{S}{2}$.

The curves obtained are compared in Fig. 2 with curves calculated by M. N. Berdichevskii (HVC reference graph) for the case when two contacting media lie on a third medium with a specific resistivity of $\varrho_3 = \infty$, where we have taken $\varrho_2 = 99\varrho_1$ instead of $\varrho_2 = \infty$ (Fig. 1, *e*).

The curves obtained practically coincide with the HVC curves.

On this basis we consider that the accuracy of the approximate construction of curves by the methods described is fully adequate for practical

* Given a cross section of this type, VEP curves may usefully be extended as far as the cross sections bounded on Fig. 2 by the horizontal line C.

purposes and the curves obtained can be used to explain the nature of distortions in probings arising from the influence of non-horizontal boundaries.

The approximate construction of curves distorted by the influence of a horizontal boundary can be extended to the more complex case shown in Fig. 1, b, when the medium at the VEP point is a triple-layered cross-section.

Fig. 3 shows curves obtained for this case:

$$\varrho_0 = 9\varrho_1,\ h_0 = 1\ h_1.$$

In this case ϱ_k^H has already been determined on an SN–20 triple-layered comparison curve for each separation taken; the value of S has been approximately determined with the same degree of error as in the double-layered case cited above. The ordinate of the minimum point is increased under the influence of the vertical contact. Its abscissa remains practically constant. In this case the variation in the co-ordinates of the minimum point and the value of S in relation to the distance $\frac{d}{H}$ is the same as would obtain if instead of sudden increase in the resistivity at the contact there were to be a gradual increase in the resistivity of the conducting horizon.

In connection with this, it is obvious that a fictitious rise of the marker horizon may be obtained in interpreting VEP curves when fixing the parameter which corresponds to the conducting horizon above the marker horizon. For VEP curves parallel to the contact, the position of this contact may be defined either from the beginning of the deviation of ϱ_k from $\varrho_{1,k}^H$ or from the alteration in the type of curve as the VEP point approaches the contact (transition from a double-layered curve to a triple-layered curve of type A), while for a triple-layered cross-section it may be defined from the increase in the ordinates of the minimum points. It is obvious that these criteria may not be of use in all cases as the electric cross-section at the VEP point is not sufficiently studied in the majority of cases. A more accurate determination of the position of the vertical contact may be made from VEP curves in which the spacings are perpendicular to the contact.

By using the approximate method described above for constructing curves for VEP in which the spacings are orientated perpendicular to the surface of the contact, let us make a preliminary comparison of certain of the curves obtained with the curves of the HVC reference graphs. The comparison shows that the calculated curves coincide with the approximated curves for a double-layered cross-section.

Approximated curves for a triple-layered cross-section of type H, are shown in Fig. 4 and for a double-layered cross-section in Fig. 5. A value

for S determined from the first rise in the VEP curves is close to its true value (when $d > 2H$) for both double and triple-layered cross-sections.

When $d \leqslant 2H$ the first rise of the asymptotic branch of the VEP curves is brought about by the influence of the vertical contact and the value of S determined from this rise is considerably less than the true transverse conductivity, this divergence being the greater for the SN–1 type of VEP the smaller is the ratio $\frac{d}{H}$.

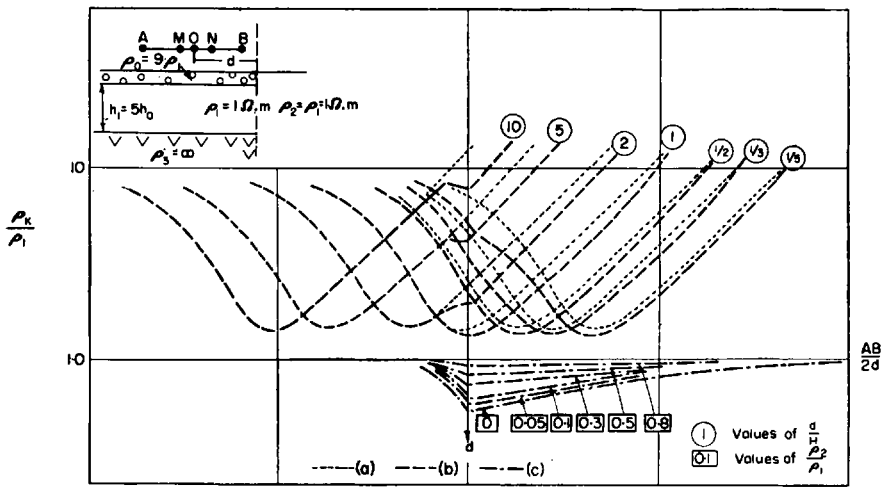

FIG. 4. *a*—VEP curves for a horizontally homogeneous medium; *b*—approximately constructed VEP curves; *c*—curves of the CV–3s reference graph.

If the values of S are determined for the terminal branches of observed VEP curves, these values will be very slightly lowered and the lowering will decrease as the ratio $\frac{d}{H}$ decreases.

The maximum increase of ϱ_k in relation to $(\varrho_{1,k})$ is observed for separations in which the feed electrode intersects the surface of separation between the media. We may therefore establish the position of the vertical contact by plotting the abscissae of the maximum increase of ϱ_k in relation to $(\varrho_{1,k})_L$ along the profile from the centre of each VEP.

In the case of a triple-layered cross-section a considerable deviation of ϱ_k from $(\varrho_{1,k})_L$ at the minimum of the curve is to be observed. The greatest deviation in the minimum is to be observed in VEP curves obtained when d is close to the abscissa of the minimum.

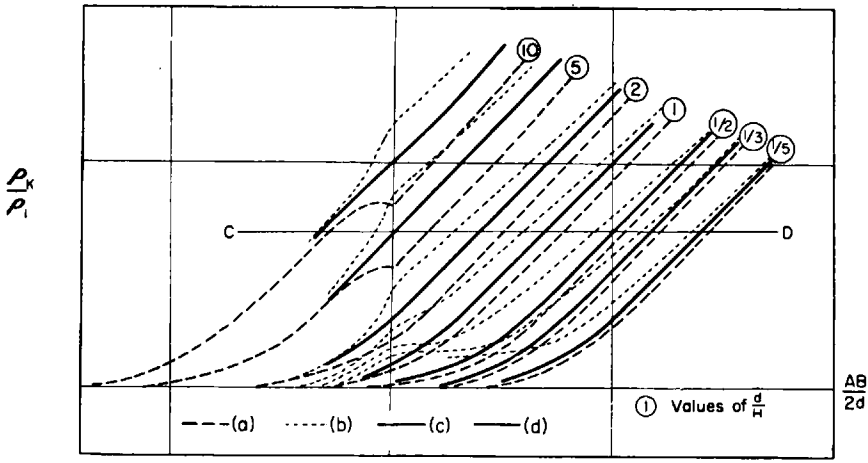

FIG 5. *a*—approximately constructed curves for $\varrho_2 < (\varrho_{1,k})_L$; *b*—approximately constructed curves for $\varrho_2 < (\varrho_{1,k})_L$; *c*—VEP curves for a horizontally homogeneous medium; *d*—line connecting the points on VEP curves for the maximum separations of AB used in practical work.

The deviation of $\varrho_{k\,\min}$ from $(\varrho_{1,k})_L$ of the minimum is insignificant for distances d being greater or smaller than the abscissa of the minimum.

The maximum deviation on the VEP curves in the cross-section under consideration is observed when $d = H$. The observed deviation can be largely utilized for qualitative evaluation of the depth at which a reflecting horizon is lying.

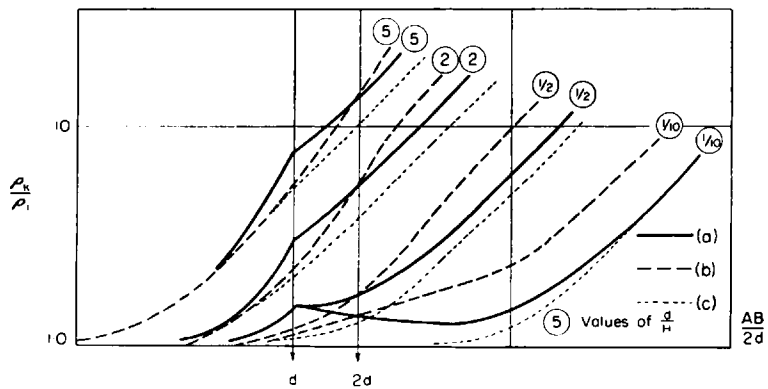

FIG 6. *a*—approximately constructed ⊥ VEP curves; *b*—approximately constructed ||VEP curves; *c*—VEP curves for a horizontally homogeneous medium.

When interpreting the distorted VEP by using parameters of the conducting horizon the deviation in the ordinate of the minimum and the value of S already noted may considerably influence the accuracy with which the depth at which the electrically reflecting horizon lies can be determined. In this case the influence of the vertical contact may lead to a fictitious rise in the reflecting horizon, the axis of the rise being situated at a distance d from the vertical contact.

Calculation of the influence of the contact is facilitated if cross VEP are made with spacings parallel and vertical to the contact. Such investigations give us two curves $\perp$ VEP and $\parallel$ VEP. The approximately constructed cross VEP curves for various values of $\frac{d}{H}$ are compared in Fig. 6.

This comparison yields the following diagnostic features for the curves when $\varrho_2 > \varrho_1$.

(1) The magnitude of S (determined from the VEP curve $\parallel$ for $d < 2H$) is approximately twice less than the analogous value obtained from the VEP curve $\perp$, and the value obtained from the latter is closer to the true value.

(2) The abscissa of the sharp maximum increase of ϱ_k on the $\perp$ VEP curve relative to ϱ_k on the $\parallel$ VEP curve is equal to d.

(3) Both curves intersect to the right of the line d. The abscissa of the point of intersection is approximately equal to $2d$.

Fig. 7 shows VEP curves obtained from a drill hole (Pribel'skaia zone, Alakaevskii sector) near the contact $\left(d = \frac{1}{5} H\right)$ where the angle of its dip exceeds 45°. VEP Nos. 67 and 324 were carried out with the spacings of AB respectively orientated parallel and perpendicular to the contact.

The approximately constructed $\perp$VEP and $\parallel$ VEP curves for case 1, $a\left(\text{when } \frac{d}{H} = \frac{1}{5}\right)$ are introduced in the lower part of Fig. 7. Comparison shows that the left-hand branches of these curves and the other curves are the same in type. A certain difference is to be observed in the form of the initial branches of the VEP curves and this is, no doubt, caused in the upper part by the complex geological cross section. The characteristic differences between $\perp$ and $\parallel$ VEP curves are revealed with sufficient clarity here, and this enables one to establish values of d and S (d = 23 m, $S = \Omega$m).

We shall now clarify the nature of the distortions brought about by the influence of the vertical contact when the cross VEP are arranged over

a medium with resistivity $(\varrho_{1,k})_L > \varrho_2$ (Fig. 1, *c* and *d*). A similar case may be encountered when working over an anticlinal fold, the core of which is composed of rocks of high resistivity while the overlaying strata of anticlinal crest and limbs are of reduced resistivity.

Use is also made in this case of approximately constructed curves and the error in construction for the case $\varrho_2 < (\varrho_{1,k})_L$ is preliminarily estimated by comparison of the approximated curve with an HVC reference graph.

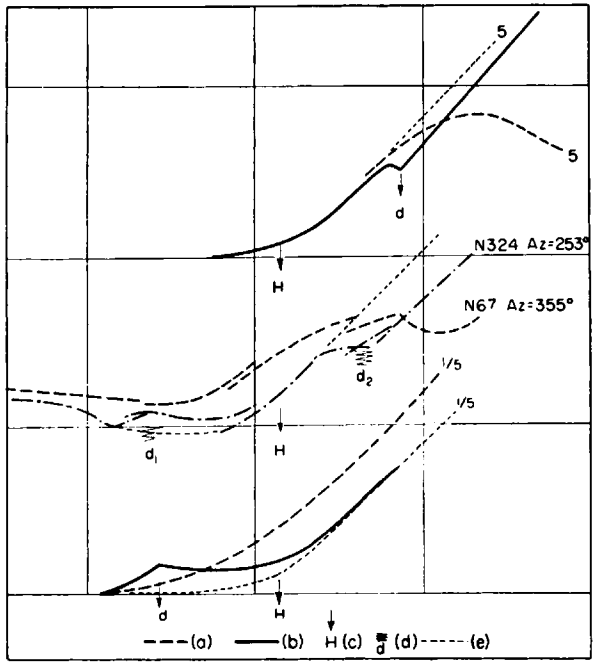

FIG. 7. *a*—approximately constructed || VEP curve; *b*—approximately constructed ⊥ VEP curve; *c*—H line; *d*—position of the non-horizontal contacts; *e*—VEP curve for a homogeneous horizontal medium.

Let us examine the special case of the HVC reference graph when $\varrho_1 = 99\varrho_2$ (Fig. 1, *d*). This case may be identified with the case which we adduce in Fig. 1, *c*, if one allows in the latter case that the thickness of the layer with a resistivity ϱ_1 at the VEP point is small in comparison with the dimensions of the arrangement.

A cross-section consisting of a two-layered medium disposed on both sides of the vertical contact is taken for the HVC reference graph (Fig. 1, *e*).

It is necessary, when constructing approximated curves, to determine the

ratio $\frac{(\varrho_2, k)_L}{(\varrho_1, k)_L}$, which we adopt for the case given in Fig. 1, *e* provided that the following assumptions are made

$$\frac{(\varrho_2, k)_L}{(\varrho_1, k)_L} = \frac{\varrho_2}{(\varrho_1, k)_L},$$

since for small spacings of the probes it is possible to treat the medium ϱ_2 as being of infinite thickness.

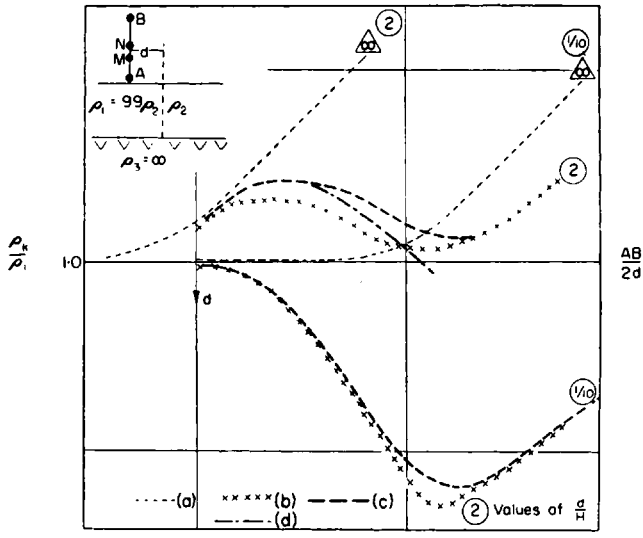

FIG. 8. *a*—VEP curves for a horizontally homogeneous medium; *b*—HVC comparison curves; *c*—approximately constructed curves for $\frac{\varrho_2}{\varrho_1} = 1/99$; *d*—approximately constructed curves for $\frac{\varrho_2}{\varrho_1} = \frac{\varrho_2}{(\varrho_1, k)_L}$

The equation

$$\frac{(\varrho_2, k)_L}{(\varrho_1, k)_L} = \frac{\varrho_2}{\varrho_1} = \frac{1}{99}$$

is adduced for the spacings which correspond to the asymptotic part of the curve.

Both variants of an approximately constructed curve for the case *d* (Fig. 1) for $\varrho_1 = 99\,\varrho_2$ $\left(\text{ratios } \frac{d}{H} = 2 \text{ and } \frac{d}{H} = \frac{1}{10}\right)$ and spacings of AB parallel to the contact are given in Fig. 8.

A curve constructed for the ratio $\frac{(\varrho_2, k)_L}{(\varrho_1, k)_L} = \frac{1}{99}$, coincides with the calculated curve in its initial and final parts. In the central portions the minimum of the constructed curve rises higher

We were unable to construct a curve for the ratio $\frac{(\varrho_2, k)_L}{(\varrho_1, k)_L} = \frac{\varrho_2}{(\varrho_1, k)_L}$ for sufficiently large spacings of AB, owing to the absence of curves with modulus $\frac{\varrho_2}{(\varrho_1, k)_L} < 0.01$ on the CV–2S reference graph.

In the part for which the construction was made, the least divergence from HVC curve was observed for $\frac{d}{H} = 2$, while for $\frac{d}{H} = \frac{1}{10}$ complete coincidence with the HVC curve was observed. If the distance of the separations of AB is increased the approximately constructed curve for the condition $\frac{(\varrho_2, k)_L}{(\varrho_1, k)_L} = \frac{\varrho_2}{(\varrho_1, k)_L}$ deviates considerably, as would be expected, from the HVC curve, since $(\varrho_2, k)_L \to \infty$, for $\frac{AB}{2} \to \infty$.

When the spacings of AB are orientated perpendicular to the plane of the contact the approximately constructed curve is observed to coincide completely with the calculated curves owing to the fact that the influence of the vertical contact diminishes as the spacings of AB increase.

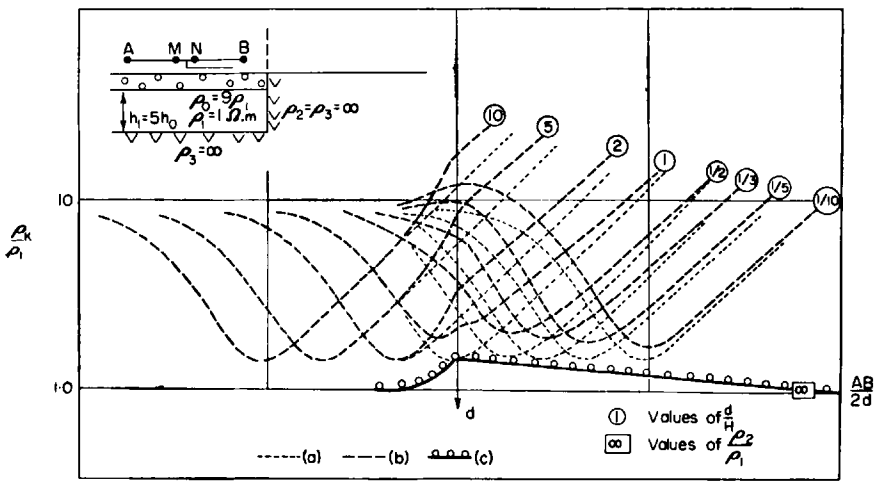

FIG. 9. *a*—VEP curves for a horizontally homogeneous medium; *b*—approximately constructed VEP curves; *c*—curves of the CV–3S reference graph.

Basing ourselves on the comparison of calculated and approximately constructed VEP curves for $\varrho_2 < (\varrho_{1,k})_L$ we can therefore consider that up to the limits of spacings AB used in practice the accuracy of the approximate construction of curves is also fully adequate to enable us to explain relative variations in the form of VEP graphs.

Curves for perpendicular orientation of the AB for spacings the cases c and d (Fig. 1) and various values of $\frac{d}{H}$ are given in Figs. 9 and 5. A satisfactory value of S may be obtained by analogy with the previous cases from the first asymptote of the VEP curves when $d > 2H$.

For $d \leqslant 2H$ up to $d = \frac{1}{2}H$, values of S obtained from the final branch of the curve will be increased in relation to their true value by anything from 15–30 %. For $d < {}^1/_2 H$ the values of S obtained will fall within the limits of accuracy of the observations.

Here, as in the case of a vertical contact for $(\varrho_{1,k})_L < \varrho_2$, the abscissa of maximum deviation of ϱ_k is equal to d. The position of the vertical contact may therefore be obtained and the depth at which the reference horizon lies be estimated by profiling the abscissae of the maximum deviation of

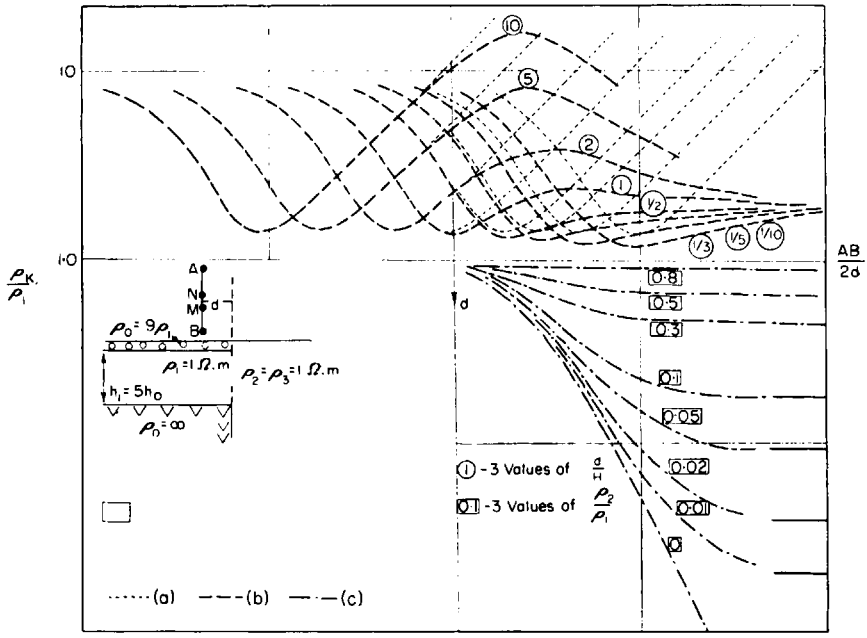

FIG. 10. *a*—VEP curves for a horizontal homogeneous medium; *b*—approximately constructed VEP curves; *c*—curves of the CV–2S reference graph.

ϱ_k from $(\varrho_{1,k})_L$ from the VEP points, since this sharp deviation of ϱ_k from $(\varrho_{1,k})_L$ should be lacking for curves in which $d < 2H$.

When the separations are orientated parallel to the plane of contact, the VEP curves for cases *c* and *d* on Fig. 1 are given for a double-layered cross-section in Fig. 11 and for a triple-layered cross-section $\left(\varrho_0 = 9\varrho_1\,;\ h_0 = \frac{1}{5}h_1\right)$ in Fig. 10. The VES curves are so distorted that a change in the type of curve is observed as the ratio $\frac{d}{H}$ decreases. The observed deformation in the curves is smooth and comes about as a result of variation in the electric cross-section in the direction of the contact.

A double-layered curve for $\varrho_2 = \infty$ and $d < \frac{H}{2}$ is transformed into a three-layered curve with $\varrho_3 < \varrho_2$, and for $d < \frac{1}{2}H$ into a two-layered curve with terminal restivity $\varrho_2 = 2\varrho_1$.

A three-layered curve of type *H* with $\varrho_3 = \infty$ for $d > \frac{1}{2}H$ is transformed into a four-layered curve with $\varrho_4 < \varrho_3$, and for $d < \frac{1}{2}H$ into a three-layered curve of type *H* but with terminal resistivity $\varrho_3 = 2\varrho_1$.

The nature of the deformations on VEP curves for $(\varrho_{1,k})_L > \varrho_2$ described above corresponds to the case when the medium ϱ_2 is homogeneous. In practice one has to deal with contacts with inhomogeneous media on both sides, and, in particular, with a two-layered medium.

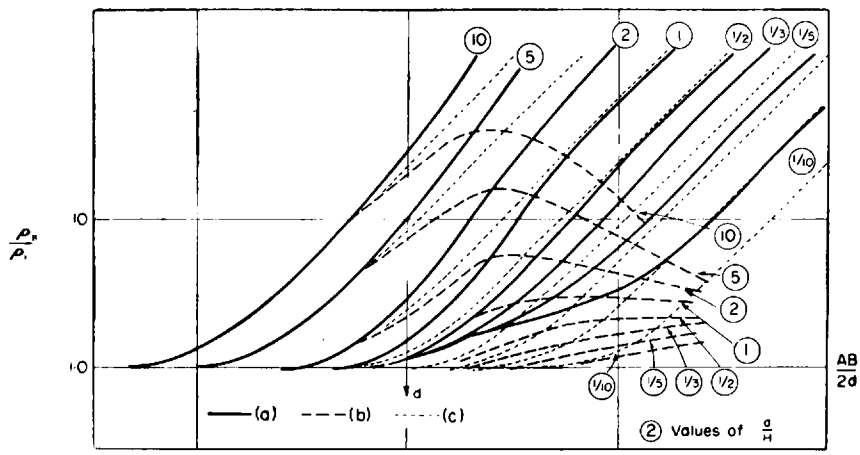

FIG. 11. *a*—approximately constructed curves for $\varrho_2 > (\varrho_{1,k})_L$; *b*—approximately constructed curves for $\varrho_2 < (\varrho_{1,k})_L$; *c*—VEP curves for a horizontally homogeneous medium.

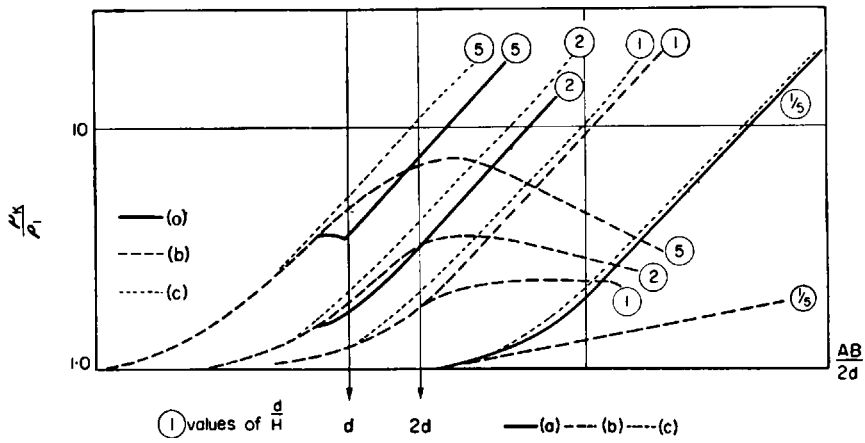

FIG. 12. *a*—approximately constructed ⊥ VEP curves; *b*—approximately constructed || VEP curves; *c*—VEP curves for a horizontally homogeneous medium.

In this case it is clearly possible to consider the medium as being homogeneous up to the spacings used in practice and to make the construction for the ratio $\frac{\varrho_2}{(\varrho_{1,k})_L}$.

Thus, the following characteristic changes are to be observed in cross VEP curves for the case $(\varrho_{1,k})_L > \varrho_2$, made near the vertical contact (Fig. 12):

(1) the absence of an asymptotic branch ascending at an angle of 45° in the || VEP curve:

(2) the abscissa of the maximum diminution of ϱ_k on the asymptotic branch of the ⊥ VEP curves is equal to d;

(3) The abscissa of the point of intersection of the ⊥ and || VEP curves (or of their convergence for small values of d) is approximately equal to 2 d.

Let us turn our attention to the observed deviations in the right-hand parts of the experimental VEP curves Nos 324 and 67 (Fig. 7), which are similar to the deviations obtained on approximately constructed curves for the case $(\varrho_{1,k})_L > \varrho_2$ $\left(\text{for } \frac{d}{H} = 5\right)$.

A somewhat different correlation between ϱ_k for experimental and approximately constructed VEP cross curves will evidently be produced by the influence of a preceded non-horizontal boundary with $\frac{\varrho_2}{(\varrho_{1,k})_L} > 1$.

A second non-horizontal surface of separation of the media with

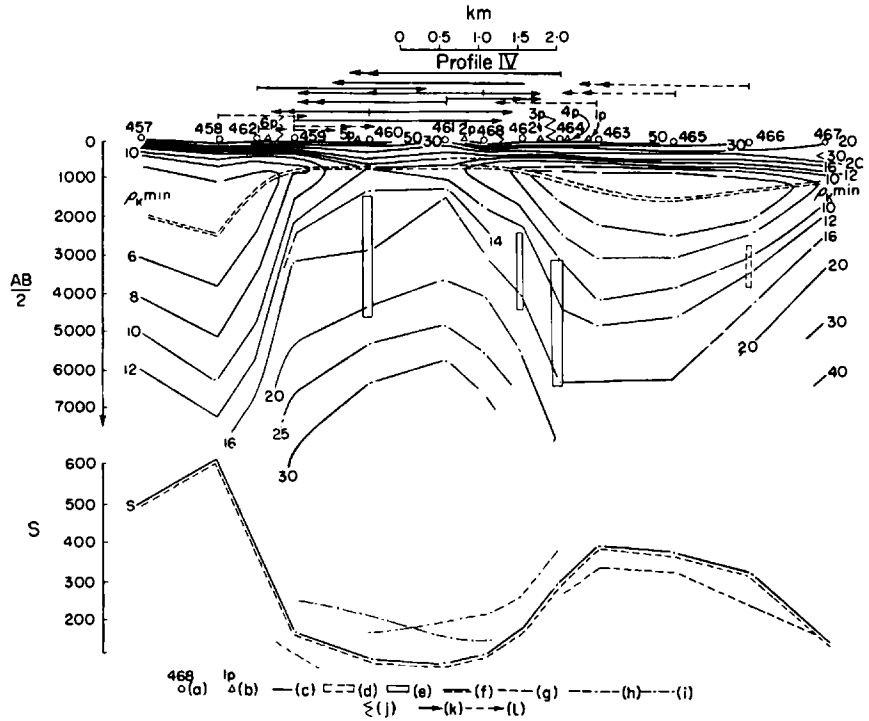

FIG. 13. *a*—VEP points; *b*—deep drilling holes; *c*—line of equal ϱ_k; *d*—areas of increase in ϱ_k; *e*—areas of decrease in ϱ_k; *f*—line of true values of S; *g*—line of reduced values of S; *h*—line of increased values of S due to the influence of the western non-horizontal boundary; *i*—line of increased values of S due to the influence of the eastern non-horizontal boundary; *j*—position of the non-horizontal boundaries; *k*—abscissae of the maximum decrease in ϱ_k; *l*—abscissae of the maximum increase in ϱ_k.

$(\varrho_{1,k})_L > \varrho_2$, at a distance approximately 400–500 m from the VEP point can be assumed on the basis of the diagnostic features of the cross VEP curve.

We can obtain an idea of the relative variations in the forms of VEP curves along the profile by comparing the approximately constructed curves for cases *a* and *c* with respect to *b* and *d* for various values of $\frac{d}{H}$ (Fig. 1.) and this enables us to determine the position of the non-horizontal contact and of the right-hand asymptotic branches of the VEP curves (cf. Fig. 5)*.

* It is here assumed that the thickness of the layer h_1 in the raised block (case *c* in Fig. 1) is sufficiently small by comparison with the thickness of this layer in the lowered block (case *a* in Fig. 1).

It is obvious from Fig. 5 that when the AB are spacings orientated perpendicular to the plane of contact on the VEP curve for all values of $\frac{d}{H}$, the true position of the right-hand asymptotic branch can be defined as the mean of the right-hand branches of VEP curves with equal $\frac{d}{H}$.

For values of $\frac{d}{H} \geqslant 2$, the true position of the right-hand asymptotic branch can be defined by the line running at an angle of 45° from the point of divergence of curves with equal $\frac{d}{H}$.

The position of the contact is fixed by the abscissae of the maximum deviations of ϱ_k in opposed directions.

When the separations of AB are orientated parallel to the plane of the contact for $\frac{d}{H} \geqslant 2$, the true position of the asymptotic branch running at an angle of 45° from the point of divergence of curves with equal $\frac{d}{H}$ is depicted on Fig. 11.

If all the characteristic variations in VEP curves along profiles mentioned above are used in the interpretation of VEP curves, one can indicate zones in which the horizontal homogeneity is disturbed and the corresponding tectonic dislocations and also establish the true position of the asymptotic branch of the VEP curve. An example of the interpretation of VEP curves in one of the regions is given in Fig. 13.

The VEP profile is disposed transversely to the direction of the anticlinal fold axis. As has been shown above, the position of the non-horizontal boundaries is determined by the analysis of the distortions in VEP curves.

Despite the fact that there are two non-horizontal boundaries in the given case, the total influence of which creates a much more complicated picture in the distortions on the VEP curves true values of S were determined by painstaking analysis of all the VEP curves along the profile and the depth at which the reflecting horizon lay was established. These results were subsequently confirmed by drilling (the drilling points are plotted on the profile).

The abscissae of the maximum deviations of ϱ_k from $(\varrho_{1,k})_L$ are indicated (by arrows) in the upper part of this profile.

In sectors where the abscissae of ϱ_k converge with deviations of different direction one can assume the presence of a non-horizontal contact. It is not difficult in this case to show that the smaller the area of convergence of

the abscissae the greater is the angle of inclination of the contact to the diurnal surface (when the strata overlaying the contact are of equal thickness).

In the given case the western limb of the anticline dips at a greater angle than the eastern. At the same time the latter obviously exhibits a step structure. The vertical cross-section of the resistivities constructed from the VEP curves gives a qualitative confirmation of the above hypothesis (Fig. 13). Here the region of increased values corresponds to the anticlinal upfold. On the western and eastern flanks of the anticline the character of the behaviour of the isolines varies. One might consider that the vertical electric cross-section gave a sufficiently good qualitative indication (by the transition from low to high resistivity) of the position of non-horizontally inclined strata and that there was no necessity for detailed analysis of the abscissae of the maximum deviations of ϱ_k from $(\varrho_{1,k})_L$.

Determination of the position of the inclined contact by means of the vertical cross-section is, however, not always sufficiently precise. In addition the value and direction of the anomalous variation in ϱ_k can be evaluated as a result of analysis of the abscissae of the maximum deviations of ϱ_k.

In practice the points of maximum deviation in ϱ_k, the abscissae of which are depicted above the profile, do not always correspond to a sufficiently clearly defined anomalous break in the isolines. In VEP No. 466 (Fig. 14), for example, an area of anomalous increase in ϱ_k is to be noted. Its abscissa is equal to 5 km, which corresponds to the distance from VEP No. 466 to the eastern non-horizontal contact (Fig. 13). There is, however, no anomalous behaviour of the ohm isolines to be observed in the vertical cross-section at VEP point 466 and the position of the right-hand asymptotic branch of VEP No. 466 can therefore be taken to be true. The position of the right-hand asymptotic branch of VEP curve No. 466 should also be determined from the analysis of the abscissae of the maximum deviations of ϱ_k, as is shown in Fig. 14.

At VEP point No. 460, situated at the peak of an anticline (Fig. 13), the anomalous lowering of ϱ_k is denoted by the course of the isolines for 16Ωm and above. This lowering can be treated as an alteration in the electric cross-section at the area of VEP No. 460 (inclusion of an additional conducting horizon). This lowering is, however, conditioned by the influence of the western and eastern non-horizontal boundaries (as may be seen from the disposition of the abscissae of the maximum deviations of ϱ_k over the profile).

The corrections indicated in Fig. 14 must be introduced into the VEP curve on this basis.

In VEP No. 464 (Fig. 14), the point of maximum decrease in ϱ_k is given

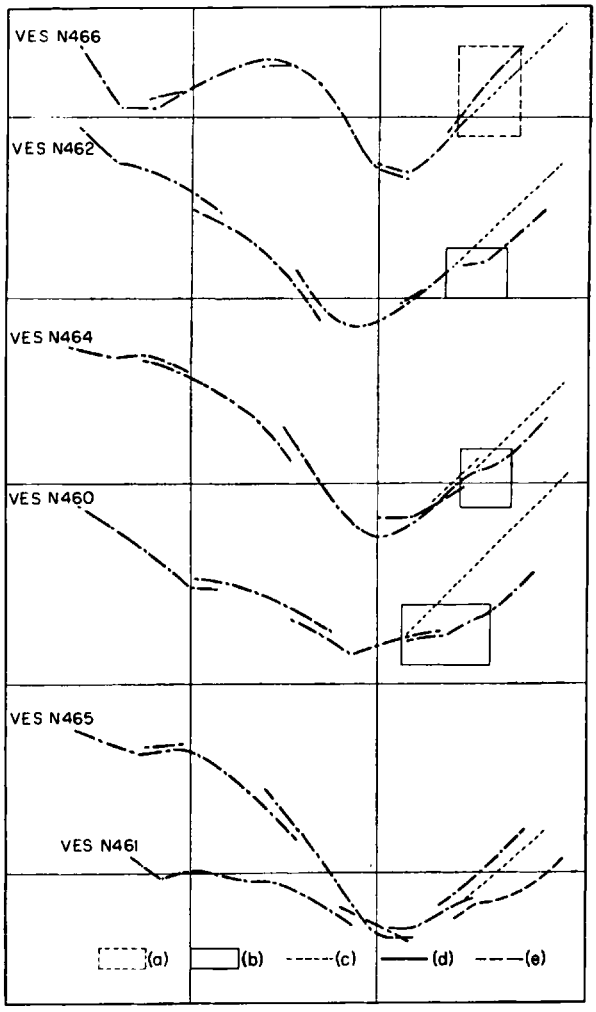

FIG. 14. *a*—section of the VEP curve with increased values of ϱ_k; *b*—section of the VEP curve with decreased values of ϱ_k; *c*—VEP curve for a horizontally homogeneous medium; *d*—VEP curve in a lowered block; *e*—VEP curve in a raised block.

by the abscissa equal to 5 km which is due to the influence of the western non-horizontal contact. At the same time, the degree of variation in the configuration of the 12 and 16Ωm isolines brought about by this lowering beneath VEP point No. 464 may be mistakenly ascribed to the result of the influence of the eastern non-horizontal contact as a result of which the right-hand branch of the VEP curve should be corrected in the direction of a decrease in ϱ_k. The analysis of the maximum deviations of ϱ_k of VEP

curves along the profile allows us to determine the true position of the asymptotic branch of VEP curve No. 464 as depicted in Fig. 14. The first asymptotic rise is, in all probability, due to the influence of the eastern contact which increases the value of ϱ_k The further lowering in the values of ϱ_k with increase in the separations of AB is due to the influence of the western contact.

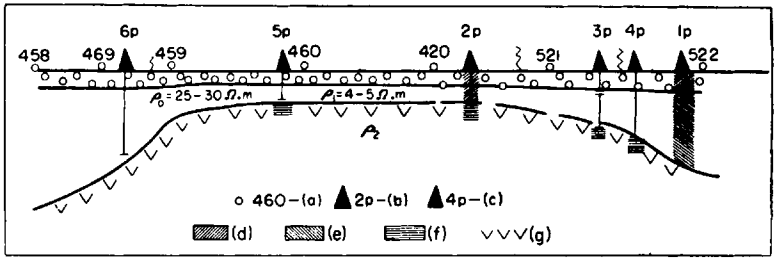

FIG. 15. *a*—VEP points; *b*—drill holes in existence at the moment when the materials were being studied; *c*—drillings made after the materials had been studied; *d*—Upper Cretaceous deposits C_{r2}; *e*—lower Cretaceous deposits C_{r1}; *f*—Paleozoic deposits P_z; *g*—top of the reflecting horizon of infinitely high resistivity from electro-prospecting data.

We obtain confirmation of this hypothesis by examining VEP point No. 462, which comes next on the profile, since the sharp increase in the ordinate of the minimum which is to be observed on the curve points to the siting of the point close to the edge of the eastern contact. The distance d for this VEP point is close to the depth H. On the other hand the abscissa of the maximum decrease in ϱ_k, which denotes the western contact, is decreased in passage between points 464 and 462 by comparison with point 464. Its right-hand asymptotic branch should be corrected in conformity with this, as is shown in Fig. 14.

The analysis of distortions in VEP curves thus carried out enables us to determine the position of the non-horizontal contact and the right-hand branch of the VEP curve with greater reliability and from this, the value of S. Possible values of S obtained from VEP curves are given in the lower portion of the drawing. The most reliable values established by the analysis of the distorted curves are joined by a continuous line.

Fig. 14 gives an example of the comparison of VEP curves sited on both sides of the contact for approximately equal values of $\frac{d}{H}$. This type of juxtaposition of the curves enables one to determine the true path of the asymptotic branch as a line running at an angle of 45° from the point of

divergence of the curves. The results obtained by interpretation were confirmed by drilling.

The method for analysing distortions in VEP curves which has been examined can also be applied to dipole quadrilateral probing (DQP)*, for which the characteristic distortions from non-horizontal boundaries will be more sharply reflected.

We shall examine distortions in DQP curves brought about by passage

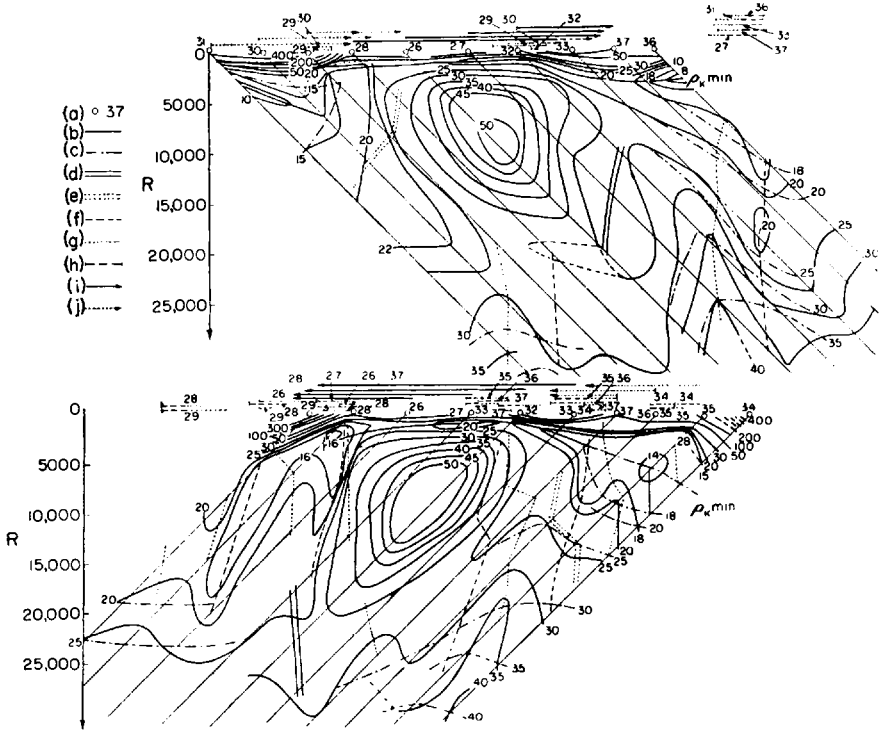

FIG. 16. *a*—VEP points; *b*—ohm isolines of ϱ_k; *c*—ohm isolines of ϱ_k compensated for the influence of surface distortions; *d*—lines of maximum decrease in ϱ_k from deep non-horizontal boundaries; *e*—lines of maximum increases in ϱ_k from deep non-horizontal boundaries; *f*—lines of minima of ϱ_k from surface non-horizontal boundaries; *g*—lines of the maxima of ϱ_k from surface non-horizontal boundaries; *h*—position of the dipole *MN* for maximum deviations of ϱ_k from $(\varrho_{1,h})_L$—influences of surface non-horizontal boundaries; *i*—abscissa of the maximum decrease in ϱ_k from the influence of deep non-horizontal boundaries; *j*—abscissa of the maximum increase in ϱ_k from the influence of deep non-horizontal boundaries.

* Literally dipole equatorial sonding or (DES) in Russian. [Editor's footnote].

of the dipole MN across the contact, the position of the dipole AB being considered as constant.

In analysing the distortions of DQP curves we make use of a vertical cross-section ϱ_k, which is constructed in the following manner; the abscissa of the values of ϱ_k taken from the plus and minus DQP curves are plotted on an arithmetical scale on lines orientated vertically from the centres of the corresponding MN dipoles.

When the same vertical and horizontal scales are used, the values of ϱ_k of DQP curves are distributed along lines at an angle of 45° to the line of the profile.

If we make separate use of the plus and minus branches of the DQP curves we obtain vertical cross-sections from which we can obtain a qualitative idea of the character of the variations in the values of ϱ_k along the profile in both the vertical and the horizontal directions.

If there is a non-horizontal boundary along the profile, we shall not observe a zone of increase or decrease in the values of ϱ_k [relative to $(\varrho_{1,k})_L$ of the horizontally layered medium] in constructing the vertical cross-section in this manner, at the site of the non-horizontal contact. In this case the line which connects maximum deviations of ϱ_k with the same sign will coincide approximately with the position of the surface of the non-horizontal boundary. Reciprocal signs of the deviations of ϱ_k will be observed at the site of the non-horizontal contact in vertical cross-sections constructed from the plus and minus branches of DQP curves.

Vertical cross-sections for the plus and minus branches of DQP curves are given in Fig. 16 for the region in which an electric prospecting party of the Spetsneftgeofizika Office (Penza province) carried out investigations.

A region of decrease in ϱ_k is to be seen quite clearly in the eastern part of the upper profile for the DQP branches. The characteristic DQP curve No. +27 given in Fig. 17 shows an area in which ϱ_k is decreased.

The abscissae of the maximum decreases in ϱ_k are plotted over the vertical cross-sections as in VEP studies*.

In that part of the profile which is being examined there are two further sections with anomalous deviations of ϱ_k, initially increasing and subsequently decreasing, and consequently giving rise to subsidiary maxima and minima. The lines which connect the abscissae of these points form vertical zones

* It is not always essential to depict the abscissae of the deviations of ϱ_k from $(\varrho_{1,k})_L$ when analysing distortions of DQP, since in the majority of cases the anomalous region of deviation on the cross-section manifests itself with sufficient clarity and is always sited in the immediate vicinity of the vertical contact owing to the principle upon which the profile is constructed.

within the limits of the measurement interval. The positions of the dipoles *MN* have been plotted in pairs over the profile for the maximum and minimum deviations of ϱ_k. DQP curves No. +32; +27; +30 are typical examples of distortions of this type. The sharp deviations in the magnitudes of ϱ_k which are obtained are (as is obvious from the vertical cross section given in Fig. 16) brought about by the non-horizontal boundaries in the uppermost part of the cross-section (they may possibly be revealed in the diurnal surface)*.

When the position of the surface non-horizontal boundaries has been established (from analysis of the DQP curves), these distortions can be removed from the DQP curves, as is shown in Figs. 16 and 17. Areas in which ϱ_k is increased on account of the buried contact can then be isolated.

An anomalous region of increase in ϱ_k (on the minus branches of the DQP) will correspond to an anomalous region of decrease in ϱ_k (on the plus branches of the DQP) in the vertical cross-section. Sections in which ϱ_k is increased are indicated on DQP curves No. −35; −36; −37 (Fig. 17).

An anomalous region of decrease in ϱ_k is also to be observed in the left-hand part of the profile from the minus branches of the DQP. This decrease is to be seen quite clearly in DQP curve No. −32 (Fig. 17) while on DQP curve No. −26 it is complicated by surface distortions. On the plus DQP given above the profile a region of increase in ϱ_k should correspond to this region of decrease in ϱ_k. A region of this type (left-hand side of the upper profile) cannot be isolated out from the ohm isoline configuration, as was possible in the previous case; it merges with a region of high values in ϱ_k which correspond to the high resistivity horizon of a layered medium in a raised block.

An anomalous increase in ϱ_k due to the influence of a western non-horizontal contact is, however, revealed with sufficient clarity on the DQP curves and may be isolated by joining the abscissae of the maximum deviation of ϱ_k in the DQP along the profile (Fig. 17, DQP curve No. +30).

There is no justification for ascribing the increases in ϱ_k in this instance to surface distortions, since deviations in ϱ_k on the side of decrease are possible from the nature of the behaviour of the ohm isolines in the upper part of the cross-section.

Having thus isolated distortions in the magnitudes of ϱ_k due to buried non-horizontal boundaries, it is possible to establish the position of the latter as the mean the lines of maxima and minima. In the DQP profile which we have examined, the position of the eastern non-horizontal boundary

* In what follows these distortions will be called surface distortions.

should lie between DQP points 37 and 33, and of the western between DQP points 29 and 28.

The configuration of the ohm isolines should be the same for the plus

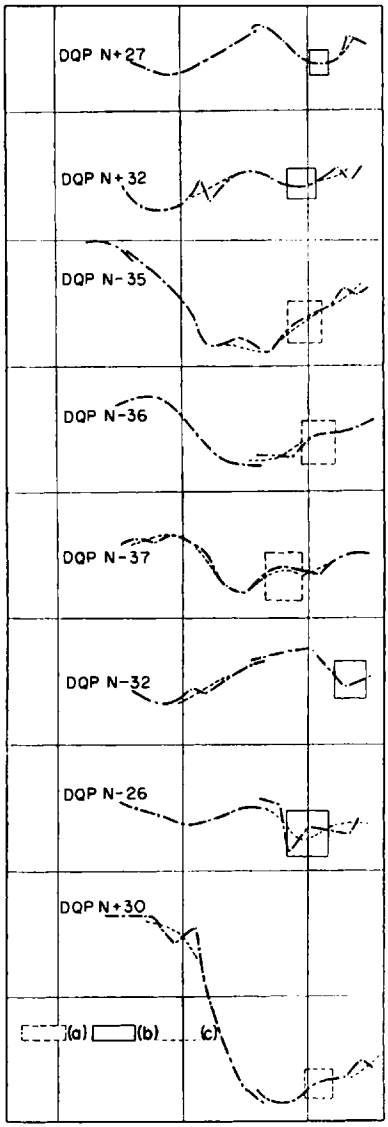

FIG. 17. *a*—area of a DQP curve with increased values of ϱ_k ; *b*—area of a DQP curve with decreased values of ϱ_k ; *c*—DQP curve corrected for the influence of surface non-horizontal boundaries.

and minus branches of the DQP in the absence of distortions from buried contacts. This is not to be observed on the profiles under consideration, owing to considerable distortions.

In calculating the influence of distortions from buried contacts we make use of the fact that the deviations ϱ_k from $(\varrho_{1,k})_L$ are of reciprocal sign for the plus and minus branches.

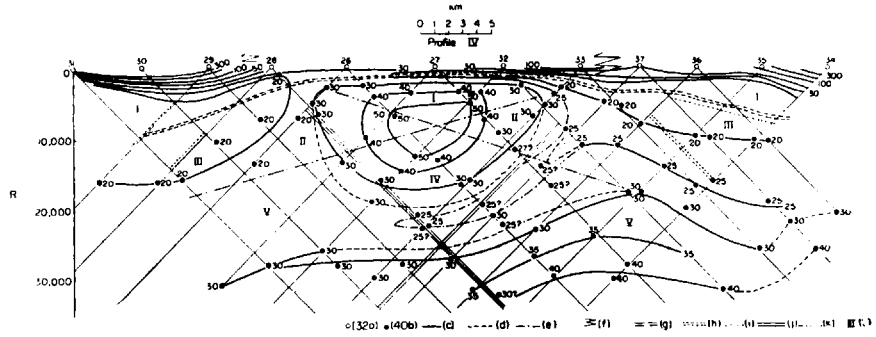

FIG. 18. *a*—DQP points; *b*—values of ϱ_k; *c*—lines of equal values of ϱ_k; *d*—lines of equal values of ϱ_k (variant); *e*—lines of equal values of ϱ_k, the configuration of which is conditioned by the influence of buried non-horizontal boundaries; *f*—the position of the buried non-horizontal boundaries; *g*—the line $\varrho_{k\,\min}$ of VEP curves of a horizontally homogeneous medium; *h*—lines of the maximum values of ϱ_k relative to $(\varrho_{1,k})_L$; *i*—lines of origin of the increase of $\varrho_{k\,\min}$ relative to $(\varrho_{1,k})_L$; *j*—lines of maxima in the increases of ϱ_k relative to $(\varrho_{1,k})_L$; *k*—line of origin of the decrease of ϱ_k relative to $(\varrho_{1,k})_L$; *l*—regions of distortions of ϱ_k.

We compile a single vertical cross-section of the plus and minus DQP branches for surface inhomogeneities of the strata. In this case the abscissae of the values of ϱ_k are laid off along the vertical lines from the central point between the dipoles *AB* and *MN*.

If the vertical cross-section is constructed in this way, the anomalous values of ϱ_k $\left(\text{beginning with values of } R \text{ close to } \frac{d}{2}\right)$ will be found in a zone in which the line of the maximum deviations of ϱ_k from $(\varrho_{1,k})_L$ is inclined to the line of the profile at an angle the tangent of which equals the ratio between the vertical and horizontal scales, while the line of origin of the deviation of ϱ_k lies along the bisectrix of this angle. The values of ϱ_k from the various DQP branches will fail in varying degrees to coincide in this region (Fig. 18). The line of origin of the distortions of ϱ_k divides the vertical cross-section into 5 regions in relation to the degree and direction of the deviation of ϱ_k, as follows:

I—Distortions of ϱ_k are lacking for any directions of the DQP branches.

II—For one direction of the DQP branches a deviation of ϱ_k on the side of increase is observed; values of ϱ_k on the opposite branches of the DQP are not distorted.

III—For one direction of the DQP branches a deviation of ϱ_k on the side of increase is observed; values of ϱ_k on the opposite branches of the DQP are not distorted:

IV—A deviation of ϱ_k on the side of decrease is observed for any directions of the DQP branches; deviations from the opposite DQP branches are equal in the central part of the region:

V—A deviation of ϱ_k on the side of decrease is observed for one direction of the DQP branches and on the side of increase for the other direction (in the central part of the region the deviations are of equal magnitude but of opposed sign). In addition, there is a very slight decrease in ϱ_k in this region due to the other non-horizontal contact which can clearly be ignored.

If we take a graphic mean of ϱ_k and allow for the possible level of its deviation from $(\varrho_{1,k})_L$, we obtain the behaviour of the isolines in the lower part of the cross-section which describes the relative variation in the value of ϱ_k along the profile. It is not possible to obtain more or less reliable values of ϱ_k in region IVowing to the fact that the directions of the deviations of ϱ_k here coincide on the opposite DQP branches because of the presence of two non-horizontal contacts. The isolines of ϱ_k are therefore given as a dashed line (two variants) in region IV.

These variants do not, however, significantly alter our general view of the qualitative features of the change in the electric cross-section along the line of the profile.

The method for calculating distortions in DQP therefore enables us to establish the position of the buried contacts and to obtain values for the total conductivity which are closer to the true values from the distorted curves and thus to improve the quantitative interpretation of DQP curves.

REFERENCES

1. V. N. Dakhnov, *Electric Prospecting for Oil and Gas Deposits.* Gostoptekhizdat (1953).
2. "*Elkageer,*" 1/2, *1938.* Articles on materials from the firm SPE. CV-1S, CV-2S and CV-3S reference graphs. GSGT, 1938.
3. E. N. Kalenov, The C-1-S reference graph. "*Elkageer,*" 3/4, GSGT, 1938.
4. A. M. Pylaev, *A Guide to the Interpretation of VEP.* Gosgeolizdat (1948).

CHAPTER 12

SOME PROBLEMS OF GAS LOGGING ESTIMATION OF GAS SATURATION OF ROCKS

L. A. GALKIN

THE object of gas logging is the detection of productive beds in the section of a well. However, the currently used methods of gas logging do not permit reliable evaluation of a bed. This is associated with the fact that, as a result of gas logging, one determines the content of hydrocarbon gases in a gas–air mixture, obtained by degasifying the drilling fluid. This content largely depends on the method of degasification and the properties of the drilling fluid being degasified. Thus, the degree of extraction of hydrocarbon gases from the drilling fluid will oscillate within wide limits, depending on the viscosity, static shear stress, temperature and salinity of the fluid. Therefore a direct relationship is not always observed between the gas measurements on the gas log and the concentration of hydrocarbon gases in the fluid. In its turn, the gas saturation of the drilling fluid depends not only on the gas content of the bed but also on many other factors, the main ones being rate of boring, rate of circulation of the drilling fluid and the nature of the bed.

It is quite clear that exact evaluation of the bed from the gas log data can be given only when the above factors are taken into consideration.

In order to establish the relationship between the readings obtained in gas logging and the actual gas saturation* of the drilling fluid, we analysed the results of gas logging conducted in various regions, by the simultaneous application of a floating degasifier and a TVD degasifier, whose degree of degasification is about 100 per cent. It was established that in most cases a direct correspondence is observed between the actual gas saturation of the drilling fluid in cm^3/l. (data of TVD instrument) and the readings of a station, the reading being obtained in working with a floating degasifier. However, in some cases this regularity is not maintained, and quite different readings are obtained for the same gas saturation, the readings being lower

* By actual gas saturation we understand the amount of gas (in cm^3) contained in 1l. of drilling fluid.

at low temperature for slightly saline fluids than for less viscous and more saline fluids, and for high temperature fluids.

It is obvious that, in order to allow for the degree of degasification of the degasifier used, and to exclude the effect of drilling fluid properties on the results of the gas logging, it is essential to perform a calibration—a determination by experimental means of the dependence of gas readings on the gas content of the drilling fluid. Such a calibration should be carried out before each operation and on every occasion in case of changes in the properties of the drilling fluid.

In calibration, a sample of drilling fluid is taken, it is degasified by means of a TVD instrument, and its content of hydrocarbon gases is determined. Then the gas saturation of the drilling fluid in $cm^3/l.$ is determined from the formula

$$F = 10K\frac{C}{Q}, \tag{1}$$

where K is amount of gas–air mixture in the gas container of the TVD degasifier in cm^3; C is the concentration of combustible gases in the gas–air mixture in per cent; Q is volume of the degasified solution in cm^3.

At the same time as the sample is taken, the readings of the gas analyser of the station are noted.

The results of the calibration are plotted on a graph with percentage gas indications as abscissae and the gas saturation F, obtained by the method described above, as ordinate (both after allowance has been made for background values). By drawing a straight line through the origin of coordinates and the point obtained on the graph, we obtain the calibration curve. By making use of this curve it is possible to arrive from the gas indications in per cent, obtained in the gas logging (after allowance for background values), at the actual gas saturation of the solution.

In practice it is recommended to choose a calibration curve from those drawn on Fig. 1 according to the results of comparison of gas readings with data on the actual gas saturation of the drilling fluid, obtained by the method described above.

Using data on the actual gas saturation of the fluid one can make a qualitative estimation of the gas contained in a bed, which is marked on the gas log by high gas readings. The gas content of a bed can be expressed by the gas factor—the content of gas in 1 m^3 per volume of porous space in 1 m^3.

The mechanism whereby hydrocarbon gases enter the drilling fluid has hitherto not been studied. Various points of view are held on this problem. Most investigators consider that gas and oil are transferred to the drilling fluid principally from the pores of rock which has been drilled through;

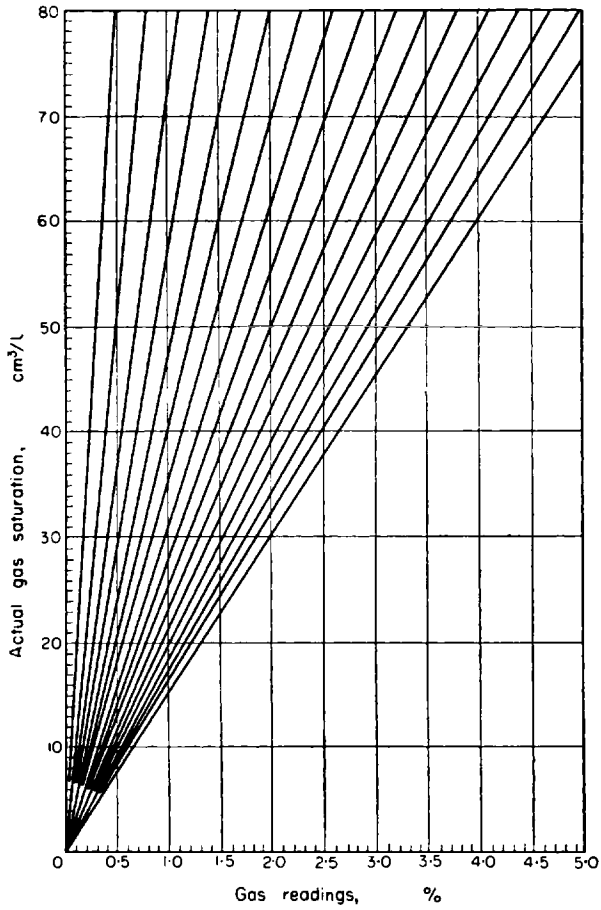

FIG. 1. Calibration curves for determination of gas saturation of the drilling fluid from readings obtained in gas logging with a floating degasifier.

the amount of gas entering the drilling fluid as a result of diffusion through the walls of the well is very small and has no practical significance and in most cases infiltration does not occur since the pressure in the bed is below that of the column of drilling fluid.

In contradiction to this, E. M. GELLER considers that gas enrichment of the drilling fluid is largely caused by infiltration of oil or gas from the bed, arising as a result of a reduction of pressure in the well during rotation of the drill bit*. According to GELLER, a favourable condition for this

* E. M. GELLER. On the conditions of passage of gas and oil into clay solution of wells during drilling. Sb. "Geokhimicheskie metody poiskov nefti i gaza" *Geochemical methods of prospecting for oil and gas* 2nd ed. Gostoptekhizdat, 1954.

is a high rate of circulation of the drilling fluid at rates of boring not exceeding 5 m/hr. However, this point of view is incorrect; this follows if only from the fact that in regions of the Ural-Volga province productive beds of the Naryshevskian Beds and sediments of the Upper Givetian substage, despite the occurrence of the favourable conditions indicated above, are quite often not shown up by gas sampling. Neither is confirmation obtained for the possibility of creating the pressure difference—necessary for filtration—between the bed and the bore-hole during rotation of the bit.

Assuming that gas and oil enter the drilling fluid from the rock that has been drilled out, the following formula can be written for the gas factor a:

$$a = \frac{FQ_n t}{V_n m} = \frac{FQ}{V_n m} \tag{2}$$

where: m is the coefficient of porosity;
Q_n is the pump capacity;
V_n is the volume of rock drilled out in the time t;
Q is the consumption of drilling fluid in the time t.

This formula can be used to determine the gas factor.

In calculating the gas factor it is convenient to use Table 1, which has been constructed from formula (2) for the most probable values of effective porosity ($m = 0.2$) and well diameter ($11\frac{3}{4}$ in.).

In order to find the gas factor, using Table 1, for a selected portion of the gas log showing high gas readings, the consumption Q of drilling fluid corresponding to the drilling time for an interval of 0.5 m is determined; against the value found for Q and the actual gas saturation of the drilling fluid, found as described above, the gas factor is obtained from the top line*.

If the consumption of drilling fluid is known for a penetration of 0.25 or 1 m, then the same course is followed as in the previous case, but the result obtained is respectively multiplied or divided by two.

If the bit diameter is different from $11\frac{3}{4}$ in. (the diameter for which the table is calculated) then we obtain the gas factor by multiplying the value obtained from the table by a coefficient K, which has the following value+.

Drilling bit	$7^3/_4$ in.	$9^3/_4$ in.	$10^3/_4$ in.	$13^3/_4$ in.
K	0.46	0.72	0.84	1.44

* In calculations the coefficient of oil and gas saturation is taken as unity, and therefore the gas factor obtained must be multiplied by the coefficient of oil saturation.

+ The correction factor for a core drill is not derived: it is the same as for an ordinary drill.

If the actual value of the gas saturation exceeds those given in Table 1, then it must be reduced by a factor of five or ten and the result obtained must be increased by the same factor.

Example—The consumption Q of drilling fluid during the time taken to penetrate 0.5 m through the bed is 40,800 l.; the gas saturation of the drilling fluid is 21 $cm^3/l.$; the porosity of the bed is 20 per cent; the diameter of the drill bit is $11\frac{3}{4}$ in. It is required to find the gas factor for the bed.

Because a gas saturation of 21 $cm^3/l.$ does not appear in Table 1, we reduce it ten times; for a gas saturation of 2.1 $cm^3/l.$ and the nearest value of Q to the actual consumption of 40,800 l. the gas factor will be between 10 and 15 (more precisely 12.4); thus the gas factor of the bed will be 124 m^3/m^3.

Table 1 is calculated for a bed porosity of 20 per cent. If the porosity of the bed has some other value, the gas factor is calculated from the formula

$$a_1 - \frac{ma}{20}$$

where: a is the gas factor obtained from the tables;

a_1 is the required gas factor;

m is the porosity (per cent) of the rocks for the given bed.

Conclusions as to the nature of the bed are reached by comparison of the gas factor obtained with values of the gas factor for known beds of the given and neighbouring localities.

Usually gas factors below 3 m^3/m^3 correspond to waterbearing strata, containing dissolved hydrocarbon gases; beds with residual gas and oil saturation have gas factors roughly three to four times less than productive beds. The gas factor for gas-bearing beds is numerically equal to the bed pressure.

In practice it is not rare to find cases where waterbearing beds with residual gas and oil saturation have the same gas factor as productive strata. In order to avoid errors in such cases, it is necessary to know the composition of the gas or the quality of the bitumen.

On the basis of the foregoing it can be concluded that interpretation using the calibration curves and Table 1 permits the effect of physicochemical properties of the drilling fluid, and also the effect of drilling conditions on the results of gas logging to be excluded; it also allows a more correct result for the gas saturation of the rocks which are being drilled.

GAS ENRICHMENT AND DEGASIFICATION OF THE DRILLING FLUID

The gas saturation of the drilling fluid during boring of a productive bed depends very much on the rate of boring. Table 2 shows rates of boring

TABLE 1. VALUE OF GAS SATURATION F (cm^3/l) OF DRILLING FLUID FOR VARIOUS VARIOUS GAS FACTORS (m^3/m^3). $11^3/_4$

Q	Gas factor											
	1	2	3	4	5	10	15	20	25	30	35	40
200000	0.1	0.1	0.1	0.1	0.2	0.3	0.5	0.7	0.9	1.0	1.2	1.4
140000	0.1	0.1	0.1	0.2	0.2	0.5	0.7	0.9	1.2	1.5	1.8	1.9
100000	0.1	0.1	0.2	0.3	0.3	0.7	1.0	1.4	1.7	2.0	2.4	2.8
72000	0.1	0.1	0.3	0.4	0.4	0.9	1.5	1.9	2.4	2.9	3.4	3.9
69600	0.1	0.2	0.3	0.4	0.5	1.0	1.5	2.0	2.5	3.0	3.5	4.0
67200	0.1	0.2	0.3	0.4	0.5	1.0	1.6	2.0	2.6	3.1	3.6	4.2
64800	0.1	0.2	0.3	0.4	0.5	1.0	1.6	2.1	2.7	3.2	3.7	4.3
62400	0.1	0.2	0.3	0.4	0.6	1.1	1.7	2.2	2.8	3.4	3.9	4.5
60000	0.1	0.2	0.4	0.5	0.6	1.2	1.8	2.3	2.9	3.5	4,2	4.7
57800	0.1	0.2	0.4	0.5	0.6	1.2	1.8	2.4	3.0	3.6	4.2	4.8
55200	0.1	0.3	0.4	0.5	0.6	1.3	1.9	2.5	3.2	3.8	4.4	5.1
52800	0.1	0.3	0.4	0.5	0.7	1.3	1.9	2.6	3.3	3.9	4.6	5,3
50400	0.1	0.3	0.4	0.5	0.7	1.4	2.1	2.8	3,5	4.1	4.8	5.5
48000	0.1	0.3	0.4	0.6	0.7	1.5	2.2	2.9	3.6	4.4	5.0	5.8
45600	0.2	0.3	0.5	0.6	0.8	1.5	2.3	3.1	3,8	4.6	5.3	6.1
43200	0.2	0.3	0.5	0.6	0.8	1.6	2.4	3.2	4.1	4.9	5.7	6.5
40800	0.2	0.3	0.5	0.7	0.9	1.7	2.6	3.4	4.3	5.1	5.9	6.8
38400	0.2	0.4	0.5	0.7	0.9	1.8	2.7	3.6	4.5	5.4	6.3	7.2
36000	0.2	0.4	0.6	0.8	0.9	1.9	2.9	3.9	4.9	5.8	6.8	7.8
33600	0.2	0.4	0.6	0.8	1.0	2.1	3.1	4.2	5.2	6.2	7.3	8.3
31200	0.2	0.4	0.7	0.9	1.1	2.2	3.4	4.5	5.6	6.7	7.8	8.9
28800	0.2	0.5	0.7	0.9	1.2	2.4	3.6	4.8	6.1	7,3	8.5	9.7
26400	0.3	0.5	0.8	1.1	1.3	2.6	3.9	5.3	6.6	7.9	9.2	10.6
24000	0.3	0.6	0.9	1.2	1.5	2.9	4.4	5.8	7.3	8.7	10.2	11.6
21600	0.3	0.6	0.9	1.3	1.6	3.2	4.8	6.5	8.1	9.7	11.3	12.9
20000	0.3	0.7	1.0	1.4	1.7	3.5	5.2	6.9	8.7	10.5	12.2	13.9
19200	0.4	0.7	1.1	1.5	1.8	3.6	5.5	7.3	9.1	10.9	12.7	14.6
18800	0.4	0.7	1.1	1.5	1.9	3.7	5.6	7.4	9.3	11.1	13.0	14.9
18400	0.4	0.8	1.1	1.5	1.9	3.8	5.7	7.6	9.5	11.4	13.3	15.2
18000	0.4	0.8	1.2	1.6	1.9	3.9	5.8	7.8	9.7	11.6	13.6	15.5
17600	0.4	0.8	1.2	1.6	1.9	3.9	5.9	7.8	9.9	11.8	13.9	16.0
17200	0.4	0.8	1.2	1.6	2.0	4.1	6.1	8.1	10.2	12.2	14.2	16.2
16800	0.4	0.8	1.2	1.7	2.1	4.2	6.2	8.3	10.4	12.5	14.6	16.6
16400	0.4	0.9	1.3	1.7	2.1	4.3	6.4	8.5	10.6	12.8	14.9	17.0
16000	0.4	0.9	1.3	1.7	2.2	4.4	6.5	8.7	10.9	13.1	15.3	17.5

CONSUMPTIONS Q (l) OF DRILLING FLUID DURING 0.5 m PENETRATION AND FOR IN. BIT, 20% EFFECTIVE POROSITY

Gas factor											
45	50	55	60	65	70	75	80	85	90	95	100
1.6	1.7	1.9	2.1	2.3	2.5	2.6	2.8	2.9	3.1	3.3	3.5
2.2	2.5	2.7	2.9	3.2	3.5	3.7	3.9	4.2	4.5	4.7	4.9
3.1	3.5	3.8	4.2	4.5	4.9	5.2	5.6	5.9	6.3	6.6	6.9
4.3	4.8	5.3	5.8	6.2	6.7	7.3	7.8	8.2	8.6	9.1	9.7
4.5	5.0	5.5	6.0	6.5	7.0	7.5	8.3	8.5	9.0	9.5	10.0
4.7	5.2	5.7	6.2	6.8	7.3	7.8	8.3	8.8	9.4	9.9	10.4
4.8	5.3	5.8	6.7	6.9	7.4	7.9	8.6	9.0	9.5	10.1	10.7
5.0	5.6	6.2	6.7	7.3	7.8	8.4	8.9	9.5	10.1	10.6	11.2
5.2	5.8	6.4	7.0	7.5	8.3	8.7	9.4	9.9	10.4	11.0	11.7
5.4	6.0	6.6	7.3	7.8	8.4	9.0	9.7	10.2	10.8	11.4	12.1
5.7	6.3	6.9	7.6	8.2	8.8	9.5	10.2	10.7	11.3	11.9	12.7
5.9	6.6	7.3	7.9	8.6	9.2	9.9	10.6	11.2	11.9	12.5	13.2
6.2	6.9	7.6	8.5	8.9	9.7	10.4	11.0	11.7	12.4	13.1	13.8
6.5	7.2	7.9	8.7	9.4	10.1	10.8	11.6	12.2	12.9	13.7	14.5
6.8	7.6	8.4	9.2	9.9	10.6	11.4	12.2	12.9	13.7	14.4	15.3
7.3	8.1	8.9	9.7	10.5	11.3	12.2	12.9	13.8	14.6	15.4	16.2
7.7	8.5	9.4	10.3	11.1	11.9	12.8	13.7	14.5	15.3	16.2	17.1
8.1	9.6	9.9	10.9	11.7	12.6	13.5	14.5	15.3	16.2	17.1	18.1
8.7	9.7	10.7	11.6	12.6	13.6	14.6	15.5	16.5	17.5	18.4	19.4
9.4	10.4	11.4	12.5	13.5	14.6	15.6	16.6	17.7	18.7	19.8	20.8
10.1	11.2	12.3	13.4	14.6	15.7	16.8	17.9	19.0	20.2	21.3	22.4
10.9	12.1	13.3	14.5	15.7	16.9	18.2	19.4	20.6	21.8	22.9	24.2
11.9	13.2	14.5	15.8	17.2	18.5	19.8	21.1	22.4	23.8	25.1	26.4
13.1	14.5	15.9	17.5	18.1	20.3	21.8	23.3	24.7	26.1	27.6	29.1
14.5	16.1	17.7	19.4	20.9	22.5	24.2	25.8	27.4	28.9	30.6	32.3
16.0	17.5	19.1	20.9	22.6	24.5	25.2	27.9	29.6	31.4	33.1	34.9
16.4	18.2	19.9	21.8	23.5	25.5	27.2	29.1	30.8	32.8	34.4	36.4
16.7	18.6	20.4	22.2	24.1	26.0	27.8	29.7	31.5	33.4	35.2	37.1
17.1	18.9	20.8	22.7	24.6	26.3	28.5	30.3	32.1	34.1	35.9	37.9
17.5	19.4	21.3	23.3	25.2	27.2	29.1	31.0	32.9	34.9	36.9	38.8
17.9	19.8	21.8	23.5	25.7	27.9	29.8	31.4	33.7	35.3	37.6	39.2
18.3	20.3	22.3	24.4	26.4	28.4	30.8	32.5	34.5	36.5	38.6	40.6
18.7	20.8	22.8	24.9	26.9	29.1	31.2	33.3	35.2	37.4	38.9	41.6
19.2	21.3	23.3	25.6	27.6	29.8	31.9	34.1	36.0	38.3	40.3	42.6
19.6	21.8	23.9	26.2	28.3	30.5	32.7	34.9	37.1	39.2	41.4	43.6

Table 1 *(continued)*

Q	Gas factor											
	1	2	3	4	5	10	15	20	25	30	35	40
15600	0.4	0.9	1.3	1.7	2.2	4.5	6.7	8.9	11.1	13.4	15.5	17.9
15200	0.5	0.9	1.4	1.8	2.3	4.6	6.9	9.2	11.5	13.8	16.0	18.4
14800	0.5	0.9	1.4	1.9	2.4	4.7	7.1	9.4	11.8	14.2	16.5	18.9
14400	0.5	0.9	1.5	1.9	2.4	4.9	7.3	9.7	12.1	14.6	16.9	19.4
14000	0.5	0.9	1.5	1.5	2.5	4.9	7.5	9.9	12.5	14.9	17.5	19.9
13600	0.5	1.0	1.5	2.1	2.6	5.1	7.7	10.3	12.9	15.4	18.1	20.5
13200	0.5	1.1	1.6	2.1	2.6	5.3	7.9	10.6	13.2	15.9	18.5	21.2
12800	0.5	1.1	1.6	2.2	2.7	5.5	8.2	10.9	13.6	16.4	19.1	21.8
12400	0.6	1.1	1.7	2.3	2.8	5.6	8.4	11.3	14.1	16.9	19.7	22.5
12000	0.6	1.2	1.7	2.3	2.9	5.8	8.7	11.6	14.6	17.5	20.4	23.3
11600	0.6	1.2	1.8	2.4	3.0	6.0	9.0	12.0	15.1	18.1	21.7	24.1
11200	0.6	1.2	1.9	2.5	3.1	6.2	9.4	12.5	15.6	18.7	21.8	24.9
10800	0.6	1.3	1.9	2.6	3.2	6.5	9.7	12.9	16.2	19.4	22.6	25.8
10400	0.7	1.3	2.0	2.7	3.4	6.7	10.1	13.4	16.8	20.2	23.5	26.9
10000	0.7	1.4	2.1	2.8	3.5	6.9	10.5	13.9	17.5	20.9	24.4	27.9
9600	0.7	1.5	2.2	2.9	3.6	7.3	10.9	14.6	18.2	21.8	25.5	29.1
9200	0.8	1.5	2.3	3.0	3.8	7.6	11.4	15.2	18.9	22.8	26.6	30.4
8800	0.8	1.6	2.4	3.2	3.9	7.9	11.9	15.9	19.8	23.8	27.8	31.7
8400	0.8	1.7	2.5	3.3	4.2	8.3	12.5	16.6	20.8	24.9	29.1	33.3
8000	0.9	1.7	2.6	3.5	4.4	8.7	13.1	17.4	21.8	26.2	30.6	34.9
7600	0.9	1.8	2.8	3.7	4.6	9.2	13.8	18.4	22.9	27.6	32.1	36.8
7200	0.9	1.9	2.9	3.9	4.9	9.7	14.6	19.4	24.3	29.1	34.0	38.8
6800	1.0	2.1	3.1	4.2	5.1	10.3	15.4	20.6	25.7	30.8	35.9	41.1
6400	1.1	2.2	3.3	4.4	5.5	10.9	16.4	21.8	27.3	32.8	38.2	43.6
6000	1.2	2.3	3.5	4.7	5.8	11.6	17.5	23.3	29.1	34.9	40.7	46.6
5600	1.2	2.5	3.7	4.9	6.2	12.5	18.7	24.9	31.2	37.4	43.7	49.9
5200	1.3	2.7	4.0	5.4	6.7	13.4	20.2	26.9	33.6	40.3	46.9	53.7
4800	1.5	2.9	4.4	5.8	7.3	14.6	21.8	29.2	36.4	43.7	50.9	58.2
4400	1.6	3.2	4.8	6.3	7.9	15.9	23.8	31.8	39.6	47.6	55.4	63.4
4000	1.7	3.5	5.2	6.9	8.7	17.5	26.2	34.9	43.7	52.4	61.1	69.8
3600	1.9	3.9	5.8	7.8	9.6	19.4	29.1	38.8	47.9	58.2	67.1	77.6
3200	2.2	4.4	6.6	8.7	10.9	21.9	32.8	43.7	54.6	65.5	76.4	87.3
2800	2.5	4.9	7.5	9.9	12.5	24.9	37.4	49.9	62.4	74.9	87.3	99.9
2400	2.9	5.8	8.7	11.7	14.6	29.1	43.7	58.2	72.8	87.3	101.9	116,6
2000	3.5	6.9	10.5	13.9	17.5	34.9	52.4	69.9	97.3	104.8	122.2	139.7
1600	4.4	8,7	13.1	17.5	21.8	43.7	65.5	87.4	109.1	131.0	152.7	174.6
1200	5.8	11.6	17.5	23.3	29.1	58.2	87.4	116.5	145.5	174.7	203.7	232.8
800	8.7	17.5	26.2	34.9	43.7	87.4	131.0	174.7	218.3	262.1	305.2	349.2
400	17.5	34.9	52.4	69.8	87.3	174.7	262.1	349.4	436.5	524.2	581.1	698.4

Gas factor

45	50	55	60	65	70	75	80	85	90	95	100
20.2	22.1	24.3	26.9	28.7	30.9	33.2	35.8	37.6	40.3	41.9	44.8
20.7	22.9	25.2	27.5	29.8	32.0	34.4	36.7	38.9	41.3	43.5	45.9
21.5	23.6	25.9	28.3	30.1	33.0	35.4	37.8	39.9	42.5	44.7	47.2
21.8	24.3	26.6	29.1	31.5	33.9	36.4	38.8	41.1	43.7	45.9	48.5
22.5	24.9	27.4	29.9	32.4	35.0	37.4	39.9	42.3	44.9	47.3	49.9
23.1	25.8	28.3	30.8	33.4	36.1	38.6	41.0	44.7	46.2	48.8	51.3
23.8	26.5	29.0	31.7	34.3	36.9	39.7	42.3	44.9	47.6	50.2	52.9
24.6	27.3	29.9	32.8	35.9	38.2	40.9	43.7	46.2	49.1	51.7	54.6
25.3	28.2	30.9	33.8	36.5	42.2	45.0	45.0	47.8	50.7	53.4	56.3
26.2	29.1	32.0	34.9	37.9	40.7	43.7	46.6	49.5	52.4	55.3	58.2
27.1	30.1	33.1	36.1	39.1	42.1	45.2	48.2	51.2	54.2	57.2	60.2
28.1	31.2	34.2	37.4	40.4	43.7	46.8	49.9	52.9	56.2	59.1	62.4
29.2	32.3	35.5	38.8	41.9	45.2	48.5	51.8	54.9	58.2	61.4	64.7
30.2	33.6	36.8	40.3	43.6	47.0	50.4	53.8	56.9	60.5	63.7	67.2
31.5	34.9	38.4	41.9	45.4	48.9	52.4	55.8	59.3	62.8	66.3	69.8
32.7	36.4	39.9	43.7	47.2	50.9	54.5	58.2	61.7	65.5	68.9	72.8
34.2	37.9	41.7	45.5	49.3	53.2	56.9	60.7	64.4	68.3	72.0	75.9
35.7	39.7	43.6	47.6	51.5	55.6	59.5	63.5	67.3	71.5	75.2	79.4
37.4	41.5	45.7	49.9	53.9	58.1	62.3	66.6	70.6	74.9	78.9	83.2
39.3	43.7	47.9	52.3	56.7	61.2	65.3	69.8	74.1	78.5	82.8	87.2
41.4	45.9	50.5	55.1	59.7	64.3	68.9	73.5	78.0	82.7	87.2	91.9
43.7	48.6	53.5	58.2	63.2	68.0	72.9	77.6	82.6	87.3	92.3	97.0
46.2	51.4	56.4	61.7	66.7	71.8	76.9	82.2	87.2	92.5	97.5	102.8
49.1	54.6	59.9	65.5	70.8	76.4	81.8	87.4	92.6	98.3	103.4	109.2
52.4	58.2	64.0	69.0	75.7	81.5	87.3	93.1	98.9	104.8	110.6	116.4
56.8	62.4	68.5	74.9	80.9	87.4	93.5	99.8	105.9	112.3	118.4	124.8
60.4	67.2	73.8	80.6	87.2	93.9	100.7	107.5	114.1	120.9	127.5	134.4
65.5	71.8	79.9	87.4	94.5	101.8	109.1	116.1	123.6	131.0	138.1	145.6
71.4	79.2	87.0	95.3	102.8	110.9	118.7	127.0	134.5	142.9	150.3	158.8
78.6	87.3	96.0	104.8	112.5	122.2	130.9	139.8	148.4	157.2	165.9	174.7
87.3	95.9	105.4	116.4	124.5	134.3	143.8	153.3	162.9	174.7	182.0	194.1
98.2	109.1	120.0	131.0	143.8	152.7	163.7	174.7	185.5	196.6	207.3	218.4
112.2	124.7	137.8	149.8	162.1	174.6	187.1	199.7	211.9	224.6	236.9	249.6
130.9	145.5	160.0	174.6	189.2	203.7	218.3	232.8	247.4	261.9	276.5	291.0
157.1	174.6	192.1	209.6	226.9	244.4	261.9	279.5	296.9	314.5	331.7	349.4
196.4	218.3	240.0	262.1	283.7	305.5	327.4	349.4	370.9	393.1	414.6	436.8
261.9	291.0	320.1	349.4	378.3	407.4	436.5	465.9	494.7	524.2	552.9	582.4
392.8	436.5	480.5	524.2	567.7	610.4	654.8	698.9	742.6	786.2	829.9	873.6
785.7	873.0	960.9	1048.32	1135.7	1162.2	1309.5	1397.8	1485.1	1572.5	1659.8	1747.2

of productive strata of the coal bearing sequence of the Tournaisian stage, of the Naryshevskian Beds and of the Upper Givetian substage of the Bashkiriyan strata (Shkapov and Stakhanov areas). It can be seen that the penetration rate varies within wide limits.

Table 2. RATES OF BORING IN PRODUCTIVE BEDS IN CERTAIN WELLS

No. well.	Coal-bearing sequence			Tournaisian stage			Naryshevskian Beds			Upper Givetian substage		
	Rate of boring (m/hr)											
	min	av	max	min	av	max	min	av	max	min	av	max
						Shkapovka area						
7	—	—	—	1.2	3.8	7.6	0.3	1.0	2.0	—	—	—
9	0.5	3.2	7.6	0.6	2.5	5.5	—	—	—	0.3	1.4	2.8
10	1.2	2.5	5	1.6	7.4	14.5	1.2	4.2	7.8	1.2	5	11.6
13	1	4	7.4	0.6	7.5	15	1	4.1	7.5	0.5	5	11.2
15	2	7	13.2	1.5	6.8	13.6	0.3	3	6.2	0.5	2.5	5
18	1.2	8	14.6	1	7.5	15	0.4	5.6	11.2	0.4	1.4	2.8
29	0.8	3	6	2	11	22.8	1	6.2	13	—	—	—
31	1.8	1.5	15	1.2	3.6	7.4	0.4	2	4.6	0.4	1.2	2.4
						Stakhanovka area						
3	0.5	4.5	10	0.5	5	10	0.4	4	10	0.4	7.6	15
4	—	—	—	0.8	6.2	13.8	0.4	0.8	1.6	0.4	0.5	1
11	0.5	1.7	3.4	0.8	3.8	7.6	0.6	3.4	7.7	0.5	2.2	4.5
15	0.6	3.2	6.7	1	2	4	1.2	6.4	13.6	1.2	4	9.4
						Average of Shkapovka and Stakhanovka areas						
	0.8	4	8.2	1	5.2	10.7	0.6	3.6	7.8	0.5	3.1	6.8

It follows from formula (2) that the gas saturation of the drilling fluid is inversely proportional to the duration of boring and is therefore directly proportional to the rate of boring. In correspondence with the wide range of variation of the boring rate, the gas saturation of the drilling fluid can also vary within very wide limits—by ten times or more. It varies within narrower limits with pump output, which varies from 20 to 60 l/sec during the boring of productive beds.

Table 3 gives calculated values of gas saturation of the drilling fluid for some values of the rate of boring and pump output, illustrating the considerable variation of the gas saturation of the drilling fluid with rate of boring.

It should be noted that, as experience of gas logging shows, actual values for the gas saturation of the drilling fluid often lie below the calculated

Table 3. VALUE OF GAS SATURATION OF THE FLUID AT VARIOUS RATES OF BORING AND MUD-PUMP CAPACITIES

Rate of boring m/hr	Mud-pump l/sec	Gas saturation ($cm^3/l.$) of drilling fluid at gasifactor (m^3/m^3) of:							
		30	40	50	60	70	80	90	100
1	20	2.9	3.8	4.7	5.2	5.6	7.6	8.5	9.5
	40	1.3	1.8	2.2	2.7	3.1	3.6	4.05	4.5
	60	0.9	1.2	1.5	1.8	2.1	2.4	2.7	3.0
5	20	14.5	19.4	24.2	29.1	33.9	38.8	43.6	48.5
	40	7.2	8.6	12	14.4	16.8	19.2	21.6	24.0
	60	4.8	6.4	8	9.6	11.2	12.8	14.4	16.0
10	20	29.0	38	47.5	52	56.5	76	85.5	95
	40	13.5	18	22.5	27	31.5	36	40.5	45
	60	9	12	15	18	21	24	27	30
15	20	40.5	54	67.5	81	94.5	108	126.5	135
	40	21	28	35	42	46	56	63	70
	60	14.5	19.4	24.2	33.9	29.1	38.8	43.6	48.05

values given in Table 3. This is evidently explained by the driving of the gas back into the bed during the process of drilling.

With a knowledge of the gas factor of the productive beds, it is possible to form a preliminary idea of the possibility of detecting them by gas logging under the drilling conditions that are used in boring productive beds.

As follows from Tables 2 and 3, for some regions of Bashkiria the gas saturation of the drilling fluid in exploring the productive deposits will often be less than 16 cm^3/l. This is below the sensitivity possessed by a gas-logging station with a floating PG degasifier. As a result of this, a whole series of productive beds is not indicated on the gas logs.

In order to record productive beds in the Bashkirian regions, the sensitivity of the apparatus employed must be increased between seven and ten times. This can be done by increasing the degree of degasification of the drilling fluid. In this connection the DP* degasifier, with a higher degree of degasification than the floating degasifier, was developed and tested.

The DP degasifier consists of a metal cylinder, inside which is fixed a hollow drum together with a wire brush. The drum is rotated by means of an electric motor fixed above the degasifier. The latter is placed in the

* The degasifier was put forward by B. V. VLADIMIROV and L. A. GALKIN (inventor's certificate No. 90747 of 28 June 1950).

trough containing the drilling fluid (as close as possible to the bore hole opening) on two floats which hold the degasifier in the same place relative to the level of the drilling fluid.

Forced agitation of the drilling fluid stream and splashing of the fluid by the wire brush bring about a considerable increase in the degree of degasification of the drilling fluid and the release not only of the free, but also of the dissolved gas. Changing the rate of rotation of the rod permits some measure of variation in the degree of extraction of gas from the drilling fluid

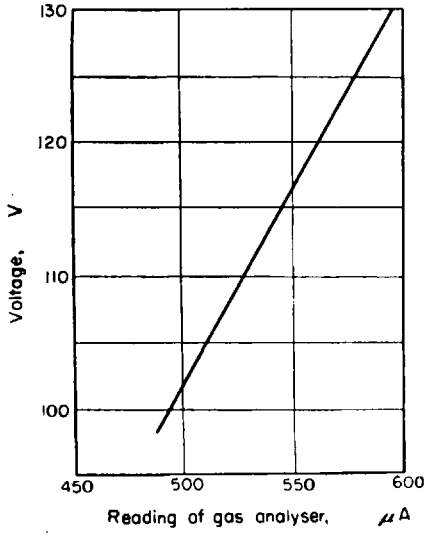

FIG. 2. Dependence of gas analyser readings on the voltage V supplied to the electric motor in the DP degasifier.

by the degasifier. This is illustrated in Fig. 2, which shows the increase in gas indications when the voltage applied to the electric motor is increased, thus producing an increase in speed. In this case the gas saturation of the fluid remained constant, this being controlled by means of a floating degasifier.

Changing the degree of degasification by adjusting the speed of the brush is of great value because it allows the amount of degasification to be suitably selected for the given geological conditions (different gas factors and reservoir properties of the rocks) and the drilling fluid used.

We will examine the results of gas logging by means of the DP degasifier, conducted in order to show the possibility of using gas logging in detecting strata with a low gas factor (15–20 m^3/m^3).

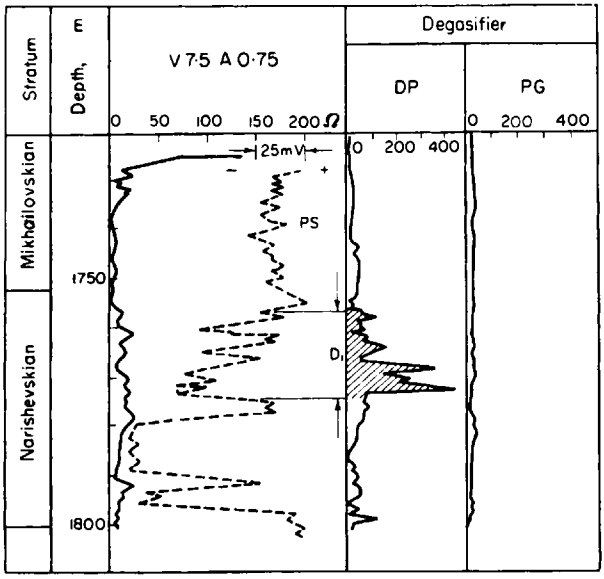

FIG. 3. Results of gas logging by means of DP and PG degasifiers (total content of hydrocarbon gases is given).

Case 1—Fig. 3 shows the results of gas logging with DP and PG degasifiers against productive Devonian beds in one of the wells.

According to the curve of total gas content, obtained with the PG degasifier, the whole interval is characterized by low gas indications (background values). When using the DP gasifier, the bed D_1 is marked by readings of 100–450 μA, which corresponds to a drilling fluid content of 2.6–13.5 cm^3/l. The gas factor for this case is 3–15 m^3/m^3. According to available data the gas factor of the bed D_1, when it is oil-bearing, is equal to 35–45 m^3/m^3, and consequently, in the given case the bed can be described as water-bearing, containing residual petroleum.

The bed D_1 on the gas log obtained with the DP degasifier is shown by individual peaks, in quite good agreement with the mechanical log and the deviations of the curve PS. Even the thin layers, separated by sections of clay, are distinguished.

Case 2 (Fig. 4)—A well was developed in the Tournaisian deposits. On the total gas content curve, obtained when using the DP degasifier, a series of intervals with a high content of combustibles can be detected. At the same time on the corresponding curve obtained by using the floating PG degasifier, only small increases are shown against these intervals. The whole curve is very smooth.

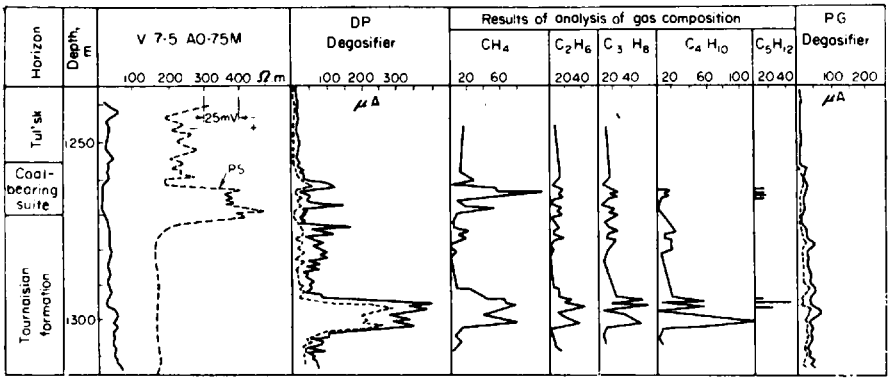

FIG. 4. Results of gas logging by means of DP and PG degasificrs (continuous curve-total hydrocarbon gases; broken curve-total heavy hydrocarbons). Content of individual hydrocarbon gases is given from the results of an analysis on a GST-2 instrument.

The intervals of increased gas content (1257–1285 m) detected by means of the DP degasifier can be described as water-bound and oil-bearing, since the gas factor for them is 5–10 m^3/m^3, while the oil beds of the coal-bearing sequence and the overlying Tournaisian limestones are characterized by a gas factor of 15–30 m^3/m^3.

The intervals (1257–1260 m and 1273–1283 m) were tested and a flow of water was obtained. A core sample taken from a depth of 1258–1259.8 m consists of quartz sandstone, evenly permeated with oil.

The interval with high gas readings at a depth of 1293–1303 m, situated 20 m from the top of the Tournaisian stage, has a gas factor of 15–20 m^3/m^3. This provides a basis for assuming that the given interval is oil-bearing, which is also supported by analysis of the gas composition, which differs markedly from the gas composition in the intervals mentioned above*.

The following conclusions may be reached on the basis of the foregoing:

(1) the DP degasifier possesses a considerably higher degree of degasification than the floating degasifier;

(2) in working with the DP degasifier it is possible to detect oil-bearing strata which have a small gas factor and are often missed when working with a floating degasifier.

* Separate analysis was conducted on a GST-2 instrument (see B. V. VLADIMIROV, The GST-2 gas analyser for determining gas composition during gas logging. *Neft. Khoz. No. 8, (1956)*.

CHAPTER 13

LUMINESCENCE LOGGING

T. V. SHCHERBAKOVA

BITUMENS, including petroleums and petroleum products, possess the ability to luminesce. This property of bitumens is used to determine the content of petroleum in rock samples and the drilling fluid. Systematic luminescence analysis of the drilling fluid during well drilling, carried out with the object of singling out oil-bearing beds penetrated by the well, is called luminescence logging.

At the present time, luminescence logging is carried out by taking samples of the drilling fluid every 1–3 m of penetration and viewing them in ultra-violet light. For this a luminoscope is used, which consists of a light-tight chamber equipped with a source of ultra-violet light (UFO–2 or PARK–4 lamp with a filter passing only ultra-violet rays). The sample of drilling fluid, which is sometimes specially treated, is placed in the ultra-violet light, while the luminescent glow is observed through a window in the chamber (the viewing window). The luminescence is arbitrarily characterized by some relative quantity, for example by the fraction of the surface area of the sample occupied by luminescent spots. Together with this, during the examination of the drilling fluid samples, the colour of the luminescent radiation is determined.

Curves, showing the variation in luminescence capacity of the drilling fluid with variation in depth of the well drilling, are constructed from the data obtained, and constitute a luminescence log. These curves, to greater or lesser extent, represent the content of oil in beds penetrated by the well.

The main drawback of luminescence logging is the subjectiveness of the evaluation of the intensity and colour of the drilling fluid luminescence, which precludes the possibility of a reliable determination of the content of oil in the drilling fluid from the data obtained in luminescence logging. Moreover, the method employed for observing the luminescence makes automatization of luminescence logging difficult.

In this connection, work was carried out to elucidate the possibility of evaluating luminescence objectively and, on the basis of this, to determine from luminescence analysis data the oil content in a drilling fluid.

APPARATUS FOR OBSERVING LUMINESCENT RADIATION

Observations on the intensity and spectral constitution of the luminescent radiation from the drilling fluid were conducted on an apparatus developed by N. O. CHECHIK. The apparatus consists of a measuring and a power unit.

The measuring unit consists of a source of ultra-violet radiation and a photosensitive element placed in a light-tight chamber.

A UFO–4A lamp with a UFS–3 filter, transmitting rays with wavelengths less than 420 mμ (maximum about 365 mμ), is used as the source of ultra violet radiation. In order to ensure constant illumination, the supply to the lamp is stabilized by a baretter.

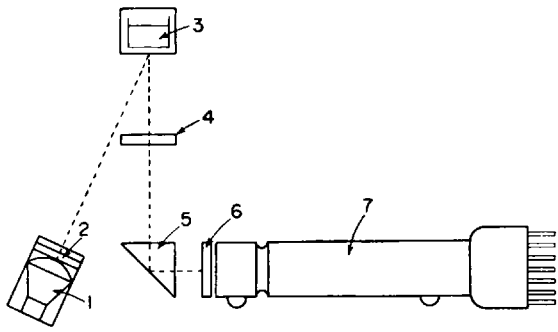

FIG. 1. Optical scheme of photoelectric luminoscope. 1—source of ultra-violet radiation UFO-4A; 2—filter UFS-2; 3—vessel containing fluid; 4—narrow-band filter; 5—prism; 6—filter; 7—photomultiplier.

The sample of liquid under investigation is placed in a quartz cell which is put into the chamber so that its bottom is irradiated by ultra-violet rays. The luminescent emission thus excited is detected by the photosensitive element, for which an FEU–19 photomultiplier is used (Fig. 1). The photomultiplier cathode is protected from the ultra-violet radiation by a yellow-green filter, which stops rays with wavelengths less than 420 mμ and transmits radiation in the visible region of the spectrum.

The radiation received by the photomultiplier is converted into an electric current, which is amplified by a direct-current amplifier (Fig. 2).

The direct-current amplifier consists of a bridge, two arms of which are the internal resistances of the anode circuit of the valve L_9 and the resistances $R_{35}-R_{39}$ and the two other arms are the anode resistances R_{27} and R_{28}. The current from the output of the photomultiplier varies the

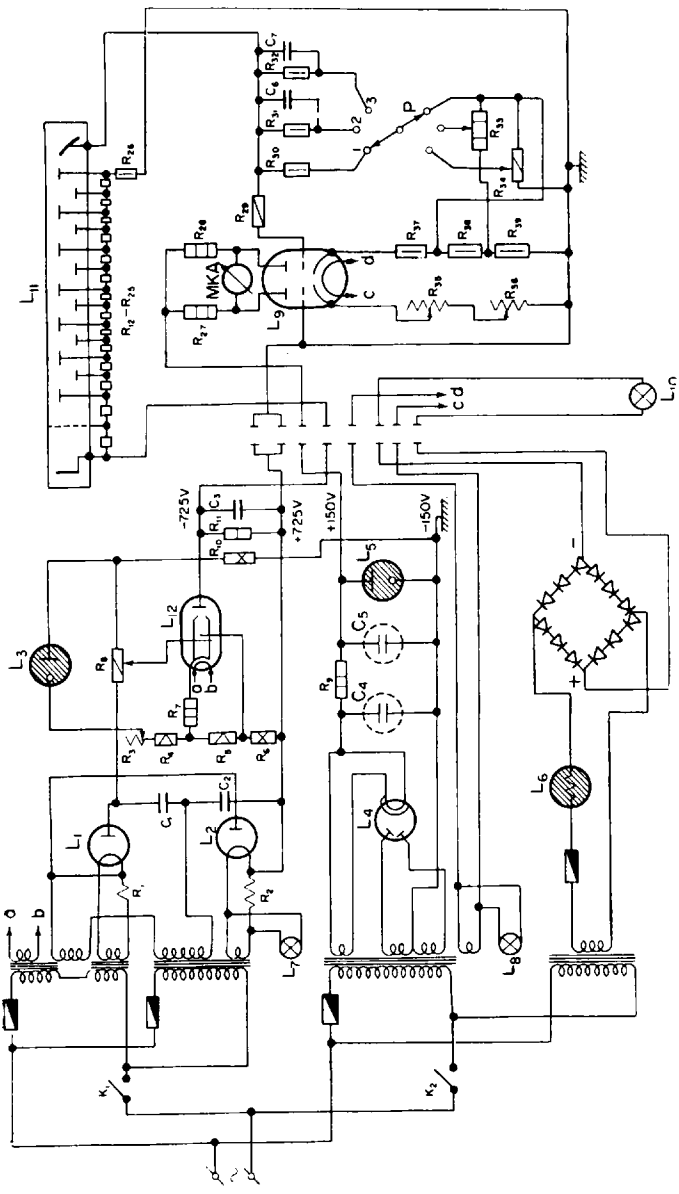

FIG. 2. Electrical scheme of photoelectric luminoscope.

Tubes: L_1—2Ts2S; L_2—2Ts2S; L_3—SG-3S; L_4—5Ts4S; L_5—SG-4S; L_6—0.3B17-35; L_7 and L_8—signal lamps; L_9—6N8S; L_{10}—UFO-4A; L_{11}—FEU-19; L_{12}—6P6S. Resistors: R_1, R_2—1.47 Ω; R_3, R_4—20 kΩ; R_5—1000 kΩ; R_6—1.0 MΩ; R_7—240 KΩ; R_9—200 kΩ; R_9—10 kΩ; R_{10}—1.0 MΩ; R_{11}—2MΩ; R_{14}—R_{26}—0.3 MΩ; R_{27}, R_{28}—16 kΩ; R_{29}—3.0 MΩ, R_{30}—2.0 MΩ; R_{31}—1.0 MΩ; R_{32}—100 MΩ; R_{33}, R_{34}—0.1 MΩ; R_{35}—700 Ω; R_{36}—20 Ω; R_{37}—430 Ω; R_{38}—25 Ω; R_{39}—100 Ω. Capacitors: C_1—C_3—0.5 μF, 1000 V; C_4, C_5—20 μF, 400 V; K_1—high tension switch; K_2—low tension switch; P—sensitivity selector switch of instrument.

voltage on the grid of one of the triodes. A 300 μA microammeter (MKA) is connected across the measuring diagonal of the bridge. The switch P permits selection of one of three values for the amplification factor of the amplifier -1100, 5500 and 27,500 (positions 1,2 and 3 respectively).

The power unit contains sources of supply for the photomultiplier and the amplifier. A voltage of 725 V, obtained from a twin rectifier assembled about the two valves L_1 and L_2 (type 2Ts2S), is used for the photomultiplier supply. The voltage is stabilized by an electronic stabilizer assembled about the 6P6S valve L_{12}. The comparatively low supply voltage for the photomultiplier is chosen with the object of obtaining a low value for the intensity of the dark current (of the order 10^{-10}A).

The supply to the anode circuits of the direct-current amplifier is obtained from a rectifier, assembled as a full-wave rectification circuit about the 5Ts4S valve L_4.

Just before the measurement, with a completely darkened photomultiplier, the current intensity in the anode circuit of the right-hand half of the 6N8S valve is adjusted by means of the rheostats R_{35} and R_{36} so that the measuring instrument indicates zero. If light falls on the cathode of the photomultiplier, the balance of the bridge is upset and a current begins to flow through the MKA instrument. The instrument readings I_n will be proportional to the intensity of the luminescent radiation reaching the cathode of the photomultiplier.

In order to ensure that it is possible to compare the readings obtained at different times for different settings of the instrument, with the readings I_n due to luminescent radiation from the sample of petroleum under investigation, the readings I_e from a standard are determined. The standard used is a mixture of luminophors giving out a bluish-white light. The ratio $\frac{I_n}{I_e}$ is taken as the quantity defining the relative intensity of the luminescent radiation.

By putting into the light path a filter transmitting a narrow region of the visible spectrum (in the range 420–640 mμ), it is possible to determine the intensity of the radiation in any part of the spectrum. Thus, by using a green filter, it is possible to measure the relative intensity $\frac{I_z}{I_e}$ of the green light ($\lambda = 530$ mμ) in the luminescent radiation.

By means of a set of filters the complete spectral characteristics of the radiation (the dependence of intensity of the radiation on wave length) from the sample under investigation can be obtained.

When using light filters, the absorption coefficient of the filter must be

allowed for; the value of I obtained from measurements must be multiplied by the absorption coefficient K.

The coefficients K of the filters were determined by comparison of four petroleum samples with the results of direct luminescence measurements conducted in the spectral laboratory of the All-Union Scientific Research Institute for Petroleum and Geological Survey under the direction of A. A. IL'INA.

In testing the apparatus described above, the following data were obtained:

(a) a threshold sensitivity of the order 1.3×10^{-10} lumen;

(b) a mean error of 2.5 per cent in ten measurements, the greatest being 8 per cent;

(c) radiation intensity, as determined by the apparatus, proportional to the actual intensity of the luminescent radiation.

The last of these was established by comparing the readings of the instrument with the results of luminescent radiation intensity determinations made in the laboratory with a visual photometer (see Table).

Petroleum samples	1	2	3	4	5	6
Relative intensity of green light, found on instrument	0.31	0.78	1.04	1.2	1.82	2.6
Intensity of green light, found with visual photometer	0.9	3.0	4.3	5.3	8.0	11.5

Luminescence of Petroleum and Drilling Fluids.

Presented below are the results of an investigation of the luminescence from petroleum, solutions of petroleum in chloroform, and drilling fluid containing petroleum, using the apparatus described above.

Figure 3 gives the results of measurements of the luminescent emission from samples of various petroleums.

It can be seen that the lower the specific gravity of the petroleum, and consequently the higher the gum content, the greater is the intensity of the luminescence. With an increase in specific gravity and reduction in gum content, the maximum of the luminescence spectrum is displaced towards longer wavelengths, i. e. towards the yellow region of the spectrum. These regularities are well known from the practice of luminescense–bituminological analysis of petroleum.

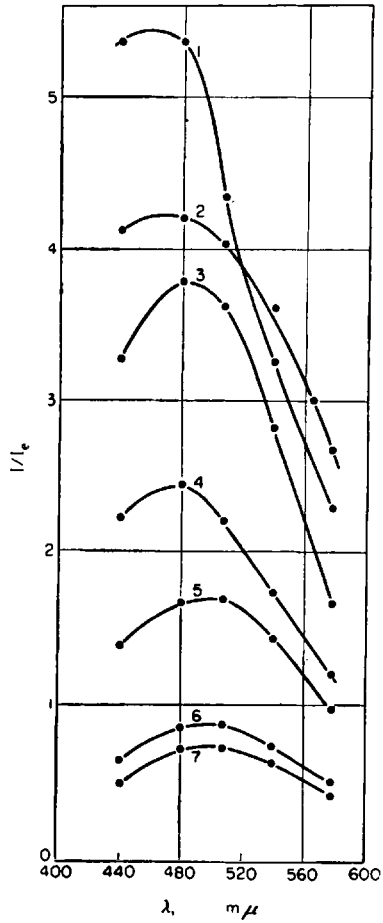

FIG. 3. Luminescence spectra of petroleums of different specific gravity: 1—0.797; 2—0.801; 3—0.813; 4—0.820; 5—0.831; 6—0.853; 7—0.861.

Figure 4 shows the results of determining the luminescence of solutions of petroleum in chloroform.

As can be seen, the luminescence spectrum of petroleum changes little with addition of chloroform, but the intensity of the radiation increases considerably. The intensity of the green radiation changes in proportion to the concentration of petroleum in the chloroform up to one hundredth of one per cent (Fig. 5). With further increase of the amount of petroleum in the chloroform the intensity of the luminescence changes little and even begins to decrease (region of concentration extinction [1, 3, 6]).

Figure 6 shows the dependence of instrumental readings (in μA) on the

content of different petroleums in a clay suspension. The clay suspension was of such viscosity that oil drops did not move about in it. The petroleum was carefully mixed with the clay suspension until a stable emulsion was

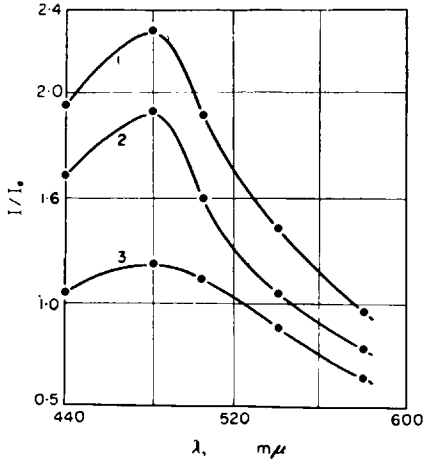

FIG. 4. Luminescence spectra. 1—solution of petroleum in chloroform with a concentration of 8×10^{-3} %; 2—the same with a concentration of 2×10^{-3} %; 3—undiluted petroleum.

formed, this being checked visually under ultra-violet light. Suspensions were prepared from two clays (light and dark) and from petroleum with different intensities of luminescence.

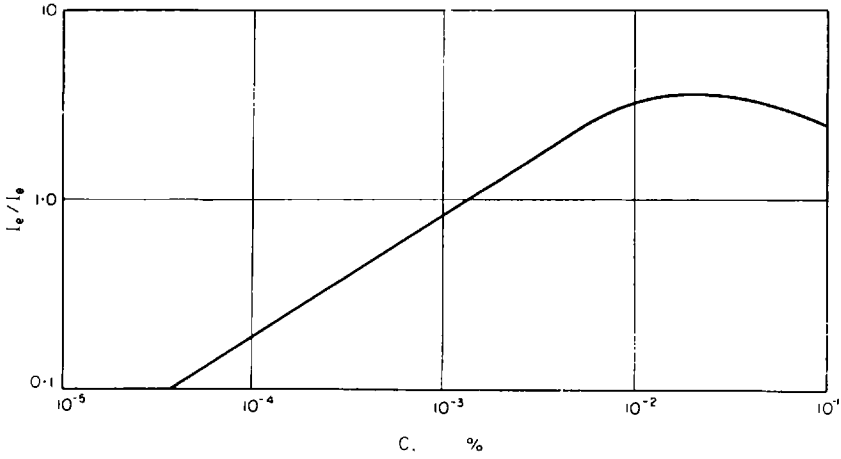

FIG. 5. Intensity of luminescence of a solution of petroleum in chloroform as a function of concentration.

It can be seen that, by means of the apparatus described above, it is possible to detect petroleum in the clay suspension down to a content of 0.5–1 cm^3 per litre, i.e. approximately as much as can be detected by visual examination of clay suspension samples in ultra-violet light in the luminoscope.

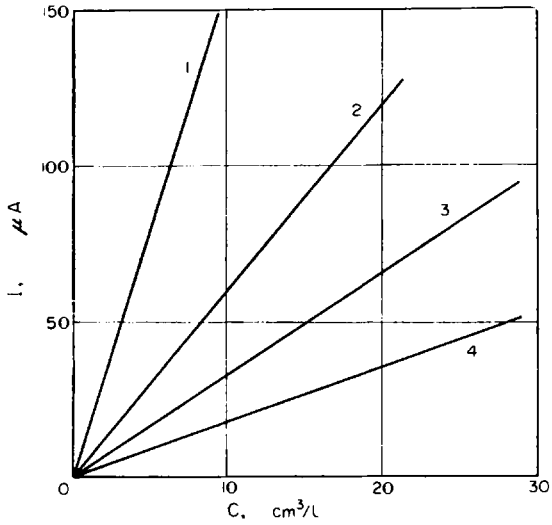

FIG. 6. Intensity of luminescence of petroleum in drilling fluid as a function of concentration. 1—petroleum with intensity $I_g/I_e = 30.0$, dark clay suspension; 2—petroleum with intensity $I_g/I_e = 2.62$, same suspension; 3—petroleum with intensity $I_g/I_e = 1.74$, light clay suspension; 4—the same petroleum, dark clay suspension.

For the concentrations of petroleum in clay suspensions which we have examined, the intensity of the luminescent emission is proportional to the amount of petroleum and no concentration extinction has been noticed. The coefficient of proportionality depends strongly on the nature of the petroleum and the clay suspension. However, it can be expected that, for a given type of clay suspension and petroleum, it is possible to obtain a quantitative estimation of the amount of petroleum in the clay suspension from the instrument readings.

SPECTRAL CHARACTERISTICS OF PETROLEUM AND PETROLEUM PRODUCTS

In luminescence logging it becomes necessary to differentiate between the luminescence of explored petroleum and the luminescence of petroleum products that have entered the drilling fluid in the process of drilling. It is

proposed that this can be done by studying the spectral characteristics of the luminescent radiation. In order to check this, the spectral characteristics of petroleum and petroleum products were determined and are shown in Figs. 7 and 8.

As can be seen, the principal petroleum products, which can enter the drilling fluid (lubricating materials—motor oil, solidol, machine oil, graphite grease), have a sharp maximum in the left-hand part of the spectral characteristic (wavelength about 480 mμ), which differs markedly from the spectral luminescence characteristics of heavy petroleums.

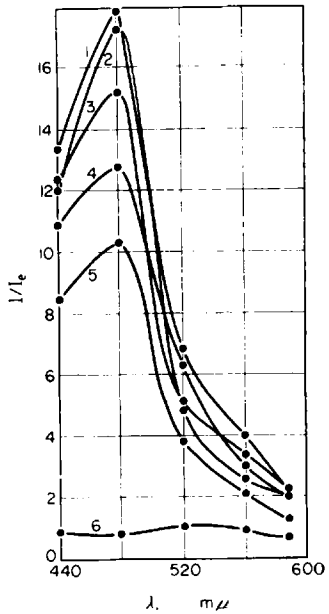

FIG. 7. Luminescence spectra. 1—motor oil No.13; 2—motor oil No. 6; 3—machine oil; 4—solidol; 5—graphite grease; 6—fuel oil No. 350.

Figure 8 shows the spectral characteristics of luminescence from a clay suspension, to which petroleum and lubricating materials had been added. It can be seen that the spectral characteristics of the luminescence from the clay suspension correspond to the spectral characteristics of bitumen contained in the clay suspension. When motor oil is added to the clay suspension, the maximum shifts to the left and, as the concentration of motor oil is increased, approaches more and more closely to the motor oil characteristic.

Thus, in the case when the explored petroleum is heavy and contains a fair amount of resinous components, it can be distinguished from lubri-

cating materials which have entered the drilling fluid from the surface. To this end it is sufficient in many cases to conduct observations with a filter, which absorbs the blue and transmits the yellow region of the spectrum, i.e. to determine mainly the luminescence of only the resinous components

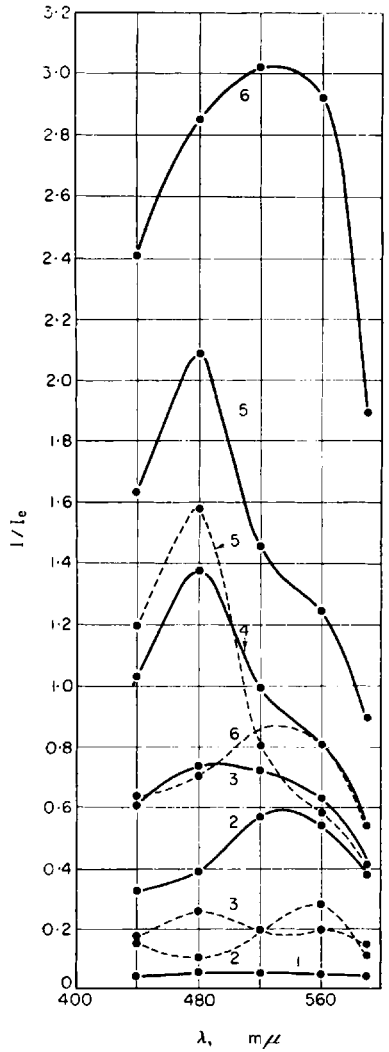

FIG. 8. Luminescence spectra. 1—drilling fluid; 2—drilling fluid with 10% petroleum; 3—drilling fluid with 10% petroleum and 5% motor oil No. 6; 4—drilling fluid with 10% petroleum and 25% motor oil No. 6; 5—drilling fluid with 10% petroleum and 50% motor oil; 6—petroleum. Continuous lines—Tuimazin petroleum. Broken lines—Kued petroleum.

of the petroleum. However, it is difficult to distinguish on spectral characteristics between the explored petroleum, containing a large quantity of light fractions or lubricating oil components, and petroleum products which have entered the drilling fluid.

Figure 9 shows results of luminescence analysis of drilling fluid samples taken while drilling one of the wells of the Aleksandrov area (Bashkiria).

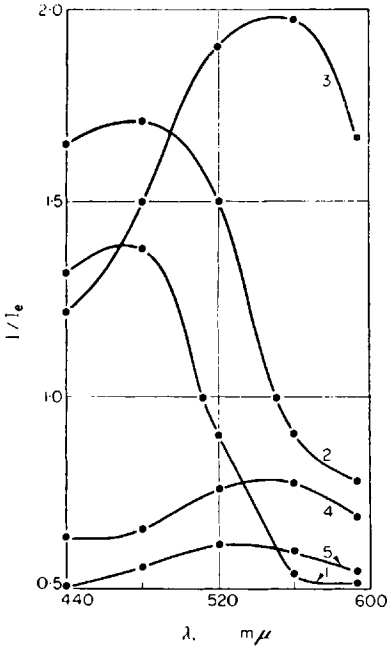

FIG. 9. Luminescence spectra. 1 and 2—drilling fluid with addition of graphite grease; 3—drilling fluid with petroleum; 4—oil-bearing sandstone; 5—drilling fluid.

Samples of fluid, taken while drilling an interval of 1600–1730 m, give fairly intense luminescence; the spectral characteristics 1 and 2 have a maximum about 480 mμ, i.e. at the same place as for lubricating materials. This indicates that the luminescence of the given samples of drilling fluid is due to lubricating materials which have fallen in. The spectral characteristic of drilling fluid sample taken at a depth of drilling greater than 1750 m has a maximum in the region of 540 mμ, which corresponds to the maximum in the spectral characteristic of petroleum in the bed. This indicates the discovery of a petroleum-bearing bed. A core sample taken from this depth proved to be oil-bearing sandstone. The spectral characteristic of this sandstone is the same as that of the drilling fluid, sampled during the drilling of this interval.

VIEWING WINDOW

To provide for continuous observation of the luminescence of the drilling fluid coming from the well, the apparatus must be equipped with a viewing window immersed in the drilling fluid. To avoid distortion of the results of the observations it is essential that the petroleum from the drilling fluid should not stick to the viewing window and remain on it. Thus, the surface of the viewing window must be hydrophylic.

Trials of various materials showed that it is best to use glass* with a degreased surface for the viewing window. The drilling fluid easily washes oil drops from the surface, and the petroleum does not leave traces on it. This was checked by the following method.

The usual clay suspension was poured into a narrow bath 1 m long; in one part this was replaced by a fluid containing petroleum, the boundary between the ordinary clay suspension and the clay suspension containing petroleum being made as sharp as possible. Observations were conducted with the aid of an optical arrangement containing a suorce of ultra-violet light and a photoelement; optical contact with the clay suspension was achieved by means of a window, covered in one case by glass and in another by Plexiglas.

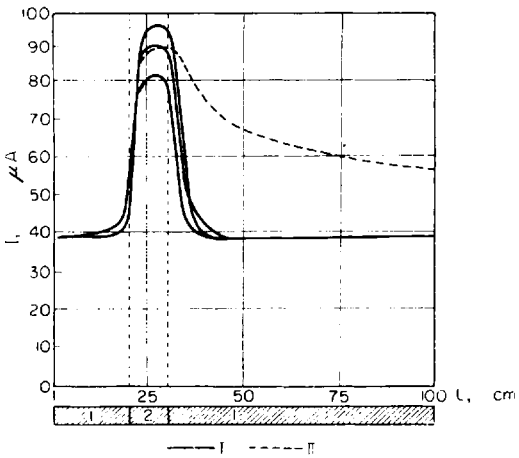

FIG. 10. Record of the luminescence intensity when glass is moved through drilling fluid. 1—drilling fluid; 2—drilling fluid with petroleum. I—measurement with degreased glass; II—measurement with organic glass.

* The glass partially absorbs ultra-violet rays, and this leads to a reduction in the sensitivity of the apparatus. However, this does not create any fundamental difficulty in the operation of the apparatus.

Observation consisted in immersing the window in the clay suspension and slowly moving the whole apparatus along the bath; every 5 to 10 cm the instrument was stopped and the intensity of the luminescence was measured. Values of intensity were obtained as a result of the measurements (Fig. 10). It can be seen that, in going from the clay suspension containing petroleum to the ordinary suspension, the petroleum ceases being detected at a distance of roughly 10 cm; with the Plexiglas window, on further displacement of the apparatus, the petroleum is washed from the window very poorly.

CONCLUSIONS

1. An apparatus for studying the luminescence of samples of drilling fluid allows petroleum present in the fluid to be detected at concentrations down to 0.5 cm^3/l.

Thus device may serve as a basis for automatizing the process of luminescence logging according to the drilling fluid.

2. Study of the spectral characteristics of the luminescence makes it possible in most cases to distinguish between the luminescence arising from the petroleum in the bed and the luminescence arising from lubricating materials that have fallen into the drilling fluid.

REFERENCES

1. A. A. Il'ina, *Study of dispersed and concentrated types of bitumens by spectral and chemical methods.* Report on topic No. 50. Documents VNIGNI (1954).
2. M. Kh. Kleinman, Distinguishing petroleum from oils and resins and determining the content of bitumen in a core sample and in drilling fluid. *Razvedka nedr.* No. 6, (1941).
3. M. A. Konstantinova-Shlezinger, *Luminescence analysis.* Izd. Akad. Nauk SSSR, (1948).
4. P. A. Levshunov, *Oil and gas logging.* Exploratory and production geophysics, Ed. 2. Gostoptekhizdat (1950).
5. V. N. Florovskaya, *An introduction to luminescence bituminology.* Gostoptekhizdat (1946).
6. V. N. Florovskaya, *Luminescent-bituminological method of studying and prospecting for petroleum deposits.* Gostoptekhizdat (1954).
7. F. M. Efendiev and E. I. Mamedov, *Spectroscopic investigation of the luminescence of petroleum.* Izd. Akad. Nauk Azerbaidzhan SSR, No. 1, (1952).

CHAPTER 14

OPTICAL METHODS OF BORE-HOLE INVESTIGATION

T. V. SHCHERBAKOVA

IN order to determine the sequence of stratification and the nature of beds penetrated by a well use is currently made of geophysical methods, of bore hole investigation, the chief of which are electric and radioactivity logging. However, in many cases the data from electric and radioactivity logging do not give a sufficiently complete representation of the rocks penetrated by the well, either because of unfavourable conditions of logging (for example, strongly saline clay suspensions) or because certain lithological and petrographical features of the beds, important for geologists, are not indicated by electric and radioactivity logging. In this connection it is necessary to work out new methods for studying the geological sections of wells.

The so-called optical methods of photographing the rocks along the well walls, and possibly also direct examination by means of television deserve much attention as possible methods of studying the lithological and petrographical nature of beds penetrated by a bore-hole.

Some problems connected with the photography of rocks along the wall of a well are reviewed below, and the results of work carried out along these lines are presented.

OPTICAL PROPERTIES OF DRILLING FLUID

The bore-hole is filled with a liquid (the drilling fluid), which may be clay suspension, very muddy water or, in extremely rare cases, clear water. When the wall of a well is being photographed there will be between it and the objective lens of the camera a layer of drilling fluid which impairs visibility. Therefore in examining the problem of photography in a well it is first of all necessary to find the effects of the layer of clay suspension or muddy water on the image of the well wall. For this it is necessary to know certain optical properties of clay suspensions.

Clay suspensions used in drilling consist of solid mineral particles suspended in water. According to the degree of division of the particles, clay suspensions can be referred to as polydisperse solutions containing particles

of different dimensions — from fractions of a micron to tenths of a millimetre with particles from 0.1 to 10 mμ being most frequently encountered.

Clay suspensions are classed as very turbid media. When light passes through such a medium it is weakened, mainly because of scattering and to a negligible extent because of absorption. In this connection the attenuation of a light beam by the clay suspension layers of various thickness was determined.

Measurements were conducted on an CF-4 specrophotometer and consisted of the following. An empty cylinder was placed in the path of the light beam coming from the monochromator and the light intensity was noted. Then in the path of the beam, in place of the empty cylinder, was placed a cylinder with a layer of clay suspension of the required thickness, and the width of the slit limiting the light beam was adjusted so that the light intensity was the same as in the first case. The ratio of the slit width in the absence of the clay suspension to the slit width in the presence of the layer of suspension, equal to the ratio of the strength of the light beam in air to the light beam which has passed through the suspension, gives the quantity T called the transmittance (a quantity the inverse of attenuation). The transmittance is usually expressed in per cent.

To obtain a layer of clay suspension of the necessary thickness (from 0.03 to 1 mm) cylinders from 4.03 to 5 mm in length were chosen. Part of the cylinder was filled with a quartz plug of length 4 mm and the rest with clay suspension forming the thin layer.

Measurements were carried out with reference to an incandescent lamp used in the spectrophotometer, and possessing wavelengths from 320 to 1100 mμ. The wavelength was determined from the position of the monochromator prism. To improve the monochromatism there were fitted filters of UFS glass for wavelengths of 300–400 mμ, and of OS-19 glass for wavelengths of 600–1100 mμ.

Clay suspensions of different specific gravity ($\gamma = 1.2-1.02$), obtained by means of diluting the initial clay suspensions, were subjected to the investigation.

The investigations were mainly carried out with clay suspensions prepared from dark Buguruslanskian clay with the addition of 1 per cent Na_2CO_3*. Data for this suspension are: viscosity 30 sec; specific gravity 1.2; water yield 9 cm^3; thickness of the crust 3 mm. The fractional composition of the clay suspension is given in Table 1.

* The sample of clay suspension was given by the clay suspensions laboratory of the Gubkin Moscow Petroleum Institute.

TABLE 1. PARTICLE COMPOSITION OF CLAY SUSPENSION IN PER CENT

Determination	Particle diameter (μ)							
	1	1—2	2—3	3—4	4—5	5—6	Above 7	Sum
First	50	26	7.5	4.5	3	3	6	100
Second	49	24	8	5	4	2	8	100
Average	49.5	25	7.25	4,75	3.5	2.5	7	100

In addition, investigations were carried out with clay suspensions prepared from light clay (kaolin).

Measurements were carried out with a light beam intensity equal to 2.5 lumens; for samples of clay suspensions with $\gamma = 1.013$, 1.026 and 1.045 measurements were made with different light intensities. Variation of the light intensity was achieved by interposing a photographic film with different degrees of blackening between the light source and the sample. The attenuation coefficient of the film had been determined beforehand.

From the results of the measurements curves of the value of the transmittance T as a function of the thickness h of the layer of clay suspension were constructed for various wavelengths λ of light (Fig. 1).

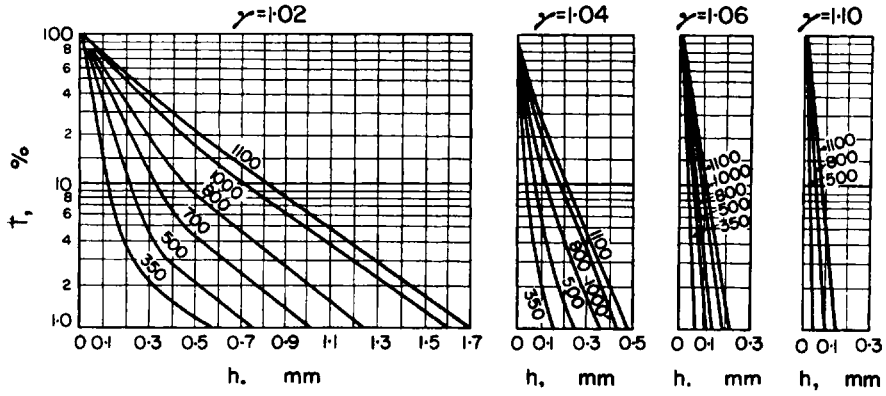

FIG. 1. Dependence of attenuation of light on specific gravity γ of the suspension, thickness h of the layer and wavelength λ of light.

It can be seen that clay suspensions are indeed very turbid media and even in thin layers transmit very little light. Thus, even when the thickness of the layer of clay suspension is only some tenths of a millimetre the transmittance of the light is only about 1 per cent.

The value of the transmittance T falls sharply as the specific gravity of the drilling fluid increases, and becomes a little lower as the wavelength is reduced.

For not very large thicknesses of the layer of fluid the connection between the transmittance T and the thickness of the layer h of the clay suspension can be expressed approximately by the formula

$$T = 100^{-kh}, \tag{1}$$

where k is a certain coefficient, called the attenuation coefficient, representing the rate of reduction of light transmission with increase in layer thickness.

For monochromatic light the attenuation coefficient (see Fig. 2) is:

$$k = (\gamma - 1)\frac{a}{\lambda^n}. \tag{2}$$

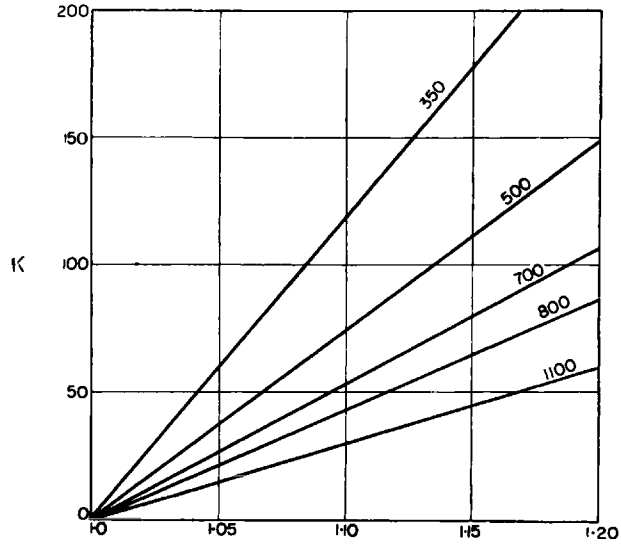

FIG. 2. Dependence of attenuation coefficient K on the specific gravity γ of the suspension and the wavelength λ of the light.

For the dark-coloured clay suspensions investigated $a = 1.4$ and $n = 1.5$.

A suspension prepared from the light clay transmits light better than a suspension from the dark clay, the average difference being 50 per cent (see Fig. 3). The difference in the transmission of light by suspensions

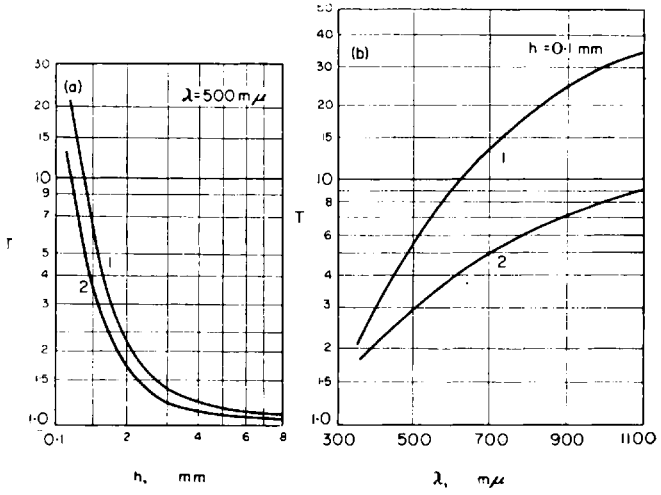

FIG. 3. Dependence of attenuation of light, for light and dark drilling fluid, on the thickness h of the layer of fluid and the wavelength λ of the light.

prepared from light and dark clays is apparently associated with the fact that the particles of the two clays have different reflection coefficients.

The values for the light transmittance shown in Figs. 1–3 were obtained for the case when the angle φ between the principal optical axis of the photometer and the direction of the light beam was equal to zero. Scattering of light at angles φ differing from zero was investigated by TIMOFEEVA on particles from 3 to 20 μ in milk solutions of low concentration and in rosin suspensions [5]. Figure 4 shows the curves obtained by TIMOFEEVA for the ratio of the intensity I of the light passing through the layer of suspension to the intensity I_0 of the light in air (i.e. values of the transmittance of the light) as a function of the thickness of the layer of suspension for various φ. As can be seen, for $\varphi = 0$ and at not very large layer thickness h the value of the transmittance decreases according to an exponential law, i.e. just as in the analogous case for a clay suspension. At angles φ differing from zero the value of the transmittance varies according to another law. In this case for small h values of I/I_0 are considerably less than for $\varphi = 0$; the curve has a maximum which is particularly sharply defined for $\varphi = 30-60°$.

It should be noted that in clay suspensions attenuation of the light with change of wavelength is observed to a much smaller extent than in the usual turbid media with small particle dimensions, in which attenuation according to the Rayleigh law is inversely proportional to the fourth power of the wavelength of the light [4]. Thus, in a clay suspension no significant

improvement in visibility is observed in the infra-red region, such as takes place, for example, in fogs. This has already been theoretically predicted by SHULEIKIN and AMBARTSUMYAN [6, 7].

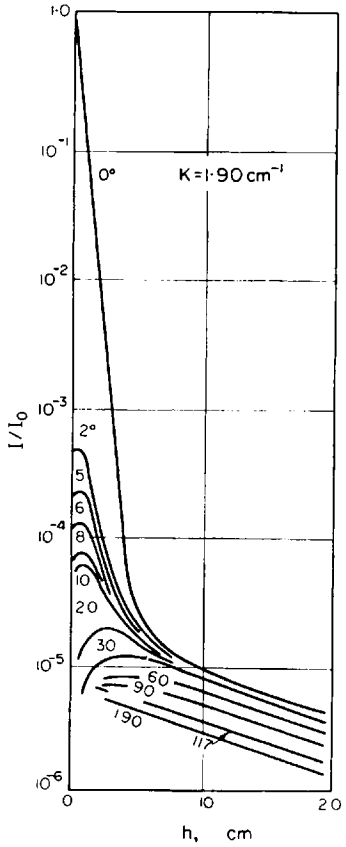

FIG. 4. Dependence of relative intensity of light passing through a suspension, on the thickness h of the layer of suspension and on the angle φ.

Together with attenuation of light in a turbid medium the phenomenon called loss of contrast, which consists of variation of the ratio between the brightness of parts of the object examined is also observed. Loss of contrast is characterized by a coefficient K which is the relative reduction in the ratio of the brightness of the white and dark backgrounds in the presence of a turbid medium.

$$K = \frac{B_w - B_d}{B_d + B_w} 100\% \tag{3}$$

where B_w and B_d are the values of the brightness of the white and dark backgrounds in air;

$B_{w'}$ and $B_{d'}$ are the values of the brightness of the white and dark grounds in a turbid medium.

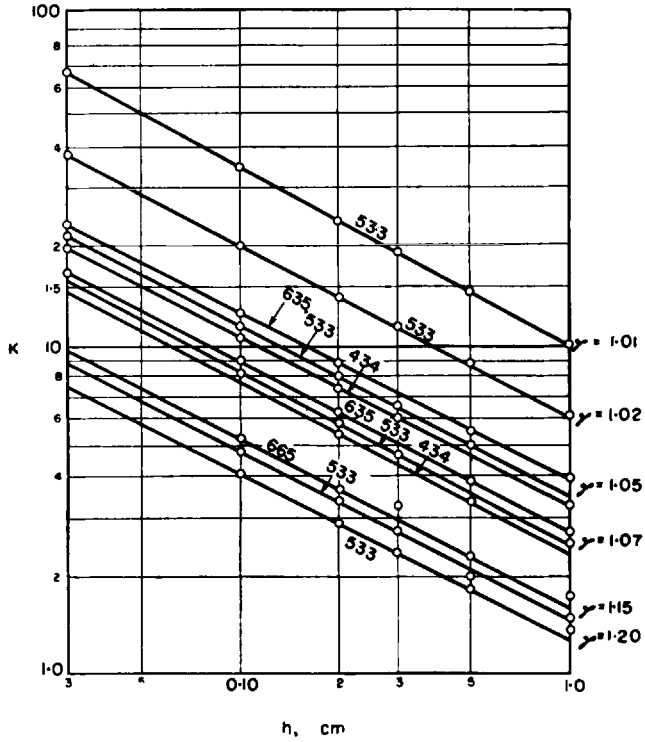

FIG. 5. Dependence of loss of contrast on the thickness of the layer of suspension, the specific gravity γ of the suspension, and the wavelength λ of the light.

To determine the reduction in degree of contrast in drilling fluid, coefficients of loss of contrast were determined for layers of clay suspension of various thickness. Determinations were made with an FM-2 photometer in the following manner.

With the aid of the photometer the brightness of the white ground (a sheet of white paper) $B_{w'}$ and B_w in the presence of a layer of clay suspension and without it was compared in turn with the brightness of the dark ground (black paper) $B_{d'}$ and B_d with and without a layer of clay suspension in front of it. In each of these cases the brightness of the white and dark grounds was obtained in units of light flux from a standard, for which a baryta disk (reflection coefficient 91 per cent) was used.

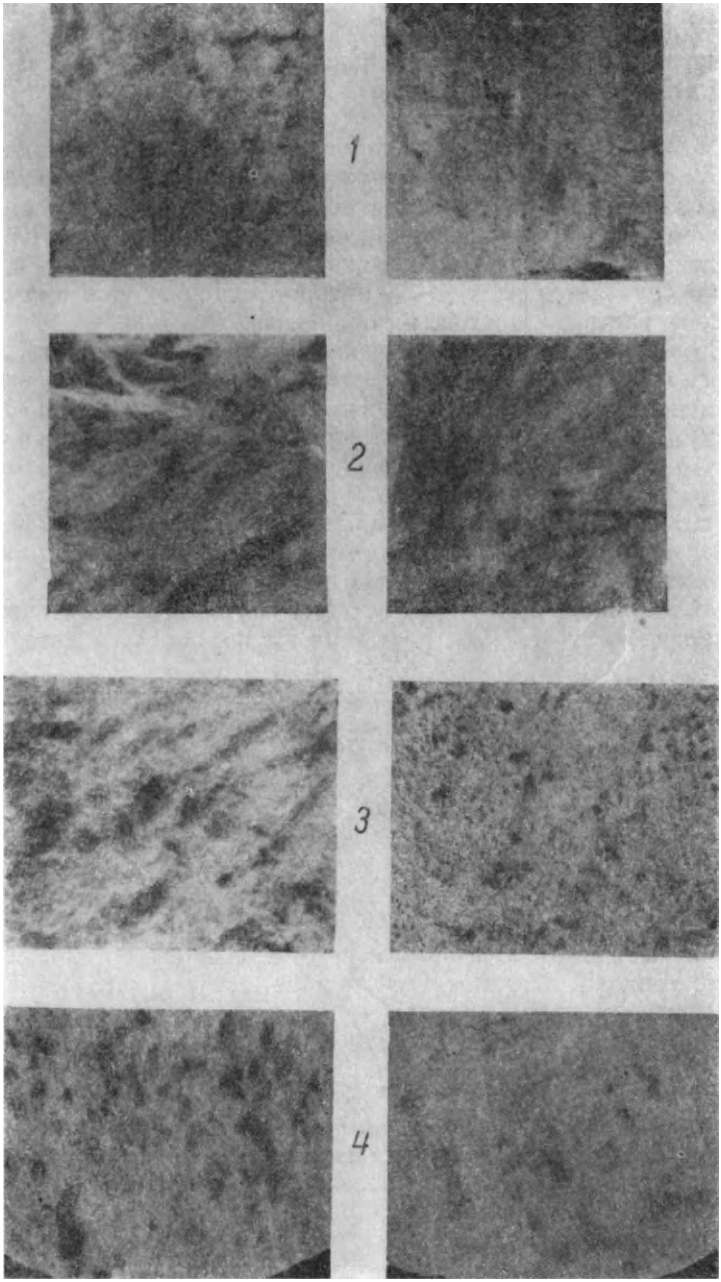

FIG. 6. Photographs of rock samples. 1—sandstone in ordinary (left) and infra-red (right) light; 2—dolomite (same conditions of photography); 3—sandstone without magnification (left) and ten-fold magnification; 4—sample of dolomite with lateral illumination (left) and direct illumination (right).

The coefficient of loss of contrast was determined from formula (3). Determination of the coefficient of loss of contrast was conducted with the same samples of clay suspension with which the transmission of light was determined; the layer of clay suspension was obtained in the same way. Measurements were made with monochromatic light of wavelength varying within the limits of 430 to 730 mμ.

Curves showing the dependence of the coefficient of loss of contrast K on the thickness of the layer of suspension h for various wavelengths λ of light were constructed from the results of the measurements (Fig. 5).

As can be seen from Fig. 5, the contrast falls sharply with increase in thickness of the layer and in specific gravity of the clay suspension. The contrast also decreases, although comparatively slightly, with decrease in the wavelength of light. In practice variation of contrast with variation of wavelength of the light can be neglected over the visible region of the spectrum.

Curves of the dependence of K on h, when both quantities are plotted on logarithmic scales, are quite close to straight lines and, consequently, the dependence of K on the thickness of the layer h can be represented in the following manner:

$$K = Ch^{-m} \tag{4}$$

The coefficient m is approximately constant and equal to 0.54; the coefficient C depends on the specific gravity of the clay suspension samples

$$C = \frac{D}{(\gamma - 1)^p} \tag{5}$$

For the clay suspensions, on which the investigations were carried out, $p = 0.7$ and $D = 2.5$.

For clear reproduction of an object it is most important in photography to convey its contrasts. However, in the passage of light rays through the layer of clay suspension a reduction of contrast is observed. Loss of contrast is the main factor obstructing the possibility of photography. Therefore in examining the possibility of photography in a clay suspension it is first of all necessary to get an idea of the loss of contrast.

Starting from the data obtained, one must determine the permissible thickness of the layer of drilling fluid between the viewing window of the camera and the wall of the well, and the permissible turbidity of the drilling fluid (Table 2).

The main factor in the sharpness of the image is the resolving power of the system, which specifies the number of lines in 1 mm that can be distinguished on the photographic film.

In the case of photography of rocks in a well the resolving power must be such that it is possible to discern the grain of sandstones having grain dimensions of 0.2 mm; for this it is obviously necessary to have a resolving power of 5 lines per mm.

It is well known [3] that resolving power is equal to

$$N = N_{\max}\sqrt{\frac{K}{2-K}},$$

where K is the coefficient of reduction (loss) of contrast; $N_{\max}$ is the resolving power for $K = 1$.

We obtain the permissible coefficient of loss of contrast K by putting into the formula $N = 5$ and $N_{\max} = 30$ lines per mm (the most probable value of $N_{\max}$ for the Industar 22 objective). Hence we obtain

$$K = 0.05 = 5\%$$

It is obvious that the permissible thickness of the layer of drilling fluid $h_{\max}$ between the viewing window of the well camera and the wall of the well is equal to that at which the coefficient of loss of contrast has a value less than $K = 0.05$. The value of $h_{\max}$ can be obtained from Fig. 5.

TABLE 2.

Specific gravity of suspension	Turbidity %	Maximum thickness (mm)
1.01	1.6	27
1.025	4	13
1.05	8	5
1.07	11	2.5
1.15	20	0.8
1.2	32	0.6

In evaluating the properties of clay suspensions it is best to use, instead of the specific gravity, the content of solid particles in the solution, expressed in weight per cent. This quantity η, which may be called the turbidity of the suspension, is connected with the specific gravity of the drilling fluid by the relationship

$$\eta = \frac{\delta(\gamma-1)}{\delta-1}100\%, \tag{6}$$

where δ is the mineralogical density, which can be taken as equal to 2.65.

As can be seen, even a thin layer or film of clay suspension excludes the possibility of photographing the bore-hole walls. Consequently, for photo-

graphy in a well, the clay suspension or turbid drilling fluid must be replaced by clear water.

In well cameras the viewing window is put as close as possible to the wall of the well, but for one reason or another (constructional shortcomings of the instrument, unevenness of the walls of the well) the distance from the viewing window to the rock in many cases will be of the order 10–20 mm. Hence it follows that, to provide for photography of the well, the liquid filling it must have a turbidity not greater than 4 per cent. If the well is filled with ordinary drilling fluid of specific gravity 1.2, then before photography this clay suspension must be diluted to more than ten times with clean water*.

In photography the necessity to have the barrel of the well filled with comparatively clear water is a real disadvantage of the method, but this does not exclude its application where it is necessary to study the geological section of a well.

SOME PROBLEMS OF PHOTOGRAPHING ROCK SAMPLES

In order to investigate some problems connected with photographing rocks along the walls of a well, photography of some samples was carried out at the surface.

1. Light of different spectral composition has different absorptive and reflective capacity. In connection with this photographs of rock samples will differ somewhat, depending on the light in which the photography takes place. To find out the difference in the nature of photographs taken in different light, photographs of rock samples were taken in ordinary light, infra-red and ultra-violet rays.

Samples of sandstones, clays, siltstones, gypsum, dolomite and anhydrite were photographed; some of the samples which were photographed in ultra-violet illumination contained petroleum.

The source of infra-red rays in photographing the rock samples was an ordinary 500 W incandescent lamp with a dark-red filter. The films used in this case were two types, produced at the Scientific Research Institute for Cinematography and Photography, of infra-red film sensitive respectively to rays of wavelengths 840 and 960 mμ.

As a result of comparing photographs taken with illumination by ordinary and infra-red rays, the following was established.

* Actually, depending on the method of illuminating the fluid, considerably greater dilution may be required.

(a) In infra-red light, details of the rock are reproduced less clearly than in ordinary light; so, in infra-red light the clarity with which grains of sandstone and lamination of clays (Fig. 6) are determined is less.

(b) No additional data are detected on photographs obtained in infra-red light.

As was shown above, increasing the wavelength of the light improves the transmittance a little, but the contrast is practically unchanged. Thus a large effect in going to long waves in not observed. Considering what has been stated above, and also that photography with infra-red rays is technically more difficult, the conclusion can be reached that photography of rocks along the walls of a well should be carried out in ordinary light.

In photographing the samples a mercury–quartz lamp with a filter of Wood glass was used as the source of ultra-violet rays. The photography was carried out on isopanchromatic film; a yellow filter, absorbing the ultra-violet rays, being placed in front of the objective lens. In connection with this, luminescent radiation was mainly recorded on the photographs of rock samples in ultra-violet rays. Photographs of rock samples exposed to ultra-violet radiation indicate the presence of bitumens and their distribution through the rock. Since the distribution of bitumen in the rock depends to some extent on the structure of the rock, photography of bituminous rock conducted in ultra-violet rays conveys to some extent the structure of the rock. On photographs of non-bituminous (for example, extracted) rocks, the structure of the rock is not shown up clearly enough.

If the question of studying the bituminosity of rock is excluded from the investigation, illumination by ultra-violet rays in photography of rocks does not offer any advantages over illumination by ordinary light in the study of rocks by photographs, because, owing to wide scattering, ultra-violet rays are transmitted worse by the drilling fluid and possess a greater capacity for loss of contrast.

It is obvious that there is no sense in photographing rock in order to study the bituminosity; for this it is sufficient to record the total intensity of luminescent radiation.

2. To find out how the position of the source of illumination affects the clarity of the rock image, some rock samples were photographed with illumination by direct and oblique (at an angle of 45%) rays. Comparison of the photographs obtained shows that with illumination of the rock sample by direct rays the photographs are "blank" (see Fig. 6); the grain of the rock is more poorly defined, and the rock projections are less noticeable. Therefore photography of rock should as far as possible be conducted with side illumination.

THE WELL CAMERA

Photography of wells was first carried out by D. G. ATWOOD in 1907 [8]. However, this work had no great practical significance.

In 1924 REINHOLD in Holland made a camera for examining the walls of artesian wells of large diameter [2]. The camera permits several hundred photographs to be obtained. Simultaneously with photography of the well wall the position of a compass is fixed, permitting determination of the clements of the bed sequence. The instrument is lowered in the tubes which are used to replace the drilling fluid by clear water.

In reference (9) there is a description of a well camera used in the U.S.A. The camera consists of two parts. One of them is filled with clear water and contains an electric lamp to illuminate the object, an inclined mirror and a viewing window; the actual camera and a winding mechanism are located in the other part. Photography is carried out with a 16 mm cine-film and 450 shots can be taken. The camera is lowered into the well on a cable; a spring presses the side of the instrument where the viewing window is situated to the wall of the well.

In the Soviet Union development of a well camera was undertaken in 1935 at the Central Scientific Research Institute of Geological Survey but was not concluded.

Since 1954 in investigations of shallow dry wells borescopes [1] have been used, consisting of a light source and mirror directing the image of the well wall to an observer situated at the mouth of the well.

In 1955 at the All-Union Scientific Research Institute for Geophysics an experimental model of a well camera was designed and constructed. Its technical features are the following:

(1) The camera is lowered on a three-strand coring cable.

(2) The winding mechanism of a photo-inclinometer is used as the winding mechanism; the width of the film is 35 mm, frame dimension 18 mm by 13 mm, and the number of frames about 120.

(3) The size of the viewing window is 5.7 cm $\times$ 4 cm.

(4) The size of instrument is: length 1.5 m, diameter (without spring) 70 mm, weight 50 kg.

Fig. 7 shows a general view of the well camera, in the lower part of which the light source, mirror and viewing window are located.

The light source consists of three type SM-29 bulbs (the light flux from each lamp is 28 lumens) equipped with hoods to protect the camera, situated in the upper part, from the direct light of the bulbs. Light from the bulbs passes by way of the mirror and viewing window on to the wall of the well.

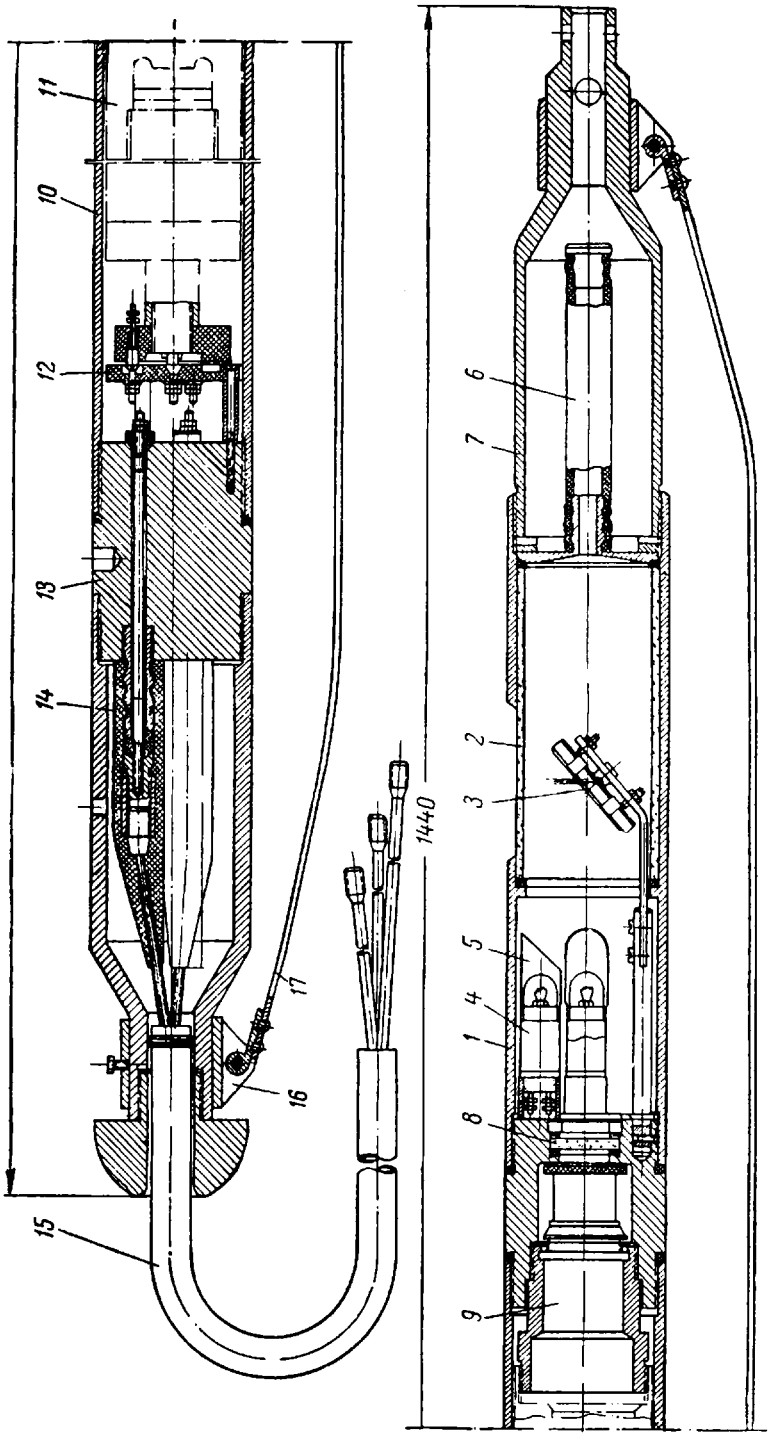

FIG. 7. General view of well camera. 1—body of optical attachment; 2—glass; 3—mirror; 4—bulbs; 5—hoods; 6—pressure compensator; 7—casing of compensator; 8—protective window; 9—objective; 10—body of film-winding mechanism; 11—film-winding mechanism; 12—plate with contacts; 13—light bridge; 14—terminal; 15—cable; 16—holder; 17—spring.

Owing to constructional considerations it was not possible to provide oblique illumination to the wall of the well. The rock is transmitted to the camera of the upper part of the instrument through the same window.

The position of the mirror can be varied within certain limits; being chosen so that light flashes, reflected from various parts of the camera, do not fall on to the photographic film.

The light source and mirror are put into a glass cylinder; in the casing opposite the mirror there is an opening 5.4 cm ×7.8 cm forming the viewing window. The lower part of the instrument is filled with distilled water; a pressure compensator serves to equalize the pressures outside and inside the chamber. The lower part of the instrument is separated from the upper part by thick glass; hermetic sealing is provided by rubber packing.

The objective lens and film-winding mechanism are situated in the upper part. An Industar-22 lens (focal length 52.4 mm, aperture 1:3.5) was chosen as the objective lens.

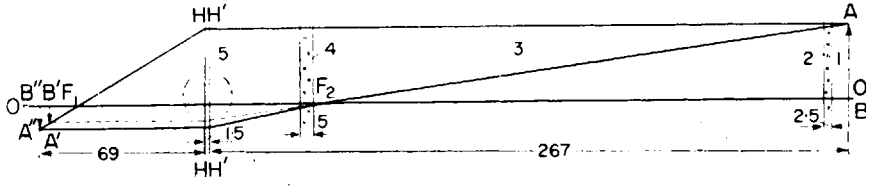

FIG. 8. Path of rays in well camera. 1—drilling fluid; 2—viewing glass ($n = 1.46$); 3—water ($n = 1.33$) filling part of instrument; 4—protective glass ($n = 1.5$); 5—air ($n = 1$); HH'—principal planes of objective; OO'—axis of optical system; F_1, F_2—forward and rear foci of objective.

The instrument is enclosed in steel casing; in the lower part the casing of the compensator with a head for the load is screwed in, and above it there is a light bridge with the three lamp leads. On the instrument are fixed springs which press the side of the instrument on which the viewing window is located to the wall of the well.

The instrument is lowered on a three-strand cable. One strand carries the supply for the electric motor of the film-winding mechanism, another carries the supply to the series-connected lamps of the light source, and the third strand is common to both circuits. The contact located on the film-winding mechanism switches a certain resistance into parallel with the electric motor when the film is wound-on the length of one frame. The winding-on of the film is controlled by the increase in current intensity associated with this switching.

Fig. 8 shows the paths of rays in the well camera, obtained by means of graphical construction; the ray paths and image of AB are shown by a broken line for the case when the medium is wholly air, and the actual path is shown by continuous lines, where account is taken of the fact that part of the medium is water and glass, which have refractive indices different from unity. It is evident that this circumstance leads to displacement of the image by $B'B'' = 5$ mm relative to that observed in air. The image is produced with fourfold reduction.

A very important quantity for the camera is the depth of field which is the distance within the limits of which objects at different distances from the objective lens will appear sufficiently sharply on the image. It is obvious that, in order to obtain a sharp image of the usually uneven surface of a well wall, it is necessary to have as large a depth of field as possible. Increase in depth of field can be obtained by increasing the distance from the objective lens to the subject of the photograph and reducing the effective aperture of the lens.

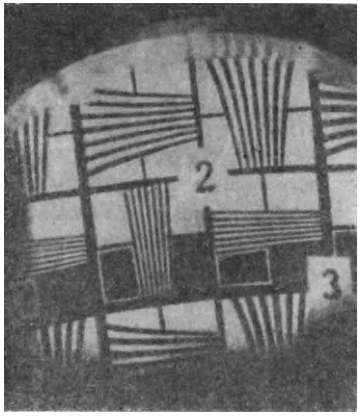

FIG. 9. Test plate.

The distance from the subject of the photograph to the objective lens is taken as equal to 267 mm; further increase in the distance is undesirable, since this would lead to considerable lengthening of the camera.

In choosing the effective aperture of the objective lens it should be remembered that reducing it leads to a sharp increase in exposure time. In the well camera the relative aperture of the objective lens is taken as 1:5.6, calculated for a depth of field of about 2 cm; in the majority of cases the distance from the viewing window to the rock wall lies within the limits of this distance.

For the lamps installed in the camera (the power of a single lamp is 5 candle power) and the distance of 20 cm from them to the subject of the photograph, the illumination of the subject (allowing for absorption) is about 6 lux. For this illumination the exposure time with a film speed of 45 GOST units equals 7 sec.

Test photographs of plates showed that the resolving power of the well camera with the lower part of the instrument not filled with water is about 30 lines per mm, and when filled with water about 10 lines per mm. This resolving power ensures that rock grains of size 0.1 mm and greater can be distinguished. The reduction of resolving power when the lower part of the instrument is filled is associated with the scattering of light in the water filling the lower part of the instrument.

Figure 9 shows a photograph by the well camera of a test plate (photograph taken in water).

Corrosion of components in the lower part of the instrument filled with water caused great difficulties. To avoid this and to increase the resolving power it is proposed in the future not to fill this part of the instrument with water but to fix thick glass into the viewing window and provide it with reliable hermetic sealing.

PHOTOGRAPHY OF ROCKS ALONG THE WALL OF A WELL

The well camera described above was used to take photographs in wells 8, 9 and 10 of one of the sites of the South Kazakhstan region and in well 2089 in part of the work of the Kamenskaia geological survey party in Donbass. The wells were filled with clear water.

In wells of a site in the South Kazakhstan region the well diameter is 90 mm. Photographs were taken at depths from 40 to 150 m in wells 8 and 9, and from 23 to 80 m in well 10; in all, one hundred photographs of the rock were obtained. The section consists mainly of dolomites and argillites.

From the photographs it is usually possible to establish the lithological nature of the rock. Dolomites are distinguished by nodular irregularities with sharp contours, associated with the special nature of the fractures of this rock. In some cases the fine-grain structure of dolomite is overlooked.

The argillites are distinguished by the presence of erosion, marked by shadows and breaks in the sharpness of the image.

Brecciated rocks are clearly detected; on a photograph the rock fragments

(dark grey dolomite, light grey limestone) constituting the breccia are easily visible; the dimensions, shape and mutual disposition of these fragments can easily be discerned (Fig. 10, 1–3).

In the photographs the stratification, presence of veins and seams in the rock, and the fissuring of the rock can be easily seen. Here it is possible to distinguish the cracks filled with some cementing material, in the given case white calcite (Fig. 10, 6–8), from those not filled with cement (gaping) (Fig. 10, 4–5).

In well 2589 in the Kamenskaia region, having a diameter of 90 mm, forty-five photographs were taken at depths from 42 to 90 m. In these photographs it is also possible to establish the lithological character of the bed.

Sandstones are distinguished by their clearly visible individual grains (Fig. 11, 4); coarse-grained sandstones being distinguishable from fine-grained sandstones. The greater the grain size, then, naturally, the more accurately is the grain structure of the sandstone recorded and the more distinctly can the individual grains be distinguished.

Clayey rocks are marked by irregularities in the wall, which are due to erosion of the rock (Fig. 11, 3), and by stratification.

Coals (in the given region close to anthracites) are well distinguished by alternation of dark and light regions which are due to the presence of sharp boundaries at the fracture of specimens; often these regions are extended in one direction, corresponding to the stratification of the rock (Fig. 11, 1 and 2).

On the basis of an analysis of the photographs the following conclusions can be reached.

1. From the photographs of the rock it is possible to form an idea — although not always unambiguous — of the lithological character of the rock.

2. Photography of the rock permits the petrographic character of the rock — structure, grain, presence of cementation, etc. — to be defined more accurately.

As a result of photography of the rocks along the walls of wells, problems of elucidating the structural features of the rock (the presence of inclusions, stratifications, fissures) are solved most successfully.

It should be noted that geophysical methods at present employed for well surveying do not permit detection of the degree of fissuring of rock, while such fissuring is a very important property of the rock. In a series of reservoirs the reservoir properties of the beds are connected with the fissuring.

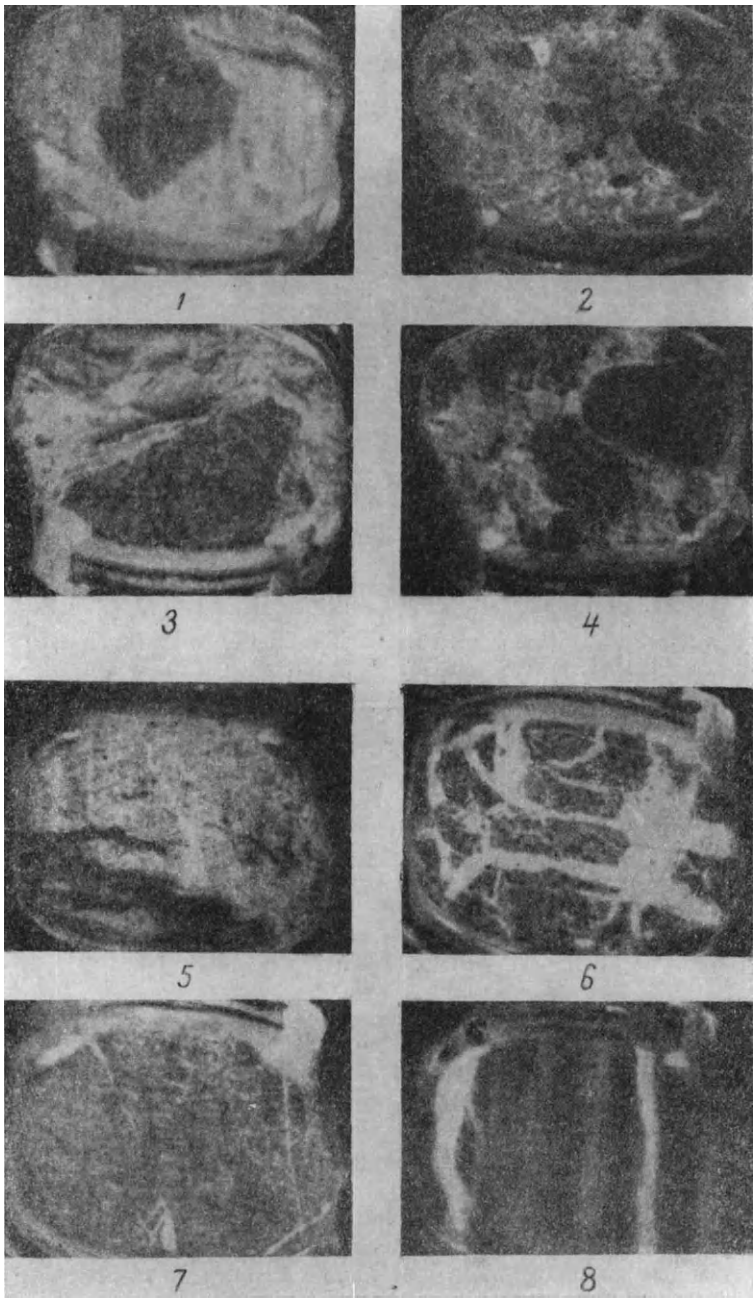

FIG. 10. Photographs of well walls (South Kazakhstan region). 1–3—brecciated rock with pieces of dark-grey dolomite and light-grey limestone; 4 and 5—light-grey limestone with open crack and dolomite inclusion; 6–8—fissured dolomite, cracks filled with calcite.

CONCLUSION

In a well with a sand-clay section (or in part of a well penetrating sand–clay deposits), from photographs of the well walls it is possible to distinguish approximately between clays and sand beds and for the latter to identify medium and coarse-grained sands and sandstones. However, generally speaking, this is not of particular interest. These problems are more successfully solved by other geophysical methods of investigation or by sampling ground by a lateral core-lifter. At the same time the drilling fluid is

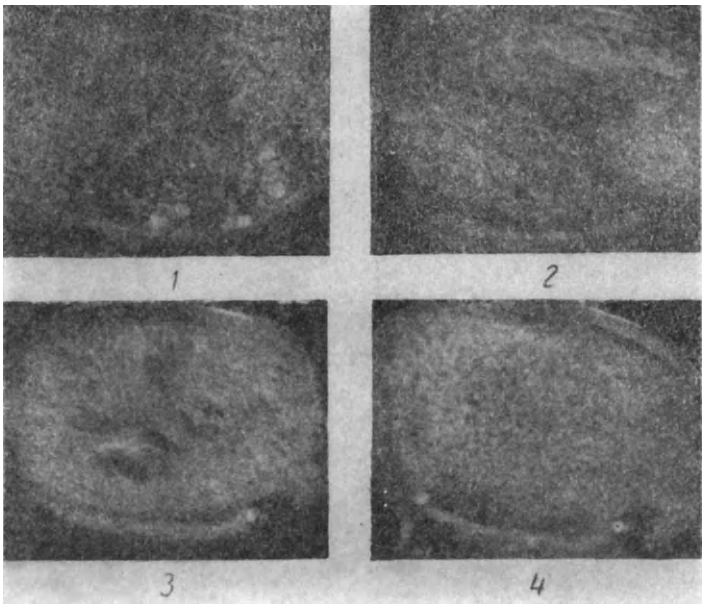

FIG. 11. Photographs of well walls (Donbass region). 1–2—coals; 3—clay rock; 4—sand rock.

cloudy in sand–clay deposits, and on the walls of the well there is a thick clay crust which is difficult to remove. Therefore at the present time optical methods of surveying wells can be recommended for application in those wells where the section consists of dense, finely grained rock; dense sandstones, carbonate rocks and hydrochemical sediments. In such wells the drilling fluid is often transparent; if necessary, it can easily be made transparent. From the photographs in such wells it is possible to identify fissured reservoir rock and to determine the nature and structure of various beds. To solve these problems by geophysical means is difficult and sometimes even impossible.

REFERENCES

1. A. M. VICTOROV, *Well Borescopes.* Gosgeoltekhizdat, (1954).
2. I. B. VIL'TER, Photographs of borc-holes. *Mastering the technique of the coal and slate industry*, No. 6 (1932).
3. A. A. LAPAURI, *Photographic Optics.* Iskusstvo, (1955).
4. J. W. STREET, *The wave theory of light.* Gostekhteoretizdat, 1940.
5. V. A. TIMOFEEVA, Multiple scattering of light in turbid media. *Trudy Morskogo Gidrofizicheskogo Instituta Akad. Nauk SSSR*, Vol. 3 (1953).
6. V. V. SHULEIKIN, The physics of the Sea. *Izd. Akad. Nauk SSSR*, (1953).
7. K. S. SHIFRIN, *Scattering of Light in a Turbid Medium.* Gostekhteoretizdat, (1951).
8. I. O. YACOBI, *Methods, Instruments and the Work of Bore Hole Surveying.* United Scientific and Technical Press, 1938.
9. O. E. BARSTOW, C. M. BRYANT, Deep well camera. *Oil Weekly*, 5 May, 1947.

CHAPTER 15

DETERMINING THE PERMEABILITY OF OIL-BEARING STRATA FROM THE SPECIFIC RESISTANCE

S. G . KOMAROV AND Z. I. KEIVSAR

THE method for determining the permeability of oil-bearing strata from the specific resistance was proposed in 1947 by G. S. MOROZOV. On the basis of experimental studies at the Research Institute for Geophysical Survey Methods, he established a relationship between the coefficient of increase in resistance and the permeability. This relationship was recommended for the determination of permeability.

A number of papers and in particular those of DOLINA [5,6] have been devoted to the determination of permeability of oil-bearing rocks from the specific resistance. As a result of this work, DOLINA developed a procedure for determining from their specific resistance [4], the permeability of the oil-bearing Devonian sandstones.

We give here an account of the method for determining the permeability of the Devonian petroleum-bearing sandstones from their specific resistance.

THE METHOD FOR DETERMINING THE PERMEABILITY OF THE PETROLEUM-BEARING DEVONIAN SANDSTONES FROM THEIR SPECIFIC RESISTANCE

To determine the permeability of the stratum, at first a determination is made of the coefficient of water saturation of the petroleum and gas-bearing stratum.

The coefficient of water saturation refers to the ratio K_w of a part of the volume of the pores, filled with water, to the total volume of the pores. Let us note that with the coefficient of petroleum and gas saturation (or, having in mind only the petroleum-saturated strata, the coefficient of petroleum saturation) K_p refers to the ratio of the volume of pores filled with petroleum to the total volume of pores. Obviously,

$$K_p + K_w = 1$$

The coefficient of water saturation is determined by the coefficient of increase in resistance

$$Q = \frac{\varrho_s}{\varrho_w}, \tag{1}$$

where ϱ_s is the specific resistance of the stratum;

ϱ_w is the specific resistance of this stratum with 100% filling of its pores by water (water-bearing stratum).

The specific resistance of the oil-bearing stratum ϱ_s, necessary for calculating the coefficient of increase in resistance Q, is determined from the data of *VKZ**.

The specific resistance of the water-bearing stratum is calculated for the formula

$$\varrho_w = F\varrho_{s.w} \tag{2}$$

where $\varrho_{s.w}$ is the resistance of the stratum water, at the temperature of the stratum;

F is the relative resistance of the rock.

The stratum water of the Devonian sandstones of the Uralo-Volzhsk province has about 260 g/l. of salts; in agreement with this its specific resistance can be taken as being equal to 0.034 Ω/m at a temperature of 30° (according to MOROZOV 0.03 Ω/m [13], according to DOLINA 0.05 Ω/m [14]).

To determine the relative resistance of the Devonian sandstones according to their porosity DOLINA recommends [4] the use of the relationship obtained from the results in determining porosity of pores and the *VKZ* data in structure contoured wells;

$$F = 0.65\, m^{-1,83}, \tag{3}$$

where m is the coefficient of porosity in relative units.

For this purpose, it is also possible to use other results [3,10].

For comparatively homogeneous strata in the absence of results on the porosity of the stratum, the specific resistance of the water-bearing stratum ϱ_w is taken as the average value of the resistance of the stratum for the structure contoured wells.

Thus, DOLINA, at one of the Tataria deposits, from the *VKZ* results for 154 structure contoured wells obtained an average value for the resistance of the water-bearing Devonian sandstone of 0.7 Ω/m. This value was recommended for use in calculating the coefficient of increase in resistance.

The coefficient of water saturation is determined from the coefficient of increase in resistance Q from the curve $Q = f(K_w)$, obtained on the basis of experimental studies of rock samples.

It is assumed that the water contained in an oil-bearing stratum cannot take part in the general movement of the liquid in the stratum and is interstitial (connate). In this case, the water saturation determined from the curve $Q = f(K_w)$ is the residual interstitial water saturation $K_{r.w}$.

* *VKZ* — All-Union Commission on mineral Resources.

Figure 1 gives the curve recommended by DOLINA[4] for determining the permeability of petroleum-bearing Devonian sandstone by the specific resistance. The curve *1* shows the dependence of the coefficient of increase in resistance Q on the coefficient of oil-bearing K_p and water saturation K_w; curve *2* shows the dependence of the residual interstitial water saturation on the permeability. Both curves are drawn from the results of experimental studies on rock samples carried out by MOROZOV. The curve *3* expresses the

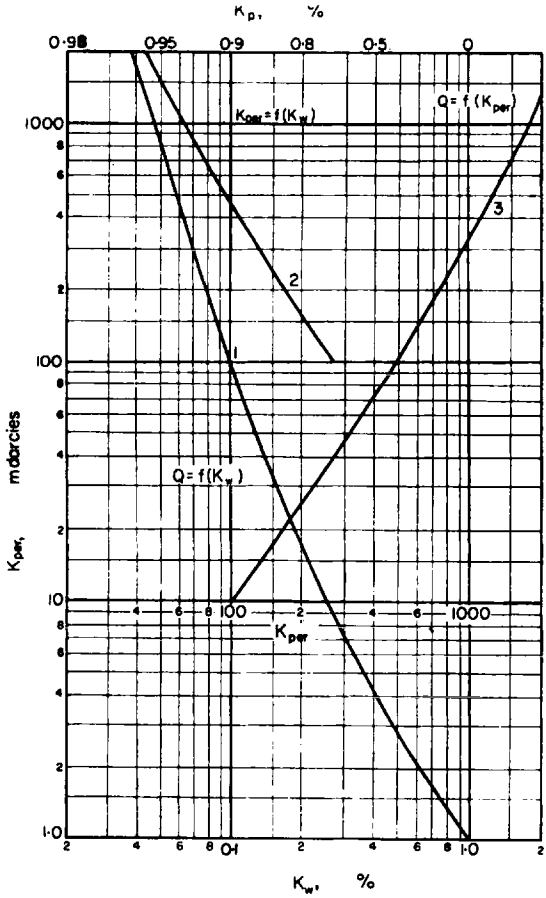

FIG. 1. Graphs for determining the permeability of the petroleum-bearing Devonian sandstones according to their specific resistance (according to DOLINA). 1—dependence of the coefficient of increase of resistance on the coefficient of water saturation K_w or the coefficient of petroleum saturation K_p; 2—the dependence of the coefficient water saturation K_w on the permeability K_{per}; 3—dependence of the coefficient of increase in resistance Q on the permeability K_{per}.

direct connection between the coefficient of increase in resistance Q and the permeability K_{per}.

To determine the permeability of the petroleum-bearing Devonian sandstone the appropriate value of permeability K_{per}, after having determined its coefficient of increase in resistance Q, should be determined from curve *3* (Fig. 1).

The method of determining permeability from the specific resistance in principle is applicable only in those cases where the studied petroleum-bearing stratum is at a distance from the contour of petroleum-bearing deposits. This is connected with the fact that close to the contour of the petroleum-bearing deposits or the intermediate zone in the stratum the water content will exceed the residual water saturation.

In thick strata containing bottom water, the method is applicable only to the upper part of the stratum at a considerable (for example, greater than 10 m) distance along the vertical from the surface of the water, or if the petroleum-bearing part of the stratum is separated from the water-bearing part by a layer of clay.

AN ANALYSIS OF THE REASONS FOR ERRORS IN THE DETERMINATION OF PERMEABILITY BY SPECIFIC RESISTANCE

The error in the determination of the permeability of the petroleum-bearing strata by the specific resistance is due to the error in determining the coefficient of the interstitial water saturation and the insufficiently close connection between the coefficient of the interstitial water saturation and the permeability of the stratum. The coefficient of the interstitial water saturation is determined from the coefficient of increase in resistance Q. The relative error dQ/Q in determining the coefficient of increase in resistance is equal to the sum of the relative error $d\varrho_s/\varrho_s$, in determining the specific resistance of the stratum and the relative deviation $d\varrho_w/\varrho_w$, taken for calculations of the value of the resistance of the water-bearing stratum from its actual value.

The error in determining the specific resistance from the results from the data of lateral electrical logging is caused by the inaccuracy of the results of the measurements of the apparent resistance, by the difference between the actual probe curve and the calculated curve chosen for it and the insufficiently accurate consideration of the various factors (the well diameter, the zone of penetration, heterogeneity of the stratum). On the whole, this error is appreciable and can reach up to 30% ($d\varrho_s/\varrho_s = 0.3$).

The relative deviation of the accepted value ϱ_w from the actual reaches a value of the order of 0.1–0.3, especially in the case when the average value is taken for the specific resistance of the water-bearing stratum.

The connection between the coefficient of increase in resistance and the coefficient of water saturation $K_{r.w}$ is approximately expressed by the formulae (3,10)

$$Q = \frac{1}{K_{r.w}^n} \quad \text{or} \quad K_{r.w} = Q^{-1/n}, \tag{4}$$

where n is a certain power close to two.

If dQ is the error in determining the coefficient of increase in resistance, and dn the deviation of the value for the power from its actual value, the error in determining the coefficient of residual water saturation will be*

$$dK_{r.w} = \frac{\partial Q^{-\frac{1}{n}}}{\partial Q} dQ + \frac{\partial Q^{-\frac{1}{n}}}{\partial n} dn = \frac{1}{n} Q^{-\frac{n-1}{n}} dQ + \frac{1}{n^2} Q^{-\frac{1}{n}} \ln Q dn.$$

In accordance with this the relative error in the coefficient of residual water saturation will be

$$\frac{dK_{r.w}}{K_{r.w}} = \frac{1}{n} \frac{dQ}{Q} + \frac{1}{n^2} \ln Q dn.$$

If we assume that $n = 2$, the deviation of the actual value from that taken $dn = 0.1$, the coefficient of increase in resistance $Q = 100$ and the relative error in its determination $\frac{dQ}{Q} = 0.3$, then we obtain

$$\frac{dK_{r.w}}{K_{r.w}} = \frac{0.3}{2} + \frac{0.1 \ln 100}{2^2} \approx 0.26.$$

As can be seen, despite the considerable errors in the original data, the coefficient of the residual water saturation (providing there are no large errors) is determined comparatively accurately†.

To determine the closer connection of the coefficient of the residual water saturation with the permeability of the strata let us compare the results in determining permeability with the data of permeability established from measurements on samples.

* We will only take the value of error without considering its sign.

† If n differs considerably from 2, then the error in determining $K_{r.w}$ is greater.

A COMPARISON OF THE RESULTS IN DETERMINING THE PERMEABILITY BY THE SPECIFIC RESISTANCE WITH DATA FOR CORE ANALYSIS

For a number of strata of Bashkiria, Tataria and Nizhnii Povolzh'e deposits the values of permeability of the strata determined, according to the instructions [4], from their specific resistance were compared with data on the permeability of strata established by measurements on samples.

The permeability of strata of the Tuimazinskian and Romashkinskian deposits was determined by DOLINA [5,6]*. The specific resistance of the waterbearing stratum, was taken, as shown above, to be 0.7 Ω/m.

GUZANOVA determined the permeability of the strata for the Shkapovskian deposit [11]. The specific resistance of the water-bearing stratum was also taken as being 0.7 Ω/m.

For the Nizhnii Povolzh'e the permeability of the strata was determined by SUSLOVA [15]; the specific resistance of the water-bearing stratum was determined from the porosity of the strata; the resistance of the stratum water was taken as 0.04 Ω/m. The permeability of the samples was taken from the data of the appropriate laboratories.

The permeability from the specific resistance was determined for strata removed from the water–petroleum contact.

In comparing the results of determining permeability from the specific resistance with the results of core analysis, all the wells, in which samples were taken from the stratum and its specific resistance measured, were selected.

For each well:

(a) K^0_{per} the permeability derived from the specific resistance according to the curve *3* of Fig. 1 was determined;

(b) The mean arithmetic value of the permeability of the stratum was determined from measurements on samples taken from the same well, K^k_{per};

(c) The absolute value for the difference was found

$$x = \left| K^0_{per} - K^k_{per} \right|$$

Since the values of the permeability K^k_{per} from the large number of determinations are more accurate than the values obtained from a small number of determinations then the "weight" of the difference x for a different number of determinations of permeability from the cores will be different. We considered that for four or more determinations, the weight of the

* From these data the conclusion was previously made that the mean error in determining the permeability is close to 20–25% [4].

TABLE 1. THE COMPARISON OF THE RESULTS FOR DETERMINING PERMEABILITY BY THE SPECIFIC RESISTANCE WITH THE DATE OF CORE ANALYSIS

Deposit	Stratum	No. of wells (cases)	Results of determination of permeability from specific resistance					Data of core analysis				
			Mean value millidarcies	Mean error		Mean square error		Mean value millidarcies	Mean error		Mean square error	
				millidarcies	%	millidarcies	%		millidarcies	%	millidarcies	%
Tuimazinskian (Bashkiriya)	D_I	97	475	200	65	260	117	485	210	45	270	60
ditto	D_{II}	39	415	155	50	215	80	410	110	30	170	43
Shkapovskian (Bashkiriya	D_I	11	395	190	62	290	110	460	205	45	270	92
ditto	D_{IV}	5	421	73	13	112	19	435	88	17	133	25
Romashkinskian (Tatariya)	D_{Ia}	12	460	215	65	290	102	460	160	36	215	40
ditto	D_{Ib}	33	510	206	45	285	171	550	220	45	275	55
ditto	D_{Ic}	30	470	215	35	325	48	600	220	37	260	45
Sokolovogorsk (Nizhnie Povolzhe)	D_V	23	635	508	111	673	187	738	403	58	529	71

difference x is equal to unity. For three, two and one determination the weight of the difference x is equal to 0.86, 0.71 and 0.5 respectively.

In all the wells for a given stratum, according to the obtained differences $x_1, x_2, \ldots, x_n$, in the values of the permeability, found from the specific resistance and cores, and the weights of these differences $P_1, P_2, \ldots, P_n$, each of which has one of the above four values, the following calculations were made[17]:

(a) the mean error in a separate determination

$$\eta = \frac{x_1P_1 + x_2P_2 + \ldots + x_nP_n}{P_1 + P_2 + \ldots + P_n}; \tag{6}$$

(b) the mean square error of a separate determination

$$\varepsilon = \sqrt{\frac{x_1^2P_1 + x_2^2P_2 + \ldots + x_n^2P_n}{n_1 + 0.86n_2 + 0.71n_3 + 0.5n_4 - 1}}, \tag{7}$$

where n_1, n_2, n_3, n_4 are the numbers of wells in which the difference x has the weight of 1.0; 0.86, 0.71, 0.5 respectively.

The error was expressed in millidarcies and relative units in percentages with respect to the value K^k_{per}.

As can be seen from Table 1, the error in the determination of permeability from the specific resistance is rather high, being 170–200 millidarcies or about 50%. This indicates the presence of errors in the method for determining the permeability by the specific resistance or the insufficiently close connection between the residual water saturation and permeability.

The strata are characterized by a comparatively high degree of homogeneity: the permeability K^k_{per} obtained from the cores from separate wells is close to the average value for the permeability for the stratum as a whole. In connection with this, determinations were made of:

(a) The actual mean permeability of the stratum

$$K^k_{av} = \frac{K^k_1P_1 + K_2P_2 + \ldots + K^k_nP_n}{P_1 + P_2 + \ldots + P_n},$$

where $K^k_1, K^k_2, \ldots, K^k_n$ are the values for the permeability of the stratum, obtained from cores for separate wells; $P_1, P_2, \ldots, P_n$ the weights of the separate values of the permeability taken for four or more, three, two and one determination respectively equal to 1, 0.86, 0.71 and 0.5;

(b) $K^k_1 - K^k_{av}, K^k_2 - K^k_{av}, \ldots, K^k_n - K^k_{av}$ are the deviations of the values for the permeability of the stratum obtained from the cores of separate wells, from the actual mean value of the permeability for the stratum K^k_{av};

TABLE 2. MEAN AND MEAN SQUARE ERRORS IN DETERMINING PERMEABILITY BY SPECIFIC RESISTANCE FROM VARIOUS CURVES

Deposit	Stratum	No. of wells	Mean value of permeability, millidarcie					Mean errors								Mean square errors							
								Millidarcie				%				Millidarcie				%			
			From cores	Dolina	Dolina (accurate)	Morozov	Sultanov	Dolina	Dolina (accurate)	Morozov	Sultanov	Dolina	Dolina (accurate)	Morozov	Sultanov	Dolina	Dolina (accurate)	Morozov	Sultanov	Dolina	Dolina (accurate)	Morozov	Sultanov
Tuimazinskian	D_I	97	485	475	470	603	466	200	155	245	197	64	60	65	57	260	270	325	256	115	100	138	91
Tuimazinskian	D_{II}	39	410	415	405	525	440	155	150	200	138	50	45	58	42	215	210	240	192	80	70	80	68
Shkapovskian	D_I	11	490	395	350	340	321	190	173	215	216	62	45	62	57	292	276	304	153	110	69	98	81
Romashkinskian	D_{Ib}	33	550	510	480	540	475	210	210	190	207	45	45	40	48	290	260	250	267	70	68	60	65
Romashkinskian	D_{Ic}	30	600	470	400	450	400	215	210	200	192	37	27	32	27	325	380	380	301	48	97	34	35
Sokolovogorsk	D_V	23	738	635	1082	722	631	508	684	430	414	111	179	73	79	673	792	490	525	187	284	96	120

(c) The mean and mean square values of these deviations, calculated from formulae similar to (6) and (7).

These mean and mean square deviations characterize the error introduced when, instead of the actual value of permeability for the stratum, we take the mean value of permeability for the stratum.

There are small differences between the errors in determining the permeability of the stratum from the specific resistance and the errors which are obtained when, for the permeability of the stratum of a given section, we take the mean value of permeability for the stratum.

Thus, the use of the method for determining permeability from the specific resistance, in accordance with the existing instructions, does not lead to a noticeable improvement in accuracy of the data on stratum permeability. The stratum permeabilities obtained by averaging the values are used more effectively since it is not necessary to process a large amount of material.

Thus, the method for determining permeability by the specific resistance in the variant recommended for the Devonian sandstones of the Bashkiria, Takaria and Nizhnii Povolzh'e deposits lead to large errors.

CERTAIN PROBLEMS IN THE METHOD FOR DETERMINING PERMEABILITY FROM THE SPECIFIC RESISTANCE

It was assumed that the large error in determining permeability from the specific resistance for the Tuimazinskian, Shkapovskian and Romashkinskian deposits is connected with the incorrect choice of the same specific resistance of the water-bearing stratum for all cases (0.7 Ω/m). Consequently for the deposits mentioned, a second determination of the permeability from the specific resistance was conducted; the specific resistance of the water-bearing stratum being taken as its value obtained for each separate well.

Calculations showed that the values of the errors are about the same (see Table 2, corrected by DOLINA results). Apparently, the main reason for the error is not the initial geophysical data, but the poor connection between the interstitial water saturation and the permeability or the error in determining it.

The determination of permeability of petroleum strata by the specific resistance is based on the assumption that in the petroleum stratum there is only interstitial (connate) water.

Apparently, apart from interstitial water in the petroleum stratum there is also the so-called free water, the quantity of which near the top surface of petroleum-bearing deposits or water–petroleum contact can be sufficiently

large, and as a consequence the water saturation of the stratum will not correspond to its permeability. The method for determining permeability by the specific resistance is therefore applicable only to a stratum (or part of a stratum), which is much higher than the water–petroleum contact.

MOROZOV[13] considers that the determination of permeability by the specific resistance can be carried out for strata 16 m above the water–petroleum contact, since only then is the water saturation of the petroleum stratum interstitial. This condition represents a very great limitation of the method.

Evidently, depending on the surface properties of the particles making up the stratum, the properties of the stratum water and petroleum this distance will be different. According to DOLINA[4] the possibility of determining the permeability from the specific resistance should be established in each individual case, depending on the position of the water–petroleum contact and the characteristics of the stratum.

To establish the effect of the water–petroleum contact on the accuracy in determining permeability from the specific resistance the above mentioned determinations were made for strata at varying distances from the water–petroleum contact. The results are given in Table 3.

As follows from Table 3, there is no systematic reduction in permeability and no large error in its determination at a small distance of the stratum from the water–petroleum contact. This indicates that the effect of the water–petroleum contact on the results of determining permeability is small.

MOROZOV[13] considers it possible to determine the permeability at a distance of less than 16 m from the stratum to the water petroleum contact. He recommends that the obtained values K_{per} should be multiplied by a correction coefficient

$$\mu = \frac{4}{\sqrt{h}}, \tag{8}$$

where h is the distance along the vertical from the middle of the studied zone to the water–petroleum contact.

However, the use of this correction is clearly undesirable for the following reasons.

1. It is insufficiently well established* and it is obviously faulty. The water saturation of an oil-bearing stratum depends not only on its distance to the water–petroleum interface, but also on a large number of other values: the density of the petroleum and water, their capillary properties, the character

* Morozov does not give the basis of the correction coefficient μ.

TABLE 3. THE VALUES OF THE ERRORS IN DETERMINING THE PERMEABILITY FROM THE SPECIFIC RESISTANCE FOR VARIOUS DISTANCES ALONG THE VERTICAL FROM THE MIDDLE OF THE STRATUM TO THE WATER–PETROLEUM CONTACT (VNK)*

Deposit	Stratum	Distance to WPC, m	No. of cases	Mean value of permeability, millidarcie		Mean error		Mean quadration error	
				from core	from resistance	Millidarcie	%	Millidarcie	%
Tuimazinsk	D_I	up to 10	15	516	376	252	69	840	80
		>16	7	519	517	317	86	312	118
Romashkinsk	D_{Ia}	0—16	3	410	533	219	37	370	50
		16—25	9	289	536	335	156	396	220
		>25	2	295	395	175	72	175	72
	D_{Ib}	0—16	20	416	424	274	65	342	103
		16—25	7	288	338	213	37	278	52
		>25	3	681	704	166	73	224	78
	D_{Ic}	0—16	30	531	517	351	92	465	168
		16—25	2	1030	762	274	25	542	51
		>25	2	542	505	107	20	160	28
Sokolovgorsk	D_V	0—10	6	953	499	543	85	782	217
		10—16	4	1014	541	539	43	861	63
		16—25	9	787	593	312	38	551	61
		>25	16	830	674	663	87	840	122

of the surface of the solid phase[8, page 259]. The simplified formula (8), which does not give this fact, will not correspond in the majority of cases to the actual state of affairs.

2. Due to the heterogeneity of the stratum, the distribution of water will deviate considerably from an even course, determined by the coefficient μ.

As recommended by DOLINA it is much better to use stratum characteristics, and to exclude from consideration all doubtful cases. As follows from Table 3, the usual method can give results free from the effect of the water-petroleum contact even at a distance of less than 16 m from it.

CURVES FOR THE DEPENDENCE OF THE COEFFICIENT OF INCREASE IN RESISTANCE ON PERMEABILITY

The DOLINA curve (*1* on Fig. 2) can be expressed approximately by the formula

$$Q = 7 \times 10^{-3} K_{per}^{1.56}, \tag{9}$$

where K_{per} is the permeability in millidarcies.

* a Russian transliteration is used [Editor's note].

As well as this curve, DAKHNOV recommended for the Devonian sandstones the curve $Q = f(K_{per})$ (Fig. 2, curve 2) which "was drawn by the MOROZOV method"[3, page 424]. Since this curve differs little from the DOLINA curve, the determination of permeability from it was not carried out and the errors in the determinations of the permeability were not calculated.

According to MOROZOV[13, page 58] the connection between the coefficient of increase in resistance Q and the reservoir properties of the strata (permeability K_{per}, porosity m) for the Devonian sandstones is expressed as shown by dotted lines in Fig. 3 (Morozov does not give the basis for the curve in this figure).

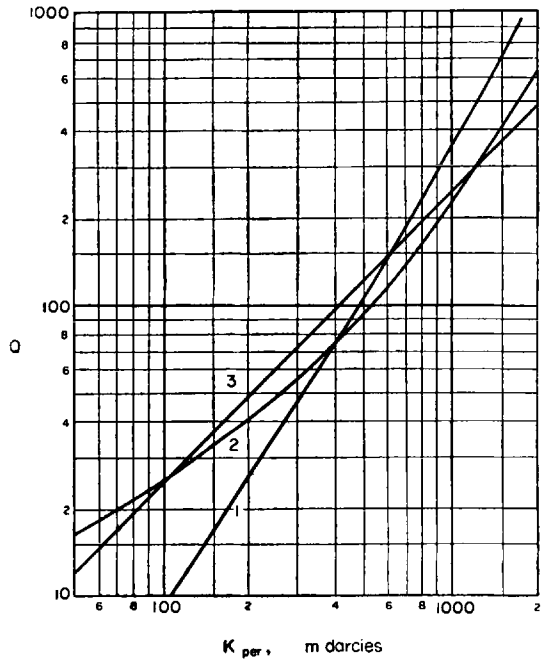

FIG. 2. Various curves for the dependence of the coefficient of increase of resistance Q on the permeability K_{per}. 1—according to DOLINA[4]; 2—according to DAKHNOV[3, page 424]; 3—according to WYLLIE and ROSE for $c = 10$[19].

Using these curves, the permeability of a number of strata was determined by employing the same values of the coefficient for the increase in resistance, that serve for the calculation of permeability by the Dolina curve (the accurate curve).

Table 2 shows the mean and mean square errors for the separate determinations of permeability from the specific resistance by means of the MOROZOV curves. These errors were calculated by the already mentioned method from formulae (6) and (7).

It can be seen that the use of the relationship between the coefficient for increase in resistance and the reservoir properties as proposed by Morozov, means that in some cases (for example, the D_{Ib} and D_{Ic} strata of the Romashkinskian deposit) the error in the results decreases, in the other cases (for example, the D_I, D_{II} strata of the Tuimazinskian deposit) it increases in comparison with that observed in determining permeability by the Dolina curve. The MOROZOV curves do not give favourable results, the error in determining permeability by the specific resistance being rather large.

Considering the curve suggested by MOROZOV $Q = f(K_{per,m})$, we find that they are obtained on the assumption that the interstitial water saturation and consequently the coefficient of increase in resistance depend not only on the permeability of the rock, but also on their porosity, depending to a much greater extent on porosity than on permeability.

In fact, the Morozov curves $Q = f(K_{per,m})$ are represented approximately by the formula

$$Q = \frac{7 \times 10^{-11}}{m^{10}} K_{per}^2 \tag{10}$$

It follows that the relative change in the coefficient of increase in resistance $\frac{dQ}{Q}$ is connected with the relative changes in permeability dK_{per}/K_{per} and porosity $\frac{dm}{m}$ in the following way (neglecting the sign of the error):

$$\frac{dQ}{Q} = 2\frac{dK_{per}}{K_{per}} + 10\frac{dm}{m}. \tag{11}$$

Any relative change in porosity causes a 5 times greater change in the coefficient of increase in resistance than the same relative change in permeability. Therefore, despite the comparatively large changes in permeability, the porosity will have a much greater effect on the coefficient of increase in resistance, than the permeability.

Thus, if the curves proposed by MOROZOV are correct then in view of the large effect of porosity and the impossibility of an exact allowance for its effect, we would still be unable to obtain from the specific resistance sufficiently accurate values of permeability.

The unusually high power-index of porosity and the shape of the curves

at their extreme parts cast doubts on their validity. According to the Morozov's curves, in a low porosity rock in a number of cases there will be very small values for the interstitial water saturation and very large values for the coefficient of increase in resistance; for example, for $m = 0.1$ and $K_{per} = 10$ millidarcies we should have $Q \approx 70$ and an interstitial water saturation of only 10%. However, this is not very probable.

SULTANOV and DOBRYNIN [14] propose for the determination of permeability of the Devonian sandstone from the specific resistance the use of the relationship between the coefficient of increase in resistance and the reservoir properties of the strata, represented by continuous curves on Fig. 3.

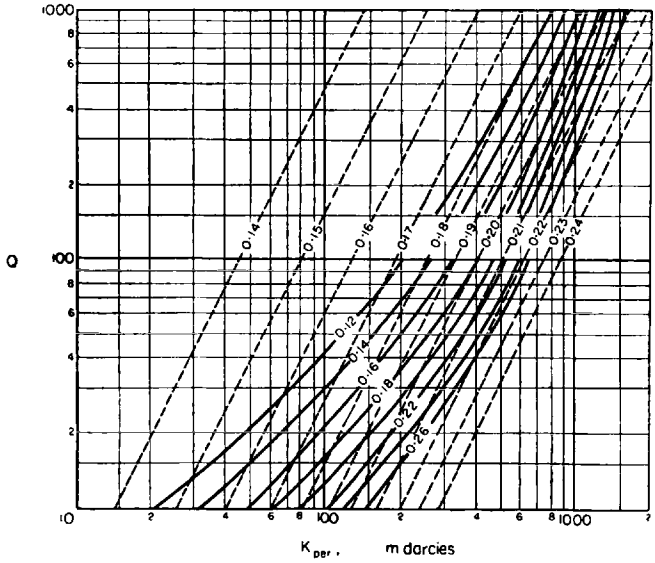

FIG. 3. Curves for the dependence of the coefficient of increase in resistance Q on the permeability K_{per} for sandstones of the Povolzh'ye Paleozoic. Curve symbols—porosity m. Dashed curves—according to MOROZOV[13, Fig. 6]; continuous curves—according to SULTANOV and DOBRYNIN[14].

Table 2 gives the mean and mean square errors for individual determinations of permeability by specific resistance using the SULTANOV–DOBRYNIN curves. The coefficient of increase in resistance was represented by those values for which determinations were made of the permeability according to the DOLINA curve (corrected). The values for the coefficient of increase in resistance were obtained from the value of resistance of the stratum, corrected by the use of the porosity data of a stratum with 100% filling of its pores with water.

As can be seen from Table 2, the use of the curves suggested by SULTANOV and DOBRYNIN $Q = f(K_{per,m})$ does not lead to a noticeable reduction in the errors; therefore, these curves have no advantages over the DOLINA and MOROZOV curves.

The justice of this conclusion will be apparent if we study carefully the curves, which were suggested by SULTANOV and DOBRYNIN, and which express the relationship between the coefficient of increase in resistance and the permeability and porosity. As can readily be seen, this relationship can be approximately represented by the formula

$$Q = 4K_{per}^{3\cdot3\cdot10^{-3}m^{-1.1}}K_{per}^{2m} \tag{12}$$

The possibility of the connection of such an artificial character is doubtful.

TIKS'E,* WYLLIE and ROSE [16, 19], starting from theoretical considerations, give the following expression for the interstitial water saturation $K_{r.w}$:

$$K_{r.w.} = C\frac{m}{\sqrt{K_{per}}}, \tag{13}$$

where K_{per} is the permeability in millidarcies:

m is the porosity in relative units;

C is a constant usually taken as ten.

It is shown that in the general case, C is the following function of the porosity:

$$C = 10\frac{m^2}{\cdot(0.2)^2}. \tag{14}$$

Assuming that $Q = K_{r.w.}^{-2}$, we obtain

$$Q = \frac{K_{per}}{C^2m^2}. \tag{15}$$

This dependence for $C = 10$ and $m = 0.2$ is shown by the curve *3* on Fig. 2. The formula was not checked. However, starting from the fact that the corresponding curve has the same character as the other curve (DOLINA, DAKHNOV, MOROZOV, SULTANOV–DOBRYNIN), it can be considered that the use of the formula of Wyllie and Rose will not lead to an improvement in the results for determining permeability from the specific resistance.

FURTHER ANALYSIS OF THE CAUSES OF ERRORS IN THE DETERMINATION OF PERMEABILITY FROM THE SPECIFIC RESISTANCE

The large error in the determination of permeability by the specific resistance can be connected with a systematic error due to the fact that the

* Possibly a transliteration of a French name.

curves for $Q = f(K_{per})$ differ considerably from the positions which they should in fact have. From this point of view, it is of considerable interest to compare the average values for the permeability of a stratum, determined from the specific resistance (K^0_{av}) and cores (K^k_{av}). These data are given in Table 2.

As follows from Table 2, the average value of the permeability of a stratum determined from the specific resistance is sufficiently close to the average

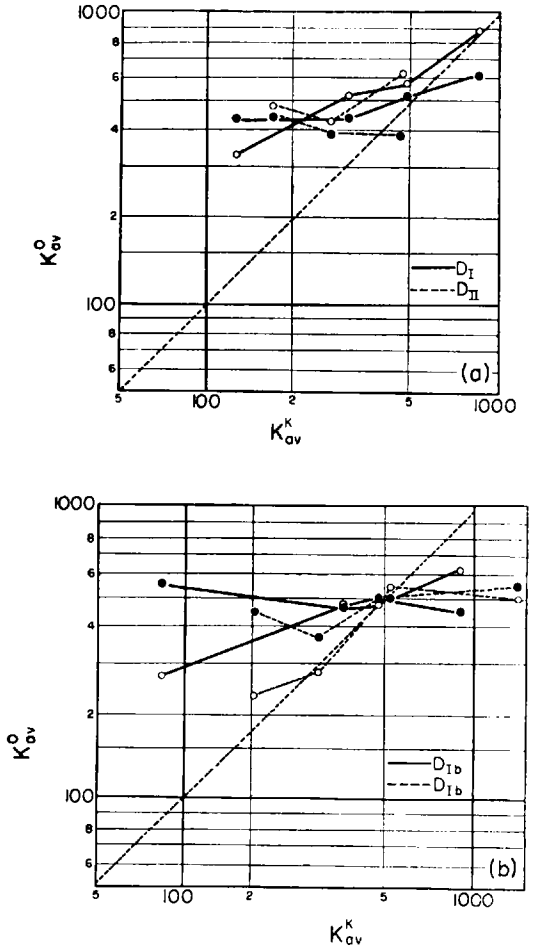

FIG. 4. A comparison of the mean values of permeability (in millidarcies), determined from the specific resistance (K^0_{av}) and from the core (K^k_{av}). (a)—Tuimazinskian deposit (strata — D_I and D_{II}); (b)—Romashkinskian deposit (strata — D_{Ib}, D_{Ic}); the black permeability determined from the Dolina curve; the open points—from the points—Morozov curves.

value for the permeability of a stratum, determined from a core; while in some cases (the strata D_I and D_{II} of the Tuimazinskian deposit, D_{Ib} of the Romashkinskian deposit) they practically coincide.

However, the difference between the values of the permeability determined from the specific resistance and from cores, increases sharply, if we compare them separately for large and small permeabilities of the stratum. This is illustrated in Fig. 4, where the average values of the permeability K^0_{av}, determined from the specific resistance, are compared with the average value for the permeability K^k_{av}, obtained from cores for different ranges of permeability values; 0–200, 200–400, 400–600 and above 600 millidarcies. The comparison was carried out for the D_I and D_{II} strata of the Tuimazinskian deposit and the D_{Ib} and D_{Ic} strata of the Romashkinskian deposit; the original data are the same as those from which the mean values of permeability were calculated in Table 1.

Evidently only for a permeability close to the average value for the stratum does the method for determining permeability by the specific resistance, based on the use of the above curves $Q = f(K_{per})$, give favourable results. For large and small permeabilities, a large systematic error is observed — increasing for the small permeabilities, and decreasing for the large permeabilities. There is a sort of levelling out of the readings. This error is very dangerous, since in an individual well it can lead to a distortion of even the qualitative idea of the permeability of the strata.

The possibility of the method for determining permeability by the specific resistance can be shown by comparing directly the coefficient of increase in resistance with the actual value of the permeability.

Fig. 5 gives the results of these comparisons for the D_I stratum of the Tuimazinskian deposit. On the graph they are points, the abscissae of which are the values of the permeability K^k_{per}, determined from the core, and the ordinates — the corresponding values for the coefficient of increase in resistance Q. For the values of Q were taken those values which were used in calculating the errors given in Table 1. The points are divided into two groups; one group (marked on the graphs with circles) includes points for which the values of the permeability were not very accurate (small number of cores, for which the permeability was measured; a large difference in the results); the other group (black) includes points for which the values of the permeability were determined with a sufficiently high degree of reliability. On each of the graphs an "empirical" curve for the dependence of the coefficient of increase in resistance Q on the permeability K_{per} was drawn through the points. This is done in the following way: the abscissa is divided into a number of separate intervals and for each of them

the most probable value for the coefficients of increase in resistance (the value with respect to which a half of the points has the greatest, and a half, the least value of Q) is determined. Through the points corresponding to these average values is drawn, with a certain amount of averaging, the curve $Q = f(K_{per})$.

On the graphs, the dotted curves give the probable deviations* ("probable error") of the coefficient of increase in resistance from its value corresponding

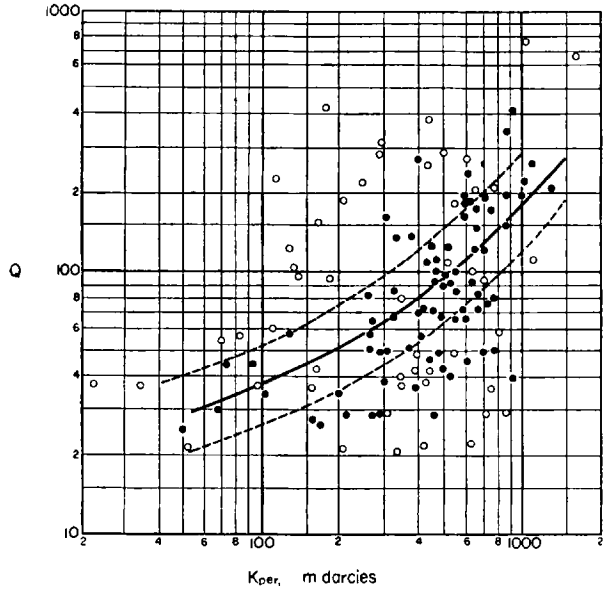

FIG. 5. Comparison of the ceofficient of increase in resistance Q with the values of the permeability K_{per} Tuimazinsk deposit, stratum D_I.

to a given permeability according to the curve $Q = f(K_{per})$. These curves are drawn so that between each of them and the curve $Q = f(K_{per})$ there is a quarter of all the points on the graph.

Similar comparisons were carried out for the D_{II} stratum of the Tuimazinskian deposit and also for the D_{Ib} and D_{Ic} strata of the Romashkinskian deposit and the stratum D_V of the Sokolovogorsk location.

The actual curves for the dependence of the coefficient of the increase in resistance of the permeability for the given regions are shown in Fig. 6.

* The probable deviation is conditional by the fact that for a half of the cases the deviation is greater, and for the other half smaller than the probable.

An opinion is widely held [13, 14, 19], that the residual water saturation, and consequently the coefficient of increase in resistance depend on the porosity of the stratum. In connection with this it is interesting to compare the values for the coefficient of increase in resistance against the permeability and also the porosity of the stratum. However, a comparatively small number of points, related to a small number of wells, where the cores were selected, and the wide scatter of the points does not allow this. It should be noted that in view of the comparative homogeneity of the strata and the

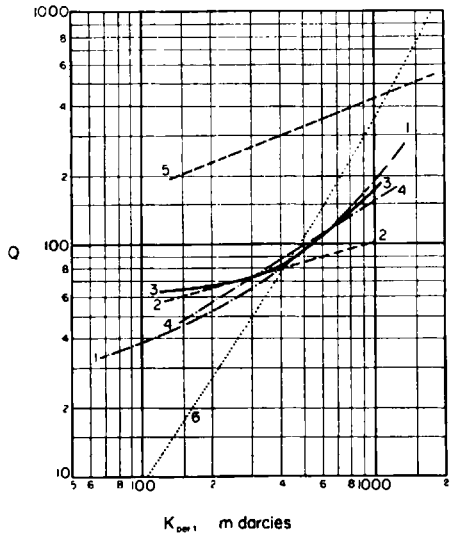

FIG. 6. Empirical curves for the dependence of the coefficient of increase in resistance Q on the permeability $K_{per.}$ 1—Tuimazinskian deposit, stratum D_I; 2—Tuimazinskian deposit, stratum D_{II}; 3—Romashkinskian deposit, stratum D_{Ib}; 4—Romashkinskian deposit, stratum D_{Ic}; 5—Sokolovogorsk deposit, stratum D_V; 6—DOLINA curve.

small change in porosity, a large change in the coefficient of increase in resistance on the porosity cannot be expected in practice. This is illustrated in Fig. 7 where for the D_I stratum of the Tuimazinskian deposits, points are given separately for the large and small values of porosity. In both cases, the regularity of distribution of points differs little from that given in Fig. 5 where points are given without considering the porosity of the stratum.

The method for determining permeability by the specific resistance, developed for the Devonian sandstones, of other regions (petroleum-bearing strata of the Groznyi, Turkmen, Baku, Krasnodar and other deposits) led

to values which did not correspond to the actual values for the permeability (Table 4).

This is due to the fact that the most probable values for the coefficient of increase in resistance of a number of deposits is much less than the most probable value of the coefficient of the increase in resistance for the Devonian sandstone of the Bashkirian and Tatarian deposits (Fig. 8).

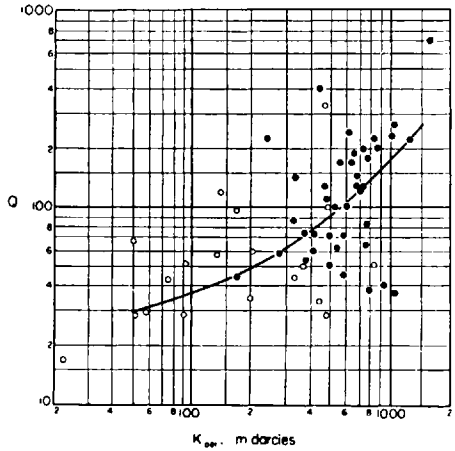

FIG. 7. A comparison of the values of the coefficient for the increase in resistance with permeability for different porosities. Tuimazinskian deposit, stratum D_I. Circles—porosity up to 19%; black points—porosity above 22%; the curve corresponds to the dependence $Q = f(K_{per})$ for the D_I stratum (according to Fig. 5).

The following conclusions can be drawn from a consideration of Figs. 6 and 8.

1. For different strata there are different curves for the dependence of the coefficient of increase in resistance on the permeability. Even for the Devonian sandstone, and in the same oil field the difference between the curves $Q = f(K_{per})$ is so great that for each stratum, it is necessary to use its own curve for the dependence of the coefficient of increase in resistance on the permeability.

The reasons for the difference between the curves $Q = f(K_{per})$ for different strata are:

(a) The difference in the values for the interstitial water saturation of separate strata and in the character for the change in the interstitial water saturation on the permeability;

(b) The absence of a unique dependence of the coefficient of increase

TABLE 4. A COMPARISON OF THE MOST PROBABLE VALUES FOR THE PERMEABILITY K^0_{per}, DETERMINED FROM THE SPECIFIC RESISTANCE, WITH THE AVERAGE VALUES OF THE PERMEABILITY K^k_{per} OBTAINED FROM THE CORE (FROM EXISTING DATA)

Deposit	Stratum	Probable values for the coefficient of increase in resistance	K^0_{av} from Dolina curve	K^k_{av} from cores
Tuimazinskian	D_I	80	500	510
Tuimazinskian	D_{II}	90	380	420
Shkapovskian	D_I	60	395	490
Romashkinskian	D_{Ib}	85	580	550
Romashkinskian	D_{Ic}	110	480	585
Sokolovogorsk	D_I	500	635	738
Turkmenia	—	5	70	—
Groznyi	—	4	50	150
Baku	—	8	80	300
Perm	—	10	100	350

in resistance on the interstitial water saturation, as a result of which, for approximately the same value of water saturation, there are different values for the coefficient of increase in resistance.

The latter is confirmed by the sharp change in the most probable values

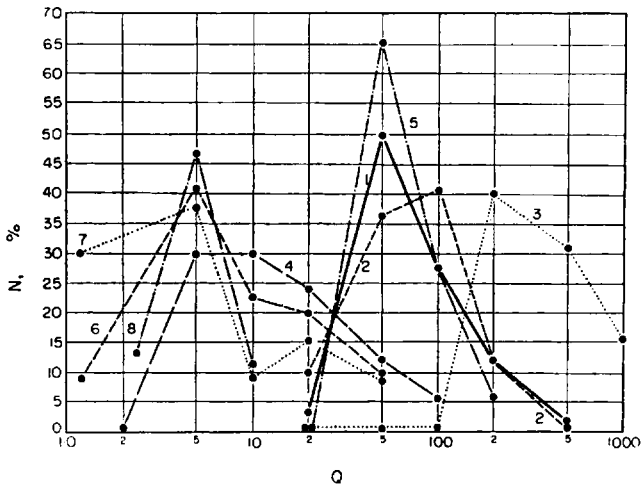

FIG. 8. Curves of the distribution of coefficients of increase in resistance Q. (N—percentage of values of Q corresponding to the interval of changes). 1—Tuimazinskian deposit, strata D_I and D_{II}; 2—Romashinskian deposit, stratum D_I; 3—Sokolovogorsk deposit, stratum D_v; 4—Perm Priural'e; 5—Shkapovskian deposit, strata D_I and D_v; 6—Baku, productive stratum; 7—Groznyi, sandstones of the Karagano-Chokrakskian deposits; 8—Nebit-Dag deposits; Turkmen.

of the coefficient of increase in resistance for petroleum strata of different deposits (see Fig. 8).

2. The curves proposed for the Devonian sandstones for the dependence of the coefficient of increase in resistance on the permeability [3, 4, 13, 14] differ considerably from the actual curves (Fig. 6). As a result, in the determination of permeability from the specific resistance using the DOLINA curve or similar curves (see Figs. 2 and 3) there is a large systematic error, considerably distorting the results (see Fig. 4).

The main error which is introduced in establishing a connection between the coefficient of increase in resistance and the permeability, consists of the fact that the effect of the permeability on $K_{r,w}$, and consequently, on Q; is over-read. In other words, it is assumed that the coefficient of increase in resistance is connected with the permeability by the relationship:

$$Q = \beta K_{per}^{q}$$

where q is a very large value.

Thus, according to DAKHNOV $q \approx 1$, according to DOLINA $q = 1.56$, according to MOROZOV $q = 2$. In actual fact, as follows from the curves given in Fig. 6, $q = 0.3$–0.66.

Of the curves $Q = f(K_{per})$ suggested for the Devonian sandstones the closest to actuality of the empirical curves is the DAKHNOV curve (2 on Fig. 2), although it also differs considerably from them.

3. It can be seen from Fig. 5 that the connection between the coefficient of increase in the resistance and the permeability are insufficiently close. Therefore, even with the help of the curve $Q = f(K_{per})$ there is a considerable error in determining the permeability from the specific resistance. Table 5 gives the probable and mean square errors in the separate determinations of permeability from the specific resistance using empirical curves $Q = f(K_{per})$ for a number of strata.

The probable error is calculated directly from Fig. 5 and from similar curves for other regions (the distance along the abscissa between the dotted and continuous curves), the mean square error was taken as 1.48 of probability [17, page 180].

The error in determining the permeability from the specific resistance even in the most favourable case is high (35–50%).

In some cases, for example, when the coefficient of increase in resistance changes little with variations in permeability (a small slope of the curve $Q = f(K_{per})$ relative to the abscissa axis), the error is so great that the determination of permeability from the specific resistance loses all meaning; as for example, for the D_V stratum of the Sokolovogorsk deposit.

TABLE 5. ERRORS IN THE DETERMINATION OF PERMEABILITY FROM EMPIRICAL CURVES $Q = f(K_{per})$

Deposit	Stratum	Errors as fractions of the true value of permeability		Errors obtained in the case when the permeability is taken as the mean value for the stratum	
		Probable	Mean square	Probable	Mean square
Tuimazinskian	D_I	1.3—0.5	1.9—0.74	0.4	0.6
Tuimazinskian	D_{II}	1.5	2.2	0.29	0.43
Romashkinskian	D_{Ib}	1.2—0.4	1.8—0.6	0.37	0.55
Romashkinskian	D_{Ic}	0.35	0.50	0.3	0.45
Sokolovogorsk	D_V	1.8	2.7	0.48	0.71

A comparison of the error in determining the permeability of the stratum from the specific resistance, using the empirical curves $Q = f(K_{per})$ with the errors which are obtained when, for the permeability of the stratum in a given well, the mean value of the permeability for the stratum (see Table 5) is taken, shows that the method of determining permeability from the specific resistance is insufficiently accurate and not very effective.

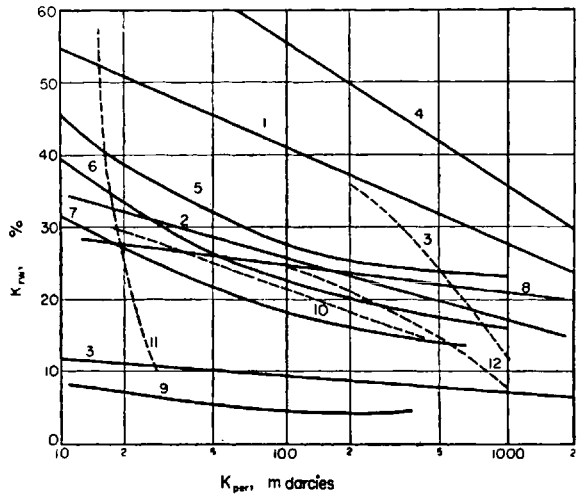

FIG. 9. Interstitial-water content K_{rw} in the rocks of different permeability K_{per} from the results of studies of samples. 1, 2, 3—the proposed value for fine grain sandstones, medium grain sandstones, dolomites and limestones, respectively, according to JONES[7]; 4–9—for different deposits in the U.S.A. from the data of MASKET[12]; 4–7—sandstones; 8—limestone; 9—dolomite; 10—Kartashevo deposit, limestone; 11—Novo-Stepanovsk deposit, dolomites (indirect determination); 12, 13—sandstones, Tuimazinskian deposit, I and II groups; (10–13 according to the data of ZAKS[8]); 10, 12, 13—determined by the method of capillary displacement.

4. Starting from erroneous notions on the high accuracy of determining permeability from the specific resistance of the Devonian sandstone, incorrect conclusions were drawn as to the most favourable possibilities of this method for the Devonian sandstones in comparison with other sediments. It is obvious however, that the method for determining permeability from the specific resistance in other deposits will give the same results as in the Devonian sandstones, and that there is apparently no reason to limit the field of application of the method.

In any case, this problem should always be solved separately for each stratum and independently of the type of deposit and the region.

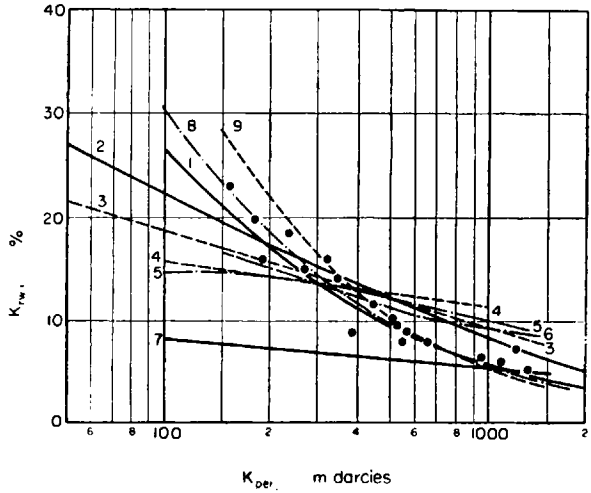

FIG. 10. Curves for the dependence of the coefficient of residual water saturation $K_{r.w}$ on the permeability K_{per}. 1—according to the DOLINA curve (1—curve from Fig. 2); 2—from the Dakhnov curve (2—curve from Fig. 2); 3–7 from the empirical curves of the dependence of Q on the permeability K_{per} (Fig. 6); 3—Tuimazinsk deposit, stratum D_I; 4—Tuimazinskian deposit, stratum D_{II}, 5—Romashkinskian deposit, stratum D_{Ib}; 6—Romashkinskian deposit, stratum D_{Ic}; 7—Sokolovogorsk deposit, stratum D_V; 8—from experimental data by Morozov, obtained from samples of the Devonian sandstone (results of separate measurements are given by points); 9—from the curves of Morozov for porosity $m = 0.2$[13].

ESTABLISHING THE CONNECTION BETWEEN THE COEFFICIENT OF INCREASE IN RESISTANCE AND THE PERMEABILITY

To use the method of determining permeability from the specific resistance, it is essential first of all to establish the connection between the interstitial water saturation and the permeability.

Fig. 9 gives some results on the interstitial water saturation of rocks of

different permeabilities. The curves *1–3* are well-known curves of JONES[7], the curves *4–9* were constructed by MASKET[12], the other curves were taken from the work of ZAKS[8].

Fig. 10 shows the curves for the dependence of the residual water saturation on the permeability, drawn from the curves for the dependence of the coefficient of increase in resistance on the permeability.

The curves are drawn from the data of Figs. 2 and 3 and the actual curves $Q = f(K_{per})$ (Fig. 6).

The value of thecoefficient of interstitial water saturation $K_{r.w}$, was determined from the coefficient of increase in resistance Q from the formula

$$K_{r,w} = \frac{1}{\sqrt{Q}}.$$

For the curves *1* and *2* of Fig. 2 the interstitial water saturation was determined from the curves proposed by DAKHNOV and DOLINA $Q = f(K_w)$ [4, 3].

A comparison of the curves on Figs. 9 and 10 shows that the values obtained when studying samples for the interstitial water saturation (Fig. 9) differ considerably from the so-called empirical value of the interstitial water saturation, with which we start in determining permeability from the specific resistance (Fig. 10)*.

Let us note that methods of determining the interstitial water saturation lead to different results. The data for the interstitial water saturation obtained by analysing cores, cannot be used to establish the dependence of the coefficient of increase in resistance on the permeability†.

It follows from Fig. 10, that the residual water saturation for different rocks has a different value. This is in full agreement with our conclusion reached above that each stratum should have its own curve $Q = f(K_{per})$. The curves for the dependence of the coefficient of increase in resistance on the permeability, which are necessary to determine the permeability from the specific resistance, should be constructed for each stratum from the results of comparing the actual coefficient of increase in resistance with the values of permeability obtained in the study of cores, as was done for example, in Fig. 5. Since the connection between these values is insufficiently close, it is necessary to have a sufficiently large number of results (large number of points), at the same time bearing in mind the porosity of the strata.

* An exception is provided by the experimental results of MOROZOV (*8* on Fig. 10), casting some doubt in this connection.

† Furthermore, in deducing from the interstitial water saturation the coefficient for increase in resistance an extra error would be introduced which would lead to a decrease in the accuracy of the curve $Q = f(K_{per})$.

The obtained curve $Q = f(K_{per})$ should be considered from the point of view of the possibility of using it to evaluate the permeability from the specific resistance, since there can be cases when, due to the wide scatter of the points or the small inclination of the curve $Q = f(K_{per})$, it cannot be used to evaluate the permeability from the specific resistance with acceptable accuracy. On the basis of what has been said above, we conclude that the determination of the permeability of the stratum from its specific resistance in any single bore-hole is undesirable for the following reasons:

(a) A preliminary curve for the dependence $Q = f(K_{per})$ is necessary and can only be obtained if, after the appropriate treatment there is sufficient material on the permeability of the stratum for individual bore-holes.

(b) The results may contain considerable errors, due to the incorrect calculation of the coefficient for the increase in resistance (errors in the determination of the specific resistance of the stratum and the stratum water, the evaluation of porosity of the stratum and the relative resistance), as well as errors connected with the influence of the water-petroleum contact.

There is a probability of a considerable increase in the number of incorrect conclusions for individual bore-holes, (at the present time, generally speaking, comparatively small) due to a large error in the results for determining permeability. It is apparent, however, that in the interpretation of material for geophysical studies of single wells, it is useful to compare the obtained value of the coefficient of the increase in resistance with its values for the wells where the permeability of the stratum is known and to consider it in the interpretation.

The method of evaluating permeability from the specific resistance is applicable in determining the mean value of permeability for the whole stratum.

The above conclusions are based on a comparison of data obtained from the material of geophysical investigations of wells with the results of core analysis. Opinion exists that derived comparison of the results for the determinations of the reservoir properties of the strata obtained in the course of geophysical studies, with the data of core analysis are not convincing and do not make it possible to define the accuracy of the determinations of reservoir properties of the strata from geophysical results, since cores do not characterize a stratum as a whole, and their properties can differ considerably from those of the stratum.

In actual fact, the accuracy of the determination of the reservoir properties of the strata from measurements on samples is relatively high and even with a small number of cores from the stratum they give a more accurate idea of the properties of the stratum than geophysical data. Furthermore,

it should be remembered that the methods for determining reservoir properties of the strata from geophysical data, on the whole or for separate stages, are based on a comparison of the geophysical data with the results of core analysis. Thus, from the very start we assume that the true properties of the strata are characterized by the core.

Evidently the data of core analysis characterize the actual permeability of the stratum sufficiently well and therefore the result of comparing them to the permeability obtained from the specific resistance is very important. This is confirmed by the following:

(a) the small difference in the values of the mean and mean square errors in determining the permeability from the specific resistance for a different number of cores from the stratum (Table 6);

(b) the more or less identical mean values for the permeability of the stratum obtained from the data of core analysis and determinations of specific resistance.

The permeability of a stratum can be determined from the results of logging. It is necessary to compare the results for determinations of permeability from the specific resistance with values for the permeability obtained from the logging data.

THE BASES OF THE METHOD FOR DETERMINING THE PERMEABILITY FROM THE SPECIFIC RESISTANCE

Opinion exists that separate strata (for example the Devonian sandstones) have a close (approaching the functional) connection between the interstitial water saturation of the oil-bearing layers and their permeability. A conclusion is therefore drawn suggesting the possibility of the method of determining permeability from the specific resistance (3, 4, 13). However, of the actual data confirming the existence of a close connection of the interstitial water saturation with the permeability, there are only the experimental data of Morozov (see Fig. 10) which, however, are clearly insufficient to prove this affirmation.

More widespread is the point of view, according to which the interstitial water saturation is a complex function of a number of factors and that therefore a close connection cannot be expected between the interstitial water saturation and permeability.

Thus, according to KOTYAKHOV (9, page 110), although a general tendency is observed of the increase in water saturation in the oil-bearing strata with the decrease in their permeability, there is no single and universal connection between the residual water saturation and permeability of the rocks. Further-

TABLE 6. A COMPARISON OF THE RESULTS OBTAINED FOR DIFFERENT NUMBERS OF CORES FROM THE STRATUM

Indices	Tuimazinskian deposit D_I					Romashkinskian deposit D_{Ib}				
	No. of cores					No. of cores				
	1	2	3	More than 3	Mean	1	2	3	More than 3	Mean
No. of wells	16	16	19	46	97	6	3	4	20	33
Data of core analysis:										
mean value of permeability, (millidarcies)	610	400	390	510	485	350	625	460	590	550
mean deviation, (millidarcies)	300	285	185	185	210	110	200	145	250	270
%	50	70	47	36	44	36	30	35	50	45
mean square deviation, (millidarcies)	390	370	240	240	270	170	270	184	310	275
%	64	90	60	48	59	50	43	42	65	57
The values of permeability determined from the specific resistance (according to Dolina):										
mean value, (millidarcies)	615	455	440	450	475	530	400	480	520	510
mean error, (millidarcies)	210	230	205	185	127	250	250	165	200	200
%	60	120	100	40	65	90	29	40	40	46
mean square deviation, (millidarcies)	300	310	290	240	260	285	495	235	290	240
%	110	170	180	60	117	122	55	60	65	70

more, even in rocks of one category, there is no single dependence between the water saturation and permeability. According to KOTYAKHOV, the content of buried water in the strata depends not only on the physical properties of the rocks, but also on other factors, the most important being the "conditions of expulsion of water from the reservoirs by petroleum and gases, and also the physical and physico-chemical properties of the petroleum, water and gas". In this connection, Kotyakhov considers that "it is incorrect to determine the permeability of the rocks from the data of water saturation and specific electrical resistance" [9].

In Baku in recent years a considerable amount of work has been done on the study of interstitial water saturation. These results are given more fully by BABALYAN [2]. This work indicates that the interstitial water saturation increases with the decrease in permeability. However, the degree of activity of the petroleum and the type of stratum water has a considerable effect on the

value of the interstitial water saturation. Analogous opinions are also held by AVANESOV[1]: "The interstitial water saturation can be different both in the type of water and the quantity of the pore content, which is conditioned by the capillary and adsorption phenomena, and also by the physical properties of the liquids, the rocks and the structural features of the reservoirs".

It follows from these remarks that the structural features of the reservoirs, including the permeability, usually play a less important role than the properties of the petroleum, the stratum water and the adsorption phenomena. This is illustrated by results on the residual water saturation (Fig. 11), recommended by BABALYAN for practical use.

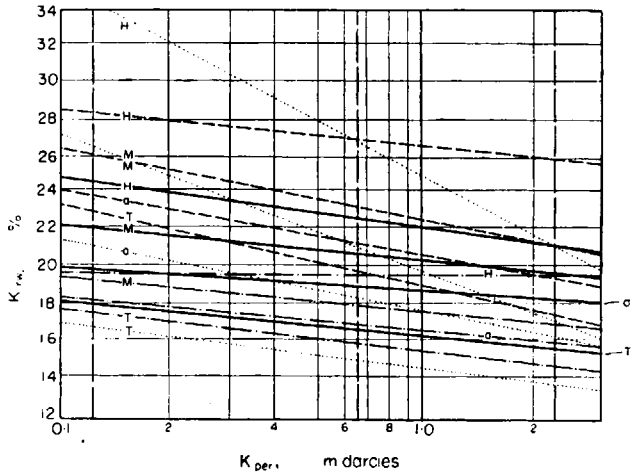

FIG. 11. Curves for the dependence of coefficient of residual water saturation $K_{r.w}$ on the permeability K_{per} for sandstone (from the data of (2)). The rock was saturated with fresh (tap water) *T*, distilled *D*, laboratory alkaline *A* and stratum alkaline (water of the PK suite) *S* water; the extraction was carried out with inactive, *i*, low active *l*, active *a* and highly active *h* petroleum (petroleum with different content of polar impurities).

JONES[7] and MASKET[12], indicating the decrease in water saturation of petroleum-bearing strata with increase in their permeability, observed that this connection does not have a general character. According to MASKET "the value of the water saturation in the oil-bearing rocks changes within wide limits for different reservoirs, even if their physical characteristics (for example, porosity and permeability) are close to one another". However, for individual rock types MASKET admits the possibility of a closer connection between the interstitial water saturation and the permeability and also

the possibility of some practical use for it. For example, this can be done in evaluating the total mean water saturation of a reservoir under the condition of established distribution of the permeability.

WYLLIE and ROSE [19] suggested the determination of permeability of petroleum-bearing strata from the specific resistance and gave formula [13] which expresses the dependence of the residual water saturation on the permeability. However, this method has not been used. WALSTROM [18] justifies this in the following way: "It is possible to evaluate the lower limit of the mean permeability from the interstitial water saturation and the relative resistance, obtained from data of electrical logging. In exploratory drilling, however, the relative resistance is determined from the core taken from the productive sandstones, in which the permeability can be measured directly. Consequently, it is not necessary to try to determine permeability from the data of electrical logging, since cores must be used for this.

"Tiks'e shows that at the present time there is no method of logging which would make it possible to determine the permeability of rocks cut in a borehole" [16, page 349].

The data given fully agreed with the conclusion which we obtained in testing the method for determining permeability from the specific resistance.

Let us consider the possibility of determining permeability from the specific resistance from another point of view.

It is generally known that the permeability varies considerably along the stratum and over wide limits. This is readily supported by the large differences in the values of permeability of separate cores from the stratum. Fig. 12 shows a core diagram illustrating the sharp change in permeability along the stratum.

In contrast to this, the curve for the resistance against the petroleum-bearing stratum differs comparatively gently; it does not have any sharp changes of apparent and specific resistances, typical of changes in permeability. The deviations of the curve of resistance against the petroleum-bearing stratum are caused by the form of the resistance curve against the high resistance strata. This serves as an indirect indication of the fact that the change in permeability of the stratum is not reflected in the variations of the specific resistance and that between the permeability, the interstitial water saturation and the coefficient of increase in resistance there is no direct unambiguous connection. Thus, the shape of the resistance curves indicates unfavourable conditions for using the specific resistance method in measuring the permeability.

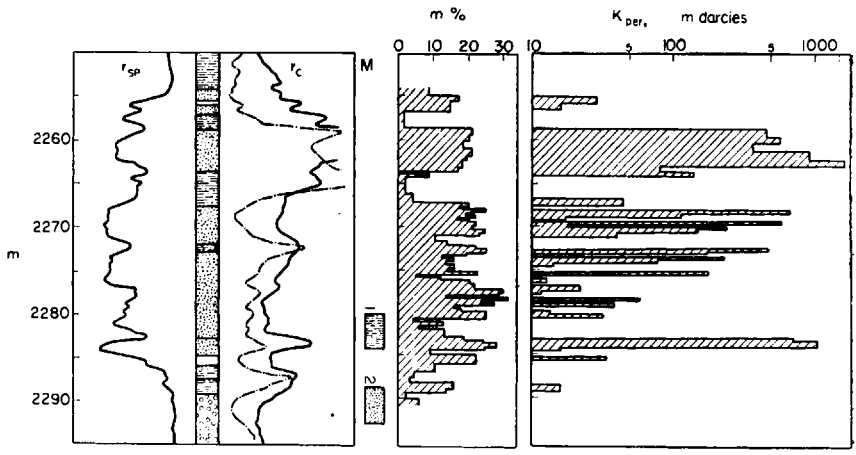

FIG. 12. Core diagram of a part of a typical sand-clay cross-section (Chili)(20, page 97). 1—clay; 2—sandstones.

It should be noted that if from the data of electrical logging, it would be possible to determine a certain mean permeability of the stratum, it cannot necessarily be considered sufficiently characteristic of the stratum. Thus neither fractures nor the very thin beds, including some which are very permeable, are depicted on a log. On the other hand, the clayey beds show a greater effect on the resistance curve than on the permeability data of the stratum. Therefore, the obtained mean value of permeability gives an insufficiently accurate idea on the permeability of the stratum, which is determined by a few very permeable members.

As a result of what has gone before a method can be recommended for determining the permeability from the specific resistance in accordance with instructions which are given below, instead of conclusions.

METHOD FOR DETERMINING PERMEABILITY OF PETROLEUM-BEARING STRATA FROM THE SPECIFIC RESISTANCE

1. The method for determining the permeability of petroleum-bearing strata from the specific resistance is based on the presence of a connection between the interstitial water saturation and the permeability. It is also assumed that the water saturation of the petroleum-bearing stratum, determined from the data of an electrical log, corresponds to the interstitial water saturation.

2. To use the method of determining permeability from the specific resistance for any bed, it is necessary to construct for this stratum the curve

of the dependence of the coefficient of increase in resistance Q on the permeability K_{per}. This is done in the following way:

(a) For all wells in which cores of the given stratum were selected and the permeability determined, the mean values of the permeability and the coefficient of increase in resistance are determined.

(b) Points, the coordinates of which correspond to the average value of the permeability K_{per} and the coefficient of increase in resistance Q obtained from each of the wells are plotted on logarithmic paper.

(c) The axis which has the values of permeability, is split up into intervals (for example, 10–20, 20–50 etc.) and for each interval the most probable value of Q is found (that value, with respect to which a half of the points in the given interval is above, and half below); this value is carried on to the middle of the interval;

(d) From the points obtained in this way and with some averaging (to obtain a smooth curve) a curve is drawn for the dependence $Q = f(K_{per})$.

In order to obtain the curve $Q = f(K_{per})$ with sufficient accuracy, the number of points on the graph should be sufficiently large (not less than 15).

On both sides of the main curve $Q = f(K_{per})$ auxiliary curves are drawn so that between them and the main curve there is a quarter of the total number of points on the graph. The distance from the main curve to the auxiliary curve in a direction parallel to the K_{per} axis gives the probable error in the results of determining the permeability.

3. To determine the permeability from the specific resistance the coefficient of increase in resistance, Q, is found, and then from the curve $Q = f(K_{per})$ for a given stratum, the corresponding value of permeability K_{per} is calculated.

4. In principle the method for determining permeability from the specific resistance is applicable only to those cases where the petroleum-bearing stratum is at a distance from the upper surface of the petroleum reservoir and where this stratum has no bottom water or an intermediate zone (the transition zone from the purely petroleum to the purely water part of the stratum).

The method of determining permeability from the specific resistance of the strata containing an intermediate zone in the upper part is applicable only to thick strata provided:

(a) It is separated from the water-bearing part by a bed of clay;

(b) It is at a considerable (for example, more than 10 m) distance along the vertical from the upper surface of the water.

Usually the error in the determination of permeability from the specific resistance is 30–50% and greater. For some strata the error is so great that

the values obtained for the permeability are of no practical interest. As a rule, the values for the permeability from the specific resistance are obtained with less accuracy than the values selected using the mean values of permeability for the strata.

The main area of application of this method is in studying the distribution of permeability over a stratum as a whole. The preliminary processing of the material makes it possible in this case to improve the accuracy of certain original assumptions (the resistance of the stratum with 100% filling of its pores with water, the position of the water — petroleum contact, etc.) and to exclude the possibility of large errors arising due to this. In processing the data for separate wells, deviations appear between the obtained values of permeability and the actual value of permeability.

In view of the insufficiently high accuracy of the results, it is not advisable to use this method in individual wells when they are in the process of being drilled.

REFERENCES

1. E. T. AVANESOV, The Role of water saturation in the Mechanism of Reservoir Yield. *Trudy AzNII DN No. 2*, Aznefteizdat, (1955).
2. G. L. BABALYAN, *Problems of the Mechanism of Petroleum Yield.* Aznefteizdat, (1956).
3. V. N. DAKHNOV, *The Interpretation of Results of Geophysical Studies of Wells.* Gostoptekhizdat, (1955).
4. L. P. DOLINA, *The Determination of Petroleum Saturation and Permeability of Devonian Reservoir, from the Specific Resistance.* Temporary instruction. Documents of the VNII geofizika, (1955).
5. L. P. DOLINA, *The Study of Reservoir Properties of Strata from the Data of Electrical Logging.* Report on the topic No. 421. Documents of the VNII geofizika (1954).
6. L. P. DOLINA, *Improving the Method of Studying the Reservoir Properties of Productive Strata from the Data of Industrial-Geophysical Studies.* Report on the topic No. 531. Documents of the VNII geofizika, (1955).
7. P. D. JONES, *Mechanics of a Petroleum Stratum.* Gostoptekhizdat, (1947).
8. S. O. ZAKS, The method of studying the connate waters in the oil reservoirs. Proceedings of the Conference on the Development of Research in the Field of Secondary Methods of Petroleum Exploitation. *Izv. Akad. Nauk AzSSR*, (1953).
9. F. I. KOTYAKHOV, *The Principles of the Physics of a Petroleum-bearing Stratum.* Gostoptekhizdat, (1956).
10. S. G. KOMAROV, Determining the porosity specific resistance. *Appl. Geophysics* No. 14, Gostoptekhizdat (1955).
11. S. G. KOMAROV, *et al.*, *Improving and Introducing Methods for Determining the Reservoir Properties of Strata from Geophysical Data.* Account on the Topic No. 132. Documents of VNIIgeofizika, (1956).
12. M. MASKET, *Principles of the Technology of Petroleum Exploitation.* Gostoptekhizdat, (1953).

13. G. S. Morozov, Methods for studying the reservoir properties of the Devonian sandstones from the data of electrical logging. *Uch. zap. Kaz. gos. universiteta im. Ul'yanov-Lenin.* Geology, Volume 114, Book 7 (1954).
14. S. A. Sultanov, *The Analysis of Data of Industrial and Geophysical Studies of Well Sections in Order to Study the Reservoir Properties and the Petroleum and Water Saturation of Productive Deposits in the Devonian of the Western Bashkiria and Eastern Tataria.* Thesis. Documents of the Moscow Petroleum Institute (1956).
15. L. L. Suslova, *The Study of Reservoir Properties of Productive Horizons in the Devonian of Saratov-Volga Basin from the Data of Industrial and Geophysical Studies.* Report of a party on the topic No. 132. Documents of VNII geofizika, (1956).
16. M. P. Tiks'e, *The Determination of Permeability of Rocks Revealed in Well Drilling.* IV International Petroleum Congress, Vol. 2, Geophysical Methods of Prospecting. Gostoptekhizdat (1956).
17. K. P. Yakolev, *Mathematical Treatment of the Results of Measurements,* Gostoptekhizdat (1953).
18. J. E. Walstrom, The quantitative aspects of electric log interpretation, *Transactions AIME,* Vol. 195 (1952).
19. M. R. J. Wyllie, W. D. Rose, Some theoretical considerations related to the quantitative evaluation of the physical characteristics of reservoir rock from electrical log data. *Petroleum development and technology, Apr.,* Vol. 189 (1950).
20. A. I. Levorsen, *Geology of Petroleum.* Freeman Co., San Francisco, (1956).

CHAPTER 16

NEW TYPES OF WELL RESISTIVITY-METERS

E. A. POLYAKOV

THE specific electrical resistance of the drilling fluid (water solution of salts or a mud suspension which fills a bore-hole) is normally determined with the aid of a well resistivity-meter, of which the principal part consists of a small logging probe. The measurements are made according to a procedure analogous to that used in the electrical resistance logging. The specific electrical resistance ϱ of the drilling fluid is determined according to the following formula

$$\varrho = K\frac{\Delta v}{I}, \tag{1}$$

Where I is the current strength, passing through the feeding electrode A; Δv is the potential measured between the electrodes M and N and K is the resistivity-meter coefficient.

It is usually assumed that the resistivity-meter coefficient remains constant, which is not true in the existing resistivity-meters, since their probe coefficient varies depending on the specific resistance of the drilling fluid, and on the conditions of measurement, and is generally unstable. In determining the specific resistance of the drilling fluid, this circumstance leads to inaccuracies, often reaching 50 per cent.

CAUSES OF VARIATIONS IN THE RESISTIVITY-METER COEFFICIENT

Variations in the resistivity-meter coefficient can be evoked by the following causes.

(1) Changes in the mutual positions of the constituent parts of the resistivity-meter and in the dimensions of the probe.

It is obvious that any change in the mutual positions of the constituent parts of the instrument and of the distances between them leads to a redistribution of the electric field produced by the current electrodes of the probe, consequently causing a change in the resistivity-meter coefficient and therefore errors in the results of measurements. Owing to the shortness

of the sonde, changes in the shape of the electrodes and in the distance between them have an especially considerable influence. In order to ensure the stability of the resistivity-meter coefficient the device should be sturdily constructed and the junctions—and in particular the probe electrodes—should not change their respective positions or size when the apparatus is being used.

(2) Influence of the surrounding medium.

The readings of the open* resistivity-meters are sometimes influenced by the surroundings such as the walls of the well (metal of the cylindrical casing tubes, practically non-conductive rocks of a high resistance, etc.).

Obviously the shorter the probe the less is the influence exerted by the surrounding medium and the possibility of distortion of the results of the measurements.

The following experiments were made in order to determine the length of the probe so that an open resistivity-meter would not reflect the influence of the well walls. A probe with its electrodes on one side of an insulating disc was immersed in a relatively large tank filled with water, then the electrode-bearing surface of the disc was moved towards the water surface, which represented an insulating screen.

When the disc is at some considerable distance away from the screen the latter, naturally, has no influence on the measurements, but as the electrode-bearing disc approaches the screen the readings begin to rise, becoming

TABLE 1. PERCENTAGE DEVIATIONS OF THE READINGS WITH A SCREEN FROM THE READINGS WITH A DISTANT SCREEN.

L—the length of the probe; *H*—the distance from the disc on which the electrodes are placed to the screen (the screen is parallel to the disc). The insulator electrode-bearing disc has a size of 10×20 cm; $AM = 5$ cm, $MN = 5$ cm, the diameter of the electrodes 1 cm; the screen 150×150 cm.

L/*H*	0	0.5	0.6	0.7	0.8	0.9	1	1.2	1.5	2
Deviation with the screen made of insulating material	0	0	1.1	2.6	5.2	8.1	11.5	20.7	38.8	74
Deviation with the screen made of conducting material	0	0	0.74	1.8	3.3	5.2	7.4	12.2	19.6	33
1. Readings increase										
2. Readings decrease										

* The open resistivity-meter is one in which the probe is not protected by a metallic or a non-conducting screen, while the influence of the bore-hole wall is minimized by the use of a short probe situated along the axis of the device.

progressively higher as the movement towards the screen (Table 1) proceeds. Similar observations were made on moving the probe-bearing disc towards a conductive screen. In this case, however, the influence of the screen is demonstrated by the decline of the readings. From Table I it follows that, in order to prevent the bore-hole walls having any influence on the results of the measurements, the probe should be separated from the walls by not less than 1.25 times its size. In such a case the error in the results does not exceed 5 per cent.

The length of the probe in the open resistivity-meter of the type GML BGK (Oufa) equals 25 mm. The container of this resistivity-meter consists of three tension shackles, which have an external diameter of about 60 mm and the probe electrodes can approach the bore-hole walls up to a distance of 25 mm. Consequently, in this resistivity-meter $\frac{L}{H} < 1.25$ the influence of the walls is likely, which is actually recorded in practice.

In order to remove the influence of the well walls the resistivity-meter probe is commonly placed inside a flat cylinder made of a good conductor or insulating material. This, however, interferes with the drilling fluid circulating through the resistivity-meter, when the latter is moved along the bore-hole shaft. As a consequence the usefulness of the instrument is impaired.

(3) Change of the resistivity-meter coefficient depending on the salinity of the drilling fluid.

The coefficients of the bore-hole resistivity-meters in current usage change strongly depending on the degree of salinity of the fluid. This is represented in Fig. 1, which shows the values of the coefficients of certain serial resistivity-meters placed in fluids of variable salinity (curves *2–4*).

Obviously, in this case, the reason for the changes in the resistivity-meter coefficient is due to a rearrangement of the electric field, produced by the changes in the salinity of the fluid. To verify this a water-filled Plexiglas tank of variable resistance was used. The bottom of the tank was covered with a sheet of zinc-plated iron. Observations on the electric field were made with the aid of two small gradient probes, which had common current electrodes (Fig. 2) and were pointing in mutually perpendicular directions x and z. As a result the following equation was determined.

$$\gamma = \frac{\Delta v_z}{\Delta v_x}, \tag{2}$$

where: Δv_z is the potential difference between the electrodes M_z and N_z of the probe placed along the z axis.

Δv_x is the potential difference between the electrodes M_x and N_x of the probe placed along the x axis. (The same current was used).

As a consequence of these observations it was established that the value of γ changes from 7 to 10 with the change of the specific resistance of the fluid from 0.5–20 Ω m, confirming the notion that a rearrangement of the electric field is caused by changes in the salinity of the fluid. In the quoted example, judging from the nature of the change of γ, it follows that, as salinity of the fluid decreases the current-density along the x axis decreases in comparison with the current density along the z axis.

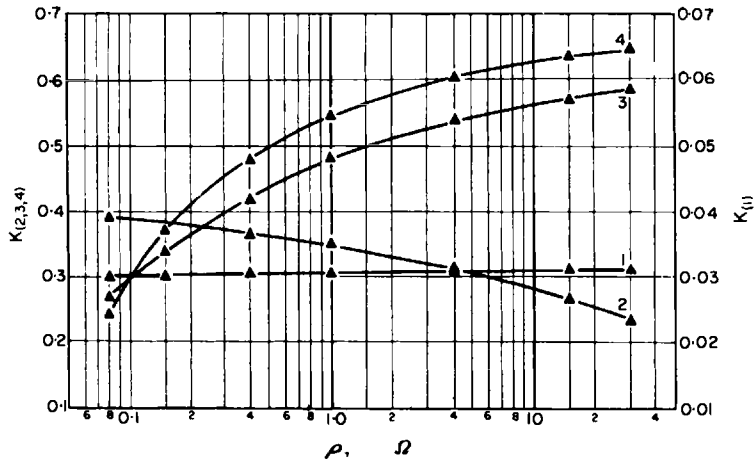

FIG. 1. The dependence of the well resistivity-meter coefficients on the specific electric resistance of the fluid. 1—REU type of resistivity-meter; 2—RA-3 type of a serial resistivity-meter; 3—PTL VOGSGT (Ufa) serial resistivity-meter; 4-GML BGK (Ufa) serial resistivity-meter.

The reason for the rearrangement of the field with the change in the salinity of the fluid should, evidently, be sought in the phenomena which occur at the electrolite-metal interface, and in particular in the so-called contact resistance of this boundary.

The contact resistance is not proportional to the specific resistance of the electrolite and with the decrease in the salinity of the fluid the contact resistance increases much less than the specific resistance. It is this that causes a rearrangement of the electric field consequent upon a change in the specific resistance of the fluid.

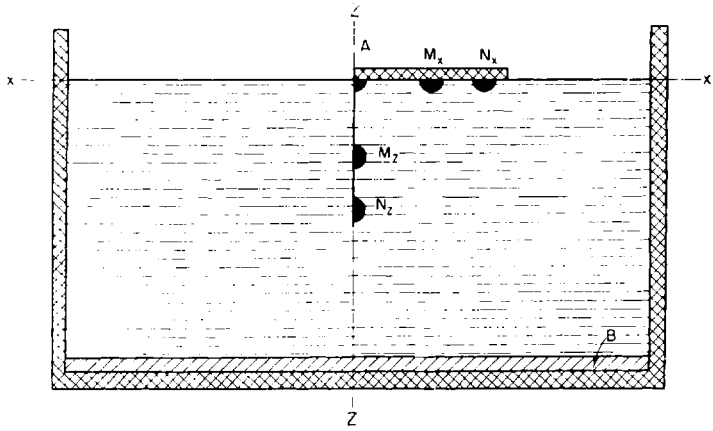

FIG. 2. A scheme of placing of probes in an electrolyte-containing tank in testing the nature of the electric field.

The resistivity-meter and many of its constituent parts are enclosed in a metallic container. Furthermore, certain of the metallic parts are situated in the immediate vicinity of the probe electrodes. As the specific resistance of the drilling fluid alters, the ratio of the contact resistance of the metallic parts to the resistance of the fluid changes as well, bringing about a rearrangement in the electric field of the probe, since with the decrease in the salinity of the drilling fluid the intensity of the electric field grows in the direction of the shortest distance from the metallic parts of the resistivity-meter and *vice versa*. The rearrangement of the field leads to a change in the relative current density and correspondingly to a change in the resistivity-meter coefficient.

It follows from (1) that:

$$K = \frac{I\varrho}{\Delta v}. \tag{3}$$

The potential difference Δv is proportional to the specific resistance ϱ of the fluid, to the distance l between the potential electrodes and to the modulus j being the vector component of the current density at the middle point between the measuring electrodes. Consequently equation (3) can be written as follows:

$$K = \frac{K'}{l} \cdot \frac{1}{j_0}, \tag{3a}$$

where $j_0 = \frac{J}{I}$ is the relative current density.

K' is a certain constant determined by the geometric parameters of the resistivity-meter.

It follows that with a rearrangement of the electric field a change in the relative current density the resistivity-meter coefficient also changes.

The rearrangement of the electric field in a well resistivity-meter with a change in the salinity of the fluid is shown in Fig. 3, where there are shown diagrammatically the lines of force in a resistivity-meter GML BGK placed in a strongly and a weakly saline fluid, respectively.

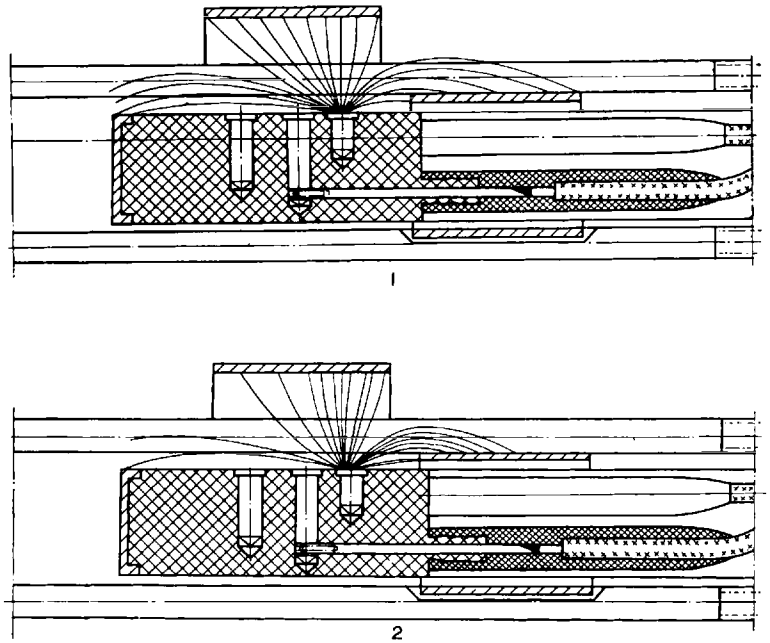

FIG. 3. The distribution of the lines of force in an electric field depending on the salinity of the fluid in a well resistivity-meter GML BGK (diagrammatic plan). 1—in a strongly saline fluid; 2—in a weakly saline fluid.

In a strongly saline fluid the lines of force of the electric field are distributed relatively uniformly. In changing over to the weakly saline fluid, when its specific resistance grows much faster than the contact resistance, the lines of force of the probes electric field become denser in the direction of the shortest distance to the metallic surfaces. This leads to a decrease in current density in the region of the measuring electrodes and consequently to the lowering of the potential difference being measured, thus causing the growth of the coefficient. The considerable increase of the GML BGK resistivity-meter

coefficient with the growth of the fluids resistance is a fact illustrated by the data shown in Fig. 1.

It is necessary to point out that the contact resistance also depends on the purity of the metallic surface concerned. Oxidation and pollution of the metallic parts as well as their corrosion can lead to a rearrangement of the electric field and to a change of the coefficient of the device. This explanation evidently applies to the majority of sharp oscillations of the resistivity-meter coefficient such as are observed in practice. In order to achieve a constant coefficient it is necessary to remove the influence of the instrumental metallic parts on the probe.

SELECTION OF THE ELECTRICAL ARRANGEMENT.

Various probes, differing in their sizes, shapes and mutual positions of the electrodes, will obviously have different degrees of coefficiental inconstancy. By using a suitable probe one can attain a constant resistivity meter-coefficient, and ensure the possibility of getting accurate results in measuring the specific resistance of the drilling fluid.

In order to select the most suitable probe a series of electrical devices involving probes with different shapes of electrodes were constructed and investigated.

The probe electrodes were mounted on ebonite discs. Thus, as is usually done in resistivity-meters, a gradient-probe was used in every instance. Fig. 4 shows some typical electrode devices, which can be divided into three groups.

1. The electrodes are discs in a linear arrangement (*1* in Fig. 4).

2. The measuring electrodes are concentrically arranged rings (*2* and *3* in Fig. 4).

3. The measuring electrodes are rings with loops. It can be considered that a spherical surface with large cut-outs is adopted for one (N) or both (N and M) of the potential electrodes. Consequently, the electrodes of the latter group of devices (*4—8* in Fig. 4) can be called three dimensional.

With the exception of the first device the current electrode is placed in the centre of the rings, which are the potential electrodes of the probe represented by the spheres formed from the loops.

Using these electrode arrangements measurements were made in a tank having (1) a metallic body as the second current electrode B, (2) a body made of insulating material with the second current electrode being represented by a metallic disc at the bottom of the tank. The tank was filled with sodium chloride solutions of varying concentrations. The electrode device

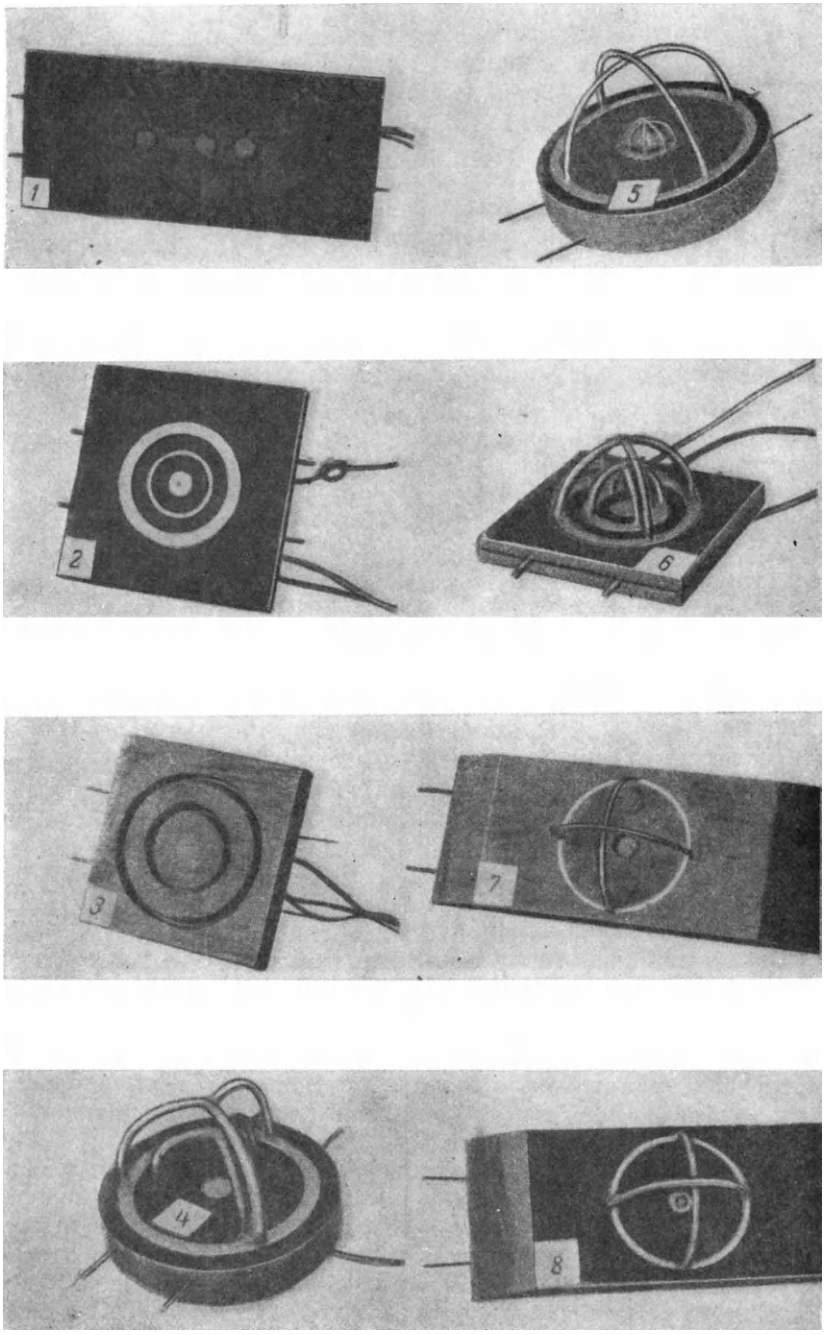

FIG. 4. Diverse types of electrical devices used in investigating their properties.

was placed on the surface of the solution, so that, the probe electrodes were in the liquid, while their leads were in the air.

The results of measuring the electrode coefficients in solutions of different concentrations are given in Table 2. The coefficient for the arrangements 7 and 8 is evidently less than for the other devices.

TABLE 2. PERCENTAGE INCREASE OF THE COEFFICIENTS OF THE ELECTRICAL DEVICES WHEN THE SPECIFIC RESISTANCE IS MEASURED FROM 0.1 TO 20 Ω m

Number of the electrical device	In the tank 1; the coefficient is fixed at 100 per cent at 2050 m	In the tank 2; the coefficient is fixed at 100 per cent at 0.1 m
1	40	18.5
2	34	16
3	20	—
4	50	20
5	25	—
6	31	11.5
7	7	3
8	5	2

To determine the influence of the external medium, changes in the readings of the electrode devices, on approach to a screen of insulating or conducting material, were taken. The results of these observations are given in Table 3.

TABLE 3. THE LEAST DISTANCE FROM THE ELECTRICAL DEVICE TO THE SCREEN WHEN THE INFLUENCE OF THE LATTER IS NOT NOTICED

L—the length of the probe; r—the radius of the outer loop.

Number of the electrical device	Conductive screen		Screen of insulating material	
	Tank 1	Tank 2	Tank 1	Tank 2
1	$0.9L$	$1.35L$	$1.15L$	$1.75L$
2	$1.3L$	$2.0L$	$1.6L$	$2.5L$
5	r*	$1.25r$	$1.1r$	$1.55r$
6	r	$1.45r$	$1.2r$	$1.6r$
7	r	r	r	r
8	r	r	r	r

(*) The screen is brought up to the outer loop.

Table 3 shows that the arrangements 7 and 8 are again the least influenced by the external medium, so that even when the screen touches the loops the readings of these devices do not change.

Obviously 7 and 8 are the most useful of the electrode devices shown on Fig. 4.

The constancy of the coefficient and the small influence of the external medium on these devices are due to the mutual positions of the electrodes A and M (the electrode M is situated on the body of the current electrode) and especially due to the shape of the electrode N. Consequent upon the shape of the electrode N the electric field inside the sphere (outlined by the electrode loops) is stable and is not influenced much by changes in resistance and rearrangements in the electric field outside the sphere. It may appear that the electrodes A and M could be placed at the same point. In such a case, however, the measured potential difference would include the potential drop produced by the contact resistance of the electrode A. This would lead to a large error in the determination of the specific resistance, affecting the constancy of the resistivity-meter coefficient. Thus, in designing a resistivity-meter one should start from a sonde corresponding to the electrode devices 7 and 8.

THE DESIGN OF THE RESISTIVITY-METERS

The well resistivity-meters REU–57 and RSE–3–57* were designed and manufactured on the basis of the most suitable electrode devices. The general shape of the resistivity-meter REU–57 is shown in Fig. 5.

The principal part of this resistivity-meter, which is open, is an electrode device built analogously to the electrode arrangement 8.

The body of the resistivity-meter consists of an upper (*5*) and a lower (*3*) parts connected by three tension shackles (*4*). The electrode device (*1*) is tightened in a holder (*2*) which is welded to the middle of two tension shackles (*9*) with circular cross-sections. In the upper part of the resistivity meter there is a plug bridge (*7*) protected by a cylinder (*6*) and a hood (*8*).

The general shape of the resistivity-meter RSE–3–57 adopted for the bore-hole gear OKS is shown in Fig. 6.

The resistivity-meter consists of an upper (*4*) and a lower (*5*) cap a container with large (75°) longitudinal windows, and a brass tube (*1*) passing through the centre.

The brass tube with the exception of its middle parts is insulated and protected from the body by a rubber insulator (*3*), while its bare part serves as the electrode A. Along a spiral groove of the middle part of the tube lies a live wire (*2*) which is insulated from the tube and serves as a measuring electrode M. The enclosure of the resistivity-meter serves as the electrode N.

To avoid the influence of the terminal parts of the resistivity-meter on

* The construction of the resistivity-meters has been carried out by Ya. A. Magnoushevskaya and L. O. Globus.

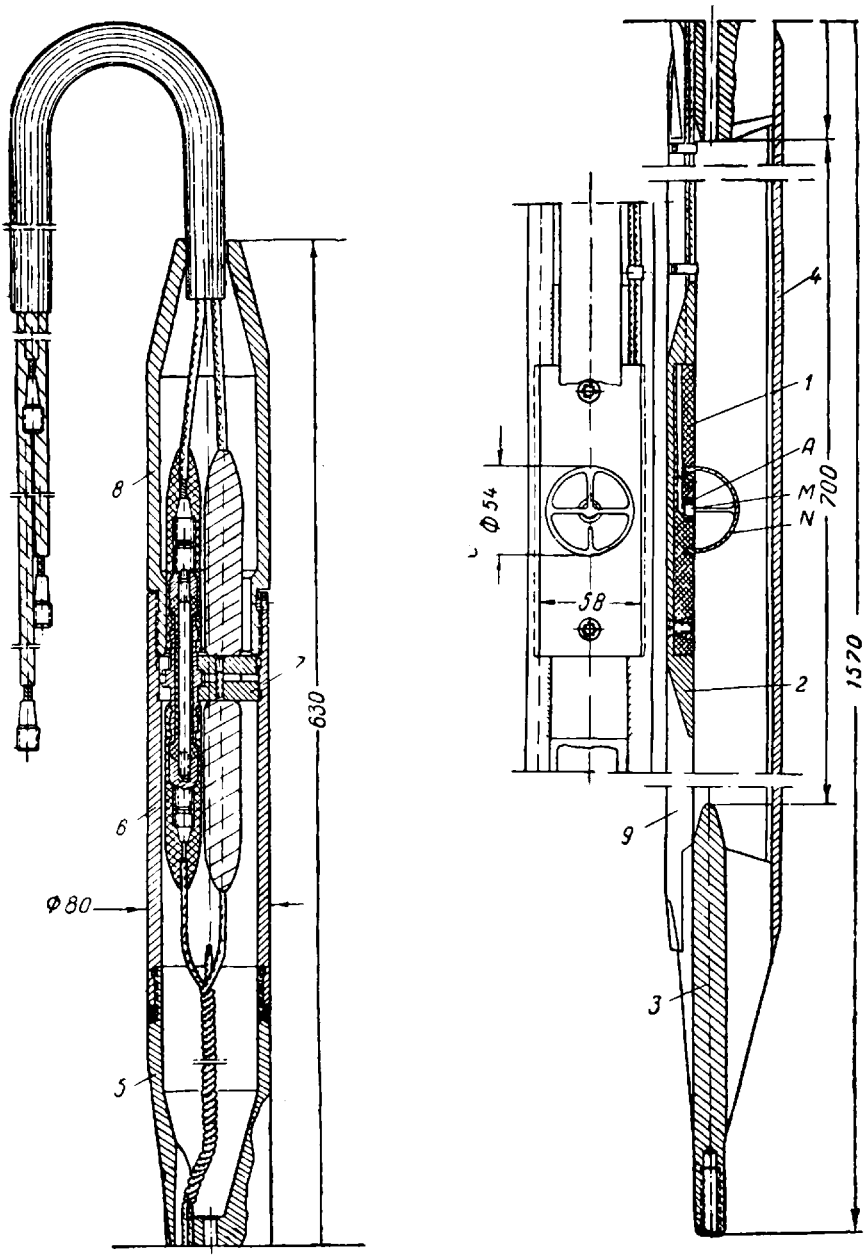

FIG. 5. The well resistivity-meter of the type REU-57.

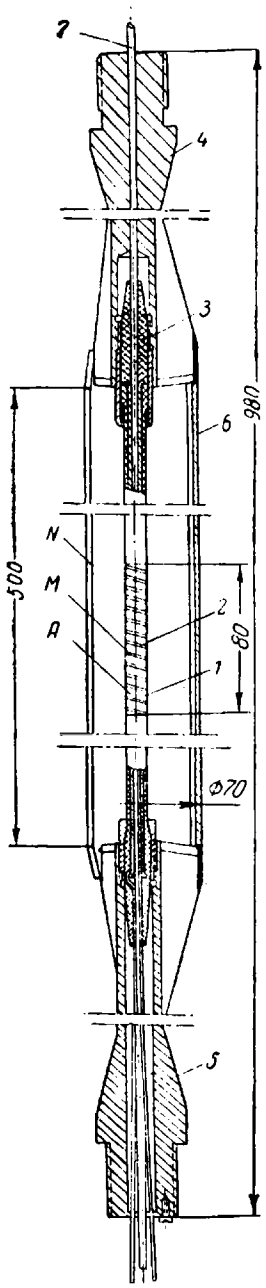

FIG. 6. The well resistivity-meter of the type RCE-3-57.

the electrode device the latter is placed away from the terminations for a distance approximately equal to three diameters of the container.

The upper part of the cap (*4*) has an affixed standard cable head, while the lower cap (*5*) is connected to the probe by a special joint. The resistivity-meter caps have channels through which—as well as through the median brass tube—passes the central strand of the cable.

In the resistivity-meter RSE-3–57 the electrode N again has a three dimensional shape and encloses the electrodes A and M, which are near to each other. As a result the measuring device of this resistivity-meter does not, in principle, differ from the arrangement 8, although superficially they appear to be very different.

In order to avoid dirtying the resistivity-meter by grease and to simplify the circulation of the drilling fluid near the electrode device all the parts of both resistivity-meters are streamlined and any corners which may preclude the motion of the drilling fluid have been eliminated. To stabilize the influence of the metallic parts of the resistivity-meter on the probe the containers and the terminal parts of the instruments are made of stainless steel, and all the instrumental parts are nickel plated to decrease sticking of clay particles. The resistivity-meters RSE–3–57 and REU–57 can be used as independent instruments in the existing logging installations, as well as parts of complex bore-hole devices.

In certain cases it is necessary to alter the terminal parts of their bodies.

Figure 1 shows the results of determining the coefficient of REU–57 in fluids of different specific resistance. It is clear that the REU–57 resistivity-meter coefficient changes much less than the coefficients of the existing resistivity-meters. With the increase in the specific resistance of the fluid from 0.1 to 30 the REU–57

resistivity-meter coefficient changes only by 6 per cent which is quite acceptable.

Investigations of the prototypes of the REU–57 and RSE–3–57 resistivity-meters in bore holes have given good results, the specific resistance of the drilling fluid being accurately determined, the walls not affecting the instrumental readings and the instruments staying clean and uncontaminated by the drilling fluid or grease. Thus the REU–57 and RSE–3–57 resistivity-meters can be recommended for serial reproduction.

CONCLUSIONS

(1) The existing resistivity-meters have an inconstant coefficient, which causes errors in the results of measurements.

(2) The causes of alterations of the resistivity-meter coefficient K are:

(a) Mutual displacement of constituent parts of the resistivity-meter and changes in the size of the probe.

(b) The influence of the surroundings.

(c) Rearrangements of the electric field owing to changes in the fluids salinity, since the contact resistance of the metallic parts of the resistivity-meter has no direct relationship to the resistance of the fluid.

(3) In order to achieve a constant resistivity-meter coefficient its electrode arrangement must have the electrodes A and M near to each other (the electrode M is placed on the current electrode), while the electrode N must enclose the electrodes A and M and must have a three-dimensional shape.

(4) Based on the electrode arrangement described two bore-hole resistivity-meters REU–57 and RSE–3–57 have been constructed. These achieve an accurate determination of the specific resistance of drilling fluid.

CHAPTER 17

THE USE OF ACCELERATORS OF CHARGED PARTICLES IN INVESTIGATING BORE-HOLES BY THE METHODS OF RADIOACTIVE LOGGING

V. M. ZAPOROZHETZ and E. M. FILIPPOV

RECENTLY an increasing number of announcements of research, involving the use of radioactive logging [12, 14] in bore-hole investigations, have been appearing in the overseas periodicals. With us similar studies are also being conducted. Hence, it is timely to discuss certain problems of utilizing the well accelerators and to consider what new techniques and methods can be introduced into the radioactive logging (RL) of bore-holes.

Of all the varieties of radiation, which can be obtained by using accelerators, there is no sense considering any but the strongly penetrative rays, since the instrument to be lowered into a bore-hole must be securely safeguarded in a strong container; implying that the emergence of proton, deutron, alpha particles radiation, etc., out of the instrument will be in practice impossible. Consequently we will consider the use of the well accelerators as possible sources of neutrons, gamma rays and electrons.

Before going on to consider the use of individual types of accelerators let us determine their general superiority over natural sources of radiation, which are commonly used in contemporary radioactive logging.

The most obvious, although not the most important advantage of accelerators rests in the possibility of obtaining with their aid a much stronger radiation than is possible with natural sources, whose strength for safety considerations has to be limited. An accelerator radiates only on being switched on and therefore can be rendered safe when it is brought up to the surface. Moreover, a considerable strength of the source radiation will allow a sharp increase in the speed of the radioactive investigations of bore-holes. In order to avoid inaccuracies in a case where natural sources are being used this speed has to be very small. This advantage can in principal be very important, and has a significant bearing on production; thus, justifying the use of bore-hole accelerators. No less important an advantage is the possibility of obtaining considerable energy from the radiation accelerators, whereas in the case of the natural sources such energy is always limited

to a relatively small magnitude. Thus, for instance, the maximum energy of the gamma rays from natural sources does not exceed 3 MeV, whereas with the aid of a betatron with a heavy element target one can obtain gamma quanta with an energy of tens of millions of electron-volts. The energy of most neutrons produced by the commonly used Po+Be or Ra+Be sources does not exceed 8 to 9 MeV whereas with the use of a neutron generator it is not difficult to obtain neutrons with an energy of the order of 14 MeV.

The third feature of the accelerators, which is advantageous in radioactive logging, consists of the possibility of obtaining with their aid, a monoenergetic radiation, or at any rate a radiation with a distinctly limited maximum energy. This provides a basis for the development of new methods of bore-hole investigation.

However, the most important advantage of the accelerators of charged particles is the possibility of governing their radiation. This allows investigation of bore-holes using a variable intensity of the source and the working out of a vast variety of intermittent methods of investigation.

NEUTRON GENERATOR

In investigating bore-holes the use of the so-called neutron generators, which produce beams of neutrons, is of a paramount interest. The most promising is the use of a neutron generator in neutron-gamma logging (NGL).

In interactions involving the high energy neutrons and the nuclei of the rock forming atoms the principal role is played by the inelastic collisions which produce gamma radiation. A fast neutron as a result of inelastic collisions loses a considerable part of its energy and thereafter, owing to a large number of elastic collisions, it is slowed down to a thermal state. Afterwards, it gets captured by some atomic nucleus, frequently involving the emission of one or several gamma quanta.

The gamma rays produced by the initial inelastic collision of the neutrons with the nuclei of rock-forming atoms can be considered to come into existance instantaneously. Retardation of the neutrons to the thermal state is a relatively lengthy process. Its continuity depends on the nature of the decelerator and is inversely proportional to the hydrogen content of the latter. For instance, in lead the average life of the neutrons with an energy of 14 MeV is 500–3000 μ sec [1] whereas in water it is 2–5 μ sec [3]. In consequence, the gamma rays produced by the capture of the slow neutrons are separated from the gamma rays produced by inelastic collisions with atomic nuclei by relatively long intervals of time. Thus, if during NGL the rocks are subjected to short duration (of the order of microseconds) spurts

of neutron radiation, separated by intervals of time (several hundreds or tens of microseconds) sufficient for the capture of all the generated neutrons, and the scintillometer is switched on for a short period after each spurt then it is possible to register only the gamma rays produced by the initial inelastic collisions of neutrons with atomic nuclei.

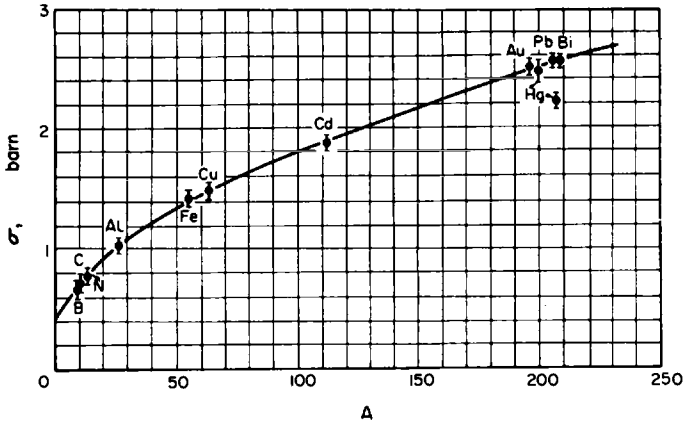

FIG. 1. Cross-section of an inelastic scattering of the neutrons with an energy of 14 MeV.

The cross-section σ of the inelastic scattering of the neutrons with an energy of 14 MeV increases with the growth of the mass number A of the scattering target. Experimental studies [3] show that the relationship between these quantities is well approximated by the following equation.

$$\sigma = \pi R^2,$$

where:

$$R = (2.5 + 1.1A^{1/3}) \times 10^{-13} \text{ cm}.$$

For the light nuclei — to which category belong most of the rock-forming elements — σ lies within the limits of 0.5 to 1.2 barns (Fig. 1) [3]. The relatively small range of σ in the rock-forming elements permits consideration of the inelastic scattering to be approximately equally likely for all of them. This circumstance precludes the possibility of carrying out neutron-neutron logging with the aid of high energy neutrons. The situation is different in the case of neutron-gamma logging.

Experiments, carried out on specimens of pure elements and rocks, have shown that the intensity and the energy of the gamma rays spectrum, produced by the initial inelastic collisions of neutrons with atomic nuclei of various rock-forming elements have characteristic features [12]. This is obvious in

Fig. 2 where there are shown the characteristic spectra of gamma rays produced during the irradiation of specimens of various elements by neutrons with an energy of 14 MeV. There is also shown the background curve (*8*) obtained in the absence of the scattering target. The study of hydrogen and sulphur has revealed somewhat weak gamma rays with the corresponding energies of 2.2 and 2.3 MeV.

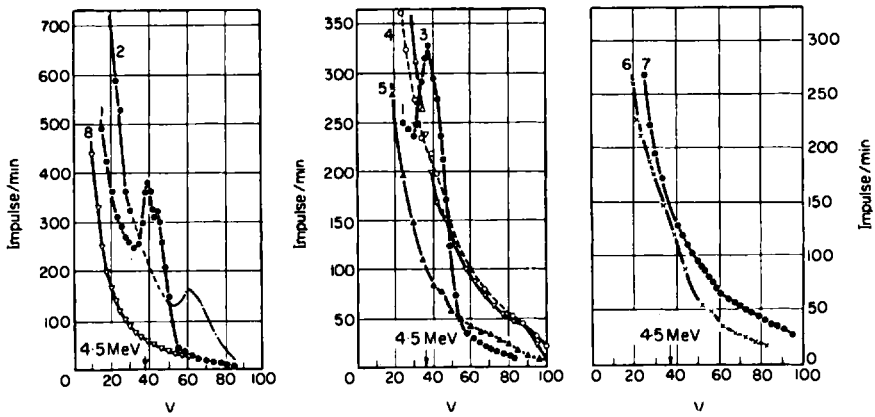

FIG. 2. Differential spectra of the gamma radiation produced in inelastic collisions of the neutrons with an energy of 14 MeV with the atomic nuclei of diverse substances. 1—graphite; 2—water; 3—aluminium; 4—magnesium; 5—iron; 6—calcium; 7—silicon; 8—background curve, obtained in the absence of the scattering agent.

Of all the rock-forming elements only carbon (4.5 MeV) and oxygen (6.5 MeV) produce considerable gamma radiation in inelastic collisions. This allows us to anticipate the possibility of direct detection of carbon, and consequently under favourable geological conditions of petroleum, with the aid of the NGL method involving a neutron generator.

The capture of the fast neutrons occurs at the same time as their elastic and inelastic scattering. Of a neutron with an energy of 14 MeV approximately 0.1 part is captured in collisions with nuclei, giving rise to radioactive nuclei.

Experiments with activation of rock specimens by fast neutrons have shown that their radioactivity is connected with the formation of the radioactive isotopes O^{19} (half-life of 27.5 sec and the gamma rays energy of 1.2 and 1.6 MeV), Al^{28} (half-life of 2.3 min and the gamma rays energy 1.8 and 2.3 MeV) and Na^{24} (half-life of 15 hr and the gamma rays energy of 1.4 and 2.76 MeV). Al is formed as a result of activation of silicon, Na of alumin-

ium, etc. It is established that a few minutes after the end of irradiation by fast neutrons the gamma rays activity in sandstones is already considerably higher than in shales, limestones, etc.

Since under the conditions prevalent in bore-holes the activation of rocks will happen both due to the fast and to the retarded neutrons, in order to develop the fast neutron rock activation method of investigation it is necessary to use an intermittently-operating neutron source.

PRINCIPAL CONSTRUCTION PROBLEMS OF A WELL NEUTRON GENERATOR

A normal well neutron generator is shown diagrammatically in Fig. 3. Its principal constituent parts consist of an ion source, an acceleration tube, a generator of high potential and a target. The ions which form in the ion generator fall into the acceleration tube. Here they are accelerated in the electric field, produced by the high-voltage generator, and bombard the target. Depending on the nature of the target and the ionized gas selected a certain nuclear reaction occurs, which results in the production of a specific radiation. The most widely used neutron generators are those in which ions of deuterium bombard a zircon–tritium target to produce the reaction $H^3(d, n)He^4$, evolving neutrons, with an energy E_n on average near to

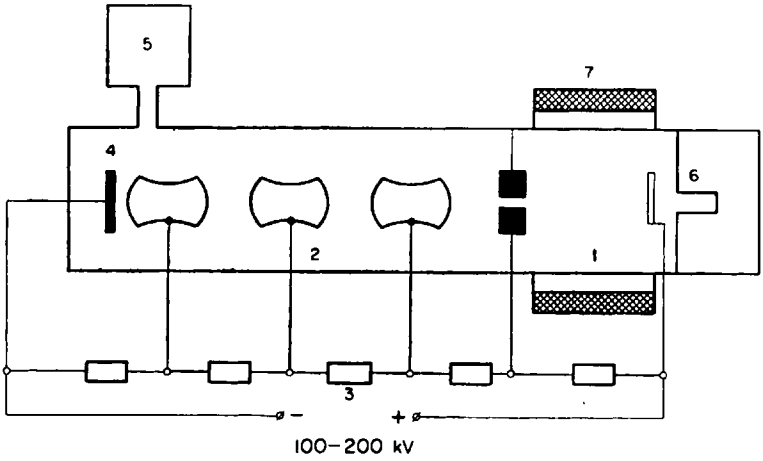

FIG. 3. A basic construction scheme of a neutron generator. 1—an ion source with gas pressure of 10^{-2}–10^{-3} mm Hg; 2—an acceleration tube with gas pressure of 10^{-5}–10^{-6} mm Hg; 3—a generator of high potential; 4—zirconium—tritium target; 5—vacuum pump; 6—a tritium filled cavity, connected via a palladium ventilator, with the ionization chamber; 7—ionizer.

14 MeV. The high efficiency of the reaction $H^3(d, n)$ He^4 and the high energy of the resultant neutrons, as well as the small values of the accelerating potential necessary for it, make this reaction the most useful among all the reactions known to be used to generate neutrons for radioactive logging.

For the sake of comparison let us consider the reaction $H^2(d, n)$ He^3 produced by bombarding a deuterium target. This reaction previously has been very widely used to generate neutrons, but the quantity of neutrons formed in this reaction is much less than in the previous reaction. The neutron energy is also much less. For instance, when $E_d = 0.2$ MeV the value of E_n, which depends on the angle of motion of the neutrons, varies within the limits of 2–3 MeV.

The neutron energy associated with the reaction $H^3(d,n)$ H^4, in general, depends on the angle of emission of the neutrons out of the target, but this dependence weakens as the energy E_d of the accelerated ions of deuterium, or in other words the accelerating potential, decreases. With the present day techniques of electrification of bore-hole instruments it is difficult to obtain potentials higher than 150–200 kW. The corresponding deutron energy will produce a neutron energy of radiation within the limits of 13–16MeV[3].

If the deutron energy is $\leqslant 0.5$ MeV the cross-section of the reaction $H^3(d, n)He^4$ is determined by the following formula[8]:

$$\sigma = \frac{58 \exp\left[-1.72\, E_d^{-0.5}\right]}{E_d\left[1 + 5705\,(E_d - 0.096)^2\right]},$$

where E_d is expressed in mega-electron-volts and σ in barns. Table 1 shows the dependence of the cross-section of this reaction on the energy of the deutrons. The reaction has a sharply developed maximum $\sigma = 4$ barns when $E_d \approx 0.26$ MeV. Since in the target a neutron is relatively rapidly slowed down, it would be sensible to accelerate the deutrons up to energies higher than those which would promote the maximum efficiency of the reaction. This, however, is precluded by difficulties of insulating the high-voltage electrical mechanism in the well apparatus. This circumstance limits the highest possible potential to the maximum of 250 kW.

Let us consider the requirements to be satisfied in the construction of a well neutron generator.

The well generator bas limited dimensions. At any rate its diameter must not exceed 15 cm. The planning of a generator within these limits is a difficult technical problem. In the first place it is difficult to ensure dependable insulation of high-voltage links; and a high voltage is necessary for the working of the acceleration tube. Even a greater difficulty appears owing to the

necessity to maintain vacuum in the acceleration tube (10^{-4} to 10^{-5} mm Hg). To this end the following methods can be employed.

TABLE 1. COMPARISON OF THE EFFECTIVENESS OF THE REACTIONS H^2 (d,n) He^3 AND H^3 (d,n) He^4

The energy of a deutron in MeV.	0.025	0.05	0.1	0.2	0.3	0.5	1	1.5	2	3
Cross section of the reaction $H^2(d,n)He^3$ in barns.	0.005	0.01	0.02	0.04	0.05	0.07	0.09	0.105	0.105	0.1
Cross-section of the reaction $H^3(d,n)He^4$ in barns.	0.3	0.7	4	3.3	2	0.75	~0.2	~0.2	~0.2	~0.2
Ratio of the reaction cross-sections $H^3(t,n)He^4$ and $H^2(d.n)He^3$	60	70	200	82	40	10.7	~2	~2	~2	~2

1. *Pumping out the gas using a vacuum pump*

The use of an ordinary—for instance a steam oil—vacuum pump in a well generator is unsuitable for the following reasons: (a) the need for a vacuum cylinder which would occupy a lot of space in the well instrument; (b) the difficulty of cooling the pump. Since, as a rule, the drilling fluid in the borehole has an elevated temperature it would be necessary either to introduce a cooling device (e.g. a semiconductor) or to introduce a cold substance (solid carbon dioxide, ice, etc,). However, the use of cooling devices which are inefficient demands a considerable power transmission through the cable of the apparatus, whereas the use of a cold substance involves operational invonvenience, such as a frequent necessity of taking apart and reassembling the instrument, etc. Consequently, it is advisable to find other less cumbersome means of maintaining vacuum in the acceleration tube.

2. *The use of a sealed tube*

It is possible to avoid the necessity of pumping the gas out if a sealed acceleration tube—necessary for the acceleration process—is filled with a suitably rarified gas. The construction scheme of such a tube is shown in Fig. 4 [14].

Positive ions, which spontaneously form around the electrode *4*, are accelerated by the potential difference E_1 existing between the electrode and the grid *3* and enter the acceleration interval and then the target. As the target *1* is being bombarded by the accelerated neutrons nuclear reactions occur. These depend on the nature of the target and the gas with which

the tube is filled. The grid *2* prevents the electrons ejected from the target *1* to fall on to the grid *3*.

The distance between the electrodes and the grid is chosen so as to exceed considerably the average free path of the gas ions under a particular pressure. As a result on the way from the electrode to the grid the ions undergo many collisions with the gas molecules, thus evoking its additional ionization.

The distance between the grid and the target is chosen so that it is smaller than the free path of an ion.

The difficulty of producing such a tube lies in the fact that with the minimum gas pressure, which is necessary to ensure a sufficiently energetic running of the process of ionization (10^{-2} to 10^{-3} mm Hg), the average free path

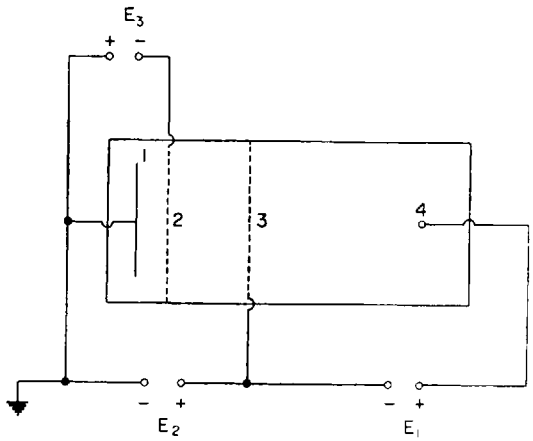

FIG. 4. A basic plan of a sealed acceleration tube with equal pressures at the ion source and the tube.

of the ions becomes smaller and the target *1* and the grid *3* of the tube have to be so near to each other that it is difficult to insulate them from each other owing to the high potential necessary for the effective running of the nuclear reactions.

Another disadvantage of such a tube is its lower efficiency compared with the tubes of normal type. Whereas in the normal tubes the ratio of the intensity of neutron radiation to the current strength of the accelerated ions is usually equal to 10^8 n/sec μA in tubes with deficient discharge it does not exceed 10^6 n/sec μA.

It is necessary to point out that if the sealed tube is filled with deuterium

and a tritium target is being used, as a result of the change in the gas content in the tube, conditioned by the diffusion exchange of the target and the tube hydrogen, there arises a certain degree of instability in the working conditions of the tube. This can be avoided if a mixture of deuterium and tritium is introduced into the tube. In such a case, when small accelerating potentials are employed, the principal role is played by the reaction $H^3(d, n)He^4$ since on collision with deutrons the cross-section of this reaction is considerably smaller. Evidently the filling of the tube with a mixture of H^2 and H^3 lessens the neutron emission by approximately half, per unit of strength of the ion current, in comparison with values obtained when the tube is filled with a single-component gas, since in the former case nearly half of the collided hydrogen atoms would be used up in useless reactions $H^2(d, n)He^3$ and $H^3(d, n)H^3$. On the whole we consider the testing of a sealed tube in a well neutron generator to be important.

3. Use of absorbents

It is possible to avoid the installation of a vacuum pump in a well neutron generator by placing an absorbent in the acceleration tube. Titanium, tantallum, zirconium and certain other substances can be used as absorbents of hydrogen. For instance, it is known that under a pressure of $\sim 10^{-4}$ mm Hg titanium on heating up to 200°C (optimal temperature of absorption) is capable of absorbing up to 1700 cm^3/g of hydrogen.

As a result of experiments conducted by G. D. GLEBOVA [4] it follows that at a temperature of about 40°C the velocity of absorption of hydrogen by metallic titanium is approximately equal to 60 cm^3 H/cm^2 Ti sec. Obviously the velocity of absorption of deuterium would be $\sqrt{2}$ times less.

Let us determine the probable velocity of arrival of hydrogen—derived from an ionic source—into the acceleration tube.

Experience of using neutron generators shows that the relationship between the intensity of the neutron radiation and the current strength of accelerated ions is usually equal to 10^8n/sec μA. Consequently, to obtain a radiation of 10^9n/sec a current of 10 μA is necessary in which case $6.25 - 10^{13}$ ions per second are transported. Thus, $\frac{10^9 \text{ n/sec}}{6.25 \times 10^{13} \text{ ions/sec}} \times 100\% = 1.5 \times 10^3$ per cent ions of deuterium react with the tritium of the target. Adopting the ratio of the atomic to the molecular ions to be equal to 0.5 and an ionic source as given above, we obtain the velocity of arrival of the gas into the acceleration tube to be $3.6 \times 10^{13} D$/sec or 1.7×10^5 cm^3/sec under atmospheric pressure. This implies that the increase in the gas content of the acceleration tube in operating a neutron generator is so small that with the aid of an

absorbent it is possible to rely on the possibility of supporting the necessary vacuum in the tube during a 6–8 hour working day. This interval of time is completely sufficient to investigate a bore-hole. Afterwards the absorbing substance can be changed.

It is completely sufficient to maintain pressures of the order of 10^{-4} mm Hg in an acceleration tube. In order to ensure the absorption of the gas flowing into the tube under this pressure the necessary surface of the absorber should be of an order of $\frac{1.7\times10^{-5}}{60}\times7.6\times10^{6}\times\sqrt{2}\approx3$ cm^2. Considering the unavoidable contamination of the constituent parts of the tube and also its imperfect hermetic qualities this figure should evidently be increased several times. An absorber possessing such a surface can be used in a bore-hole device.

It is considered quite desirable to test the use of absorbers.

4. The use of an ion pump with an absorber

In order to maintain vacuum in an acceleration tube it is also possible to use an ion pump with an absorber. This is a device in which gas molecules are ionized in an electric field and are directed towards an absorbing surface. However, such a method of maintaining vacuum is evidently only slightly more effective than the use of an absorber by itself[22].

5. The use of an ion pump to extract the gas

Figures 5 and 6 show two types of sealed acceleration tubes.

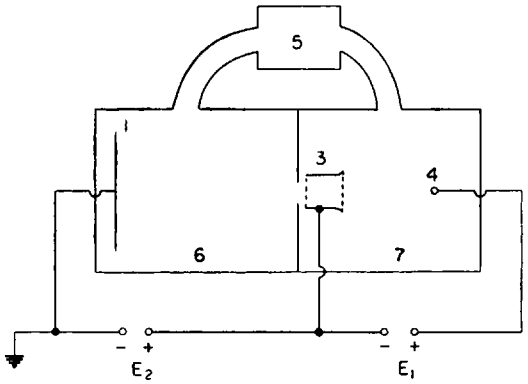

FIG. 5. A basic construction scheme of a sealed acceleration tube with different pressures at the ion source and the tube. 1—target; 3—an electrode extracting the ions; 4—an electrode; 5—a device ensuring the pressure difference between the chambers 6 and 7; other notations are the same as in Fig. 4.

In the tube shown in Fig. 5 there are two chambers (6 and 7) with different concentrations of gas in them. The necessary difference of pressure between the two chambers is maintained by the device 5, which is an ion pump with a cathode which does not absorb the ionized gas. Experimentation with an ion pump of this type has shown that with a relatively small expenditure of effective power it can ensure a pressure difference of 10^{-2} to 10^{-6} mm Hg [7].

TABLE 2. EXPENDITURE OF DEUTERIUM IN THE ACCELERATION TUBE

Pressure in mm Hg	Molecular free path in cm	Expenditure of deuterium					
		To form 10^6 neutrons	Source power when working is 10^9 n/sec			The quantity of the gas used in 10 hrs	
			1 sec	1 hour	10 hours	In the acceleration tube (1 l)	In the ion source (0.5 l)
760	$11.77 \cdot 10^{-6}$	$2.1 \cdot 10^{-14}$	$2.1 \cdot 10^{-11}$	$7.5 \cdot 10^{-8}$	$7.5 \cdot 10^{-7}$	$7.5 \cdot 10^{-10}$	$1.5 \cdot 10^{-9}$
1	0.009	$1.6 \cdot 10^{-11}$	$1.6 \cdot 10^{-8}$	$5.7 \cdot 10^{-5}$	$5.7 \cdot 10^{-4}$	$5.7 \cdot 10^{-7}$	$1.15 \cdot 10^{-8}$
10^{-1}	0.09	$1.6 \cdot 10^{-10}$	$1.6 \cdot 10^{-7}$	$5.7 \cdot 10^{-4}$	$5.7 \cdot 10^{-3}$	$5.7 \cdot 10^{-6}$	$1.15 \cdot 10^{-5}$
10^{-2}	0.9	$1.6 \cdot 10^{-9}$	$1.6 \cdot 10^{-6}$	$5.7 \cdot 10^{-3}$	$5.7 \cdot 10^{-2}$	$5.7 \cdot 10^{-5}$	$1.15 \cdot 10^{-4}$
10^{-3}	9	$1.6 \cdot 10^{-8}$	$1.6 \cdot 10^{-5}$	$5.7 \cdot 10^{-2}$	$5.7 \cdot 10^{-1}$	$5.7 \cdot 10^{-4}$	$1.15 \cdot 10^{-3}$
10^{-4}	90	$1.6 \cdot 10^{-7}$	$1.6 \cdot 10^{-4}$	$5.7 \cdot 10^{-1}$	5.7 —	$5.7 \cdot 10^{-3}$	$1.15 \cdot 10^{-2}$
10^{-5}	900	$1.6 \cdot 10^{-6}$	$1.6 \cdot 10^{-3}$	5.7 —	57 —	$5.7 \cdot 10^{-2}$	$1.15 \cdot 10^{-1}$
10^{-6}	9000	$1.6 \cdot 10^{-5}$	$1.6 \cdot 10^{-2}$	57 —	570 —	$5.7 \cdot 10^{-1}$	1.15 —

Figure 6 shows an interesting variety of sealed acceleration tube in which a single device performs the functions of an ion pump and an ion source for the acceleration tube.

In Table 2 there are presented the results of an estimate of expenditure

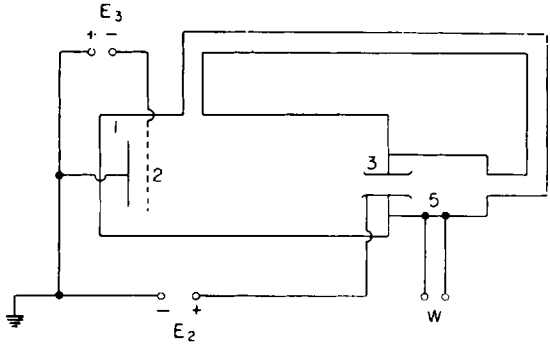

FIG. 6. A basic construction scheme of a sealed acceleration tube in which the ion pump 5 also serves as an ion source. *W*—power source of the ion pump; other notations are the same as in Figs. 4 and 5.

of deuterium in an acceleration tube. The following factors were considered in this calculation.

(a) The average molecular free path in a deuterium or hydrogen atmosphere is equal to 11.77×10^{-6} cm at 760 mm Hg pressure.

(b) There are 6×10^{23} diatomic molecules in 22 litres of deuterium at 0 temperature and 760 mm Hg pressure.

(c) The volume of an acceleration tube in a well neutron generator equals 1000 cm^3; the volume of an ion source is 500 cm^3 and the operational temperature 40 °C, while the duration of an uninterrupted run of the mechanism (until it is filled with gas) is 10 hours. The neutron emission is 10^9n/sec, namely 100 times more than is normally obtained in logging with Po+Be sources.

As is evident from the Table 2 the expenditure of deuterium in a nuclear reaction of the type $H^2(t,n)He^4$ is very small. Even if the source produces 10^9n/sec in a sealed acceleration tube which is shown diagrammatically in Figs. 5 and 6, the expenditure of deuterium, with the gas pressure at the ion source being not less than 10^{-3}–10^{-4} mm Hg, does not exceed 1 per cent per eighteen working hours. Thus, the tube is capable of working for a long time without renewal of the gas that fills it.

GAMMA QUANTA GENERATOR

Well accelerators are used as sources of gamma particles.

First let us consider what new data can be obtained by using these accelerators in gamma-gamma logging.

The contemporary demands of safety in working on bore-holes do not allow the use of natural uninterrupted radiating sources stronger than 30 m Cu. The relative safety of working with an accelerator allows the use of much more powerful gamma quanta in gamma-gamma logging. This makes it possible to increase the velocity of running GGL without lowering its accuracy and to conduct investigations involving considerable distances (provided the distance between the mid-points of the source and the indicator is large).

A source of gamma quanta no stronger than 30 mCu allows us to conduct the GGL method of bore-hole investigations with the aid of the standard apparatus RARK (containing one discharge counter of the type VS–9) with an additional device which screens the counter from the radiation scattered by the drilling fluid. In such a case the deflection of the registered GGL curve from statistical fluctuations will be no more than 1% if the device is raised at a velocity no higher than 500 m/hr.

The use of powerful accelerators of gamma quanta presents a possibility

of increasing the speed of measurement and of making measurements with large sondes. This, as is known from theory and from experimental bore-hole investigations [9, 10], involves a diminution in the influence of the bore-hole, leading to an increase in the sensitivity of the GGL method to the density variations of rocks.

The second circumstance favourable for GGL is the possibility of obtaining a high energy with the aid of gamma ray accelerators. The desirability of using high energy sources during GGL is obvious from the following considerations.

The use of cobalt sources of gamma quanta with an energy of 1.25 MeV in GGL allows the investigation of a rock stratum (density 2.4–2.8 g cm^3) no thicker than 5–7 cm [9, 10] in a bore-hole. Consequently, the presence of a mud crust on the bore-hole wall and a layer of drilling fluid between the crust and the body of the apparatus leads to a considerable diminution in the accuracy of determining the density of the rock.

The increase in the gamma quanta energy increases the depth of investigation* and considerably diminishes the influence of the above mentioned factors on the results of investigations.

Calculations have shown that if the energy of the gamma quanta source is increased from 1 to 15 MeV the average free path of a gamma quantum in the rocks possessing a density of 2–3 g/cm^3 increases four to five-fold and correspondingly the depth of investigation also increases.

The increase in the source energy of the gamma quanta to over 15 MeV is useless since in conjunction with such an increase the phenomenon of formation of electron-position pairs [10] also increases and the penetration depth does not grow much.

In order to obtain more accurate information on the rocks investigated in bore-holes by the GGL method with a high energy gamma quanta generator it is necessary to register the soft part of the spectrum of the scattered gamma ray (0.05–0.07 MeV) by using, for instance, a differential gamma spectrometer. This helps to increase the depth of investigating the rocks. This is connected with the fact that the soft gamma radiation reaching the gamma quanta recorder arrives from those rock strata which are the most distant from the instrument.

GAMMA-NEUTRON LOGGING (GNL)

To study the geological sections of bore-holes and to determine the constitution of certain elements in the rocks gamma neutron logging may

* In this context implies the power of penetration of the rays. [Editor's footnote]

TABLE 3. PHOTONUCLEAR REACTIONS*

Periodic number of the element	Elemental symbol	Atomic weight of the element	Abundance in percents	Reaction threshold (γ, n) MeV	Maximal Reaction output (γ, n)
1	H	2	0.015	2.23	—
2	He	4	100	20.6	24.0
3	Li	6	7.52	5.35	—
		7	92.47	7.15	17.5
4	Be	9	100	1.67	30
5	B	10	18.45	8.55	—
		11	81.35	11.50	—
6	C	12	98.89	18.7	22.4
7	N	14	99.64	10.5	22.5
8	O	16	99.76	15.5	22.5
9	F	19	100	10.4	22.2
10	Ne	20	90.92	16.9	21.5
		22	8.82	10.4	—
11	Na	23	100	12.05	—
12	Mg	24	78.60	16.4	—
		25	10.11	7.25	—
		26	11.29	11.15	—
13	Al	27	100	12.75	19.6
14	Si	28	92.27	16.8	—
		29	4.68	8.45	—
15	P	31	100	12.05	17.19
16	S	32	95.1	14.8	—
		34	4.2	10.85	—
17	Cl	35	75.4	9.95	19.0
		37	24.6	9.5	—
18	Ar	40	99.6	9.8	20.0
19	K	39	93.08	13.2	—
20	Ca	40	96.97	15.9	19.6
22	Ti	46	7.95	13.3	—
		48	73.45	11.6	—
		49	5.51	8.7	—
23	V	51	99.76	11.15	17.7
24	Cr	50	4.31	13.40	19.0
		52	83.76	11.80	17.5
		53	9.55	7.75	19.7

* This table is composed principally from the data given by SEGRE [8] with certain other additions (11, 16, 17, 19, 21).

Table 3 continued.

Periodic number of the element	Elemental symbol	Atomic weight of the element	Abundance in percents	Reaction threshold (γ, n) MeV	Maximal reaction output (γ, n)
25	Mn	55	100	10.1	18.4
26	Fe	54	5.84	13.8	18.3
		56	91.68	11.15	—
		57	2.17	7.75	—
27	Co	59	100	10.25	17.3
28	Ni	58	67.75	11.17	18.5
		60	26.16		16.0
		61	1.25	7.5	—
29	Cu	63	69.1	11.0	17.5
		65	30.9	10.0	19.0
30	Zn	64	48.98	11.65	18.5
		66	27.81	11.15	—
		67	4.11	7.0	—
		68	18.56	10.15	—
		70	0.62	9.2	—
31	Ga	69	60.2	10.1	—
		71	39.8	9.05	—
33	As	75	100	10.2	17.3
34	Se	82	9.19	9.8	—
		?	—	7.3	—
		?	—	9.35	—
35	Br	79	50.52	10.65	16.0
		81	49.48	10.1	16.0
37	Rb	87	27.85	9.3	17.5
38	Sr	86	9.86	9.5	—
		87	7.02	8.4	—
		88	82.56	11.15	—
40	Zr	90	51.46	12.2	18.0
		91	11.23	7.2	—
41	Nb	93	100	8.7	17.0
42	Mo	92	15.86	13.28	18.7
		97	9.45	7.1	—
		—	—	6.75	—
		—	—	7.95	—
44	Ru	?	—	7.05	—
		?	—	9.50	—
45	Rh	103	100	9.35	16.5
46	Rd	?	—	7.05	—
		?	—	9.35	—
47	Ag	107	51.35	9.5	16.0
		109	48.65	9.05	16.0

Table 3 continued.

Periodic number of the element	Elemental symbol	Atomic weight of the element	Abundance in percents	Reaction threshold (γ, n) MeV	Maximal Reaction output (γ, n)
48	Cd	113	12.26	6.5	—
49	In	115	95.77	9.05	—
50	Sn	118	24.01	9.10	—
		119	8.58	6.55	—
		124	5.98	8.50	—
51	Sb	121	57.25	9.25	14.5
		123	42.75	9.3	14.5
52	Te	?	—	6.5	—
		?	—	8.55	—
53	I	127	100	9.3	15.5
55	Cs	133	100	9.05	—
56	Ba	?	—	6.80	—
		?	—	8.55	—
57	La	138	0.09	—	15.5
		139	99.01	8.8	13.8
58	Ce	140	88.48	9.05	—
		142	11.07	7.15	—
59	Pr	141	100	9.4	—
60	Nd	150	5.6	7.4	—
73	Ta	181	100	7.6	13.5
74	W	?	—	6.25	—
		?	—	7.15	—
75	Re	187	62.93	7.8	—
77	Ir	193	61.5	7.8	—
78	Pt	194	32.8	9.5	—
		195	33.7	6.1	—
		196	25.4	8.2	—
79	Au	197	100	8.0	13.5
80	Hg	201	13.22	6.25	—
				6.60	—
81	Tl	203	29.5	8.8	—
		205	70.5	7.5	—
82	Pb	206	23.6	8.25	—
		207	22.6	6.88	—
		208	52.3	7.40	—
83	Bi	209	100	7.40	13.3
90	Th	232	100	6.35	—
92	U	238	99.27	5.97	13.9

be found suitable. In this method the bore-hole wall is irradiated by a powerful beam of gamma quanta of high energy while photo-neutrons, which are knocked out by the gamma quanta from the atomic nuclei, are registered with the aid of a neutron recorder.

Table 3 gives a list of rock-forming elements, which participate in photo-nuclear reactions, the threshold values of the gamma quanta energy which may lead to the appearance of photo-neutrons, and also the maximal energy of the gamma quanta which produce the maximum emission of neutrons.

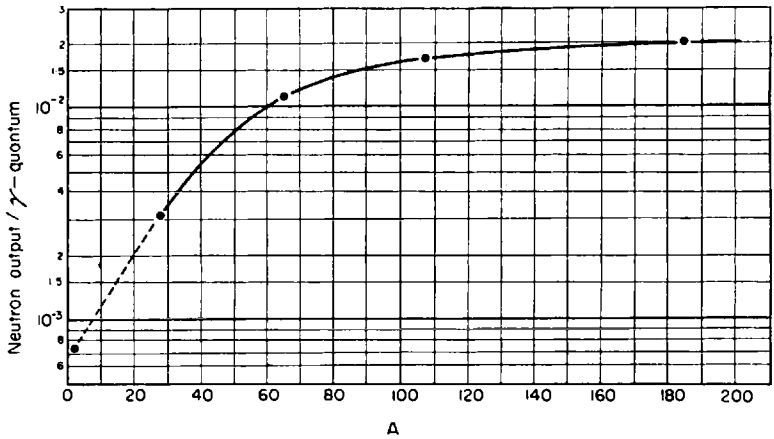

FIG. 7. The dependence of the neutron output per one gamma quantum on the elemental atomic weight A for thick targets of these elements. The gamma-quanta energy of the low atomic weight elements (up to 20) is 2.76 MeV and for the other elements is 17.6 MeV.

Table 3 shows that the values for the energy of the gamma quanta—which cause the knocking of neutrons out of the elemental nuclei—is least for beryllium (1.67 MeV) and deuterium (2.23 MeV). For all the other elements the value of this energy is no less than 6 MeV.

Table 4 and Fig. 7 show the emission of neutrons for 1 gamma quantum. Evidently with the increase in the atomic weight of an element the production of neutrons per one gamma quantum at first grows and then becomes constant and approximately equal to 2×10^{-2} neutrons per 1 gamma quantum. The diminution of the gamma quantum energy leads to the diminution of the production of neutrons per 1 gamma quantum.

Thus, for silver the diminution of the gamma quanta energy from 17.6 to 10 MeV leads to a 70 times lower neutron production per 1 gamma quantum [8].

The most promising outlook for the GNL method exists in the possibility of discovering oil-bearing strata from a higher content of deuterium in oil (1.5–3 times exceeding that in water [6]). Since the threshold energy of photo-splitting of deuterium is not high (2.23 MeV) an accelerator is used which has a relatively low energy of gamma quanta. The building of such an instrument will not involve unsurpassable difficulties. In particular, in such a case, no confusion will arise as a result of the formation of photo-neutrons in the material from which the instrument is constructed or the material of the bore-hole casing tubes for which the threshold energy exceeds 6 MeV.

TABLE 4. NEUTRON OUTPUT PER GAMMA QUANTUM

Periodic number of the element	Elemental symbol	Atomic weight of the element	Neutron output per gamma quantum	Gamma-quantum energy in MeV
1	H	2	$7 \cdot 10^{-4}$	2.76
4	Be	9	$3 \cdot 10^{-4}$	2.76
13	Al	27	$3 \cdot 10^{-3}$	17.6
47	Ag	109	$1.7 \cdot 10^{-2}$	17.6
74	W	?	$2 \cdot 10^{-2}$	17.6

The measurement of the density of photo-neutrons can be made on the background formed by the natural neutron radiation of the rocks. However, the intensity of the latter is very small and it will not preclude the detection of photo-neutrons.

To confirm let us make the following estimate. In petroleum there is 13 per cent of hydrogen; in which the average content of deuterium will be 4×10^{-2} per cent [6]. If we accept the porosity of sandstones to be 30 per cent we will see that deuterium forms $4 \times 10^{-2} \times 0.13 \times 0.3 = 1.6 \times 10^{-3}$ per cent of the mass of the oil-bearing stratum. Since the production of neutrons per one gamma quantum is of the order of 7.4×10^{-4} (with a thick target) for deuterium, the probability of obtaining photo-neutrons in an oil bearing layer will be $7.4 \times 10^{-4} \times 1.6 \times 10^{-3} \times 10^{-2} = 1.2 \times 10^{-8}$ per gamma quantum.

Since the investigation depth in the bore-hole rocks is of the order of 10 cm the probability of the photo-neutrons, which are formed in the stratum and have an energy of about 2 MeV, to reach the recorder will conform to the following rule.

$$P = \frac{e^{-r/\lambda}}{4\pi r^2},$$

where: λ is the average free path of the fast neutrons in the substance under investigation.

r is the average distance of the centre of formation of photo-neutrons from the recorder.

Accepting according to S. A. KANTOR (Private communication) $\lambda = 5$ cm and $r = 10$ cm we obtain $P = 1.1 \times 10^{-4}$.

The volume of the rock with which the gamma radiation (in the instance of a beam of gamma quanta) will interact, will be no less than 1000 cm^3. Consequently, the probability of the photo-neutrons reaching the recorder of the fast neutrons will be:

$$1.2 \times 10^{-8} \times 1.1 \times 10^{-4} \times 10^3 = 1.3 \times 10^{-9}$$

The effectiveness of the fast neutron scintillation counters (diameter 4 cm; length 10 cm) used in bore-hole investigations is approximately 0.1 per cent. Consequently, the probability of registering one neutron will be $P_3 = 1.3 \times 10^{-12}$.

The following values of intensity of natural neutron radiation are known: sedimentary rocks in the presence of the cosmic background -230; extrusive rocks (at depth) -610; pegmatites -3000 n $\times$ cm$^{-2} \times$ day^{-1}. Based on these data it is possible to consider that in oil wells the natural neutron background will not exceed 0.003 n $\times$ cm$^{-2} \times$ sec^{-1}, whereas in a rock layer with a cross-section of 100 cm^2 the natural neutron background I_{bg} affecting the readings in GNL the neutron stream should exceed several-fold the natural neutron background. For this it is necessary to have a source possessing the following power

$$M = I_{bg} m / P_3,$$

where: m is the demanded increase of the induced neutron radiation over the natural;

M is the power of the source measured in gamma quanta per second. Substituting the previously quoted values for I_{bg} and P_3 and assuming $m = 20$, we obtain $M = 4.6 \times 10^{12}$.

It is interesting to examine the possibility of using the gamma-neutron log for the following purposes.

1. Prospecting for beryllium-bearing rocks. Using a method similar to the one used above it is possible to show that to distinguish rocks containing up to 5 per cent of beryllium a source with a power of the order of 10^{11} gamma quanta per sec is necessary. In this connection it is necessary to notice that V. N. DAKHNOV's suggestion about beryllium prospecting using the GNL method with an antimony source of gamma quanta from the point of view of safety of bore-hole working is not easily realizable.

2. Recognition of sandstone layers from their content of the isotope of

silicon with an atomic weight of 29. In this case a gamma quanta source of up to 10^{12} gamma quanta per second is necessary.

3. Recognition of rocks containing rare elements with the atomic weight of an order of 200 in a bore-hole section.

In order to recognize the rare elements of such a high atomic weight when their content in the rock varies from tenths to hundredths of one per cent it is necessary to use a power source of an order of 10^{10} gamma quanta per second.

Scintillation neutron counters used in radioactive logging, besides the neutrons, register also gamma quanta. Let us consider how the scattering of the gamma ray will influence the results of gamma-neutron logging in bombarding the deuterium of a water–oil contact.

The effectiveness of the scintillation neutron indicators using the gamma quanta with energy of an order of 1 MeV is approximately 100 times less than their effectiveness in using neutrons.

Let us assume that the generator produces a directed beam of gamma quanta with an energy of 3 MeV. In reaction with the electrons of the rock atoms this radiation as a result of one act of scattering will lose an average of 50 per cent of energy [10], i.e. it will diminish to 1–1.5 MeV. By a proper selection of the displacement potential in the network of the amplifiers input cascade it is possible to succeed having the non-corresponding impulses unrecorded by the registering instrument. However, owing to the great power of the gamma quanta source there will be a certain number of corresponding impulses which would influence the readings. If the source power is 4.6×10^{12} gamma quanta per sec, and the resolution time of the electronic device of the apparatus used in radioactive logging of an order of 10 μ/sec, and the effectiveness of the recorder towards the gamma quanta is of an order of 10^{-5}, then the number of corresponding impulses is of an order of $10 \times 10^{-6} \times 10^{-5} \times 4.6 \times 10^{12} = 460$ per sec.

When the power of the gamma quanta source is 4.6×10^{12} gamma quanta per sec then $m = 20$. The speed of the photo-neutron count will be equal to 0.3 n/sec $\times 20 = 6$ n/sec. Thus the influence of the synchronously corresponding impulses of the scattered gamma radiation will considerably exceed the effect measured by GNL. To surpass such an influence it is necessary to increase the network displacement of the spectral input into the amplifier so as to distinguish completely between the synchronously corresponding impulses. This is done by increasing the potential twice in comparison with such as is necessary to suppress the non-corresponding impulses. This leads to a slight, but only slight, diminution in the speed of the neutron count.

TABLE 5. NUCLEAR REACTIONS, USED IN OBTAINING GAMMA QUANTA*

Nature of the reaction	Nature of the target	Resonance energy of protons and alpha particles	Gamma-quanta energy in MeV	Gamma-quanta output per proton	Maximal available power of the source in Cu†
$B^{11}(p,\gamma)C^{12}$	B_4C	0.162	16.3 11.8	$4.2 \cdot 10^{-11}$ $1.7 \cdot 10^{-10}$	$6 \cdot 10^{-7}$
$F^{19}(p,\alpha,\gamma)O^{16}$	CaF_2, NaF	0.338	6.3	$1.74 \cdot 10^{-8}$	$5 \cdot 10^{-5}$
$Li^7(p,\gamma)Be^8$	Li (metal)	0.460	17.6 14.8	$1.9 \cdot 10^{-8}$ $0.95 \cdot 10^{-8}$	$8 \cdot 10^{-5}$
$Si^{29}(p,\gamma)P^{30}$	$Si^{29}O_2^{16}$	0.326 0.414	5.86 5.27 0.7	— — —	— — —
$Na^{23}(p,\gamma)Mg^{24}$	NaCl	0.310	4.24	$1.3 \cdot 10^{-11}$	$\sim 4 \cdot 10^{-8}$
$Na^{23}(p,\alpha)Ne^{21}$	— —	0.287–0.539	— —	$2.0 \cdot 10^{-12}$	— —
$Mg^{24}(p,\gamma)Al^{25}$	— —	0.226 0.418	— —	$7 \cdot 10^{-11}$ $2 \cdot 10^{-10}$	$\sim 2 \cdot 10^{-7}$ $3 \cdot 10^{-7}$
$Mg^{25}(p,\gamma)Al^{26}$	— — —	0.317 0.391 0.496	— — —	$3 \cdot 10^{-11}$ $1 \cdot 10^{-10}$	$1 \cdot 10^{-7}$ $3 \cdot 10^{-7}$
$H^3(p,\gamma)He^4$	— —	0.1–6.2	20	$7 \cdot 10^{-11}$	$2 \cdot 10^{-7}$
$H^3(\alpha,\gamma)He^5$ $H^3(\alpha,n)He^4$	— —	0.16 0.16	— —	$2 \cdot 10^{-12}$	$5 \cdot 10^{-9}$

* Composed from the data in [23, 13, 20, 2].

† Number of gamma quanta equals the strength in Curies multiplied by 3.7×10^{10}.

BASIC PROBLEMS IN CONSTRUCTION OF A BORE-HOLE GAMMA QUANTA GENERATOR

A normal acceleration tube or a betatron is used as a gamma quanta generator.

The construction of a gamma quanta generator using a normal acceleration tube in principle does not in any way differ from the construction of a neutron generator which is shown diagrammatically on Fig. 3. However, in order to obtain gamma quanta unstead of neutrons it will be necessary to use other targets and ionized gas.

Nuclear reactions which can be used to obtain gamma quanta are given in Table 5.

The data on the possible power of a gamma quanta source, which are given in Table 5 are based on the following deductions. From the data on

the well neutron generators it is known that currents of charged particles in such generators cannot exceed 10 μA, which corresponds to $\sim 10^{14}$ protons per sec. Knowing the relative output of gamma quanta per proton it is easy to obtain the power of the gamma quanta per second. Knowing the relative output of gamma quanta per proton it is easy to obtain the power of the gamma quanta source. From the Table 5 it is evident that from the point of view of a maximum output of gamma quanta and of obtaining the necessary energy for this the best targets are of lithium and fluor. The use of the former target allows obtaining gamma quanta energy up to 17.6 MeV; while the use of the latter up to 6.3 MeV. Let us consider whether these sources are sufficiently powerful for GGL and GNL.

For GGL with scintillation counters of gamma quanta it is necessary to have the activity of the gamma quanta source in the proximity of the counter of not less than 10^{-9}Cu. The distribution of the scattered gamma radiation in a homogeneous medium is expressed by the formula

$$I = \frac{Qe^{-\tau_{av} l}}{4\pi l^b},$$

where: Q is the power of the gamma quanta source; τ is the average coefficient of gamma radiation weakening in the rock.
l is the sonde length.
b is a coefficient which is a function of the rock density.

TABLE 6. THE SOURCE-POWER NECESSARY FOR GGK IN CURIES

Gamma-quanta energy in MeV	Length of the probe in cm					
	20	30	40	50	60	70
10.0	$2.7 \cdot 10^{-5}$	$8.2 \cdot 10^{-5}$	$1.6 \cdot 10^{-4}$	$4.3 \cdot 10^{-4}$	$7.9 \cdot 10^{-4}$	$1.4 \cdot 10^{-3}$
17.6	$2.9 \cdot 10^{-5}$	$8.6 \cdot 10^{-5}$	$2.0 \cdot 10^{-4}$	$4.0 \cdot 10^{-4}$	$6.8 \cdot 10^{-4}$	$1.14 \cdot 10^{-3}$

Table 6 shows the power of the gamma quanta source with energies of 10 and 17 MeV calculated for different lengths of the sonde according to the above mentioned formula. In the table the quantities of τ_{av} and b are adopted from [9]. Comparing the data of this table with the data of the Table 5 it is evident that the gamma quanta generator with an acceleration tube can be used only with GGL probe of no more than 40 cms.

As has been shown already, to carry out GNL gamma radiation sources with a power of 10^{10}–10^{12} gamma quanta per second (1–10 Cu) are necessary. This exceeds the permitted power of a gamma quanta generator with an acceleration tube.

Consequently, at present, charged particle accelerators which can accelerate protons up to energies of 0.5 MeV, cannot be used in the construction of a gamma quanta generator useful for GGL and GNL. This can be achieved only when it becomes technically possible to accelerate protons up to 1 MeV and more, within the framework of the deep RL apparatus, which circumstance will lead to a sharp increase of neutron output per 1 gamma quantum [13].

To obtain powerful sources of gamma quanta the well betatrons can be used. Using such betatrons it is possible to produce impulses of an order of 10^{18}–10^{10} gamma quanta with a duration of an order of 1 μsec with the upper limit of the gamma quanta energy higher than the natural gamma radiations. The gamma quanta flow per second in such betatrons depends on the current frequency. For instance, when the current frequency is 300 c/s it is possible to generate an output of 10^{10} to 3×10^{12} gamma quanta per sec, which is quite sufficient for operating GGL as well as GNL.

The relationship between the kinetic energy W_{max} (in eV) of accelerated electrons, caused by an inductive force B (in gauss) and orbital radius (in centimetres) can be expressed by the following formula:

$$W_{max} = 300Br.$$

The size of the orbit r will determine the dimensions of the well betatron. The diminution of the orbital radius, necessary in construction, will demand an increase of the magnetic field so that the radiation energy is maintained. For instance, if the orbital radius is taken to be 10 cm, then in order to obtain gamma quanta with an energy of $W_{max} = 3$ MeV it is necessary to generate a field with an inductive force of 1000 G, and for a radius of 5 cm 2000 G, which is quite possible.

ELECTRON LOGGING

Having obtained an electron beam from a betatron it is possible to build an electron log, which involves irradiating the bore-hole walls by a powerful beam of electrons, while the reactive gamma radiation of the rocks is registered.

The energy E and the electron path R in a substance of density ϱ are connected (for $E > 0.8$ MeV) by the formula

$$\varrho R = 0.542E - 0.133.$$

The connection between the energy spent by the electrons on the reaction radiation, and the parameters characterizing the medium (density ϱ and effective atomic number Z_{ef}) can be seen from the following relationship.

$$E_\gamma = E_e \exp\left(-\frac{R}{\varrho Z}\right),$$

where: E is the energy of an electron;

R is the penetration path of the electron in a substance.

TABLE 7. PENETRATION OF ELECTRONS WITH DIFFERENT ENERGY IN SUBSTANCES OF DIFFERENT DENSITIES (cm)

E_e MeV \ ϱ g/cm³	2.0	2.6	3.0
5	1.3	1.0	0.86
10	2.65	2.0	1.8

TABLE 8. THE ENERGY USED BY AN ELECTRON (WITH E_e ENERGY) TO PRODUCE REACTION RADIATION OVER AN INTERVAL R cm (MeV).

E_e MeV \ ϱZ	2 · 12.7	2.6 · 13	3 · 15.7
5	0.25	0.15	0.1
10	1.3	0.6	0.4

TABLE 9. THE ENERGY E_γ, USED BY AN ELECTRON (WITH E_e ENERGY TO PRODUCE REACTION RADIATION OVER AN INTERVAL $r < R$ (MeV)

E_e MeV	ϱZ \ r, cm	2 · 12.7	2.6 · 13	3 · 15.7
5	0.5	0.1	0.008	0.05
10	1.0	0.4	0.2	0.2

The penetration paths of electrons and the energy used by electrons over different path-intervals in the rock, as calculated in terms of these formulae, are shown in the Tables 7–9.

These tables show the following:

(a) The increase in the density of the rock leads to the diminution in the penetration path of an electron in it.

(b) The increase in the electron energy leads to the increase of its penetration path in rocks.

(c) The increase in the density of a rock and of its effective atomic number leads to the generation of a harder reaction radiation.

The reaction radiation, produced in the irradiated medium has its beam near to the direction of the electron beam. At the same time the higher the

electron energy the smaller is the deviation of the reaction radiation, generated in the irradiated medium, from the direction of movement of electrons. Hence in order to distinguish the rocks, their mineral composition and density, with the aid of electron logging, it is necessary to lodge the betatron in the core device so that the hard radiation produced in the rock would reach the gamma quanta counter directly or after the least number of scatterings.

The possible use of electron logging is in dry bore-holes. In bore-holes filled with drilling fluid this method cannot be used owing to its small penetrative power and technical considerations, such as that an electron beam emerges from the vacuum chamber of the betatron via a thin slit which can be easily closed by the liquid filling the bore-hole.

CONCLUSION

The use of the neutron-generators and the gamma quanta in radioactive logging allows a considerable improvement in the effectiveness of neutron logging and gamma-gamma logging, and will also bring about new methods of gamma-neutron and electron types of logging, which will widen considerably the circle of problems solved with the aid of radioactive logging.

The possibility of radioactive methods of investigation can also be considerably widened when a powerful controllable neutron source is constructed as a small size well-reactor.

REFERENCES

1. A. A. BERGMAN, et *al.*, *Physical Studies* (A collection of papers). Izd. Akad. Nauk SSSR, (1956).
2. N. A. VLASOV, *et al.*, *Zh. eksp. teor. fiz.*, (1955).
3. N. A. VLASOV, *Neutrons*, Gosteortizdat, (1955).
4. G. D. GLEBOVA, *An investigation of the Kinetics of Absorption of Hydrogen by Barium and Other Metals.* Candidate thesis, Lenin State Library, (1955).
5. V. N. DAKHNOV, Contemporary Position and the Outlook for Further Development of Well Radiometry. *Exploration and Conservation of Minerals, No. 6,* (1956).
6. *Isotopes in Geology* (A collection of papers). Foreign Literature Publishing House, (1954).
7. E. M. REIKHRUDEL, G. V. SMIRNITSKAIA, A. I. BORISYENKO, *Radiotechnics and Electronics*, No. 12, (1956).
8. E. SEGRE, *Experimental Nuclear Physics*, Vols. I and II, Foreign Literature Publishing House, (1955).
9. E. M. FILIPPOV, A Contribution to the Theory of the Gamma-gamma logging Method *(GGK). Applied Geophysics*, No. 18, Gustoptekhisdat, (1957).
10. E. M. FILIPPOV, *Gamma-gamma Logging. The Use of Radioactive Isotopes in the Oil Industry.* Gostoptekhisdat, 1957.

11. *Photonuclear Reactions* (A collection of papers), part 1, Foreign Literature Publishing House, 1953.
12. R. L. COLDWELL, *World Petroleum.*, **27** (1956).
13. P. M. ENDT, *Phys. Rev.*, **95**, 580 (1954).
14. R. E. FEARON, I. M. THAYER, United States Patents, No. 2712, 0.81, (1955).
15. G. D. FERGUSSON, *Phys. Rev.* **95**, 776 (1954).
16. I. GOLDENBERG, L. KATZ, *Canad. Journ. Phys.*, **32**, 49 (1954); *Phys. Rev.*, 95, 464 (1954).
17. H. E. JOHNES, *et al.*, *Phys Rev.*, **80**, 1062, (1950).
18. L. KATZ, *Phys. Rev.*, **82, 271**, (1591).
19. R. NOTHENS, J. MOLJERU, *Phys. Rev.*, **33**, 437, (1954).
20. J. E. PERRY, S. J. BAME, *Phys. Rev.*, **99**, 1368, (1955).
21. R. SHAR, *Phys. Rev.*, **84**, 387, (1951).
22. V. STONT, M. GIFFOUS, *Appl. Journ. Phys.* (1955).

AUTHOR INDEX

A

Aleinikova, P. K. 268
Alekseev, A. M. 196, 206, 214
Al'pin, L. M. 195, 197, 222, 223, 240
Ambartsumyan, 333
Andreev, B. A. 139, 165
Anurov, B. A. 269
Arkhangel'skaia, A. D. 247, 268
Atwood, D. G. 340
Avanesov, E. T. 378, 382

B

Babalyan, G. L. 377, 378, 382
Bame, S. J. 422
Barstow, O. E. 348
Berdichevskii, M. N. 196, 206, 222, 223
Bergman, A. A. 421
Berzon, I. S. 97, 119
Bessonova, N. 45
Bordovskii, V. P. 196, 223
Borisyenko, A. I. 421
Bortfeld, R. 86, 98
Bryant, C. M. 348
Bulanov, N. A. 214
Bulanzhe, Yu. D. 139, 165
Burgsdorf, V. V. 170, 195
Bursian, V. R. 268

C

Chechik, N. O. 316
Chetaev, D. P. 270
Coldwell, R. L. 422

D

Dakhnov, V. N. 195, 241, 269, 361, 364, 371, 373, 374, 382, 412, 421
Didura, I. G. 241
Dikgof, Yu. A. 269
Dix, C. H. 98
Dobrynin, 363, 364
Dolina, L. P. 349, 350, 351, 354, 358, 359, 360, 361, 362, 363, 364, 368, 371, 373, 374, 382
D'yackhov, N. P. 269

E

Efendiev, F. M. 327
Ellsworth, J. P. 98
Endt, P. M. 422
Epinat'yeva, A. M. 43

F

Fearon, R. E. 422
Fedorova, D. P. 270
Fergusson, G. D. 422
Filippov, E. M. 421
Flathe, K. 195
Florovskaya, V. N. 327
Fomina, V. I. 271
Frolova, A. V. 44

G

Galkin, L. A. 301, 311
Gal'perin, E. I. 44
Gamburtsev, G. A. 119
Geller, E. M. 303
Giffous, M. 422
Glebova, G. D. 405, 421
Goldenberg, I. 422
Gorbatova, V. P. 11
Grushinskii, N. P. 139, 166
Gubkin, I. M. 268
Gumarov, K. S. 268
Gurvich, I. I. 82, 97
Guzanova, 354

H

HANSEN, R. F. 85, 98

I

IL'INA, A. A. 319, 327
IVANKIN, B. N. 82, 98

J

JOHNSON, 83
JONES, P. D. 374, 378, 382

K

KALENOV, E. N. 241, 297
KANTOR, S. A. 415
KATZ, L. 422
KEIVSAR, Z. I. 349
KHARKLVICH, A. A. 120
KHOMENYK, Yu. V. 222
KLEINMAN, M. K. 327
KLIMAREV, A. A. 269
KOMAROV, S. G. 349
KONSTANTINOVA-SCHLEZINGER, M. A. 327
KOPELEV, Yu. S. 210, 270
KOTLIAREVSKII, B. V. 139
KOTYAKHOV, F. I. 376, 377, 382
KRASIL'SHCHIKOVA, G. A. 44
KREY, T. 120
KROLENGO, I. I. 241, 258, 269
KROLENKO-GORSHKOVA, N. G. 269
KUPALOV-YAROPOLK I. K. 98
KURNYSHEV, A. G. 269
KUZNETS, G. 222

L

LAPAURI, A. A. 348
LEVORSEN, A. I. 383
LEVSHUNOV, P. A. 327
LIPILIN, V. A. 200
LITVINOV, S. Ya. 169, 195
LUKAVCHENKO, P. I. 139, 166
LYAMSHEV, L. M. 82, 98
LYCHAGIN, G. A. 269

M

MAIE, R. 195
MAIMIN, Z. L. 270
MALINOSKAIA 18
MALOVICHKO, A. K. 139, 166
MAMEDOV, E. I. 327
MASKET, M. 372, 374, 378, 382
MIGO, L. 222
MILLER, Q. 120
MIRONOVA, V. I. 44
MISHCHENKO, G. L. 270
MOLJERU, J. 422
MOROZOV, G. S. 241, 350, 351, 359, 361, 362, 363, 364, 365, 371, 373, 374, 376, 383
MURATOV, M. V. 270

N

NAZARENKO, O. V. 169, 200
NOTHENS, R. 422

O

OBLOGINA, T. I. 99
OGURTSOV, K. I. 86
OSIPOV, M. F. 270
OSLOPOVSKII, A. N. 270

P

PANTELEYEV, V. L. 123
PERRY, J. E. 422
PETRASHEN', G. I. 11, 15, 21, 43, 98
PETROVSKII, A. D. 222, 240
POLYAKOV, E. A. 384
POPOV, Yu. N. 196
POULTER, 76
PUZYREV, N. N. 139, 166
PYLAEV, A. M. 297

R

REIKHRUDEL, E. M. 421
REINHOLD, 340
RIEBER, F. 120
ROBINSON, W. B. 120
ROSE, W. D. 361, 364, 379, 383

S

SAFONTSEV, E. G. 270
SAMOILOV, M. Ya. 169
SCHLUMBERGER, K. 206
SEGRE, E. 410, 421
SERZHANT, A. A. 161
SHAR, R. 422
SHCHERBAKOVA, T. V. 315, 328
SHEINMAN, S. M. 206, 270
SHIFRIN, K. S. 348
SHULEIKIN, V. V. 333, 348
SHUSHAKOV, S. D. 75
SLOAT, J. 98
SMIRNITSKAIA, G. V. 421
SMIRNOV, V. I. 112, 119
SOBOLEV, S. L. 112, 119
SOKOLOV, P. T. 119
SOROKIN, L. V. 138
SREBRODOL'SKII, D. M. 213
STEFANESKO, S. 185
STONT, V. 422
STREET, J. W. 348
SULTANOV, S. A. 363, 364, 383
SUSLOVA, L. L. 354, 383

T

TAL'VIRSKII, D. B. 43
TEREKHIN, E. I. 169
THAYER, I. M. 422
TIKHONOV, A. N. 270
TIKS'E, M. P. 364, 379, 383
TIMOFEEVA, V. A. 322, 348
TROITSKAYA, V. A. 222
TSEKOV, G. D. 190, 195
TVALTVADZE, G. K. 119

V

VAN MELLER, F. A. 98
VAN'YAN, L. L. 169, 191, 195
VARENTSOV, M. K. I. 268
VASLIL'EV, V. N. 268
VENING MEINISZ, F. L. 123, 138
VESELOV, K. Y. 123, 138
VICTOROV, A. M. 348
VIL'TER, I. B. 348
VLADIMIROV, B. V. 311, 314
VLASOV, N. A. 421
VOLODARSKII, R. F. 139, 160, 165
VUL'F 47

W

WALSTROM, J. E. 379, 383
WATERMAN, J. C. 98
WEATHERBURN, K. R. 98
WYLLIE, M. R. J. 361, 364, 379, 383

Y

YACOBI, I. O. 348
YAKOLEV, K. P. 383
YEPINAT'YEVA, A. M. 76, 97, 106, 119

Z

ZABOROVSKII, A. I. 190, 195, 241
ZAGARMINSTER, A. M. 196
ZAKS, S. O. 372, 374, 382
ZAPOROZHETZ, V. M. 397
ZAVADSKAYA, T. N. 223
ZVOLINSKII, N. V. 97

SUBJECT INDEX

A

Absorbancy of media, effect on seismic wave intensity, 93
Acoustic rigidity, effect on seismic wave reflection, 27–8, 38, 41
Anisotrophy coefficient, of sedimentary deposits, 244
Anticlinal folds, effect on electrical probing, 289–91
Azimuthal-dipole probes, 198–206, 223–40
  arrangement, 223
  errors in, 231–6
  practical procedure, 236–40
  theory of, 224–31

B

Berezovka gas deposits, 210
Beryllium, detection by radiation, 415
Boreholes,
  camera for, 340–4
  optical studies of, 328–48
Boring rate,
  effect on gas saturation of drilling fluid, 311
  variation in, 310

C

Camera, for boreholes, 340–4
Caspian Sea area, geology of, 254–6
Cis-Baltic depression, geoelectric survey, 198
Cis-Carpathian depression, seismic wave reflection in, 75, 85
Clay suspensions,
  effect on oil detection, 320-2
  optical properties, 328–38
Cretaceous deposits, and multiple wave reflection, 75
Crimean steppes, geology of, 252

D

Damping of seismic waves, with distance, 29 37, 38–9, 90–4
Density, effect on seismic wave intensity, 30
Devonian sandstones,
  oil-bearing, permeability, 349
  specific resistance, 335, 350, 354, 361, 363
Diffracted seismic waves, 99–119
  dynamic properties, 108–110
  kinematic properties, 100–8
Diffraction,
  structural formation causing, 99
  from tapering strata, 110–9
Dipole probes,
  azimuthal, 197, 223–40
  effect of non-horizontal rock boundaries on, 292–7
  for inaccessible country, 214
  practical application, 196–206
  theory of, 169–95
DP degasifier, for drilling fluid analysis, 311–2
Drilling fluid,
  degasification, 311
  gas saturation,
    estimation, 302
    factors affecting, 302, 305, 310
  luminescence of, 289–92, 319–22
  luminescent spectral properties, 322–5
  optical properties, 308, 328–38

E

Echoes, single/double comparison, 40, 42
Elastic properties of media, 12
Electrical probing,
  distortion by non-horizontal rocks, 271–97
  in inaccessible country, 214, 223
    Western Siberia, 196–222
    strata relief studies, 201–6

at sea, theoretical curves for, 183–95
at sea, theory of, 170–8
two-way, 196–206
Electrical surveys,
by loop method (see Loop method)
mobile units for, 214–21
Electron logging,
of rock strata, 419–21

G

Gamma–gamma logging, of rock strata, 408–9
Gamma–neutron logging, 381–9, 409–17
for oil, 414
Gamma quanta generator, construction of, 417–9
Gas factor, of oil-bearing strata, 313
Gas logging, factors affecting, 301–5
Gas saturation,
of drilling fluid, effect of boring rate on, 280, 305, 310
estimation of, 302
fluid, factors affecting, 302
of rocks, estimation, 302–5
Gravimeter, static, for use at sea, 123–38
Gravimetric surveys,
accuracy of, 140–2
of Kerch peninsular, 248
observational errors, 144–6
of Russian basins, 160–1
source of errors in, 144–7
Grazing rays, spatial direction, 52
Gypsum-anhydrite, and multiple wave reflection, 85

H

Head waves, intensity, 28–30, 33–35
Hodographs,
construction for reflected waves, 55–73
of diffracted waves, 101, 114–7
theoretical, for multiple reflections, 82

I

Infra-red photography, of rocks, 338
Intensity of seismic waves, 14–43
Isochrone chart, for waves reflected from dome, 62

K

Kaolin, optical properties, 330
Kerch peninsula,
geophysical data, 241–2, 244–5, 247, 263
gravitational field, 248
seismic exploration, 250

L

Lamé constants, 15
Leningrad tables, 27
Light transmittance, of clay suspensions, 331
Logging,
gamma–gamma, 408–9
gamma neutron, 409–17
gas, 84, 301–14
luminescence, 315–27
radioactive, 397–421
Longitudinal seismic waves, intensity, 11–43
Loop method,
developments in, 244–63
economics of, 265
errors in, 251
geological surveys by, 244–59
principles of, 241
uses of, 242–4, 251, 266
Luminescence,
of drilling fluid, 319
of oil, 319–20
of oil–chloroform solutions, 320–1
oil deposit logging by, 285–97, 315–27
Luminoscope, photoelectric, design of, 286–9, 316–319, 326

M

Mesozoic deposits, 201, 204, 210, 250
Mobile units, for electrical surveys, 214–21
Moscow synclinal basin, gravimetric survey, 160–1
Multi-layered media,
reflected wave intensity in, 40
refracted primary waves in, 40
surface hodograph for reflected waves in, 62–73

N

Neutron–gamma logging in, 398–401
Neutron generators,
  for borehole logging, 398–401
  construction of, 373–80, 401–8
  theory of, 401–2
Neutron radiation, of rock strata, 415

O

Oil,
  –chloroform solutions, luminescence of, 320–1
  luminescence of, 298–90 318–20
  spectral characteristics, 322–5
Oil-bearing strata,
  detection by gas logging, 283–4, 313–4
    by loop method, 244, 248, 252, 256
      luminescence logging, 285–97 315–27
      permeability, 352–4, 380–2
      radiation, 414
      seismical data, 251
  permeability, determination, 321–5, 349–53
Oscillations, of multiple reflections, 82–4
Oscillograph, for electrical exploration 217–9

P

Paleozoic deposits, electrical surveys of, 202–4, 209–10, 213
Permeability,
  determination, errors in, 324–5, 330–2, 352–3, 358–60, 364–73
    from core analysis, 354–8, 365, 375–7
    from specific resistance, 349–52, 352–8, 360, 365, 376–82
  of Devonian sandstones, 349–52, 376
  of oil-bearing strata, 349–52, 380
  –specific resistance increase, 332–6, 340–8 360–4, 368–76
  –water saturation, of oil strata, 353, 358–60
Photography,
  of rock samples, 338, 344
  of wells. 336–8, 340–7
Porosity, –specific resistance of rock strata, 362, 368
Primary seismic waves,
  intensity of, 15–18, 28–37
  in multi-layered media, 29–37
  in two-layered media, 28–29

R

Radioactive logging, of boreholes, 397–421
Reflected multiple waves, 75–97
  damping of, 90–4
  dynamic properties, 80–95
  intensity of, 18–27
  interference with single waves, 75–95
  kinematic properties, 76–80
  oscillation intensity, 85–90
Reflected single waves,
  intensity of, 18–27, 37–43
  interference by multiple waves, 75–95
  in multi-layered media, 40–3
  in two-layered media, 37–9
Reflection coefficients, calculation, 18, 21–4, 26–7
Reflective rays, spatial direction, 51
Refracted rays, spatial direction, 52
Refracted waves, 15–18, 28–37
Refraction coefficients, 15, 17, 31
  calculation, 17, 21, 26–7
Resistivity meters,
  coefficient variation, 384–90
  design of, 393–6
  electrode design, 390–3
Rock density, effect on seismic wave intensity, 30
Rock strata,
  disturbance, effect on electrical probes, 271–97
  identification by gamma radiation, 400–1, 409
    by photography, 344–6
  natural neutron radiation values, 415

S

Salinity, effect on resistivity measurements, 358–62, 386–90

Sandstone, detection by radiation, 415
Sea probes, electrical apparatus for, 169–83
Seismic rays, spatial direction, 44–73
Seismic waves,
damping with distance, 29, 37–9
diffracted, dynamic properties, 108–110
kinematic properties, practical, 105–8
properties, theoretical, 100–5
doubly reflected, 39–40, 91
intensity calculation, 15–27
longitudinal, intensity, 11–43
multiple reflected, damping with distance, 90–4
reflected, dynamic properties, 80–95
intensity, 18, 20, 85–90
interference by, 75
kinematic properties, 76–80
primary, in multi-layered media, 28–37
factors affecting, 30–7
intensity of, 15–8, 28–37
reflected, hodograph construction for, 55–73
intensity of, 18–27, 37–43
in multi-layered media, 40, 55–73
refracted, intensity of, 28–37
simple reflected, 18
Seismical studies,
comparison with loop method, 250–4
with telluric currents, 212
of Kerch peninsular, 250
Siberia, west,
electro-geological survey, 196–222, 256
gravimetric survey, 161–3
telluric current fields in, 209
Specific gravity of clay suspensions,
effect on light transmittance, 331
Specific resistance,
of Devonian sandstones, 350, 354, 361, 363
drilling fluid, errors in measurement, 384–90
marine electrical probe instruments, 178–83
Mezo-Cenezoic deposits, 204
oil-bearing strata, 349–53
measurement (see Resistivity meters)
–permeability of rock strata, 360–4, 368–82
–porosity of rock strata, 368–73
Spectral characteristics,
of oil products, 323
Stereographic nets, construction of, 46–7
Stereographic projections, 44–73

T

Taman peninsula,
geology of, 254
Telluric currents,
electronic measuring apparatus, 219–21
in geological surveys, 206–13
in Western Siberia, 209
Transverse waves, effect on longitudinal wave intensity, 30, 39–40
Turkmenia, geology, 256
Two-layered media, wave intensity in, 28–9, 37

U

Ust-Urt plateau,
geology of, 258, 267

V

Volcano-sedimentary strata,
effect on electrical surveys, 199, 204, 210

W

Water saturation,
–permeability of rock strata, 373–4, 377–8, 380–2
–specific resistance of oil strata 351, 353, 358–60
theoretical value, 364
Well camera,
design of, 340–4
Wulff net, 45, 55, 57
accuracy of, 73
uses of, 47–53, 65, 68–9